

Geological Sequestration of Carbon Dioxide in Deep Saline Aquifers: Coupled Flow-Mechanical Considerations

By

Tharaka Dilanka Rathnaweera

BSc. Eng. (Hons)

Supervised by

Professor Ranjith Pathegama Gamage



MONASH University

**A thesis submitted in fulfilment of the requirements for the degree of
Doctor of Philosophy**

Department of Civil Engineering

Faculty of Engineering

Monash University

Melbourne, Australia

August 2016

Copyright notice

© Tharaka Dilanka Rathnaweera (2016).

I certify that I have made all reasonable efforts to secure copyright permissions for third-party content included in this thesis and have not knowingly added copyright content to my work without the owner's permission.

Dedication

To my beloved parents, sister and brother

**This thesis is with publication, in
accordance with section 17.2 of the
Research Graduate School Committee
regulations (Doctorate)**

General declaration

Monash University

In accordance with Monash University Doctorate Regulation 17.2 Doctor of Philosophy and Research Master's regulations the following declarations are made:

This thesis contains no material which has been accepted for the award of any other degree or diploma at any university or equivalent institution and that, to the best of my knowledge and belief, this thesis contains no material previously published or written by another person, except where due reference is made in the text of the thesis.

Signature: 

Print Name: Tharaka Dilanka Rathnaweera

Date: 09/08/16

Thesis including unpublished works declaration

I hereby declare that my unpublished works contain no material which has been accepted for the award of any other degree or diploma at any university or equivalent institution and that, to the best of my knowledge and belief, these works contain no material previously published or written by another person, except where due reference is made in the text of this thesis.

Chapters 2, 3 (partially), 5 and 7 report my unpublished works resulted during the studies undertaken for this degree.

[The inclusion of co-authors reflects the fact that the work came from active collaboration between researchers and acknowledges input into team-based research.]

In the case of Chapters 2, 3 (partially), 5 and 7 my contribution to the work involved the following:

Thesis Chapter	Publication title	Publication status*	Nature and extent of candidate's contribution	Co-author names, nature and % of co-authors contribution
2	A review of the effect of CO ₂ sequestration on hydro-mechanical properties of deep saline aquifers and factors affecting it	Submitted	Initiation, key ideas, literature review, conduct of experiments, data	1) Ranjith PG- key ideas 10% 2) Perera MSA

			analysis and writing up: 85%	-reviewing the manuscript 5%
2	A review of chemical and mineralogical concerns of CO ₂ sequestration in deep saline aquifers	Submitted	Initiation, key ideas, literature review, conduct of experiments, data analysis and writing up: 85%	1) Ranjith PG-key ideas 10% 2) Perera MSA -reviewing the manuscript 5%
3	Stress state and stress path evaluation to address uncertainties in reservoir rock failure in CO ₂ geo-sequestration in deep saline aquifers: An experimental study	Submitted	Initiation, key ideas, literature review, conduct of experiments, data analysis and writing up: 85%	1) Ranjith PG-key ideas 10% 2) Perera MSA -reviewing the manuscript 5%
5	An experimental investigation of coupled chemico-mineralogical and mechanical changes in varyingly-cemented sandstones upon CO ₂ injection in deep saline aquifer environments.	Submitted	Initiation, key ideas, literature review, conduct of experiments, data analysis and writing up: 85%	1) Ranjith PG-key ideas 10% 2) Perera MSA -reviewing the manuscript 5%
7	Development of laboratory-scale numerical model to simulate the mechanical behaviour of deep saline reservoir rocks under varying salinity conditions under uniaxial and triaxial test environments.	Submitted	Initiation, key ideas, literature review, conduct of experiments, data analysis and writing up: 85%	1) Ranjith PG-key ideas 10% 2) Perera MSA -reviewing the manuscript 5%
7	Investigation of relative flow characteristics of brine-saturated reservoir rock: A numerical study of Hawkesbury formation	Submitted	Initiation, key ideas, literature review, conduct of experiments, data analysis and writing up: 85%	1) Ranjith PG-key ideas 10% 2) Perera MSA -reviewing the manuscript 5%
7	Injection and storage of CO ₂ in deep saline aquifers: A numerical study of Hawkesbury formation	Submitted	Initiation, key ideas, literature review, conduct of experiments, data analysis and writing-up: 85%	1) Ranjith PG-key ideas 10% 2) Perera MSA -reviewing the manuscript 5%

I have renumbered sections of unpublished papers in order to generate a consistent presentation within the thesis.

Student signature:



Date: 09/08/16

The undersigned hereby certify that the above declaration correctly reflects the nature and extent of the student's and co-authors' contributions to these unpublished works.

Main Supervisor signature:



Date: 09/08/16

Thesis including published works declaration

I hereby declare that my published works contain no material which has been accepted for the award of any other degree or diploma at any university or equivalent institution and that, to the best of my knowledge and belief, these published works contain no material previously published or written by another person, except where due reference is made in the text of this thesis.

This thesis includes 8 original papers published in peer-reviewed journals and 7 unpublished publications. The core theme of the thesis is geological sequestration of carbon dioxide in deep saline aquifers: coupled flow-mechanical considerations of the potential Gosford carbon capture and storage site. The ideas, development and writing up of all the papers in the thesis were the principal responsibility of myself, the candidate, working with the Department of Civil Engineering, Monash University, under the supervision of Professor Ranjith Pathegama Gamage.

Chapters 3 (partially), 4 and 6 report my published works resulted during the studies undertaken for this degree.

[The inclusion of co-authors reflects the fact that the work came from active collaboration between researchers and acknowledges input into team-based research.]

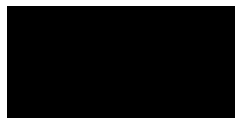
In the case of Chapters 3 (partially), 4 and 6 my contribution to the work involved the following:

Thesis Chapter	Publication title	Publication status*	Nature and extent of candidate's contribution
3	Salinity-dependent strength and stress-strain characteristics of reservoir rocks in deep saline aquifers: An experimental study	Published	Initiation, key ideas, literature review, conduct of experiments, data analysis and writing up: 85%
3	Non-linear stress-strain behaviour of reservoir rock under brine saturation: An experimental study	Published	Initiation, key ideas, literature review, conduct of experiments, data analysis and writing up: 85%
3	CO ₂ -induced mechanical behaviour of Hawkesbury sandstone in the Gosford basin: An experimental study	Published	Initiation, key ideas, literature review, conduct of experiments, data analysis and writing up: 85%

4	Effect of salinity on effective permeability in reservoir rock determined by pressure transient methods: An experimental study on Hawkesbury sandstone	Published	Initiation, key ideas, literature review, conduct of experiments, data analysis and writing up: 85%
4	Determination of effective stress parameters in deep saline aquifers: An experimental study	Published	Initiation, key ideas, literature review, conduct of experiments, data analysis and writing up: 85%
4	Laboratory measurement of deformation-induced hydro-mechanical properties of reservoir rock in deep saline aquifers: An experimental implication of CO ₂ sequestration	Published	Initiation, key ideas, literature review, conduct of experiments, data analysis and writing up: 85%
4	Experimental investigation of geochemical and mineralogical effects of CO ₂ sequestration on flow characteristics of reservoir rock in deep saline aquifers	Published	Initiation, key ideas, literature review, conduct of experiments, data analysis and writing up: 85%
6	Influence of CO ₂ -brine co-injection on CO ₂ storage capacity enhancement in deep saline aquifers: An experimental study on Hawkesbury sandstone formation	Published	Initiation, key ideas, literature review, conduct of experiments, data analysis and writing up: 85%

I have renumbered sections of published papers in order to generate a consistent presentation within the thesis.

Student signature:



Date: 09/08/16

The undersigned hereby certify that the above declaration correctly reflects the nature and extent of the student's and co-authors' contributions to these published works. In instances where I am not the responsible author I have consulted with the responsible author to agree on the respective contributions of the authors.

Main Supervisor signature:



Date: 09/08/16

Acknowledgement

It is my pleasure to acknowledge the roles of several individuals who have been instrumental in the completion of my PhD research. This dissertation would not have been possible without the guidance and help of these people.

First of all, I would like to express my sincere gratitude to my PhD supervisor, Prof. Ranjith Pathegama, who encouraged me to pursue my PhD study and taught me the art of geo-engineering. I am deeply grateful to him for his guidance, support, stoic patience and encouragement during my entire candidature. I am also thankful to him for the treasured advice he gave me about achieving success in my future professional career. I have truly enjoyed working in a research environment that stimulates original thinking and initiative, which he created. In addition, I am extremely thankful to my associate supervisor, Dr. Asadul Haque for his valuable assistance and innovative ideas at various stages of my research work.

Secondly, I appreciate with indebted heart, the help and guidance provided by my associate supervisor, Dr. Samintha Perera. I have been privileged to work with her for around three years and I am truly thankful to her for her tremendous assistance, especially with writing up journal papers, reports and this dissertation. My journal publications would not have been possible without her support.

This acknowledgement would not be complete without thanking the administrative staff of the Civil Engineering department of Monash University, Mrs. Jenny Manson, Miss Tara Fry and Mr. Christopher Powell for their help and support. My heartfelt thanks also go to the technical staff of the Civil Engineering department of Monash University, especially Mr. Long Goh, Mr. Zoltan Csaki, Mr. Alexander Benjamin, Mr. Michael Leach, Mr. Jeff Doddrell, Mr. Kevin Nievaart and Mr. Mark Taylor. It was a great pleasure working with them and I appreciate their ideas, help and good humour. Dr. Alex McKnight is also greatly acknowledged for his continuous support with proofreading my journal papers and this thesis.

I would also like to thank my colleagues Daniel, Navinda, Piyal, Charitha, Nasvi, Gayani, Ranmalee, Nadeesha, Suranj, Dilanth, Arunodi, likhitha, Ashani, Ayal, Pabasara, Dharshana, Arooran, Radhika, Rukshan, Gary, ShiShi, Harsha and Tanvirul for giving such true companionship and creating a friendly environment for me to work in during my journey. Last, but not least, I owe my deepest appreciation to my beloved parents, sister and brother for their priceless support and love given to me throughout my candidature.

Thesis synopsis

Global warming is an extremely crucial challenge for 21st century researchers and numerous climate change policies and mitigation options have been initiated throughout the world during the last few decades. After much research on these approaches to mitigate global climate change, CO₂ sequestration has been identified as the only technology which can reduce CO₂ emissions on a significant scale from fossil fuel power plants and other industrial processes like steel, cement and chemical production in an economically and environmentally friendly way. Sequestration involves the long-term storage of captured CO₂ in deep subsurface geologic reservoirs such as oil/gas fields, deep saline aquifers, unmineable coal seams and mineral sequestration. Of these methods, deep saline aquifers have been identified as an effective geological formation for sequestering anthropogenic CO₂ emissions and isolating them from the earth's atmosphere. However, long-term interaction between injected CO₂ and aquifer brine causes its chemical and mineralogical properties to be significantly changed, resulting in altered hydro-mechanical performance compared to its natural condition. Ultimately, these altered hydro-mechanical properties affect the efficiency and safety of the sequestration process. In relation to the safety of the sequestration process, CO₂-induced reservoir performance maximizes the CO₂ leakage risk by the fracturing or reopening of pre-existing non-transmissive faults in the reservoir. The efficiency of the storage process may be significantly jeopardized due to the fluctuation of the reservoir permeability induced due to rock mineral alterations. Therefore, it is important to understand the reservoir's chemical, mineralogical and hydro-mechanical performances induced due to CO₂ injection before beginning any sequestration project. In addition, the long-term integrity of a potential aquifer formation should be investigated thoroughly, taking into account a number of operational and reservoir variables. Of these variables, CO₂ flow rate, injection pressure and number of injection wells are important operational variables, while depth, salinity, aquifer pH, rock mineralogy and aquifer chemical composition are reservoir variables that should be considered in reservoir performance analysis. Therefore, the main aim of this thesis is to investigate the influence of CO₂/aquifer brine/reservoir rock interactions on the chemical, mineralogical and hydro-mechanical behaviours of deep saline reservoir rock masses under deep reservoir conditions.

In the present study, a comprehensive literature review of the chemical, mineralogical and hydro-mechanical processes involved in deep saline sequestration was carried out, highlighting some factors (operational and reservoir variables) and theories related to the mechanical and

flow behaviours of deep saline formations. Based on identified research gaps, the objectives of this study were defined. This study has two components: experimental which is the major component of the study, followed by some numerical studies. The experimental part is achieved by the comprehensive chemical, mineralogical, micro-structural, mechanical and permeability investigations of CO₂ flow-related properties of intact reservoir rock specimens obtained from the Gosford Basin in New South Wales, Australia. The Gosford formation mainly consists of sandstone and it is known as Hawkesbury sandstone. The numerical section reports the results of investigations of the mechanical and flow-behaviour of the Hawkesbury formation under both laboratory- and field-scale conditions.

The experimental study started by investigating the mechanical behaviour of natural aquifer formations prior to CO₂ injection under both unconfined and confined environment. First, the influence of different salinity conditions on the mechanical properties of reservoir rock in an unconfined stress environment was investigated. Three different salinity conditions (10, 20 and 30% NaCl concentration by weight) were used to saturate the samples and the saturation was done in desiccators under vacuum for one month. After reaching full saturation, a series of unconfined compressive strength tests was performed on brine-saturated reservoir rock samples. In order to identify the influence of salinity on the fracturing process of the reservoir rock, acoustic emission (AE) and ARAMIS technologies were also incorporated in the strength tests. The effect of salinity on the mechanical behaviour of reservoir rock was checked by comparing the results of water-saturated specimens tested under the same conditions. After evaluating the salinity effect in an unconfined environment, experimental testing under confined stress conditions was initiated to understand the effect of confining stress and salinity on rock failure under reservoir conditions. The same salinity conditions were used for the confined stress series. The results of these brine-saturated sandstone strength tests revealed some important characteristics of their failure strength and fracturing mechanisms under natural aquifer conditions. In general, it was observed that brine saturation can considerably increase the reservoir rock strength compared to water saturation, and the reason for this was confirmed by the results of scanning electron microscopy (SEM) analysis, where a significant number of NaCl crystals were observed in the brine-saturated reservoir rock pore space.

After evaluating the mechanical behaviour of natural aquifers, experimental testing under CO₂-reacted conditions was started to evaluate the influence of CO₂/brine/rock interaction on the mechanical properties of reservoir rock. The prepared samples were first saturated with brine

and then reacted with CO₂ using a specially-designed reaction rig. Finally, CO₂-reacted samples were tested under both unconfined and confined stress conditions. A series of unconfined compressive strength tests coupled with AE and ARAMIS was initially conducted to understand the influence of CO₂ on the mechanical properties of reservoir rock. SEM, X-ray diffraction (XRD) and X-ray fluorescence (XRF) analyses were carried out to evaluate the rock mineral alterations induced due to CO₂ injection. A comprehensive mechanical investigation was carried out by performing a series of tri-axial strength tests on these CO₂-reacted samples for a range of injection (0.25-16MPa) and confining (2.5-20MPa) pressures at a constant temperature of 35°C. According to the results, CO₂/brine/rock interaction causes reservoir rock failure strength to be considerably reduced compared to its natural condition. In addition, the tri-axial strength test results revealed the influence of injection and confining pressures on the mechanical properties of reservoir rock during sequestration.

After the mechanical tests, the flow behaviour of reservoir rock was investigated by performing undrained and drained high-pressure permeability tests for both brine-saturated and CO₂/brine-reacted samples. The brine-saturated samples were tested in order to identify the effect of salinity on the flow behaviour of reservoir rock. In addition, the influence of CO₂-phase change, injection and confining pressures on the permeability characteristics of reservoir rock were evaluated. The tests on brine-saturated samples showed that salinity has a significant influence on the permeability of reservoir rock. According to the results, high salinity conditions tend to reduce the aquifer permeability by NaCl crystallisation. The effective stress coefficient for CO₂ permeability also showed a significant correlation to salinity. The experimental testing performed on CO₂/brine-reacted samples indicated the influence of CO₂/brine interaction on the overall flow performance of the reservoir rock. The inductive-coupled plasma mass spectroscopy (ICP-MS) and inductive-coupled plasma atomic emission spectroscopy (ICP-AES) analyses confirmed the dissolution/precipitation of rock minerals upon exposure to CO₂ and brine.

In the case of different sandstone formations, the hydro-mechanical behaviour was observed to be governed mainly by the rock mineralogy. Two types of sandstone: carbonate- and silicate-cemented were therefore chemically, mineralogically and mechanically tested in order to understand the influence of rock mineralogy on CO₂ sequestration. In addition, it is important to identify CO₂ storage enhancement techniques in deep saline sequestration. Therefore, the

present study proposes a potential CO₂ storage enhancement technique: enhancement of CO₂ storage through the co-injection of CO₂ and brine into saline aquifers.

Mechanical and permeability experimental results were used to develop laboratory- and field-scale models using the COMSOL Multiphysics tool. First, a triaxial strength model at laboratory scale was developed using experimental data. After the model was validated, it was further extended to study the failure behaviour of brine-saturated reservoir rock under high confining pressure conditions. According to the results, the numerical model developed considering the stiffness degradation mechanism of reservoir rock can accurately simulate its salinity-dependent stress-strain behaviour under laboratory condition. Interestingly, the predicted results under high confining pressure conditions revealed that this rate of strength increment reduces as the confining pressure increases. Importantly, the model clearly showed a reduction of the pore fluid salinity on reservoir rock strength characteristics with increasing reservoir depth or confinement, mostly due to the more significant effective stress at such extreme depths. This indicates an important insight on CO₂ sequestration in deep saline aquifers: the salinity-dependent strength alterations are not as important for extremely deep aquifers as for shallow aquifers.

After simulating mechanical behaviour, a 2-D axisymmetric relative flow model was developed using the pore-elastic module available in COMSOL Multiphysics, and Buckley-Leverett flow theory was applied to the model using pre-defined partial differential equations. The developed model was first validated using experimental permeability data conducted under triaxial drained conditions and the model was then extended to predict the relative flow characteristics such as brine and CO₂ saturation and CO₂ pressure distribution along the sample length under different injection pressure conditions, including both sub- and super-critical conditions. The results revealed that CO₂ phase change has a significant influence on the final distribution of brine and the CO₂ saturation profile in the reservoir rock sample and this can be simply identified by comparing the shapes of the saturation profiles obtained under both sub- and super-critical conditions.

The relative flow model proposed under laboratory-scale conditions was finally extended to field-scale conditions by coupling geochemical and mineralogical reactions. The PDE interface available in the COMSOL (mathematical module) Multiphysics simulator was used to define the governing processes in reservoirs using partial differential equations. After developing the model, the Dogger aquifer data from the Paris basin were used to validate the model and finally

the model was extended to simulate the Hawkesbury formation. According to the results, long-term interaction of CO₂ causes the Hawkesbury formation's pore structure to significantly change during CO₂ sequestration.

Table of contents

General declaration	iv
Acknowledgement	viii
Thesis synopsis	ix
Table of contents	xiv
List of publications	xxiv
Notations and abbreviations	xxviii
Chapter 1: Introduction	1-1
1.1 Why CO ₂ sequestration is important?	1-2
1.2 Current states of CO ₂ sequestration	1-3
1.3 CO ₂ sequestration in deep saline aquifers	1-7
1.4 Statement of problem, motivation and objective of the thesis	1-10
1.5 Thesis outline	1-16
1.5.1 Introduction-Chapter 1	1-16
1.5.2 Literature review-Chapter 2	1-16
1.5.3 Experimental investigation of the effect of CO ₂ sequestration on mechanical properties of deep saline reservoir rocks - Chapter 3	1-17
1.5.4 Experimental investigation of the effect of CO ₂ sequestration on flow behaviour of deep saline reservoir rocks - Chapter 4	1-18
1.5.5 Experimental investigation of Chemical, mineralogical and mechanical stability of carbonate- and silicate-cemented formations under deep saline sequestration environment - Chapter 5	1-20
1.5.6 Experimental investigation of process enhancing technologies in deep saline CO ₂ storage process - Chapter 6	1-20
1.5.7 Numerical investigation of the effect of CO ₂ sequestration on deep saline reservoir hydro-mechanical properties - Chapter 7	1-21
1.5.8 Conclusions and suggestions for future research - Chapter 8	1-21
1.6 References	1-22
1.7 Summary of Chapter 1	1-27
Chapter 2: Literature Review	2-1
2.1 Introduction	2-2
2.2 The effect of CO ₂ sequestration on hydro-mechanical properties of deep saline aquifers and factors affecting it	2-3

2.2.1 Introduction	2-4
2.2.2 Mechanisms of the CO ₂ storage process in saline aquifers	2-6
2.2.3 Effect of CO ₂ sequestration on chemico-mineral-structure of the aquifer rock mass	2-8
2.2.4 Effect of CO ₂ sequestration on hydro-mechanical properties of saline aquifer	2-11
2.2.4.1 Effect of CO ₂ sequestration on mechanical properties	2-11
2.2.4.1.1 Factors affecting CO ₂ sequestration-induced strength reduction	2-14
2.2.4.2 Effect of CO ₂ sequestration on permeability	2-19
2.2.4.2.1 Factors influencing CO ₂ sequestration-induced permeability alteration	2-22
2.2.5 Risks associated with CO ₂ storage in saline aquifers	2-32
2.2.6 Conclusions	2-33
2.2.7 References	2-35
2.3 The influence of aquifer characteristics and rock mineralogy on deep saline sequestration process	2-47
2.3.1 Introduction	2-48
2.3.2 Role and behaviour of the rock mineral structure upon CO ₂ sequestration	2-51
2.3.3 Prediction models for mineral dissolution and precipitation kinetics in saline aquifers	2-55
2.3.4 Effect of mineral composition on mechanical properties of reservoir rock	2-56
2.3.5 Effect of mineral composition on permeability characteristics of reservoir rock	2-58
2.3.6 Influence of other aquifer characteristics on hydro-mechanical properties of reservoir rock	2-60
2.3.6.1 Effect of pH variation on mechanical properties of reservoir rock	2-61
2.3.6.2 Effect of ionic composition of pore fluid on hydro-mechanical properties of reservoir rock	2-64
2.3.6.3 Effect of distance from injection well on aquifer characteristics	2-65
2.3.7 Existing risk and potential applications	2-68
2.3.8 Conclusion	2-69
2.3.8.1 Scope for future studies	2-70
2.3.9 References	2-71
2.4 Theories of rock failure and flow concepts	2-79
2.4.1 Overview	2-79
2.4.2 Rock failure criteria	2-79

2.4.2.1 The Hoek-Brown failure criterion	2-80
2.4.2.2 Mohr-Coulomb criterion	2-82
2.4.2.3 Modified Mohr-Coulomb criterion	2-83
2.4.2.4 The Drucker-Prager criterion	2-84
2.4.2.5 Modified Lade failure criterion	2-84
2.4.2.6 Modified Wiebols and Cook failure criterion	2-86
2.4.3 Flow concepts for porous media	2-86
2.4.3.1 Scheidegger permeability function for porous media	2-86
2.4.3.2 Davies and Davies's modified exponential relationship	2-87
2.4.3.3 Leverett modified stress-induced permeability formula	2-88
2.4.3.4 Corey's relative permeability function	2-89
2.4.3.5 The Klinkenberg effect for gas permeability measurements	2-90
2.4.3.6 Buckingham Reiner equation for Bingham flow effect	2-91
2.5 References	2-93
2.6 Summary of Chapter 2	2-98
Chapter 3: Experimental Investigation of the Effect of CO₂ Sequestration on Mechanical Properties of Deep Saline Reservoir Rock	3-1
3.1 High-pressure triaxial test apparatus	3-7
3.2 The effect of salinity on mechanical behaviour of deep saline reservoir rock under uniaxial stress environment	3-11
3.2.1 Introduction	3-12
3.2.2 Experimental methodology	3-13
3.2.2.1 Sample preparation	3-13
3.2.2.2 Mechanical properties of rock	3-14
3.2.2.3 Digital image correlation system	3-14
3.2.2.4 Acoustic emission methodology	3-14
3.2.2.5 Experimental procedure	3-14
3.2.3 Results and discussion	3-14
3.2.3.1 Stress–strain behaviour	3-15
3.2.3.2 Acoustic emission (AE) response	3-17
3.2.3.3 ARAMIS photogrammetry response	3-19
3.2.3.4 Scanning electron microscopy (SEM) analysis	3-19
3.2.3.5 Salinity-dependent stress relationship	3-19

3.2.4 Conclusion	3-20
3.2.5 References	3-20
3.3 The effect of salinity on mechanical behaviour of deep saline reservoir rock under reservoir stress environment	3-23
3.3.1 Introduction	3-24
3.3.1.1 Applicability of Mohr–Coulomb failure criterion to saline aquifers	3-26
3.3.2 Methodology	3-26
3.3.2.1 Sample preparation	3-26
3.3.2.2 Triaxial tests	3-29
3.3.3 Results and discussion	3-29
3.3.3.1 Overall stress–strain responses	3-29
3.3.3.2 Effect of water and NaCl saturations on mechanical properties of Hawkesbury sandstone	3-29
3.3.3.3 Applicability of conventional Mohr–Coulomb failure criterion to NaCl-saturated reservoir rocks	3-32
3.3.3.4 Modified Mohr–Coulomb failure criterion for nonlinear behaviour of water- and NaCl-saturated sandstone	3-32
3.3.3.5 Applicability of proposed failure criterion to NaCl-saturated Sandstones	3-35
3.3.3.6 Dilatancy behaviour of reservoir rock under brine saturation	3-35
3.3.3.7 Mineralogical and microstructural aspects	3-38
3.3.4 Conclusions	3-39
3.3.5 References	3-40
3.4 CO ₂ -induced mechanical behaviour of reservoir rock under uniaxial stress condition	3-41
3.4.1 Introduction	3-42
3.4.2 The CO ₂ -water/brine system and its influence on rock properties	3-43
3.4.3 Experimental procedure	3-44
3.4.3.1 Sandstone samples	3-44
3.4.3.2 Sample preparation	3-44
3.4.3.3 Testing procedure	3-45
3.4.3.4 Acoustic emission (AE) methodology	3-46
3.4.3.5 X-ray diffraction (XRD) methodology	3-46
3.4.3.6 Scanning electron microscopy (SEM) methodology	3-46
3.4.4 Results and discussion	3-46

3.4.4.1 Rock mass mineral structure alterations with CO ₂ injection	3-46
3.4.4.2 Geo-mechanical effects	3-52
3.4.4.3 Effect of CO ₂ saturation on the fracture formation pattern of the reservoir rock	3-54
3.4.5 Conclusions	3-55
3.4.6 References	3-55
3.5 The effect of interaction between injected CO ₂ , aquifer brine and reservoir rock on overall mechanical performance of the formation under in situ stress conditions	3-57
3.5.1 Introduction	3-59
3.5.2 Experimental procedure	3-60
3.5.2.1 Sample preparation	3-60
3.5.2.2 Brine saturation process	3-61
3.5.2.3 Brine+CO ₂ reaction	3-61
3.5.2.4 Design of triaxial tests	3-62
3.5.3 Results and discussion	3-65
3.5.3.1 CO ₂ injection-induced stress-strain characteristics in reservoir rocks	3-65
3.5.3.2 Change of effective stress behaviour in deep saline reservoir rock upon CO ₂ injection	3-71
3.5.3.3 Change of reservoir shear strength parameters under various stress environments	3-74
3.5.3.4 Evaluation of mechanical stability of reservoir rock using triaxial data	3-78
3.5.4 Conclusions	3-84
3.5.5 References	3-86
3.6 Summary of Chapter 3	3-91
Chapter 4: Experimental Investigation of the Effect of CO₂ Sequestration on Flow Behaviour of Deep Saline Reservoir Rock	4-1
4.1 Effect of salinity on effective CO ₂ permeability in reservoir rock	4-7
4.1.1 Introduction	4-8
4.1.2 Literature review	4-9
4.1.2.1 Effect of brine concentration	4-9
4.1.2.2 Existing reservoir permeability evaluation measures	4-10
4.1.2.3 Klinkenberg effect for gas permeability measurement	4-11
4.1.3 Experimental program	4-12

4.1.3.1 Sample preparation	4-12
4.1.3.2 The triaxial apparatus and experimental procedure	4-12
4.1.3.3 Porosity measurement of tested samples	4-14
4.1.4 Results and discussion	4-15
4.1.4.1 Effect of salinity on effective CO ₂ permeability	4-16
4.1.4.2 Influence of effective stress on effective CO ₂ permeability in brine-saturated sandstone	4-19
4.1.4.3 The Klinkenberg effect	4-21
4.1.4.4 Corresponding variations in the rock mineral structure	4-22
4.1.5 Conclusions	4-23
4.1.6 References	4-23
4.2 The effect of salinity on effective stress parameters for effective CO ₂ permeability in deep saline aquifers	4-26
4.2.1 Introduction	4-27
4.2.1.1 The concept of effective stress law for permeability of reservoir rock	4-28
4.2.2 Relevant literature	4-28
4.2.3 Experimental methodology	4-29
4.2.3.1 Rock samples	4-29
4.2.3.2 Sample preparation	4-29
4.2.3.3 Permeability tests	4-30
4.2.4 Results and discussion	4-31
4.2.4.1 Effect of injection pressure on effective CO ₂ permeability of brine-saturated Hawkesbury sandstone	4-31
4.2.4.2 Effect of confining pressure on effective CO ₂ permeability of brine-saturated Hawkesbury sandstone	4-33
4.2.4.3 Importance of evaluating effective stress coefficient for the CO ₂ sequestration process in deep saline aquifers	4-35
4.2.4.4 Variation of effective stress coefficient for permeability of brine-saturated Hawkesbury sandstone with pressures	4-36
4.2.4.5 The corresponding variations in rock mass mechanical properties and seismic behaviour	4-38
4.2.4.6 Effect of effective confining pressure on effective CO ₂ permeability of brine-saturated Hawkesbury sandstone	4-40
4.2.5 Conclusions	4-40
4.2.6 References	4-41
4.2.7 Nomenclature	4-41

4.3 Overburden stress effect on flow behaviour of deep saline reservoir rock	4-43
4.3.1 Introduction	4-44
4.3.2 Sample preparation and saturation process	4-46
4.3.2.1 Experimental procedure	4-47
4.3.2.2 Data processing and permeability calculation	4-48
4.3.3 Results and discussion	4-49
4.3.3.1 Stress-strain behaviour	4-49
4.3.3.2 Deformation-induced permeability variation	4-52
4.3.3.3 Further investigation of the influence of rock mass damage development (dilatancy) on its permeability	4-53
4.3.4 Conclusions	4-55
4.3.5 References	4-56
4.4 CO ₂ -induced flow behaviour of reservoir rock under reservoir conditions	4-57
4.5 Summary of Chapter 4	4-70
Chapter 5: Experimental Investigation of Chemical, Mineralogical and Mechanical Stability of Different Sandstone Formations under Deep Saline Sequestration Environment	5-1
5.1 Influence of reservoir mineralogy on deep saline storage process	5-2
5.1.1 Introduction	5-4
5.1.2 Experimental procedure	5-5
5.1.2.1 Sample description	5-5
5.1.2.2 Sample preparation and reaction process	5-7
5.1.2.3 Mechanical testing	5-8
5.1.3 Results and discussion	5-9
5.1.3.1 Reactions between injected CO ₂ and aquifer pore fluid	5-9
5.1.3.2 Reactions between dissolved CO ₂ and aquifer rock minerals	5-13
5.1.3.3 Chemical equilibrium and kinetic evaluation of rock mineral reaction upon exposure to CO ₂	5-19
5.1.3.4 Mineralogical alteration-induced mechanical behaviour in reservoir rock formations	5-27
5.1.4 Conclusions	5-30
5.1.5 References	5-32
5.2 Summary of Chapter 5	5-36

Chapter 6: Experimental Investigation of Process-Enhancement Technologies in Deep Saline CO₂ Storage	6-1
6.1 Influence of CO ₂ -brine co-injection on deep saline storage	6-4
6.1.1 Introduction	6-5
6.1.2 Experimental procedure	6-6
6.1.2.1 Sample preparation	6-6
6.1.2.2 Relative permeability tests	6-6
6.1.3 Results and discussion	6-8
6.1.3.1 Application of Darcy's law and Klinkenberg correction	6-8
6.1.3.2 Two-phase flow behaviours of CO ₂ and brine co-injection	6-10
6.1.3.3 Single- and two-phase flow behaviours of conventional CO ₂ injection	6-10
6.1.3.4 Influence of CO ₂ -brine co-injection on solubility and mineral trapping in saline aquifers	6-13
6.1.3.5 Influence of depth and CO ₂ phase change on solubility and mineral trapping in saline aquifers	6-14
6.1.3.6 Alteration of relative permeability behaviour in saline aquifers through co-injection and its influence on the long-term stability of CO ₂ sequestration	6-15
6.1.3.6.1 Influence of CO ₂ phase change on relative permeability behaviour in saline aquifers	6-15
6.1.3.6.2 Influence of other influencing factors on flow behaviour in saline aquifers	6-16
6.1.3.7 Comparison of co-injection process with other innovative concepts	6-17
6.1.4 Conclusions	6-18
6.1.5 Nomenclature	6-18
6.1.6 References	6-18
6.2 Summary of Chapter 6	6-20
Chapter 7: Numerical Investigation of Effect of CO₂ Sequestration on Deep Saline Reservoir Hydro-mechanical Properties	7-1
7.1 Development of a laboratory-scale numerical model of mechanical behaviour of deep saline reservoir rock under high salinity conditions	7-2
7.1.1 Introduction	7-4
7.1.2 Stiffness degradation model for reservoir rock	7-5
7.1.2.1 Previous studies on stiffness degradation mechanism	7-5
7.1.2.2 Model development	7-7

7.1.3 Experimental data used for model validation	7-12
7.14 Model geometry, parameters, boundary and reservoir conditions and loading	7-13
7.15 Basic assumptions	7-16
7.1.6 Results and discussion	7-16
7.1.6.1 Pore fluid salinity-dependent strength variation in reservoir rock in simple stress environment (uniaxial compressive stress)	7-18
7.1.6.2 Reservoir rock behaviour in real in situ environment (triaxial stress)	7-21
7.1.7 Conclusions	7-24
7.1.5 References	7-27
7.2 Investigation of relative flow characteristics of Hawkesbury formation under laboratory conditions	7-30
7.2.1 Introduction	7-31
7.2.2 Model concept and governing equations	7-36
7.2.3 Model development	7-38
7.2.3.1 Basic assumptions	7-38
7.2.3.2 Geometry, boundary conditions and input parameters	7-38
7.2.3.3 Model validation using experimental data	7-40
7.2.4 Results and discussion	7-41
7.2.5 Conclusions	7-46
7.2.6 Nomenclature	7-47
7.2.7 References	7-49
7.3 Development of a field-scale numerical model of hydro-mechanical, mineralogical and geochemical behaviour of deep saline reservoir rock	7-52
7.3.1 Introduction	7-53
7.3.2 Model development	7-57
7.3.2.1 COMSOL Multiphysics	7-57
7.3.2.2 Governing equations	7-58
7.3.2.3 Model geometry and boundary conditions	7-61
7.3.2.3 Model parameters and variables	7-63
7.3.3 Model validation	7-67
7.3.4 Results and discussion	7-69
7.3.4.1 Chemical and mineralogical response of Hawkesbury formation upon exposure to CO ₂	7-69
7.3.4.2 CO ₂ sequestration-induced hydro-mechanical behaviour of Hawkesbury formation	7-75

7.3.5 Conclusions	7-77
7.3.6 Nomenclature	7-78
7.3.7 References	7-82
7.4 Summary of Chapter 7	7-86
Chapter 8: Conclusions and Suggestions for Future Research	8-1
8.1 Conclusions	8-2
8.1.1 Conclusions regarding mechanical behaviour of deep saline reservoir rock in natural and CO ₂ sequestrated environments	8-2
8.1.1.1 Experimental work	8-2
8.1.1.2 Numerical work	8-7
8.1.2 Conclusions regarding flow behaviour of deep saline reservoir rock in natural and CO ₂ sequestrated environments	8-7
8.1.2.1 Experimental work	8-7
8.1.2.2 Numerical work	8-10
8.2 Suggestion for future research	8-11

List of publications

The following publications have resulted during the studies undertaken for this degree.

Peer-reviewed journal papers

1. **Rathnaweera TD**, Ranjith PG, Perera MSA. 2014. Salinity-dependent strength and stress-strain characteristics of reservoir rocks in deep saline aquifers: An experimental study. *Fuel* 2014; 122:1-11.
2. **Rathnaweera TD**, Ranjith PG, Perera MSA, Yang SQ. Determination of effective stress parameters for effective CO₂ permeability in deep saline aquifers: An experimental study. *Journal of Natural Gas Science and Engineering* 2015; 24: 64-79.
3. **Rathnaweera TD**, Ranjith PG, Perera MSA. Effect of Salinity on Effective CO₂ Permeability in Reservoir Rock Determined by Pressure Transient Methods: An Experimental Study on Hawkesbury Sandstone. *Rock Mechanics and Rock Engineering* 2015; 48(5): 2093-2110.
4. **Rathnaweera TD**, Ranjith PG, Perera MSA, Haque A, Lashin A, Al Arifi N, Chandrasekharam D, Yang SQ, Xu T, Wang SH, Yasar E. CO₂-induced mechanical behaviour of Hawkesbury sandstone in the Gosford basin: An experimental study. *Materials Science and Engineering: A* 2015; 641: 123-137.
5. **Rathnaweera TD**, Ranjith PG, Perera MSA, Lashin A, Al Arifi N. Non-linear stress-strain behaviour of reservoir rock under brine saturation: An experimental study. *Measurement* 2015; 71: 56-72.
6. **Rathnaweera TD**, Ranjith PG, Perera MSA. Experimental investigation of geochemical and mineralogical effects of CO₂ sequestration on flow characteristics of reservoir rock in deep saline aquifers. *Nature Scientific Reports* 2016; 6: 19362.
7. **Rathnaweera TD**, Ranjith PG, Perera MSA, Haque A. Influence of CO₂-brine co-injection on CO₂ storage capacity enhancement in deep saline aquifers: An experimental study on Hawkesbury sandstone formation. *Energy and Fuels* 2016; 30(5): 4229-4243.
8. Perera MSA, **Rathnaweera TD**, Ranjith PG, Wanniarachchi WAM, Nasvi MCM, Haque A. Laboratory measurement of deformation-induced hydro-mechanical properties of reservoir

rock in deep saline aquifers: An experimental implication of CO₂ sequestration. *Marine and Petroleum Geology* 2016; 77: 640-652.

9. **Rathnaweera TD**, Romain, L, Ranjith PG, Perera MSA. Deformation mechanics and acoustic propagation in reservoir rock under brine and oil saturation: An experimental study. *Energy Procedia* 2016; 88: 544-551.

10. Perera MSA, Gamage RP, **Rathnaweera TD**, Ranathunga AS, Koay A, Choi X. A Review of CO₂-Enhanced Oil Recovery with a Simulated Sensitivity Analysis. *Energies* 2016; 9(7): 481-492.

11. Lee B, **Rathnaweera TD**. Stress threshold identification of progressive fracturing in bukit timah granite under uniaxial and triaxial stress conditions. *Geomechanics and Geophysics for Geo-Energy and Geo-Resources* (Accepted).

12. Nasvi MCM, **Rathnaweera TD**, Padmanabhan E. Geopolymer as well cement and its mechanical integrity under deep down-hole stress conditions: Application for carbon capture and storage wells. *Geomechanics and Geophysics for Geo-Energy and Geo-Resources* (Accepted).

13. Wanniarachchi WAM, Ranjith PG, Perera MSA, Wickramarathne MHNDP, **Rathnaweera TD**. Effect of pore fluid saturation characteristics on mechanical properties of low permeable reservoir rocks. *Rock Mechanics and Rock Engineering* (Accepted).

14. **Rathnaweera TD**, Ranjith PG, Perera MSA, Wanniarachchi WAM. Stress state and stress path evaluation to address uncertainties in reservoir rock failure in CO₂ geo-sequestration in deep saline aquifers: An experimental study. *Rock Mechanics and Rock Engineering* (Under review).

15. **Rathnaweera TD**, Ranjith PG, Perera MSA, Wanniarachchi WAM, Haque A. An experimental investigation of coupled chemico-mineralogical and mechanical changes in varyingly-cemented sandstones upon CO₂ injection in deep saline aquifer environments. *Contribution to Mineralogy and Petrology* (Under review).

16. **Rathnaweera TD**, Ranjith PG, Perera MSA, Wanniarachchi WAM. A review of the effect of CO₂ sequestration on hydro-mechanical properties of deep saline aquifers and factors affecting it. *Environmental Earth Science* (Under review).

17. **Rathnaweera TD**, Ranjith PG, Perera MSA, Wanniarachchi WAM. A review of chemical and mineralogical concerns of CO₂ sequestration in deep saline aquifers. *Fuel* (Under review).
18. **Rathnaweera TD**, Ranjith PG, Perera MSA, Haque A, Wanniarachchi WAM. Development of lab scale numerical model to simulate the mechanical behaviour of deep saline reservoir rocks under varying salinity conditions under uniaxial and triaxial test environments. *Rock Mechanics and Rock Engineering* (Under review).
19. **Rathnaweera TD**, Ranjith PG, Perera MSA, Wanniarachchi WAM, Haque A. Investigation of relative flow characteristics of brine-saturated reservoir rock: A numerical study on Hawkesbury formation. *Fuel* (Under review).
20. **Rathnaweera TD**, Ranjith PG, Perera MSA, Haque A. Injection and storage of CO₂ in deep saline aquifers: A numerical study on Hawkesbury formation. *Rock Mechanics and Rock Engineering* (Under review).
21. Perera MSA, Ranjith PG, **Rathnaweera TD**, Ranathunga AS, ZeTM, Choi SK, Wu B. Effects of reservoir and well properties on sand production during the extrusion of hydrocarbons from geological formations. *Energies* (Under review).
22. Perera MSA, Ranjith PG, **Rathnaweera TD**, Ranathunga AS, Liu T, Wu B. An experimental study to quantify sand production during oil recovery from conventional shallow geological formations. *Energy and Fuels* (Under review).
23. Perera MSA, Ranjith PG, **Rathnaweera TD**. Effect of pore fluid saturation on fracability of shale gas reservoirs. *The International Journal of Energy Engineering* (Under review).
24. Wanniarachchi WAM, Ranjith PG, Perera MSA, **Rathnaweera TD**, Zhang DC, Zhang C. Investigation of depth and injection pressure effects on breakdown pressure and fracture permeability of shale reservoirs: An experimental study. *Applied Energy* (Under review).
25. Wanniarachchi WAM, Ranjith PG, Perera MSA, **Rathnaweera TD**. Attenuation of seismic waves in intact rock samples: An experimental study. *Materials Science and Engineering: A* (Under review).

Peer-reviewed conference papers

1. **Rathnaweera TD**, Ranjith PG, Perera MSA. Attenuation of Seismic Waves in Brine-Saturated Hawkesbury Sandstone: An Experimental Study. In 49th US Rock Mechanics/Geomechanics Symposium. American Rock Mechanics Association, 2015: 257-266.
2. **Rathnaweera TD**, Ranjith PG, Perera MSA. Experimental perspectives of deep saline reservoir flow performance due to CO₂/rock/brine interaction. International conference of Geomechanics, Geoenergy and Georesources (IC3G), Melbourne, 2016 (Accepted).

Notations and abbreviations

Notations

k	Permeability
ϕ	Porosity
α	Biot's Effective Stress Coefficient
T	Temperature
\mathcal{G}	Volumetric Expansion Coefficient
k_+	Dissolution Rate Constant
a_i	Activity of the Relevant Species
Ω	Ratio of Activity Quotient to Equilibrium Constant for a Reaction
n, m	Partial Orders of Reaction
k_H	Rate Constants for Proton
k_{OH}	Rate Constants for Hydroxyl
r'	Mineral Dissolution Rate
ν_i	Stoichiometric Coefficient of the Reaction
t	Time
q_i	Charge of the Aqueous Species
k_n	Rate Constant Depending on the Temperature
A_n	Specific Reactive Surface Area
Ω_n	Saturation Index of the Minerals
η, θ	Experimental Based Parameters
E	Activation Energy
R	Gas Constant
$f(\Delta G_r)$	Gibbs Free Energy Term
σ_1'	Major Principal Effective Stress at Failure
σ_3'	Minor Principal Effective Stress or Confining Pressure
m, s	Material Constants
σ_c	Uniaxial Compressive Strength

σ_1	Major Principal Stresses at Failure
σ_3	Minor Principal Stresses at Failure or Confining Pressure
C_i	Cohesion
θ_i	Friction Angle
σ_{crit}	Critical Confining Pressure
C_{i0}	Initial Cohesion
θ_{i0}	Initial Friction Angle
τ_{oct}	Octahedral Shear Stress
σ_{oct}	Octahedral Normal Stress
P_a	Atmospheric Pressure
I_1	First Invariants of the Stress Tensor
J_2	Second Invariants of the Stress Tensor
J_3	Third Invariants of the Stress Tensor
m', η_1	Material Constants
S	Internal Friction
μ_g	Viscosity Coefficient of the Gas
L	Length of the Core Sample
A	Cross Sectional Area of the Core Sample
P_u	Upstream Pore Pressure
P_d	Downstream Pore Pressure
k_0	Zero Stress Permeability
ϕ_0	Porosity at Zero Stress
ϕ_r	Residual Porosity
σ_m'	Mean Effective Stress
P	Average Pore Pressure
S_l	Degree of Liquid Saturation
P_l	Pore Liquid Pressure

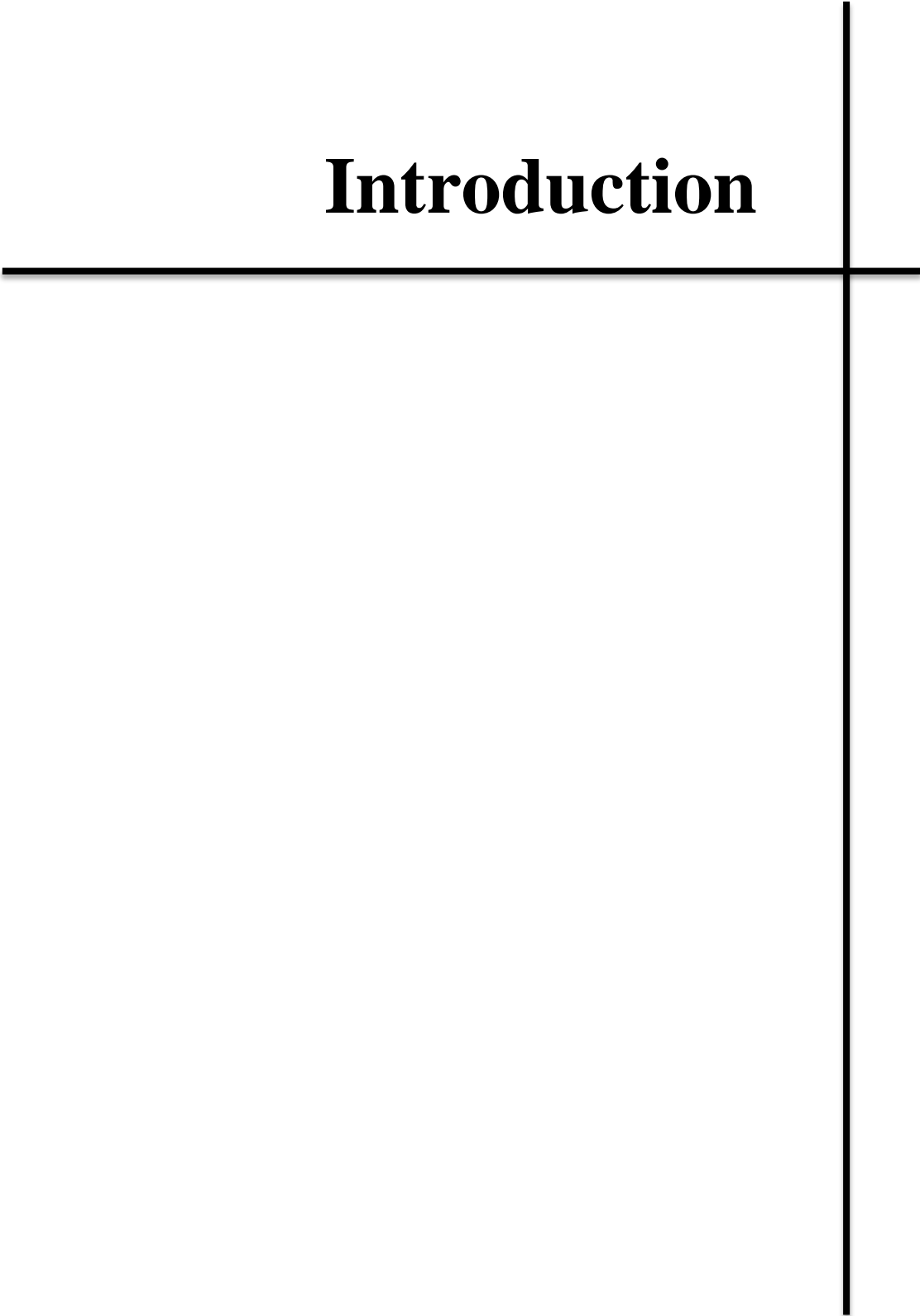
P_g	Pore Gas Pressure
k_{rw}	Relative Permeability of Wetting Phase
S_w	Saturation of Wetting-phase
S_{wr}	Residual Saturation of Wetting-phase
k_{rnw}	Relative Permeability of Non-wetting-phase
S_{wir}	Irreducible Wetting-phase Saturation
S_{nwir}	Non-wetting-phase Saturation
k_{in}	Intrinsic Permeability
ρ	Fluid Density
g	Gravitational Acceleration
k_a	Apparent Permeability
l	Mean Free Path of the Gas Molecules
b	Klinkenberg Slip Factor
Q	Volumetric Flow Discharge
ΔP	Pressure Difference
τ_0	Critical Yield Strength
K	Stress Path Coefficient
T_s	Slip Tendency
φ	Brine Saturation-induced Porosity
z_i	Valence of the Ion i
ε	Dielectric Constant
C_i	concentration
I	Ionic Strength of the Ion
Y_i	Activity Coefficient
E_r	Elastic Modulus at the Residual Stage
E_0	Elastic Modulus at Pre-peak Stage
E_s	Unloading Modulus at Post-peak Stage
γ	Poisson's ratio

Abbreviations

IEA	International Energy Agency
UNFCCC	The United Framework Convention on Climate Change
IPCC	The Intergovernmental Panel on Climate Change
CCS	CO ₂ Capture and Storage
EOR	Enhance Oil Recovery
CO ₂ -ECBM	CO ₂ Enhanced Coal Bed Methane
DEERL	Deep Earth Energy Research Laboratory
SEM	Scanning Electron Microscopy
XRD	X-ray Diffraction
XRF	X-ray Fluorescent
ICP	Inductive-coupled Plasma Mass Spectroscopy
UCS	Uniaxial Compressive Strength
CT	Computerized Tomography
GSI	Geological Strength Index
IPA	Ion Activation Product
SI	Saturation Index

CHAPTER 1

Introduction



1 Introduction

1.1 Why is CO₂ sequestration important?

With the rapid expansion of industrialization, primary energy demand in the world has begun to increase and will continue to rise. Of the various primary energy options (hydro, wind, solar, tide, nuclear, etc.), fossil fuels currently provide around 80% of primary energy demand in the world (IEA, 2014), and due to the low relative cost and abundance of fossil fuels, it is likely that energy production for the foreseeable future will remain dominated by fossil fuels (Johns et al., 2003; Pruess et al., 2004). According to the International Energy Agency's (IEA) 2015 report, even with concentrated action by the United Framework Convention on Climate Change (UNFCCC) to limit temperature increases to under 2°C, fossil fuels will still provide 60% of the world's primary energy demand by 2040 (IEA, 2015). Due to the abundant use of fossil fuel combustion, such as coal, oil and natural gas, the levels of atmospheric carbon dioxide (CO₂), an important greenhouse gas that modulates global climate change, have increased and to date around a 35% increment in the CO₂ level has been recorded in the heavily industrialized areas of the world (Le Treut et al., 2007). In addition, over the past century, the atmospheric CO₂ level has increased more than 39% from 280ppm during pre-industrial times to the record high level of 400ppm in May 2013 (IPCC, 2007). Moreover, the Emission Database for Global Atmospheric Research revealed that the recorded global CO₂ emission value of 33.4 billion tonnes in 2011 was 48% higher than that of the value record two decades ago (IEA, 2014). Perhaps even more important is what will happen due to this uncontrollable global emission of anthropogenic CO₂. To understand the adverse effects of this uncontrollable emission of CO₂ on the environment, many researchers have conducted studies and predicted that an industrial sources-related increase in atmospheric CO₂ could cause an increase in the average global temperature (Alley, 2007; Le Treut et al., 2007), and Alley (2007) showed that the global average temperature may rise by 1.4 to 5.8°C by the end of the 21st century. As a result of this global warming, the Earth's climate and weather patterns may significantly change, leading to extremes of drought and rainfall. Sea levels may be raised due to the melting of polar glacier ice.

Therefore, global warming is an extremely crucial challenge for 21st century researchers and numerous climate change policies and mitigation options have been initiated throughout the world during the last few decades. According to the IPCC special report on emission scenarios

in 2015 (IEA, 2014), without climate change policies, global greenhouse gas emissions in 2030 will increase by 25-90% over the year 2000 level. Therefore, it is necessary to have appropriate CO₂ emission control policies and techniques to create a safer atmosphere for human beings.

1.2 Current state of CO₂ sequestration

To date, the mitigation of uncontrollable emissions of greenhouse gases has become a critical concern among researchers, particularly anthropogenic CO₂ emission, as CO₂ is one of the major greenhouse gases responsible for global warming. Due to this growing awareness, different approaches have been considered and adopted by different countries to control their CO₂ emissions (Leung et al., 2014), including

1. Improved energy efficiency and promotion of energy conservation
2. Promotion of use of low carbon fuels, including hydrogen and nuclear power
3. Increased use of renewable energies, such as solar, wind, hydropower and bioenergy
4. Introduction of geo-engineering approaches, such as afforestation and reforestation
5. CO₂ sequestration or CO₂ capture and storage (CCS)

After much research on these approaches to the mitigation of global climate change (Li et al., 2006; Leung et al., 2014; IEA, 2015), CO₂ sequestration has been identified as the only technology which can reduce CO₂ emissions on a significant scale from fossil fuel power plants and the other industrial processes like steel, cement and chemical production in an economically and environmentally friendly way (IEA, 2014). Interestingly, the Intergovernmental Panel on Climate Change (IPCC) 5th Assessment Synthesis Report (2014) revealed that without CO₂ sequestration, it may not be possible to meet the emission reduction target of limiting global warming to below 2°C relative to pre-industrial levels. In addition, the panel concluded that without CO₂ sequestration, the cost of mitigation will rise by an average of 138%, which is more than double the cost.

Fig. 1.1 shows the growth of large-scale CO₂ sequestration projects in operation by year. According to Fig. 1.1, there are 15 large-scale CO₂ sequestration projects now in operation globally compared with seven at the start of the decade. This reveals the current status of CO₂ sequestration and the maturity of CO₂ sequestration technologies and the number is expected to grow to 22 over the next two years (IEA, 2015). This also highlights the important role of CO₂ sequestration in mitigating global CO₂ emissions. The current total capacity of these 15 large-

scale CO₂ sequestration projects in operation around the world is around 28 million tonnes of CO₂ per year (Mt/year) (IPCC, 2007). However, according to IEA's (2015) study, to achieve the mitigation target of limiting global warming to below 2°C relative to pre-industrial levels, the potential global CO₂ storage capacity needs to be increased to around 4,000 million tonnes in 2040 and 6,000 million tonnes in 2050.



Figure 1.1. Large-scale CO₂ sequestration projects in operation by year (The Global Status of CCS Summary Report, 2015).

In order to maximise the storage capacity, researchers and scientists have considered various types of geological formations to store and isolate captured anthropogenic CO₂ from the surface environment. Three major potential geological formations have recently attracted the attention of the scientific community and the general media due to their many advantages. They are:

1. Depleted oil and gas reservoirs
2. Unmineable coal beds
3. Deep saline aquifers

Fig. 1.2 shows the three major storage options available for CO₂ sequestration (Steadman et al., 2006). These three geological settings have different criteria for consideration for their reliability as potential candidates for storing CO₂ and these are discussed below.

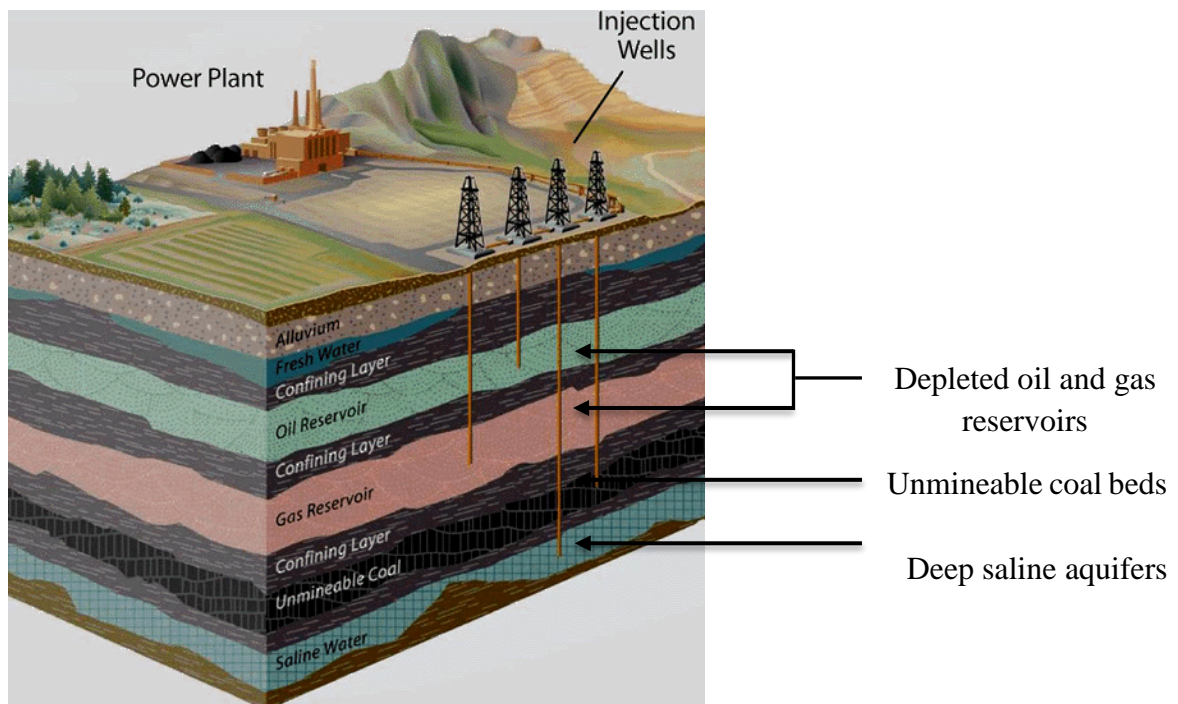


Figure 1.2. CO₂ sequestration in three major geological formations (Steadman et al., 2006).

Of the above, CO₂ sequestration in depleted oil and gas reservoirs has unique advantages. In general, CO₂ is normally injected into depleted oil and gas reservoirs to increase the reservoir pressure and provide the driving force to displace residual oil and gases in tiny pores in reservoirs, while the injected CO₂ remains stored there permanently. According to Blunt et al. (1993), up to 40% of the residual oil and gas trapped in an active reservoir can be successfully extracted after the initial injection of CO₂. In fact, this method has been in use in the oil and gas extraction industry for decades to enhance the recovery of residual oil and gases. Therefore, this practice not only provides a solution to mitigate global warming, it also has economic value which can be used to recover the high cost of carbon capture and storage (CCS). Although this method is considered as the most mature technology for injection of CO₂ for enhanced oil recovery (EOR), the limited available capacity, potential leakage risks and high production costs involved in the process, may limit its feasibility as a CO₂ storage site. However, several EOR projects for CO₂ storage are ongoing and expected to be in operation in the next few years, as shown in Table 1.1.

Table 1.1. List of current and planned CO₂-EOR projects.

Project name	Location	Year of operation start	Max. CO ₂ injection rate Mt/year	Reference
Jilin Oil Field	Jilin, China	-	0.1	Yun et al. (1998)
Weyburn-Midale	Saskatchewan, Canada	2000	2.2	Emberley et al. (2005)
Paradox Basin	Utah, USA	2005	0.14	Kane (2010)
Salt Creek	Wyoming, USA	2006	2.2	Rai et al. (2008)
Williston Basin	North Dakota, USA	2011	1.0	Bachu and Shaw (2004)
South Heart	North Dakota, USA	2012	0.6	Rai et al. (2008)
Oologah	Oklahoma, USA	2012	1.5	Westmark et al. (2006)
Masdar	Abu Dhabi, United Arab Emirates	2012	1.7	Rai et al. (2008)
Hatfield	Hatfield, USA	2013	6.5	Westmark et al. (2006)
California (DF2)	California, USA	2014	5	Nader (2009)
Mongstad	Mondstad, Norway	2014	1.5	Rai et al. (2008)
Trailblazer	Texas, USA	2014	4.3	Rai et al. (2008)
Greengen	China	2015	0.7	Rai et al. (2008)
Genesee (EPCOR)	Alberta, Canada	2015	3.6	Rai et al. (2008)
Kemper County	Mississippi, USA	2016-2017	3.0	IEA (2015)
W. A. Parish plant	Houston, Texas, USA	2016-2017	1.4	IEA (2015)
Emirates Steel Plant	Abu Dhabi, United Arab Emirates	2016-2017	0.8	IEA (2015)
Peterhead	North-east Scotland	2016-2017	1.0	IEA (2015)
White Rose	North Yorkshire, UK	2016-2017	2.0	IEA (2015)
Yanchang Integrated	Shaanxi, China	2016-2017	0.4-0.5	IEA (2015)

Unmineable coal beds can be used to permanently store injected CO₂ due to the adsorption capability of CO₂ to the coal matrix. In addition, this method is widely used in the industry to recover the methane which is trapped in the porous structure of coal seams. This process is called CO₂ enhanced coal bed methane (CO₂-ECBM). The ability to offset the operational costs by using the valuable energy product methane (CH₄) is a unique advantage associated with this process. However, a comprehensive review of CO₂ sequestration in deep unmineable coal beds with the recovery of methane gas by White et al. (2003) highlighted several key issues associated with this process, including limited global storage capacity, storage integrity, physical and chemical processes, and environmental health and safety. Moreover, Stenvens et al. (1998) revealed that many of the potential coal seams have relatively low permeability, causing this process not to be feasible as a good CO₂ storage candidate. A field study of the

Yubari site in Japan confirmed this, and revealed that reservoir permeability must be solved in order to make this method economically viable (Fujioka et al., 2010). Although the process has disadvantages, CO₂ sequestration in deep unmineable coal beds with simultaneous methane gas recovery has been successfully carried out in several coal bed sites in the world since there are economic incentives. A list of current and planned CO₂-ECMB projects in the world is given in Table 1.2.

Table 1.2. List of current and planned CO₂-ECBM projects.

Project name	Location	Year of operation start	Max. CO ₂ injection rate Mt/year	Reference
San Juan Basin	New Mexico, USA	1996	0.1	Stenvens et al. (1998)
Fenn Big Valley	Alberta, Canada	1998	0.02	Gunter (2000)
Recopol	Poland	2003	0.0004	Rai et al. (2008)
Qinshui Basin	China	2003	0.01	Rai et al. (2008)
Yubari	Japan	2004	0.004	Rai et al. (2008)
Permian Basin	Texas, USA	2005	0.3	Esser et al. (2010)
Uinta Basin	Utah, USA	2005	0.9	Van Alphen et al. (2010)
Hokkaido	Japan	2015	0.01	Rai et al. (2008)

Although CO₂ sequestration plays a vital role in reducing global CO₂ emissions, there is a high risk associated with the process, as the injected CO₂ may back-migrate into the atmosphere sometime after injection. However, compared with the other two CO₂ sequestration approaches, long-term storage of CO₂ in deep saline aquifers has more advantages and has also been identified as a safe, practical and economically attractive approach to store captured anthropogenic CO₂. The present study therefore mainly focuses on this particular CO₂ sequestration method.

1.3 CO₂ sequestration in deep saline aquifers

Deep saline aquifers are the most abundant geological reservoirs in the subsurface and can be found both on- and off-shore (Singh, 2008). According to a comprehensive review of several concurrent projects by White et al. (2003), CO₂ sequestration in deep saline aquifers is the most technically feasible approach with few or no negative environmental impacts. In addition to these advantages, deep saline aquifers have the largest storage capacity of all geological media (Bruant et al., 2002) and it is estimated that up to 10,000GtCO₂ could be stored worldwide in

aquifers (IPCC, 2015). A comparison of the available storage capacity of three major geological storage options is shown in Table 1.3. Although it has the greatest storage potential, CO₂ sequestration in deep saline aquifers has no economic benefits, which is the major drawback associated with this method compared to depleted oil and gas reservoirs and unmineable coal seams.

Table 1.3. Storage capacity of three major geological storage options (IPCC, 2005).

Reservoir type	Storage capacity (GtCO ₂)	
	Lower estimation	Upper estimation
Depleted oil and gas	675	900
Unmineable coal beds	3-15	200
Deep saline aquifers	1000	10,000

Suitable geological formations for CO₂ storage have to be carefully selected and fulfil several requirements, including appropriate porosity, thickness, and permeability of the reservoir rock, have a cap rock with good sealing capacity and be in a stable geological environment (Solomon et al., 2008). Reservoir rocks located in deep saline aquifers fit these criteria perfectly, as they generally consist of sedimentary rocks, mainly sandstone. Saline aquifers that have sandstone with high porosity, high permeability and high strength are the ideal geological settings for deep saline sequestration as they allow safe dispersion of CO₂ injection-induced reservoir and fluid pressures. However, the most suitable deep saline aquifers are those at depths greater than 800m, as at this depth, the injected CO₂ behaves as a super-critical fluid, allowing more CO₂ to be safely stored (Perera and Ranjith, 2013). Generally, deep saline aquifers at 800m below ground level often host high salinity brine, and according to past studies (Bachu and Bennion, 2008; Shukla et al., 2013), the brine concentration in deep saline aquifers is in the range of 20,000 to 200,000mg/l. This highly saline brine contains a mixture of ions (Na^+ , Mg^{2+} , Ca^{2+} , Cl^- , HCO_3^- and SO_4^{2-} , etc.) with a greater proportion of $NaCl$ than others (Hem, 1959). Rosenbauer et al. (2005) illustrated the advantages of having mineralized brine as a host fluid, and proved the possibility of enhancement of the storage process of CO₂ by the mineralized brine and injected CO₂-induced chemically-coupled mineralogical phenomena during deep saline sequestration.

Precise understanding of the CO₂ sequestration process in deep saline aquifers, including the geochemical, hydro-mechanical and economic aspects, is important for accurate and reliable storage estimations and the long-term safety of project. This requires substantial experimental and numerical studies. Although a number of studies have set out to evaluate the performance of deep saline aquifers, there is still comparatively little knowledge about CO₂ sequestration in deep saline aquifers compared to other geological sites, such as unmineable coal seams and depleted oil and gas fields (Leung et al., 2014).

Over the past two decades, several pilot and commercial projects on CO₂ sequestration in deep saline aquifers have been launched and are functioning today. Of these projects, Statoil's Sleipner project in the Utsira formation in the North Sea, launched in 1996, is one of the oldest and most successful CO₂ sequestration projects in the world (Arts et al., 2000) and has already injected more than 8 million tonnes of CO₂ successfully (Torp and Gale, 2004). Other current and approved deep saline sequestration projects of different scales (commercial, pilot and demonstration) are summarized in Table 1.4.

Table 1.4. Current and planned projects on CO₂ sequestration in deep saline aquifers.

Project name	Location	Year of injection start	Max. CO ₂ injection rate Mt/year	Scale
Alberta basin	Alberta and B. C., Canada	1990	0.1	Commercial
Statoil's Sleipner	North Sea, Norway	1996	1.0	Demonstration
Frio	USA	2004	0.1	Pilot
In Salah	Krechba, Algeria	2004	1.3	Demonstration
Snohvit	Barents Sea, Norway	2008	0.7	Demonstration
MRCSP-Michigan basin	Gaylord, MI, USA	2008	0.2	Pilot
MRCSP-Cincinnati arch	Kentucky, USA	2009	0.2	Pilot
SECARB early	Cranfield, USA	2009	1.0	Demonstration
Mountaineer	West Virginia, USA	2009	0.1	Commercial
MGSC Decatur	Decatur, II, USA	2010	0.4	Demonstration
ZeroGen	Queensland, Australia	2012	0.7	Pilot
Brindisi	Italy	2012	1.2	Pilot
Latrobe valley	Victoria, Australia	2015	3.0	Commercial

Nagaoka	Japan	2015	0.007	Pilot
Edwards port	Indiana, USA	2015	1.0	Pilot
Gorgon	Barrow Island, WA, Australia	2016-2017	3.4-4	Commercial
Illinois	Illinois, USA	2016-2017	1.0	Commercial

According to Table 1.4, it can be observed that there are significant developments in projects in deep saline aquifers, revealing a steady stream of projects demonstrating the technology in action around the world. For example, previous projects (before 2012) are of small CO₂ injection rates (<1.0Mt/year) but later projects have much larger CO₂ injection rates (>1.0Mt/year). In addition, the Gorgon CO₂ injection project in Western Australia will be the world's largest injection project in deep saline aquifers after it is launched in 2017. When this project is launched, it will inject between 3.4 to 4.0Mt/year of CO₂ in a deep saline formation at a depth of more than 2km.

Another important consideration when selecting a CO₂ sequestration method is the economics of the process. It is obvious that the CO₂ storage cost varies for different storage options. Of these options, CO₂ sequestration in deep saline aquifers does not have any economic benefits, which makes it less economically attractive than others (IPCC, 2007). According to the IPCC (2007) report, the cost of CO₂ storage in deep aquifers normally falls between 0.5 and 7.7US\$/tCO₂ stored. Since offshore deep saline sequestration requires special platforms or sub-sea facilities and deeper drilling equipment, the costs involved in offshore storage are significantly higher than for onshore sequestration. Table 1.5 presents the CO₂ storage cost estimates for both onshore and offshore sequestration in deep saline aquifers.

Table 1.5. CO₂ storage cost estimates for onshore and offshore sequestration in deep saline aquifers (IPCC, 2007).

On or offshore	Location	US\$/tCO ₂ stored		
		Low	Mid	High
Onshore	Australia	0.2	0.5	5.1
Onshore	Europe	1.9	2.8	6.2
Onshore	USA	0.4	0.5	4.5
Offshore	Australia	0.5	3.4	30.2
Offshore	North Sea	4.7	7.7	12.0

1.4 Statement of problem, motivation and objective of the thesis

This study is important, as it is concerned with one of humanity's most critical challenges, mitigating the threat posed by anthropogenic global warming. This study will contribute to national efforts to develop solutions to significantly reduce Australia's greenhouse gas emissions. At the 15th United Nations Framework Convention on Climate Change (UNFCCC), held in Copenhagen, Denmark in 2009, Australia agreed to set its greenhouse emission reduction target 5 to 25% of 2000 levels by 2020. Currently, 93% of Australia's power generation is from fossil fuels, mainly the burning of coal and natural gas (ESAA, 2010). With these levels of dependence on fossil fuels, it is difficult to achieve the CO₂ emission target without technology for geological CO₂ sequestration. Of these technologies, deep saline aquifers have the greatest potential to reduce greenhouse gas emissions, and at levels beyond the targets set at Copenhagen.

However, the injection of CO₂ into a deep saline aquifer causes its physical and mineralogical structure to be significantly changed, and this occurs due to the complex interaction between injected CO₂, brine and the host reservoir formation (Rathnaweera et al., 2015). According to past studies (Busch et al., 2009; Fleury et al., 2010; Rathnaweera et al., 2016), this interaction creates an altered pore structure in the reservoir rock matrix and the resulting microstructural and mineralogical changes then significantly affect the hydro-mechanical behaviour of reservoir rock. Recent field studies conducted by many researchers (Kharaka et al., 2006; Mito et al., 2008; Rutqvist et al., 2010) confirm the possibility of complex variations in the physical, mechanical and chemical behaviour of aquifer formations during long-term sequestration in deep saline aquifers. Therefore, to ensure the long-term integrity of deep saline aquifer CO₂ sequestration, a comprehensive understanding of the coupled mechanical-flow behaviour of reservoir rock and sealing cap rocks is essential prior to CO₂ injection. This understanding cannot be gained only from field trials, and high-precision experiments that simulate the reservoir environment are also required.

Potential deep saline aquifers for CO₂ sequestration are located at depths of 0.8 to 3km (Winter and Bergman 1993). Therefore, the pressures and temperatures at these depths are generally higher than the critical pressure and temperature values of CO₂. The critical pressure and temperature of CO₂ are 7.38MPa and 31.8°C, respectively (Perera et al., 2011). Since both of these parameters normally exceed the critical point of CO₂ at these depths, injected CO₂ exists in its super-critical state during the deep saline sequestration process. Super-critical CO₂ has

gas-like compressibility and liquid-like density and viscosity values (Qu et al., 2010). Therefore, the viscosity and density of injected CO₂ in to deep saline aquifers varies greatly with depth, due to the variation of the pressure and temperature with depth. In addition, super-critical CO₂ displays higher solubility characteristics in aquifer brine compared to sub-critical (gaseous) CO₂ (Liu et al., 2003), which reveals the different behaviours of super-critical CO₂ and sub-critical CO₂. Due to this thermodynamic difference between sub- and super-critical CO₂, the interaction between injected CO₂, aquifer brine and reservoir rock changes with the phase change of injected CO₂, resulting in different chemical and hydro-mechanical responses under the two different conditions. To date, no detailed study has been reported regarding the chemical and hydro-mechanical behaviour of deep saline reservoir rocks under these two conditions. Therefore, a comprehensive study was conducted to understand the effect of CO₂ phase change on the chemical and hydro-mechanical characteristics of reservoir rock in deep saline aquifers by examining the 1) strength variation 2) flow behaviour 3) chemical response and 4) mineralogical response of reservoir rock under both states of CO₂.

Potential deep saline aquifers for CO₂ sequestration contain highly saline brine, and the salinity increases with increasing depth of the aquifer. Due to this salinity effect, different hydro-mechanical and microstructural behaviours are expected in deep saline reservoir rock compared to dry or water-saturated sandstone. Shukla et al. (2013) studied the mechanical behaviour of reservoir rock under different brine-saturated conditions and confirmed the significant effect of brine saturation on the mechanical properties of reservoir rock. Therefore, the effect of salinity on reservoir rock mechanical properties is an important topic for investigation. However, few studies have been carried out to date on this aspect, and it is important to note that the studies which have been conducted have not focussed on high salinity effects, which is the expected situation in real field conditions. Therefore, a series of mechanical tests was conducted to examine the high salinity effect on deep saline reservoir rock in the range of 10 to 30% concentrations of NaCl (% by weight) under both triaxial and uniaxial stress conditions.

In addition to the alteration of mechanical properties of deep saline reservoir rock, salinity has a significant influence on the effective and relative permeability characteristics of reservoir rock. The permeability reduction associated with the deposition of NaCl crystals and the salt dry-out effect during CO₂ injection is a threat in terms of the long-term CO₂ trapping process, because it reduces CO₂ movement through the rock pore space, which eventually affects the overall injectivity. A detailed knowledge of the flow behaviour of natural formations is therefore

important to enhance the safety and effectiveness of CO₂ storage in deep saline aquifers. In order to understand the effect of salinity on the flow behaviour of reservoir rocks, a comprehensive experimental study was conducted under reservoir conditions.

As the CO₂ sequestration process in deep saline aquifers is a long-term process, the interactions between injected CO₂, brine, and reservoir rock in deep saline aquifers alter their natural hydro-mechanical properties, affecting the safety and efficiency of the sequestration process. To date, a number of studies have set out to evaluate the effect of CO₂ interaction on reservoir rock behaviour, but most studies have focused only on the chemical and mineralogical components, with little attention to how reservoir mechanical and flow is influenced by long-term CO₂ interaction. The results of these studies (Emberley et al., 2005; Hovorka et al., 2006; Kharaka et al., 2006; Rutqvist et al., 2010) suggest that dissolution of injected CO₂ brine has considerable effects on the chemical diffusion and mineral structure in the rock. The interaction between the resulting acidic environment from the solubility reaction of CO₂ in brine and the reservoir rock causes both dissolution and precipitation of primary and secondary rock minerals, resulting in altered minerals and micro-structures in the rock pore space. These changes significantly affect the hydro-mechanical properties of reservoir rock. The impact on mechanical and flow properties in deep saline aquifers can only be evaluated by the combined use of geochemical, mineralogical and hydro-mechanical experiments. Therefore, combined long-term geochemical, mineralogical and hydro-mechanical experiments were conducted to identify the interaction-induced mineralogical changes in aquifers, and their impact on reservoir rock mechanical and flow properties.

Generally, deep saline sequestration is a highly time-consuming process and therefore, the incorporation of short-term (relative to real field) laboratory data with the real field case is one of the major challenges. Although many field-scale simulations have been developed to evaluate the flow behaviour in reservoir rock in deep saline aquifers using different computer software packages, including TOUGH 2, COMSOL, FEMLAB, COMET 3, MSFLOW and METSIM2, little attention has been given to the application of these software programs on laboratory-scale studies (Class et al., 2000; Audigane et al., 2007; Bielinski et al., 2008). All the experimental studies reported to date have been limited to the short-term effects of CO₂ injection in deep saline aquifers, and reveal nothing about hydro-mechanical behaviour under long-term CO₂ sequestration. Therefore, it is important to have laboratory-scale simulations to predict the long-term variation of short-term experimental data and extend the findings to field

conditions. Therefore, a comprehensive study was conducted to develop an appropriate laboratory-scale model to simulate CO₂ permeability and strength variation in reservoir rock under different salinity, temperature, injection and confining pressure conditions. First, a basic model of CO₂ movement in sandstone under triaxial test conditions was developed using the COMSOL simulator, and this model was finally modified to model the possible chemical and mineralogical reactions that can occur during interaction between injected CO₂, brine and reservoir rock minerals.

In order to investigate the real field behaviour of CO₂ sequestration in deep saline aquifers, there is a need for the development of coupled mechanical-flow field numerical simulations that incorporate the influence of chemical, mineralogical and microstructural changes that occur during CO₂ sequestration in deep saline aquifers on rock hydro-mechanical behaviour. More general approaches to the coupling between chemical, mineralogical and hydro-mechanical effects in geomaterials for a variety of environment problems have been discussed by Hueckel (2005). According to this study, current modelling approaches include coupling through a swell strain linked to CO₂ adsorption, assume elastic behaviour, and link volume strain to changes in hydro-mechanical characteristics through empirical relationships. In these approaches, material parameters are introduced to allow for the evaluation of hydro-mechanical properties due to changes in pore fluid chemistry. However, the scarcity of relevant data on how hydro-mechanical properties in typical reservoir and sealing rocks for CO₂ sequestration are likely to evolve limits the application of such an approach. To date, many field simulations have been developed to investigate the complex interactions of the various physical, hydro-mechanical and chemical processes that occur in deep saline sequestration, but fully-coupled models that can handle the time and length scales involved in the different processes both accurately and efficiently are not available. Therefore, the present study developed a fully-coupled numerical field scale model and validated it based on the results obtained from experimental data and past studies. The validated model was then used to investigate the parameter space for CO₂ sequestration in deep saline aquifers, in terms of the influence of reservoir variables (depth, temperature, brine chemistry and reservoir rock type) and operational variables (injection rates, injection periods and injection strategies) on the system's overall performance. The model will help to advance knowledge with respect to reservoir types and depths and operational variables that will produce optimal performance in deep saline aquifer CO₂ sequestration. This in turn will help to provide information for planning and policy development.

The research methodologies employed in this experimental and numerical modelling work will contribute to the advancement of knowledge, as they can be adopted or modified for new investigations in a variety of deep CO₂ sequestration applications. Finally, this study will also provide a springboard for future investigations of the hydro-mechanical, chemical and mineralogical aspects of deep saline sequestration through comprehensive and carefully-designed laboratory- and numerical-based studies.

The main objectives of the thesis can be outlined as follows:

1. To investigate the effects of salinity on the mechanical behaviour of deep saline reservoir rock using uniaxial and triaxial experiments.
2. To evaluate the effects of salinity on the permeability of deep saline aquifers using high-pressure triaxial experiments.
3. To investigate the effects of injection and confining (depth effect) pressures on the mechanical flow of deep saline aquifers during CO₂ injection and storage.
4. To evaluate the chemical, mineralogical and microstructural changes that occur in reservoir rocks following the injection of CO₂ into deep saline aquifers and the manner by which these changes influence the hydro-mechanical properties of these rocks.
5. To distinguish the mechanical and permeability behaviour of deep saline reservoir rock under sub-critical and super-critical CO₂ flow conditions using triaxial experiments.
6. To distinguish the chemical, mineralogical and hydro-mechanical behaviour of silicate- and carbonate-cemented reservoir rock under deep saline sequestration conditions.
7. To investigate the process-enhancement technologies in deep saline CO₂ storage and how they can be employed in the sequestration process in the most effective way, including the control of effective factors and the best injection scenarios.
8. To develop an experimentally-validated laboratory-scale numerical model using the COMSOL simulator to model CO₂, chemical, mineralogical and hydro-mechanical behaviour in deep saline reservoir rock using triaxial experiments.
9. To develop a field-scale numerical model using the COMSOL simulator to study the coupled chemico-mineralogical-mechanical flow behaviour of deep saline reservoir rock during CO₂ sequestration.

1.5 Thesis outline

This thesis comprises of eight chapters as follows:

1.5.1 Introduction - Chapter 1

Chapter 1 gives a general introduction to the entire research program. This chapter begins with a brief description of the current situation in relation to the greenhouse gas effect, global warming and the importance of the adoption of CO₂ sequestration technologies. Then, it outlines the current situation of CO₂ sequestration, giving brief introductions to three different major CO₂ sequestration approaches, including deep saline aquifers. This chapter also summarises the gaps in the existing research and the contribution of the present study to fill these gaps. Finally, the chapter gives the thesis outline.

1.5.2 Literature review - Chapter 2

The second chapter is the literature review and presents a critical and comprehensive literature review and comparison of past studies conducted on deep saline reservoir rock. This chapter consists of four main sections. The first section gives the introduction. The next section is a submitted journal paper entitled “*A review of the effect of CO₂ sequestration on hydro-mechanical properties of deep saline aquifers and factors affecting it*”. This paper presents a basic introduction to deep saline sequestration, the trapping mechanisms of the CO₂ sequestration process in deep saline aquifers, the effect of CO₂ sequestration on the chemico-mineral-structure of the aquifer rock mass, the effect of CO₂ sequestration on the hydro-mechanical properties of deep saline aquifers and factors affecting it and finally, the risks associated with CO₂ sequestration in deep saline aquifers.

The third section of this chapter is a submitted journal paper named “*A review of chemical and mineralogical concerns of CO₂ sequestration in deep saline aquifers*”. This section of the chapter reviews the role and behaviour of the reservoir rock mineral structure upon CO₂ sequestration, available models for the prediction of mineral dissolution and precipitation kinetics in deep saline aquifers, the influence of aquifer characteristics on the hydro-mechanical behaviour of deep saline aquifers, including the mineral composition of reservoir rock, and the effect of distance from the injection well on overall aquifer performance. The final section of the chapter presents a brief introduction to the constitutive and empirical relationships and

concepts involved in the investigation of the hydro-mechanical behaviour of deep saline reservoir rocks and documents future research requirements in the field.

1.5.3 Experimental investigation of the effect of CO₂ sequestration on mechanical properties of deep saline reservoir rocks - Chapter 3

The third chapter presents some results of strength tests conducted using both the uniaxial compressive strength and the triaxial strength testing equipment available in the Civil Engineering Department at Monash University. The main aim of this experimental series was to investigate the mechanical behaviour of natural reservoir rock before CO₂ injection and the behaviour after CO₂ injection under different reservoir conditions. The Gosford sandstone (known as Hawkesbury sandstone) formation was selected as a potential reservoir rock for the investigation, due to its favourable conditions for CO₂ sequestration in deep saline aquifers and the lack of data on this aspect for the Gosford formation. This chapter starts (Section 3.1) with a description of the newly-developed high pressure triaxial set-up available in the Deep Earth Energy Research Laboratory (DEERL) in the Civil Engineering Department at Monash University, which was used to conduct strength and permeability tests for reservoir rock under high injection pressure, confining pressure, axial loads and temperature conditions. Section 3.1 includes a detailed description of the set-up, including the experimental procedure, and a brief description of the applications and capabilities of the set-up. In addition to this section, there are other four sections in Chapter 3.

Section 3.2 reports on a mechanical study performed to evaluate the natural aquifer behaviour under uniaxial stress conditions. This is a published journal paper entitled “*Salinity-dependent strength and stress-strain characteristics of reservoir rocks in deep saline aquifers: An experimental study*”. The paper compares the mechanical performance of deep saline reservoir rock under different salinity conditions and describes the associated basic theory which accounts for the different behaviour compared to dry and water-saturated reservoir rock.

Section 3.3 of the chapter describes the mechanical behaviour of a natural aquifer formation in a triaxial stress environment using the newly-developed high pressure triaxial set-up. This section is a published journal paper, “*Non-linear stress-strain behaviour of reservoir rock under brine saturation: An experimental study*”. Triaxial tests were conducted on Gosford sandstone samples which had been saturated under different salinity conditions (0, 10, 20 and 30% NaCl concentration of brine) under different confining pressures. In addition, this study

proposes an experimental data-based non-linear model to simulate the stress-strain behaviour of reservoir rock under water and brine saturation conditions, especially at high confinements, which cannot be precisely represented by the conventional linear Mohr-Coulomb failure criterion.

Section 3.4 reveals the mechanical behaviour of Hawkesbury sandstone due to CO₂ sequestration in a uniaxial stress environment. First, samples were reacted with brine and CO₂ under in-situ pressure and temperature conditions using the reaction rig available in DEERL. This section is a published journal paper entitled “*CO₂-induced mechanical behaviour of Hawkesbury sandstone in the Gosford basin: An experimental study*”. The paper compares the mechanical behaviour of the natural formation (only brine-saturated) with that of the CO₂ sequestration-induced reservoir formation to understand the mechanical integrity of the deep saline formation during the sequestration process.

The last section of this chapter refers to a study conducted to investigate the effect of CO₂ injection on the mechanical behaviour of reservoir rock in a triaxial stress environment. In addition, the results were used to visualise the mechanical behaviour of reservoir formations under effective stress by developing a stress-deformation model as a function of stress state and stress path. The proposed model distinguishes three stress-strain domains based on the experimental observations: near-elastic, inelastic and failure. These are then used to predict the mechanical failure of reservoir rock in a CO₂-interaction-induced effective stress field. This section is a submitted journal paper entitled “*Stress state and stress path evaluation to address uncertainties in reservoir rock failure in CO₂ geo-sequestration in deep saline aquifers: An experimental study*”.

1.5.4 Experimental investigation of the effect of CO₂ sequestration on flow behaviour of deep saline reservoir rocks - Chapter 4

The fourth chapter presents some results of permeability tests conducted using the triaxial set-up on both natural and CO₂-reacted reservoir rock samples. In order to combine the CO₂ reaction-induced mineralogical and chemical changes with the altered flow characteristics of the reservoir formation, comprehensive chemical, microstructural and mineralogical experiments were also carried out by performing pH, scanning electron microscopy (SEM), X-ray diffraction (XRD), X-ray fluorescent (XRF) and Inductive-coupled Plasma Mass Spectroscopy (ICP) analyses.

There are four main sections in Chapter 4. Section 4.1 reports the influence of different salinity conditions on effective permeability variation in Hawkesbury sandstone under 20MPa confining pressure. These type of studies are important for the selection of desirable aquifers for CO₂ sequestration in deep saline aquifers, as salinity changes with location and depth. The section consists of a published journal paper entitled “*Effect of salinity on effective permeability in reservoir rock determined by pressure transient methods: An experimental study on Hawkesbury sandstone*”. The paper also describes the influence of injection pressure and effective stress on the variation of effective permeability of reservoir rock by using detailed microstructural analysis. In addition, this section also describes how the effective permeability of CO₂ varies when it converts to the super-critical state from its sub-critical state.

Section 4.2 is represented by a published journal paper entitled “*Determination of effective stress parameters in deep saline aquifers: An experimental study*”. This paper shows how the effective stress parameters for effective CO₂ permeability vary with salinity under in-situ stress conditions. Furthermore, the section presents a detailed discussion of the effects of injection pressure and confining pressure on effective CO₂ permeability, the importance of evaluating the effective stress coefficient for CO₂ sequestration in deep saline aquifers and the corresponding variations in rock mass mechanical properties and seismic behaviour.

Section 4.3 shows how the flow characteristics of reservoir rock vary with the changing overburden stress of the formation. Due to the unsteady nature of surrounding factors, and the time-dependent nature of the aquifer’s overburden load (which may vary with natural causes such as landslides and man-made activities such as building construction), the evaluation of the coupled hydro-mechanical performance of reservoir rock under different overburden loads becomes critical. Therefore, this section aims to identify the influence of overburden load variations on the long-term integrity of CO₂ storage in deep saline aquifers. High-pressure triaxial strength and permeability tests, coupled with acoustic emission (AE) and SEM analyses, were conducted on Hawkesbury sandstone obtained from the Gosford basin. This section is a published journal paper entitled “*Laboratory measurement of deformation-induced hydro-mechanical properties of reservoir rock in deep saline aquifers: An experimental implication of CO₂ sequestration*”.

To date, very few experimental studies have been performed to evaluate the combined geochemical, mineralogical and permeability effects on deep saline reservoir rocks during CO₂ sequestration, and the studies which have been reported have focused on short-term effects.

This section relates to the experimental results of the geochemical and mineralogical effects of CO₂ sequestration on the flow characteristics of deep saline reservoir rock, which are presented in a published journal paper entitled “*Experimental investigation of geochemical and mineralogical effects of CO₂ sequestration on flow characteristics of reservoir rock in deep saline aquifers*”. This paper discusses the flow characteristics of CO₂ injection-induced reservoir rock, showing how the variation adversely affects the long-term integrity of CO₂ sequestration. In order to investigate this aspect, combined chemical, mineralogical, microstructural and permeability experiments were carried out.

1.5.5 Experimental investigation of chemical, mineralogical and mechanical stability of different sandstone formations under deep saline sequestration environment - Chapter 5

Chapter Five reports the results of an experimental study conducted to distinguish the behaviours of silicate- and carbonate-cemented sandstone in the CO₂ sequestration environment. To identify the behaviours, comprehensive chemical, mineralogical and mechanical tests were conducted on CO₂+brine-reacted reservoir rock samples. In addition, the influence of sub- and super-critical CO₂ injection on the chemical, mineralogical and mechanical characteristics of reservoir rocks was investigated. This chapter of the thesis is a submitted paper entitled “*An experimental investigation of coupled chemico-mineralogical and mechanical changes in varyingly-cemented sandstones upon CO₂ injection in deep saline aquifer environments*”.

1.5.6 Experimental investigation of process-enhancement technologies in deep saline CO₂ storage - Chapter 6

The extensive time required for CO₂ mixing in brine is one of the major issues in CO₂ sequestration in saline aquifers process and addressing this issue by injecting CO₂ and brine simultaneously into the aquifer is a novel concept. This practice will enhance the mixing process by offering more easy contact surfaces and the high-pressure condition of brine and CO₂ is expected to create a significant enhancement in the mixing process by increasing the kinetic energy of the molecules of the two phases (brine and CO₂). This study provides a new data set relating to this area and assesses the likely success of industrial-scale geo-sequestration in saline aquifers considering the issues of sustainability and safety. This chapter is a published journal paper entitled “*Influence of CO₂-brine co-injection on CO₂ storage capacity*”.

enhancement in deep saline sequestration: An experimental study on Hawkesbury sandstone formation”.

1.5.7 Numerical investigation of the effect of CO₂ sequestration on deep saline reservoir hydro-mechanical properties - Chapter 7

The seventh chapter presents the numerical component of this thesis and has three main sections, which cover the numerical simulations developed for both laboratory-scale and field-scale conditions to simulate the coupled hydro-mechanical behaviour of deep saline reservoir rock under CO₂ sequestration. COMSOL Multiphysics was used for the model development.

Section 7.1 of the chapter provides a detailed discussion of the development of a laboratory-scale model to simulate the salinity-dependent mechanical behaviour of reservoir rock in deep saline aquifers. Salinity-dependent mechanical behaviour under both uniaxial and triaxial stress conditions was simulated and validated using experimental data. The results were used to predict the mechanical behaviour under conditions which are difficult to achieve in the laboratory, such as high pressures. The development of the basic model is represented by a submitted journal paper entitled “*Development of a laboratory-scale numerical model to simulate the mechanical behaviour of deep saline reservoir rocks under varying salinity conditions in uniaxial and triaxial test environments*”.

Section 7.2 relates to a CO₂ flow model, which was developed to simulate the relative permeability behaviour of deep saline reservoir rock under laboratory conditions. The model was then used to predict the behaviour of CO₂ flow through reservoir rock under high injection pressure (8-14MPa). In order to simulate the experimental conditions, the cylindrical sample was modelled based on 2-D axial symmetric conditions and the Buckley-Leverett flow concept was incorporated to simulate CO₂ flow through brine-saturated reservoir rock. This section of the thesis is a submitted journal paper entitled “*Investigation of relative flow characteristics of brine-saturated reservoir rock: A numerical study of the Hawkesbury formation*”.

The last section of this chapter provides a detailed description of the field-scale model developed to investigate the effect of CO₂ sequestration on the chemical, mineralogical and hydro-mechanical behaviour of deep saline reservoirs. This section is a submitted journal paper entitled “*Injection and storage of CO₂ in deep saline aquifers: A numerical study of the Hawkesbury formation*”.

1.5.8 Conclusions and suggestions for future research - Chapter 8

Chapter Eight presents the main conclusions drawn from the experimental and numerical studies and suggestions for future research work.

1.6 References

1. Alley R. Climate change 2007: The physical science basis, summary for policymakers, Contribution of working Group I to the Fourth Assessment Report of the Intergovernmental Panel on Climate Change. Intergovernmental Panel on Climate Change, Geneva 2007; 1-78.
2. Arts R, Zweigel P, Lothe A. Reservoir geology of the Utsira Sand in the Southern Viking Graben area- a site for potential CO₂ storage. In: 62nd EAGE meeting, paper B-20. Glasgow; 2000; 1-34.
3. Audigane P, Gaus I, Czernichowski LI, Pruess K, Xu T. Two-dimensional reactive transport modelling of CO₂ injection in a saline aquifer at the Sleipner site, North Sea. American Journal of Science 2007; 307(7): 974-1008.
4. Bachu S, Shaw J. CO₂ storage in oil and gas reservoirs in Western Canada: effect of aquifers, potential for CO₂-flood enhanced oil recovery. In: Proceedings of the 7th International Conference on Greenhouse Gas Control Technologies 2004; 1-17.
5. Bachu S, Bennion B. Effects of in-situ conditions on relative permeability characteristics of CO₂-brine systems. Environmental Geology 2008; 54(8): 1707-1722.
6. Bielinski A, Kopp A, Schütt H, Class H. Monitoring of CO₂ plumes during storage in geological formations using temperature signals: numerical investigation. International Journal of Greenhouse Gas Control 2008; 2: 319-328.
7. Blunt M, Fayers FJ, Orr FM. Carbon dioxide in enhanced oil recovery. Energy Conversion and Management 1993; 34:1197-204.
8. Bruant RG, Guswa AJ, Celia MA, Peters CA. Safe storage of CO₂ in deep saline aquifers. Environmental Science and Technology 2002; 36(11): 240A-245A.
9. Busch A, Alles S, Krooss BM, Stanjek H, Dewhurst D. Effects of physical sorption and chemical reactions of CO₂ in shaly cap rocks. Energy Procedia 2009; 1: 3229-3235.

10. Class H, Helmig R, Bastian P. Numerical simulation of non-isothermal multiphase multicomponent processes in porous media-1. An efficient solution technique. *Advanced Water Resources* 2002; 25: 533-550.
11. Emberley S, Hutcheon I, Shevalier M, Durocher K, Mayer B, Gunter WD, et al. Monitoring of fluid-rock interaction and CO₂ storage through produced fluid sampling at the Weyburn CO₂-injection enhanced oil recovery site, Saskatchewan, Canada. *Applied Geochemistry* 2005; 20: 1131-57.
12. The Energy Supply Association of Australia. (ESAA) Australia's Energy Supply Industry: Facts in Brief. 2011; 1-23.
13. Esser R, Levey R, Mcpherson B, O'Dowd W, Litynski J, Plasynski S. (Geology conference series 2010). Preparing for a carbon constrained world: overview of the United States regional carbon sequestration partnerships programme and its South-west Regional Partnership, vol.7. London, Petroleum: Geological Society 2010:1189-1195.
14. Fleury M, Pironon J, Le Nindre YM, Bildstein O, Berne P, Lagneau V, et al., Evaluating sealing efficiency of cap rocks for CO₂ storage: an overview of the Geocarbone Integrity programme and results. *Oil and Gas Science Technology* 2010; 65: 435-444.
15. Fujioka M, Yamaguchi S, Nako M. CO₂-ECBM field tests in the Ishikari Coal Basin of Japan. *International Journal of Coal Geology* 2010; 82: 287-98.
16. Gunter WD. CO₂ sequestration in deep unmineable coal seams. In: *Conference Proceedings; CAPP/CERI Industry Best Practices Conference 2000*: 1-19.
17. Hem JD. Study and interpretation of the chemical characteristics of natural water. *U.S. Geology Survey and Water Supply* 1959; 34: 1431-1473.
18. Hovorka SD, Doughty C, Benson SM, Pruess K, Knox PR. The impact of geological heterogeneity on CO₂ storage in brine formations: a case study from the Texas Gulf Coast: *Geological storage of carbon dioxide: Geological Society* 2006; 233: 147-163.
19. Hueckel T. Chemo-mechanics of geomaterials. *Revue Europeenne de Genie Civil* 2005; 9: 689-711.

20. International Energy Agency (IEA). CO₂ storage; Part 1: sources of CO₂. IEAGHG, Cheltenham, Gloucestershire, Report PH1/9 2014; 1-48.
21. International Energy Agency (IEA). CO₂ storage; Part II: sources of CO₂. IEAGHG, Cheltenham, Gloucestershire, Report PH1/9 2015; 1-68.
22. Intergovernmental Panel on Climate Change (IPCC). IPCC Special Report on CO₂ Capture and Storage prepared by Working Group III of the Intergovernmental Panel on Climate Change. Cambridge University Press, Cambridge 2007; 1-442.
23. Johns TC, Gregory JM, Ingram WJ, Johnson CE, Jones A, Lowe JA, Mitchell et al. Anthropogenic climate change for 1860 to 2100 simulated with the HadCM3 model under updated emissions scenarios. *Climate Dynamics*. 2003; 6: 583-612.
24. Kane B. CO₂ sequestration capability: where are we? An overview of the advances being made in CO₂ geologic storage by DOE/NETL's regional carbon sequestration partnership. US Carbon Sequestration Council 2010.
25. Kharaka YK, Cole DR, Hovorka SD. Gas-water-rock interactions in Frio formation following CO₂ injection: implications for the storage of greenhouse gases in sedimentary basins. *Geology* 2006; 34: 577-580.
26. Le Treut H, Somerville R, Cubasch U, Ding Y, Mauritzen C, Mokssit A, Peterson T, Prather M. Historical overview of climate change, In: Solomon S, Qin D, Manning M, Chen Z, Marquis M, Averyt KB, Tignor M, Miller H (Eds) *Climate Change 2007: The Physical Science Basis. Contribution of Working Group 1 to the Fourth Assessment Report of the Intergovernmental Panel on Climate Change*, Cambridge University Press, Cambridge 2007; 97-124.
27. Leung DY, Caramanna G, Maroto-Valer M. An overview of current status of carbon dioxide capture and storage technologies. *Renewable and Sustainable Energy Reviews* 2014; 39: 426-443.
28. Li Q, Wu Z, Lei X, Murakami Y, Satoh T. Experimental and numerical study on the fracture of rocks during injection of CO₂-saturated water. *Environmental Geology* 2006; 51(7): 1157-1164.

29. Liu L, Suto Y, Bignall G, Yamasaki N, Hashida T. CO₂ injection to granite and sandstone in experimental rock/hot water systems. *Energy Conversion and Management* 2003; 44(9), 1399-1410.
30. Mito S, Xue Z, Ohsumi T. Case study of geochemical reactions at the Nagaoka CO₂ injection site, Japan. *International Journal of Greenhouse Gas Control* 2008; 111: 122-135.
31. Nader S. Paths to a low-carbon economy: the Masdar example. *Energy Procedia* 2009; 1: 3951-3958.
32. Perera MSA, Ranjith PG, Choi SK, Airey D. Numerical simulation of gas flow through porous sandstone and its experimental validation. *Fuel* 2011; 90: 547-554.
33. Perera MSA, Ranjith PG. Effects of gaseous and super-critical carbon dioxide saturation on the mechanical properties of bituminous coal from the southern Sydney basin. *Applied Energy* 2013; 110: 73-81.
34. Pruess K, Garcia J, Kovscek T, Oldenburg C, Rutqvist J, Steefel C, Xu T. Code inter-comparison builds confidence in numerical simulation models for geologic disposal of CO₂. *Energy* 2004; 29(9): 1431-1444.
35. Qu HY, Liu JS, Pan ZJ, Connell L. Impact of thermal processes on CO₂ injectivity into a coal seam. In: *IOP Conf. Series: Materials Science and Engineering* 2010; 10: 1-10.
36. Rai V, Chung NC, Thurber MC, Victor DG. PESD carbon storage project database. Working paper 76, the Program on Energy and Sustainable Development, Stanford University, Available at SSRN: <http://dx.doi.org/10.2139/ssrn.1400118> 2008.
37. Rathnaweera TD, Ranjith PG, Perera MSA, Haque A, Aref L, Nassir AA, Chandrasekharam D, et al. CO₂-induced mechanical behaviour of Hawkesbury sandstone in the Gosford basin: An experimental study. *Materials Science and Engineering* 2015; A 641: 123-137
38. Rathnaweera TD, Ranjith PG, Perera MSA. Experimental investigation of geochemical and mineralogical effects of CO₂ sequestration on flow characteristics of reservoir rock in deep saline aquifers. *Scientific Reports* 2016; 6: 19362-19374.

39. Rosenbauer RJ, Koksalan T, James LP. Experimental investigation of CO₂-brine-rock interactions at elevated temperature and pressure: Implications for CO₂ sequestration in deep-saline aquifers. *Fuel Processing Technology* 2005; 86(14): 1581-1597.
40. Rutqvist J, Vasco DW, Myer L. Coupled reservoir-geomechanical analysis of CO₂ injection and ground deformation at In Salah, Algeria. *International Journal of Greenhouse Gas Control* 2010; 4: 225-230.
41. Shukla R, Ranjith PG, Choi SK, Haque A, Yellishetty M, Hong L. Mechanical Behaviour of Reservoir Rock Under Brine Saturation. *Rock Mechanics and Rock Engineering* 2013; 46(1): 83-9.
42. Singh N. Deep saline aquifers for sequestration of carbon dioxide. In: *International Geological Congress, Oslo; August 2008: 3-25.*
43. Solomon S, Carpenter M, Flach TA. Intermediate storage of carbon dioxide in geological formations: a technical perspective. *International Journal of Greenhouse Gas Control* 2008; 2: 502-510.
44. Steadman EN, Daly DJ, de Silva LL, John A, Harju JA, Melanie D, Jensen MD, O'Leary EM, Peck WD, Smith SA, Sorensen JA. *Plains CO₂ Reduction (PCOR) Partnership (Phase 1) Final report, U. S. Department of Energy, 2006.*
45. Stenvens SH, Kuuskraa VA, Spector D, Riemer P. CO₂ sequestration in deep coal seams: pilot results and worldwide potential. In: *Proceedings of the 4th International Conference on Greenhouse Gas Control Technologies (GHGT). Interlaken, Switzerland, August 30-September 2, 1998, Elsevier; 1998: 175-180.*
46. *The Global Status of CCS Summary Report. Global CCS Institute CCS legal and regulatory indicator. <http://www.globalccsinstitute.com/publications/policy-update> 2015.*
47. Torp AT, Gale JJ. Demonstrating storage of CO₂ in geological reservoirs: the Sleipner and SACS projects, In: JJ Gale, Y Kaya, (Eds.) *Proceedings of the 6th International Conference on Greenhouse Gas Control Technologies, Volume 1, Pergamon, Amsterdam, 2003: 311-316.*

48. Van Alphen K, Noothout PM, Hekkert MP, Turkenburg WC. Evaluating the development of carbon capture and storage technologies in the United States. *Renewable and Sustainable Energy Review* 2010; 14: 971-986.
49. Westermarck RE, Schmeling J, Dauben DL, Robinowitz S, Weyland HV. Application of horizontal water flooding to improve oil recovery from old fields. In: *SPE/DOE Symposium on Improved Oil Recovery*. Oklahoma, USA; 22-26 April 2006. ISBN: 978-1-55563-157-4, 2006.
50. White CM, Strazisar BR, Granite EJ, Hoffman JS, Pennline HW. Separation and capture of CO₂ from large stationary sources and sequestration in geological formations-coal beds and deep saline aquifers. *Journal of Air and Waste Management Association* 2003; 53: 645-715.
51. Winter EM, Bergman PD. Availability of depleted oil and gas reservoirs for disposal of carbon dioxide in the United States. *Energy Conversion and Management* 1993; 34: 1177-1187.
52. Yun G, Liu D, Wu T, Wu J, Ji X, Zhuang L. CO₂ capture and utilization for enhanced oil recovery (EOR) and underground storage: a case study in Jilin Field, China. *Studies in Surface Science and Catalysis* 1998; 114: 201-216.

1.7 Summary of Chapter 1

This chapter provides a general introduction to the thesis, including the problem, motivation and thesis outline. Global warming has become a challenge for 21st century scientists, and numerous greenhouse gas mitigation and global warming control programs have therefore been initiated throughout the world. Of the various atmospheric CO₂ mitigation methods, CO₂ sequestration in deep saline aquifers has recently attracted the attention of the world due to its many advantages. Deep saline aquifers are the most widely-available option and have the ability to store huge amounts of CO₂ in an economically and environmentally friendly way. However, the interaction between injected CO₂, aquifer brine and reservoir rock causes chemical and mineralogical changes in the rock matrix, resulting in altered hydro-mechanical properties during long-term CO₂ sequestration, which leads to unpredictable CO₂ storage capacities in deep saline aquifers. In addition, precise understanding of injected CO₂ behaviour in deep saline environments is important, as CO₂ likely exists in its super-critical state at these depths, and behaves quite differently from sub-critical CO₂. Moreover, the presence of saline brine in the reservoir rock pore space has a significant influence on the hydro-mechanical behaviour of deep saline reservoir rocks. While there has been considerable research into the chemical interaction of CO₂ and reservoir rocks, it has been mainly limited to low pressures and salinities, and the impact of CO₂ on the hydro-mechanical properties and the determination of the CO₂ storage capacity enhancing strategies of such reservoir rock have received little attention. This in turn leads to considerable uncertainty about the viability of large-scale geo-sequestration in deep saline aquifers. Since CO₂ sequestration in deep saline aquifers is a long-term process, laboratory experimental studies alone may not have the ability to fill the existing gaps in knowledge. Therefore, numerical models are required which are capable of simulating the field scenario in deep saline aquifers. Although many field-scale simulations have been developed on this aspect, to date only minor consideration has been given to laboratory-scale model development, which is important in identifying CO₂ flow behaviour in rock matrix under triaxial conditions. In order to evaluate the long-term behaviour of deep saline reservoir rock, it is important to develop appropriate field-scale numerical models, which couple the chemical, mineralogical and hydro-mechanical behaviours of reservoir rock in the sequestration environment.

The main objectives of the present thesis are to 1) investigate the effects of salinity on the mechanical behaviour of deep saline reservoir rock, 2) evaluate the effects of salinity on

permeability using high-pressure triaxial experiments, 3) investigate the effects of injection and confining pressures on the mechanical-flow behaviour during CO₂ injection and storage, 4) evaluate the chemical, mineralogical and microstructural changes that occur in reservoir rocks following the injection of CO₂ in deep saline aquifers, 5) distinguish the mechanical and permeability behaviour of deep saline reservoir rock under sub-critical and super-critical CO₂ flow conditions, 6) distinguish the chemical, mineralogical and hydro-mechanical behaviour of silicate- and carbonate-cemented reservoir rocks, 7) investigate process-enhancement technologies in deep saline CO₂ storage, 8) develop an experimentally-validated laboratory-scale numerical model using the COMSOL simulator to model CO₂ chemical, mineralogical and hydro-mechanical behaviour, and 9) develop a field-scale numerical model using the COMSOL simulator to study the coupled chemico-mineralogical-mechanical flow behaviour of deep saline reservoir rock.

CHAPTER 2

Literature Review

2 Literature Review

2.1 Introduction

Over the past two decades, a significant amount of research has been undertaken in the field of CO₂ sequestration in deep saline aquifers (Koide et al., 1992; Ormerod, 1994; Koide et al., 1995; Bruant et al., 2002; Johns et al., 2003; Wu et al., 2005; Egerman et al., 2006; Rao et al., 2007; Bachu, 2008; Zhang et al., 2009; Ranjith et al., 2012; Berg et al., 2013; Shukla et al., 2013; Rathnaweera et al., 2015). Although the scientific knowledge has been developed regarding the processes involved in deep saline sequestration, some critical aspects related to mechanical and flow behaviour of deep saline reservoir rocks are yet to be explored and understood completely. These include the mechanical and permeability behaviour of natural aquifers, the mechanical and permeability behaviour of reservoir rock upon exposure to CO₂, CO₂ storage-enhancement techniques and the influence of CO₂-induced rock mineral alteration on CO₂ storage. Therefore, extensive research should be undertaken to understand the complete picture of the impacts of CO₂/brine/rock interaction on the chemical, mineralogical, mechanical and flow characteristics of reservoir rock. The main objective of this chapter is to present a detailed literature review and identify the gaps to be addressed during the present study.

2.2 The effect of CO₂ sequestration on hydro-mechanical properties of deep saline aquifers and factors affecting it

CO₂ sequestration in deep saline aquifers is a potential anthropogenic CO₂ mitigation measure that has been received growing recognition. However, the injection of CO₂ into deep saline formations may affect the strength and permeability of the host rock and overlying caprock due to the dissolution/precipitation of the primary and secondary rock minerals. Therefore, it is important to investigate the effect of CO₂ sequestration on reservoir rock strength and permeability. The effect of CO₂ sequestration may vary due to many factors, including aquifer brine concentration, temperature, rock mineralogy, CO₂ injection pressure and aquifer depth. Therefore, this section provides a comprehensive review of the potential changes in aquifer strength and permeability characteristics caused by injected CO₂ under in-situ conditions, highlighting the factors affecting the integrity of sedimentary rock properties. The following submitted journal paper entitled “*A review of the effect of CO₂ sequestration on hydro-mechanical properties of deep saline aquifers and factors affecting it*” makes up this section of the thesis.

A Review of the Effect of CO₂ Sequestration on Hydro-mechanical Properties of Deep Saline Aquifers and Factors Affecting It.

T. D. Rathnaweera¹, P.G. Ranjith¹, M. S. A. Perera¹

¹Department of Civil Engineering, Monash University, Building 60, Melbourne, Victoria, 3800, Australia.

Abstract

Sequestration of carbon dioxide (CO₂) in deep saline aquifers is one of the most feasible approaches to the mitigation of global warming. However, dissolution of injected CO₂ in brine has some effects on chemical diffusion and permeability in the reservoir rock. There is also a significant variation in the mineral composition of reservoir rock upon exposure to CO₂, which changes the mineralogical and micrological structure of the rock mass and consequently changes the mechanical properties of the rock. Therefore, this paper provides a comprehensive review of the potential changes in aquifer strength and permeability characteristics caused by injected CO₂ under in-situ conditions, highlighting the factors affecting the integrity of sedimentary rock properties. The factors considered are temperature, brine concentration, injection pressure, depth, and clay content of the sedimentary rock. It is clear that the permeability of the aquifer increases with increasing injection pressure and decreasing salinity, depth and clay composition. However, the behaviour of aquifer strength is still unclear due to the lack of studies related to CO₂-induced rock strength. It is also clear that the temperature effect is negligible in sequestration in deep saline aquifers. In addition, the consequences of leakage and the mechanisms of failure of the cap rock due to changes in permeability and strength are also discussed. The review identifies major research gaps and the need for further study of the hydro-chemical and hydro-mechanical interactions of reservoir rock, CO₂ and brine.

Keywords: Saline aquifer, sequestration of carbon dioxide, hydro-mechanical properties, effective factors, long-term safety

2.2.1 Introduction

Carbon dioxide (CO₂) is one of the main greenhouse gases released to the atmosphere mainly from the burning of fossil fuels, such as coal, oil and natural gas, which currently supply around 85% of the world's energy needs. Moreover, due to the low relative cost and abundance of

fossil fuels, it is likely that fossil fuels will govern the economy for at least the next 25 to 50 years (Koide et al., 1992; Ormerod, 1994; Koide et al., 1995; Johns et al., 2003; Pruess et al., 2004). Therefore, it is necessary to have appropriate CO₂ emission control techniques to create a safer atmosphere for human beings. Currently, CO₂ sequestration is one of the most promising means of reducing anthropogenic CO₂ emissions in the atmosphere. Sequestration involves the long-term storage of captured CO₂ in deep sub-surface geologic reservoirs such as oil/gas fields, deep saline aquifers, unmineable coal seams and mineral sequestration (Nasvi et al., 2012; Perera and Ranjith, 2013). Of these options, sequestration in deep saline aquifers has recently attracted the attention of the scientific community and the general media due to its many advantages. Deep saline aquifers have the largest storage capacity of all geological media, the process of capture is quick, unlike oil and gas reservoirs that have to wait for production first, and capture requires simpler technology than coal beds (Farrar et al., 1999). For example, Koide et al. (1995) and Bruant et al. (2002) have estimated the total storage capacity of deep saline aquifers to be between 320 Gt CO₂ and 200,000 Gt CO₂, with the potential to store the world's anthropogenic CO₂ emissions for hundreds of years.

Sequestration in deep saline aquifers involves a number of steps, including CO₂ capture, transport and injection deep underground via wells. The CO₂ is stored in the geological reservoir, where the process needs to be clearly monitored (Farrar et al., 1999; Pruess et al., 2004). CO₂ capture can be carried out through three main types of activities: industrial processes, electricity generation, and hydrogen production. However, it is notable that one third of total CO₂ emissions come from fossil fuel power production (Bruant et al., 2002). In addition, it has been found that the production of hydrogen (H₂) used in turbines to produce electricity and in fuel cells to power cars will also become a potentially large future source of CO₂ (Ormerod, 1994).

CO₂ transport requires the transport of the captured CO₂ from the source to the geological storage site. Typically, the CO₂ is transported in a compressed form via a pipeline as a super-critical phase fluid. At a temperature of 31.4⁰C and a pressure of 7.38MPa, CO₂ exists in the super-critical phase (Bruant et al., 2002). In this phase, CO₂ has a relatively higher density than gaseous or liquid CO₂.

CO₂ injection involves injecting CO₂ into a reservoir rock via a single well or array of wells and CO₂ storage involves keeping the CO₂ secured deep underground in a geological reservoir.

In addition, it is important to have a comprehensive monitoring system to ensure that the CO₂ remains in the subsurface. This is highly important in terms of safety.

Of these processes, our concern is with CO₂ storage and monitoring processes, as according to current studies, there remains a lack of understanding related to the physio-chemical reactions that occur in the saline aquifer during this process and their effect on CO₂ back-migration into the atmosphere through the cap rock. This indicates the importance of a clear understanding of the mechanical and chemical behaviour of reservoir rock and the integrity of the caprock in the process of CO₂ storage in saline aquifers. Hence, this paper aims to provide a comprehensive overview of CO₂ storage in saline aquifers and the factors affecting it, including temperature, depth, injection pressure, clay content and the salinity of the aquifer.

2.2.2 Mechanisms of the CO₂ storage process in saline aquifers

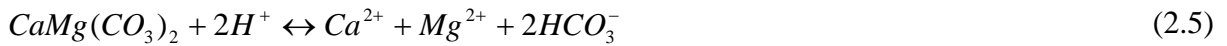
The process of trapping plays a very important role in CO₂ storage in saline aquifers, because the injected CO₂ is less dense than the formation water and therefore, it will easily migrate to the top of the reservoir due to buoyancy forces (Winter and Bergman, 1993; Kongsjorden et al., 1998; Oldenburg and Benson, 2002; Emberley et al., 2004; Shukla et al., 2010). Hence, a trap is needed to ensure that it does not reach the surface. CO₂ injected into deep saline aquifers can be trapped by a number of different mechanisms (Ozah et al., 2005), including solubility trapping, mineral trapping, residual gas trapping and mobility trapping. The dissolution of CO₂ in the formation water is referred to as solubility trapping (Rosenbauer et al., 1983; Rosenbauer et al., 1992; Rosenbauer et al., 1993; Sass et al., 2002) which produces carbonic acid due to the reaction of CO₂ with formation water (Eq. 2.1). This reaction is fundamentally important because the aqueous, not the molecular, form of CO₂ is reactive to aquifer rocks (Kaszuba et al., 2003).



In addition, the resulting dissociation of carbonic acid into reactive hydrogen ions and bicarbonate (Eq. 2.2) enhances the reaction between aquifer fluids and formation rocks to fix the CO₂ in the aqueous and mineral phases (Rosenbauer at al., 1983; Rosenbauer at al., 1992; Rosenbauer at al., 1993).



For example, dissolution of calcite, dolomite and magnesite in carbonic acid causes an additional mole of CO₂ to be stored as bicarbonate (Eqs. 2.3-2.5, respectively) (Kaszuba et al., 2003).



Mineral trapping is another important mechanism that occurs in deep saline aquifers. The mineral trapping mechanism results from the formation of weak carbonic acid, which can react with minerals in the aquifer to form solid carbonate minerals over a long period of time (Gunter et al., 2004). According to a past study of arkosic sandstone, it is clear that the available H⁺ ions resulting from the dissociation of carbonic acid can enhance mineral trapping by the dissolution of silicates (Eq. 2.6) (Kaszuba et al., 2003).



Once the CO₂ plume develops, it goes through the porous rocks and a small amount of CO₂ is trapped in the pore space due to surface tension. This process is known as residual gas trapping. Past studies have shown that residual gas trapping is more important when the aquifer is low permeable and becomes more predominant after the cessation of CO₂ injection (Bachu, 2008; Nghiem et al., 2009).

Mobility or structural and stratigraphic trapping mechanisms also play an important role in the CO₂ storage process in deep saline aquifers. Mobility trapping is the dominant form of trapping initially, and is a form of static trapping where the injected super-critical CO₂ percolates through the porous rock and is trapped by the impermeable caprock (Bachu et al., 2007; Yang et al., 2010).

Fig. 2.1 shows the amount of CO₂ stored by each mechanism with respect to time. According to Fig. 2.1, most CO₂ is stored in saline aquifers through the processes of solubility and mobility trapping, while mineral trapping plays a minor role. In addition, mineral trapping does not occur in the first few years and it slowly increases only after around 200 years. During the injection period, mobility trapping dominates the CO₂ trapping process and solubility trapping contributes only slightly. In addition, Fig. 2.1 clearly shows that after 4000 years of CO₂

injection, both mobility and mineral trapping became almost stable. However, solubility trapping appears to be active for another few thousand years. It is also clear that over 90% of CO₂ storage is completed within the first 4000 years. Hence, the active period for carbonation can be taken as being 4000 years.

According to Fischer et al. (2011), the injection of CO₂ into a saline aquifer disturbs its physico-chemical equilibrium and the subsequent CO₂-brine-rock interaction, including the dissolution of certain minerals and the precipitation of carbonates, not only affects the chemical properties, but also the physical properties of the reservoir rocks. Therefore, CO₂ sequestration-induced chemico-mineral-structural change in the aquifer is considered in the following section.

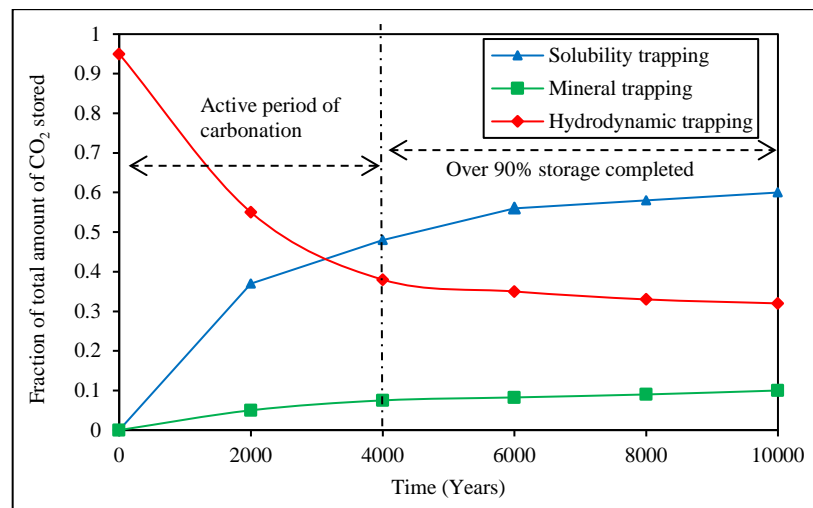


Figure 2.1. Fractions of total amount of captured CO₂ by solubility, mobility and mineral trapping (Ranganathan et al., 2011).

2.2.3 Effect of CO₂ sequestration on chemico-mineral-structure of the aquifer rock mass

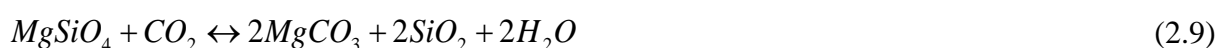
Understanding of the chemical reactions of the aquifer with the injected CO₂ during the sequestration process is essential in studying the major changes in the rock structure and chemical composition of the reservoir and cap rock during the sequestration process. Some research reports regarding short-term exposure to a mixture of brine and super-critical CO₂ (scCO₂) changes to rock-forming minerals and the reactions, including the dissolution and precipitation of rock-forming minerals, have been published (Svec and Grigg, 2001; Schutt et al., 2004). It has been concluded that it is necessary to carry out experiments on geological formations under in-situ pressure and temperature conditions, describing the mineral reactions which occur after the injection of CO₂ (Shukla et al., 2013). Sandstones are generally classified

according to the relative proportion of quartz to other grain types, as well as according to the ratio of feldspar grains to finely crystalline lithic fragments (Moore et al., 2005). The mineral composition of sandstone can be identified by performing X-ray diffraction testing (Dunning and Miller, 1985; Shukla et al., 2012). According to past studies, the typical mineralogical composition of reservoir sandstone cores can be summarised as quartz, feldspar, dolomite, pyrite, calcite, albite, mica, muscovite, tourmaline, plagioclase, kaolinite, chlorite, illite and smectites (Schutt et al., 2004; Moore et al., 2005). Sandstones rich in clay usually have a considerably higher compressive strength than those which lack clay (Knauss et al., 2005). Moreover, the presence of clay minerals has a significant impact on the engineering properties of the rocks, due to the formation of a weak bond between the grains. However, it may also enhance the re-crystallization of intergranular bonds (Shukla et al., 2013).

To date, much research effort has focussed on the mineralization reactions which occur in sandstone formations during CO₂ sequestration via the dissolution of CO₂ with rock minerals (Kaszuba et al., 2003). Silicate minerals, such as olivine, serpentine, pyroxene, and plagioclase, have the potential to react with CO₂ to produce metal carbonate, which is deposited in the faults and cracks of the reservoir rocks (Oelkers et al., 2008). Mineralization is restricted to the vicinity of faults (Naylor et al., 1988), and is observed all around the Mercia Mudstone Group outcrop and elsewhere (Ford and King, 1968; Holmes et al., 1983). Regnault et al. (2009) showed evidence of dissolution and massive secondary precipitation of smectites and calcite and suggested that the reaction mechanism is a function of the water- scCO₂ phase state. The reactions of common minerals like calcite or magnesite can be expressed by Eq. 2.7 and have the potential to convert naturally-occurring silicate minerals to geologically-stable carbonate minerals and silica.



Eq. 2.8 illustrates the reaction of the common silicate mineral serpentine and CO₂. The transformation of the end member of the common silicate mineral olivine, forsterite (Mg₂SiO₄), is given by Eq. 2.9. However, these reactions take thousands of years to form geologically stable carbonate.



Giammar et al. (2005) performed forsterite dissolution experiments in CO₂-rich solutions. In this experiment, the authors found that a substantial degree of super-saturation is required for magnesite nucleation, suggesting a limitation of the precipitation process. A more complex chemical system was studied by Kaszuba et al. (2003), who found that the presence of the common industrial waste gas SO₂ can alter the quantity of CO₂ trapped in carbonate minerals in an oxidizing environment, while H₂S has negligible effects on the CO₂ carbonation process (Knauss et al., 2005). They also showed that the total quantity of CO₂ trapped in carbonate minerals mainly depends on the composition of the reservoir rock. Xu et al. (2005) considered the injection of CO₂ into a common sedimentary basin and found that for a representative composition, 90kg/m³ of CO₂ can be trapped over 100,000 years, mainly in the sandstone.

The dissolution of low permeability rocks by acidic CO₂-rich fluids has been studied by Moore et al. (2005). They observed the coupled mechanisms of the dissolution of detridal feldspar and the precipitation mechanisms of dawsonite and kaolinite. The researchers concluded that only a small percentage of CO₂ is trapped in secondary carbonates. White et al. (2005) also studied the precipitation mechanisms of calcite and dawsonite and found that CO₂ trapping is mainly due to the dissolution of CO₂ in the formation fluid and the precipitation of carbonate minerals.

Numerical simulation of the effect of mineralisation on reservoir rocks has been carried out by Ranganathan et al. (2011) to evaluate the feasibility of a potential site within the Rotliegend sandstone formation in Holland at a depth of around 3000m using the numerical simulator CMG-GEM. The simulation results allow the following conclusions. The injected CO₂ is first converted into kaolinite and a small amount into dolomite which then precipitates. The dissolution of aluminosilicates like feldspar provides an aluminium-rich region for kaolinite precipitation. In order for dolomite to precipitate, clay minerals of divalent cations such as Ca²⁺, Mg²⁺ and Fe²⁺ need to be present. According to Ranganathan et al.'s (2011) simulation, the change of the number of moles of several minerals over a period of 10,000 years is shown in Fig. 2.2. This figure clearly shows an increment of kaolinite with time, while dolomite slightly increases and feldspar shows the same variation. The moles change in kaolinite composition shows a sharp gradient of about 1.25×10^7 gmole/year for the first 4000 years of CO₂ injection. However, the precipitation rate of kaolinite decreases after 4000 years due to complete dissolution of feldspar. It can be seen that illite decreases strongly with time, showing a gradient of 1.35×10^7 gmole/year for the first 4000 years. At the same time, the quartz concentration increases in the same manner as kaolinite, showing a gradient of approximately 1.2

$\times 10^7$ gmole/year for the first 4000 years. It is concluded that in order to sequester CO_2 by mineralisation it is important to dissolve CO_2 to form HCO_3^- ions and dissolve quartz to form $\text{SiO}_2(\text{aq})$. Therefore, based on Ranganathan et al.'s (2011) study, it can be concluded that CO_2 sequestration in a saline aquifer by means of mineralization is limited.

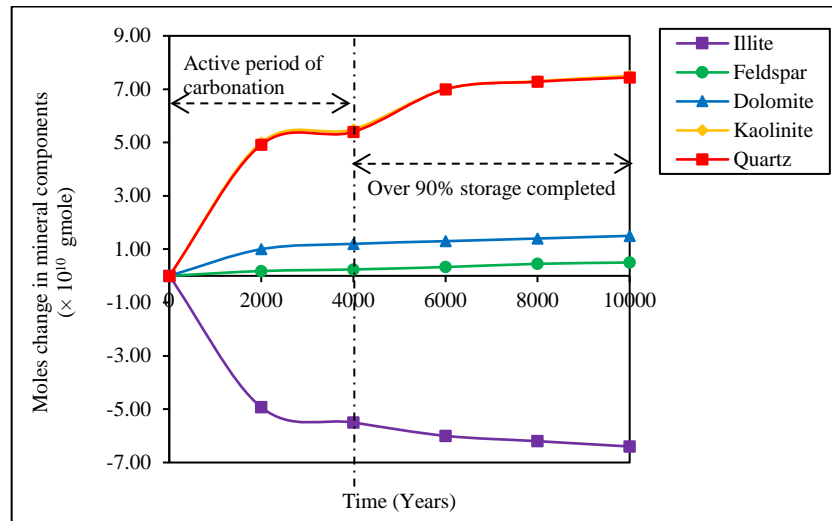


Figure 2.2. Base case of mineralization as a function of time (Ranganathan et al., 2011).

Many researchers have found that CO_2 sequestration may cause the permeability and compressive strength of reservoir rock to increase or decrease, depending on the mineralogical composition of the rock (Knauss et al., 2005; Xu et al., 2005). This is considered in the next section.

2.2.4 Effect of CO_2 sequestration on hydro-mechanical properties of saline aquifers

2.2.4.1 Effect of CO_2 sequestration on mechanical properties

The effect of CO_2 sequestration in deep saline aquifers on reservoir rock (sandstone) mechanical properties is still not completely understood. A number of researchers have carried out uniaxial compressive strength testing (UCS) to evaluate the changes in failure strength that salinity causes to sandstones (Mungan, 1965; Gray and Rex, 1966; Ford and King, 1968; Holmes et al., 1983; Dynning and Miller, 1985; Naylor et al., 1988; Omar, 1990; Dahab et al., 1992; White et al., 2005; Xu et al., 2005; Hangx et al., 2013). The interaction between CO_2 and reservoir rock (Goss, 1987; Wu et al., 2005; Egerman et al., 2006; Rao et al., 2007; Zhang et al., 2009; Ranjith et al., 2012; Berg et al., 2013; Shukla et al., 2013) under in-situ pressure and temperature conditions is a relatively unknown phenomenon, since it leads to the carbonation

of the sandstone pore matrix. This interaction mainly consists in the chemical reaction of calcium and magnesium in the sandstone pores, with the CO₂ resulting in the initial matrix leaching and the formation of calcium and magnesium carbonates. Since the carbonates that precipitate are different from the initial matrix of the reservoir rock and may exhibit higher mechanical properties than that of the sandstone matrix that is dissolved, this carbonation reaction is known to increase or decrease the mechanical strength of the reservoir rock. In addition, there is a significant variation in the mineral composition of reservoir rocks such as quartz (1.2×10^7 gmole/year), feldspar (0.125×10^7 gmole/year), kaolinite (1.2×10^7 gmole/year), illite (1.35×10^7 gmole/year) and dolomite (0.25×10^7 gmole/year) upon exposure to CO₂ (Ranganathan et al., 2011), which changes the mineralogical and micrological structure of the reservoir rock mass and consequently changes the mechanical strength of the reservoir rock.

Hangx et al. (2013) conducted conventional triaxial creep experiments combined with fluid flow to investigate the effect of carbonate cement dissolution on the mechanical and ultrasonic properties, as well as on the failure strength of reservoir sandstones. The researchers concluded that the total dissolution of calcite did not affect the rock strength. This is mainly because grain-to-grain contacts are quartz-cemented and quartz is not affected by CO₂-rich brine. However, it is possible that fast dissolution of calcite cement at grain contacts may weaken the rock on a diminutive timescale (Hangx et al., 2013). Fig. 2.3 below clearly shows that the failure strength obtained under CO₂ exposure conditions is consistent with unexposed failure conditions. Therefore, according to their results, the injection of CO₂ does not affect the material strength. However, based on Stevens and Smectic sandstone studies, Mohan et al. (1993, 1999) have also shown that high ionic strength brines can cause detrimental formation damage to the rocks. According to Mohan et al. (1999), the permeability decreases with increasing ionic strength of brines due to the re-crystallization of expandable clay minerals, and this crystallization effect adds additional strength to reservoir rocks during CO₂ sequestration. Dahab et al. (1992) recorded formation damage of sandstone and showed that the failure strength of reservoir rock is dependent on the rock mineralogy and on the ionic concentration of the saline aquifer. Shukla et al. (2013) also concluded that the changes in UCS values are mainly due to the mineralogical interaction of the brine and the reservoir rock minerals and also due to the crystallization of the NaCl crystals in the rock pores, which may add to the strength of reservoir rocks. Table 2.1 below shows a brief summary of strength variation in different reservoir rock types. It is clear

that various rock types have different peak strengths under the same test conditions, due to different mineralogical compositions.

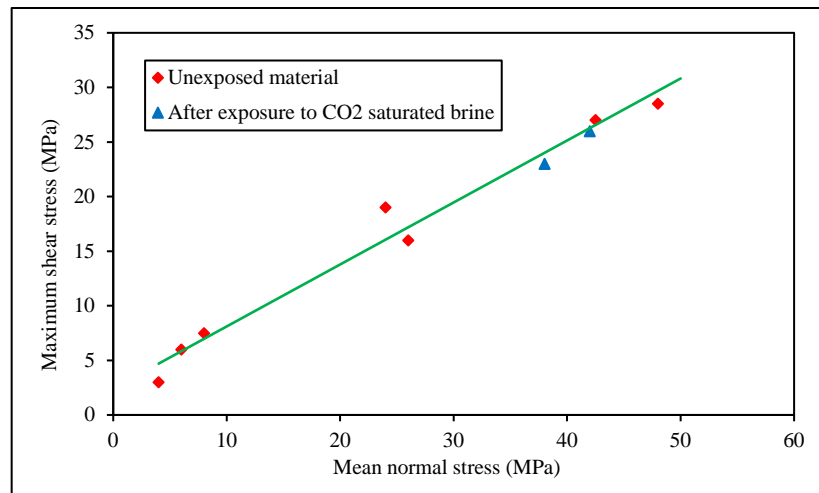


Figure 2.3. Mohr-Coulomb failure envelope showing maximum shear stress versus mean normal stress for unexposed sandstone as well as after exposure to CO₂-saturated brine (Mungan, 1965).

Table 2.1. Summary of experimental studies performed on rock strength.

Reference	Rock type	Test condition	Peak strength (MPa)
		UCS test	
Shukla et al., (2013)	Sandstone (quartz, muscovite and tourmaline)	1) Dry	82.6
		2) Water	32.2
		3) 2% NaCl	31.0
		4) 5% NaCl	29.8
		5) 10% NaCl	30.7
		6) 15% NaCl	34.2
	Sandstone (quartz, muscovite and plagioclase)	1) Dry	174
		2) Water	133
		3) 2% NaCl	128
		4) 5% NaCl	97
		5) 10% NaCl	109
		6) 15% NaCl	130
		Triaxial test	
Marbler et al., (2013)	Bunter sandstone	1) Dry	
		i 5MPa confinement	65
		ii 10MPa confinement	80
		iii 15MPa confinement	104
		2) CO ₂ /brine-reacted	
		i 5MPa confinement	50
ii 10MPa confinement	67		
iii 15MPa confinement	76		
Wasantha et al., (2013)	Hawkesbury sandstone	UCS test	

		1) Dry	21.1
		Triaxial test	
		1) Dry	
		i 5MPa confinement	40
		ii 10MPa confinement	58
		iii 25MPa confinement	95
		Triaxial test	
		1) Dry	
		i 5MPa confinement	65
Wong et al., (1997)	Adamswiller sandstone	ii 20MPa confinement	97
		iii 40MPa confinement	113
		iv 60MPa confinement	128
		Triaxial test	
		i 10MPa confinement	125
	Doddington sandstone	ii 25MPa confinement	222
Santarelli et al., (1989)		iii 50MPa confinement	326
		i 10MPa confinement	120
	Carboniferous sandstone	ii 25MPa confinement	180
		iii 50MPa confinement	230

2.2.4.1.1 Factors affecting CO₂ sequestration-induced strength reduction

Effect of brine concentration

Identification of the effect of brine concentration is an essential criterion when addressing the sequestration of CO₂ in deep saline aquifers. Past studies have indicated that the effect can be addressed in terms of critical salt concentration. Critical salt concentration is an indicator of equilibrium between the reservoir rock and the pore fluid (brine) (Omar, 1990). Typically, brine is a solution of NaCl in water. Since NaCl concentration plays a major role in brine composition, it is important to understand the effect of NaCl on the mechanical properties and the geochemical characteristics of the reservoir rock under brine saturation. The detrimental effects of NaCl concentration on sandstone properties have been studied by many researchers in the past and it is now established that high ionic strength brines can cause irreversible formation damage to rocks (Ranjith et al., 2013; Shukla et al., 2013). Formation damage can be studied based on the mechanical behaviour of sandstone, including crack propagation, and monitoring various failure criteria such as crack initiation, crack closure and failure. Acoustic emission (AE) testing and stress-strain curve analysis are methods commonly used in analysing failure criteria (Shukla et al., 2013). It is also important to identify the effect of NaCl concentration on the uniaxial compressive strength, deformability and permeability of sandstones. The geomechanical effects of high salinity brine on sandstone are still not completely understood,

but a number of studies have published formation damage and permeability variations that salinity causes to clay rich sandstones (Mungan, 1965; Dahab et al., 1992).

Shukla et al.'s (2013) test results suggest that the mechanical properties change significantly with the change in NaCl concentration in the pore fluids. Their testing was conducted on two different sandstone samples, called S-type and M-type sandstones. The differences between two rock cores can be identified using mineralogical analysis. According to Shukla et al.'s (2013) test results, S-type samples contain quartz, muscovite and tourmaline and M-type samples contain plagioclase, quartz and muscovite. The researchers concluded that average ultimate uniaxial compressive strength initially decreases with the increment of NaCl concentration and then it increases again with the increase of NaCl concentration for both types. Fig. 2.4 below clearly shows the relationship between salinity and average uniaxial compressive strength for both S- and M-type sandstone specimens. The initial reduction of the strength is due to the water sensitivity or softening of the sandstone specimens in the brine. The observed increase in average peak strength of the sandstones is due to the crystallization of NaCl molecules from the brine in the pores of the sandstones (Akai, 1997; Bachu, 2000; Agustawijaya, 2001). Moreover, the strength difference of the two types of sandstones results from the difference of porosities, and S-type sandstones have greater porosity than M-type sandstones. The greater porosity provides more pore space for the formation of NaCl crystals and hence produces greater strength, while lower porosity provides lower strength (Omar, 1990; Shukla et al., 2013).

According to Fig. 2.4, it is clear that the UCS of the rocks starts increasing somewhere between the 5% and 10% NaCl concentration. This variation can be identified as softening of the reservoir rocks caused by the crystallization of the NaCl in the pore fluids. Dunning and Miller (1985) studied the effect of chemically-active solutions on the rock strength of porous Berea sandstone and Tennessee sandstone and concluded that the Berea rock's strength reduces due to the chemical solution, producing gouge more quickly. However, the same trend was not found for Tennessee sandstone. Presumably, the differences occur due to the higher porosity which offers more surface area for the fluids. Swolfs (1971) proposed a hypothesis to explain the effect of different pore fluids on reservoir rock fracture strength. The hypothesis is that the reduction in fracture strength due to the adsorption of ions or molecules onto the rock surface reduces the surface free energy of rocks.

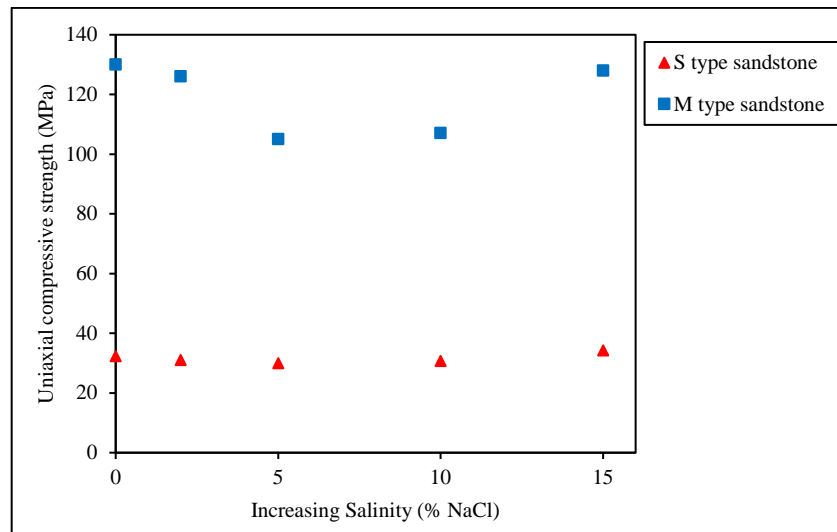


Figure 2.4. Average stress change with increasing NaCl concentration in brine for both types of sandstones (Shukla et al., 2013).

To evaluate the effect of chemically-active solutions on the strength properties of quartz- rich sandstone, Feucht and Logan (1990) performed triaxial compression tests on sandstone saturated with distilled water solutions of NaCl, CaCl₂, and Na₂SO₄ at varying ionic strengths and pH values. According to these researchers, the strength of rocks depends on the chemical composition of the reservoir pore fluid. The composition of most saline aquifers consists primarily of six ions: Na⁺, Mg²⁺, Cl⁻, HCO₃⁻, and SO₄²⁻. In conclusion, Feucht and Logan (1990) showed that the chemistry of the reservoir fluid may weaken a fault zone at high and low concentrations, but strengthen it at intermediate concentrations (Fig. 2.5).

Under brine concentration, we have only discussed the failure strength of the aquifer due to different brine concentrations. However, under CO₂ sequestration, we are mainly interested in CO₂-induced rock strength rather than pure compressive strength. However, it is clear that there are no data available on CO₂-induced rock strength. Therefore, further experimental and theoretical studies of CO₂-induced rock strength during the injection of CO₂ are necessary.

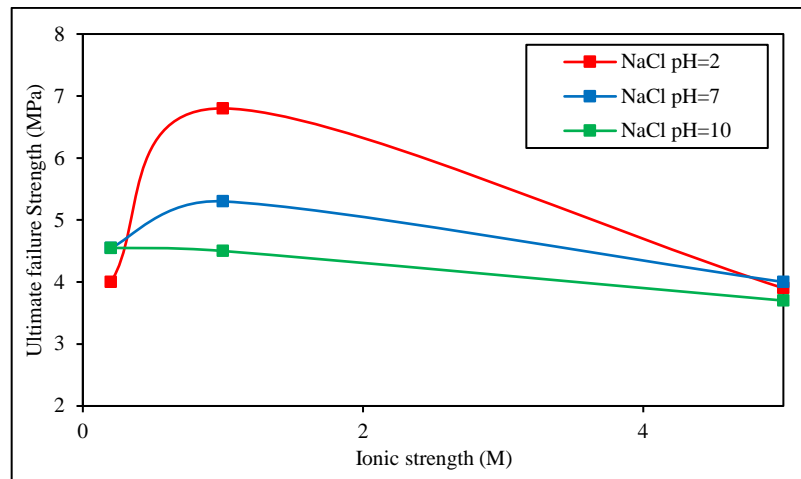


Figure 2.5. Relationship between ultimate failure strength and ionic strength (Feucht and Logan, 1990).

Effect of temperature

An understanding of the influence of temperature on reservoir rock strength is important when evaluating safe and effective methods of CO₂ sequestration. The influence of temperature on reservoir rock strength is extremely significant for engineering applications. In recent years, a considerable number of studies have been carried out to evaluate the impact of temperature on the mechanical behaviour and strength of reservoir rocks (Fig.2.6) (Czanderna, 1958; Byerlee, 1968; Dmitriyev et al., 1972; Fredrich et al., 1989; Duclos and Paquet, 1991; Bellotto et al., 1995; Gibb, 1999). However, it is important to note that there are no results available on CO₂ sequestration-induced rock strength and all the data are based on the pure compressive strength of reservoir rock. It is clear that CO₂ sequestration-induced mineralogical changes mainly depend on the reservoir temperature and that the strength of the reservoir depends on the mineral structure of the host rock. Therefore, rock strength can be extensively changed due to the mineralogical changes in reservoir rock during the injection of CO₂ and a comprehensive study of this effect is essential.

Wu et al. (2005) considered the influence of temperature on sedimentary rocks, conducting uniaxial compressive strength (UCS) tests on sandstone at temperatures between 25 and 600 °C. The researchers found that compressive strength decreases significantly with increasing temperature at temperatures higher than 400°C and that temperature does not affect compressive strength for temperatures lower than 400°C. Rao et al. (2007) also carried out UCS tests, evaluating the strengthening and stiffening processes of sandstone at temperatures between 25

and 300⁰C. According to these researchers, compressive strength increases with increasing test temperature up to 250⁰C and a sudden decrease of the trend was observed for temperatures greater than 250⁰C. Zhang et al. (2009) conducted UCS tests on sandstone at temperatures between 25 and 800⁰C. These researchers found that compressive strength decreases with increasing temperatures from 25 to 200⁰C, then increases with increasing temperatures from 200 to 800⁰C. Moreover, Ranjith et al. (2012) carried out UCS tests on Hawkesbury sandstone at different temperatures between 25 and 950⁰C and found that compressive strength increases with increasing temperature up to 600⁰C, whereas the opposite scenario was observed for temperatures greater than 600⁰C. In addition, this study showed that there were significant changes in sandstone mineralogy with heating, mainly due to the dehydroxylation of kaolinite. The researchers also concluded that the dehydroxylation of kaolinite can be used to explain the observed changes in mechanical properties with increasing temperature at temperatures greater than 500⁰C.

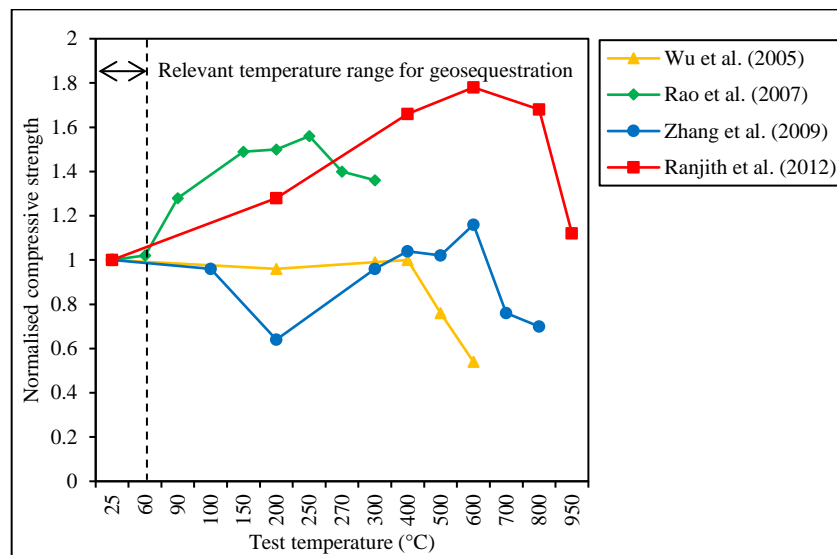


Figure 2.6. Normalised compressive strength versus test temperature curves reported in the literature.

The observed changes in the mineralogy of Hawkesbury sandstone can be summarised as shown in Table 2.2 below. According to Table 2.2, kaolinite dissolves significantly at 950⁰C and the precipitation rate of quartz and illite also increase at 950⁰C. However, there are no significant changes in smectite, goethite, haematite, anatase and rutile. The coupled behaviour of sandstones due to the injection of CO₂ and brine were observed by Hangx et al. (2013) at two different temperatures, 20⁰C and 60⁰C. As a consequence, the dissolution of calcite was

observed. It is clear that this temperature change did not affect the rock mechanical properties, even though it changed the mineralogical properties.

Table 2.2. Summary of mineralogical composition of specimens following UCS testing (Ranjith et al., 2012).

Testing temperature	Quartz	Haematite	Goethite	Illite/muscovite	Kaolinite	Smectite	Anatase	Rutile
25°C	85	-	2	3	7	2	1	-
950°C	91	1	-	7	-	-	<1	1

2.2.4.2 Effect of CO₂ sequestration on permeability

Over the last decade, several experimental studies on CO₂-brine flow systems in various rock samples have been performed. Researchers have used unsteady-state and steady-state and core-flooding techniques to evaluate relative permeabilities, and other system properties under different CO₂ injection pressures, temperatures, depths and salinity levels. Table 2.3 below shows a summary of these experimental studies.

Table 2.3. Experimental studies performed on the permeability of CO₂/brine flow in porous media in relation to geologic storage of carbon dioxide.

Reference	Rock samples	Measured parameters	Process
Bennion and Bachu(2005)	Basal Cambrian Sandstone, Niksu Carb., Cooking Lake Carb., Ellerslie SS., Viking Sandstones, Wabanum Carb.	K_r	Drainage
Bennion and Bachu(2008)	Calmar and Colorado group shales	Threshold P_c IFT and K_r	Drainage imbibition
Bennion and Bachu(2008)	Muskeg anhydrite	IFT, K_r	Drainage imbibition
Bennion and Bachu(2006)	Cardium Sandstone	IFT, K_r	Drainage imbibition

Suekane et al.(2008)	Fired Berea Sandstone	Trapped saturations	Drainage imbibition
Perrin et al. (2010a) and (2010b)	Sandstone from Australia and fired Berea Sandstone	Trapped saturations and K_r	Drainage
Krevor et al. (2011)	Mt. Simon Sandstone	Initial and trapped sat.	Drainage imbibition
Zuo et al. (2012)	Mt. Simon Sandstone and fired Berea Sandstone	Exsolution of CO ₂ and solubility, K_r	Drainage pressure drop
Shi et al. (2009)	Tako Sandstone	Initial saturation	Drainage
Pentland et al. (2011)	Berea Sandstone	Initial and residual CO ₂ sat.	Drainage imbibition
Akbarabadi and Piri (2013)	Berea SS. Nugget Sandstone	Initial and residual CO ₂ sat. Dissolution K_r	Drainage imbibition Dissolution
Akbarabadi and Piri (2013)	Berea Sandstone	K_r , Hysteresis	Drainage imbibition

According to past studies, the permeability of CO₂-brine systems depends on the in-situ conditions of brine concentration, temperature and pressure, and on the pore size distribution of the sedimentary rocks. Since pore size distribution is a function of permeability, it is important to study the effect of the mineralization process of CO₂ sequestration on the permeability of the saline aquifer in order to mitigate migration of CO₂ into the atmosphere. Moreover, it is clear that single-phase fluid flow in porous media can be described by the porosity and permeability of the formation rock, and the fluid viscosity (Berg et al., 2013). Multiphase flow (the CO₂-brine system) can be described by the relative permeability, capillary pressure and saturation functions (Egermann et al., 2006). Baudracco (1990) studied the relationship between the time-resolved changes in the sandstone rock composition, and the permeability and porosity induced by the mineralogical reactions during the CO₂ sequestration process in saline aquifers (Fig. 2.7). The dissolution of feldspars, laumontite and chamosite were observed throughout the research. In addition, the precipitation of silica and kaolinite were also noticed and the researchers concluded that permeability decreases of about one order of magnitude occurred due to the localization of the kaolinite precipitation. The researchers also showed that the limitation of the injection rate and the spreading of the CO₂ in the reservoir are

due to permeability reduction. Baudracco and Aoubonazza (1990) studied the variation in permeability in unconsolidated Triassic sandstones submitted to saline circulation. The authors noticed that the permeability of sandstone decreased as a function of time for all the samples. According to Baudracco and colleagues (Baudracco et al., 1988; Baudracco and Aoubouazza, 1990; Baudracco and Aoubouazza, 1995), the reduction of the permeability of sandstones results from to the displacement of free fine particles, which block the finest pores. In addition, the swelling of clays, the interaction of colloids and adsorption phenomena of the liquid on the walls of the porous environment may be reasons for reduced permeability.

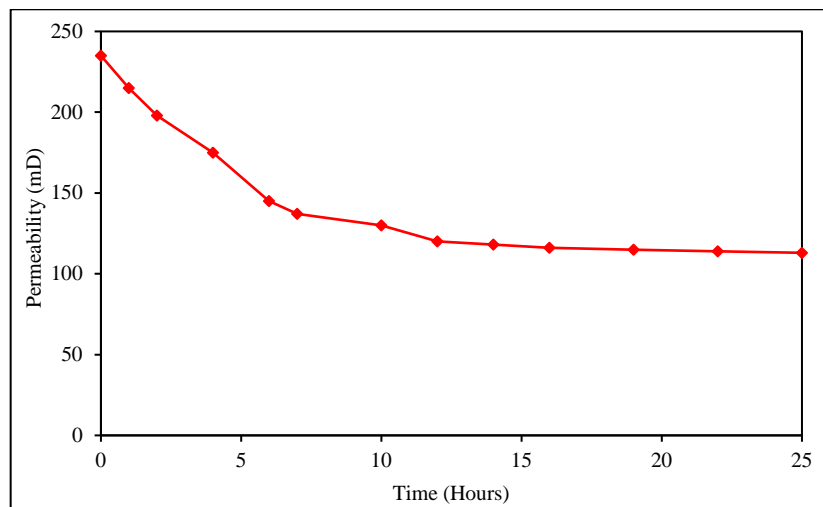


Figure 2.7. Variation of the permeability coefficient of reservoir rock with time ($T = 20^{\circ}\text{C}$, I (Brine) = 0.01 M) (Baudracco, 1990).

The effects of clay precipitation of reservoir sandstones were studied by Matthews et al. (1996) and Hovorka et al. (2004). They observed local decrease in permeability. Imbus et al. (2006) showed the importance of relative permeability data for CO_2 brine systems, considering the critical sub-surface issues in CO_2 storage in deep saline aquifers. Berg et al. (2010) conducted a series of core flood experiments to evaluate the process of displacement and mass transfer between CO_2 and brine by developing relative permeability and capillary pressure curves for Berea sandstone rock. Kuo et al. (2010), Perrin et al. (2010), and Perrin and Benson (2010) measured the CO_2 brine relative permeability of Berea sandstone in south-west Australia. These authors found that the permeability of aquifers is adversely affected due to the injection of CO_2 .

Perrin et al. (2010) conducted steady-state experiments on brine CO_2 relative permeability. Brine permeability was measured at several flow rates while recording the pressure drop. Finally, the permeability was calculated applying Darcy's law using fluid viscosity and

densities at reservoir temperature and pressure, and the process was continued up to 100% of CO₂ injection. The experiment confirmed that the spatial distribution of CO₂ under steady-state conditions significantly affects the permeability of reservoir rock. Egermann et al. (2006) and Chalbaud et al. (2010) conducted unsteady-state N₂ brine and CO₂ brine relative permeability experiments using carbonate samples, and found that CO₂ brine relative permeability decreased with time, and no significant variation was observed in N₂ brine permeability.

2.2.4.2.2 Factors influencing CO₂ sequestration-induced permeability alteration

Effect of brine concentration

Understanding the mechanisms of CO₂ permeability reduction in relation to the brine concentration of reservoir fluid is of great interest in environmental engineering, geothermal exploration and the petroleum industry. To date, few studies are available on the effect of brine concentration on the CO₂ permeability of reservoir rocks (Probst, 2008; Ranjith et al., 2013).

Probst (2008) observed that aquifer permeability decreases with increasing concentration of brine, and explained this using the evaporation effects of salt in the aquifer. In addition, this study also illustrated the “salting out effect”, whereby evaporation can make the water phase denser and reduce CO₂ solubility in water. The increase of density of water due to salinity is up to almost 20% and the H₂O-CO₂ system makes aqueous phase denser in the order of 2-3% (Julio, 2001). Fig. 2.8 below shows the salinity and temperature effects on CO₂ solubility in water. According to Fig. 2.8, the solubility of CO₂ in water decreases with increasing salinity and temperature (Hangx, 2005). Ranjith et al. (2013) also studied the effect of high salinity level on CO₂ permeability in the saline aquifer, changing the salinity level to 100,000, 110,000, 120,000, 130,000, 140,000, 150,000 and 160,000 ppm. These researchers concluded that high salinity levels reduce CO₂ permeability in aquifers, while reducing the total CO₂ storage capacity by 1.8%.

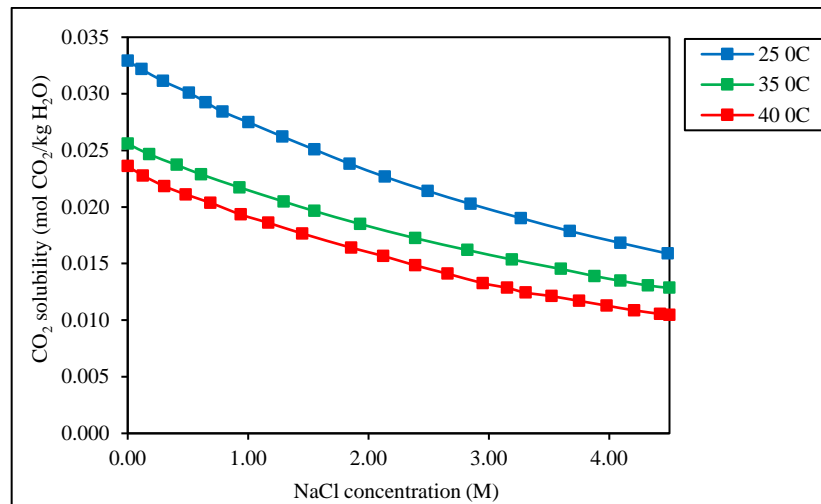


Figure 2.8. Relationship between CO₂ solubility and brine concentration (Hangx, 2005).

Many researchers have discussed the effect of brine concentration on water permeability (Baudracco and Tardy, 1988; Mohan et al., 1999). For example, Mohan et al. (1999) studied the effect of different high ionic strength brines on the absolute permeability of smectitic sandstones. The results of this study show that the permeability of sandstone decreases with increasing concentration of salt solution, and the damage to the formation is irreversible. Formation damage can be described as the permeability reduction of host rock due to contact with foreign fluids (Mohan et al., 1999).

Baudracco and Tardy (1988) showed that for a given cation, permeability decreases with increasing concentration of brine. The authors interpreted the changes in permeability as permanent changes of the flocculation-deflocculation state of the colloidal clay fraction available in reservoir rocks.

Four sets of experiments were conducted by Dahab et al. (1992) to study the effect of different ionic concentrations of the host fluid on the relative permeability of Saudi cores under different temperature and pressure conditions. Three types of cores were examined: Berea sandstone, Saudi sandstone and Aramco. These researchers concluded that the reduction in the permeability of reservoir rocks depends on the amount of change in the ionic concentration as well as the nature of the ions which are causing formation damage.

In general, permeability damage has been determined by using initial and final permeability, and the reduction is expressed as the permeability drop ratio, which is equal to $(k_1 - k)/k_1$, where k_1 and k are initial and final permeability, respectively (Omar, 1990).

After testing three different sandstones in Saudi Arabia, Omar (1990) showed that permeability damage is a function of NaCl concentration in the pore fluid in saline aquifers. The test results clearly illustrated that water sensitivity also increased when the cores were aged in NaCl solution. In sandstones, the swelling clay minerals can easily adsorb water (highly water-sensitive) and can result in changes in porosity, permeability, modulus of elasticity, deformability, tensile strength and uniaxial compressive strength of the rock mass. The correlation between the change in water and the permeability drop ratio was evaluated using milliequivalents of exchangeable ion values. Fig. 2.9 shows the variation between the permeability drop ratio and the milliequivalents of exchangeable ion capacity.

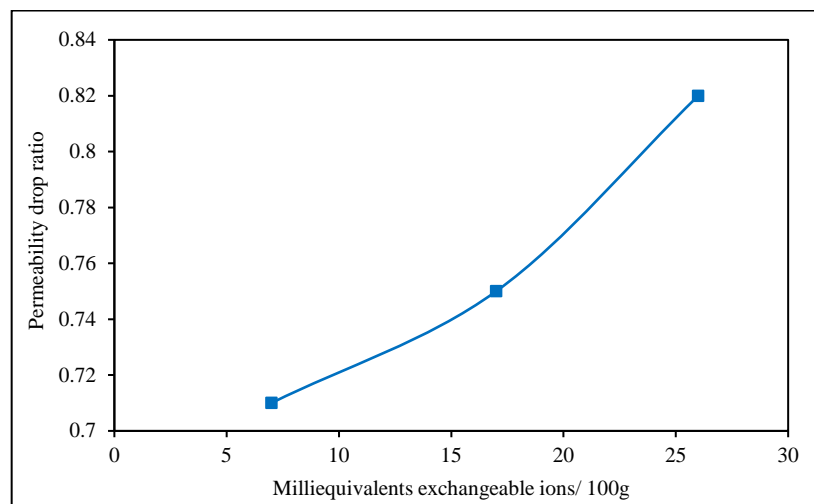


Figure 2.9. The variation between permeability drop ratio and the milliequivalents of exchangeable ion capacity (Omar, 1990).

Effect of clay composition

Another important factor affecting the permeability of aquifers is the clay composition of the reservoir rocks. Permeability damage to sandstone cores due to the presence of clay particles has been extensively studied by many researchers (Wilson and Pittman, 1977; McHardy et al., 1982; Pallat et al., 1984; Baudracco and Tardy, 1988; Baudracco and Auobouazza, 1990; Omar, 1990; Oelkers and Cole, 2008). Omar (1990) conducted permeability damage experiments on three types of sandstone cores. X-ray diffraction results showed that cores containing varying amounts of clay have different impacts on permeability. The interaction between brine solution and reservoir rock can be explained using injected electrolyte reactions and the double layer effect of clay particles. According to Omar (1990), a decrease in electrolyte concentration results in a decrease in the thickness of the double layer and the flocculation of clay crystals

will result in a decrease in the permeability of the reservoir rock. Moreover, the research demonstrated that the degree of reduction of permeability depends upon the abundance of swelling, the amount of movable clay (kaolinite, chlorite, illite and smectites) in the formation, the nature of the ions, and the number of exchangeable ions in the clay.

According to Baudracco and Terdy (1990), sandstones which contain clay particles or unconsolidated sandstones have been less studied. The effect of authigenic clay minerals on the water permeability of reservoir rocks has been shown by Wilson and Pittman (1977). These authors observed the reduction of water permeability due to the presence of clay minerals. The effects of clay inclusions and formation damage have been studied by McHardy et al. (1982) and Pallatt et al. (1984). However, both groups of researchers have identified that few theories interpret the effect of inclusions of clay due to the complex nature of the void spaces in sandstones. Matthews et al. (1996) assessed the heterogeneity of the hydrodynamic properties and its possible changes during the injection and storage of CO₂, particularly in terms of clay precipitation during sequestration. The authors observed permeability reduction due to clay precipitation and fine clay particle migration. Luquot et al. (2012) conducted CO₂ percolation experiments on chlorite-zeolite-rich sandstone by reproducing in-situ reservoir conditions during CO₂ injection. According to these researchers, aquifer permeability reduces due to the precipitation of kaolinite and they concluded that the permeability reduction function mainly depends on the composition of clay particles (Fig. 2.10). Moreover, these researchers discussed the different behaviour of the permeability function due to the presence of kaolinite, illite, chlorite and smectite.

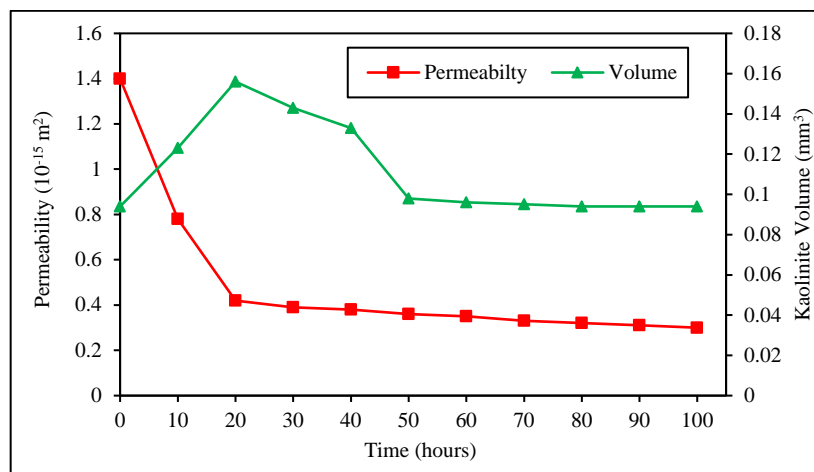


Figure 2.10. Permeability and precipitated kaolinite volume versus elapsed time (Luquot et al., 2012).

Effect of temperature

In this section, the effect of temperature on CO₂ permeability during the storage of CO₂ in deep saline aquifers is discussed. The effect of temperature on CO₂ permeability in saline aquifers was studied by Ranjith et al. (2013), over 15 years of CO₂ injection with changing temperatures of 20, 40, 60, 80, 100 and 110⁰C. The researchers found that CO₂ permeability decreased with increasing temperature. Furthermore, Bachu and Bennion (2008) measured the relative permeability and other displacement characteristics of CO₂ brine systems for sandstone. The results showed that relative permeability depends on the in-situ temperature and concluded that CO₂ permeability decreases as temperature increases.

The effects of temperature on the water permeability of sandstones in saline aquifers have been extensively studied over the last 50 years (Somerton et al., 1965; Somerton and Gupta, 1965; Akton and Farouk, 1975; Sydansk, 1980; Khilar, 1981; Miller and Ramey, 1986; Jing et al., 1992; Baudracco and Aoubouazza, 1995; Matthews et al., 1996; Hovorka et al., 2004). These studies showed that changes in sandstone permeability due to temperature variation depend on the materials, the composition of the fluids and the experimental conditions. Permeability can decrease, remain constant or, in special cases, increase with increasing temperature, depending on the above conditions. In contrast, it is difficult to predict changes in sandstone permeability. In past studies, Berea sandstone has been the most frequently examined (Aktan and Farouk, 1975).

Baudracco and Aoubouazza (1995) examined the behaviour of two samples of Berea and Vosges sandstones at different temperatures under the circulation of different ionic strengths and solutions of different natures. The temperatures were taken in the increasing and then decreasing directions to correlate the effect of temperature on sandstone permeability. According to the test results, it can be seen that thermal expansion has practically no effect on permeability. Nevertheless, the effects of thermal expansion between T and $T + \Delta T$ on measured permeability should be corrected. The relationship is expressed as follows:

$$\frac{\Delta k}{k} = \frac{3\mathcal{G}\Delta T}{\phi - 1} \quad (2.10)$$

where k is the permeability, ϕ is the porosity and \mathcal{G} is the volumetric expansion coefficient.

However, Baudracco and Aoubovazza (1995) noticed that all increases in temperature caused a steep decrease in permeability, and all decreases in temperature caused a sharp increase in permeability for both cases. For 0.1M NaCl saturated Berea sandstone, the permeability decreased about 81.75% with increasing temperature from 20⁰C to 90⁰C and permeability increased about 89.29% with decreasing temperature from 90⁰C to 20⁰C. The authors concluded that permeability is inversely proportional to temperature. In addition, the different behaviour of sandstones due to temperature is explained by the flocculation and deflocculation of the clay particles in porous media.

The effect of in-situ heating on the permeability of dry and saturated Berea sandstone and Boise sandstone was studied by Aktan and Farouk (1975). They calculated permeability by using a Ruska permeameter. In the in-situ heating experiment, the increasing trends of the permeabilities of sandstones were identified upon heating to 300 and 500⁰F respectively. Sydansk (1980) conducted flooding experiments in two fired Berea sandstone plugs, one at 450⁰C and the other at 1000⁰C, and each was flooded at 22 and 85⁰C. The results showed that brine absolute permeability in fired Berea sandstones does not vary considerably with temperatures between 22 and 85⁰C. Furthermore, the permeability reduction of Berea sandstone with increasing flooding temperature was observed to be due to the migration of clay particles at higher flooding temperatures.

Fig. 2.11 below shows the trend observed by Jing et al. (1992) for the normalised permeability versus temperature of two different sandstone samples at a confining pressure of 13.8MPa. The results clearly illustrate that permeability decreases with increasing temperature from ambient to 93⁰C. The decrease in rock permeability may be caused by the thermal expansion of rock-forming materials under confining pressure, which reduces the pore size, and changes the effective rock tortuosity and roughness.

Some previous studies have found that permeability increases with increasing temperature for clean clay-free sandstones (Somerton et al., 1965; Somerton and Gupta, 1965). The increase of permeability is explained by thermally- induced micro-crack opening and the change in degree of rock fluid interaction caused by increasing free pore space.

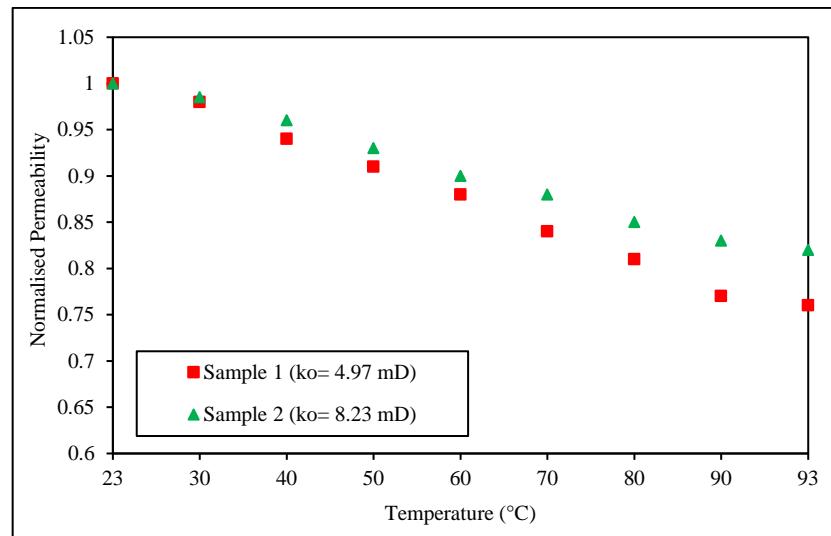


Figure 2.11. Plot for normalised permeability versus temperature of two different sandstone samples at a confining pressure of 13.8 MPa (Jing et al., 1992).

Effect of depth

The effect of depth on the permeability of reservoir rocks can be simulated with different confining pressure conditions at a laboratory scale. According to past studies, it is clear that the stress-dependent model of fluid flow properties (rock permeability, porosity and storage capacity) for reservoir rocks remains debatable (David et al., 1994; Wibberley, 2002; Heikamp and Nover, 2003; Kwon et al., 2004; Lion and Skoczylas, 2004; Ghabezloo et al., 2009; Tanikawa and Shimamoto, 2009). Furthermore, permeability and porosity are a function of both current loading condition and past loading condition (stress history) within a sedimentary basin (Kwon et al., 2004). The effect of confining or overburden pressure on the permeability of various porous media with various pore fluids has been studied by several researchers (Somerton et al., 1965; Somerton and Gupta, 1965; Morrow et al., 1984; Shi and Wang, 1988; Gavrilenko and Gueguen, 1989; Jing et al., 1992; David et al., 1994; Evans et al., 1997; Wibberley, 2002; Heikamp and Nover, 2003; Lion and Skoczylas, 2004; Ghabezloo et al., 2009; Tanikawa and Shimamoto, 2009; Dong et al., 2010; Shukla et al., 2012). All these past studies show that the permeability of sandstones decreases with increasing confining pressure.

Jing et al. (1992) carried out novel experiments to evaluate the permeability of five sandstone samples at elevated pressure with 50g/l NaCl brine as the flow fluid. Fig. 2.12 shows the variation of the normalised permeability of five sandstones at different confining pressures ranging from atmospheric to 30MPa. According to this research, normalized permeability is

defined as the permeability at elevated pressure over that under atmospheric conditions. Based on their experimental results, the authors concluded that permeability decreases with increasing confining pressure for all five rocks tested. However, the amount of reduction in permeability is mainly dependent on the porosity and the initial permeability of the rock samples. The observed reduction in the permeability of rocks with confining pressure was explained by rock deformation, which reduces the pore size and alters the internal surface roughness.

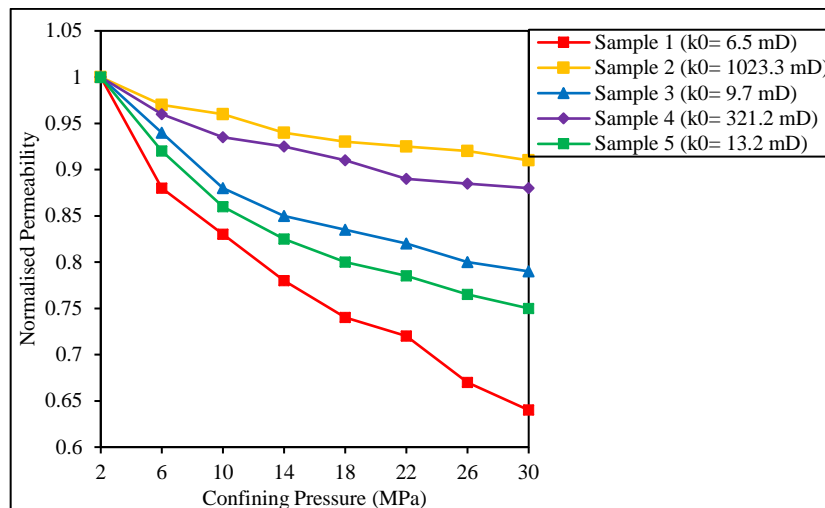


Figure 2.12. Plot of normalised permeability versus confining pressure for five sandstone samples (Jing et al., 1992).

A deep drilling project was conducted in the western foothills of Taiwan to study fluid flow properties including stress-dependent permeability under different effective confining pressures (Kaszuba et al., 2003). Dong et al. (2010) conducted experiments to measure the permeability and porosity of Pleistocene sandstone from a 2000m borehole under different loading and unloading pressures. Permeability was reduced when the confining pressure was increased (Fig. 2.13). Models for describing the effective confining pressure-dependency of permeability have been discussed by a number of researchers (Shi and Wang, 1988; Gavrilenko and Gueguen, 1989; David et al., 1994; Evans et al., 1997). David et al. (1994) suggested that an exponential relationship is suitable for calculating stress-dependent permeability. The same relationship was noted by Evans et al. (1997). Based on Morrow et al.'s (1984) experimental results, Shi and Wang (1988) proposed that the relationship between effective pressure and rock permeability could be evaluated by power law models.

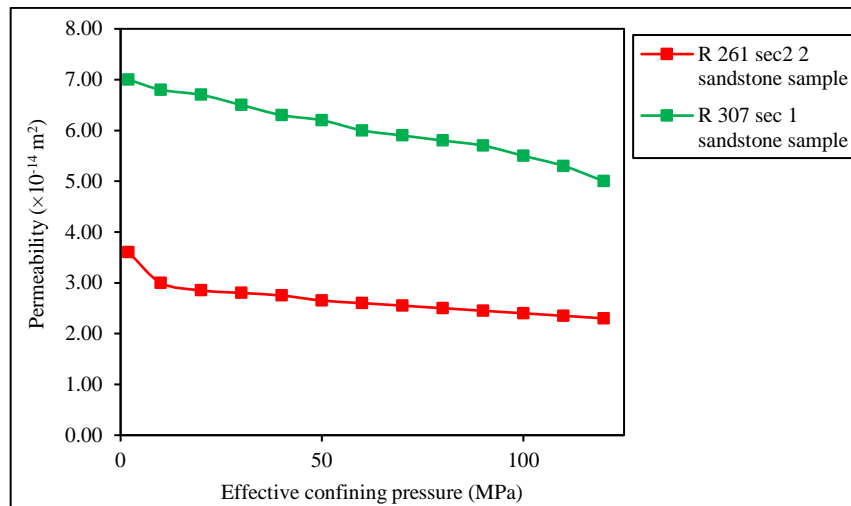


Figure 2.13. Variation of stress-dependent permeability of sandstone with effective confining pressure (Dong et al., 2010).

The dominant mechanisms controlling the evaluation of rock permeability with effective confining stress have been proposed by different researchers. According to David et al. (1994), permeability reduction occurs mainly because of micro-crack closure, particle rearrangement and crushing. In addition, these authors introduced three types of permeability evaluation techniques, depending on mechanical compaction for low porosity crystalline rock, porous clastic rock and unconsolidated materials. The sandstones tested indicated that no particle crushing mechanism was available for sandstones. Therefore, the observed reduction of permeability was mainly because of the relative movement of grains (Shi and Wang, 1988). In summary, David et al. (1994) showed the applicability of power law models to predict the permeability and porosity of porous sandstones at depths where no particle crushing mechanism is involved. Shukla et al. (2013) concluded that the permeability of reservoir rock decreases with increasing confining pressure. This observation is consistent with several past studies. Shukla et al. (2013) also showed that the time taken by the rock specimen to reach pore pressure equilibrium increased with increasing confining pressure. This may be mainly because of decreasing pore throat size with increasing confining stress in the initial phase, but when pore pressure crosses the breakthrough pressure, pressure starts to dissipate through the rock again. According to Ranjith et al. (2013), changing depth has a significant influence on CO_2 permeability and storage capacity in a saline aquifer. In addition, this research studied the surrounding confinement environment of rock mass and the effect of aquifer pore pressure by

investigating 15 years of CO₂ injection with changing depths (0.8, 1, 1.1, 1.2, 1.4 and 1.8km). The researchers found that CO₂ permeability exponentially reduces with increasing depth.

Effect of injection pressure

To date, very few studies have reported the effect of injection pressure of CO₂ and its potential impacts on CO₂ permeability. Ranjith et al. (2013) have clearly shown the effect of injection pressure on CO₂ permeability by considering 15 years of injection with changing injection pressures of 15, 17, 19, 20, 21 and 23MPa. The authors concluded that CO₂ permeability increases with increasing CO₂ injection pressure due to the reduction of effective stress acting on the aquifer, which results in the expansion of pore space. Shukla et al. (2012) conducted novel tests for the hydro-mechanical investigation of reservoir rocks. The rock samples were injected with water, gaseous CO₂ and liquid CO₂ while the confining pressures were varied during the experiment. The results demonstrated that there is a linear relationship between downstream fluid flow rate and injection pressure for water. However, for gaseous CO₂ injection, the curves showed a non-linear relationship (Shukla et al., 2012; Ranjith et al., 2013). It is clear that for both cases, the downstream flow rate increases with increasing injection pressure. Fig. 2.14 below shows the relationship between injection pressure and flow rate at constant confining pressure for (a) water and (b) gaseous CO₂. The nonlinear behaviour of gaseous CO₂ may be because of the higher compressibility of the CO₂ at low pressure. Hence, at lower injection pressure (upstream pressure), the gas is more compressible and the downstream flow rate is reduced. At higher upstream pressure, the gas is less compressible and the flow rate is therefore much higher (Dong et al., 2010).

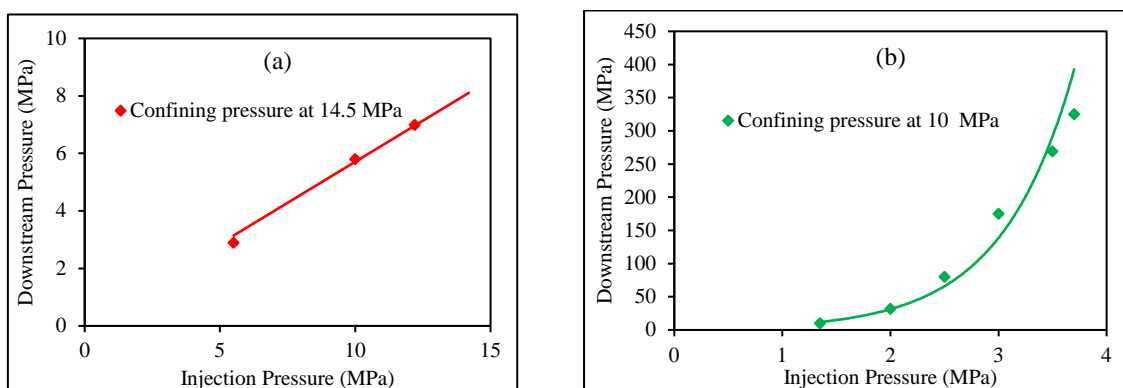


Figure 2.14. Variation of flow rate with injection pressure change for a) water and b) gaseous CO₂ at constant confining pressure (Shukla et al., 2012).

2.2.5 Risks associated with CO₂ storage in saline aquifers

Back-migration of the injected CO₂ into the atmosphere after some time of injection is the greatest risk associated with CO₂ sequestration in saline aquifers and the reservoir caprock plays an important role in preventing this leakage by acting as a barrier. Therefore, it is of utmost importance to study the effect of CO₂ sequestration on caprock stability. Past studies indicate that the geological interaction between CO₂, brine, and reservoir rock can have effects on caprock stability during and after the injection of CO₂ (Bieniawski, 1967; Martin and Chandler, 1994; Eberhardt et al., 1997; Rutqvist and Tsang, 2002; Sminchak et al., 2002; Bouchard and Delaytermoz, 2004; Peacock and Mann, 2005; Li et al., 2007). It is also possible to react scCO₂ with the organic contents of the caprock, which affects the permeability and porosity of the caprock (Rutqvist and Tsang, 2002). It is therefore, important to have a thorough knowledge of the caprock and its long-term integrity to ensure that the injected CO₂ will be stored safely during the sequestration process.

However, according to current studies, there is no considerable leakage or adverse impact on the caprock formation when the caprock is free of faults and fractures (Peacock and Mann, 2005; Li et al., 2007). These studies considered the fracture mechanics, the level of crack formation, the dependence of deformations, and the characteristics of lateral and axial deformations with injecting excessive pressure on the rocks to develop confining pressure (Bieniawski, 1967; Martin and Chandler, 1994; Eberhardt et al., 1997; Sminchak et al., 2002; Peacock and Mann, 2005; Li et al., 2007). Super-critical CO₂ injection tests were also carried out to identify the variation of porosity and the permeability of caprock. The test results found a change of less than 1% in permeability and an inconsequential increase in porosity (Okamoto et al., 2005). It is also concluded that the availability of secondary minerals can accelerate CO₂ leakage into the caprock (Liu et al., 2003). Rutqvist and Tsang (2002) studied the response of the hydraulic, mechanical and hydro-mechanical behaviours of caprock and the reservoir rock and found that the changes in permeability of the caprock and the aquifer are proportional to the effective mean stress changes. The lower part of the caprock and the upper part of the basement are also affected, with the most relevant changes being in permeability and the stress field (Eberhardt et al., 1997). According to these researchers, a change in stress field may adversely affect the performance of an injection site in many ways. The high permeability leakage path through fractured rock and the opening of pre-existing faults, fractures and slip displacement-associated permeability changes are the most devastating catastrophes which may

occur. In addition, the reduction in effective stress field in the aquifer can cause the ground surface to heave. It is therefore, important to study rock deformation stresses, including changes in pore pressure due to multi-phase flow and heat transfer. However, to date there have been few studies of the effect of CO₂ injection pressure on the hydro-chemical and hydro-mechanical properties of reservoir rock. Therefore, these properties should be further considered in future studies.

2.2.6 Conclusions

A comprehensive review was conducted to identify the effect of CO₂ sequestration on the mechanical properties and permeability characteristics of saline aquifers and factors affecting them, with special consideration of leakage through the cap rock due to changes in its hydro-mechanical parameters and permeability during CO₂ injection. It is clear that the mechanical properties and permeability of the aquifer vary significantly with brine concentration, injection pressure, depth, clay composition and the mineralogical structure of the reservoir rock. However, uncertainties remain concerning the behaviour of CO₂-induced rock strength due to the lack of studies related to the interaction between brine, CO₂ and reservoir rock. According to past studies, CO₂ permeability increases with increasing injection pressure due to the expansion of pore structure, resulting in the decrease of effective stress acting on the rock skeleton. It is also clear that aquifer permeability decreases with increasing concentration of brine, due to the evaporation effects of the salt. Furthermore, the clay composition of the sandstone significantly reduces the aquifer permeability, due to clay precipitation and migration of the fine clay particles. In addition, past studies have concluded that aquifer permeability decreases with increasing depth, due to the reduction of pore size and the internal surface roughness. However, when the factors affecting the CO₂ injection-induced mechanical properties and permeability variations in aquifers are considered, it is notable that temperature is not a critical factor in the CO₂ sequestration process. This is mainly because, in sequestration the temperature varies with respect to the injection depth and the most preferable aquifers for CO₂ sequestration lie at depths between 800 and 2000m and the corresponding temperature conditions are in the range of 50 to 60°C.

On the basis of this review, the permeability and strength of aquifers have a great influence on the final outcome of CO₂ sequestration. Therefore, detailed hydro-chemical and hydro-mechanical evaluations should be conducted before planning a CO₂ sequestration project in any saline aquifer. However, there are few studies related to the interaction between brine, CO₂ and

reservoir rock in CO₂ sequestration. In particular, the role of faults and joints related to the injection of CO₂ requires research. In addition, an appropriate constitutive model to describe the failure criteria of reservoir rock is essential, due to the absence of appropriate failure models such as those which are commonly used in rock mechanics. Therefore, more elaborate laboratory experiments should be conducted on CO₂-induced aquifer strength and CO₂ permeability under conditions representative of natural reservoir conditions. The chemical interaction of carbon dioxide with rock minerals and the aquifer should be studied, with special consideration of the effects of temperature, depth, brine concentration and CO₂ injection pressure.

The effect of these factors on the integrity of the caprock should also be carefully studied to ascertain the long-term safety of sequestration projects. Regarding the risks associated with CO₂ sequestration in saline aquifers, geological interaction between CO₂, brine, and reservoir rock affects cap rock stability. The rate of this interaction depends on the CO₂ injection pressure, which is higher for super-critical CO₂ compared to gas or liquid CO₂. In addition, scCO₂ has more ability to react with the organic contents of the cap rock, which also affects the permeability and porosity of the cap rock and consequently causes CO₂ leakage. However, according to current studies, there is no considerable leakage or adverse impact on the cap rock formation when the cap rock is free of faults and fractures. Hence, it is concluded that, if sufficient attention is given to the points identified in this review, the planning and execution of a carbon sequestration projects will be more efficient.

2.2.7 References

1. Agustawijaya DS. The development of design criteria for underground excavations in Coober Pedy arid soft rocks. PhD dissertation, University of South Australia, 2001.
2. Akai K. Testing methods for indurated soils and soft rocks-Interim report. In: Geotechnical Engineering of hard soils–soft rocks, Proceedings of the First International Conference on Hard Soils and Soft Rocks Balkemam, Rotterdam 1997; 3: 1707-1737.
3. Akbarabadi M, Piri M. Relative permeability hysteresis and capillary trapping characteristics of supercritical CO₂/brine systems: An experimental study at reservoir conditions. *Advanced Water Resource* 2013; 52: 190-206.
4. Aktan T, Farouk ASM. Effect of cyclic and in situ heating on the absolute permeabilities, elastic constants and electrical resistivities of rocks. Presented at the 50th Annual Fall Meeting of the SPE of AIME, Dallas, TX SPE 1975; 5633: 1-10.
5. Bachu, S. Sequestration of CO₂ in geological media: criteria and approach for site selection in response to climate change. *Energy Conversion Management* 2000; 41(9): 953-970.
6. Bachu S, Bonijoly D, Bradshaw J, Burruss R, Holloway S, Christensen NP, Mathiassen OM. CO₂ storage capacity estimation: Methodology and gaps. *International Journal of Greenhouse Gas Control* 2007; 1(4): 430-443.
7. Bachu S. CO₂ storage in geological media: Role, means, status and barriers to deployment. *Progress in Energy Combustion Science* 2008; 34(2): 254-273.
8. Bachu S, Bennion B. Effects of in-situ conditions on relative permeability characteristics of CO₂-brine systems. *Environmental Geology* 2008; 54(8): 1707-1722.
9. Baudracco J. Variations in permeability and fine particle migrations in unconsolidated sandstones submitted to saline circulations. *Geothermics* 1990; 19(2): 213-221.
10. Baudracco J, Tardy Y. Dispersion and flocculation of clays in unconsolidated sandstone reservoirs subjected to percolation with NaCl and CaCl₂ solutions at different temperatures. *Applied Clay Science* 1988; 3(4): 347-360.
11. Baudracco J, Aoubouazza M. Study of the variations in permeability and cationic exchange kinetics during solution changes in clay sandstone. *Chemical Geology* 1990; 84(1-4): 235-238

12. Baudracco J, Aoubouazza M. Permeability variations in Berea and Vosges sandstone submitted to cyclic temperature percolation of saline fluids. *Geothermics* 1995; 24(5): 661-677.
13. Bellotto M, Gualteri A, Artioli G, Clark SM. Kinetic study of the kaolinite mullitereaction sequence. Part I: kaolinite dehydroxylation. *Physics and Chemistry of Minerals* 1995; 22: 207-214.
14. Bennion B, Bachu S. Relative permeability characteristics for supercritical CO₂ displacing water in a variety of potential sequestration zones in western Canada sedimentary basin. In SPE 95547, *Proceedings of the SPE Annual Technical Conference and Exhibition*, Dallas, Texas, 2005.
15. Bennion D, Bachu S. Dependence on temperature, pressure, and salinity of the IFT and relative permeability displacement characteristics of CO₂ injected in deep saline aquifers. In *SPE Annual Technical Conference and Exhibition*, 2006.
16. Bennion B, Bachu S. Drainage and imbibition relative permeability relationships for supercritical CO₂/brine and H₂S/brine systems in intergranular sandstone, carbonate, shale, and anhydrite rocks. *SPE Reservoir Evaluation and Engineering* 2008; 11(3): 487-496.
17. Berg S, Oedai S, Landman AJ, Brussee N, Boele M, Valdez et al. Miscible displacement of oils by carbon disulfide in porous media: Experiments and analysis. *Physics of Fluids* 2010; 22: 102-113.
18. Berg S, Oedai S, Ott H. Displacement and mass transfer between saturated and unsaturated CO₂-brine systems in sandstone. *International Journal of Greenhouse Gas Control* 2013; 12: 478-492.
19. Bieniawski ZT. Stability concept of brittle fracture propagation in rock. *Environmental Geology* 1967; 2(3): 149-162.
20. Bouchard R, Delaytermoz A. Integrated path towards geological storage. *Energy* 2004; 29:1339-1346.
21. Bruant RG, Guswa AJ, Celia MA, Peters CA. Safe storage of CO₂ in deep saline aquifers. *Environmental Science and Technology* 2002; 36(11): 240A-245A.
22. Byerlee JD. Brittle-ductile transition in rocks. *Journal of Geophysical Research* 1968; 73: 4741-4750.

23. Chalbaud C, Robin M, Lombard JM, Bertin H, Egermann P. Brine/CO₂ interfacial properties and effects on CO₂ storage in deep saline aquifers. *Oil and Gas Science Technology* 2010; 65 (4): 541-555.
24. Czanderna AW, Ramachandra RCN, Honig JM. The anatase-rutile transition. Part I: kinetics of the transformation of pure anatase. *Transactions of the Faraday Society* 1958; 54: 1069-1073.
25. Dahab AE, Omar El, Gassier MM, Kariem HA. Formation damage effects due to salinity, temperature and pressure in sandstone reservoirs as indicated by relative permeability measurements. *Journal of Petroleum Science and Engineering* 1992; 6(4): 403-412.
26. David C, Wong TF, Zhu W, Zhang J. Laboratory measurement of compaction- induced permeability change in porous rocks: implication for the generation and maintenance of pore pressure excess in the crust. *Pure Applied Geophysics* 1994; 143: 425-456.
27. Dmitriyev AP, Kusyayev LS, Protasov YI, Yamschchikov VS. *Physical properties of rocks at high temperatures*. Nedra Press, Moscow, 1972.
28. Dong JJ, Hsu JY, Wu WJ, Shimamoto T, Hung JH, Yeh et al. Stress-dependence of the permeability and porosity of sandstone and shale from TCDP Hole-A. *International Journal of Rock Mechanics and Mining Science* 2010; 47: 1141-1157.
29. Duclos R, Paquet J. High-temperature behaviour of basalts – role of temperature and strain rate on compressive strength and K_{Ic} toughness of partially glassy basalts at atmospheric pressure. *International Journal of Rock Mechanics and Mining Science* 1991; 28: 71-76.
30. Dunning JD, Miller ME. Effects of ore fluid chemistry on stable sliding of Berea sandstone. *Pure Applied Geophysics* 1985; 122(2-4): 447-462.
31. Eberhardt E, Stead D, Stimpson B, Read RS. Changes in acoustic event properties with progressive fracture damage. *International Journal of Rock Mechanics and Mining Science* 1997; 34: 621- 633.
32. Egermann P, Chalbau C, Duquerroix JP, Le Gallo Y. An integrated approach to parameterize reservoir models for CO₂ injection in aquifers. *Society of Petroleum Engineers* 2006; 102: 1-9.
33. Emberley S, Hutcheon I, Shevalier M, Durocher K, Gunter WD, Perkins EH. Geochemical monitoring of fluid-rock interaction and CO₂ storage at the Weyburn CO₂ injection enhanced oil recovery site, Saskatchewan, Canada. *Energy* 2004; 29(9): 1393-1401.

34. Evans JP, Forster CB, Goddard JV. Permeability of fault-related rocks and implications for hydraulic structure of fault. *Journal of Structural Geology* 1997; 19(11): 1393-1404.
35. Farrar CD, Neil JM, Howele JFUS. Geological survey water-resource investigation report. U. S. Geological Survey: Sacramento, CA, 1999; 43: 1-17.
36. Feucht LJ, Logan JM. Effects of chemically active solutions on shearing behavior of a sandstone. *Tectonophysics* 1990; 175(1-3): 159-176.
37. Fischer S, Zemke K, Liebscher A, Wandrey M. Petrophysical and petrochemical effects of long-term CO₂ exposure experiments on brine-saturated reservoir sandstone. *Energy* 2011; 4: 4487-4494.
38. Ford TD, King RJ. Mineralization in the Triassic rocks of south Derbyshire. *Mineral Processing and Extractive Metallurgy* 1968; 77: B42-B44.
39. Fredrich JT, Evans B, Wong TF. Micromechanics of the brittle to ductile transition in Carrara marble. *Journal of Geophysics Research* 1994; (B4): 4129-4145.
40. Gaus I, Azaroual M, Czernichowski-Lauriol I (2005). Reactive transport modelling of the impact of CO₂ injection on the clayey cap rock at Sleipner (North Sea). *Chemical Geology* 2005; 217: 319-337.
41. Gavrilenko P, Gueguen Y. Pressure dependence of permeability: a model for cracked rocks. *International Journal of Geophysics* 1989; 98: 159-172.
- [42]. Ghabezloo S, Sulem J, Guedon S, Martineau F. Effective stress law for the permeability of a limestone. *International Journal of Rock Mechanics and Mining Science* 2009; 46: 297-306.
43. Giammar DE, Bruant Jr RG, Peters CA. Forsterite dissolution and magnesite precipitation at conditions relevant for deep saline aquifer storage and sequestration of carbon dioxide. *Chemical Geology* 2005; 217: 257-276.
44. Gibb SE. High-temperature, very deep geological disposal: a safer alternative for high-level radioactive waste. *Waste Management* 1999; 19: 207-211.
45. Goss CJ. The kinetics and reaction mechanism of the goethite to hematite transformation. *Mineral Magazine* 1987; 50: 437-451.

46. Gray DH, Rex R. Formation damage in sandstones caused by clay dispersion and migration. *Proceedings of 14th National Conference of Clays and Clay Minerals, Bailey (SW) 1966*; 14: 355-366.
47. Gunter WD, Bachu S, Benson S. The role of hydrogeological and geochemical trapping in sedimentary basins for secure geological storage of carbon dioxide. *Journal of Geological Society* 2004; 233(1): 129-145.
48. Hangx SJT. Behaviour of the CO₂-H₂O system and preliminary mineralisation model and experiments. Shell International Exploration and Production (leader CATO WP 4.1). Work performed in the framework of Shell contract 4600002284, 2005.
49. Hangx S, Van der Linden A, Marcellis F, Bauer A. The effect of CO₂ on the mechanical properties of the Captain Sandstone: Geological storage of CO₂ at the Goldeneye field (UK). *International Journal of Greenhouse Gas Control* 2013; 201: 5-17.
50. Heikamp S, Nover G. An integrated study on physical properties of a KTB gneiss sample and marble from Portugal: pressure dependence of the permeability and frequency dependence of the complex electrical impedance. *Pure Applied Geophysics* 2003; 160: 929-936.
51. Holmes I, Chambers AD, Ixer RA, Turner P, Vaughan DJ. Diagenetic processes and the mineralization in the Triassic of Central England. *Mineral Processing and Extractive Metallurgy* 1983; 18: 365-377.
52. Hovorka SD, Doughty C, Benson SM, Pruess K, Knox PR. The impact of geological heterogeneity on CO₂ storage in brine formations: a case study from the Texas Gulf Coast: Geological storage of carbon dioxide. *Geological Society* 2004; 233: 147-163.
53. Imbus S, Orr FM, Kuuskraa VA, Kheshgi H, Bennaceur K, Gupta et al. Critical issues in CO₂ capture and storage: findings of the SPE advanced technology workshop (ATW) on carbon sequestration. *Society of Petroleum Engineering* 2006; 102968: 1-7.
54. Jing XD, Archer JS, Daltaban TS. Laboratory study of the electrical and hydraulic properties of rocks under simulated reservoir conditions. *Marine and Petroleum Geology* 1992; 9(2): 115-127.
55. Johns TC, Gregory JM, Ingram WJ, Johnson CE, Jones A, Lowe JA, Mitchell et al. Anthropogenic climate change for 1860 to 2100 simulated with the HadCM3 model under updated emissions scenarios. *Climate Dynamics* 2003; 6: 583-612.

56. Julio GE. Density of aqueous solutions of CO₂. Lawrence Berkeley National laboratory, <http://escholarship.org/uc/item/6dn022hb>, 2001.
57. Kaszuba JP, Janecky DR, Snow MG. Carbon dioxide reaction processes in a model brine aquifer at 200°C and 200 bars: implications for geologic sequestration of carbon. *Applied Geochemistry* 2003; 18(7): 1065-1080.
58. Khilar KC. Water sensitivity of sandstone. PhD thesis, University of Michigan, 1981.
59. Knauss KG, Johnson JW, Steffel CI. Evaluation of the impact of CO₂, co-contaminant gas, aqueous fluid and reservoir rock interactions on the geologic sequestration of CO₂. *Chemical Geology* 2005; 217: 339-350.
60. Koide HG, Tazaki Y, Noguchi M. Subterranean containment and long-term storage of carbon dioxide in unused aquifers and in depleted natural gas reservoirs. *Energy Conversion Management* 1992; 33: 619-626.
61. Koide H, Takahashi M, Tsukamoto H, Shindo Y. Self-trapping mechanisms of carbon dioxide in the aquifer disposal. *Energy Conversion Management* 1995; 36(6): 505-508.
62. Kongsjorden H, Karstad O, Torp TA. Saline aquifer storage of carbon dioxide in the Sleipner project. *Waste Management* 1998; 17(5): 303-308.
63. Krevor SCM, Pini R, Li B, Benson SM. Capillary heterogeneity trapping of CO₂ in a sandstone rock at reservoir condition. *Journal of Geophysics* 2011; 38: 23-31.
64. Kuo CW, Perrin JC, Benson SM. Effect of gravity, flow rate and small scale heterogeneity on multiphase flow of CO₂ and brine. *Society of Petroleum Engineering* 2011; 132607: 1-13.
65. Kwon O, Kronenberg AK, Gangi AF, Johnson B, Herbert BE. Permeability of illite-bearing shale: Anisotropy and effects of clay content and loading. *Journal of Geophysics* 2004; 10: 102-112.
66. Li Q, Wu Z, Lei X, Murakami Y, Satoh T. Experimental and numerical study on the fracture of rocks during injection of CO₂-saturated water. *Environmental Geology* 2006; 51(7): 1157-1164.
67. Lion M, Skoczylas F. Determination of the main hydraulic and poro-elastic properties of a limestone from Bourgogne France. *International Journal of Rock Mechanics and Mining Science* 2004; 41: 915-925.

68. Liu L, Suto Y, Bignall G, Yamasaki N, Hashida T. CO₂ injection to granite and sandstone in experimental rock/hot water systems. *Energy Conversion Management* 2003; 44(9): 1399-1410.
69. Luquot L, Andreani M, Gouze P, Camps P. CO₂ percolation experiment through chlorite/zeolite-rich sandstone (Pretty Hill Formation, Otway Basin, Australia). *Chemical Geology* 2012; 294-295: 75-88.
70. Marbler H, Erickson KP, Schmidt M, Lempp C, Pollmann H. Geomechanical and geochemical effects on sandstone caused by the reaction with supercritical CO₂: an experimental approach to in situ conditions in deep geological reservoirs. *Environmental Earth Science* 2013; 4: 123-132.
71. Martin CD, Chandler NA. The progressive failure of Lac du Bonnet granite. *International Journal of Rock Mechanics and Mining Science* 1994; 31(6): 643-659.
72. Matthews GP, Ridgway CJ, Small JS. Modelling of simulated clay precipitation within reservoir sandstones. *Marine and Petroleum Geology* 1996; 13 (5): 581-589.
73. McHardy WJ, Wilson ML, Tait JM. Electron microscope and x-ray diffraction studies of filamentous Illitic clay from sandstones of the magnus field clay min. *Society of Petroleum Engineering* 1982; 17: 23- 29.
74. Miller MA, Ramey HJ. Effect of temperature on oil/water relative permeability of unconsolidated sands. *Journal of Petroleum Engineering* 1986; 34: 1945-955
75. Mohan KK, Vaidya RN, Reed MG, Fogler HS. Water sensitivity of sandstones containing swelling and non-swelling clays. *Colloids and Surfaces A: Physical and Chemical Engineering Aspects* 1993; 73:237-254.
76. Mohan KK, Reed MG, Fogler HS. Formation damage in smectic sandstones by high ionic strength brines. *Colloids and surfaces A: Physical and Chemical Engineering Aspects* 1999; 154: 249-257.
77. Moore J, Adams M, Allis R, Lutz S, Rauzi S. Mineralogical and geochemical consequences of the long-term presence of CO₂ in natural reservoirs: an example from the Springerville-St. Johns field, Arizona, and New Mexico, USA. *Chemical Geology* 2005; 217: 365-385.
78. Morrow CA, Shi L, Byerlee JD. Permeability of fault gouge under confining pressure and shear stress. *Journal of Geophysics* 1984; 89: 3193-3200.

79. Mungan N. Permeability reduction through changes in pH and salinity. *Journal of Petroleum Technology* 1965; 17(12): 1449-1453.
80. Nasvi MMC, Ranjith PG, Sanjayan J. Geopolymer as well cement and the variation of its mechanical behaviour with curing temperature. *Greenhouse Gases Science and Technology* 2012; 2: 46-58.
81. Naylor H, Turner P, Vaughan DJ, Boyce AJ, Fallick AE. Genetic studies of red bed mineralization in the Triassic of the Cheshire Basin, northwest England. *Journal of Geological Society* 1988; 146: 685-699.
82. Nghiem L, Sammon P, Grabenstetter J, Ohkuma H. Modeling CO₂ storage in aquifers with a fullycoupled geochemical EOS compositional simulator. In *SPE/DOE Symposium on Improved Oil Recovery*, 2004.
83. Nghiem L, Yang C, Shrivastava V, Kohse B, Hassam M, Card C. Risk mitigation through the optimization of residual gas and solubility trapping for CO₂ storage in saline aquifers. *Energy* 2009; 1(1): 3015-3022.
84. Oelkers EH, Cole DR. Carbon dioxide sequestration a solution to a global problem. *Elements* 2008; 4(5): 305-310.
85. Oelkers EH, Gislason SR, Matter J. Mineral carbonation of CO₂. *Elements* 2008; 4(5): 333-337.
86. Okamoto I, Li X, Ohsumi T. Effect of supercritical CO₂ as the organic solvent on cap rock sealing performance for underground storage. *Energy* 2005; 30(11-12): 2344-2351.
87. Oldenburg C, Benson S. CO₂ injection for enhanced gas production and carbon sequestration. In *SPE International Petroleum Conference and Exhibition in Mexico*, 2002.
88. Omar A. Effect of brine composition and clay content on the permeability damage of sandstone cores. *Journal of Petroleum Science and Engineering* 1990; 4(3): 245-256.
89. Ormerod MB. The disposal of carbon dioxide from fossil fuel fired power stations. *IEA Greenhouse Gas R&D Programme*, 1994.
90. Ozah R, Lakshminarasimhan S, Pope G, Sepehrnoori K, Bryant S. Numerical simulation of the storage of pure CO₂ and CO₂-H₂S gas mixtures in deep saline aquifers. In *SPE Annual Technical Conference and Exhibition*, 2005.

91. Pallat N, Wilson J, McHardy W. The Relation between permeability and the morphology of diagenic illite reservoir rocks. *Journal of Petroleum Technology* 1984; 36: 2225-2227.
92. Peacock DCP, Mann A. Evaluation of the controls on fracturing in reservoir rocks. *Journal of Petroleum Geology* 2005; 28(4): 385-396.
93. Pentland CH, El-Maghraby R, Iglauer S, Blunt MJ. Measurements of the capillary trapping of supercritical carbon dioxide in Berea sandstone. *Journal of Geophysics* 2011; 38: 64-76
94. Perera MSA, Ranjith PG. Effects of gaseous and super-critical carbon dioxide saturation on the mechanical properties of bituminous coal from the southern Sydney basin. *Applied Energy* 2013; 110: 73-81.
95. Perrin JC, Benson S. An experimental study on the influence of sub-core scale heterogeneities on CO₂ distribution in reservoir rocks. *Transport Porous Medium* 2010; 82: 93-109.
96. Perrin JC, Krause M, Kuo CW, Miljkovic L, Charoba E, Benson SM. Core-scale experimental study of relative permeability properties of CO₂ and brine in reservoir rocks. *Energy* 2010; 1(1): 3515-3522.
97. Probst P. Numerical Simulations of CO₂ Injection into Saline Aquifers: Estimation of Storage Capacity and Arrival Times using Multiple Realizations of Heterogeneous Permeability Fields, Master Thesis, 78, 2008.
98. Pruess K, Garcia J, Kavscek T, Oldenburg C, Rutqvist J, Steefel C, Xu T. Code intercomparison builds confidence in numerical simulation models for geologic disposal of CO₂. *Energy* 2004; 29(9): 1431-1444.
99. Ranganathan P, Van HP, Rudolph E, Susanne J, Zitha PZJ. Numerical modelling of CO₂ mineralisation during storage in deep saline aquifers. *Energy* 2011; 4: 4538-4545.
100. Ranjith PG, Viete DR, Chen BJ, Perera M. Transformation plasticity and the effect of temperature on the mechanical behaviour of Hawkesbury sandstone at atmospheric pressure. *Engineering Geology* 2012; 151: 120-127.
101. Ranjith P, Perera M, Khan E. A study of safe CO₂ storage capacity in saline aquifers: A numerical study. *International Journal of Energy Research* 2013; 37: 189-199.

102. Rao QH, Wang Z, Xie HF, Xie Q. Experimental study of properties of sandstone at high temperature. *Journal of Central South University of Technology (English Edition)* 2007; 14 (s1): 478-483.
103. Regnault O, Lagneau V, Schneider H. Experimental measurement of portlandite carbonation kinetics with supercritical CO₂. *Chemical Geology* 2009; 265:113-121.
104. Rosenbauer RJ, Bischoff JL, Radke AS. Hydrothermal alteration of graywacke and basalt by 4 m NaCl. *Economic Geology* 1983; 78: 1701-1710.
105. Rosenbauer RJ, Bischoff JL, Kharaka YK. Geochemical effects of deep-well injection of the Paradox Valley brine into Paleozoic carbonate rocks, Colorado, U.S.A. *Applied Geochemistry* 1992; 7: 273-286.
106. Rosenbauer RJ, Bischoff JL, Potter JM. A flexible Au-Ir cell with quick assembly for hydrothermal experiments. *American Mineralogist* 1993; 78: 1286-1289.
107. Rutqvist J, Tsang CF. A study of caprock hydro-mechanical changes associated with CO₂-injection into a brine formation. *Environmental Geology* 2002; 42: 296-305.
108. Santarelli FJ, Brown ET. Failure of three sedimentary rocks in triaxial and hollow cylinder compression tests. *International Journal of Rock Mechanics and Mining Science* 1989; 26(5): 1100-1012.
109. Sass BM, Engelhard MH, Berman P, Byrer C. Interaction of rock minerals with carbon dioxide and brine: A hydrothermal investigation. *Journal of Energy and Environment* 2002; 2: 23-31.
110. Schutt H, Wigand M, Spangenberg E. Geophysical and geochemical effects of supercritical CO₂ on sandstones. In: Benson, S. (Ed.), *The CO₂ Capture and Storage Project for Carbon Dioxide Storage in Deep Geological Formations for Climate Change Mitigation* 2004; 2: 767-786.
111. Shi T, Wang CY. Generation of high pore pressure in accretionary prisms: inferences from the Barbados Subduction Complex. *Journal of Geophysics* 1988; 93(B8): 8893-8910.
112. Shi JQ, Xue Z, Durucan S. History matching of CO₂ core flooding CT scan saturation profiles with porosity dependent capillary pressure. *Energy* 2009; 1: 3205-3211.
113. Shukla R, Ranjith P, Haque A, Choi X. A review of studies on CO₂ sequestration and caprock integrity. *Fuel* 2010; 89(10): 2651-2664.

114. Shukla R, Ranjith PG, Choi SK, Haque A. A novel testing apparatus for hydromechanical investigation of rocks: geosequestration of carbon dioxide. *Rock Mechanics and Rock Engineering* 2012; 45(6): 1073-1085.
115. Shukla R, Ranjith PG, Choi SK, Haque A, Yellishetty M, Hong L. Mechanical Behaviour of Reservoir Rock Under Brine Saturation. *Rock Mechanics and Rock Engineering* 2012; 46(1): 83-9.
116. Sminchak J, Gupta N, Byrer C, Bergman P. Issues related to seismic activity induced by the injection of CO₂ in deep saline aquifers. *Journal of Energy Environment* 2002; 2(1): 32-46.
117. Somerton WH, Gupta VS. Role of fluxing agents in thermal alteration of sandstones. *Journal of Petroleum Technology* 1965; 36: 585- 588.
118. Somerton WH, Mehta WM, Dean GW. Thermal alteration of sandstones. *Journal of Petroleum Technology* 1965; 21: 589-593.
119. Suekane T, Nobuso T, Hirai S, Kiyota M. Geological storage of carbon dioxide by residual gas and solubility trapping. *International Journal of Greenhouse Gas Control* 2008; 2(1): 58-64.
120. Svec RK, Grigg RB. Physical Effects of WAG Fluids on Carbonate Core Plugs. In *SPE Annual Technical Conference and Exhibition, SPE* 2001; 71496:1-10.
121. Swolfs H. Influence of pore fluid chemistry and temperature on fracture of sandstone under confining pressure. Ph.D. Thesis, Texas A&M University, 1971.
122. Sydansk RD. Discussion of the effect of temperature and confining pressure on single-phase flow in consolidated rocks. *Journal of Petroleum Engineering* 1980; 32: 1329-1330.
123. Tanikawa W, Shimamoto T. Comparison of Klinkenberg-corrected gas permeability and water permeability in sedimentary rocks. *International Journal of Rock Mechanics and Mining Science* 2009; 46: 229-238.
124. Wasantha PLP, Darlington WJ, Ranjith PG. Characterization of mechanical behaviour of saturated sandstone using a newly developed triaxial apparatus. *Experimental Mechanics* 2013; 53: 871-882
125. White SP, Allis RG, Moore J, Chidsey T, Morgan C, Gwynn W, Adams M. Simulation of reactive transport of injected CO₂ on the Colorado Plateau, Utah, USA. *Chemical Geology* 2005; 217: 387-405.

126. Wibberley C. Hydraulic diffusivity of fault gouge zones and implications for thermal pressurization during seismic slip. *Earth Planets Space* 2002; 54: 1153-1171.
127. Wilson M, Pittman E. Authigenic clays in sandstones: recognition and influence on reservoir properties and palaeoenvironmental analysis. *Journal of Sedimentary Petrol* 1977; 47: 3-31.
128. Winter EM, Bergman PD. Availability of depleted oil and gas reservoirs for disposal of carbon dioxide in the United States. *Energy Conversion Management* 1993; 34(9): 1177-1187.
129. Wong TF, David C, Zhu W. The transition from brittle faulting to cataclastic flow in porous sandstones: Mechanical deformation. *Journal of Geophysics Research* 1997; 102-B2: 3009-3025.
130. Wu Z, Qin Bd, Chen LJ, Luo YJ. Experimental study on mechanical character of sandstone of the upper plank of coal bed under high temperature (in English). *Chinese Journal of Rock Mechanics and Engineering* 2005; 24: 1863-1867.
131. Xu T, Apps JA, Pruess K. Mineral sequestration of carbon dioxide in a sandstone–shale system. *Chemical Geology* 2005; 217(3); 295-318.
132. Yang F, Bai B, Tang D, Shari DN, David W. Characteristics of CO₂ sequestration in saline aquifers. *Petroleum Science* 2010; 7(1): 83-92.
133. Zhang LY, Mao Xb, Lu Ah. Experimental study of on the mechanical properties of rocks at high temperature. *Science in China Series E-Technological Science* 2009; 52: 641-646.
134. Zuo L, Krevor SCM, Falta RW, Benson SM. An experimental study of CO₂ exsolution and relative permeability measurements during CO₂ saturated water depressurization. *Transport Porous Medium* 2012; 91(2): 459-478.

2.3 The influence of aquifer characteristics and rock mineralogy on deep saline sequestration process

In addition to injection pressure, confining pressure, temperature and salinity, aquifer characteristics, including pH, chemical composition, distance from the injection point and reservoir rock mineral composition are other factors in the behaviour of reservoir rock in deep saline sequestration. Generally, chemical and mineral compositions vary from aquifer to aquifer, and therefore, different aquifers exhibit different hydro-mechanical responses upon exposure to CO₂. Therefore, it is important to identify the effect of these basic factors when selecting an appropriate reservoir for CO₂ sequestration. In addition, it is essential to understand the chemical response and kinetic evaluation of reservoir rock minerals upon exposure to CO₂ in order to develop numerical simulations related to deep saline sequestration. Therefore, a comprehensive chemical and mineralogical evaluation is carried out in this section to investigate the influence of aquifer characteristics on reservoir hydro-mechanical behaviour. The following submitted journal paper discusses this aspect of the study.

A Review of Chemical and Mineralogical Concerns of CO₂ Sequestration in Deep Saline Aquifers.

T. D. Rathnaweera¹, P.G. Ranjith¹, M. S. A. Perera¹

¹Department of Civil Engineering, Monash University, Building 60, Melbourne, Victoria, 3800, Australia.

Abstract

CO₂ sequestration in deep saline aquifers offers a promising solution to the control of global warming by reducing anthropogenic CO₂ emissions into the atmosphere. During this process, the captured CO₂ is injected in its super-critical form into the aquifer via wells and stored in the aquifer using different trapping mechanisms. However, fundamental dissolution reactions occur between the injected CO₂ and the aquifer host fluid during the interaction between CO₂, brine and host rock, leading to changes in the chemical integrity of the natural aquifer formation, which consequently changes the reservoir formation, both mineralogically and chemically. These changes significantly alter the hydro-mechanical behaviour of the reservoir rock during CO₂ sequestration. Therefore, this paper provides a comprehensive review of potential changes in the chemical and mineralogical environments of saline aquifers due to CO₂ injection under in-situ conditions and the influence of these changes on the hydro-mechanical behaviour of reservoir rock. The effect of aquifer characteristics, such as pH and ionic composition, on the hydro-mechanical properties of reservoir rock are also considered. However, the CO₂ injection-induced hydro-mechanical properties in saline aquifers vary significantly with the aquifer and injecting gas properties, making the process extremely complex. As a result, to date, insufficient studies have been undertaken on this aspect. Furthermore, this study identifies the chemically corrosive nature of the different host fluids, which leads to decreased rock strength and increased crack propagation velocity during CO₂ sequestration.

Keywords: saline aquifer, hydro-mechanical properties, petrophysical properties, chemical and mineralogical changes

2.3.1 Introduction

CO₂ sequestration in deep saline aquifers has recently attracted the attention of many industrialised countries, such as Canada, the United States, the United Kingdom, Australia and a number in the Middle East, due to its unique advantages. Of these, the huge storage capacity

of saline aquifers compared to other geological media such as oil/gas fields and unmineable coal seams is critical (Bachu, 2000; Orr, 2004). According to Bruant et al. (2002), the estimated total capacities of available deep saline aquifers are between 320 Gt CO₂ and 200,000 Gt CO₂ with a life-time of more than 100 years. In addition to this huge storage capacity, CO₂ sequestration in deep saline aquifer process has a quick capture process and requires only simple technology compared to other methods, such as CO₂ storage in coal beds (Farrar et al., 1999). Therefore, this can be considered as one of the most promising means of reducing anthropogenic CO₂ emissions into the atmosphere.

However, the process needs to be well monitored and key factors must be clearly identified to ensure safe and effective long-term sequestration. CO₂ dissolution kinetics, mineral trapping kinetics, microbial interactions with CO₂ and the influence of stress change on the integrity of caprock and formation rock are the most critical factors (Ranjith et al., 2013).

Preferable aquifers for CO₂ sequestration lie between 800 to 2000 m depths, and most are highly saline and situated in sedimentary basins. According to Freeze and Cherry (1979), saline aquifers generally contain six primary ions: Na⁺, Mg²⁺, Ca²⁺, Cl⁻, HCO₃⁻ and SO₄²⁻ and the pH varies from 5.5 to 8, and between 1.9 to 9.4 according to Hem (1959).

The geo-chemical reactions that occur between the injected CO₂-brine and reservoir rock mass during the CO₂ sequestration process depend on the distance from the injection well, as the degree of CO₂ saturation varies with that distance (Azaroual et al., 2007; Gaus et al., 2008). During long-term injection of CO₂, the sedimentary rocks at the centre of the well and adjacent to the well become almost dry due to forced brine migration, and the rock mass is fully CO₂ saturated. However, the degree of CO₂ saturation becomes less than one with increasing distance from the injection well and reaches zero in more remote areas (100% brine saturation). Therefore, as shown in Fig. 2.15 there are differently saturated rock masses in the aquifer during the CO₂ injection process (Marbler et al., 2013), which can be basically divided into three main groups: CO₂/ rock reaction system, CO₂/ brine/ rock reaction system and rock/ brine reaction system.

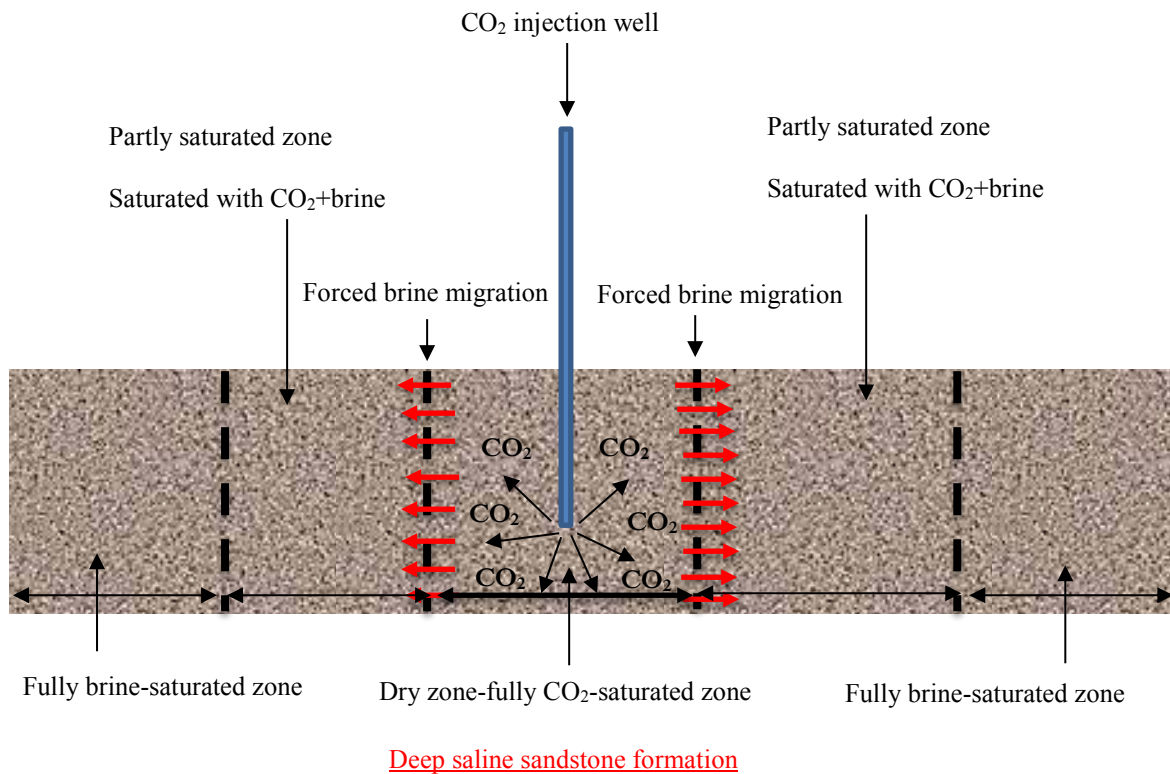


Figure 2.15. Formation of different zones during CO₂ sequestration.

This chemical interaction between CO₂, brine and rock leads to changes in the porosity, permeability and strength characteristics of the aquifer (Johnson et al., 2004). These consequently create time-dependent reservoir deformations (Madland et al., 2006; Le Guen et al., 2007; Vialle and Vanorio, 2011) and micro-cracking (Atkinson, 1979; Chester et al., 2007; Hangx et al., 2010; Liteanu et al., 2012), which affect the diffusive mass transfer in the aquifer (Schutjens, 1991; Dewers and Hajash, 1995; Renard et al., 1999; Croize et al., 2010; Hangx et al., 2013). As a consequence, detrimental effects such as back-migration of CO₂ into the atmosphere, sub-surface heaving near injection wells, aquifer compaction and contamination of CO₂ in fresh water aquifers, may occur during sequestration. Therefore, it is essential to fully understand the chemical and mineralogical behaviour of saline aquifers during and after CO₂ injection. Therefore, this study provides a comprehensive overview of the chemico-mineralogical interactions between the CO₂, brine and host rock during the CO₂ storage process, and the effects on the hydro-mechanical properties of the aquifer.

2.3.2 Role and behaviour of rock mineral structure upon CO₂ sequestration

Generally, reservoir rock is a complex medium, which contains different types of minerals. Therefore, in order to define the composition of the reservoir rock it is necessary to perform a detailed mineralogical analysis, such as X-ray diffraction (XRD) or X-ray fluorescence spectroscopy (XRF). Table 2.4 below provides the mineralogical composition of the reservoir rock in some saline aquifers located throughout the world. According to Marbler et al. (2013), reservoir rocks in saline aquifers are sedimentary rocks, which mainly have matrix and grain-supported structures and can be categorised into two main categories: silicate-cemented and carbonate-cemented sandstones. These different mineralogical compositions of reservoir rocks cause different responses of reservoir rocks upon CO₂ sequestration. For example, according to Shukla et al. (2012), S-type and M-type sandstones (two different types of sandstones) have different mechanical behaviours under brine saturation due to their different mineralogical contents.

Table 2.4. Summary of different compositions of reservoir rock.

Reference	Location	Type of Rock	Mineral composition
Feng et al. (2004)	Luoyang city, China	Carbonate-cemented sandstone	Quartz (75%), calcite (18%), hydrous mica (2%), plagioclase (1%), silica (< 0.1%), muscovite (0.1%), limonite (3%), tourmaline (< 0.1%)
Feucht and Logan (1990)	-	Tennessee sandstone: silica-cemented	Quartz (90%), kaolinite (7%), calcite and feldspar (< 1%)
Marbler et al. (2013)	Birkigt Quarry , Saxony Anhalt	Silicate-cemented sandstone (Triassic Bunter sandstone)	Quartz (75%), microline (20%), muscovite (1%), clay minerals including kaolinite, illite, smectite (3-4%)
	Uder Quarry , Thuringia	Carbonate-cemented sandstone (Triassic Bunter sandstone)	Quartz (60%), calcite (25%), muscovite (1%), siderite, orthoclase, plagioclase, clay minerals including kaolinite, illite, smectite (3-4%)
	Bebertal Quarry, Saxony Anhalt	Silicatic and carbonic sandstone (Rotliegend sandstone)	Quartz (70%), microline (20%), hematite rims, cherts, plag, orthoclase, calcite (4-5%), muscovite (1-2%), clay minerals including kaolinite, illite, smectite (3%)
Shukla et al. (2012)	Melbourne's south-eastern suburbs	S-type	Quartz, muscovite, tourmaline
		M-type	Quartz, muscovite, plagioclase
Hangx et al. (2013)	Goldeneye field, Moray Firth, UK North Sea	Captain D sandstone	Quartz (78%), K-feldspar (5.7%), plagioclase (5.6%), kaolinite (7.6%), calcite (0.3%)
Wilkinson et al. (2009)	Holland	Rotliegend sandstone	Quartz (51%), K-feldspar (7%), dolomite (14%), rock fragments

			(12%), kaolinite (3%), illite (0.6%)
Baudracco and Tardy (1988)	Sherwood area, Larne (Northern Ireland)	Triassic sandstone	Quartz (95%), feldspar (2%), halite (1%), illite (0.7%), smectite (0.2%), kaolinite (0.1%), rock fragments (1%)
Zerai et al. (2006)	Eastern Ohio, Pennsylvania, New York, and Kentucky in the Appalachian Basin	Silica-cemented sandstone	Quartz (83%), K-feldspar (10%), albite (2%), annite (1%), kaolinite (3%), siderite (1%)
Kummerow and Spangenberg (2011)	Ketzin site, Germany	Upper Triassic sandstone	Quartz (39.3%), albite (31.6%), dolomite (2.8%), orthoclase (7.4%), anhydrite (4.5%), illite (10.9%), hematite (2.1%), halite (1.4%)
Baudracco and Aoubouazza (1990)	-	Fine Berea sandstone	Quartz (85%), feldspar (5%), carbonate (1%), opaque minerals (2%), kaolinite (1%), illite (1%), montmorillonite (1%)

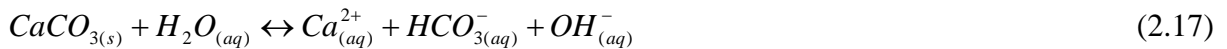
The reaction rate between the host rocks' minerals and the host fluid is a key factor when evaluating both the flow and mechanical properties of saline aquifers during CO₂ injection, according to which the reactions in saline aquifers can be categorized as: rapid dissolution of fast-reacting minerals such as carbonates (Pokrovsky et al., 2009; Liteanu et al., 2012) and slow long-term mineralisation, such as quartz, feldspars, clays, micas and Fe-oxides (Ca^{2+} , Mg^{2+} or Fe^{2+} rich minerals) (Aagaard et al., 2004; Palandri et al., 2005; Carroll and Knauss, 2005; Hangx and Spiers, 2009). For example, the chemical interaction of feldspar and clay minerals with the host fluid and the injected CO₂ during CO₂ sequestration is quite a slow process, which normally takes in the order of tens to thousands of years (Parkhurt and Appelo 1999). Carbonate dissolution is therefore the primary reaction in saline aquifers upon CO₂ injection, which is controlled by the brine-to-rock ratio, the pH of the host fluid, the chemical potential of the CO₂ and the kinetic rate of its dissolution (Zerai et al., 2006).

The possible interaction between carbonate minerals and the dissolved carbonic acid leads to the formation of bicarbonate ions during CO₂ injection, which can be written as follows for some of the major carbonate minerals in saline aquifers (Plummer et al., 1978; Rosso and Rimstidt, 2000):





In relation to these carbonate minerals, Plummer et al. (1978) discussed the dissolution reaction of calcite minerals. The following reactions occur in parallel during calcite dissolution under ambient conditions:



Moreover, the net rate of these reactions, r (Eqs. 2.15-2.17) can be evaluated by using following equation (Plummer et al., 1978), where k_1 , k_2 , k_3 and k_4 are rate constants and a_i is the activity of the relevant species.

$$r = k_1 a_{H^+} + k_2 a_{H_2CO_3^*} + k_3 a_{H_2O} - k_4 a_{Ca^{2+}} a_{HCO_3^-} \quad (2.18)$$

Understanding of calcite dissolution in the reservoir environment requires understanding of both the hydrodynamic mass transport properties of the mineral-brine system and the kinetics of heterogenous reaction at the calcite surface. According to Sjöberg (1976), calcite dissolution is controlled largely by surface reaction when the system's pH is above 4. However, Reddy (1975) revealed that this dissolution reaction is complicated by the effects of "foreign ions" present in the aquifer pore fluid. In real field conditions, foreign ions from the aquifer pore fluid and other mineral reactions can make this reaction even more complicated. Therefore, it is worth understanding the reaction kinetics of calcite dissolution and their influence on the hydro-mechanical properties of reservoir rock.

The other important rock mineral reaction in deep saline aquifers is the quartz (SiO_2) mineral reaction, since the major proportion of reservoir rock normally contains silicate-cemented quartz minerals. Quartz dissolution is known as non-stoichiometric or incongruent dissolution due to the dissolution of impurity phases or zones within the primary minerals and the secondary minerals. The non-stoichiometric reaction can be defined as "a reaction which releases elements into solution at different rates" (Brantly, 2008). According to Brantly (2004), the quartz mineral formation mechanism is a simple leaching process which occurs as a result

of surface condensation and reconstruction reactions. The natural abundance of quartz suggests the importance of this mineral reaction in the evaluation of diverse earth processes. In deep saline sequestration, the rate of quartz mineral dissolution can be used to evaluate the strength and flow alterations induced by CO₂ injection. According to Van Lier et al. (1960), quartz in deep saline reservoir rock can be dissolved even under natural aquifer conditions due to the presence of high salinity brine as a pore fluid. Moreover, the results of their study revealed that the quartz dissolution reaction rate increases with increasing NaCl concentration. This is due to the formation of *Na – Si* complexes in solution, which ultimately increases the affinity between quartz and NaCl, resulting in increased quartz solubility reaction. Knauss and Thomas (1988) revealed the influence of aquifer pH on the quartz dissolution reaction. According to their results, the dissolution rate is independent of pH up to approximately 6, but at higher pH, the dissolution rate increases with increasing aquifer pH. Icenhower and Dove (2000) investigated the rate of dissolution of quartz and the net rate of dissolution of quartz (r) with and without NaCl can be described successfully using the following rate model.

$$r = k_+ (a_{SiO_2(aq)}) (a_{H_2O})^2 (1 - \Omega) \quad (2.19)$$

where, k_+ is the dissolution rate constant, a_i is the activity of the relevant species and Ω is the ratio of activity quotient to equilibrium constant for a reaction.

In addition to carbonate and quartz minerals, feldspar minerals also play a major role in reservoir hydro-mechanical behaviour, because the dissolution of feldspar grains also causes the hydro-mechanical properties to significantly change during the sequestration process. Generally, the feldspar mineral family contains K-feldspar, albite, oligoclase, andesine, labradorite, bytownite and anorthite. The rate of feldspar dissolution can be calculated by the following empirical equation:

$$r = k_H a_{H^+}^n + k_{OH} a_{OH^-}^m \quad (2.20)$$

where, n and m are partial orders of reaction, k_H and k_{OH} are the rate constants for proton and hydroxyl and a_i is the activity of species.

According to Mukhopadhyay and Walther (2001), with respect to pH, the dissolution rate of feldspar exhibits a parabolic trend, and the dissolution rate increases under low and high pH conditions. In addition, the reservoir rock mineral structure may contain some non-framework

silicate minerals, such as kaolinite, muscovite, biotite, talc and chrysotile. According to Brantley (2008), the dissolution rate of non-framework silicate minerals can also be calculated using Eq. 2.20.

2.3.3 Prediction models for mineral dissolution and precipitation kinetics in saline aquifers

The kinetics of mineral dissolution and precipitation determine the lifetimes of reservoir minerals and therefore affect the flow and mechanical properties in saline aquifers during CO₂ sequestration (Aagaard and Helgeson, 1982). According to White and Brantley (2003), laboratory-scale results of mineral dissolution are much higher than those in the field under pre-weathered conditions. However, to date there are many kinetics models that can be used to predict the behaviour of mineral dissolution and precipitation in different environments (Lasaga, 1984; Lasaga, 1998; Lasaga, 2001; Sorai and Sasaki, 2010). In general, the dissolution reaction of a mineral $A_{v_A} B_{v_B}$ can be expressed as follows:



where, $A_{v_A} B_{v_B}$ is the reactant, A_{aq}^{qA} and B_{aq}^{qB} are the products, and v_A and v_B represent the stoichiometric numbers.

According to Brantley (2008), the mineral dissolution rate (r') can be written as the increased concentration of solute over time as follows:

$$r' = \frac{d[A_{v_A} B_{v_B}]}{dt} = \frac{1}{v_A} \frac{d[A_{aq}]}{dt} = \frac{1}{v_B} \frac{d[B_{aq}]}{dt} \quad (2.22)$$

where, $[i]$ is the concentration of species i , v_i is the stoichiometric coefficient of the reaction, t is time and q_i is the charge of the aqueous species.

According to Dove and Platt (1996), the measurement of the rate of disappearance of mass and the rate of surface retreat can also be used to measure mineral dissolution, as shown in Eq. 2.23:

$$r_n = \pm k_n A_n \left| 1 - \Omega_n^\theta \right|^\eta \quad (2.23)$$

A positive value of r_n indicates mineral dissolution where k_n is the rate constant depending on the temperature, A_n is the specific reactive surface area per kg of water, Ω_n is the saturation index of the minerals, η and θ are experimentally-based parameters which are usually taken as 1. To date, Eq. 2.23 is the most widely-used kinetic model to predict the mineral dissolution rate.

Lasaga (1998) expresses the rate of a mineral reaction as a function of the Gibbs free energy change as follows:

$$rate = kA \exp^{-E/RT} \pi a_i^{n_i} f(\Delta G_r) \quad (2.24)$$

where k is the rate constant, A is the reactive surface area, E is the activation energy, R is the gas constant, T is the absolute temperature, a_i is the activity of chemical species i and n_i signifies the reaction order of a_i and the last term $f(\Delta G_r)$ denotes the Gibbs free energy term.

According to Andre et al. (2007), the continuous injection of CO₂ causes most of the carbonates to dissolve, including calcite, dolomite and siderite located around the injection well of the aquifer, which eventually increases the reservoir porosity up to around 90%. According to these researchers, carbonate dissolution has the major influence and alumina silicates (albite, K-feldspar and illite) have only a minor impact on the porosity variation in the aquifer. Sorai and Sasaki (2010) studied the dissolution kinetics of Ca²⁺ rich feldspar mineral under scCO₂-water saturation using the mineral model proposed by Lasaga (1998). The authors found that the rates of mineral dissolution depend on the degree of saturation. Therefore, the rate of feldspar dissolution decreases with time due to the rise of saturation.

2.3.4 Effect of mineral composition on mechanical properties of reservoir rock

The interaction between CO₂, brine and host rock under in-situ pressure and temperature conditions is a complex process, which includes both mineralogical and microstructural changes of the aquifer which consequently affect the hydro-mechanical behaviour of the reservoir (Rao et al., 2007; Ranganathan et al., 2011; Berg et al., 2013). Therefore, a comprehensive review of the effect of CO₂ injection-induced mineralogical changes on the hydro-mechanical properties of saline aquifers is provided in this section.

Marbler et al. (2013) found that the alkaline earth metals Ca^{2+} and Mg^{2+} in the mineral structure initially dissolve in pore fluid and both Ca^{2+} and Mg^{2+} show similar enrichment patterns due to their similar mobility during hydrothermal alteration. The observed enrichment patterns are explained by Ellis (1959) and Gledhill and Morse (2006). According to past studies (Azaroual et al., 2007; Shukla et al., 2012; Marbler et al., 2013), rock alteration with a brine and scCO₂ system undoubtedly changes the hydro-mechanical behaviour of reservoir rock. Lombard et al. (2010) studied the effect of progressive rock alteration on the modulus of deformation under the influence of CO₂. According to Marbler et al. (2013), the alteration of clay minerals like smectite, illite, muscovite and kaolinite changes the accumulation of Mg^{2+} with Si^{4+} and Al^{3+} in the pore fluid, which causes a significant reduction of the rock strength. Kaszuba et al. (2003) showed the possible impact of decomposition of single minerals, dissolution of microcline, oligoclase and quartz crystals and the precipitation of secondary minerals on the multi-phase fluid equilibrium relationship. It is clear that the dissolution reaction of the mineral structure makes the grain-to-grain contact weaker in syntaxial quartz-cemented sandstone by dissolving the bond of primary and secondary silicate mineral rims around the quartz and feldspar. Hangx et al. (2013) performed conventional creep experiments to investigate the effect of carbonate cement dissolution on the mechanical and ultrasonic properties, as well as on the failure strength of reservoir rocks. The researchers concluded that the total dissolution of calcite cement does not affect the strength of quartz-cemented sandstones due to the strong bond between quartz grains. However, the effect may be significant on rock strength during long-term injection. In addition, Shukla et al. (2012) illustrated the effect of NaCl crystallisation on reservoir rock strength under brine saturation. These researchers found that the differences in failure strength values are mainly due to the crystallisation of the NaCl and the crack initiation threshold stress values are severely affected by the crystallisation process. According to Shukla et al. (2012), the uniaxial compressive strength values of S- and M-type sandstone initially decreased due to the water saturation from 0 to 5% (% by weight of NaCl) and increased with increasing NaCl concentration from 5 to 15 % (% by weight of NaCl). Dahab et al. (1992) studied the effect of rock mineralogy and the ionic concentration of the saline aquifer on the formation damage characteristics of the reservoir rock. The results showed that the failure strength of reservoir rock is highly dependent on the rock mineralogy and on the ionic concentration of the aquifer. Marini (2007) exemplified the effect of the volume change of the bulk mass of the rock during mineralogical changes and concluded that the observed volume change leads to decreased rock

strength by weakening the grain bonds in the pore matrix. The results of Marbler et al. (2013) are consistent with Marini's (2007) explanation. Moreover, Marbler et al. (2013) observed that the rock mass of the reservoir rock increased during the carbonation reactions of feldspar-bearing minerals and the mineral formation process.

After theoretical consideration of the dissolution of Na-bearing feldspar (albite) (Marini, 2007) and K-bearing feldspar (Baker et al., 1995), it was stated that dawsonite mineral forms as a secondary mineral in an acidic environment due to the presence of scCO₂ and brine. However, the formed dawsonite dissolves due to the thermodynamically unstable behaviour at CO₂ pressure below the critical value (Hellevang et al., 2005), leading to the formation of amorphous silica and kaolinite. As a consequence, the volume of the reservoir rock increases during this entire reaction.

On the basis of these findings, it is clear that the mineralogical changes in the rock matrix due to the interaction of brine and scCO₂ alter the pore space as well as the mineral grain boundaries and subsequently change the mechanical properties of the reservoir rock. Hence, it can be concluded that mineralogical alteration appears to play a major role in the mechanical integrity of the reservoir rock during CO₂ sequestration.

2.3.5 Effect of mineral composition on permeability characteristics of reservoir rock

According to past studies, the CO₂ sequestration-induced permeability characteristics of reservoir rock mainly depend on the in-situ conditions of brine concentration, temperature and pressure, and on the pore size distribution of the rock (Hangx et al., 2013; Marbler et al., 2013). Since pore size distribution is a function of permeability, an understanding of the effect of mineralisation during CO₂ injection is unquestionably important for the integrity of the CO₂ sequestration process. Baudracco and Aouboazza (1990) showed that the permeability of an aquifer decreases of about one order of magnitude occurred due to the localization of kaolinite precipitation. In addition, the researchers found that the dissolution of feldspars, laumontite and chamosite and the precipitation of silica also affected permeability and porosity during the CO₂ sequestration process in saline aquifers. Baudracco and colleagues (Baudracco and Tardy, 1988; Baudracco and Aouboazza, 1990; Baudracco and Aoubouazza, 1995) studied the behaviour of clay minerals and the displacement of fine particles which block the finest pores. The researchers concluded that the swelling of clay minerals, the interaction of colloids and the adsorption of the liquid on the pore walls are the reasons for reduced permeability. Hovorka et

al. (2004) also studied the effect of clay precipitation on the permeability of aquifers and observed the reduction in local permeability due to clay swelling. However, massive injection of scCO₂ into the saline aquifer significantly alters the geochemical equilibrium between porous rock and the formation fluids. The rate of dissolution and precipitation of minerals are normally controlled by the dissolution rate of scCO₂ into brine, and the consequential change of the pore volume significantly modifies the pore structure, affecting both the permeability and porosity of the reservoir rock (Andre et al., 2007). The adverse effects of the interaction of scCO₂ contaminated with SO₂, brine and reservoir rock on petrophysical properties were studied by Kummerow and Spangenberg (2011). The authors found that the permeability of reservoir rock decreases due to the precipitation of some framework minerals, and the precipitation of quartz, albite and orthoclase and the dissolution of dolomite were observed after CO₂ and SO₂ exposure.

Moreover, Dou et al. (2011) evaluated the heterogenetic properties of the permeability of the San Andre carbonate reservoir based on the extended Biot theory of poroelasticity (Sun, 2004). The researchers concluded that it is difficult to develop correlations between the permeability and porosity of reservoir rock due to variations in carbonate pore type, rock texture and mineral composition. The precipitation of anhydrite minerals was observed during the field study of the San Andre carbonate reservoir by Zerai et al. (2006). They showed that the permeability decreases due to the cementation process of anhydrite in the reservoir pore space. Moreover, Zerai et al. (2006)'s study illustrated that the majority of the rock mass increment is due to the precipitation of quartz, muscovite and microcline due to the release of silica from dissolution of K-feldspar, kaolinite and albite. As a consequence of this mass increment, the porosity of the rock mass decreases by 0.1-0.2% and increases the storage capability of caprock sealing. In addition, the porosity and permeability of the formation rock decrease due to the dissolution of calcite, which increases the precipitation of silicate minerals like quartz and microcline. In addition, the reduction of permeability due to mineralogical changes depends greatly on the location where the dissolution and precipitation occur within the pore space (Zerai et al., 2006). Generally, single-phase fluid flow in porous media can be defined based on the porosity and permeability characteristics of the formation rock and the fluid viscosity properties (Berg et al., 2013). However, it is difficult to define the multiphase flow condition (scCO₂-brine-rock) as a single flow system based on porosity and permeability. According to a past study, multiphase

flow condition can be described by the permeability, capillary pressure and saturation functions (Egermann et al., 2006).

Based on the above findings, it is clear that a thorough understanding of the mineralogical behaviour of reservoir rock during interaction with scCO₂ and brine is required to evaluate the petrophysical (permeability, porosity, etc.) characteristics of the reservoir rock.

2.3.6 Influence of other aquifer characteristics on hydro-mechanical properties of reservoir rock

The different properties of saline aquifers, including aqueous composition, concentration, conductivity and pH, also decide the hydro-mechanical behaviour of reservoir rock during CO₂ injection (Ranganathan et al., 2011; Ranjith et al., 2013; Shukla et al., 2012). Kumar et al. (2004) showed the importance of studying the effect of the salinity level of saline aquifers and concluded that the salinity level of the aquifer significantly affects the CO₂ storage capacity of the aquifer. In other words, the salinity level of the aquifer decreases the solubility trapping mechanism during CO₂ injection. Ranjith et al. (2013) also studied the effect of the salinity level of the aquifer on both permeability characteristics and the CO₂ storage capacity of the aquifer. Probst (2008) elucidated the effect of high salinity on the petrophysical properties of reservoir rock. Moreover, Zerai et al. (2006) studied the behaviour of the Cambrian Rose Run sandstone saline aquifer in Ohio, Pennsylvania, New York and Kentucky in the Appalachian basin of the eastern United States. The authors concluded that the rate of mineral trapping depends on the brine composition of the host fluid, the mineral composition of the host rock, initial CO₂ fugacity, and the temperature during CO₂ storage. These researchers highlighted the effect of brine composition and showed that it has the greatest impact on mineral trapping during CO₂ storage. According to Breen et al. (1985), the Cambrian Rose Run sandstone aquifer consists of different ions, including mainly Na^+ and Cl^- with subordinate Ca^{2+} , Mg^{2+} , Fe^{2+} , Sr^{2+} , Al^{3+} , Si^{4+} , K^+ , H^+ , Br^- , SO_4^{2-} and HCO_3^- and the total dissolved solids concentration is about 278,000mg/kg. Ranganathan et al. (2011) studied the behaviour of the Rotliegend sandstone formation in Holland using the reaction parameters from the research literature (Nghiem et al. 2004) and showed that the influence of aquifer composition on the petrophysical parameters is significant during CO₂ sequestration. Therefore, it is important to have a thorough understanding of the aquifer characteristics before selecting a sequestration site. On the basis

of the above facts, the effect of pH, aquifer composition and distance from the injection well on the hydro-mechanical properties of the reservoir rock are discussed in the following sections.

2.3.6.1 Effect of pH variation on mechanical properties of reservoir rock

Chemically-induced rock strength and its failure characteristics is one of the main factors in CO₂ sequestration in deep saline aquifers, nuclear waste disposal, oil drilling, geothermal exploration, toxic material disposal, seismic aspects, and the long-term integrity of rock engineering structures. Of these, CO₂ sequestration in deep saline aquifers attracts more attention due to the highly corrosive nature of the aquifer host fluid, mainly due to the highly saline brine. To date, many researchers have found that rock strength decreases and the failure and instability of structure increase with the increasingly chemically corrosive nature of the host fluid (Charles, 1959; Swolfs, 1972; Westwood and Macmillian, 1973; Ishido and Mizutani, 1984; Rebinder et al., 1984; Bottai and Cigni, 1985; Engelmann et al., 1987; Lajtai et al., 1987; Feucht and Logan, 1990; Karfakis and Askram, 1993; Dunning et al., 1994; Geilikman and Dusseault, 1996; Seto et al., 1998; Wilson, 1998). Moreover, it has been shown that the pH value of the reservoir fluctuates relative to the distance from the injected well (Andre et al., 2007). Andre et al. (2007) studied the pH variation with respect to the distance from the well and found that near the injection well the pH is equal to 3.6 due to the dissolution of carbonic acid. However, further away from the reservoir it becomes neutral due to minor chemical reactions. Feng et al. (2004) performed computerized tomography (CT) image analysis to evaluate the effect of ionic concentration of the host fluid on the ultimate rock strength of Xiaolangdi sandstone and the corrosive nature of the chemical solutions with different pH values on the rock micro-fracturing process. According to Feng et al. (2004), the peak stress of 160 MPa in the natural state decreased to 112 and 134 MPa for a NaCl solution of 0.01M with pH 2 and pH 12, respectively. The decreases were about 30% and 16% for pH 2 and pH 12 solutions respectively, and the observed variations were mainly due to the chemical corrosion of the pore matrix which accelerates rock failure. Meanwhile, the influence of the acidity (pH < 7) and causticity (pH > 7) of different host fluids including distilled water (pH 7), Yellow River water (pH 8.3), CaCl₂ (pH 9) and NaHCO₃ (pH 9) were also studied. Fig. 2.16 below shows the relationship between the failure strength of sandstone and the pH of the host fluid. Based on the results of Feng et al. (2004), the correlation between Young's modulus and pH was developed. As Fig. 2.17 shows, the Young's modulus initially increases with increasing pH up to 7 and then shows a sudden drop as the pH increases from 7 to 12. From this observation, it

can be concluded that the pH value of the host fluid has a great influence on the mechanical properties of sandstone.

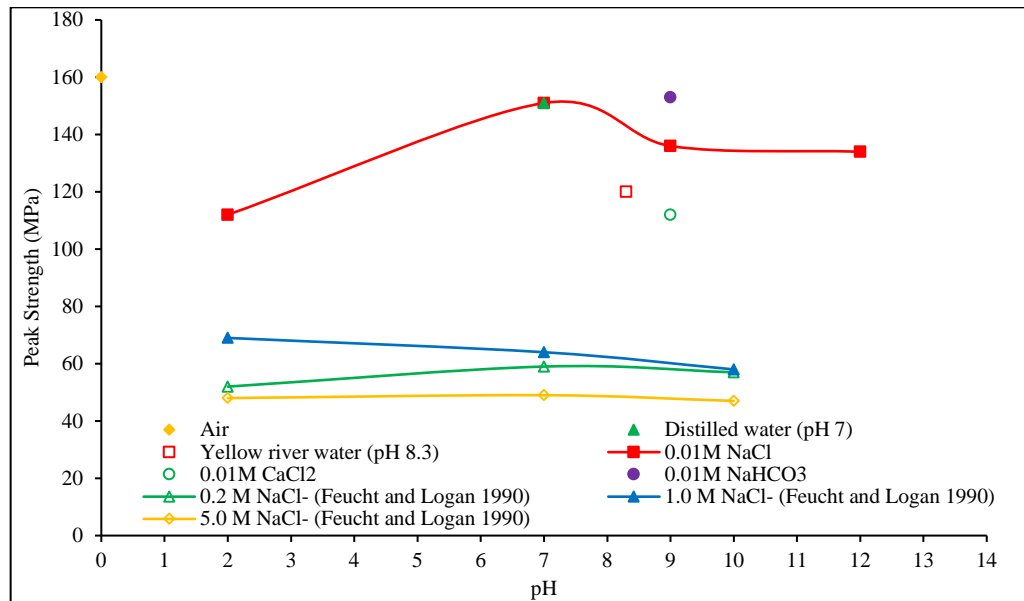


Figure 2.16. Effect of different pH values of host fluid on peak strength of sandstone specimens (Feucht and Logan, 1990; Feng et al., 2004).

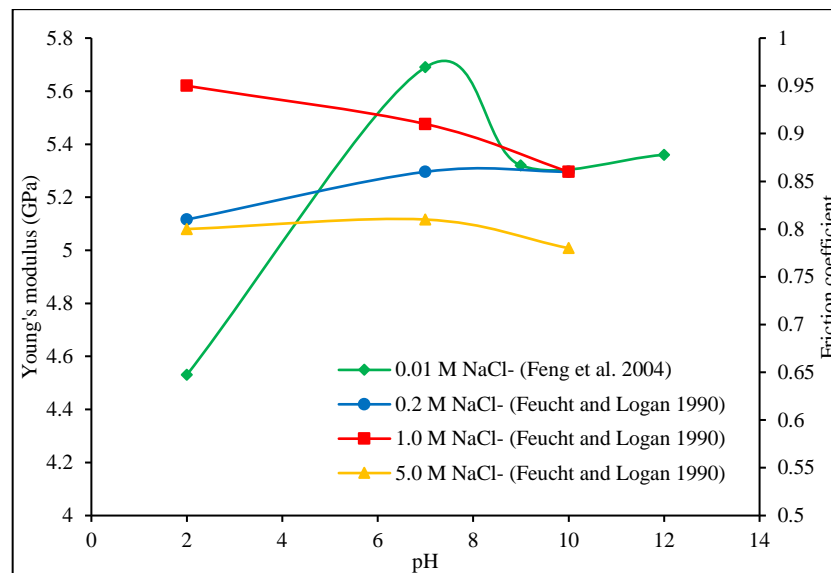


Figure 2.17. Effect of different pH values of host fluid (0.01M NaCl) on Young's modulus of sandstone specimens (Feng et al., 2004) and effect of different pH values of host fluid (NaCl) on coefficient of friction of sandstone specimens (Feucht and Logan, 1990).

Atkinson and Meredith (1981) found that the rate of crack growth in silicate-cemented sandstone increases with increasing concentration of hydroxyl (OH^-) ions in the solution. Their results also demonstrated that the causticity of the solution controls the crack growth at low crack velocities, whereas at higher velocities the composition of the rock mineral structure controls the propagation (Atkinson, 1984). The same phenomenon was suggested by Martin and Durham (1975) who introduced the silica hydration phenomenon. Furthermore, Feucht and Logan (1990) developed a relationship between pH and the shearing behaviour of sandstone to evaluate the effect of chemical solutions on the frictional properties of quartz-rich sandstone. According to Feucht and Logan (1990), the ultimate strength and the frictional resistance to sliding are primarily controlled by the ionic strength of the pore fluid and secondarily by the pH. The results of this study illustrate that the effect of pH on ultimate strength of the rock is not significant compared to the ionic strength of the pore fluid.

Figs. 2.16 and 2.17 show the effect of pH on both the failure strength and the friction coefficient. From these figures, it is clear that there is no significant variation between pH and the failure strength, and the observed maximum difference in the ultimate strengths of pH 2 and 7 solutions was 11% under low ionic strength (0.2M NaCl). The same variation was also observed for the friction coefficient. The changes may be mainly due to the mineralogical changes in the mineral structure of reservoir rock during pore fluid saturation. In CO_2 sequestration, the effect may be more significant due to the dissolution of CO_2 in the aquifer host fluid and resulting carbonic acid accelerates the degradation mechanisms of the reservoir rock (due to the formation of an acidic medium) including the dissolution rate of minerals and their primary and secondary precipitation. In addition, Swolfs (1971) introduced a new hypothesis to explain the effect of chemically-active solutions on the mechanical properties of rock mass. The author hypothesized the effect using surface free energy and showed that the adsorption and absorption phenomena of chemically-active ions or molecules reduce the surface energy of rocks. It is clear that an understanding of the effect of pH on the hydro-mechanical properties of reservoir rock is important when estimating the effective storage capacity of aquifers and the ultimate strength of reservoir rock formations.

2.3.6.2 Effect of ionic composition of pore fluid on hydro-mechanical properties of reservoir rock

Another important factor affecting the hydro-mechanical properties of aquifers is the ionic composition of the host fluid. To date, ionic composition-induced mechanical and permeability damage to sandstone cores have been extensively studied (Feucht and Logan, 1990; Omar, 1990; Feng et al., 2004). For example, Omar (1990) conducted a series of experiments on permeability damage to reservoir rock using three different types of sandstone cores saturated in different types of pore fluids: $NaCl$, $MgCl_2$, $LiCl$, $BaCl_2$ and $CaCl_2$. According to Omar's (1990) results, the maximum drop in permeability was observed in $LiCl$ saturated specimens and the reduction was 86%. However, the permeability drop was reduced to 13.5% when aqueous $BaCl_2$ solution was used. From this observation, it can be concluded that the varying cations in the aqueous solution have a large effect on the petrophysical properties of reservoir formations. In addition, this research concluded that varying the anions in the aqueous sodium salt creates minor changes in permeability reduction. This was observed by using solutions of $NaCl$, $NaOH$, $NaNO_3$ and Na_2SiO_3 . The results showed 10% reduction in permeability in specimens saturated with $NaCl$, 12% with $NaNO_3$, 13% with Na_2SiO_3 and 16% with $NaOH$, respectively. Hence, based on these results, it can be concluded that changing the cations in the aqueous solution has a greater effect on the permeability characteristics of the aquifer than changes in the anions in the host fluid.

Swolfs (1971) gave evidence for the proposed hypothesis by using solutions of $FeCl_3$ and $AlCl_3$ and found that solutions of $FeCl_3$ and $AlCl_3$ reduced the rock strength of Coconino sandstone by 8 and 15% respectively. Moreover, Atkinson and Meredith (1981) illustrated that the rate of crack propagation in semi-quartz-cemented reservoir rock can be increased by raising the concentration of OH^- ions in the aquifer fluid. Feucht and Logan (1990) found that the ultimate strength of reservoir rock is enhanced due to the presence of divalent cations and anions at low and intermediate ionic strengths. According to Feucht and Logan (1990), a reduction of 42% was observed in the failure strength of $NaCl$ -saturated specimens under low ionic strength (0.2M) and the failure strength of specimens saturated with Na_2SO_4 and $CaCl_2$ showed reductions of 20 and 28% from that of the $NaCl$ -saturated strength. For the intermediate ionic strength, the reduction of ultimate strength of $NaCl$ -saturated specimens

was 30% and for the Na_2SO_4 and CaCl_2 -saturated specimens, the reductions were about 23 and 25% respectively, from that of the NaCl -saturated strength. Considering these observations, it is clear that the NaCl -saturated specimens showed higher ultimate strength than the specimens saturated with Na_2SO_4 and CaCl_2 at given ionic strength and pH values. In addition, Feucht and Logan (1990) showed the importance of evaluating the aquifer's ionic composition by correlating the aquifer composition with pH.

Feng et al. (2004) also studied the chemically corrosive behaviour of different host fluids, including NaCl , CaCl_2 and NaHCO_3 which leads to rock strength decrease, failure acceleration and finally to instability. Their results showed a 15% reduction of rock strength in NaCl -saturated specimens compared to natural rock strength and a 30% reduction in CaCl_2 - and 4.4% reduction in NaHCO_3 -saturated specimens. These variations can be explained by using Omar's (1990) results discussed in this section above. It is clear that the chemically-induced rock strength and permeability reduction decrease with the increasing size of the cations. Therefore, the specimens saturated in CaCl_2 showed a maximum reduction in rock strength compared to other specimens.

Generally, deep saline aquifers have different ionic compositions and different levels of salinity concentrations, and most of them are highly saline. Hence, these types of observations provide detailed information about the behaviour of underground aquifers during CO_2 sequestration.

2.3.6.3 Effect of distance from injection well on aquifer characteristics

Fig. 2.18 shows the relationship between gas saturation and pore fluid saturation with respect to the distance from the injection well in the Dogger aquifer in France (Andre et al., 2007). According to Andre et al.'s (2007) analysis, the 100% CO_2 saturation zone occurs near the injection well at a distance ranging from 8-9m from the well. Furthermore, Marbler et al. (2013) refer to this region as a dry zone due to forced brine migration. As it can be seen in Fig. 2.18, a partly saturated zone occurs between 10 and 1000m from the injection well and it is important to note that most of the chemical and mineralogical changes take place in this region. This can be seen in Figs. 2.19-2.23. Figs. 2.19 and 2.20 show the variation in pH and porosity profile due to the distance effect of the injection well during 10 years of injection, respectively.

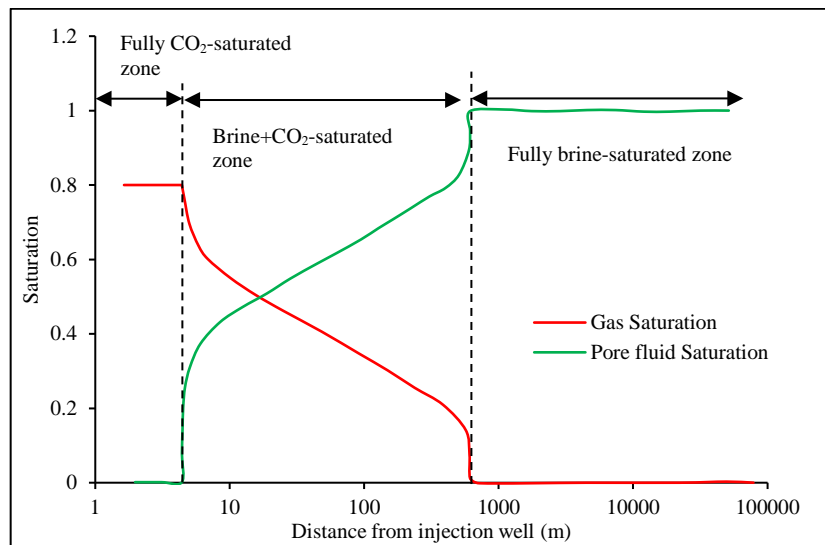


Figure 2.18. Effect of distance from injection well on gas and pore fluid saturation during injection period of 10 years in the Dogger aquifer in France (Andre et al., 2007).

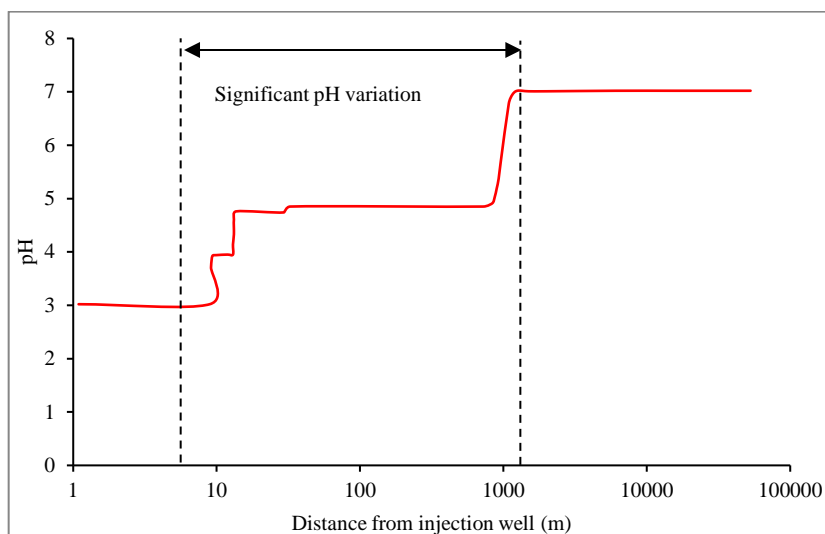


Figure 2.19. Effect of distance from injection well on pH variation during injection period of 10 years in the Dogger aquifer in France (Andre et al., 2007).

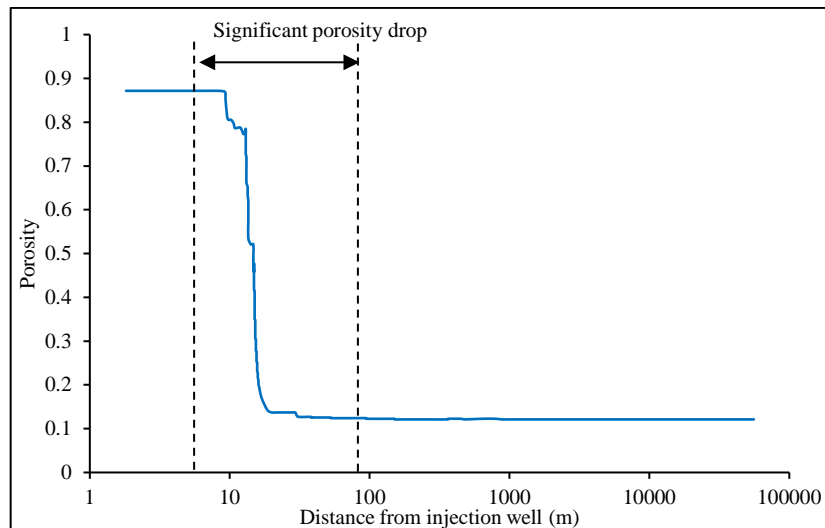


Figure 2.20. Effect of distance from injection well on porosity profile during injection period of 10 years in the Dogger aquifer in France (Andre et al., 2007).

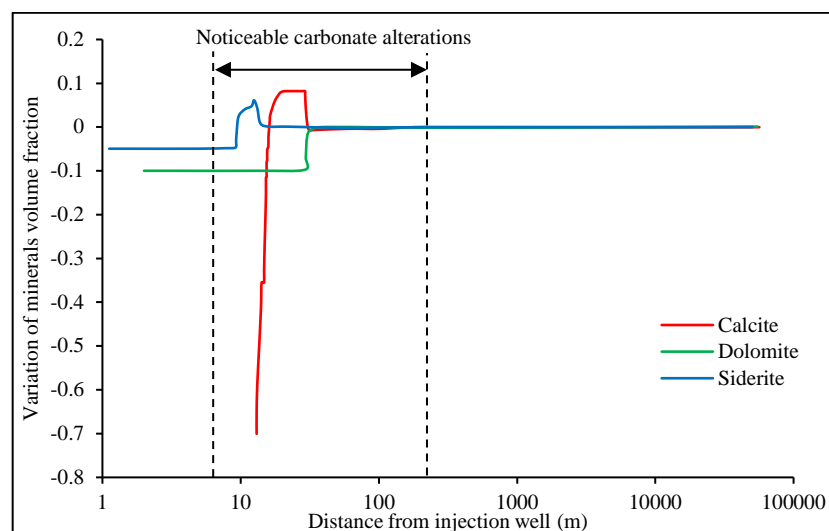


Figure 2.21. Effect of distance from injection well on the volumetric fraction of carbonate minerals during injection period of 10 years in the Dogger aquifer in France (Andre et al., 2007).

It is clear that the host fluid becomes more acidic with a pH value of 3.0 near the injection well during CO₂ injection and significant pH alteration occurs at a distance between 10 and 1000m from the injection well. According to Figs. 2.21 and 2.22, noticeable mineralogical changes can be seen in partly-saturated zones due to the interaction between CO₂, brine and host rock. As a result of carbonation and clay mineral precipitation, the porosity decreases from 0.88 to 0.13 in this partly-saturated region (Andre et al., 2007). However, in the more remote parts of the reservoir, the degree of brine saturation of the rock becomes nearly 1 and the pH becomes

almost 7.0. Therefore, it can be concluded that the effect of distance from injection well on the chemical and mineralogical characteristics is significant and more research is required in this area.

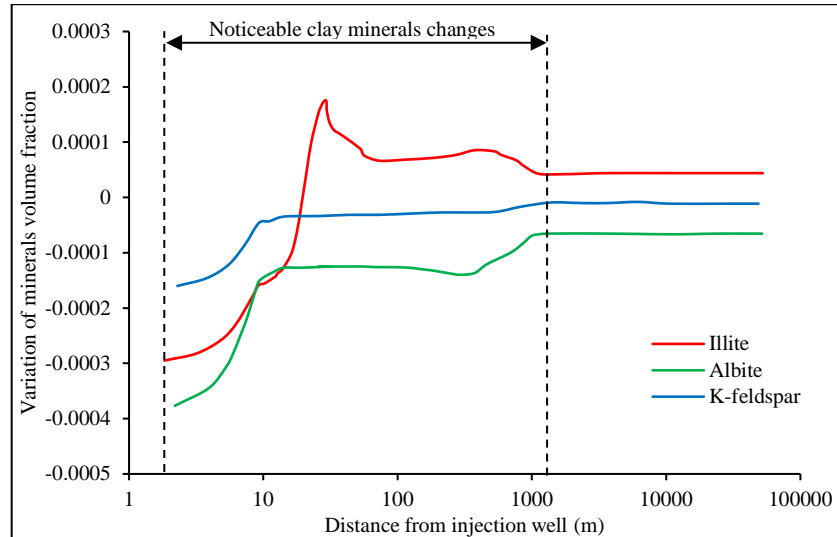


Figure 2.22. Effect of distance from injection well on the volumetric fraction of clay minerals during injection period of 10 years in the Dogger aquifer in France (Andre et al., 2007).

2.3.7 Existing risks and potential applications

Research on reservoir rock strength, permeability and failure characteristics while subjected to a chemical and mineralogical environment are the fundamental factors to be considered in evaluating the long-term integrity of CO₂ sequestration. It is obvious that the back-migration of the injected CO₂ into the atmosphere after some time of injection is the greatest risk associated with this process. Past studies indicate that the chemical and mineralogical interaction between CO₂, brine and reservoir rock can have a significant impact on the long-term stability of reservoirs during and after the injection of CO₂ (Sminchak et al., 2002; Bouchard and Delaytermoz, 2004; Peacock and Mann, 2005; Li et al., 2007). Generally, in CO₂ sequestration, the caprock plays an important role in preventing possible leakages resulting from the potential hydro-mechanical alterations by acting as a barrier. Therefore, it is of utmost importance to have a thorough understanding of aquifer behaviour during the interaction between CO₂, brine and reservoir rock. The possible chemical reactions during the dissolution of CO₂ in the formation fluid can significantly accelerate the chemical corrosion of the reservoir rock and caprock.

Chemical corrosion causes rock strength to decrease, increasing the possibility of the early occurrence of rock failure. In addition, this corrosive environment may increase the crack propagation velocity of the reservoir rock during sequestration (Li et al., 2007). According to James et al.'s (2004) evaluation of the Sleipner project, the cementation (precipitation) of dawsonite and calcite-group carbonates improves the aquifer and caprock integrity during mineral and solubility trapping. The precipitation reactions reduce the local porosity and permeability of the caprock shale and consequently reduce the possibility of leakage of injected CO₂ into the atmosphere during and after the injection of CO₂. In addition to the Sleipner project in offshore Norway, the Weyburn project in Canada, the Otway Basin pilot project in Australia and the In Salah project in Algeria are major on-going projects of CO₂ sequestration around the world, which require quantitative estimation of the possible degradation mechanisms of the reservoir formation during CO₂ sequestration.

Investigation of chemical corrosion-induced crack propagation provides valuable data on the long-term integrity of CO₂ sequestration. The long-term stability of rock caverns, seismic mechanisms and sub-critical crack propagation are the most important factors that may be of concern throughout any sequestration project (Feng et al., 2004). These factors may significantly change due to changes in the chemical and mineralogical compositions of the aquifer during and after CO₂ injection. High permeability leakage paths through fractured rock, the opening of pre-existing faults and fractures, and slip displacement-associated permeability changes are the most devastating catastrophes which can occur during CO₂ sequestration due to these chemical and mineralogical alterations. Therefore, it is important to give more attention to these possible mineralogical and chemical changes in aquifers during the interaction of CO₂/brine/rock for the long-term integrity of CO₂ sequestration.

2.3.8 Conclusion

A comprehensive review was conducted to identify the effect of CO₂ sequestration-induced chemical and mineralogical changes on the hydro-mechanical properties of saline aquifers during and after CO₂ injection. It is clear that the mechanical and petrophysical properties of the aquifer vary significantly with mineralogical interaction between brine, CO₂ and the host rock and other aquifer characteristics, such as pH and composition. However, there are still uncertainties in CO₂-induced rock hydro-mechanical properties due to the lack of studies related to the interaction between brine, CO₂ and reservoir rock. According to past studies, the mechanical and permeability properties of the aquifer primarily depend on the type of

sandstone. For example, carbonate-cemented sandstone shows higher variation in mechanical and permeability properties during the interaction of CO₂ and brine due to relatively rapid carbonate reactions in CO₂-dissolved brine. Quartz-cemented sandstone shows minor changes in its mechanical and permeability characteristics due to the presence of strong grain-to-grain contacts in the silicate bonds. Hence, it can be concluded that the mineral composition of reservoir rock is one of the key factors to be considered when selecting suitable aquifer formations for CO₂ sequestration. Moreover, the aquifer chemical composition and the pH of the formation fluid also play an important role when evaluating the mechanical and petrophysical properties of the reservoir rock during and after CO₂ injection. Finally, it can be concluded that the hydro-mechanical properties of aquifers significantly depend on the pH, the ionic composition of the host fluid, the mineral composition of the reservoir rock and the degree of saturation during CO₂ sequestration.

2.3.8.1 Scope for future studies

This review has analysed the effect of chemical and mineralogical changes in aquifers following the injection of CO₂ in deep saline aquifers and the manner by which these changes influence the hydro-mechanical properties of the reservoir rocks. In order to implement effective and safe sequestration, it is important to understand the effect of salinity and scCO₂ on the hydro-mechanical properties of the reservoir under different temperature and pressure conditions. The effect of salinity remains unclear due to different conclusions drawn by different researchers. There is another important aspect which needs to be addressed: the effect of multi-phase interaction of CO₂-brine-rock on the reservoir and caprock hydro-mechanical properties. The effect of defect densities and surface heterogeneities and impurities, as well as the degree of saturation of reservoir rock on mineralogical behaviour, including the rate of dissolution and precipitation of minerals should also be considered in future studies.

2.3.9 References

1. Aagaard P, Helgeson HC. Thermodynamic and kinetic constraints on reaction rates among minerals and aqueous solutions I. Theoretical considerations. *American Journal of Science* 1982; 282: 237-285.
2. Aagaard P, Oelkers EH, Schott J. Glauconite dissolution kinetics and applications to CO₂ storage in the subsurface. *Geochimica et Cosmochimica Acta* 2004; 68: 138-143.
3. Andre L, Audigane P, Azaroual M, Nenjoy A. Numerical modelling of fluid-rock chemical interactions at the supercritical CO₂-liquid interface during CO₂ injection into a carbonate reservoir, the Dogger aquifer (Paris basin, France). *Energy Conversion Management* 2007; 48: 1782-1797.
4. Atkinson BK. A fracture mechanics study of subcritical tensile cracking of quartz in wet environments. *Pure and Applied Geophysics* 1979; 117: 1011-1024.
5. Atkinson BK, Meredith PG. Stress corrosion cracking of quartz: a note on the influence of chemical environment. *Tectonophysics* 1981; 34: 26-36.
6. Atkinson BK. Subcritical crack growth in geologic materials. *Journal of Geophysics Research* 1984; 31: 4077-4115.
7. Azaroual M, Pruess K, Fouillac C. Feasibility of using supercritical CO₂ as heat transmission fluid in the EGS (Enhanced Geothermal Systems) integrating the carbon storage Constraints. Engine-Enhanced Geothermal Innovative Network for Europe. Workshop 2, Volterra Italy, 2007.
8. Bachu S. Sequestration of CO₂ in geological media: criteria and approach for site selection in response to climate change. *Energy Conversion Management* 2000; 41(9): 953-970.
9. Baker JC, Bai GP, Hamilton PJ, Golding SD, Keene JB. Continental-scale magmatic carbon dioxide seepage recorded by dawsonite in the Bowen-Gunnedah-Sydney Basin system. Eastern Australia. *Journal of Sediment Research* 1995; 65(3): 522-530.
10. Baudracco J, Tardy Y. Dispersion and flocculation of clays in unconsolidated sandstone reservoirs subjected to percolation with NaCl and CaCl₂ solutions at different temperatures. *Applied Clay Science* 1988; 3(4): 347-360.
11. Baudracco J, Aoubouazza M. Study of the variations in permeability and cationic exchange kinetics during solution changes in clay sandstone. *Chemical Geology* 1990; 84(1-4): 235-238.

12. Baudracco J, Aoubouazza M. Permeability variations in Berea and Vosges sandstone submitted to cyclic temperature percolation of saline fluids. *Geothermics* 1995; 24(5): 661-677.
13. Berg S, Oedai S, Ott H. Displacement and mass transfer between saturated and unsaturated CO₂-brine systems in sandstone. *International Journal of Greenhouse Gas Control* 2013; 12: 478-492.
14. Bottai A, Cigni U. Completion techniques in deep geothermal drilling. *Geomechanica* 1985; 14(2-3): 309-314.
15. Bouchard R, Delaytermoz A. Integrated path towards geological storage. *Energy* 2004; 29:1339-1346.
16. Brantley SL. Reaction kinetics of primary rock-forming minerals under ambient conditions. *Surface and Ground Water, Weathering, and Soils* 2014; 5: 73-118.
17. Brantley SL. Kinetics of mineral dissolution. In *Kinetics of water-rock interaction*. Springer New York, 2008; 151-210.
18. Breen KJ, Angelo CG, Masters RW, Sedam AC. Chemical and isotopic characteristics of brines from three oil and gas-producing formations in eastern Ohio, with applications to the geochemical tracing of brine sources: USGS Water-Resources Investigations Report 1985; 84: 4301-4314.
19. Bruant RG, Guswa AJ, Celia MA, Peters CA. Safe storage of CO₂ in deep saline aquifers. *Environmental Science and Technology* 2002; 36(11): 240A-245A.
20. Carroll SA, Knauss KG. Dependence of labradorite dissolution kinetics on CO₂(aq), Al(aq), and temperature. *Chemical Geology* 2005; 217: 213-225.
21. Charles RJ. The strength of silicate glasses and some crystalline oxides. In: *Fracture, Proceedings of International Conference on the Atomic Mechanisms of Fracture*, MIT Press, Cambridge, MA, 1959: 225-249.
22. Chester FM, Chester JS, Kronenberg AK, Hajash A. Subcritical creep compaction of quartz sand at diagenetic conditions: effects of water and grain size. *Journal of Geophysical Research* 2007; 112: 6203-6217.
23. Croize D, Bjorlykke K, Jahren J, Renard F. Experimental mechanical and chemical compaction of carbonate sand. *Journal of Geophysical Research* 2010; 115: 11204-11216.

24. Dahab AE, Omar El, Gassier MM, Kariem HA. Formation damage effects due to salinity, temperature and pressure in sandstone reservoirs as indicated by relative permeability measurements. *Journal of Petroleum Science and Engineering* 1992; 6(4): 403-412.
25. Dewers TA, Hajash A. Rate laws for water-assisted compaction and stress-induced water-rock interaction in sandstones. *Journal of Geophysical Research* 1995; 100: 13093-13112.
26. Dou Q, Sun Y, Sullivan C. Rock-physics-based carbonate pore type characterization and reservoir permeability heterogeneity evaluation, upper San Andres reservoir, Permian basin, west Texas. *Journal of Applied Geophysics* 2011; 74: 8-18.
27. Dove PM, Platt FM. Compatible real-time rates of mineral dissolution by Atomic Force Microscopy (AFM). *Chemical Geology* 1996; 127: 331-338.
28. Dunning J, Douglas B, Millar M, McDonald S. The role of the chemical environment in frictional deformation: stress corrosion cracking and comminution. *Pageoph* 1994; 143(1/2/3): 151-178.
29. Egermann P, Bemer E, Zinszner B. An experimental investigation of the rock properties evolution associated to different levels of CO₂ injection like alteration processes. Paper SCA, 2006; 34, 12-16.
30. Ellis A. The solubility of calcite in carbon dioxide solutions. *American Journal of Science* 1959; 257: 354-365.
31. Engelmann WH, Watson PJ, Tuzinski PA, Pahlman JE. Zeta potential control for simultaneous enhancement of penetration rates and bit life in rock drilling. US Bureau of Mines RI9103, 1987.
32. Farrar CD, Neil JM, Howele JFUS. Geological survey water-resource investigation report. U. S. Geological Survey: Sacramento, CA: 1999; 1-17.
33. Feng XT, Chen S, Zhou H. Real-time computerized tomography (CT) experiments on sandstone damage evaluation during triaxial compression with chemical corrosion. *International Journal of Rock Mechanics and Mining Science* 2004; 41: 181-192.
34. Feucht LJ, Logan JM. Effects of chemically active solutions on shearing behaviour of a sandstone. *Tectonophysics* 1990; 175: 159-76.
35. Freeze RA, Cherry JA. *Groundwater*. Prentice Hall, Englewood Cliffs, N.J. 1979.

36. Gaus I, Audigane P, Andre´ L, Lions J, Jacquemet N, Durst P, Czernichowski-Lauriol I, Azaroual M. *Geochemical and Solute Transport Modelling*, 2008.
37. Geilikman MB, Dusseault MB. Mechano-chemical corrosion of shales in borehole-mud contact. *Rock Mechanics Tools and Techniques* 1996; 1: 959-964.
38. Gledhill DK, Morse JW. Calcite solubility in Na-Ca-Mg-Cl brines. *Chemical Geology* 2006; 233(3-4): 249-256.
39. Hangx SJT, Spiers CJ. Reaction of plagioclase feldspars with CO₂ under hydrothermal conditions. *Chemical Geology* 2009; 265, 88-98.
40. Hangx SJT, Spiers CJ, Peach CJ. Creep of simulated reservoir sands and coupled chemical-mechanical effects of CO₂ injection. *Journal of Geophysical Research* 2010; 115: 9205-9228.
41. Hangx S, Linden AVD, Marcelis F, Baucer A. The effect of CO₂ on the mechanical properties of the captain sandstone geological storage of CO₂ at the Goldeneye field (UK). *International Journal of Greenhouse Gas Control* 2013; 19: 606-619.
42. Hellevang H, Aagaard P, Oelkers EH, Kvamme B. Can dawsonite permanently trap CO₂? *Environmental Science and Technology* 2005; 39: 8281-8287.
43. Hem JD. *Study and interpretation of the chemical characteristics of natural water*. U.S. Geological Survey and Water-Supply 1959; 11: 1473-1483.
44. Hovorka SD, Doughty C, Holtz M. Testing efficiency of storage in the subsurface: Frio brine pilot experiment. Lawrence Berkley Natl lab rep LBNL-55730, 2004.
45. Ishido T, Mizutani H. Experimental and theoretical basis of electrokinetic phenomena in rock-water systems and its applications to geophysics. *Journal of Geophysics Research* 1984; 86: 1763-75.
46. James JW, Nitao JJ, Knauss KG. Reactive transport modeling of CO₂ storage in saline aquifers to elucidate fundamental processes, trapping mechanisms and sequestration partitioning. *Geological Storage of Carbon Dioxide* 2004; 233: 107-128.
47. Johnson JW, Nitao JJ, Morris JP. Reactive transport modelling of cap rock integrity during natural and engineered CO₂ storage. In: Thomas, D.C., Benson, S.M. (Eds.), *Carbon Dioxide Capture for Storage in Deep Geologic Formations*. Elsevier, Oxford, UK, pp. 2004; 787-813.

48. Karfakis MG, Askram M. Effects of chemical solutions on rock fracturing. *International Journal of Rock Mechanics and Mining Science* 1993; 37 (7):1253-1259.
49. Kaszuba JP, Janecky DR, Snow MG. Carbon dioxide reaction processes in a model brine aquifer at 200°C and 200 bars: implications for geologic sequestration of carbon. *Applied Geochemistry* 2003; 18(7): 1065-1080.
50. Knauss KG, Thomas JW. The dissolution kinetics of quartz as a function of pH and time at 70°C. *Geochimica et Cosmochimica Acta*. 1988; 52: 43-53.
51. Kumar A, Noh M, Pope GA, Sephrnoori K, Bryant S, Lake LW. Reservoir simulation of CO₂ storage in deep saline aquifers. In *SPE/DOE Symposium on improved oil recovery*. Society of Petroleum Engineers: Tulsa, Oklahoma, 2004.
52. Kummerow J, Spagenberg E. Experimental evaluation of the interactions of CO₂-SO₂, brine and reservoir rock on petrophysical properties: A case study from the Ketzin test site, Germany. *Geochemical, Geophysics and Geosystems* 2011; 12: 134-144.
53. Lajtai EZ, Schmidtke RH, Bielus LP. The effect of water on the time-dependent deformation and fracture of a granite. *International Journal of Rock Mechanics and Mining Science* 1987; 24(4): 247-55.
54. Lasaga AC. Chemical kinetics of water-rock interactions. *Journal of Geophysics Research* 1984; 89: 4009-4025.
55. Lasaga AC. *Kinetic Theory in the Earth Sciences*. Princeton University Press, New Jersey, 1998: 581-712.
56. Lasaga AC, Luttge, A. Variation of crystal dissolution rate based on a dissolution step wave model. *Science* 2001; 291: 2400-2404.
57. Le Guen Y, Renard F, Hellmann R, Brosse E, Collombet M, Tisserand D, Gratier JP. Enhanced deformation of limestone and sandstone in the presence of high PCO₂ fluids. *Journal of Geophysical Research* 2007; 112: 5421-5437.
58. Li Q, Wu Z, Lei X, Murakami Y, Satoh T. Experimental and numerical study on the fracture of rocks during injection of CO₂-saturated water. *Environmental Geology* 2007; 51(7): 1157-1164.
59. Liteanu E, Niemeijer AR, Spiers CJ, Peach CJ, De Bresser JHP. The effect of CO₂ on creep of wet calcite aggregates. *Journal of Geophysical Research* 2012; 117: 23-37.

60. Lombard JM, Azaroual M, Pironon J, Broseta D, Egermann P, Murnier G, Mouronval G. CO₂ injectivity in geological storages: an overview of program and results of the geocarbon-injectivity project. *Oil and Gas Science and Technology Review* 2010; 65(4): 533-539.
61. Madland MV, Finsnes A, Alkafadgi A, Risnes R, Austad T. The influence of CO₂ gas and carbonate water on the mechanical stability of chalk. *Journal of Petroleum Science and Engineering* 2006; 51:149-168.
62. Marbler H, Erickson KP, Schmidt M, Lempp C, Pollmann H. Geomechanical and geochemical effects on sandstones caused by the reaction with supercritical CO₂: an experimental approach to in situ conditions in deep geological reservoirs. *Environmental Earth Science* 2013; 4: 123-132.
63. Marini L. Geological sequestration of carbon dioxide-thermodynamics, kinetics, and reaction path modelling. *Developments in Geochemistry* 2007; 11: 453-462.
64. Martin RJ, Durham WB. Mechanisms of crack growth in quartz. *Journal of Geophysics Research* 1975; 80: 4837-4844.
65. Mukhopadhyay B, Walther JV. Acid-base chemistry of albite surfaces in aqueous solutions at standard temperature and pressure. *Chemical Geology* 2001; 174: 415-443.
66. Nghiem L, Sammon P, Grabenstetter J, Ohkuma H. Modelling CO₂ storage in aquifers with a fully coupled geochemical EOS compositional simulator. *Society of Petroleum Engineers* 2004; 54: 32-47.
67. Omar A. Effect of brine composition and clay content on the permeability damage of sandstone cores. *Journal of Petroleum Science and Engineering* 1990; 4(3): 245-256.
68. Orr Jr FM. Storage of carbon dioxide in geologic formations. *Journal of Petroleum Technology* 2004; 56: 90-97.
69. Palandri JL, Rosenbauer RJ, Kharaka YK. Ferric iron in sediments as a novel CO₂ mineral trap: CO₂-SO₂ reaction with hematite. *Applied Geochemistry* 2005; 20: 2038-2048.
70. Peacock DCP, Mann A. Evaluation of the controls on fracturing in reservoir rocks. *Journal of Petroleum Geology* 2005; 28(4): 385-396.
71. Plummer LN, Wigley TML, Parkhurst DL. The kinetics of calcite dissolution in CO₂-water systems at 5 to 60°C and 0.0 to 1.0atm CO₂. *American Journal of Science* 1978; 278: 179-216.

72. Pokrovsky OS, Golubev SV, Schott J, Castillo A. Calcite, dolomite and magnesite dissolution kinetics in aqueous solutions at acid to circumneutral pH, 25 to 150 °C and 1 to 55 atm pCO₂. New constraints on CO₂ sequestration in sedimentary basins. *Chemical Geology* 2009; 260: 317-329.
73. Probst P. Numerical Simulations of CO₂ Injection into Saline Aquifers: Estimation of Storage Capacity and Arrival Times using Multiple Realizations of Heterogeneous Permeability Fields. Masters Thesis 2008.
74. Ranganathan P, Van HP, Rudolph E, Susanne J, Zitha PZJ. Numerical modelling of CO₂ mineralisation during storage in deep saline aquifers. *Energy Procedia* 2011; 4: 4538-4545.
75. Ranjith P, Perera M, Khan E. A study of safe CO₂ storage capacity in saline aquifers: A numerical study. *International Journal of Energy Research* 2013; 37: 189-199.
76. Rao QH, Wang Z, Xie HF, Xie Q. Experimental study of properties of sandstone at high temperature. *Journal of Central South University of Technology (English Edition)* 2007; 14 (s1): 478-483.
77. Rebinder PA, Schreiner LA, Zhigach KF. Hardness reducers in drilling: a physico-chemical method of facilitating mechanical destruction of rocks during drilling. Akad Naunk, USSR, Moscow, 1984 (Transl. By CSIRO, Melbourne, Australia).
78. Reddy MM. Kinetics of calcium carbonate formation. *Verh. Internat. Verein. Limnol.* 1975; 19: 429-438.
79. Renard F, Park A, Ortoleva P, Gratier JP. An integrated model for transitional pressure solution in sandstones. *Tectonophysics* 1990; 312: 97-115.
80. Rosso JJ, Rimstidt JD. A high resolution study of forsterite dissolution rates. *Geochimica et Cosmochimica Acta* 2000; 64(5): 797-811.
81. Schutjens PMTM. Experimental compaction of quartz sand at low effective stress and temperature conditions. *Journal of the Geological Society of London* 1991; 148: 527-539.
82. Seto M, Vutukuri VS, Nag DK, Katsuyama K. The effect of chemical additives on strength of rock. In: *Proceedings of Civil Engineering* 1998; 44: 157-166.
83. Shukla R, Ranjith PG, Choi SK, Haque A, Yellishetty M, Hong L. Mechanical Behaviour of Reservoir Rock Under Brine Saturation. *Rock Mechanics and Rock Engineering* 2012; 46(1): 83-89.

84. Sjoberg EL. A fundamental equation for calcite dissolution kinetics. *Geochimica et Cosmochimica Acta*. 1976; 40: 441-447.
85. Sminchak J, Gupta N, Byrer C, Bergman P. Issues related to seismic activity induced by the injection of CO₂ in deep saline aquifers. *Journal of Energy and Environment* 2002; 2(1): 32-46.
86. Sorai M, Sasaki M. Dissolution kinetics of anorthite in a supercritical CO₂-water system. *American Mineralogist* 2010; 95: 853-862.
87. Sun YF. Effects of pore structure on elastic wave propagation in rocks. *Journal of Geophysics Engineering* 2004; 1: 268-276.
88. Swolfs H. Influence of pore fluid chemistry and temperature on fracture of sandstone under confining pressure. Ph.D. Thesis, Texas A&M University, College Station, 1971.
89. Swolfs HS, Chemical effects of pore fluids on rock properties. In: Cook TD, editor. *Underground Waste Management and Environment Implications*, 1972: 224-234.
90. Van Lier JA, De Bruyn PL, Overbeek JTHG. The solubility of quartz. *Journal of Physical and Chemical* 1960; 64: 1675-1682.
91. Vialle S, Vanorio T. Laboratory measurements of elastic properties of carbonate rocks during injection of reactive CO₂-saturated water. *Geophysical Research Letters* 2011; 38: 1302-1314.
92. White AF, Brantley SL. The effect of time on the weathering of silicate minerals: Why do weathering rates differ in the laboratory and field? *Chemical Geology* 2003; 202: 479-506.
93. Wilson G. How to reduce drill string fatigue failure in a corrosive environment. *World Oil* 1998; 219(10): 40-52.
94. Zerai B, Saylor BZ, Matisoff G. Computer simulation of CO₂ trapped through mineral precipitation in the Rose Run sandstone, Ohio. *Applied Geochemistry* 2006; 21: 223-240.

2.4 Theories of rock failure and flow concepts

2.4.1 Overview

An understanding of the mechanisms behind the mechanical and flow behaviours of reservoir rocks is important in a wide range of geophysical problems encountered in deep saline sequestration. Generally, these geophysical problems occur due to the lack of basic understanding of the failure criteria of rocks, including their mechanical strength, the elastic properties of the reservoir rock mass and the relative flow behaviour of injected CO₂ and brine through reservoir rock. To date, numerous studies have been carried out on these matters and many failure criteria and permeability concepts have been introduced. The objective of this section is to investigate the applicability of these concepts to deep saline sequestration.

2.4.2 Rock failure criteria

To date, a number of failure criteria have been proposed for rocks by various researchers (Drucker and Prager, 1952; Wiebols and Cook, 1968; Mogi, 1971; Chang and Haimson, 2005). It is of note that the sound principles of rock mechanics are the basis of these failure criteria. However for practical applications, it is more important to understand how easily and accurately the parameters of a failure criterion can be obtained in the field. A full understanding of the long-term mechanical integrity of deep saline reservoir rock and its caprock is needed before large-scale carbon capture and storage is feasible. In addition, feasibility studies including environmental risk assessment are essential for the effectiveness of projects to be determined. The potential environmental impact of carbon capture and storage technologies is currently being investigated in many locations around the world, including the Sleipner field in the North Sea (Gale et al., 2001), an offshore project in Japan (Yamazaki et al., 2006) and the Otway Basin project Australia (Etheridge et al., 2005). The performance of an injection site mainly depends on the reservoir stress field. Hence, a change in the stress field can affect the injection process severely. If the injection pressure is too great, it can cause failure, causing high permeability leakage paths. In addition, the induced stress can act upon pre-existing faults and fractures and cause opening or slip displacement. Moreover, high compressed CO₂ injection pressure can heave the ground surface due to reduction in effective stress in the aquifer. These hydro-mechanical changes may damage the long-term integrity of the reservoir rock.

The interaction between CO₂, aquifer brine and reservoir rock (Knauss et al., 2005; Marbler et al., 2013) under underground pressure and temperature conditions is a relatively unknown

phenomenon, since it leads to the formation of various precipitation/dissolution reactions inside the reservoir pore matrix. This interaction mainly consists of the carbonation of rock minerals. Since the carbonates that precipitate are different from the initial matrix of the reservoir rock, they may exhibit different mechanical properties to those of the sandstone matrix that is dissolved. This carbonation reaction is known to increase or decrease the mechanical strength of the reservoir rock. It is also clear that the dissolution of carbonate minerals can increase the pore space of the reservoir rock matrix and easily create pathways to leak CO₂ along faults (Peacock and Mann, 2005; Li et al., 2007). This can lead to the contamination of freshwater aquifers used for drinking water. Another important criterion is the hydraulic fracturing during CO₂ injection. Generally, hydraulic fracturing occurs when the injection pressure (pore pressure) exceeds the overburden pressure of the surrounding well (Evans et al., 1997). However, the behaviour of the mechanical properties of reservoir rock under multi-phase flow conditions during CO₂ injection remains unclear. The impact on mechanical properties in deep saline aquifers can only be evaluated by understanding the basic principles and theories of rock failure.

2.4.2.1 The Hoek-Brown failure criterion

Generally, the Hoek-Brown failure criterion describes the brittle failure mechanism of rocks (Benz and Schwab, 2008; Lee et al., 2012). This criterion is well-known for estimating the strength of jointed rock masses. The original failure criterion was developed for underground excavation design. The failure criterion was expressed in terms of major and minor principal effective stresses acting upon the rock mass. The equation below expresses the basic failure criterion.

$$\sigma_1' = \sigma_3' + \sqrt{m\sigma_c\sigma_3' + s\sigma_c^2} \quad (2.26)$$

where, σ_1' is the major principal effective stress at failure, σ_3' is the minor principal effective stress or confining pressure, m and s are material constants and σ_c is the uniaxial compressive strength of the intact rock. The values of m and s can be calculated for intact rock using Eqs. 2.27 and 2.28 below. Here, intact rock is defined as unfractured blocks which occur between structural discontinuities in a typical rock mass.

$$m = m_i \exp\left(\frac{GSI - 100}{28}\right) \quad (2.27)$$

The value of m_i can be determined using Eq. 2.29 below.

where, m_i is the value of m for the intact rock, $x = \sigma_3'$ and $y = (\sigma_1' - \sigma_3')^2$.

$$s = \exp\left(\frac{GSI - 100}{9}\right) \quad (2.28)$$

$$m_i = \frac{1}{\sigma_c} \left[\frac{\sum xy - (\sum x \sum y / n)}{\sum x^2 - ((\sum x)^2 / n)} \right] \quad (2.29)$$

It is clear that the most reservoir rocks fail under brittle conditions (Benz and Schwab, 2008; Shukla et al., 2013). To date, many researchers have shown that the Hoek-Brown failure criterion can be successfully used to simulate the failure mechanism of sandstone reservoirs. Wasantha et al. (2013) compared triaxial test results of sandstone with the Hoek-Brown failure criterion and showed that the experimental results are consistent with the predicted results of the Hoek-Brown failure criterion. However, the behaviour of reservoir rocks under CO₂ sequestration is still unclear due to the lack of studies related to CO₂-induced rock strength. Marbler et al. (2013) studied the geochemical and geomechanical behaviour of reservoir rocks in deep saline aquifers during CO₂ injection under laboratory conditions. Fig. 2.23 shows the comparison of Marbler et al. (2013) experimental results with the predicted results using the Hoek-Brown criterion.

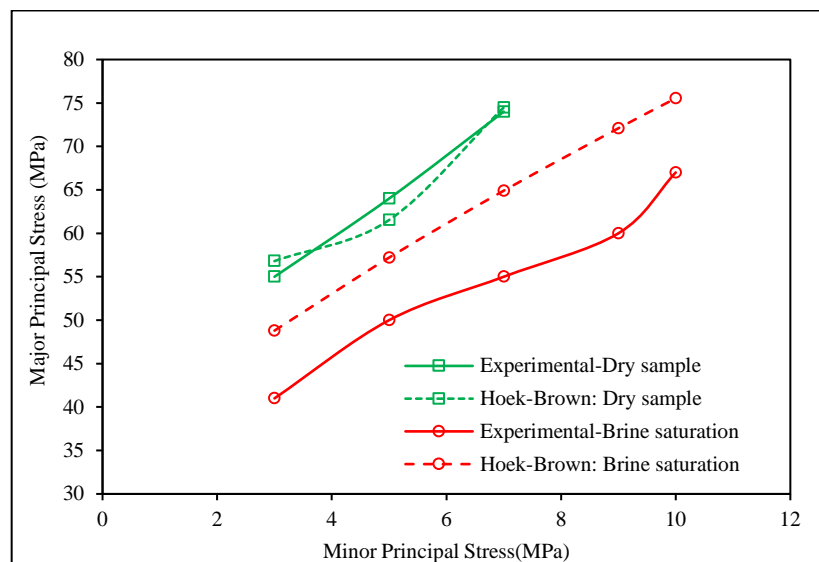


Figure 2.23. Comparison of Marbler et al.'s (2013) experimental results with predicted results using Hoek-Brown criterion.

According to Fig. 2.23, the Hoek-Brown non-linear curve shows a better correlation with the dry results of Bunter sandstone. However, the brine-saturated sandstone results show a significant deviation from the Hoek-Brown non-linear curve. The discrepancy between the dry strength and the brine-saturated strength may be caused due to the weakening of grain bonds resulting from the water softening effect and salt precipitation.

2.4.2.2 Mohr-Coulomb criterion

The conventional Mohr-Coulomb strength criterion is the most popular and widely used strength criterion in civil and mining engineering. In geotechnical engineering, it is used to define the shear strength of soils and rocks in different effective stress environments. However, it has two major limitations (Singh et al., 2011) as follows: 1) the Mohr-Coulomb criterion represents the strength of rock as a linear function of confining pressures and 2) the effect of intermediate principal stress is ignored. Generally, the Mohr-Coulomb criterion can be expressed in terms of σ_1 and σ_3 as in Eq. 2.30 below:

$$(\sigma_1 - \sigma_3) = \frac{2C_i \cos \theta_i}{1 - \sin \theta_i} + \frac{2 \sin \theta_i}{1 - \sin \theta_i} \sigma_3 \quad (2.30)$$

where C_i and θ_i are the Mohr-Coulomb shear strength parameters of the intact rock, $(\sigma_1 - \sigma_3)$ is the deviatoric stress at failure and σ_1 and σ_3 are the major and minor principal stresses at failure.

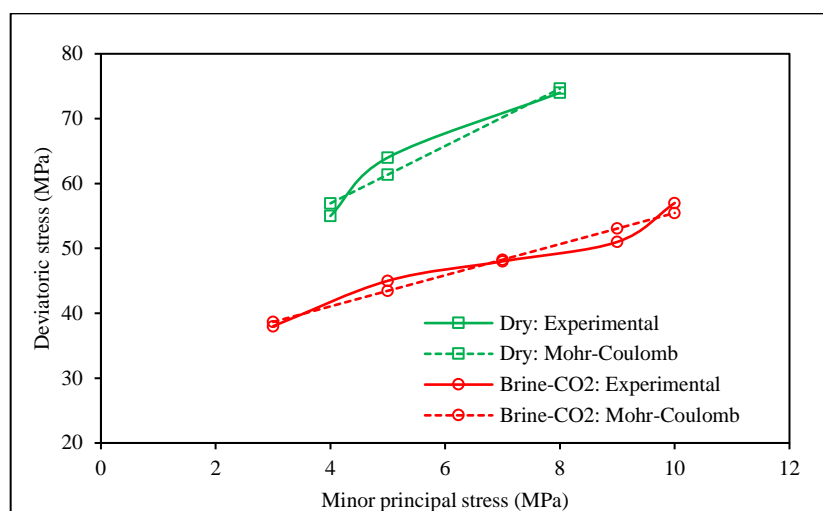


Figure 2.24. Comparison of Marbler et al.'s (2013) experimental results with predicted results using Mohr-Coulomb criterion.

Fig. 2.24 shows the experimental results of Marbler et al. (2013) with respect to the results predicted by the Mohr-Coulomb failure criterion, where two different variations, dry and brine+CO₂-induced strength of sandstone samples are plotted with the Mohr-Coulomb criterion to compare the applicability of the criterion on sequestration-induced rock failure. According to the results, the variation of the stress-strain behaviour of CO₂ interaction-induced rock is non-linear and inelastic, and depends on the magnitude of the confining pressure. Therefore, the linear behaviour of the Mohr-Coulomb criterion is not applicable to reservoir rock strength and requires appropriate corrections in order to capture the mechanical behaviour of deep saline reservoir rocks.

2.4.2.3 Modified Mohr-Coulomb criterion

To overcome the limitations of the conventional Mohr-Coulomb strength criterion Singh et al. (2011) proposed a modified Mohr-Coulomb criterion to explain the non-linear behaviour of intact rock under different confining pressures. Generally, the actual behaviour of reservoir rock is non-linear. Considering this basic non-linear behaviour, the authors introduced a non-linear term $A'\sigma_3'$ to the Mohr-Coulomb system in addition to the existing basic shear terms. The basic shear strength parameters, C_i and θ_i were modified considering the low confining stress environment ($\sigma_3 \rightarrow 0$) and the criterion was then expressed by replacing the mobilised shear parameters, C_i and θ_i with initial values, C_{i0} and θ_{i0} . According to Singh et al. (2011), the modified relationship can be used to determine the triaxial strength of a rock under high confining pressure. The modified Mohr-Coulomb criterion can be written as Eq. 2.31 below, where A' is an empirical constant for a given rock type.

$$(\sigma_1 - \sigma_3) = \frac{2C_{i0} \cos \theta_{i0}}{1 - \sin \theta_{i0}} + \frac{2 \sin \theta_{i0}}{1 - \sin \theta_{i0}} \sigma_3 - A' \sigma_3^2 \quad (2.31)$$

Using the critical state concept Gerogiannopoulos and Brown (1978) and Singh et al. (2011) defined the value of A' . If the critical confining pressure for the rock type is σ_{crit} , the modified Mohr-Coulomb criterion can be written as follows:

$$(\sigma_1 - \sigma_3) = \sigma_{ci} + \frac{2 \sin \theta_{i0}}{1 - \sin \theta_{i0}} \sigma_3 - \frac{\sin \theta_{i0}}{\sigma_{crit} (1 - \sin \theta_{i0})} \sigma_3^2 \quad (2.32)$$

where, σ_{ci} is the uniaxial compressive strength of the rock.

This non-linear expression is only applicable up to the critical state. The modified Mohr-Coulomb criterion uses two parameters σ_{crit} and θ_{i0} in addition to the uniaxial compressive strength. It is clear that the actual critical confining pressure for a given rock depends on the rock type and lithology (Colmenares and Zoback, 2002). However, obtaining an exact value of the critical confining pressure for a given rock type is still a topic for future research.

2.4.2.4 The Drucker-Prager criterion

The Drucker-Prager criterion was initially established for soil mechanics and is an extended version of the Mohr-Coulomb failure criterion (Zhang, 2002). It is based on principal stresses as follows:

$$\tau_{oct} = k + m\sigma_{oct} \quad (2.33)$$

where, τ_{oct} is the octahedral shear stress and σ_{oct} is the octahedral normal stress. τ_{oct} and σ_{oct} can be defined using Eqs. 2.34 and 2.35, respectively:

$$\tau_{oct} = \frac{1}{3} \sqrt{(\sigma_1 - \sigma_2)^2 + (\sigma_2 - \sigma_3)^2 + (\sigma_3 - \sigma_1)^2} \quad (2.34)$$

$$\sigma_{oct} = \frac{(\sigma_1 + \sigma_2 + \sigma_3)}{3} \quad (2.35)$$

where, k and m are material constants that can be estimated from the intercept and slope of the failure envelope of the τ_{oct} versus σ_{oct} plot.

2.4.2.5 Modified Lade failure criterion

Lade (1977) introduced the Lade criterion to characterise three-dimensional failure in frictional materials. This criterion is given by:

$$\left[\left(\frac{I_1^3}{J_3} \right) - 27 \right] \left(\frac{I_1}{P_a} \right)^m = \eta_1 \quad (2.36)$$

where, P_a is the atmospheric pressure, m' and η_1 are material constants and I_1 and J_3 are first and third invariants of the stress tensor, respectively.

Ewy (1999) proposed a new failure criterion based on this criterion. The modified Lade failure criterion was obtained by m' equal to zero and is used to predict the shear strength variation of rocks due to the increase of the first stress invariant. In addition, two new material constants were introduced to the initial Lade criterion as below:

$$\left[\frac{(I_1')^2}{J_3'} \right] - 27 = \eta \quad (2.37)$$

where, $I_1' = (\sigma_1 + S) + (\sigma_2 + S) + (\sigma_3 + S)$ and $J_3' = (\sigma_1 + S)(\sigma_2 + S)(\sigma_3 + S)$

The two introduced parameters, cohesion, S and internal friction, η were then correlated with the Mohr-Coulomb shear strength parameters, cohesion, S_0 and internal friction, θ to obtain the following expressions:

$$S = S_0 / \tan \theta \quad (2.38)$$

$$\eta = 4(\tan \theta)^2 (9 - 7 \sin \theta)(1 - \sin \theta) \quad (2.39)$$

According to Ewy (1999) and Colmenares and Zoback (2002), the strength of the rock initially increases with increasing intermediate stress and reaches a certain value, followed by a slight reduction in strength at higher values of intermediate stress. Ewy (1999) performed a wellbore analysis using the modified Lade criterion to study the effect of a three-dimensional stress environment on mud weight analysis and evaluate the effective orientation of the wellbore. Moreover, the author explained the limitation of the two most commonly-used rock failure criteria, the Mohr-Coulomb criterion and the Druker-Prager criterion, in wellbore analysis, emphasising the advantages of using the modified Lade failure criterion. According to Ewy (1999), the modified Lade criterion adequately explains the effect of intermediate stress on rock strength and can be used to analyse the critical mud weight in the wellbore. Furthermore, this criterion needs only two rock strength parameters, cohesion and friction angle. Colmenares and Zoback (2002) show that the modified Lade failure criterion fits the experimental data of five different rock types from the research literature.

2.4.2.6 Modified Wiebols and Cook failure criterion

In order to determine the combine effect of intermediate principal stress, Zhou (1994) modified the Wiebols and Cook failure criterion (Wiebols and Cook, 1968) correlating it with the Drucker-Prager criterion. According to Zhou (1994), the proposed criterion can be expressed as:

$$J_2^{1/2} = A + BI_1 + CI_1^2 \quad (2.40)$$

where, $I_1 = \frac{1}{3}(\sigma_1 + \sigma_2 + \sigma_3)$ and $J_2^{1/2} = \left(\frac{3}{2}\right)^{1/2} \tau_{oct}$.

Colmenares and Zoback (2002) evaluated the applicability of the modified Wiebols and Cook failure criterion to demonstrate the effect of intermediate stress on rock strength using five different rock types. According to these researchers, the predicted strength values for poly-axial states of stress are greater than those predicted by the Mohr-Coulomb criterion. The observed behaviour of poly-axial strength was then clarified by using yield envelopes projected in the π -plane. In addition, they notes that the poly-axial data fitted this criterion very well, in comparison with the Mohr-Coulomb, Hoek-Brown, and Drucker-Prager failure criteria.

2.4.3 Flow concepts for porous media

The other important consideration when considering the reservoir rock in deep saline aquifers is its flow behaviour under reservoir conditions. This is important, because CO₂ injection-induced rock mineral alteration causes the rock's pore structure to significantly change during CO₂ sequestration. These changes can occur due to mineral dissolution and precipitation in the reservoir pore structure and more details regarding the influence of rock mineral alteration on reservoir flow behaviour can be found in Sections 2.2, 2.3 and Chapter 4. The main aim of this section is to understand the applicability of existing flow concepts on reservoir rock flow behaviour.

2.4.3.1 Scheidegger permeability function for porous media

This method can be used to estimate the gas permeability of a given rock sample under steady state conditions. Eq. 2.41 below shows Scheidegger's permeability function for porous media (Scheidegger, 1958):

$$k = \frac{2Q\mu_g LP_d}{A(P_u^2 - P_d^2)} \quad (2.41)$$

where, k denotes the permeability, μ_g represents the viscosity coefficient of the gas, L and A are the length and cross-sectional area of the core sample, and P_u and P_d are the upstream and downstream pore pressure, respectively.

2.4.3.2 Davies and Davies' modified exponential relationship

Generally, the permeability of reservoir rock changes in response to varying effective stress fields during CO₂ sequestration in deep saline aquifers (Rathnaweera et al., 2015). However, the rate of permeability change with increasing stress is highly variable (Chen et al., 2007). Davis and Davis (1999) modified the permeability porosity relationship considering the isotropic behaviour of reservoir rocks to capture this stress-dependent variation. Eq. 2.42 represents the exponential function of permeability (k) modified by Davis and Davis (1999).

$$k = k_0 \exp \left[22.2 \left(\frac{\phi}{\phi_0} - 1 \right) \right] \quad (2.42)$$

where, k_0 is the zero stress permeability, ϕ is the mobilised porosity and ϕ_0 is the porosity at zero stress. The mobilised porosity function of porous rock induced due to the effective mean stress can be expressed as follows:

$$\phi = (\phi_0 - \phi_r) \exp(5 \times 10^{-8} \sigma'_m) + \phi_r \quad (2.43)$$

where, ϕ_r is the residual porosity and σ'_m is the mean effective stress. The mean effective stress is defined based on effective principal stresses:

$$\sigma'_m = \frac{1}{3} (\sigma'_1 + \sigma'_2 + \sigma'_3) \quad (2.44)$$

where, each individual effective stress component can be calculated using Biot's effective stress concept (Biot, 1941):

$$\sigma'_1 = \sigma_1 - \alpha P \quad (2.45)$$

$$\sigma'_2 = \sigma_2 - \alpha P \quad (2.46)$$

$$\sigma_3' = \sigma_3 - \alpha P \quad (2.47)$$

where, α is the Biot's effective stress parameter and P is the average pore pressure defined as:

$$P = S_l P_l + (1 - S_l) P_g \quad (2.48)$$

where, S_l is the degree of liquid saturation, P_l is the pore liquid pressure and P_g is the pore gas pressure.

Davies and Davies (1999) developed this relationship between porosity and permeability of porous rock by performing a series of comprehensive experiments on sandstone, and according to the data, permeability displayed one order of magnitude reduction with increasing effective stress from 0 to 30 MPa. Rutqvist and Tsang (2002) used this stress-induced permeability model to study the effect of 10 years of CO₂ injection on the hydro-mechanical behaviour of a deep saline sequestration site. The numerical results showed that the permeability changes in the aquifer and the caprock were proportional to the effective stress change.

2.4.3.3 Leverett's modified stress-induced permeability formula

Understanding of the theory underlying the behaviour of mixtures of fluids in porous rocks is important when addressing the problems related to CO₂ sequestration in deep saline aquifers. The objective of Leverett's (1940) research was to develop a basic theory with the assistance of well-established thermodynamic and physical principles to solve problems in petroleum production. In order to develop a theory, Leverett (1940) performed a series of relative saturation experiments to correlate saturation, capillary pressure, interfacial tension and permeability:

$$P_c = P_{c0}(S_l) \frac{\sqrt{\frac{k_0}{\phi_0}}}{\sqrt{\frac{k}{\phi}}} \quad (2.49)$$

where, k_0 is the zero stress permeability, ϕ is the induced porosity and ϕ_0 is the porosity at zero stress.

According to Eq. 2.49 above, porosity, permeability and capillary pressure are all directly dependent on the effective mean stress field. To study the caprock flow behaviour, Rutqvist and

Tsang (2002) applied this modified function to the evaluation of the effect of critical pressure that can induce shear slip of pre-existing faults.

2.4.3.4 Corey's relative permeability function

The estimation of the relative permeability of reservoir rock to each of the fluids flowing through its porous (CO₂ and brine) medium is important to understand the flow behaviour of a reservoir. Corey (1954) performed a series of relative permeability experiments on a large number of cores from several reservoir formations to find the interrelation between wetting and non-wetting relative permeabilities based on the capillary pressure technique. Based on the results of numerous measurements of the capillary pressure technique, a relationship was developed to demonstrate the relative permeability of gas and oil systems. In addition, the consistency of the observed relationship was evaluated using the Kozeny-Carman equation. Corey's proposed relative permeability function can be expressed as follows:

$$k_{rw} = S_{we}^4 \quad (2.50)$$

$$k_{rnw} = (1 - S_{we})^2 (1 - S_{we}^2) \quad (2.51)$$

$$S_{we} = \frac{(S_w - S_{wr})}{(1 - S_{wr})} \quad (2.52)$$

where, k_{rw} is the relative permeability of the wetting phase, S_w is the saturation of the wetting phase expressed as a fraction of the pore volume, S_{wr} is the residual saturation of the wetting phase, and k_{rnw} is the relative permeability of the non-wetting-phase.

Rutqvist and Tsang (2002) modified Eq. 2.52 to study the hydro-mechanical properties of caprock upon exposure to CO₂ and brine. They introduced two new two parameters to the system and modified Eq. 2.52 by replacing the residual saturation functions from the irreducible saturation term. An irreducible wetting-phase saturation (S_{wir}) and non-wetting-phase saturation (S_{nwir}) are the two new parameters introduced by Rutqvist and Tsang (2002). This modified formula was also used by Weir et al. (1995) and Pruess et al. (2002). The modified equation is given in Eq. 2.53 below.

$$S_{we} = \frac{(S_w - S_{wir})}{(1 - S_{wir} - S_{nwir})} \quad (2.53)$$

However, according to Corey's further studies, the derived formulation failed to simulate the relative flow behaviour of sandstone containing considerable amounts of dolomitic materials and the researcher also found that it failed in the case of cores with noticeable stratification. Therefore, Corey's model is only applicable when the cores are from the same formation and have no visible stratification or unusual pore size distribution.

2.4.3.5 Klinkenberg effect for gas permeability measurements

The Klinkenberg effect is one of the best ways to explain the difference between gas and water permeability of porous media. Klinkenberg (1941) discovered that permeability to gas is relatively higher than that to water and explained the reason by introducing a new phenomenon called the "slip flow" effect. The slip flow effect is defined as additional flux due to the collision of gas molecules and solid walls when a pore radius approaches the mean free path of gas molecules. This additional flux enhances the flow rate. This phenomenon is called the "Klinkenberg effect" and its effect can be expressed using Eq. 2.55 below. In addition, the author explained the difference between intrinsic permeability and apparent permeability. According to the explanation, intrinsic permeability is independent of fluid properties but permeability (hydraulic conductivity) is a function of both the medium and the fluid properties. Therefore, intrinsic permeability measured by any gas used as pore fluid should be the same as that measured by any kind of fluids. The relationship between intrinsic permeability and permeability (hydraulic conductivity) is given by:

$$k = \frac{k_{in} \rho g}{\eta} \quad (2.54)$$

where, k is the permeability (hydraulic conductivity), k_{in} is the intrinsic permeability, η is the viscosity of the fluid, ρ is the fluid density and g is the gravitational acceleration.

$$k_a = k_i \left(1 - \frac{4cl}{r} \right) = k_i \left(1 + \frac{ckT}{\pi\sqrt{2}r^3P} \right) = k_i \left(1 + \frac{b}{P} \right) \quad (2.55)$$

$$b = \frac{ckT}{\pi\sqrt{2}r^3} \quad (2.56)$$

$$l = \frac{kT}{4P\pi\sqrt{2}r^3} \quad (2.57)$$

where, k_a is the apparent permeability, k_m is the intrinsic permeability, l is the mean free path of the gas molecules, r is the Boltzmann's constant, T is the temperature, c is a constant, P is the pore pressure and b is the Klinkenberg slip factor.

Thanikawa and Shimamoto (2009) measured the intrinsic permeability of sedimentary rocks from the Western Foothills of Taiwan using nitrogen gas and distilled water as pore fluids under different effective pressure conditions. This study found that gas permeability was larger than water permeability by several times to one order of magnitude, and the gas permeability increased with increasing pore pressure. Moreover, the researchers found that the discrepancy between permeability to gas and permeability to water is caused mainly by the Klinkenberg effect. In addition, they explained the effect of pore pressure on permeability to gas and to water. They found that permeability to gas increased linearly as the inverse of the average pore pressure increased, but water permeability did not show a linear relationship with average pore pressure.

2.4.3.6 Buckingham Reiner equation for Bingham flow effect

The Buckingham Reiner equation can be used to explain the pore pressure dependency of water permeability of relatively impermeable sedimentary rocks. According to Byerlee (1990), the fluid pressure in the fault zone increases due to the Bingham flow, thus reducing the fault strength of the relatively impermeable fault zone. Sasaki (2003) also suggested that the positive pore pressure-dependence of permeability of a medium to water is caused by the Bingham plastic flow effect. The Buckingham Reiner equation describing Bingham flow in a one capillary tube model can be expressed as follows:

$$Q = \frac{\pi \Delta P R}{8L\eta_p} \left[1 - \frac{4}{3} \left(\frac{2L\tau_0}{R\Delta P} \right) + \frac{1}{3} \left(\frac{2L\tau_0}{R\Delta P} \right)^4 \right] \quad (2.58)$$

where, Q is the volumetric flow discharge, ΔP is the pressure difference, R is the radius of the capillary tube, η_p is the slope of the relationship between shear stress and the rate of shear or dynamic viscosity, L is the length of the tube and τ_0 is the critical yield strength.

Note that under Newtonian flow, τ_0 becomes zero and Eq. 2.58 reduces to the Hagen Poiseuille law (Pfritznner, 1976) as follows:

$$Q = \frac{\pi \Delta P R^4}{8L\eta_p} \quad (2.59)$$

In addition, the applicability of Buckingham Reiner equation to porous media was modified by combining Darcy's law with Bingham plastic flow, assuming that a capillary tube is analogous to a pore with radius, $r = R$ which assumes that all pores are the same size (Berg et al., 2013). The modified Buckingham Reiner equation for porous media can be expressed as:

$$k_l = \frac{\eta r^2}{8} \left[1 - \frac{4}{3} \left(\frac{2L\tau_0}{r\Delta P} \right) + \frac{1}{3} \left(\frac{2L\tau_0}{r\Delta P} \right)^4 \right] \quad (2.60)$$

where, k_l is the water permeability and r is the pore radius.

According to Eq. 2.60, the permeability increases as the pore pressure difference increases and the pressure sensitivity gradually decreases with the increase of pressure difference. However, this formulation is not applicable when the pore size distribution is taken into account. Considering the pore size distribution, Eq. 2.60 can be modified as follows:

$$k_l = n \sum f(r_i) \frac{r_i^2}{8} \left[1 - \frac{4}{3} \left(\frac{2L\tau_{i0}}{r_i\Delta P} \right) + \frac{1}{3} \left(\frac{2L\tau_{i0}}{r_i\Delta P} \right)^4 \right] \quad (2.61)$$

where, $f(r_i)$ is the volumetric ratio of a pore of radius r_i and τ_{i0} is related to pore geometry and can change with pore radius.

Moreover, it has been found that the arithmetic mean model can be used for relatively porous rocks when permeability is controlled by the larger pore size and the harmonic mean model can be used for impermeable samples when small pores govern the permeability of rock (Sasaki, 2003).

2.5 References

1. Bachu S. CO₂ storage in geological media: Role, means, status and barriers to deployment. *Progress in Energy Combustion and Science* 2008; 34(2): 254-273.
2. Benz T, Schwab R. A quantitative comparison of six rock failure criteria. *International Journal of Rock Mechanics and Mining Science* 2008; 45: 1176-1186.
3. Berg S, Oedai S, Ott H. Displacement and mass transfer between saturated and unsaturated CO₂-brine systems in sandstone. *International Journal of Greenhouse Gas Control* 2013; 12: 478-492.
4. Biot MA. General Theory of Three Dimensional Consolidation. *Journal of Applied Physics* 1941; 12(2): 155-164.
5. Bruant RG, Guswa AJ, Celia MA, Peters CA. Safe storage of CO₂ in deep saline aquifers. *Environmental Science and Technologies* 2002; 36(11): 240A-245A.
6. Byerlee J. Friction, overpressure and fault normal compression. *Geophysical Research Letters* 1990; 17(12): 2109-2112.
7. Chang B, Haimson B. Non-dilatant deformation and failure mechanism in two Long Valley Caldera rocks under true triaxial compression. *International Journal of Rock Mechanics and Mining Science* 2005; 42: 402-14.
8. Chen Y, Zhou C, Sheng Y. Formulation of strain-dependent hydraulic conductivity for a fractured rock mass. *International Journal of Rock Mechanics and Mining Sciences* 2007; 44: 981-996.
9. Corey AT. The interrelation between gas and oil relative permeabilities. *Producers Monthly* 1954; 19(1): 38-41.
10. Colmenares LB, Zoback MD. A statistical evaluation of intact rock failure criteria constrained by polyaxial test data for five different rocks. *International Journal of Rock Mechanics and Mining Sciences* 2002; 39: 695-729.
11. Davies JP, Davies DK. *Stress-dependent permeability: characterization and modeling*. Houston, TX, USA: Society of Petroleum Engineering (SPE) 1999.
12. Drucker DC, Prager W. Soil mechanics and plastic analysis or limit design. *Quart. Applied Maths* 1952; 10:157-65.

13. Egermann P, Chabau C, Duquerroix JP, Le Gallo Y. An integrated approach to parameterize reservoir models for CO₂ injection in aquifers. Society of Petroleum Engineers 2006; 102: 1-9.
14. Etheridge D, Leuning R, de Vries D, Dodds K, Trudinger C, Allison C, et al., Atmospheric monitoring and verification technologies for CO₂ storage at geosequestration sites in Australia; CO₂CRC, Report No. RPT05-0134; 2005.
15. Evans JP, Forster CB, Goddard JV. Permeability of fault-related rocks and implications for hydraulic structure of fault. Journal of Structural Geology 1997; 19(11): 1393-1404.
16. Ewy RT. Wellbore-stability predictions by use of a modified Lade criterion. SPE Drill and Complete 1999; 14(2): 85-91.
17. Gale J, Christensen NP, Cutler A, Torp TA. Demonstrating the potential for geological storage of CO₂: the Sleipner and GESTCO projects. Environmental Geoscience 2001; 8(3): 160-165.
18. Gerogiannopoulos NG, Brown ET. The critical state concept applied to rock. International Journal of Rock Mechanics and Mining Sciences 1978; 15: 1-10.
19. Hoek E, Brown ET. Practical estimates of rock mass strength. International Journal of Rock Mechanics and Mining Sciences 1997; 34(8): 1165-1186.
20. Johns TC, Gregory JM, Ingram WJ, Johnson CE, Jones A, Lowe JA, Mitchell et al. Anthropogenic climate change for 1860 to 2100 simulated with the HadCM3 model under updated emissions scenarios. Climate Dynamics 2003; 6: 583-612.
21. Lade P. Elasto-plastic stress-strain theory for cohesion less soil with curved yield surfaces. International Journal of Solids Structures 1977; 13: 1019-1935.
22. Lee KY, Pietruszczak S, Choi BH. Failure criterion for rocks based on smooth approximations to Mohr-Coulomb and Hoek-Brown failure criteria. International Journal of Rock Mechanics and Mining Sciences 2012; 56: 146-160.
23. Leverett M. Capillary behavior in porous solids. Transactions of the American Institute 1940; 23: 230-243.
24. Li Q, Wu Z, Lei X, Murakami Y, Satoh T. Experimental and numerical study on the fracture of rocks during injection of CO₂-saturated water. Environmental Geology 2007; 51(7): 1157-1164.

25. Klinkenberg, L., The permeability of porous media to liquids and gases. *Drilling and Production Practice* 1941; 12: 285-291.
26. Koide HG, Tazaki Y, Noguchi M. Subterranean containment and long-term storage of carbon dioxide in unused aquifers and in depleted natural gas reservoirs. *Energy Conversion Management* 1992; 33: 619-626.
27. Koide H, Takahashi M, Tsukamoto H, Shindo Y. Self-trapping mechanisms of carbon dioxide in the aquifer disposal. *Energy Conversion Management* 1995; 36(6): 505-508.
28. Knauss KG, Johnson JW, Steffel CI, Evaluation of the impact of CO₂, co-contaminant gas, aqueous fluid and reservoir rock interactions on the geologic sequestration of CO₂. *Chemical Geology* 2005; 217: 339-350.
29. Marbler H, Erickson KP, Schmidt M, Lempp C, Pollmann H. Geomechanical and geochemical effects on sandstone caused by the reaction with supercritical CO₂: an experimental approach to in situ conditions in deep geological reservoirs. *Environmental Earth Science* 2013; 4: 123-132.
30. Mogi K. Fracture and flow of rocks. *Tectonophysics* 1971; 13: 541-568.
31. Ormerod MB. The disposal of carbon dioxide from fossil fuel fired power stations. *IEA Greenhouse Gas R & D Programme* 1994; 23-29.
32. Peacock DCP, Mann A. Evaluation of the controls on fracturing in reservoir rocks. *Journal of Petroleum Geology* 2005; 28(4): 385-396.
33. Pfitzner J. Poiseuille and his law. *Anaesthesia* 1976; 31(2): 273-275.
34. Pruess K, García J. Multiphase flow dynamics during CO₂ disposal into saline aquifers. *Environmental Geology* 2002; 42(2): 282-295.
35. Ranjith PG, Viete DR, Chen BJ, Perera M. Transformation plasticity and the effect of temperature on the mechanical behaviour of Hawkesbury sandstone at atmospheric pressure. *Engineering Geology* 2012; 151: 120-127.
36. Rao QH, Wang Z, Xie HF, Xie Q. Experimental study of properties of sandstone at high temperature. *Journal of Central South University of Technology (English Edition)* 2007; 14 (s1): 478-483.

37. Rathnaweera TD, Ranjith PG, Perera MSA, Haque A, Lashin A, Al Arifi N, et al. CO₂-induced mechanical behaviour of Hawkesbury sandstone in the Gosford basin: An experimental study. *Material Science and Engineering A* 2015; 641: 123-137.
38. Rathnaweera TD, Ranjith PG, Perera MSA, Yang SQ. Determination of effective stress parameters for effective CO₂ permeability in deep saline aquifers: An experimental study. *Journal of Natural Gas Science and Engineering* 2015; 24: 64-79.
39. Rutqvist J, Tsang CF. A study of caprock hydromechanical changes associated with CO₂-injection into a brine formation. *Environmental Geology* 2002; 42(2): 296-305.
40. Sasaki T. A Study on Hydraulic Conductivity for Neogene Sedimentary Rocks under Low Hydraulic Gradient Condition. *Journal of the Mining and Materials Processing Institute of Japan* 2003; 119(9): 587-592.
41. Scheidegger AE. The physics of flow through porous media. *Soil Science* 1958; 86(6): 355-365.
42. Shukla R, Ranjith PG, Choi SK, Haque A, Yellishetty M, Hong L. Mechanical Behaviour of Reservoir Rock Under Brine Saturation. *Rock Mechanics and Rock Engineering* 2013; 46(1): 83-89.
43. Singh M, Raj A, Singh B. Modified Mohr-Coulomb criterion for non-linear triaxial and polyaxial strength of intact rocks. *International Journal of Rock Mechanics and Mining Science* 2011; 48: 546-555.
44. Tanikawa W, Shimamoto T. Comparison of Klinkenberg-corrected gas permeability and water permeability in sedimentary rocks. *International Journal of Rock Mechanics and Mining Sciences* 2009; 46(2): 229-238.
45. Wasantha PLP, Darlington WJ, Ranjith PG. Characterization of mechanical behaviour of saturated sandstone using a newly developed triaxial apparatus. *Experimental Mechanics* 2013; 53: 871-882.
46. Weir G, White S, Kissling W. Reservoir storage and containment of greenhouse gases. *Energy Conversion and Management* 1995; 36(6): 531-534.
47. Wiebols G, Cook N. An energy criterion for the strength of rock in polyaxial compression. *International Journal of Rock Mechanics and Mining Sciences* 1968; 5: 529-49.

48. Wu Z, Qin Bd, Chen LJ, Luo YJ. Experimental study on mechanical character of sandstone of the upper plank of coal bed under high temperature (in English). *Chinese Journal of Rock Mechanics and Engineering* 2005; 24: 1863-1867.
49. Yamazaki T, Aso K, Chinju J. Japanese potential of CO₂ sequestration in coal seams. *Applied Energy* 2006; 83: 911-920.
50. Zhang J. Dual-porosity approach to well stability in naturally fractured reservoirs. PhD dissertation, University of Oklahoma, 2002.
51. Zhang LY, Mao XB, Lu AH. Experimental study of on the mechanical properties of rocks at high temperature. *Science in China Series E-Technological Science* 2009; 52: 641-646.
52. Zhou S. A program to model the initial shape and extent of borehole breakout. *Computation and Geoscience* 1994; 20(7):1143-60.

2.6 Summary of Chapter 2

This chapter has presented the literature review related to hydro-mechanical behaviour of reservoir rock in deep saline sequestration process.

CO₂ sequestration in deep saline aquifers has recently identified as one of the most effective and economical methods to mitigate anthropogenic CO₂ emission into atmosphere. However, unpredictable behaviour resulted due to CO₂ injection causes its hydro-mechanical properties to be significantly changed during the long-term sequestration process, making CO₂ leakage risk at maximum level. Therefore, it is important to understand the hydro-mechanical behaviour of reservoir upon exposure to CO₂ for the long-term integrity of the sequestration process.

Generally, four major trapping mechanisms, solubility trapping, mineral trapping, residual gas trapping and mobility trapping involve in deep saline storage process. Most of CO₂ is initially stored in saline aquifers through the processes of solubility, residual and mobility trapping while mineral trapping plays a final role since it is a relatively slow process. Though mineral trapping is a slow process, the resulted acidic environment due to solubility reaction of injected CO₂ and brine complicates the behaviour of reservoir rock in terms of strength and permeability.

The factors affecting the integrity of reservoir rock properties (strength and permeability) can mainly divided into two categories as operational and reservoir variables. The operational variables involve injection pressure and number of wells where aquifer variables consist of temperature, brine concentration, depth, pH, aquifer pore fluid chemical composition and reservoir rock mineralogy. The results of previous studies related to the influence of these factors on reservoir hydro-mechanical behaviour have been discussed in sections 2.2 and 2.3. Finally, a critical review on the present approaches for estimating reservoir rock strength and permeability has been presented.

After comprehensively reviewing the past studies on CO₂ injection-induced reservoir rock strength and permeability, some important research gaps have been identified. These include the inadequate consideration of natural aquifer hydro-mechanical behaviour before CO₂ injection, CO₂-induced reservoir rock hydro-mechanical behaviour, the influence of rock mineralogy on CO₂ sequestration and CO₂ storage enhancing techniques in deep saline sequestration process. The present study is driven by these demands and various experimental and numerical approaches to address these issues are described in chapters 3-7 of this thesis.

CHAPTER 3

Experimental Investigation of the Effect of CO₂ Sequestration on Mechanical Properties of Deep Saline Reservoir Rock

Declaration

Three publications are included in Chapter 3 and details of the publications are given below:

Chapter 3.2

Rathnaweera TD, Ranjith PG, Perera MSA. Salinity-dependent strength and stress-strain characteristics of reservoir rocks in deep saline aquifers: An experimental study. *Fuel* 2014; 122: 1-11.

Chapter 3.3

Rathnaweera TD, Ranjith PG, Perera MSA, Lashin A, Al Arifi N. Non-linear stress-strain behaviour of reservoir rock under brine saturation: An experimental study. *Measurement* 2015; 71: 56-72.

Chapter 3.4

Rathnaweera TD, Ranjith PG, Perera MSA, Haque A, Lashin A, Al Arifi N, et al. CO₂-induced mechanical behaviour of Hawkesbury sandstone in the Gosford basin: An experimental study. *Material Science and Engineering A* 2015; 641: 123-137.

Declaration for Thesis Chapter 3.2

Declaration by candidate

Monash University

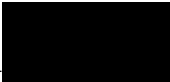
In the case of Chapter 3.2 the nature and extent of my contribution to the work was the following:

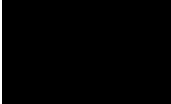
Nature of Contribution	Extent of contribution (%)
Initiation, key ideas, experimental work, analysis of data and writing up	85

The following co-authors contributed to the work. Co-authors who are students at Monash University must also indicate the extent of their contribution in percentage terms:

Name	Nature of contribution	Extent of contribution (%) for student co-authors only
Ranjith PG	Key ideas, reviewing and editing the manuscript	N/A
Perera MSA	Reviewing and editing the manuscript	N/A

The undersigned hereby certify that the above declaration correctly reflects the nature and extent of the candidate's and co-authors' contributions to this work*.

Candidate's Signature		Date 08/08/16
------------------------------	---	-------------------------

Main Supervisor's Signature		Date 08/08/16
------------------------------------	---	-------------------------

*Note: Where the responsible author is not the candidate's main supervisor, the main supervisor should consult with the responsible author to agree on the respective contributions of the authors.

Declaration for Thesis Chapter 3.3

Declaration by candidate

Monash University

In the case of Chapter 3.3 the nature and extent of my contribution to the work was the following:

Nature of Contribution	Extent of contribution (%)
Initiation, key ideas, experimental work, analysis of data and writing up	85

The following co-authors contributed to the work. Co-authors who are students at Monash University must also indicate the extent of their contribution in percentage terms:

Name	Nature of contribution	Extent of contribution (%) for student co-authors only
Ranjith PG	Key ideas, reviewing and editing the manuscript	N/A
Perera MSA	Reviewing and editing the manuscript	N/A
Lashin A	Reviewing and editing the manuscript	N/A
Al Arifi N	Reviewing and editing the manuscript	N/A

The undersigned hereby certify that the above declaration correctly reflects the nature and extent of the candidate's and co-authors' contributions to this work*.

Candidate's
Signature

		Date 08/08/16
--	--	-------------------------

Main
Supervisor's
Signature

		Date 08/08/16
--	--	-------------------------

*Note: Where the responsible author is not the candidate's main supervisor, the main supervisor should consult with the responsible author to agree on the respective contributions of the authors.

Declaration for Thesis Chapter 3.4

Declaration by candidate

Monash University

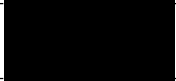
In the case of Chapter 3.4 the nature and extent of my contribution to the work was the following:

Nature of Contribution	Extent of contribution (%)
Initiation, key ideas, experimental work, analysis of data and writing up	85

The following co-authors contributed to the work. Co-authors who are students at Monash University must also indicate the extent of their contribution in percentage terms:

Name	Nature of contribution	Extent of contribution (%) for student co-authors only
Ranjith PG	Key ideas, reviewing and editing the manuscript	N/A
Perera MSA	Reviewing and editing the manuscript	N/A
Haque A	Reviewing and editing the manuscript	N/A
Lashin A	Reviewing and editing the manuscript	N/A
Al Arifi N	Reviewing and editing the manuscript	N/A
Chandrasekharam D	Reviewing and editing the manuscript	N/A
Yang SQ	Reviewing and editing the manuscript	N/A
Xu T	Reviewing and editing the manuscript	N/A
Wang SH	Reviewing and editing the manuscript	N/A
Yasar E	Reviewing and editing the manuscript	N/A

The undersigned hereby certify that the above declaration correctly reflects the nature and extent of the candidate's and co-authors' contributions to this work*.

Candidate's Signature		Date 08/08/16
----------------------------------	---	-------------------------

Main Supervisor's Signature		Date 08/08/16
--	---	-------------------------

*Note: Where the responsible author is not the candidate's main supervisor, the main supervisor should consult with the responsible author to agree on the respective contributions of the authors.

3 Experimental Investigation of the Effect of CO₂ Sequestration on Mechanical Properties of Deep Saline Reservoir Rock

3.1 High-pressure triaxial test apparatus

Overview

A major proportion of the laboratory experiments in this research study is based on the hydro-mechanical behaviour of deep saline reservoir rock in a triaxial stress environment. To simulate real field conditions, it is important to have a triaxial set-up which can operate at high temperatures and confining pressures with the ability to inject CO₂ as a pore fluid. Therefore, in this study, a newly-developed high pressure triaxial set-up available in the Deep Earth Energy Research Laboratory (DEERL) in the Civil Engineering Department at Monash University was used. A detailed description of this set-up can be found in Shukla et al. (2012). This set-up is capable of delivering gas (CO₂ and N₂) to the sample at injection pressures of up to 50MPa, confining pressures of up to 70MPa and temperatures of up to 60°C. In addition, up to 150kN axial load can be applied to the sample. Fig. 3.1 shows the configuration of this new set-up. The set-up consists of eight major units: 1) confining unit, 2) gas injection unit, 3) water/brine injection unit, 4) loading unit, 5) outlet flow measurement unit, 6) heating belt, 7) pressure cell and 8) data acquisition system.

The confining unit is used to provide the required confining pressure to the rock sample by pressurizing hydraulic oil in the pressure cell. The confining unit consists of two major units, an oil reservoir with a compressed air unit and a syringe pump. After placing the sample in the triaxial pressure cell, oil in the reservoir is pushed by compressed air to allow the injection of oil into the pressure cell. When it is completely filled with oil, the syringe pump with 50MPa capacity is used to compress the oil in the pressure cell to obtain the required confining pressure.

The gas injection unit has two main parts, a low-pressure gas injection unit and a high-pressure gas injection unit, and includes a liquid CO₂ gas bottle (5MPa bottle pressure at 20°C), a liquid CO₂ bottle (6.2MPa bottle pressure at 20°C), a N₂ bottle (12MPa bottle pressure at 20°C) and a syringe pump with 50MPa injection capacity. The low-pressure gas unit is used to inject low pressure CO₂ into the reservoir rock. The low injection pressure is controlled by the bottle regulator and it can go up to a maximum of 5MPa injection pressure. The more advanced high-

pressure injection unit with a syringe pump is used to deliver CO₂ pressure greater than 5MPa and can achieve CO₂ injection pressures up to 50MPa.

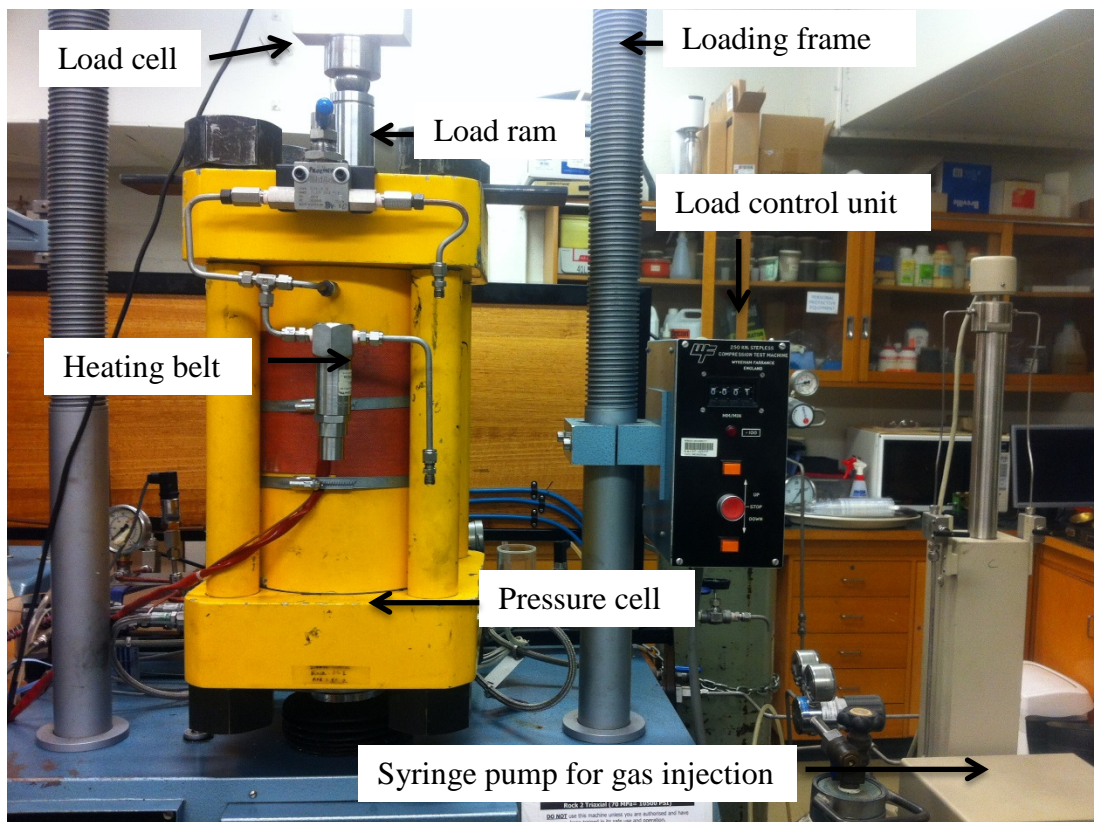


Figure 3.1. Newly-developed high pressure triaxial set-up.

As mentioned earlier, this set-up is capable of simultaneous injection of water/brine and CO₂ and this is controlled by the water/brine injection unit. The water/brine injection unit consists of a water/brine reservoir with 10 litre capacity and a compressed air- driven Haskel MS-36 injection pump.

The loading unit consists of a loading frame and load cell. The loading frame was supplied by Wykeham Farrace and is designed to withstand up to 300kN of axial load, which acts through the loading ram and the sample on a circular bottom platen. The axial load is applied to the rock specimen by movement of the circular bottom platen and the load is then measured by a load cell placed between the loading ram and the loading frame. This load cell is rated to 150kN of axial force and load readings are continuously reported to the computer from the load cell.

The outlet flow measurement unit comprises two main parts, a gas outlet measurement unit and a water/brine outlet measurement unit. The water/brine outlet measurement unit consists of a high-precision electrical balance of a minimum count of 0.01g (an EHB+3000g×0.01g (non-

trade) precision balance) and a Dreschel bottle. The flushed-out water/brine is collected using a Dreschel bottle, which allows the separation of CO₂ and water/brine coming from the sample in two-phase drained experiments. The weight of the flushed-out water/brine with time is recorded and finally, the recorded weights are converted to flow rates. The gas outlet measuring unit records the flow rate and the pressure of gas liberated from the tested rock sample at the outlet. This sub-unit consists of a pressure transducer to measure the outlet gas pressure and a digital flow meter with a capacity of 1000ml/min (digital gas flow meter type XFM-17) to measure gas flow rates. The main advantage of this outlet flow measurement unit is that it allows testing of reservoir rock under both drained and undrained triaxial conditions.

The heating unit of this set-up is a unique feature and was specially designed to ensure that injected CO₂ remains in a super-critical state during movement through the rock sample. This heating unit can be used to achieve operating temperatures up to 60°C and can therefore be used to simulate in situ high-temperature conditions during the investigation of reservoir rock. The heating unit includes a band heater (Watlow) which is wrapped around the pressure cell in order to heat the hydraulic oil in the pressure cell. In addition, one thermocouple is installed inside the pressure cell while the other thermocouple is attached to the heating belt. The PID controller, which is connected to both thermocouples, then reads the data and controls the power going to the belt to maintain the required temperature inside the rock sample. During the heating stage, the heat transfers to the rock sample and eventually to the pore fluid through convection, and this system takes about 24 hours to heat a standard reservoir rock sample (38mm diameter by 76mm height) from room temperature (around 20°C) to around 60°C.

The pressure cell has been designed to withstand pressures of up to 70MPa and temperatures up to 60°C and is made of high quality steel and nickel to avoid any corrosive damage from super-critical CO₂ injection and brine in the case of leakage. The pressure cell consists of three main parts, the cell base, cover and barrel. The cell base has four ports for CO₂ and water/brine injection, confinement oil, CO₂/water/brine outlet and electrical lines. The cell barrel comprises of a 75mm thick, 160mm internal diameter hollow cylinder, which is placed on an O-ring within a seating cut into the cell base. The cell cover provides the upper seal for the pressure cell system while the cell base acts as a bottom seal. The cell base, cover and barrel are connected using four steel rods, which have threads at top and bottom to fix them to the cell base and cell cover and ensure a tight seal.

The data acquisition system is a high-performance and multifunctional OM-DAQ-USB-2401 model with the ability to transfer data at a rate of 480 Mbps. A simple and convenient version of Omega DAQ software is used to record the data. The data acquisition system consists of several transducers to record the pressures in different lines, axial load, axial and lateral strain, outlet gas flow rate and temperature. All the inlet and outlet pressure lines are fitted with pressure transducers, which feed the pressure data to the data acquisition system and then to the computer. The axial load and variable strain rates are applied using a load control unit and axial load is measured using the load cell attached on an automated loading frame. Axial load readings are continuously reported to the computer from the load cell. The axial strain is measured using linear variable differential transducers (LVDTs) fitted to the loading ram of the pressure cell and lateral strain measurements are taken by two strain gauges installed in stainless steel circumferential clip gauges positioned around the sample in the pressure cell.

This set-up is ideal for the investigation of single- and two-phase CO₂ flow and the mechanical behaviour of both soft and hard rocks. Moreover, two-phase triaxial tests can be conducted with different combinations of water/sub-critical CO₂ and water/super-critical CO₂ (scCO₂) or brine/sub-critical CO₂ and brine/scCO₂. In order to present the mechanical investigation using this set-up in a comprehensive manner, four main sections are included in this chapter. The first two sections (3.2 and 3.3) describe the salinity-dependent mechanical behaviour of deep saline reservoir rock in both uniaxial and triaxial environments. The other two sections (3.4 and 3.5) illustrate the mechanical behaviour of reservoir rock upon exposure to CO₂ under deep saline reservoir conditions.

3.2 The effect of salinity on mechanical behaviour of deep saline reservoir rock in a uniaxial stress environment

The long-term interaction of reservoir rock with high NaCl-concentrated brine can cause precipitation of NaCl crystals in the rock pore space, creating altered mechanical behaviours compared to its natural characteristics. To date, studies related to this aspect have considered only low salinity effects for relatively short exposure periods. Therefore, the effect of salinity level on the mechanical behaviour of natural aquifer formations was investigated first. To simulate the in situ salinity levels, the present study selected 10, 20, and 30% of NaCl concentrations (% by weight) to cover the lower and upper limits of existing in situ salinity conditions. The following published journal paper makes up this section of the thesis.



Salinity-dependent strength and stress–strain characteristics of reservoir rocks in deep saline aquifers: An experimental study



T.D. Rathnaweera, P.G. Ranjith*, M.S.A. Perera

Deep Earth Energy Lab, Building 60, Monash University, Melbourne, Victoria 3800, Australia

HIGHLIGHTS

- Salinity effects on mechanical properties of deep saline aquifers are investigated.
- AE counts, SEM and ARAMIS analyses on varying brine saturated sandstone are performed.
- Crystals develop in the rock's pore structure, depending on the brine concentration.
- Increased salinity enhances rock brittleness and reduces crack initiation stress.

ARTICLE INFO

Article history:

Received 11 October 2013

Received in revised form 15 November 2013

Accepted 18 November 2013

Available online 19 December 2013

Keywords:

CO₂ sequestration
Acoustic emission
Sandstone
Strength
Brine

ABSTRACT

This paper presents an experimental study of the effects of salinity on the mechanical properties of reservoir rocks in deep saline aquifers. Nineteen sandstone specimens saturated in NaCl brines of varying salinity concentrations (0%, 10%, 20%, and 30% NaCl by weight) were tested in a uniaxial compression testing machine and the corresponding fracture propagation patterns were recorded using an advanced acoustic emission (AE) system. The stress–strain curves were analysed, with the simultaneous recording of the acoustic signals and the failure mode. In addition, a digital image correlation system, ARAMIS, was used to measure the lateral and axial strains during the loading period. Scanning electron microscopy (SEM) analysis was performed to understand the changes observed in the uniaxial compressive strength (UCS) and stress–strain behaviour of the rock specimens. According to the experimental results, the UCS and stress–strain behaviour of the rock specimens change with the increasing NaCl concentration of the host fluid. The SEM results show only minor changes in mineral structure during immersion. However, some depositions of NaCl crystals in the rock's pore space were observed. Interestingly, the growth of the NaCl crystals depends on the brine concentration, the amount of growth increasing with increasing brine concentration. The observed changes in AE analysis are also explained by the crystallisation of NaCl in the pore space, which transfers more acoustic energy from the cracks to the AE sensors due to the crushing of NaCl crystals during the compression process.

© 2013 Elsevier Ltd. All rights reserved.

3.2.1. Introduction

Geosequestration in deep saline aquifers has recently attracted the attention of the scientific community and the general media, as it is one of the most promising means of reducing anthropogenic CO₂ emissions in the atmosphere. Deep saline aquifers have the largest storage capacity, which has been estimated to be between 320 Gt CO₂ and 200,000 Gt CO₂, with the potential to store the world's anthropogenic CO₂ emissions for hundreds of years [24,7]. Geosequestration in deep saline aquifers involves a number of steps including CO₂ capture, transport and injection deep underground via wells. Of these, the injection of CO₂ plays an important role in the CO₂ storage process. Typically, CO₂ is injected into the

aquifer in a compressed form via a pipeline as a super-critical phase fluid, which exists in the super-critical phase at a temperature of 31.48 °C and a pressure of 7.38 MPa. CO₂ injection involves injecting CO₂ into a reservoir rock via a single well or array of wells. Normally, the most preferable aquifers for CO₂ sequestration lie at depths between 800 and 2000 m. Most are highly saline and situated in sedimentary basins, and can host large amounts of carbon dioxide safely due to the high formation pressures. According to past studies, it is clear that the high overburden pressure (high formation pressure) significantly affects CO₂ storage capacity during sequestration. Generally, high overburden pressure can prevent the decrease in the effective stress in the rock formation due to CO₂ injection. On the other hand, the increase of CO₂ injection pressure can significantly reduce the effective stress at low overburden pressure zones (shallower depths) and will damage the caprock sealing and reactivate existing faults, fractures and joints, even if

* Corresponding author. 

the fluid pressure is below the fracturing pressure, and this can open new pathways for CO₂ back-migration into the atmosphere. As a result of this back-migration of CO₂, the effectiveness of the storage process will decrease, reducing the storage capacity of the sequestration project [37,41,1].

The CO₂ injected into deep saline aquifers is trapped by a number of different mechanisms, including solubility, mineral, residual and mobility trapping. During the long-term injection of CO₂ into the aquifer, the sedimentary rock at the centre of the well of the aquifer becomes almost dry due to forced brine migration. However, sedimentary rocks in this area are fully CO₂ saturated. Further away from the injection well, the degree of gas saturation of the host rock becomes less than one. Generally, these areas are characterised by rocks partly saturated with brine and CO₂, and in more remote parts only brine. Therefore, it is clear that differently saturated rock masses exist at the same time during the CO₂ injection process in saline aquifers, which itself exhibits the complexity of CO₂ sequestration in saline aquifers. On the other hand, reservoir rock (sandstone) is a complex solid medium, which has many initial internal micro-cracks. Therefore, during these trapping processes, the mineralogical structure of reservoir rock is exposed to the brine in various complex ways, leading to significant changes in the hydro-mechanical properties of the host rock.

According to past studies [8–10,19,12,4,20,42,36,43,34,21], the strength of reservoir rocks mainly depends on the temperature, confining pressure, injection pressure, pore size distribution, porosity and mineralogical structure of the rock mass. The concentration of brine in the aquifer is also an important parameter in the geosequestration process, when evaluating the possible changes in the mineralogical structure of reservoir rock. The detrimental effects of NaCl concentration on sandstone properties have been studied by a number of researchers [18,17,35,38] and it is now established that high ionic strength brines can cause irreversible formation damage to reservoir rocks. For instance, [18] showed that the shear friction of sandstone decreases due to the ionic concentration of NaCl. They also revealed that the rock strength reduces, mainly due to the corrosive nature of the chemical reaction between the mineral structure and brine. Feng et al. [17] conducted triaxial tests to evaluate the risks associated with the Xiaolangdi hydraulic project due to chemical corrosion, and investigated the long-term impact of NaCl on rock strength and its fracture characteristics. They found that, under the influence of a solution of NaCl with 0.01 M, the peak stress decreased about 15% in comparison with the natural state. Swolfs [40] proposed a hypothesis to explain the effect of different pore fluids on reservoir rock fracture strength, which is that the reduction in fracture strength due to the adsorption of ions or molecules onto the rock surface reduces the surface free energy of rocks. Moreover, Dunning and Miller [13] studied the effect of chemically-active solutions on the rock strength of porous Berea sandstone and Tennessee sandstone and concluded that Berea rock's strength reduces due to the chemical solution, producing gouge more quickly, which was not observed for Tennessee sandstone. Shukla et al. [38] studied water and NaCl saturation effects on reservoir rock mass strength and found that the mechanical properties of reservoir rock change significantly with the NaCl concentration in the pore fluids, where it initially reduces, and then increases with increasing NaCl concentration. According to Shukla et al. [38], the initial reduction of the strength is due to the water sensitivity or softening of the sandstone specimens in the brine, and according to these researchers, up to about 80% of the overall reduction in the dry strength of reservoir rock may occur due to the saturation effects of the pore fluids. The additional strength gained in reservoir rock with increasing salinity concentration is related to the crystallisation effect of NaCl in the pore structure, which happens with salt evaporation [38], and the double-layer interactions of clay particles [29].

Generally, sandstones contain many pore voids which provide enough space to develop NaCl crystals during the saturation process. The growth of these NaCl crystals significantly changes the pore matrix of the reservoir rock, while adding to the compressive strength. Mohan et al. [28] also studied the effect of NaCl crystallisation on reservoir rock strength using smectitic sandstone, considering the swelling effect of the existing clay minerals in the rock samples. These researchers observed that the growth of NaCl crystals during the swelling process of clay particles causes irreversible formation damage to the reservoir rock pore structure. Probst [32] observed that aquifer hydro-mechanical properties change with increasing concentration of brine, and explained this using the evaporation effect of salt in the aquifer. In addition, this study also illustrated the salting out effect, whereby evaporation can make the water phase denser and cause formation damage. Baudracco and Aoubouazza [2] also studied the variation in aquifer properties in Triassic sandstones submitted to saline circulation. The observed changes in the mechanical properties of the aquifer were explained by the displacement of free fine particles, which block the finest pores. In addition, the swelling of clays, the interaction of colloids and the adsorption of the brine on the walls of the porous environment may be the reasons for the changes observed.

Based on these findings, it is clear that there is a direct relationship between the brine concentration and mechanical properties of the host rock. However, it is important to note that these studies were conducted for low salinity ranging between 0% and 15% (by wt) and have not presented a quantitative explanation of the salinity effect on the mechanical properties of reservoir rock. Hence, this paper aims to present the findings of a laboratory investigation into the identification and characterization of the failure patterns and damage mechanisms of fully saturated reservoir rock under high concentrations of NaCl by integrating the use of acoustic emission (AE) monitoring and ARAMIS technology. Finally, scanning electron microscopy (SEM) analysis was performed to verify the results obtained and correlate them with possible changes in the microstructure of the rock mass.

3.2.2. Experimental methodology

3.2.2.1. Sample preparation

The sandstone samples used for this study were obtained from the Gosford quarries in New South Wales and some physical and mechanical properties are shown in Table 1. The sandstone blocks were cored according to ASTM standards and cored samples were then cut into 38 mm diameter cylinders in the Monash University Civil Engineering Department Laboratory. The height was selected as 76 mm to make the diameter-to-height ratio of 1:2. Both ends of the specimen were then carefully ground to produce smooth faces, and the specimens were oven-dried for 48 h and allowed to cool before being weighed.

For the present study, the water saturation specimens were selected as control tests, and four samples were kept for saturation in distilled water. In addition, three samples were selected to deter-

Table 1
Physical and mechanical properties of the Gosford sandstone used for the test program.

Property	Value
Bulk density (ASTM C97-83)	2.22–2.5 g cm ³
Absorption by weight (ASTM C97-83)	6.57%
Modulus of rupture	8.9 MPa dry, 2.5 MPa wet
Compressive strength (ASTM C170-87)	39.05 MPa dry, 22 MPa wet

mine the dry strength of the reservoir rock (sandstone). Four replicates were selected for each condition and kept in 10%, 20% and 30% NaCl by weight brine solutions in desiccators (see Fig. 1b). The samples were left to saturate for 60 days under vacuum to ensure maximum saturation. Finally, the saturated specimens were removed from the desiccators only minutes before testing to avoid moisture loss and the saturated weights were measured before testing.

3.2.2.2. Mechanical properties of rock

Nineteen uniaxial compression (UCS) tests were performed to quantify the effect of different high salinity levels on reservoir rock strength and micro-fracturing damage with respect to the stress–strain and AE properties. The UCS tests were conducted according to the methods suggested in the ASTM standards [6]. The testing was conducted at Monash University's Deep Earth Energy Laboratory using cylindrical sandstone samples. A SHIMADZU AG 9 300 kN compression machine with maximum compression load capacity of 300 kN (Fig. 1a) was used for the experiments, and the loading rate was maintained at 0.1 mm/min for all the tests. Applied loads were recorded using an automatic data acquisition system and the corresponding strains and fracture propagation patterns were recorded using the ARAMIS technology and the AE system, respectively.

3.2.2.3. Digital image correlation system

For image analysis, the digital image correlation system (DIC) ARAMIS was used in all the experiments. The set-up consists of two high-sensitive cameras to record speckle images in pixel format. In this technique, the deformations of the surface and full-field motion of the geometry are measured in terms of axial and lateral strains. A non-contact optical 3-D metrology system was used for analysing and calculating deformations at each load step. The images obtained were filtered using the filter option provided in the ARAMIS software, selecting run time as one and pixel size as three. Displacement correction was then carried out to eliminate the effect of the bottom pedestal's relative movement during the loading stage. Fig. 10 shows the images of the strain distribution of tested samples at failure obtained using the ARAMIS system.

3.2.2.4. Acoustic emission methodology

The AE system which was used for this experiment is called the PCI (peripheral component interconnection) 2 channel data acquisition system. The AE monitoring system consists of a band-pass filter with a frequency range of 200–750 kHz and a nominal reso-

nant frequency of 500 kHz. The hardware includes two sensors and external amplifiers. In this experiment, two sensors were connected in series to the sample on either side of the specimen and were placed 10 mm below each face for effective data acquisition. The amplifiers were used to amplify the low frequency acoustic waves resulting from the crack fracturing process in the rock and were set to 60 dB to amplify the AE signals.

3.2.2.5. Experimental procedure

The samples were first collected from the fog room and all the covering polyethylene bags, which were used to minimize moisture loss, were removed. The samples were then weighed using a balance with the accuracy of 0.01 g and kept in an oven for 48 h at 100 °C. The samples were then weighed and placed in desiccators to cool. After cooling, the samples were submerged in the relevant brine solutions and kept under vacuum to saturate for 60 days in desiccators at room temperature. AE sensors were attached to each specimen using electrical tape and lubricant gel prior to UCS testing. Generally, lubricant gel is used between the sensor surface and the sample to allow better contact. The ARAMIS cameras were set to capture the axial and lateral strains. The displacement rate was set to 0.1 mm/min and all nineteen samples were tested one by one and finally stress–strain and AE data were recorded. In addition, water absorption testing was performed to obtain the porosity of each sample for later comparison with the effects of different concentrations of brine on the porosity of reservoir rock [6]. Furthermore, SEM analysis was performed to evaluate the possible mineralogical and chemical changes during the brine saturation process.

3.2.3. Results and discussion

For each sample, the axial stress–strain and AE responses were recorded during the entire testing period. Three dry sandstone samples were tested to compare the water saturation effect. The water-saturated samples were used as control specimens for the tests, which were carried out under different brine concentrations. Table 1 shows the physical and mechanical properties of all the sandstone specimens. The porosity of the tested sandstone was calculated by performing water absorption testing [6], and the value varies between 18% and 19%. Dry and wet uniaxial compressive strength were obtained by conducting UCS tests at room temperature. The dry and wet strengths obtained are 39.52 and 25.28 MPa respectively. The results of this experiment will be discussed under five categories. (1) Stress–strain behaviour, (2) acoustic emission response, (3) ARAMIS response, (4) SEM analysis and (5) salinity-dependent stress.

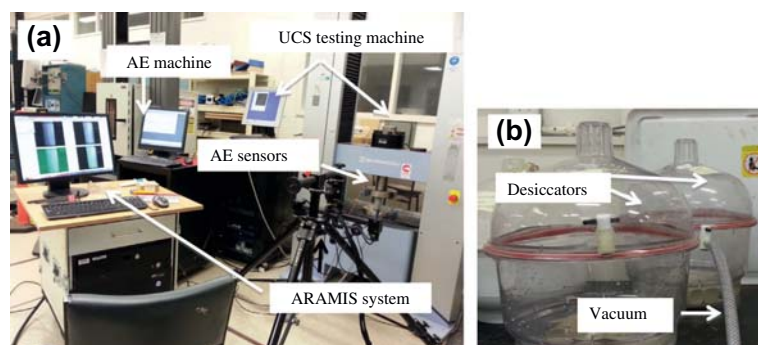


Fig. 1. (a) The UCS testing set-up with AE machine and ARAMIS system and (b) the set-up desiccators used for saturating samples.

3.2.3.1. Stress–strain behaviour

Fig. 2 shows the stress–strain behaviour of reservoir rock specimens under unconfined stress at different concentrations of NaCl (0, 10, 20 and 30% by wt). Young’s moduli (E) and Poisson’s ratios for each condition were then calculated using the elastic region of the obtained stress–strain curve (Fig. 3). Table 2 shows the UCS, Young’s modulus and Poisson’s ratio values obtained for all the tested samples. As can be seen from Table 2, the differences in the values obtained for the various mechanical properties from the initial and replicate tests were very minor. This is probably due to the careful selection of samples from a single sandstone block with minor discontinuous features. However, for the discussion, the average values are considered. The average UCS and Young’s modulus values for brine-saturated samples are compared with both dry and water-saturated values.

According to the results, with respect to the water-saturated samples, the average UCS strength of sandstone decreases from 25.28 to 23.05 MPa with the initial increment of NaCl concentration from 0% to 10%, and a sudden increase of the trend is observed for concentrations greater than 10%. The changes in UCS strength in NaCl-saturated samples were compared with the water-saturated samples to remove the water saturation effect and to check

the pure NaCl saturation effect on UCS strength. As a consequence, the average UCS value increases from 23.05 to 26.35 MPa when the NaCl concentration increases from 10% to 20%. The same trend can be observed up to 30% concentration of NaCl, where the UCS value increases from 26.35 to 27.72 MPa with increasing NaCl concentration from 20% to 30%.

Moreover, it is important to note that the total reduction of average UCS value from dry condition to fully water-saturated condition is about 36.03% (Table 2). Therefore, it is clear that water saturation creates a significant influence on the strength of the reservoir rock mass, and it probably becomes weaker due to the softening effect of the pore fluid [14,16]. This has been clearly shown in past studies, which have shown that water saturation reduces the fracture energy, capillary tension and elastic behaviour and increases the effect of pore pressure and chemical and corrosive deterioration [22,11,14].

The initial reduction of UCS strength with increasing NaCl concentration from 0% to 10% is partially related to the adsorption of ions or NaCl molecules into the rock surface, which reduces the surface energy of the rock mass, while reducing its fracture strength [40]. In addition, according to Feng et al. [17], the highly chemically corrosive behaviour of brine has a significant influence on the rock mass strength. It is therefore clear that, when the pore

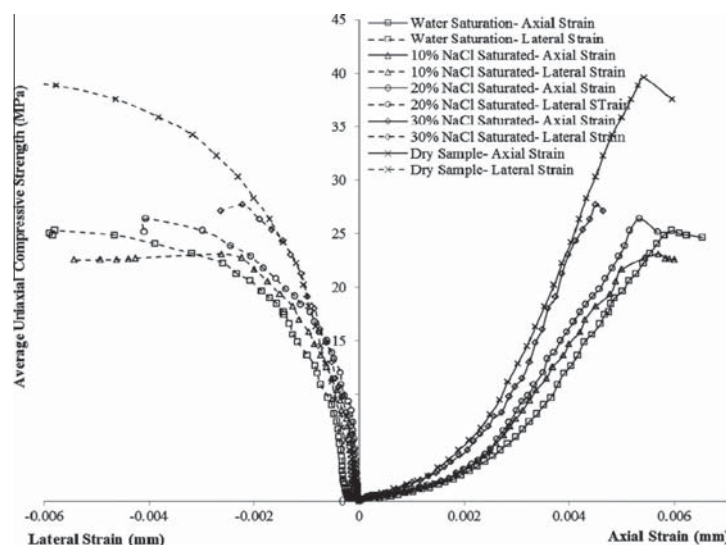


Fig. 2. Stress–strain curves for tested specimens.

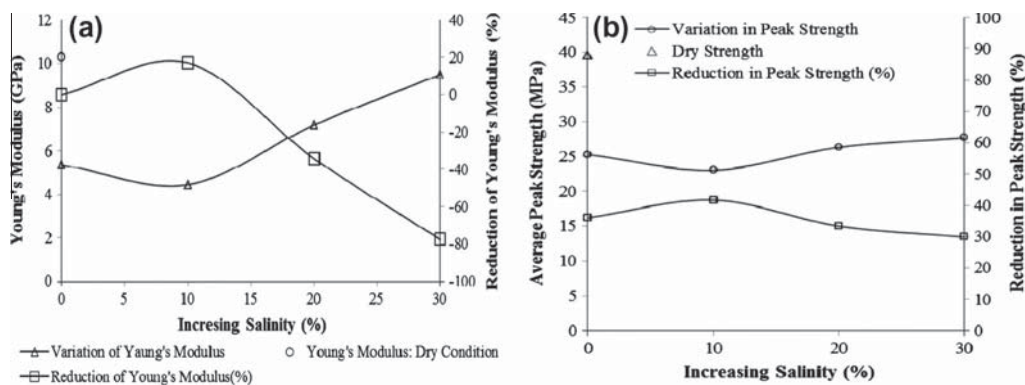


Fig. 3. Effects of NaCl concentration in brine on reservoir rock (a) uniaxial compressive strength and (b) Young’s modulus.

fluid has around 10% NaCl concentration, the strength gain due to NaCl crystals is insignificant when compared to the chemically corrosive effect of the NaCl ions. In contrast, when there is a high NaCl concentration in the pore fluid (>10%), the crystallisation process may have a more significant influence on rock mass strength compared to chemical corrosion. The SEM analysis also confirmed the above hypothesis, while giving no visible growth of NaCl in 10% NaCl saturated specimens. Fig. 3(a) shows the variation of average peak UCS due to the brine saturation and Section 3.4 gives more explanation of the strength variation observed with NaCl saturation.

The other important mechanical property when considering the mechanical behaviour of reservoir rock is the elastic modulus (Young's modulus). According to Fig. 3(b) and Table 2, it is clear that the brittleness of the reservoir rock increases with the increasing NaCl concentration, as its Young's modulus due to water saturation reduces with the addition of NaCl, and increasing the NaCl concentration from 20% and 30% causes the Young's modulus to be increased by 34.21% and 77.57%, respectively. It is important to note that here also, the Young's modulus was compared with that of the water-saturated sample to see the pure NaCl saturation effect on it. The enhancement of the reservoir rock's brittleness with increasing NaCl concentration is not favourable to the safety of the CO₂ sequestration process, and therefore needs to be considered before any fieldwork.

The effect of brine saturation on reservoir rock mass strength and brittleness can be well described by studying the crack formation behaviour of the rock mass. According to Bieniawski [5], the stress-strain curves mirror the microscopic activities of brittle rocks, such as crack development and pore closure. Therefore, the stress-strain results were used to analyse the crack propagation and to monitor the various failure stages (such as crack closure, crack initiation and crack propagation). Generally, two different methods, the volumetric stiffness and strain method and the stress-crack volumetric strain method, can be used to analyse the microscopic activities in brittle rock pore structures. In the volumetric stiffness and strain method, crack closure can be identified using the axial stiffness versus stress curve, and crack initiation and propagation can be identified using the volumetric stiffness and strain versus stress curve. In the present study, the stress-crack volumetric strain method was used to characterise the cracking phenomenon by using the experimental results. The crack volumetric strain data were calculated by using volumetric strain (ε_v) and elastic volumetric strain (ε_{ev}). For the analysis, the axial and lateral strains are defined as positive for compression and negative for expansion. These strains were calculated by using Eqs. (1)–(3) below [23,15,25]:

$$\varepsilon_v = \varepsilon + 2\varepsilon_1 \quad (1)$$

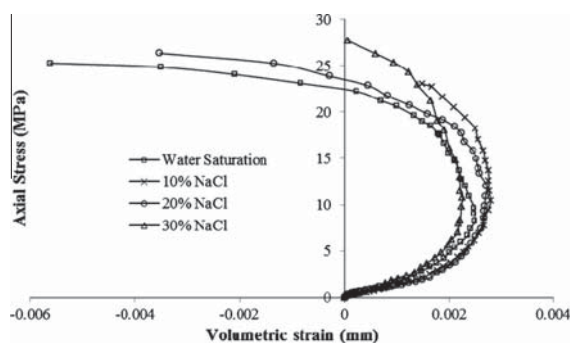


Fig. 4. Obtained stress-volumetric strain curves for tested specimens.

$$\varepsilon_{CV} = \varepsilon_v - \varepsilon_{ev} \quad (2)$$

$$\varepsilon_{ev} = (1 - 2\nu)/E\sigma \quad (3)$$

where ε_{CV} is the crack volumetric strain, ε_1 is the lateral strain, ε is the axial strain, ν is the Poisson's ratio, E is the Young's modulus and σ is the axial stress.

The three stress patterns of the stress-crack volumetric strain curves indicate three types of microscopic activities. The three patterns of deformation are dilatancy, compaction and dilatancy followed by compaction. For uniaxial compression, a negative value shows dilatancy, which is caused by crack initiation, and positive values indicate compaction [25]. According to Brace [3], dilatancy is critical for brittle failure of rocks. Fig. 4 shows the stress-volumetric strain variation of the tested specimens. As Fig. 4 shows, the curves reverse towards the negative direction with increasing axial stress. These observations are mainly due to the high magnitude of the dilatancy, which is caused by the inelastic increase in volume of the rock specimens. Considering this behaviour of the samples, the stress-crack volumetric strain curves were developed to identify the crack initiation stresses under each condition. Fig. 5 shows the stress-crack volumetric strain curves for the tested samples. For all the specimens in Fig. 5, the stress-crack volumetric strain curves are initially positive. However, the curves go through a reversal point and end with a negative value. From the viewpoints of Eberhard et al. and Martin and Chandler [15,27], this reversal point can be identified as the crack initiation point. The reversal stresses observed for this study are 11.99, 10.41, 12.65 and 13.84 MPa for water, and 10%, 20% and 30% NaCl saturations, respectively. It is important to note that the crack initiation values are approximately half of the peak stresses of each test condition. The ratio of reversal stress to failure strength for each test is also listed in Table 3, where the ratio does not appear to significantly change with test condition. According to Table 3, its mean value is 48% with the standard deviation of 2%. As the stresses increase further, the curves deviate from linearity faster. In addition, it can be seen that there is an initial reduction of crack initiation stress up to 10% NaCl concentration, probably due to the softening effect of the pore fluid, and then an increasing trend of crack initiation stress can be observed for the higher NaCl concentrations (up to 30%). Therefore, it is clear that, although the high percentage of salinity in the pore fluid of the reservoir rock increases the brittleness of the rock mass, it also causes its strength to be significantly increased. Therefore, care should be taken in both aspects before fieldwork begins.

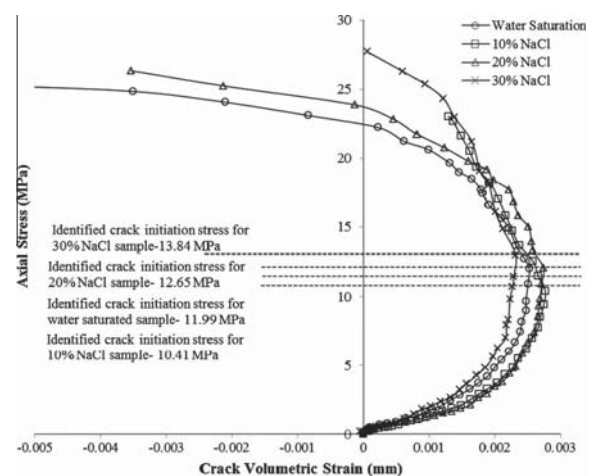


Fig. 5. Obtained stress-crack volumetric strain curves for tested specimens.

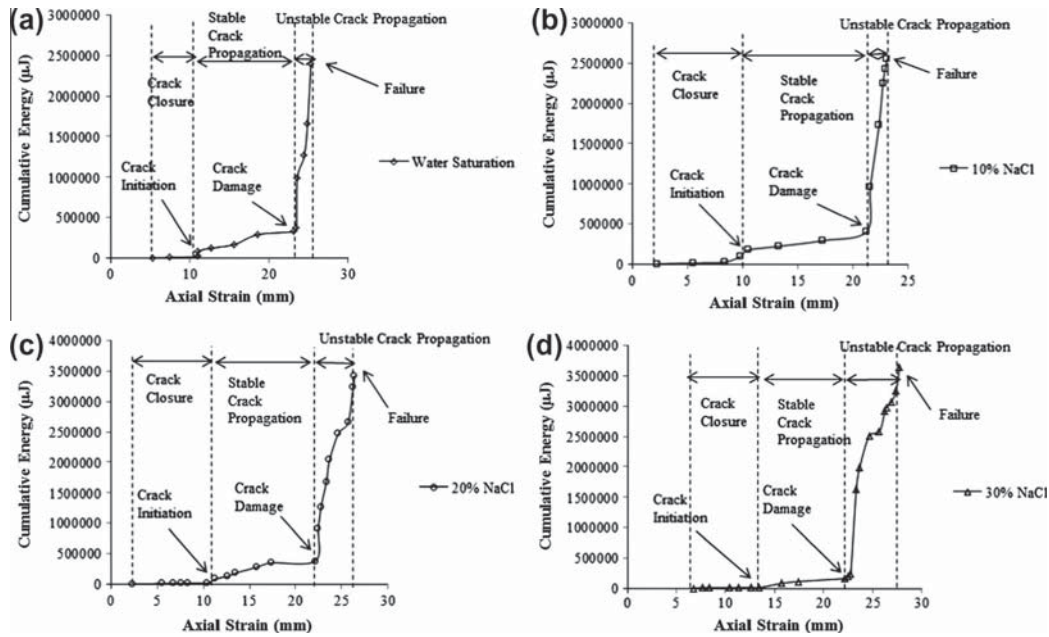


Fig. 6. Variation of cumulative AE energy with axial stress for (a) water saturation specimen, (b) 10% NaCl saturated specimen, (c) 20% NaCl saturated specimen and (d) 30% NaCl saturated specimen.

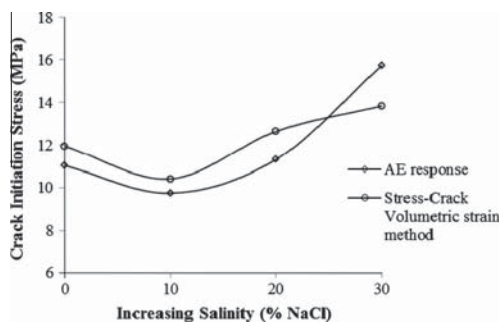


Fig. 7. Variation of crack initiation stress with increasing salinity from AE analysis and stress-crack volumetric strain methods.

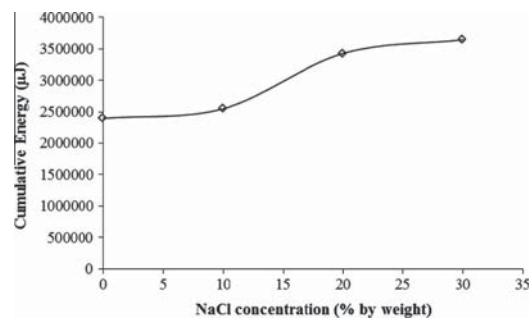


Fig. 9. Variation of cumulative AE energy with increasing salinity.

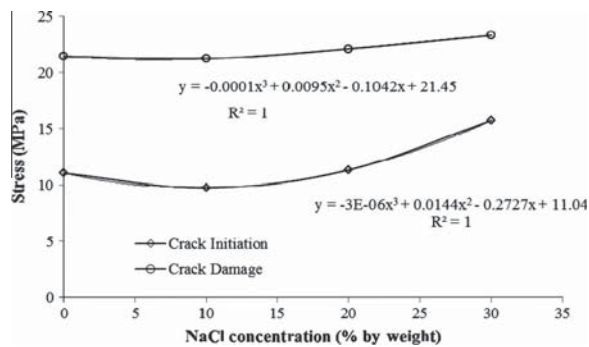


Fig. 8. Developed equations for crack initiation and crack damage in terms of salinity.

3.2.3.2. Acoustic emission (AE) response

AE analysis is a powerful tool that can be used to identify crack initiation, propagation and damage behaviours in reservoir rock [26,33,30,31,38]. If the crack formation behaviour shown by the AE system is described at the beginning of the load application, no significant AE energy release can be seen and the rock mass is at its crack closure state. Then, with the gradually increasing compressive load on the rock mass, stable crack propagation begins, which is indicated by the gradually increasing AE energy release. The further increase of the load causes unstable crack propagation in the rock mass, which is exhibited by the exponential increase in the AE energy release. This stage of the load application clearly creates significant damage to the rock mass and it eventually fails.

The present study used this concept to identify the effect of NaCl saturation on the crack formation behaviour of the reservoir rock in saline aquifers. The variation of the cumulative amount of released AE energy with axial stress for the tested samples is shown in Fig. 6 and the failure-related stress thresholds obtained

are shown in Table 4. As Fig. 6 and Table 4 show, the sample is at crack closure stress condition up to the axial stress of 10.23 MPa for water-saturated specimens (0% NaCl), which decreases up to 9.01 MPa at 10% NaCl concentration and controversially, increases up to 10.67 and 14.67 MPa at 20% and 30% NaCl concentrations, respectively. Interestingly, a similar trend can be seen for the crack initiation stress of specimens. At 0% NaCl concentration, the crack initiation stress is 11.04 MPa and the stress value reduces up to 9.75 MPa at 10% NaCl concentration, and again increases up to 11.32 and 15.73 MPa at 20% and 30% NaCl concentrations, respectively. The relationship between crack initiation and salinity can be expressed by using a polynomial function (Fig. 8) with a 100% confidence band as follows (Eq. (4)):

$$\sigma_i = -3 \times 10^{-6} C^3 + 0.0144 C^2 - 0.2727 C + 11.04 \quad (4)$$

where σ_i is the crack initiation stress and C is the NaCl concentration in percentage by weight.

Fig. 7 shows the trend pattern obtained for crack initiation stress threshold values using both AE analysis and the stress-crack volumetric strain curve method. According to Fig. 7, it is clear that the values from both methods show some slight deviation, while keeping the same trend pattern as NaCl concentration increases. Moreover, the average unstable crack propagation stress for the water-saturated specimens is around 21.45 MPa, which decreases up to 21.23 at 10% NaCl salinity and increases up to 22.12 and 23.32 MPa at 20% and 30% salinities, respectively. The influence

of salinity on crack damage stress was also studied by developing a polynomial function (Fig. 8) with a 100% confidence band, shown in Eq. (5) below.

$$\sigma_d = -0.0001 C^3 + 0.0095 C^2 - 0.1042 C + 21.45 \quad (5)$$

where σ_d is the crack damage stress and C is the NaCl concentration in percentage by weight.

Based on the results obtained, it is clear that rapid energy release can be seen near failure, and with failure it will disappear. Therefore, AE results can also be used to predict the failure strength of the reservoir rock. The observed changes in acoustic emission analysis are also explained by the crystallization of NaCl in the pore space. As Fig. 9 indicates, the salinity percentage of the pore fluid of the rock specimens has a clear influence on the AE energy release. This is partially affected by the electron conductivity of the pore fluid, which clearly increases with the increasing salinity level, as it causes the transferability of acoustic energy from the cracks to the acoustic emission sensors to increase. In addition, the crushing effect of the crystallised NaCl also produces more acoustic pulses during the period of crack closure, which is an important consideration. Fig. 9 shows that cumulative AE energy release during the whole deformation process increases with increasing NaCl concentration in brine solution, indicating the influence of NaCl crystallisation on the AE phenomena of reservoir rock, which is confirmed by both SEM and chemical analyses (see Table 5).

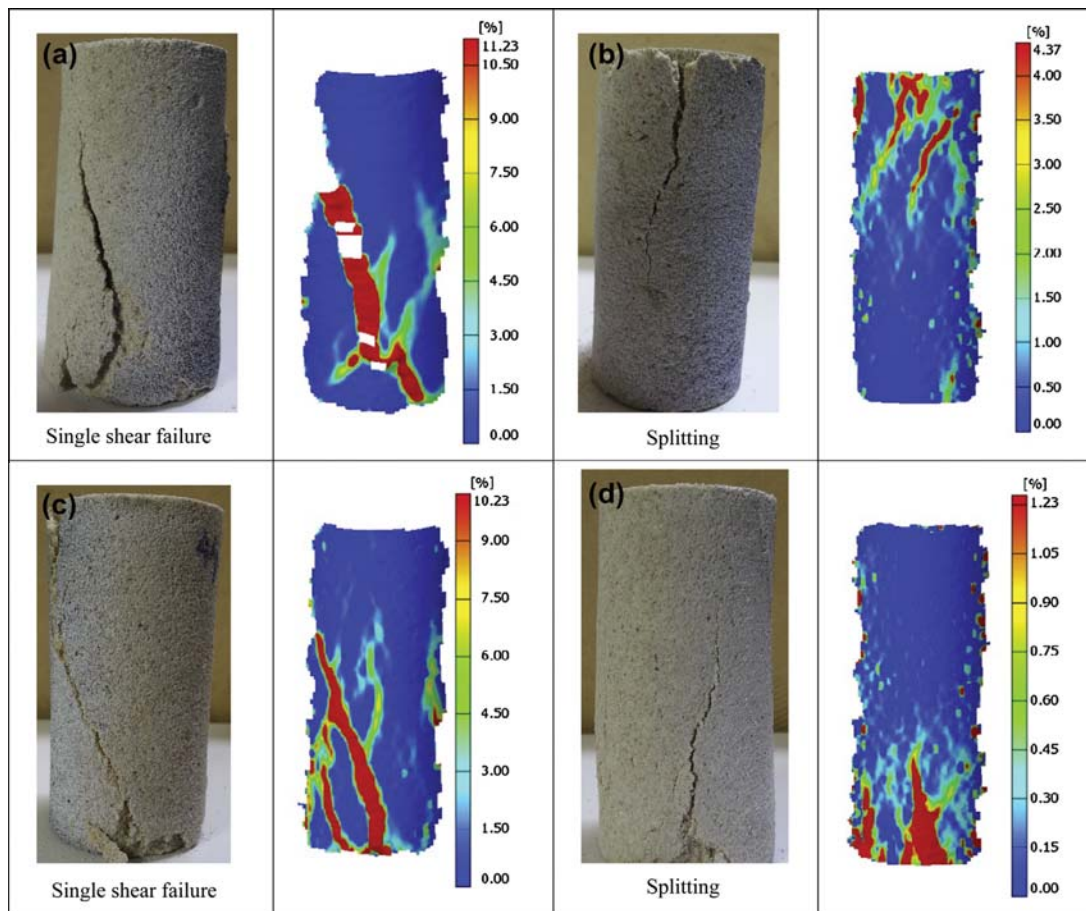


Fig. 10. The strain distribution of tested specimens at failure (a) water-saturated specimen, (b) 10% NaCl-saturated specimen, (c) 20% NaCl-saturated specimen and (d) 30% NaCl-saturated specimen.

From both methods, it is clear that although pore fluid saturation causes the reservoir rock to be weaker, the failure-related stress threshold values can be increased by increasing the NaCl concentration in the pore fluid. Therefore, the net effect decides the final behaviour of reservoir rock.

3.2.3.3. ARAMIS photogrammetry response

ARAMIS photogrammetry was also used in this study to ascertain the effect of NaCl concentration on the overall mechanical behaviour of reservoir rock under a uniaxial stress environment. Fig. 10 shows the ARAMIS photogrammetry images of the strain distributions of the reservoir rock specimens at failure. There is a range of colours on each rock mass surface, which exhibits the large variation in the strain values, and most of the points inside the darkest red zone experienced maximum stress prior to failure. According to the ARAMIS photographs, the rock samples saturated with 20% and 30% NaCl brine (or pore fluid) are highly brittle in nature (maximum strains at failure are 3.45 and 1.57), the 10%

NaCl saturated sample exhibits some quasi-brittle behaviour (maximum strain at failure is 8.73%), and the water-saturated sample shows some slight ductile behaviour (maximum strain at failure is 12.24%). Moreover, according to these digital images, shear failure dominates the failure mechanism of reservoir rock at low salinities ($\leq 10\%$) and splitting failure dominates at higher salinities (Fig. 10). Overall, this observation clearly indicates that the ductility of the brine-saturated samples tends to be reduced by the increased NaCl concentration of the pore fluid.

SEM analysis, which can be used to observe the NaCl crystal formation behaviour of the reservoir rock due to NaCl saturation, was then performed to understand the results reported in Sections 3.1–3.3.

3.2.3.4. Scanning electron microscopy (SEM) analysis

Finally a complete micro-structural analysis was carried out to understand the observed mechanical behaviour of the reservoir rock during the brine saturation. Fig. 11 shows the results

Table 2

Mean values of uniaxial compressive strength (UCS), Young's modulus (E) and Poisson's ratio obtained from testing and changes in these values relative to values obtained from testing of the water-saturated sample.

Specimen	UCS (MPa)	Average UCS	Δ UCS (%)	Young's Modulus (GPa)	Average E	ΔE (%)	Average Poisson's ratio
Dry							
Sample 1	38.95			11.24			
Sample 2	39.96	39.52	–	10.07	10.29	–	0.261
Sample 3	39.63			10.04			
Water-saturated							
Sample 1	25.66			4.89			
Sample 2	25.03			5.65			
Sample 3	25.34	25.28	–	4.98	5.35	–	0.282
Sample 4	25.04			5.77			
10% NaCl							
Sample 1	22.62			4.02			
Sample 2	23.22			4.23			
Sample 3	23.07	23.05	(–)8.82	4.21	4.44	(–)17.01	0.323
Sample 4	22.73			4.46			
20% NaCl							
Sample 1	26.08			7.24			
Sample 2	25.93			7.67			
Sample 3	26.48	26.35	(+)4.23	6.99	7.18	(+)34.21	0.305
Sample 4	26.89			6.58			
30% NaCl							
Sample 1	27.43			9.16			
Sample 2	28.61			9.45			
Sample 3	27.89	27.72	(+)9.65	8.94	9.50	(+)77.57	0.359
Sample 4	27.03			9.11			

“+” sign indicates increase trend and “–” sign indicates decrease trend.

Table 3

Summary of reversal stresses from stress-crack volumetric strain analysis method.

Specimen	Reversal stress (MPa)	Strength (MPa)	Reversal stress/strength	Reversal direction	Reversal strain
Water-saturated	11.99	25.28	0.474288	+ to –	0.00383
10% NaCl-saturated	10.41	23.05	0.451627	+ to –	0.00337
20% NaCl-saturated	12.65	26.05	0.485605	+ to –	0.00344
30% NaCl-saturated	13.84	27.72	0.499278	+ to –	0.00312

Where “+ to –” indicates dilatancy.

Table 4

Crack propagation stress thresholds values from AE analysis.

Test condition	Crack closure stress range (MPa)	Crack initiation stress (MPa)	Crack damage stress (MPa)	Failure (MPa)
Water-saturated	5.34–10.23	11.04	21.45	25.28
10% NaCl	2.32–9.01	9.75	21.23	23.05
20% NaCl	5.55–10.67	11.32	22.12	26.35
30% NaCl	6.71–14.67	15.73	23.32	27.72

Table 5
Amount of NaCl deposition from chemical analysis.

	10% NaCl-saturated	20% NaCl-saturated	30% NaCl-saturated
Amount of NaCl (ppm)	10,500	31,215	53,754

of the SEM analysis, and clearly exhibits a significant amount of NaCl crystal growth in the 20% and 30% NaCl saturated specimens and a negligible amount of NaCl crystal growth in the 10% NaCl saturated specimens. It should be noted that, according to the predicted UCS stress analysis, 20% and 30% of NaCl saturation caused the reservoir rock's UCS strength to be increased by up to 4.23% and 9.65%, respectively, with respect to the water-saturated condition. Therefore, according to this SEM analysis, the UCS increment in the rock specimen appears to be clearly related to the NaCl crystallisation process in the rock pore spaces (refer to Fig. 11(c) and (d)). In addition to SEM analysis, a chemical analysis was conducted to quantify the amount of NaCl crystals deposited in the rock pores for various NaCl concentrations by stirring a weighted quantity of the sample in demineralised water and filtering the water before analysing the solution for Na and Cl [39]. From the analysis of the solutions, it was observed that the amount of soluble salts increases with increasing NaCl concentration of brine solution. This can be clearly seen in Table 5. However, the result will not be precise, as there are most likely many soluble compounds in the sample, and Na is ubiquitous, but it will give a good indication of the amount of NaCl present in the sample. As described earlier, these NaCl crystals may add additional strength to the rock skeleton by reducing the pore space of reservoir rock. The results of this analysis are consistent with the results obtained for reservoir rock tested under low salinity conditions (0%, 2%, 5%, 10% and 15% NaCl) reported in Shukla et al. [38].

3.2.3.5. Salinity-dependent stress relationship

Overall, it is clear that the UCS strength of reservoir rock in saline aquifers exhibits a non-linear relationship with increasing NaCl concentration in the pore fluid. In this section, an effort is made to characterise the relationship between salinity and the UCS strength of the selected reservoir rock. The non-linear regression method was used to develop the basic relationship between the average failure strength and the NaCl concentration, and the least squares procedure was applied to resolve the functions (Fig. 12). As can be seen from Fig. 12, the relationship of salinity and average failure strength is best represented by a polynomial function with a 99% confidence band for the relationship, which is given in Eq. (6). However, it is important to note that the developed relationship (Eq. (6)) can only be used on the sandstones selected for the tested saline concentrations and may not be applicable to other types of rocks.

$$\sigma_f = -0.00101C^3 + 0.059C^2 - 0.7032C + 25.28 \quad (6)$$

where σ_f is the average failure strength and C is the NaCl concentration in percentage by weight.

To date, there has been no data available on the high salinity effect on the mechanical properties of reservoir rock in a uniaxial stress environment. Therefore, the findings of this study are vital for CO₂ sequestration in saline aquifers, and provide some basic knowledge of the field situation when selecting appropriate

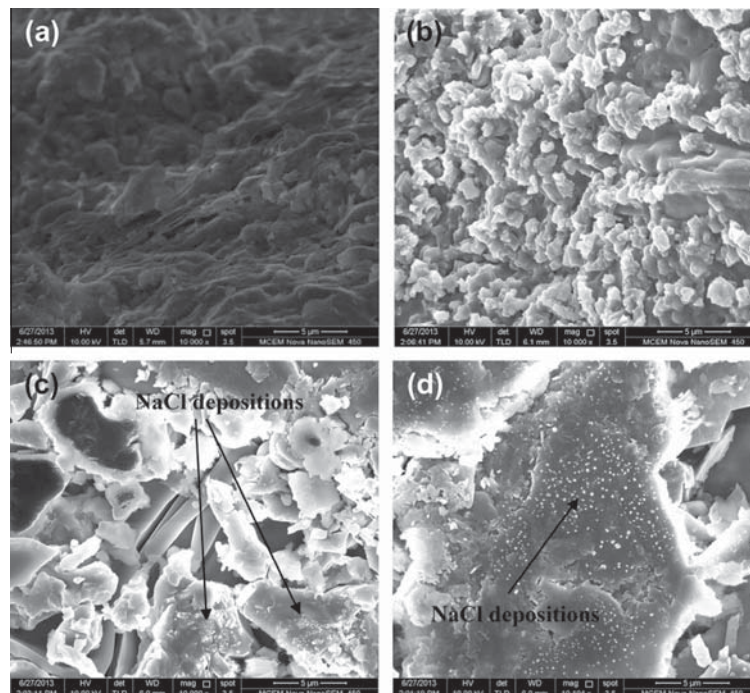


Fig. 11. SEM test results of (a) water saturation, (b) 10% NaCl-saturated specimen, (c) 20% NaCl brine-saturated specimen and (d) 30% NaCl-saturated specimen.

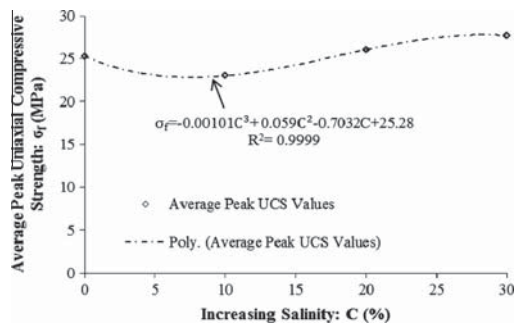


Fig. 12. Relationship between average failure strength and salinity.

sequestration sites. However, the mechanical properties of reservoir rock will also vary with the injection of CO₂. Therefore, further studies regarding CO₂ and the coupled effect of both brine and CO₂ on the mechanical properties of reservoir rock are necessary for a complete understanding of CO₂-sequestration-induced rock strength in deep saline aquifers.

3.2.4. Conclusion

The presence of NaCl in pore fluid causes the reservoir rock strength to be reduced in the CO₂ sequestration process in saline aquifers. Therefore, a comprehensive study was conducted for a range of salinity levels (0%, 10%, 20% and 30% NaCl) using a series of UCS tests. Of these different saturations, water saturation (pore fluid with 0% of NaCl) appears to play a significant role in reservoir rock strength, and it causes the dry rock mass strength to be reduced by around 36%. The effect of NaCl in the pore fluid on the rock mass strength was then investigated using a range of brine-saturated rock samples (pore fluid with 10%, 20% and 30% NaCl). Of these differently saturated rock samples, the sample saturated with 10% NaCl showed a reduction in UCS strength (8.82%) and the samples saturated with higher percentages of NaCl (20% and 30%) showed an enhancement in UCS strength (4.23% and 9.65%), compared to the water-saturated specimen. The physical phenomenon causing this observation was identified by conducting a SEM analysis. According to the SEM analysis, when the pore fluid has a higher degree of salinity (20% and 30% of NaCl), there is a considerable number of NaCl crystals in the pore structure of the rock mass, and these NaCl crystals probably improve the reservoir rock strength by reducing the number of voids. Interestingly, the 10% NaCl saturated rock mass pore space did not exhibit any noticeable number of NaCl crystals in the pore structure. However, the further reduction of strength with the 10% NaCl saturation compared to water saturation is crucial. The chemical corrosion which occurs in the rock mass surface due to NaCl ions is the reason for the strength reduction in the 10% NaCl saturated rock sample. Although this happens in the rock samples with higher percentages of NaCl (20% and 30%), the NaCl crystallization effect may be dominant at this stage.

The effect of brine saturation on the crack propagation pattern and the strain behaviour of reservoir rock were then studied by performing an acoustic emission analysis and a stress-crack volumetric strain analysis, respectively. According to the stress-crack volumetric results, an increased salinity percentage of the pore fluid causes the reservoir rock to be dilated significantly, and according to the acoustic emission analysis, this causes the crack initiation stress threshold to be increased. Therefore, it can be concluded that the salinity percentage of the pore fluid has a crucial

influence on the mechanical properties of saline aquifers' reservoir rock.

3.2.5. References

- [1] Arsyad A, Mitani Y, Babadagli T. Comparative assessment of potential ground uplift induced by injection of CO₂ into Ainoura and Berea sandstone formations. *Earth Planet Sci* 2013;6:278–86.
- [2] Baudracco J, Aoubouazza M. Study of the variations in permeability and cationic exchange kinetics during solution changes in clay sandstone. *Chem Geol* 1990;84(1–4):235–8.
- [3] Brace WF. Volume change during fractured and frictional sliding: a review. *Pure Appl Geophys* 1978;116:603–14.
- [4] Bellotto M, Gualteri A, Artioli G, Clark SM. Kinetic study of the kaolinite multiteraction sequence. Part I: Kaolinite dehydroxylation. *Phys Chem Miner* 1995;22:207–14.
- [5] Bieniawski ZT. Mechanism of brittle fracture of rock: Part I – Theory of the fracture process. *Int J Rock Mech Min Sci* 1967;4:395–406.
- [6] Brown ET. Rock characterisation, testing and monitoring. *Int Soc Rock Mech* 1981:81–5.
- [7] Bruant RG, Guswa AJ, Celia MA, Peters CA. Safe storage of CO₂ in deep saline aquifers. *Environ Sci Technol* 2002;36:240A–5A.
- [8] Byerlee JD. Brittle–ductile transition in rocks. *J Geophys Res* 1968;73:4741–50.
- [9] Czanderna AW, Ramachandra RCN, Honig JM. The anatase–rutile transition. Part I: Kinetics of the transformation of pure anatase. *Trans Faraday Soc* 1958;54:1069–73.
- [10] Dmitriyev AP, Kusyayev LS, Protasov YI, Yamschchikov VS. Physical properties of rocks at high temperatures. Moscow: Nedra Press; 1972.
- [11] Dobereiner L, DeFreitas MH. Geotechnical properties of weak sandstones. *Geotechnique* 1986;36(1):79–94.
- [12] Duclos R, Paquet J. High-temperature behaviour of basalts – role of temperature and strain rate on compressive strength and K_{1c} toughness of partially glassy basalts at atmospheric pressure. *Int J Rock Mech Min Sci* 1991;28:71–6.
- [13] Dunning JD, Miller ME. Effects of ore fluid chemistry on stable sliding of Berea sandstone. *Pure Appl Geophys* 1985;122(2–4):447–62.
- [14] Dyke CG, Dobereiner L. Evaluating the strength and deformability of sandstone. *Q J Eng Geol* 1991;24:123–34.
- [15] Eberhard E, Stead D, Stimpson B, Read RS. Identifying crack initiation and propagation threshold in brittle rock. *Can Geotech J* 1998;35:222–33.
- [16] Erguler ZA, Ulusay R. Water-induced variations in mechanical properties of clay-bearing rocks. *Int J Rock Mech Min Sci* 2009;46(2):355–70.
- [17] Feng XT, Chen S, Zhou H. Real-time computerized tomography (CT) experiments on sandstone damage evaluation during triaxial compression with chemical corrosion. *Int J Rock Mech Min Sci* 2004;41:181–92.
- [18] Feucht LJ, Logan JM. Effects of chemically active solutions on shear behaviour of a sandstone. *Tectonophysics* 1990;175:156–76.
- [19] Fredrich JT, Evans B, Wong TF. Micromechanics of the brittle to ductile transition in Carrara marble. *J Geophys Res* 1989;94(B4):4129–45.
- [20] Gibb SE. High-temperature, very deep geological disposal: a safer alternative for high-level radioactive waste. *Waste Manage (Oxford)* 1999;19:207–11.
- [21] Hangx S, Van der Linden A, Marcellis F, Bauer A. The effect of CO₂ on the mechanical properties of the Captain sandstone: geological storage of CO₂ at the Goldeneye field (UK). *Int J Greenhouse Gas Control* 2013;201:5–17.
- [22] Hawkins AB, McConnell BJ. Sensitivity of sandstone strength and deformability to changes in moisture content. *Q J Eng Geol* 1992;25:115–30.
- [23] Jaeger JC, Cook NGW. Fundamentals of rock mechanics. 3rd ed. London: Chapman and Hall; 1979.
- [24] Koide HG, Tazaki Y, Noguchi M. Subterranean containment and long-term storage of carbon dioxide in unused aquifers and in depleted natural gas reservoirs. *Energy Convers Manag* 1992;33:619–26.
- [25] Lajtai EZ. Microscopic fracture processes in a granite. *Rock Mech Rock Eng* 1998;31:237–50.
- [26] Lockner D. The role of acoustic emission in the study of rock fracture. *Int J Rock Mech Min Sci* 1993;30:883–99.
- [27] Martin CD, Chandler NA. The progressive fracture of Lac du Bonnet Granite. *Int J Rock Mech Min Sci* 1994;31:643–59.
- [28] Mohan KK, Reed MG, Fogler HS. Formation damage in smectitic sandstones by high ionic strength brines. *Colloids Surf A* 1999;154:49–257.
- [29] Omar A. Effect of brine composition and clay content on the permeability damage of sandstone cores. *J Petrol Sci Eng* 1990;4(3):245–56.
- [30] Perera MSA, Ranjith PG, Choi SK, Airey D. Investigation of temperature effect on permeability of naturally fractured black coal for carbon dioxide movement: an experimental and numerical study. *Fuel* 2011;94:596–605.
- [31] Perera MSA, Ranjith PG. Effects of gaseous and super-critical carbon dioxide saturation on the mechanical properties of bituminous coal from the southern Sydney basin. *Appl Energy* 2013;110:73–81.
- [32] Probst P. Numerical simulations of CO₂ injection into saline aquifers: estimation of storage capacity and arrival times using multiple realizations of heterogeneous permeability fields. Master Thesis: University of Stuttgart; 2008.
- [33] Ranjith PG, Pong SF, Chian W, Haque A. Characterization of fractured rocks under uniaxial loading states. *Int J Rock Mech Min Sci* 2004;4:361–72.

- [34] Ranjith PG, Viete DR, Chen BJ, Perera M. Transformation plasticity and the effect of temperature on the mechanical behaviour of Hawkesbury sandstone at atmospheric pressure. *Eng Geol* 2012;151:120–7.
- [35] Ranjith P, Perera M, Khan E. A study of safe CO₂ storage capacity in saline aquifers: a numerical study. *Int J Energy Res* 2013;37:189–99.
- [36] Rao QH, Wang Z, Xie HF, Xie Q. Experimental study of properties of sandstone at high temperature. *J Cent South Univ Technol (Engl Ed)* 2007;14(s1):478–83.
- [37] Rutqvist J, Birkholzer JT, Tsang CF. Coupled reservoir–geomechanical analysis of the potential for tensile and shear failure associated with CO₂ injection in multilayered reservoir–caprock systems. *Int J Rock Mech Min Sci* 2008;45:132–43.
- [38] Shukla R, Ranjith PG, Choi SK, Haque A, Yellishetty M, Hong L. Mechanical behaviour of reservoir rock under brine saturation. *Rock Mech Rock Eng* 2013;46(1):83–9.
- [39] Skougstad MW, Fishman MJ, Friedman LC, Erdmann DE, Duncan SS. In: Methods for determination of inorganic substances in water and fluvial sediments: techniques of Water-Resources Investigations of the United States Geological Survey, book 5, 1979;1–626 [chapter A1].
- [40] Swolfs H. Influence of pore fluid chemistry and temperature on fracture of sandstone under confining pressure. Texas A&M University; 1971.
- [41] Vilarrasa V, Bolster D, Olivella S, Carrera J. Coupled hydromechanical modelling of CO₂ sequestration in deep saline aquifers. *Int J Greenhouse Gas Control* 2010;4:910–9.
- [42] Wu Z, Qin Bd, Chen LJ, Luo YJ. Experimental study on mechanical character of sandstone of the upper plank of coal bed under high temperature. *Chin J Rock Mech Eng* 2005;24:1863–7 [in Chinese].
- [43] Zhang LY, Mao XB, Lu AH. Experimental study on mechanical properties of rocks at high temperature. *Sci China Ser E – Technol Sci* 2009;52:641–6.

3.3 The effect of salinity on mechanical behaviour of deep saline reservoir rock in reservoir stress environments

According to Section 3.2, the presence of high salinity brine in the reservoir rock pore space causes mechanical properties to significantly change. Knowledge of the mechanical properties of the reservoir rock are important to ensure the long-term integrity of the sequestration process. Therefore, the effect of salinity on the mechanical behaviour of reservoir rock in a triaxial stress environment was investigated and the results are presented in this section of the thesis. In addition to the salinity level, the effect of high confining pressure conditions (the depth effect) was also investigated. To date, a number of triaxial strength studies have been conducted on sandstone, but no stress-strain data is available on brine-saturated sandstone. Although the conventional Mohr-Coulomb failure criterion is broadly used for many engineering applications, its applicability to brine-saturated sandstone has not been investigated to date. The following published journal paper reports on this part of the study.



Contents lists available at ScienceDirect

Measurement

journal homepage: www.elsevier.com/locate/measurement

Non-linear stress–strain behaviour of reservoir rock under brine saturation: An experimental study



T.D. Rathnaweera^a, P.G. Ranjith^{a,*}, M.S.A. Perera^a, A. Lashin^{b,c}, N. Al Arifi^d

^a Deep Earth Energy Laboratory, Department of Civil Engineering, Monash University, Building 60, Melbourne, Victoria 3800, Australia

^b King Saud University, College of Engineering – Petroleum and Natural Gas Engineering Department, P.O. Box 800, Riyadh 11421, Saudi Arabia

^c Benha University, Faculty of Science – Geology Department, P.O. Box 13518, Benha, Egypt

^d King Saud University, College of Science – Geology and Geophysics Department, P.O. Box 2455, Riyadh 11451, Saudi Arabia

ARTICLE INFO

Article history:

Received 28 January 2015

Received in revised form 25 March 2015

Accepted 8 April 2015

Available online 16 April 2015

Keywords:

CO₂ sequestration

Saline aquifers

Strength

Salinity

Mohr–Coulomb criterion

Carbon storage

Reservoir rocks

ABSTRACT

CO₂ geo-sequestration process in deep saline aquifers has recently attracted attention as it addresses one of the current global issues of climate change. Suitable saline aquifers for CO₂ storage are generally located very deep underground, where the aquifer's pore fluid is highly saline. The strength of the reservoir rock mass is important to ensure safe sequestration, it is essential to check the aquifer rock mass strength in this highly saline environment. Although the Mohr–Coulomb failure criterion is widely used for many geotechnical engineering applications, its applicability to brine-saturated sedimentary rocks or saline aquifers has not been confirmed to date. This study therefore identifies the brine saturation effect on the stress–strain behaviour of saline aquifer reservoir rock (sandstone) under in-situ stress conditions, to check and if necessary modify the conventional Mohr–Coulomb failure criterion to capture the brine saturation effect on reservoir's rock strength parameters. A series of tri-axial experiments was conducted on Hawkesbury sandstone samples, obtained from the Sydney basin, for a range of confining pressures (5–20 MPa) and brine saturation conditions (0%, 10%, 20% and 30% NaCl concentrations) at 25 °C constant temperature.

According to the experimental results, the presence of NaCl in pore fluid causes the reservoir rock strength and shear parameters (friction angle and cohesion) to be increased in deep saline aquifers, and this effect increases with increasing brine concentration in the pore fluid. In addition, the presence of brine causes the dilatancy strength of saline aquifer rocks to be enhanced and the post-peak dilation (at which macroscopic shear faults may occur in the rock mass) of saline aquifer rock mass to be reduced. These enhance the micro-fracturing resistivity of the rock mass and increase the rock mass stability, both of which are favourable for the long-term integrity of the CO₂ sequestration process in deep saline aquifers. In addition, the conventional linear Mohr–Coulomb failure criterion fails to simulate the measured stress–strain data of brine-saturated Hawkesbury sandstone. This can be precisely corrected using the modified failure criterion proposed in this study.

© 2015 Elsevier Ltd. All rights reserved.

3.3.1. Introduction

Carbon dioxide geo-sequestration in deep saline aquifers has recently been identified as one of the best ways to

mitigate the global emission of CO₂ into the atmosphere [34,29]. According to current studies, deep saline aquifers have the largest CO₂ storage capacity (320–20,000 Gt [8]), which is much higher than the CO₂ storage capacity of other potential reservoirs, such as coal seams (300–1000 Gt CO₂ [43]). Generally, most preferable saline aquifers are located at depths between 0.8 and 2 km and most are in

* Corresponding author

sedimentary rocks, mainly sandstone. In addition, the salinity levels of suitable aquifers are quite high and according to Bachu and Bennion [5], the salinity level can range from 2×10^4 (2% by weight) to 2×10^5 mg/l (25% by weight). The influence of salinity can therefore be considered one of the critical factors to consider when selecting a suitable saline aquifer for any CO₂ sequestration project.

The dumping of a significant amount of CO₂ into an underground reservoir, such as a saline aquifer, is believed to considerably affect its chemico-physical structure, resulting in altered hydro-mechanical properties in the aquifer [25]. Although many studies related to this effect on the flow properties of saline aquifers have been reported [5,31] little consideration has been given to the influence of CO₂ injection on aquifer mechanical properties and understanding of this subject is therefore clearly not sufficient to confidently apply this practice in the field. In order to have a proper understanding of the effect of CO₂ sequestration on the strength of saline aquifers, it is necessary to conduct appropriate laboratory experiments, such as tri-axial experiments, on a saline aquifer's representative material such as brine-saturated sandstone, under in-situ stress condition. Such experiments will combine the influences of all the effective factors, including stress application, brine saturation, and CO₂ injection, and therefore more reliably represent the CO₂ sequestration process in saline aquifers. However, in order to understand this complex, combined influence it is essential to have a thorough knowledge of the influence of each individual factor.

The effect of brine saturation on sandstone's strength has received little attention and instead many studies have been conducted to check the water saturation effect on sandstone, as such studies can be used to understand the wetting effect created by brine saturation. Of the studies conducted to date on the effect of water saturation on sandstone strength, those conducted by Hawkins and McConnell [15], Vasarhelyi [37], Vasarhelyi [38], Vasarhelyi and Van [39], and Rathnaweera et al. [30] showed the significant strength reduction which occurs in sandstone with the softening effect created by water saturation. Rutter and Mainprice [32], Chester and Logan [11] and Baud et al. [7] proved this water saturation-induced strength reduction effect by conducting tri-axial experiments. According to Orowan [27], chemical interaction resulting from water saturation causes the surface free energy of the rock mass to be reduced and its strength to be reduced accordingly. According to Paterson [28] and Atkinson and Meredith [4], the pressurised water-induced mechanical effect causes the sandstone strength reduction. The experiments conducted by Vasarhelyi [37] on various British sandstones showed a liner correlation between the dry and water-saturated compressive strength of sandstone, where the water-saturated compressive strength was around 24.1% lower than the dry strength of the tested sandstone.

As mentioned earlier, very few studies have focussed on the brine saturation effect on the mechanical properties of reservoir rock [13,34,30], and of these, most of the laboratory experiments have been conducted under uniaxial stress conditions rather than actual field conditions (under confinement). Shukla et al. [34] performed a series of unconfined compressive strength tests to study the

influence of water and NaCl saturation on reservoir rock mass strength, and showed that the mechanical properties of reservoir rock change significantly with the NaCl concentration in the pore fluids, where it initially reduces and then increases with increasing NaCl concentration. According to Shukla et al. [34], the observed initial strength reduction is due to the water sensitivity or softening of the sandstone specimens in the brine. According to these researchers, the observed additional strength gain in the reservoir rock with increasing salinity concentration is related to the crystallisation effect of NaCl in the pore structure, which happens with salt evaporation. Rathnaweera et al. [30] also carried out a series of unconfined compressive strength tests to determine the detrimental effects of NaCl concentration on sandstone's mechanical properties. In this study, the effect of NaCl in the pore fluid on the rock mass strength was investigated using a range of brine-saturated rock samples (pore fluids with 10%, 20% and 30% NaCl). Of these differently saturated rock samples, the sample saturated with 10% NaCl showed a reduction in UCS strength (8.82%) and the samples saturated with higher percentages of NaCl (20% and 30%) showed an enhancement in UCS strength (4.23% and 9.65%) compared to the water-saturated specimen. However, these studies under uniaxial stress conditions do not represent the actual field conditions and it is therefore necessary to check the rock mass strength under confined conditions to simulate real aquifer rock mass strength behaviour under various salinity conditions.

To date, although many attempts have been made to analytically simulate the water saturation effect on sandstone's strength, none have considered the brine saturation effect, which is important for saline aquifers. However, if the available modelling studies of water saturation-induced strength property variations are considered, one of the earliest such models was proposed by Hawkins and McConnell [15], and this model can be used to predict the water saturation effect on sandstone's compressive strength:

$$\sigma_c(w) = ae^{-bw} + c \quad (1)$$

where $\sigma_c(w)$ is the rock strength, w is the water content (%), and a , b , and c are constants. Vasarhelyi and Van [39] improved Hawkins and McConnell's [15] model to the following form to more correctly predict the moisture effect on sandstone strength:

$$\sigma_c(w) = \sigma_{co} - \frac{(\sigma_{co} - \sigma_{csat})}{1 - e^{-b^*}} + \frac{(\sigma_{co} - \sigma_{csat})}{1 - e^{-b^*}} e^{-b^*w} \quad (2)$$

where the constant b^* can be determined from Eq. (3):

$$b^* = -\ln\left(\frac{0.1}{\sigma_{co} - \sigma_{csat}}\right) \quad (3)$$

where σ_{co} is the dry strength and σ_{csat} is the fully saturated strength.

Ashby and Sammis [3], Zhang et al. [46], Horii and Nemat-Nasser [19] and Zhang et al. [46] have made theoretical attempts to recognise the macroscopic and microscopic failure modes in the brittle faulting and cataclastic flow regimes in sandstone under water saturation. Of these, the sliding wing crack model developed by Horii

and Nemat-Nasser [19] can be used to investigate the dilatancy and brittle faulting behaviour of rock, and the Hertzian fracture model developed by Zhang et al. [46] can be used to model the grain crushing and pore collapse mechanisms of rock under compactive cataclastic flow. However, the applicability of these concepts for brine-saturated sandstones requires research.

An appropriate failure criterion is essential to effectively understand the rock mass strength variation with external stresses, especially in stress-changing field applications such as CO₂ injection into saline aquifers. To date, a number of strength criteria have been proposed by various researchers for intact rocks and their applicability to many engineering applications has been extensively studied [35,17,18,2,1,9]. In these studies the Mohr–Coulomb failure criterion is the most widely used criterion due to its simplicity [35]. However, the applicability of the existing Mohr–Coulomb failure criterion to simulate the coupled effect of brine and CO₂ on reservoir rock strength remains doubtful. Therefore, the investigation of the applicability of the Mohr–Coulomb failure criterion to CO₂ sequestration in saline aquifers is essential.

3.3.1.1. Applicability of Mohr–Coulomb failure criterion to saline aquifers

The conventional Mohr–Coulomb strength criterion is the most popular and widely used strength criterion in civil and mining engineering, and is used to define the shear strength of soils and rocks in different effective stress environments. However, according to existing studies, there are some major limitations of this criterion, including the linear relationship between the shear strength and confining pressure, and the non-incorporation of the intermediate principal stress effect [35]. The conventional Mohr–Coulomb failure criterion is shown in Eq. (4):

$$(\sigma_1 - \sigma_3) = \frac{2C_i \cos \phi_i}{1 - \sin \phi_i} + \frac{2 \sin \phi_i}{1 - \sin \phi_i} \sigma_3 \quad (4)$$

where C_i and ϕ_i are Mohr–Coulomb shear strength parameters of the intact rock, $(\sigma_1 - \sigma_3)$ is the deviatoric stress at failure, and σ_1 and σ_3 are the major and minor principal stresses at failure.

However, the applicability of this criterion to saline aquifers has not been properly shown. Therefore, an attempt was first made to evaluate the applicability of this criterion to sandstone, in a tri-axial stress environment, using the available strength data from past studies [33,44,25,41]. Table 1 shows the Mohr–Coulomb strength relationships obtained in some past relevant studies (the C_i and ϕ_i parameters were calculated using the data) and the corresponding model verification is shown in Fig. 1. As it Fig. 1 indicates, the experimental and predicted results for Mohr–Coulomb failure criterion are not in good agreement in most cases, and the error made by the Mohr–Coulomb criterion is much higher at high confining stresses. According to Sing et al. [35], the stress–strain behaviour of sandstone is inelastic and nonlinear, especially at high confining pressures.

Table 1

Mohr–Coulomb relationships developed for some available experimental data.

Experimental data set	Obtained relationship
Santarelli and Brown [33]: Dodderington sandstone	$(\sigma_1 - \sigma_3) = 7.25 \sigma_3 + 78.33$
Carboniferous sandstone	$(\sigma_1 - \sigma_3) = 2.2 \sigma_3 + 104.08$
Wong et al. [44]	$(\sigma_1 - \sigma_3) = 0.12 \sigma_3 + 75$
Marbler et al. [25]: Dry sandstone	$(\sigma_1 - \sigma_3) = 4.42 \sigma_3 + 39.27$
Brine–CO ₂ saturated sandstone	$(\sigma_1 - \sigma_3) = 2.4 \sigma_3 + 31.46$
Wasantha et al. [41]	$(\sigma_1 - \sigma_3) = 6.0 \sigma_3 + 22.14$

According to past studies, rock strength increases with increasing confining pressure, such that the rate of increment decreases with increasing confining pressure [6], Hoek, 1980, [18]. This is because, at low confining pressures, there is more dilation potential and the ability to open rock mass micro-cracks at the beginning of the failure is therefore higher, resulting in higher friction angle [35]. On the other hand, at high confining pressures, the tendency of micro-cracks to open and the subsequent dilation required to complete failure is suppressed, resulting in a lower friction angle. Increasing confining pressure therefore, shifts the rock failure mechanism from brittle to fully ductile and Barton [6] showed that further increase in confining pressure moves the rock to a “critical state” (Fig. 2). According to Barton [6], the critical state for an initially intact rock is defined as the stress condition, under which the Mohr envelope of peak shear strength of the rocks reaches a zero gradient that represents the maximum possible shear strength of the rock mass. For each rock, there will be a critical effective confining pressure, above which the shear strength will not increase. Rocks therefore become more ductile with reduced instantaneous friction angles at high confining pressures (Fig. 2). The approach of the Mohr envelope’s gradient to zero at high confining pressures has also been shown by Hoek [18].

The linear stress–strain behaviour of the conventional Mohr–Coulomb criterion is therefore not applicable when evaluating the rock strength in many engineering applications, especially under high stress conditions deep underground. This demonstrates the urgency of the need for an appropriate failure criterion for the CO₂ sequestration process in saline aquifers that can incorporate the non-linear behaviour of sandstone. An attempt has therefore been made in the present study to modify the Mohr–Coulomb failure criterion to simulate the CO₂ injection process into brine saturated sedimentary rocks (saline aquifers), giving special attention to the effect of salinity level on reservoir rock strength in various stress environments.

3.3.2. Methodology

3.3.2.1. Sample preparation

Sample preparation and testing were performed in the Deep Earth Energy Research Laboratory (DEERL) of the Civil Engineering Department at Monash University. The tested Hawkesbury sandstone samples were collected from the Sydney basin and the sample preparation was

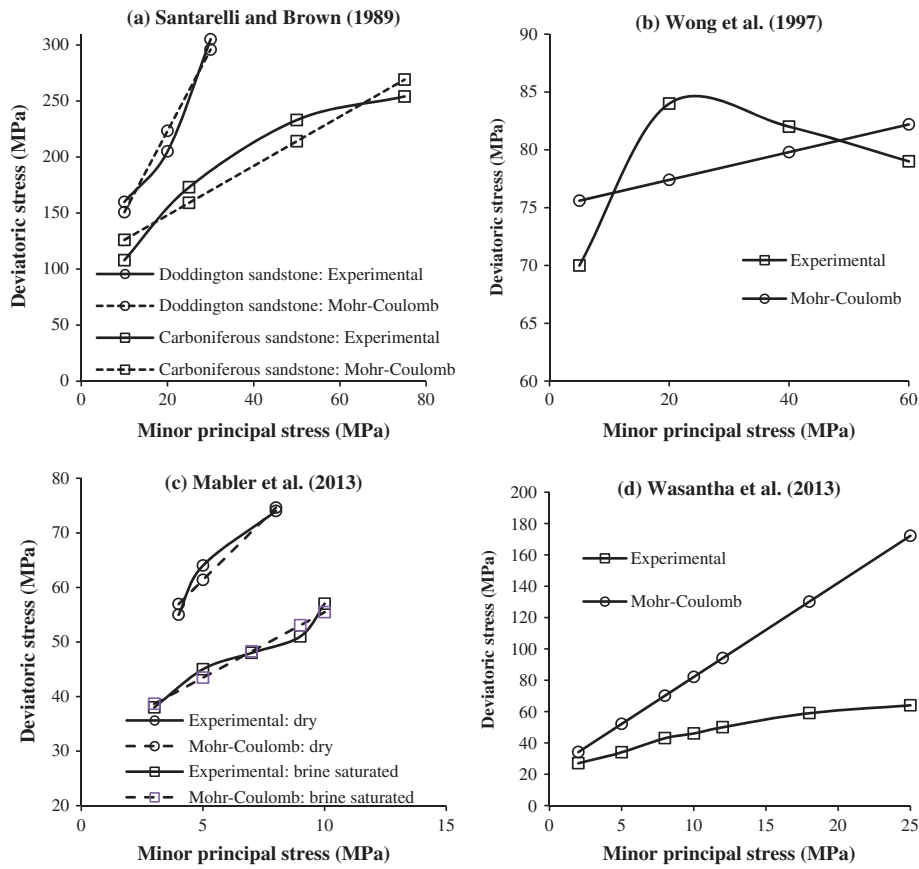


Fig. 1. Comparison of experimental and model-predicted results.

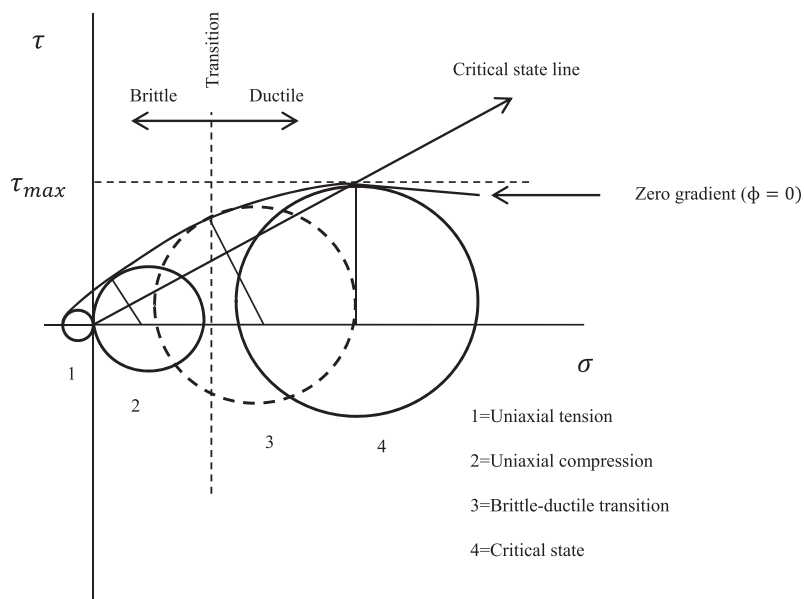


Fig. 2. Critical state of intact rocks shown in Mohr-Coulomb envelope [35].

done according to the ISRM standard [20]. All samples were cored to 38 mm in diameter at the same orientation (perpendicular to stratification). This is because the hydro-mechanical properties of sedimentary rocks are greatly dependent on its bedding plane direction [10]. Studies show significantly lower compressive strength, tensile strength and Young's modulus of sandstone normal to the bedding plane compared with the parallel plane [10] and rock orientation-dependent shear strength and internal friction coefficients in sedimentary rocks [10]. Therefore, in order to maintain consistency, rock samples were taken from the same block and care was taken to select samples with the same orientation (perpendicular to stratification). However, it should be noted that studying rock masses with different orientations is necessary to comprehensively understand the formation rock strength response to well operation in real field conditions. This will be considered in a future study.

Cored samples were then cut into 76 mm high cylinders and both ends of the samples were carefully ground to produce smooth parallel faces. The prepared samples were then oven-dried for 48 h at 25 °C, before being kept for saturation in selected saturation mediums. Both brine and water saturation conditions were considered in this study, and the water saturation was performed for comparison with the brine-saturated samples to determine the effect of pure brine saturation on rock strength (to remove the

softening effect of water saturation). In addition, in order to check the stress–strain behaviour of reservoir rock with varying pore fluid salinities, three different NaCl concentrations were used (10%, 20% and 30%, by weight). In this study NaCl was used to represent the reservoir brine because although saline aquifer brine is a mixture of ions (Na^+ , Mg^{2+} , Ca^{2+} , Cl^- , HCO_3^- and SO_4^{2-} , etc.), the NaCl percentage is much greater than others (70–90% of brine is composed of NaCl) [16]. Further, according to Bachu and Bennion [5] and Shukla et al. [34], brine concentration in saline aquifers is in the range of 2×10^4 (2% by weight) to 2×10^5 mg/l (25% by weight). Considering this range, three different NaCl concentrations were selected to cover the low to highest salinity saline aquifers, where 10%, 20% and 30% NaCl saturated samples represent low, medium and high salinity aquifers, respectively. The saturations were carried out under vacuum in desiccators (refer to Fig. 3(a)) for 18 months to ensure maximum saturation, and the weights of the samples were measured regularly to ensure the steady-state full saturation condition (until constant mass was reached). The same saturation procedure was carried out by the authors for their previously published studies, Rathnaweera et al. [30]. Rathnaweera et al. [30] performed a series of unconfined compressive strength tests following a saturation period of 60 days. However, the present study reveals the effect of long-term saturation (1.5 years) of brine on the mechanical

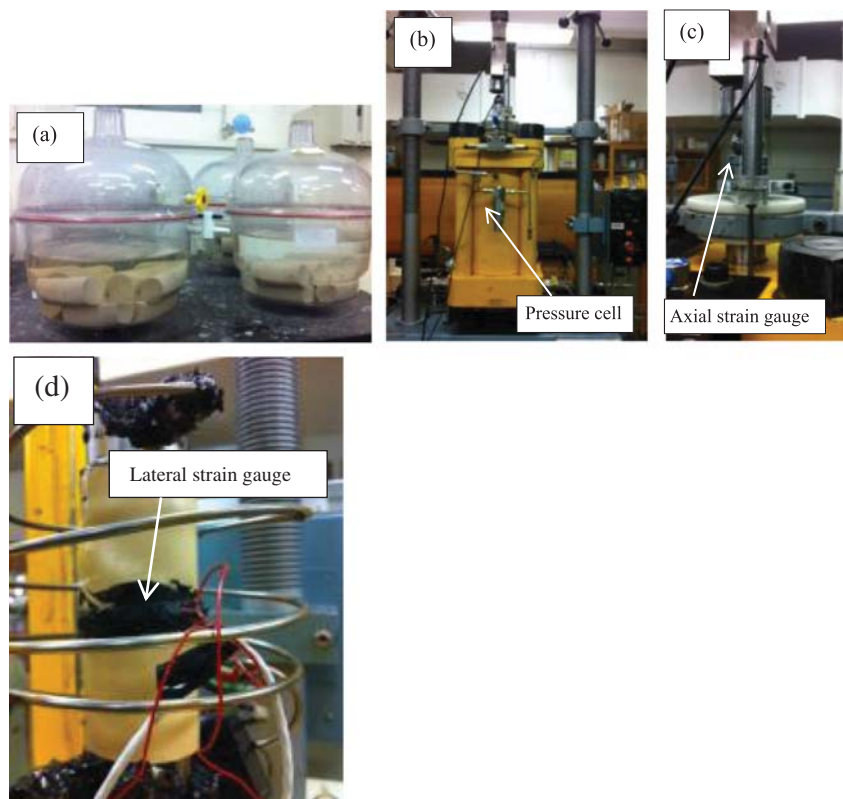


Fig. 3. (a) The desiccators used for saturating samples, (b) triaxial testing set-up, (c) axial strain gauges and (d) lateral strain gauge.

properties of reservoir rock under confined stress conditions (confining pressures of 5–20 MPa). Therefore, this research is a novel study compared to previously published work by the same authors [30].

3.3.2.2. Tri-axial tests

Undrained tri-axial experiments were conducted on both wet (water- and brine-saturated) and dry samples. The wet samples were tested under four different confining pressures (5, 10, 15 and 20 MPa) and the dry samples were also tested under four different, but lower, confining pressures (2.5, 5, 7.5 and 10 MPa) at room temperature (around 25 °C). These different confining pressure conditions were selected to simulate the reservoir depth effect. Generally, most preferable saline aquifers are located at depths between 0.8 and 2 km [8], where the corresponding confining pressures are 20 MPa to 50 MPa, respectively (assuming the reservoir rock density is equal to 2500 kg/m³). However, this exceeds the capacity of the loading frame used, considering the high strength of the tested sandstone (around 40 MPa UCS strength). Therefore, it was decided to adopt the maximum possible confining stress condition (20 MPa). The complete arrangement of the tri-axial cell is shown in Fig. 3(b). Duplicated samples were tested at each confining pressures. Prior to each test, sample porosity was determined by performing a mercury intrusion porosimetry (MIP) test and possible microstructural and mineralogical changes which occurred during 1.5 year saturation period were checked using SEM and XRD analyses.

The prepared samples were then placed inside the cell (Fig. 3(b)), the required confinement was applied using oil, and the load was applied. During the load application, the axial strain was measured using linear variable differential transducers attached to the RAM of the load cell (Fig. 3(c)) and the lateral strain was measured by two lateral strain gauges (clip gauges attached around the sample (see Fig. 3(d))).

3.3.3. Results and discussion

3.3.3.1. Overall stress–strain responses

The stress–strain responses of dry, water- and NaCl- (10%, 20% and 30% concentration of NaCl) saturated Hawkesbury sandstone samples were first checked. Fig. 4(a)–(e) show the relationships between the differential stress ($\sigma_1 - \sigma_3$) versus the axial and lateral strains for the samples tested at 25 °C constant temperature and 5, 10, 15 and 20 MPa confining pressures for water- and NaCl-saturated samples and 2.5, 5, 7.5 and 10 MPa for dry samples, respectively. Dry samples were tested for low confining pressure because at high confining pressures (more than 10 MPa) the corresponding failure load exceeds the maximum capacity of the load cell. According to Fig. 4, brine saturation causes the brittleness of sandstone to increase, and the effect increases with increasing confinement. The failure pattern of the sandstone samples under each saturation condition was then checked and the results

are shown in Fig. 5. According to this figure, regardless of saturation type, all the samples appeared to fail along a shear plane with load application. Interestingly, Rathnaweera et al. [30] found that under unconfined stress conditions, the rock samples saturated with brine tended to fail by splitting.

However, a closer examination of Fig. 4 reveals that, regardless of saturation type or applied confinement, the axial strain of the tested sandstone starts to decrease after the post-peak, which reflects a strain localisation process during the latter stage of load application. This is consistent with the findings of Sulem and Ouffroukh [36], who state that this non-homogeneous behaviour of sandstone strain is mainly due to the formation of shear bands inside the sample and eventually the rigid block sliding along the shear surface. However, according to Fig. 4, the lateral strain of the tested sandstone increases with load application, which exhibits the dilatant properties of the tested sandstone.

Fig. 6 shows the variation of differential stress with saturation condition and how it varies with the applied confinement. According to the figure, both water and NaCl saturations (including 10%, 20% and 30% concentrations of NaCl) have a significant influence on Hawkesbury sandstone's strength. However, the influence appears to reduce with increasing NaCl concentration in the pore fluid. This indicates the importance for long-term safety of the determination of the actual NaCl concentrations of the aquifer pore fluid when selecting suitable saline aquifers for CO₂ geo-sequestration in deep saline formations. The present study therefore aimed to gain comprehensive knowledge of the influence of water and brine saturation on the mechanical properties of Hawkesbury sandstone.

3.3.3.2. Effect of water and NaCl saturations on mechanical properties of Hawkesbury sandstone

According to Fig. 4, water saturation causes a significant strength reduction in Hawkesbury sandstone, which is comparable with previous findings [7,39]. According to the results, with respect to dry rock strength, 46.56% and 47.90% strength reductions were observed in water-saturated samples under 5 and 10 MPa confining pressures, respectively (Fig. 4). As mentioned earlier, this strength reduction is mainly due to the softening effect of water, which reduces the surface free energy of the rock mass, leading to failure. Importantly, according to Fig. 5, under both confinements, the water-saturated samples exhibit a brittle type of failure, which again proves the softening effect created by water saturation.

However, in addition to the water saturation effect, the NaCl-induced mechanical behaviour of reservoir rock is also important in deep saline CO₂ sequestration projects, due to the presence of highly saline brine in suitable aquifers (0.8–2.5 km deep). According to well bore data from the Wabamun Lake area in Canada, around a 10% per kilometre salinity gradient exists along the lithology [5], which implies the importance of a clear understanding of the influence of salinity level on the hydro-mechanical characteristics of reservoir rock for the long-term integrity of CO₂ sequestration projects in deep saline aquifers. Although

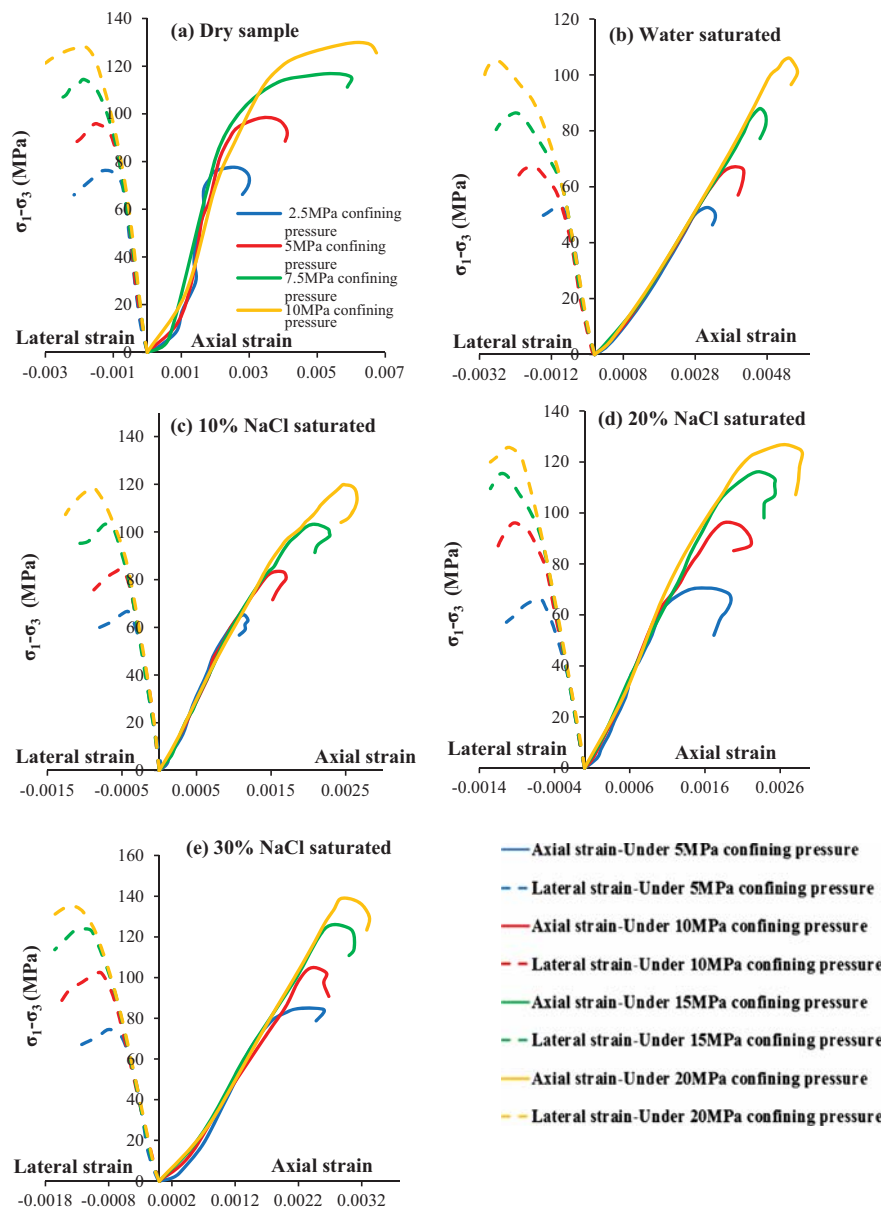


Fig. 4. The corresponding stress–strain responses of Hawkesbury sandstone, including dry, water- and NaCl- (10%, 20% and 30% concentrations of NaCl) saturated.

many studies exist related to the influence of salinity on the flow properties of reservoir rocks, little consideration has been given to its influence on the mechanical properties of reservoir rocks [26,34,30]. According to Rathnaweera et al. [30], the deposition of NaCl crystals has a considerable influence on reservoir rock strength in unconfined environments, and the strength increases with the increasing salinity of the pore fluid due to the NaCl crystallisation process in the rock mass pore structure with salt evaporation. This is consistent with a similar study conducted by Shukla et al. [34]. However, these studies

cannot represent the actual strength reduction in deep saline aquifers in confined environments and only tri-axial experiments can be used to examine real behaviour such as that considered in the present study.

Figs. 6 and 7 show the variations of differential stress with saturation condition and confining pressure. According to these figures, the rock mass strength reduction occurred due to the water saturation being clearly reduced with the presence of NaCl in pore fluid, and the influence increases with increasing NaCl concentration in the pore fluid. For example, under 5 MPa confinement,

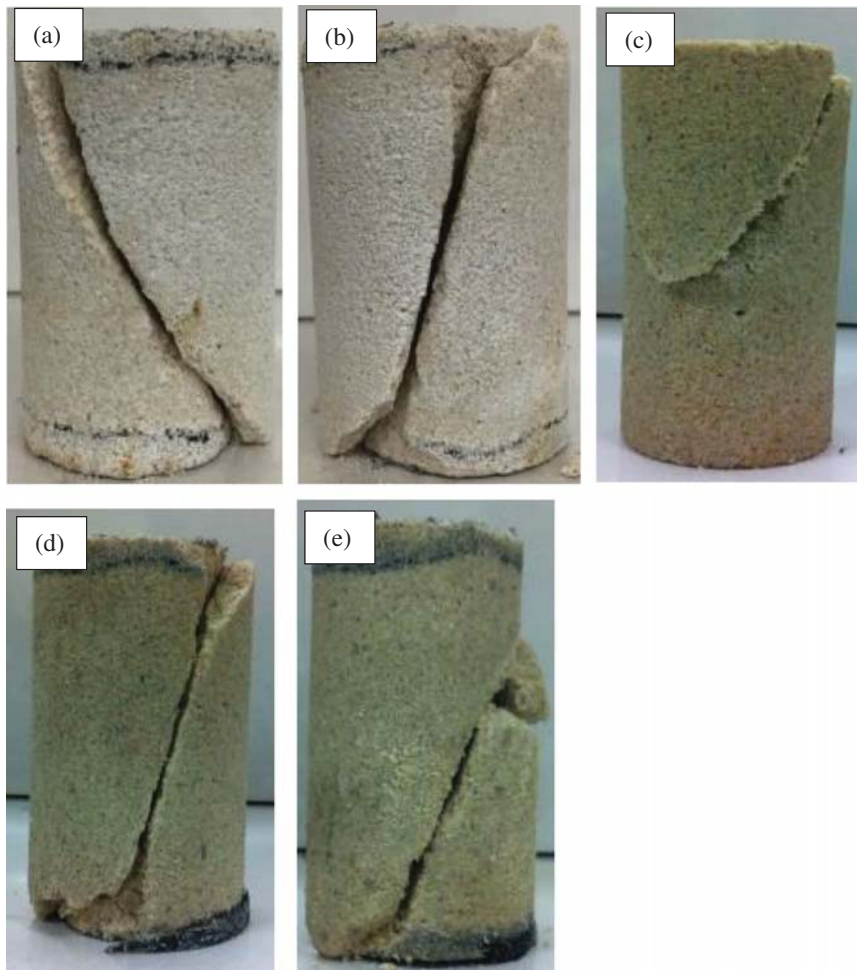


Fig. 5. Visual inspection of post-peak samples indicating that the samples failed by shear localisation (a) dry (b) water- (c) 10% (d) 20% and (e) 30% NaCl-saturated samples.

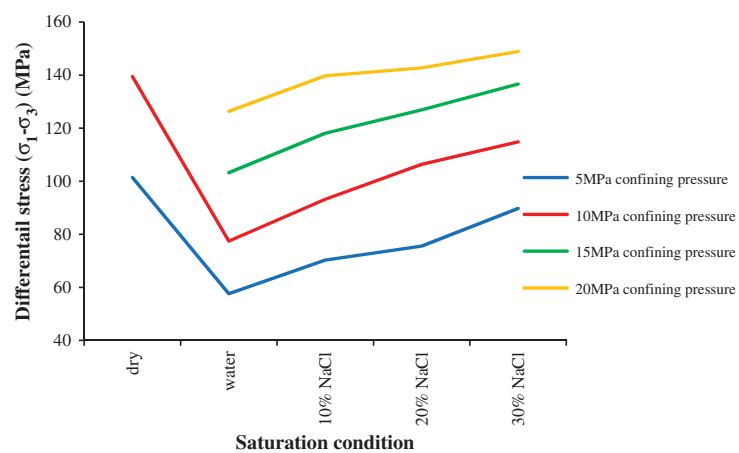


Fig. 6. Variation of differential stress with respect to the differently saturated mediums under tested confining pressure conditions.

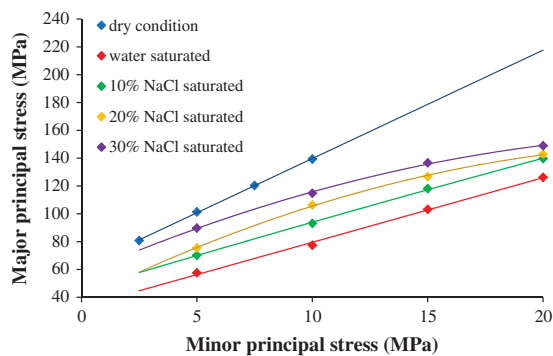


Fig. 7. Variation of differential stress versus confining pressure for each saturation condition.

the failure strength increases from 57.57 to 70.27 MPa and 75.52 to 89.76 MPa, when the NaCl concentration in the pore fluid is increased from 0% to 10% and 10% to 30%, respectively. Chemical and microstructural analysis confirmed the deposition of NaCl crystals in the pore structure under brine saturation, and this is believed to be the reason for the observed strength gain in the reservoir rock samples with the existence of NaCl in the pore fluid. According to Feucht and Logan's [13] study on the effect of chemically active solutions on the shearing behaviour of sandstone, there can be around 6–16% strength reduction and 20% strength gain in reservoir rock due to 1 M and 5 M NaCl concentrations, respectively (compared to water-saturated samples). According to these researchers, high ionic strength solutions produce significant mechanical weakening in reservoir rock and in contrast, intermediate ionic strength solutions may strengthen rocks relative to water-saturated samples. However, this result is based on very short-term saturation condition (approximately 6 h). Based on studies of the long-term saturation effects of NaCl by Shukla et al. [34] and Rathnaweera et al. [30], the existence of NaCl in the pore fluid causes strength enhancement in reservoir rock due to NaCl crystallisation in the rock mass pore space. Rathnaweera et al. [30] found 4.2% and 9.7% strength gains in 20% and 30% NaCl-saturated compared to water-saturated samples and conversely, a strength reduction of 8.7% was observed in 10% NaCl-saturated samples. The reason for this strength reduction in 10% NaCl saturated sample was explained by the chemically corrosive nature of NaCl ions, which can also happen in rock samples with higher percentages of NaCl (20% and 30%). However, according to Rathnaweera et al. [30], although corrosion occurs in rock samples with higher percentages of NaCl (20% and 30%), the NaCl crystallisation effect may enhance the rock strength in samples saturated with higher percentages of NaCl. Interestingly, the present study reveals the importance of duration of brine saturation (1.5 years saturation) on rock strength and shows controversial stress–strain behaviour in 10% NaCl saturated reservoir rock compared to Rathnaweera et al. [30], where the duration of brine saturation was about 60 days. According to the present study, compared with water-saturated samples, enhancements in rock

strength were observed in NaCl-saturated samples (10%, 20% and 30% NaCl) under all confining pressure conditions tested. For instance, under 5 MPa confining pressure, 22%, 32% and 56% strength gains were observed in 10%, 20% and 30% NaCl-saturated samples compared to water-saturated samples, respectively. As mentioned earlier, the present study was conducted on reservoir rock saturated with brine for 1.5 years, and this long-term saturation facilitates NaCl deposition, which tends to dominate the strength characteristics at this stage compared to the corrosive nature of NaCl ions.

3.3.3.3. Applicability of conventional Mohr–Coulomb failure criterion to NaCl-saturated reservoir rocks

According to Fig. 7, there is a considerable non-linear variation of failure strength in NaCl-saturated samples compared to dry and water-saturated samples. This raises a question related to the applicability of the existing Mohr–Coulomb failure criterion to model the failure of deep saline aquifer rocks which are saturated with NaCl. In order to examine this, Mohr–Coulomb failure envelopes were plotted (Fig. 8) and Eq. (5) was used to calculate the Mohr–Coulomb parameters (effective cohesion and friction angle) for each saturation condition. The results are shown in Fig. 9(a) and (b).

$$\sigma_1 = \frac{1 + \sin \theta}{1 - \sin \theta} \sigma_3 + \frac{2c \cos \theta}{1 - \sin \theta} \quad (5)$$

where c and θ are effective cohesion and friction angle.

As can be seen in Fig. 9(a), the friction angle decreases from 42.24 to 29.37° with water saturation and then increases up to 35.93°, 36.67° and 38.79° with the presence of 10%, 20% and 30% NaCl in the pore fluid, respectively. This observed friction angle gain is believed to be related to the deposition of NaCl crystals in the rock pore space. The friction between grain-to-grain contacts may be changed due to the deposition of NaCl crystals in the rock pore space, which consequently enhances the friction angle with the deposition of NaCl crystals. A similar trend can be seen in rock cohesion (Fig. 9(b)), which reduces from 10.71 to 10.67 MPa due to water saturation and again starts to increase with increasing NaCl concentration from 0% to 30%. The observed cohesion gain in the reservoir rock with the presence of NaCl in the pore fluid is because of the enhanced rock strength due to NaCl deposition. Moreover, the observed clay mineral formation by NaCl saturation enhances the cohesiveness between grain contacts. The observed cohesion gain in the reservoir rock with the presence of NaCl in the pore fluid may also be due to the clay mineral formation by NaCl, which was confirmed by XRD analysis, according to which the amount of kaolinite minerals in the rock mass increased from 8% to 13% due to the saturation of dry rock samples with 20% NaCl brine (refer to Table 2).

3.3.3.4. Modified Mohr–Coulomb failure criterion for non-linear behaviour of water- and NaCl-saturated sandstone

Although a number of strength criteria have been proposed for intact rocks, the determination of their

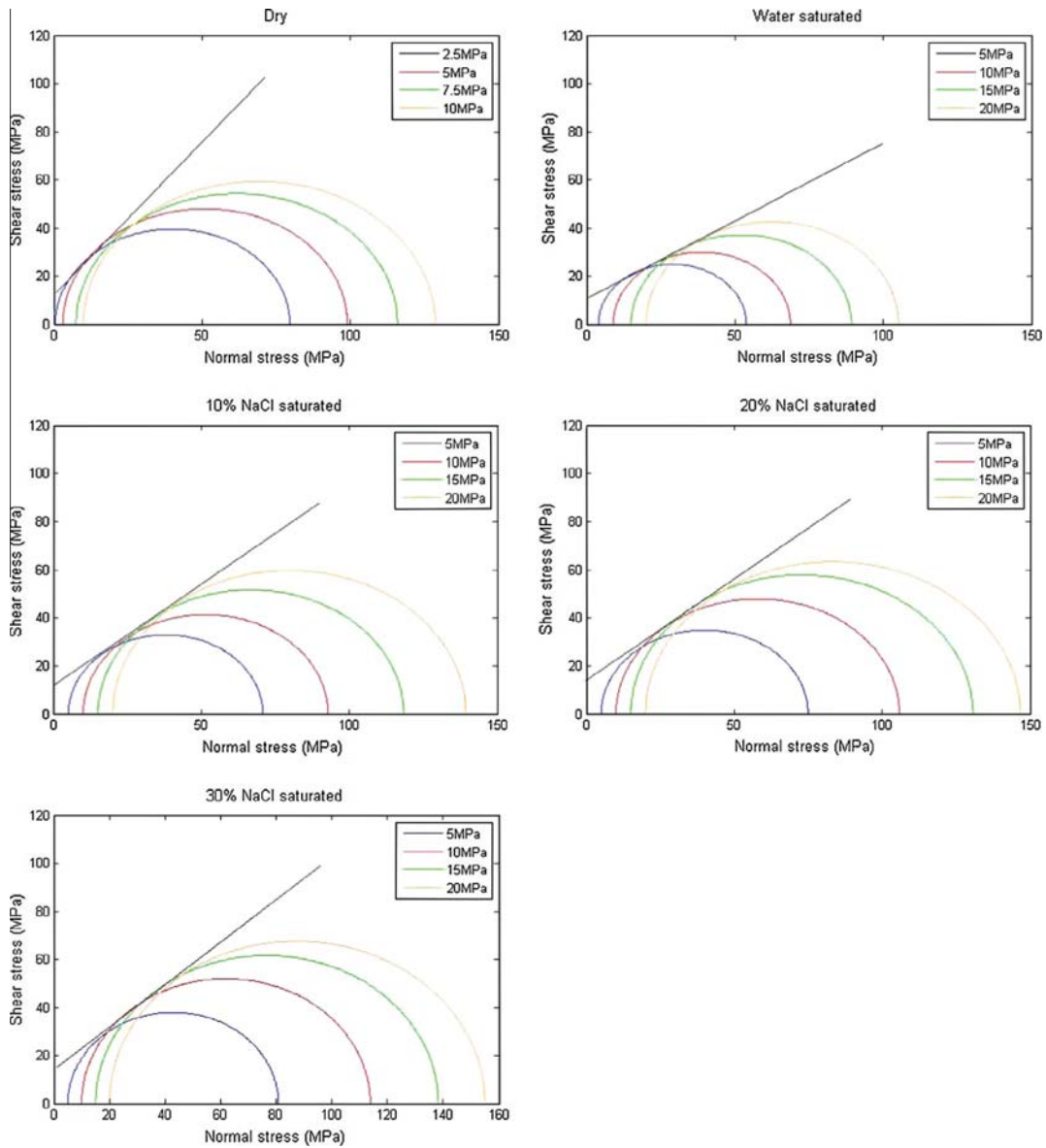


Fig. 8. The corresponding Mohr-Coulomb failure envelopes for dry, water-, 10%, 20% and 30% NaCl-saturated samples.

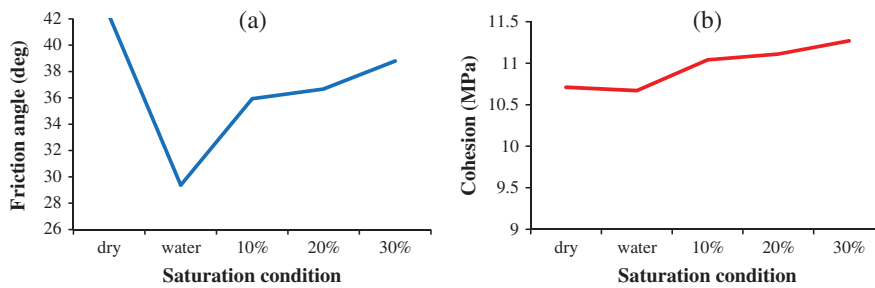


Fig. 9. The variation in (a) friction angle and (b) cohesion with respect to saturation condition.

Table 2
XRD results of dry and 20% NaCl-saturated samples.

Mineral ID	Dry sample (%)	Brine-saturated sample (20% NaCl) (%)
Alpha Quartz	82	80
Kaolinite	8	13
Calcite	4	3
Mica	1	1
Siderite	1	1
Gypsum	1	1
Halite	1	<1
Zeolite	<1	<1
Clinochlore	<1	<1
Talc	0	<1
Anatase	2	1
Dolomite	0	<1
Amphibole	<1	<1

parameters is a real challenge in actual field situations. Therefore, the conventional Mohr–Coulomb failure criterion remains the most widely-used tool for many engineering applications. However, this criterion has two major limitations: (1) it does not capture non-linear behaviour of rocks (failure strength is expressed in terms of linear function of major and minor principal stresses), and (2) it does not consider the intermediate principal stress, although it also makes a considerable contribution to rock mass failure.

According to the results (see Fig. 7), it is clear that the strength response of dry and water-saturated sandstone samples shows linear behaviour in the major (σ_1) and minor (σ_3) principal plane, which is compatible with the Mohr–Coulomb failure criterion. However, NaCl-saturated samples exhibit non-linear responses, even under low confining pressure conditions, and this non-linear behaviour is enhanced with the increasing salinity percentage in the pore fluid (Fig. 7), which is believed to be related to the crystallisation of NaCl in the rock pore space. This implies the inappropriateness of using the conventional Mohr–Coulomb failure criterion for saline aquifers that have brine-saturated rock, mainly sandstone. This was considered in the next stage of the study and the conventional Mohr–Coulomb failure criterion was modified for brine-saturated sandstone.

According to Barton [6] and Hoek [18], the strength response of rocks under high confining pressures may deviate considerably from linear to non-linear. Therefore, Sing et al. [35] modified the conventional Mohr–Coulomb linear criterion for high confining pressures as in Eq. (6).

$$(\sigma_1 - \sigma_3) = \sigma_{ci} + \frac{2 \sin \theta_{i0} \sigma_s}{1 - \sin \theta_{i0}} - \frac{\sin \theta_{i0}}{\sigma_{ci}(1 - \sin \theta_{i0})} \sigma_3^2 \quad (6)$$

Generally, low confining pressure conditions are used to determine the Mohr–Coulomb parameters. Therefore, θ_{i0} is the mobilised friction angle under low confining pressures where σ_3 reaches zero ($\sigma_3 \rightarrow 0$) [35].

It is important to note that this non-linear equation (Eq. (6)) is only applicable up to the critical state ($0 \leq \sigma_3 \leq \sigma_{crit}$). The above non-linear relationship was then modified to capture the NaCl saturation effect. According to Vernik et al. [40], the unconfined compressive

strength can be expressed as a function of porosity (ϕ) as follows:

$$\sigma_{ci} = a \exp^{b\phi} \quad (7)$$

where a , and b are material constants that can change with the physical properties of the rock materials and this relationship is only applicable for sandstones with $2 < \text{UCS} < 360 \text{ MPa}$ and $0.002 < \phi < 0.33$ [40].

The values of the constants a and b were determined based on regression analysis for all saturation conditions (10%, 20% and 30% concentrations of NaCl) combined, and then put in Eq. (7) to estimate the unconfined compressive strength at given porosity levels under tested conditions.

According to Weingarten and Perkins [42], the friction angle of sandstone can be written as a function of porosity as follows:

$$\theta_i = c - d\phi \quad (8)$$

where c and d are material constants.

The a , b , c and d values were determined by regression analysis, as explained by Erguler and Ulusay [12]. In order to determine the a and b values, a series of unconfined compressive strength tests was conducted on NaCl-saturated samples (including 10%, 20% and 30% NaCl) and the porosity measurements were taken by conducting MIP tests, as described by Rathnaweera et al. [31]. The obtained compressive strength and porosity values are shown in Table 3.

The modified Mohr–Coulomb failure criterion can now be written as:

$$(\sigma_1 - \sigma_3) = 394 \exp^{-10\phi} + \frac{2 \sin(44.78 - 112\phi) \sigma_3}{1 - \sin(44.78 - 112\phi)} - \frac{\sin(44.78 - 112\phi)}{(394 \exp^{-10\phi}) [1 - \sin(44.78 - 112\phi)]} \sigma_3^2 \quad (9)$$

It is important to note that this modified Mohr–Coulomb criterion uses only one parameter, ϕ , and this may reduce the complexity of finding Mohr–Coulomb parameters such as cohesion and friction angle. However, the modified criterion is only applicable for the type of sandstone studied under the tested conditions and not be suitable for other types of sandstone formations.

Table 3
Compressive strength and porosity values for brine-saturated samples.

10% NaCl saturated		20% NaCl saturated		30% NaCl saturated	
UCS (MPa)	Porosity	UCS (MPa)	Porosity	UCS (MPa)	Porosity
25.13	0.291	26.33	0.273	26.81	0.271
24.89	0.284	26.78	0.277	27.41	0.268
25.33	0.290	25.83	0.285	27.37	0.265
24.91	0.288	26.12	0.270	27.81	0.273
25.53	0.293	26.57	0.269	26.93	0.264
25.71	0.287	25.91	0.274	27.33	0.266

3.3.3.5. Applicability of proposed failure criterion to NaCl-saturated sandstones

The applicability of the proposed criterion to brine-saturated sandstone was then checked using the measured data. Table 4 shows the standard deviations from measured data (samples saturated with 10%, 20% and 30% concentrations of NaCl) for both the conventional Mohr–Coulomb criterion and the proposed method. As expected, the standard deviations obtained for both cases do not show any significant deviations at low confining pressures (up to 10 MPa), and this confirm the applicability of both criteria to brine-saturated sandstone at low confining pressures (Table 4). However, the situation is completely different at higher confining pressures (>10 MPa), where although the proposed criterion neatly

fits the measured data, the conventional Mohr–Coulomb criterion exhibits a significant deviation. For instance, at 20 MPa confining pressure, the conventional Mohr–Coulomb failure criterion shows standard deviations of 6.135, 13.705 and 9.52 from the experimental data for brine-saturated samples with 10%, 20% and 30% concentrations of NaCl, which are only around 1.128, 0.911 and 1.656 for the proposed criterion. It is important to note that this verification was done using another set of experimental data under confining pressures of 12, 17 and 22 MPa. Fig. 10 shows the comparison of the experimental data with the conventional Mohr–Coulomb criterion and the proposed criterion for each saturation condition. The figure suggests the applicability of the proposed criterion in determining the strength parameters of brine-saturated sandstone compared to the conventional Mohr–Coulomb failure criterion in a triaxial stress environment.

Table 4

Standard deviations with respect to experimental data results for tested samples saturated with 10%, 20% and 30% concentrations of NaCl.

Confining pressure	Standard deviation					
	Mohr–Coulomb			Proposed criterion		
	10%	20%	30%	10%	20%	30%
5	0.295	0	1E–14	0.188	0.399	0.1555
10	0.475	0.055	0	0.153	0.362	0.4675
15	1.93	5.58	3.135	0.6185	0.852	1.033
20	6.135	13.705	9.52	1.1275	0.911	1.656

3.3.3.6. Dilatancy behaviour of reservoir rock under brine saturation

A full understanding of rock fracture phenomena is highly important in many engineering applications, to prevent the collapse of rock engineering structures, to achieve effective fracturing in drilling, blasting, and mining, and to maintain the safety and effectiveness of hydraulic fracturing in oil and gas production. Dilatancy is defined as inelastic increment in rock volume due to applied compressive

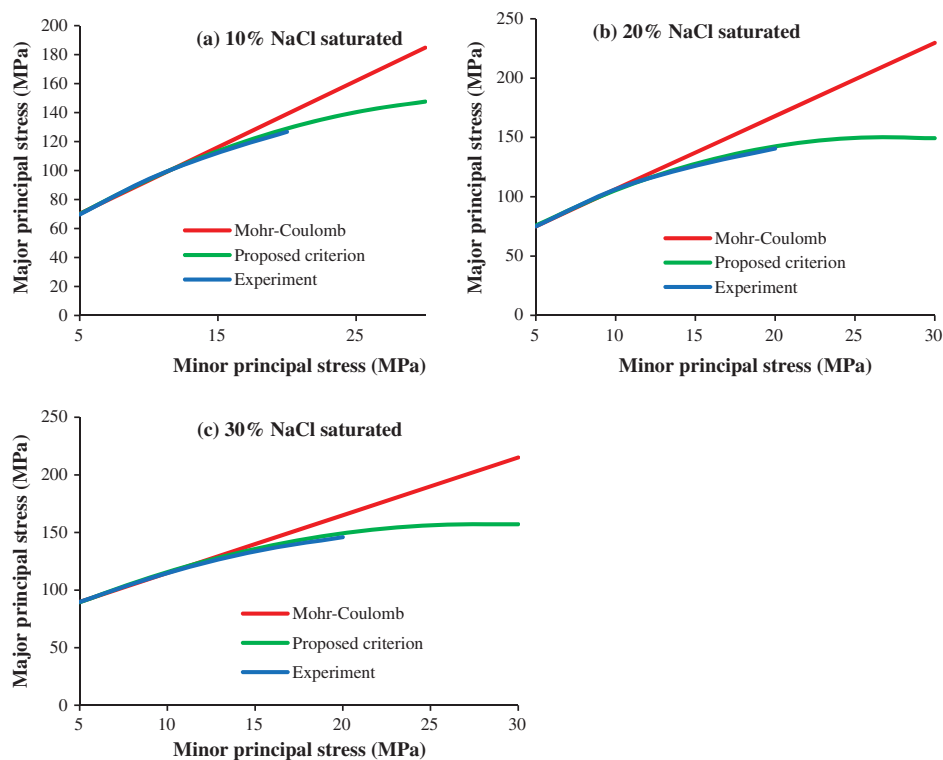


Fig. 10. Comparison of conventional Mohr–Coulomb criterion, proposed strength criterion and experimental data (a) 10% (b) 20% and (c) 30% NaCl-saturated samples.

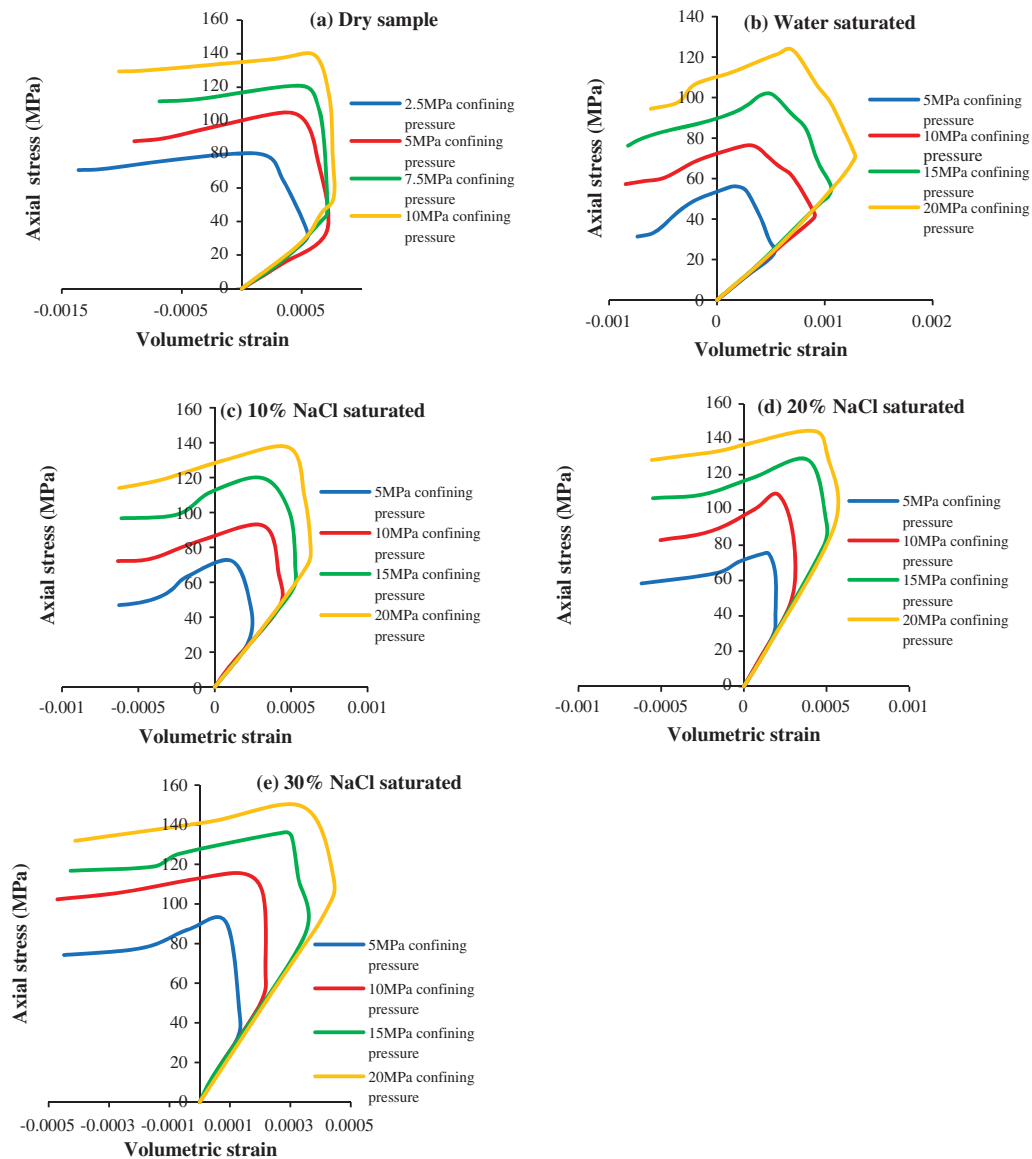


Fig. 11. Axial stress versus volumetric strain curves for each saturation condition of the reservoir rock under confining pressure up to 20 MPa.

stress [21]. This is an important aspect of the fracturing process to characterise the initiation and propagation of micro-fractures, and is very important for brittle failure of rocks [22]. The dilatancy behaviours of the tested sandstone samples were therefore considered in the next stage of the study. The axial stress versus volumetric strain curves for each saturation condition of the reservoir rock under confining pressures up to 20 MPa are given in Fig. 12, where the volumetric strain (ε_v) was calculated using Eq. (10) [21], considering the axial (ε_a) and lateral strain (ε_l). As can be seen from Fig. 12, the curves reverse towards the negative direction, showing the effect of dilation under compression. Interestingly, similar variations

were observed for each tested condition under the tested confining pressures.

$$\varepsilon_v = \varepsilon_a + 2\varepsilon_l \quad (10)$$

According to past studies, dilation initiates and accordingly fractures from when the stress–volumetric strain curve reverses towards the negative direction, and the strength of the rock mass at this point is called its dilatancy strength (σ_v) (Fig. 12) [22,24]. According to Fig. 11, at 5 MPa confining pressure, water saturation causes the dilatancy strength (σ_v) of dry reservoir rock to decrease by around 34.16%, probably due to the water softening effect that leads to the reduction of rock mass

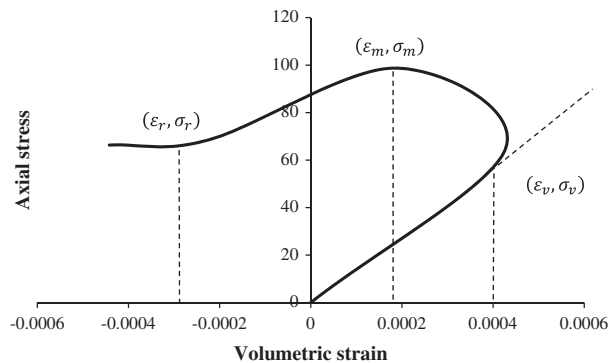


Fig. 12. Definition of dilatancy strength (σ_v), volumetric strain ε_v at σ_v , volumetric strain ε_m at σ_m , volumetric strain ε_r at σ_r and post-peak dilation ($\varepsilon_m - \varepsilon_r$).

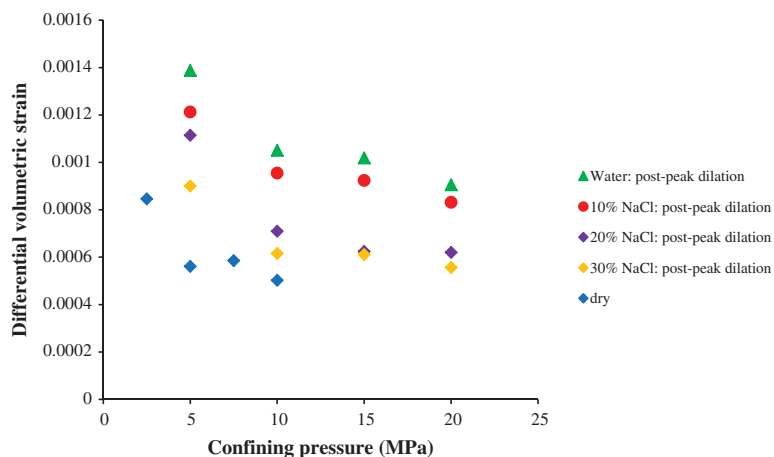


Fig. 13. Post-peak dilation as a function of confining pressures at tested saturation conditions.

surface energy which enhances the fracturing process in rock mass during load application. Interestingly, adding NaCl into water (brine) causes the dilatancy strength of water-saturated sandstone to increase, and there is around 18% increment in dilatancy strength with the addition of 10% of NaCl to the pore water. Moreover, the observed dilatancy strength gain with NaCl (brine) addition to pore water increases with increasing brine concentration, and the increase of NaCl concentration in pore fluid from 20% to 30% causes around 10% dilatancy strength increment in brine-saturated sandstone. Deposition of NaCl crystals seals the pore voids in the rock mass, which reduces its porosity and consequently enhances the micro-fracturing resistivity of the rock mass, resulting in higher dilatancy strength of the reservoir rock. The effect increases with the increase of NaCl concentration in the pore fluid. This is a favourable fact for the long-term integrity of CO₂ sequestration in deep saline aquifers, as decreasing the possibility of micro-fracturing in the reservoir rock (through deposited NaCl crystals) leads to reduction of CO₂ back-migration into the atmosphere.

According to Gowd and Rummel [14], dilation of rocks under low confining pressures (<40 MPa) leads to considerable permanent volume increase in the post-failure region through the development of macroscopic shear faults and the dilation of fault segments during frictional sliding at reduced strength. In order to identify this phenomenon, the term post-peak dilation is used, which is the difference between the mobilised strain and the residual strain (Fig. 12). This extreme condition of the tested samples was checked in the next stage of the study by plotting the values of post-peak dilation against confining pressure (see Fig. 13). According to Fig. 13, the post-peak dilation of the brine-saturated samples is lower than that of the water-saturated samples, and the dilations generally reduce with increasing brine concentration in the pore fluid (10–30% NaCl) and increasing confining pressure. These results indicate that the development of macroscopic shear faults also reduces with increasing NaCl concentration of the pore fluid, which is also favourable for the field CO₂ sequestration process in saline aquifers in terms of safety.

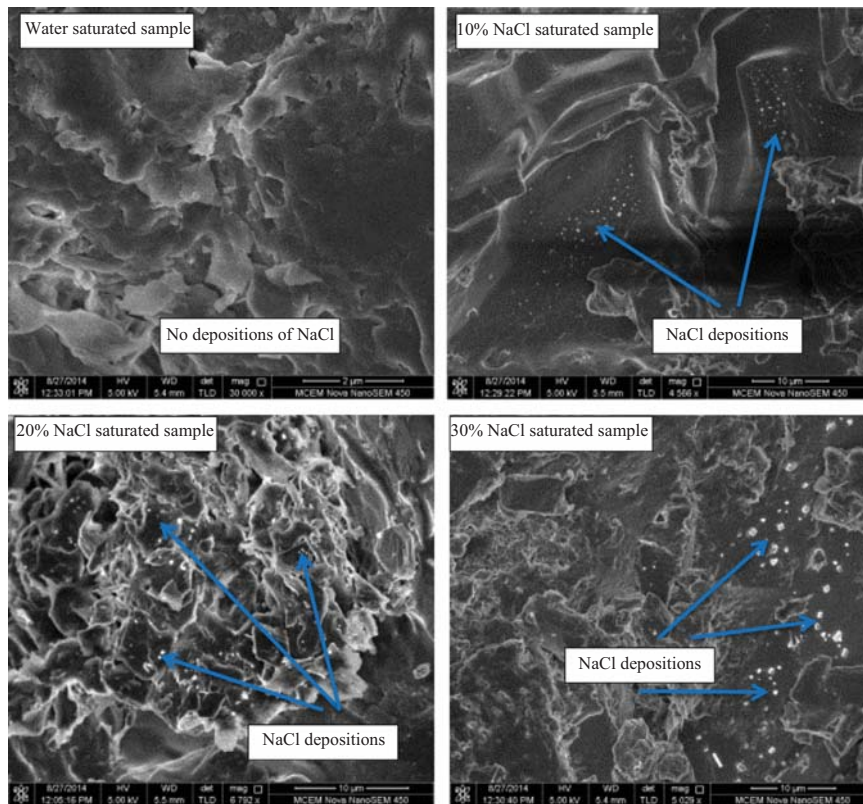


Fig. 14. NaCl depositions in 10%, 20% and 30% NaCl-saturated samples compared to water-saturated sample.

3.3.3.7. Mineralogical and microstructural aspects

Mineralogical and microstructural changes in sandstone due to water/brine saturation were then examined by performing comprehensive micro-structural analyses using XRD and SEM. As expected, a significant amount of NaCl crystals was observed in the rock pore space of brine-saturated samples (Fig. 14). According to the SEM results (Fig. 14), the amount of NaCl crystals clearly increases with the increase of brine concentration (10–30% NaCl). Therefore, the observed stress increment in the brine-saturated samples compared to water-saturated samples clearly relates to the NaCl crystallisation process. For example, at 5 MPa confining pressure, 22.06%, 31.18% and 55.91% axial stress increments and 22.34%, 24.86% and 32.07% friction angle increments were observed in 10%, 20% and 30% NaCl-saturated samples compared to water-saturated samples, respectively. Although this mechanical properties gain with increasing brine concentration has been well shown in existing studies [13,34,30], these studies were conducted under unconfined environments that cannot represent the in situ stress conditions in deep saline aquifers. Therefore, the findings of this study provide a novel data set related to the effect of brine concentration on the strength of reservoir rock under in situ conditions, which is important for field-scale projects.

Further, brine–rock mass interaction made quartz and other mineral deposition and dissolution and NaCl crystallization may cause the surface roughness along the rock matrix to be enhanced, where the effect should be increased with increasing NaCl concentration due to the greater deposition of NaCl and enhanced rock minerals alteration process. This rock mineral alternation is confirmed by the SEM and XRD analyses. The XRD analysis shows significant reductions in quartz and calcite minerals and increments in clay minerals in brine-saturated samples compared to the dry samples (Table 2) and SEM images exhibit rather rough surfaces in brine-saturated samples compared to water-saturated samples (Fig. 15). According to Worden and Morad [45], the morphology of the rock matrix has a significant influence on rock strength and therefore, the expected changes in surface roughness upon brine–rock mass interaction should change the overall strength of the rock mass. Water saturation lubricates the mineral grains, making it easier for them to slip past each other, while creating lower frictional resistance, resulting in reduced strength. However, NaCl crystals deposited in brine-saturated samples reduce this lubrication effect of water and therefore should enhance the frictional strength of the rock mass. This sliding surface topography effect on strength reduction in brittle rocks has been well documented [23,45].

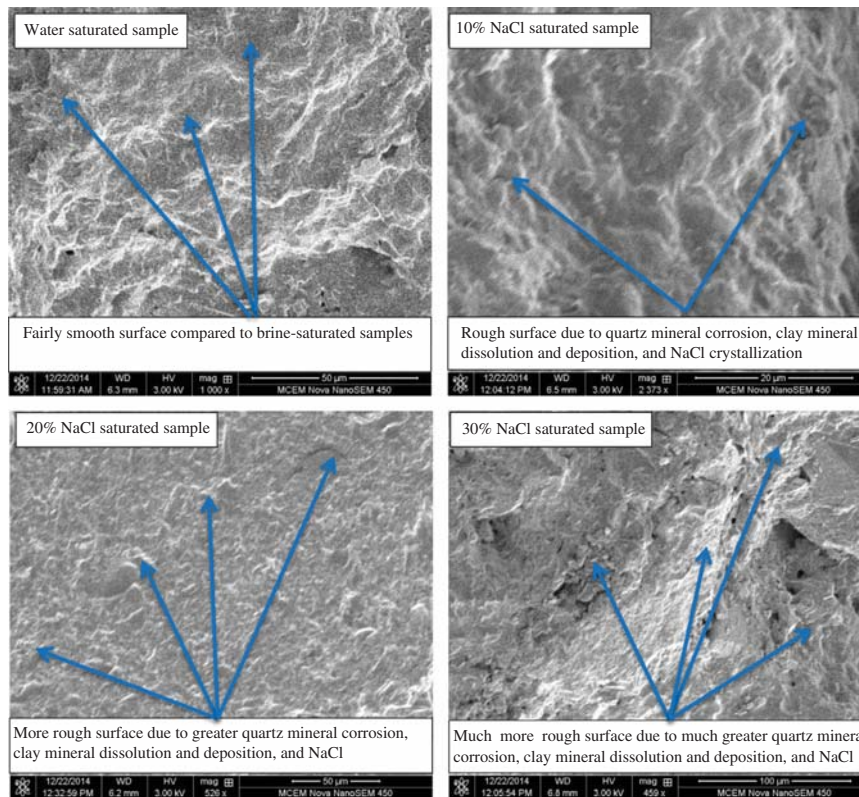


Fig. 15. Development in surface morphology of samples saturated with solutions ranging from 0% (water) to 30% NaCl concentration.

3.3.4. Conclusions

The understanding of the stress–strain behaviour of rocks under in situ stress environments is required in many rock engineering applications, and the Mohr–Coulomb failure criterion is the most commonly used criterion. However, this simple criterion not only neglects the effect of intermediate principal stress, but also assumes a linear behaviour of strength in confined stress environments. These lacks mean that it is inappropriate to use the conventional Mohr–Coulomb failure criterion to simulate the actual non-linear behaviour of deep reservoir rocks and it needs modification depending on the application. In this study, the conventional Mohr–Coulomb failure criterion was modified to account for the non-linear behaviour of brine-saturated reservoir rocks in deep saline aquifers, and model calibration and verification were achieved by conducting a series of tri-axial strength tests. The following conclusions can be drawn based on the results:

- The conventional linear Mohr–Coulomb failure criterion creates a considerable deviation from the measured stress–strain data of Hawkesbury sandstone under brine saturation conditions, especially at high confinements, which can be precisely corrected using the modified failure criterion proposed in this study.
- The presence of NaCl in pore fluid causes the reservoir rock strength to increase in deep saline aquifers, mainly due to the deposition of NaCl crystals in the rock mass pore structure, and this effect increases with increasing brine concentration in the pore fluid and reducing aquifer depth (confinement). For instance, the strength of the tested Hawkesbury sandstone is increased by up to around 21%, 34% and 52% with the presence of 10%, 20% and 30% NaCl in the pore fluid at low confining pressures (5–10 MPa), and these increments are reduced to around 13%, 18% and 25% at high confining pressures (15–20 MPa).
- The presence of NaCl in pore fluid also enhances the shear parameters (friction angle and cohesion) of the reservoir rock. For instance, the cohesion and friction angle of the tested Hawkesbury sandstone increase by around 3.5%, 4% and 5.6% and 22%, 25% and 32% in the presence of 10%, 20% and 30% NaCl concentrations in the pore fluid. The presence of brine causes kaolinite to precipitate in the rock mass, and this affects the cohesion of the rock mass. In contrast, the presence of brine causes NaCl crystals in the rock mass pore structure which affect its friction angle, are both effects increase with increasing brine concentration in the pore fluid.
- The presence of brine causes the dilatancy strength of saline aquifer rocks to be enhanced, and the presence of 10%, 20% and 30% NaCl in the pore fluid under

5 MPa confining pressure causes the dilatancy strength of the tested brine-saturated Hawkesbury sandstone to increase by around 18%, 25% and 29% compared to water-saturated samples, respectively. This is because the deposition of NaCl crystals in the reservoir rock mass pore structure reduces its porosity, and consequently enhances the micro-fracturing resistivity of the rock mass. This is favourable for the long-term integrity of CO₂ sequestration in deep saline aquifers, as it leads to the reduction of CO₂ back-migration into the atmosphere.

- In addition, the presence of NaCl in the pore fluid reduces post-peak dilation (at which macroscopic shear faults may occur in the rock mass) of the saline aquifer rock mass, and the effect increases with increasing brine concentration in the pore fluid and increasing depth (confining pressure). This is also favourable for the safety of CO₂ sequestration in saline aquifers.

3.3.5. References

- [1] A.M. Ajmi, R.W. Zimmerman, Stability analysis of vertical borehole using the Mogi–Coulomb failure criterion, *Int. J. Rock Mech. Min. Sci.* 43 (2006) 1200–1211.
- [2] A.M. Al-Ajmi, R.W. Zimmerman, Relation between the Mogi and the Coulomb failure criteria, *Int. J. Rock Mech. Min. Sci.* 42 (2005) 431–439.
- [3] M.F. Ashby, C.G. Sammis, The damage mechanics of brittle solids in compression, *Pure Appl. Geophys.* 133 (1990) 489–521.
- [4] B.K. Atkinson, P.G. Meredith, Experimental fracture mechanics data for rocks and minerals, *Fract. Mech. Rock* 23 (1987) 477–525.
- [5] S. Bachu, B. Bennion, Effects of in-situ conditions on relative permeability characteristics of CO₂–brine systems, *Environ. Geol.* 54 (2008) 1707–1722.
- [6] N. Barton, The shear strength of rock and rock joints, *Int. J. Rock Mech. Min. Sci.* 13 (1976) 255–279.
- [7] P. Baud, W. Zhu, T. Wong, Failure mode and weakening effect of water on sandstone, *J. Geophys. Res.* 105 (2000) 16371–16389.
- [8] R.G. Bruant, A.J. Guswa, M.A. Celia, C.A. Peters, Safe storage of CO₂ in deep saline aquifers, *Environ. Sci. Technol.* 36 (2002) 240A–245A.
- [9] B. Chang, B. Haimson, Non-dilatant deformation and failure mechanism in two Long Valley Caldera rocks under true triaxial compression, *Int. J. Rock Mech. Min. Sci.* 42 (2005) 402–414.
- [10] M.E. Chenevert, C. Gatlin, Mechanical anisotropies of laminated sedimentary rocks, *Soc. Petrol. Eng. J.* 5 (1965) 221–232.
- [11] F.M. Chester, J.M. Logan, Implication for mechanical properties of brittle faults from observations of the punchbowl fault zone, *Pure Appl. Geophys.* 124 (1986) 79–126.
- [12] Z.A. Erguler, R. Ulusay, Water-induced variations in mechanical properties of clay-bearing rocks, *Int. J. Rock Mech. Min. Sci.* 46 (2009) 355–370.
- [13] L.J. Feucht, J.M. Logan, Effect of chemically active solutions on shearing behaviour of a sandstone, *Tectonophysics* 175 (1990) 159–176.
- [14] T.N. Gowd, F. Rummel, Effect of confining pressure on fracture behaviour of a porous rock, *Int. J. Rock Mech. Min. Sci.* 17 (1980) 225–229.
- [15] A.B. Hawkins, B.J. McConnell, Sensitivity of sandstone strength and deformability to changes in moisture content, *Eng. Geol.* 25 (1992) 115–130.
- [16] J.D. Hem, Study and interpretation of the chemical characteristics of natural water. U.S. Geology Survey and Water-Supply; vol. 54, 1959, pp. 1473–1482.
- [17] E. Hoek, E. Brown, Empirical strength criterion for rock masses, *J. Geotech. Eng. ASCE* 106 (GT9) (1980) 1013–1035.
- [18] E. Hoek, Strength of jointed rock masses, *Geotechnique* 23 (3) (1983) 187–223.
- [19] H. Horii, S. Nemat-Nasser, Brittle failure in compression: splitting, faulting and brittle-ductile transition, *Philos. Trans. R. Soc. Lond.* 319 (1986) 337–374.
- [20] ISRM, ISRM suggested methods: rock characterization, testing and monitoring, in: E.T. Brown (Ed.), Pergamon, London, 1981.
- [21] J.C. Jaeger, N.G.W. Cook, *Fundamentals of Rock Mechanics*, 3rd ed., Chapman and Hall, London, 1979.
- [22] E.Z. Lajtai, Microscopic fracture processes in a granite, *Rock Mech. Rock Eng.* 31 (1998) 237–250.
- [23] J.M. Logan, L.W. Teufel, The effect of normal stress on the real area of contact during frictional sliding of rocks. In: T. Tullis (Ed.), *Frictional Properties of Rocks and Fault Zones*. Pure Applied Geophysics, vol. 124, 1987, pp. 471–486.
- [24] L. Ma, J.J.K. Daemen, Strain rate dependent strength and stress-strain characteristics of a welded tuff, *Eng. Geol. Environ.* 65 (2006) 221–230.
- [25] H. Marbler, K.P. Erickson, M. Schmidt, C. Lempp, H. Pollmann, Geomechanical and geochemical effects on sandstone caused by the reaction with supercritical CO₂: an experimental approach to in situ conditions in deep geological reservoirs, *Environ. Earth Sci.* 69 (2013) 1981–1998.
- [26] K.K. Mohan, M.G. Reed, H.S. Fogler, Formation damage in smectitic sandstones by high ionic strength brines, *Colloids Surf. A* 154 (1999) 49–57.
- [27] E. Orowan, The fatigue of glass under stress, *Nature* 154 (1944) 341–343.
- [28] M.S. Peterson, *Experimental Rock-deformation-the Brittle Field*, Springer Verlag, New York, 1978.
- [29] P. Ranjith, M. Perera, E. Khan, A study of safe CO₂ storage capacity in saline aquifers: a numerical study, *Int. J. Energy Res.* 37 (2013) 189–199.
- [30] T.D. Rathnaweera, P.G. Ranjith, M.S.A. Perera, Salinity-dependent strength and stress–strain characteristics of reservoir rocks in deep saline aquifers: an experimental study, *Fuel* 122 (2014) 1–11.
- [31] T.D. Rathnaweera, P.G. Ranjith, M.S.A. Perera, Effect of salinity on effective CO₂ permeability in reservoir rock determined by pressure transient methods: an experimental study on Hawkesbury sandstone, *Rock Mech. Rock Eng.* (2014), <http://dx.doi.org/10.1007/s00603-014-0671-0>.
- [32] E.H. Rutter, D.H. Mainprice, The effect of water on stress relaxation of faulted and unfaulted sandstone, *Pure Appl. Geophys.* 116 (1978) 634–654.
- [33] F.J. Santarelli, E.T. Brown, Failure of three sedimentary rocks in triaxial and hollow cylinder compression tests, *Int. J. Rock Mech. Min. Sci.* 26 (5) (1989) 1100–1012.
- [34] R. Shukla, P.G. Ranjith, S.K. Choi, A. Haque, M. Yellishetty, L. Hong, Mechanical behaviour of reservoir rock under brine saturation, *Rock Mech. Rock Eng.* 46 (1) (2013) 83–89.
- [35] M. Sing, A. Raj, S. Bhawani, Modified Mohr–Coulomb criterion for non-linear triaxial and polyaxial strength of intact rocks, *Int. J. Rock Mech. Min. Sci.* 48 (2011) 546–555.
- [36] J. Sulem, H. Ouffroukh, Shear banding in drained and undrained triaxial tests on saturated sandstone: porosity and permeability evolution, *Int. J. Rock Mech. Min. Sci.* 43 (2006) 292–310.
- [37] B. Vasarhelyi, Some observations regarding the strength and deformability of sandstone in case of dry and saturated conditions, *Eng. Geol.* 62 (2003) 245–249.
- [38] B. Vasarhelyi, Statistical analysis of the influence of water content on the strength of the Miocene limestone, *Rock Mech. Rock Eng.* 38 (2005) 69–76.
- [39] B. Vasarhelyi, P. Van, Influence of water content on the strength of rock, *Eng. Geol.* 84 (2006) 70–74.
- [40] L. Vernik, M. Bruno, C. Bovberg, Empirical relations between compressive strength and porosity of siliciclastic rocks, *J. Rock Mech. Min. Sci.* 30 (1993) 677–680.
- [41] P.L.P. Wasantha, W.J. Darlington, P.G. Ranjith, Characterization of mechanical behaviour of saturated sandstone using a newly developed triaxial apparatus, *Exp. Mech.* 53 (2013) 871–882.
- [42] J.S. Weingarten, T.K. Perkins, Prediction of sand production in gas wells: methods and Gulf of Mexico case studies, *J. Petrol. Technol.* 14 (1995) 596–600.
- [43] C.U. White, B.R. Strazisar, E.J. Granite, J.S. Hoffman, H.W. Pennline, Separation and capture of CO₂ from large stationary sources and sequestration in geological formations-coalbeds and deep saline aquifers, *J. Air Waste Manag. Assoc.* 53 (6) (2003) 645–715.
- [44] T.F. Wong, C. David, W. Zhu, The transition from brittle faulting to cataclastic flow in porous sandstones: mechanical deformation, *J. Geophys. Res.* 102-B2 (1997) 3009–3025.
- [45] R.H. Worden, S. Morad, Clay minerals in sandstones: controls on formation, distribution and evaluation, *Int. Assoc. Sedimentol.* 34 (2003) 3–41.
- [46] J. Zhang, T.F. Wong, D.M. Davis, Micromechanics of pressure-induced grain crushing in porous rocks, *J. Geophys. Res.* 95 (B1) (1990) 341–352.

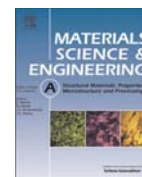
3.4 CO₂-induced mechanical behaviour of reservoir rock under uniaxial stress conditions

According to Sections 3.2 and 3.3, it is now clear that salinity has considerable effects on deep saline reservoir rock and therefore, understanding of these effects is important prior to any CO₂ sequestration project. However, with CO₂ injection, a deep saline aquifer undergoes a variety of chemical and mineralogical effects, which may create CO₂-induced mechanical changes and time-dependent reservoir deformation during deep saline sequestration. In CO₂ sequestration, the injected CO₂ first reacts with the aquifer brine and produces weakly acidic carbonic acid. The resulting acidic environment then reacts with reservoir rock minerals and creates completely different mineral and microstructures compared to the natural conditions. Therefore, a comprehensive study was conducted to evaluate the CO₂ injection-induced mechanical behaviour of Hawkesbury sandstone and the results are presented in this section. First, reservoir rock samples were reacted with super-critical CO₂ and brine, and complete mineralogical and microstructural analyses were conducted on the samples. After mineralogically characterisation of the samples, a series of uniaxial strength tests was carried out, integrating the use of acoustic emission (AE) monitoring and digital image correlation technology. This study is reported in a published journal paper entitled “*CO₂-induced mechanical behaviour of Hawkesbury sandstone in the Gosford basin: An experimental study*”.



Contents lists available at ScienceDirect

Materials Science & Engineering A

journal homepage: www.elsevier.com/locate/msea

CO₂-induced mechanical behaviour of Hawkesbury sandstone in the Gosford basin: An experimental study



T.D. Rathnaweera^a, P.G. Ranjith^{a,*}, M.S.A. Perera^a, A. Haque^a, A. Lashin^{b,c}, N. Al Arifi^d, D Chandrasekharam^{d,e}, SQ Yang^{a,f}, T Xu^g, SH Wang^g, E Yasar^h

^a Department of Civil Engineering, Monash University, Building 60, Melbourne, Victoria 3800, Australia

^b King Saud University, College of Engineering–Petroleum and Natural Gas Engineering Department, P.O. Box 800, Riyadh 11421, Saudi Arabia.

^c Benha University, Faculty of Science–Geology Department, P.O. Box 13518, Benha, Egypt

^d King Saud University, College of Science–Geology and Geophysics Department, P.O. Box 2455, Riyadh 11451, Saudi Arabia.

^e Department of Earth Sciences, Indian Institute of Technology Bombay, 400076 India

^f State Key Laboratory for Geomechanics and Deep Underground Engineering, China University of Mining and Technology, Xuzhou 221116, PR China

^g Center for Rock Instability & Seismicity Research, Northeastern University, Shenyang 110819, PR China

^h Iskenderun Technical University, Faculty of Mechanical Engineering, Dept. of Petroleum & Natural Gas Engineering, 31200, Turkey

ARTICLE INFO

Article history:

Received 24 March 2015

Received in revised form

11 May 2015

Accepted 11 May 2015

Available online 11 June 2015

Keywords:

CO₂ sequestration

Saline aquifers

Strength

Crack formation

Microstructure

CO₂ storage in Australia

ABSTRACT

Carbon dioxide (CO₂) sequestered in saline aquifers undergoes a variety of chemically-coupled mechanical effects, which may cause CO₂-induced mechanical changes and time-dependent reservoir deformation. This paper investigates the mineralogical and microstructural changes that occur in reservoir rocks following injection of CO₂ in deep saline aquifers and the manner in which these changes influence the mechanical properties of the reservoir rocks. In this study, cylindrical sandstone specimens, 38 mm in diameter and 76 mm high, obtained from the Gosford basin, were used to perform a series of unconfined compressive strength (UCS) tests. Different saturation conditions: dry, water- and brine-saturated sandstone samples with and without scCO₂ (super-critical carbon dioxide) injection, were considered in the study to obtain a comprehensive understanding of the impact of scCO₂ injection during the CO₂ sequestration process on saline aquifer mechanical properties.

An acoustic emission (AE) system was employed to identify the stress threshold values of crack closure, crack initiation and crack damage for each testing condition during the whole deformation process of the specimens. Finally, scanning electron microscopy (SEM), X-ray diffraction (XRD) and X-ray fluorescence (XRF) analyses were performed to evaluate the chemical and mineralogical changes that occur in reservoir rocks during CO₂ injection. From the test results, it is clear that the CO₂-saturated samples possessed a lower peak strength compared to non-CO₂ saturated samples. According to SEM, XRD and XRF analyses, considerable quartz mineral corrosion and dissolution of calcite and siderite were observed during the interactions of the CO₂/water/rock and CO₂/brine/rock systems, which implies that mineralogical and geochemical rock alterations affect rock mechanical properties by accelerating the collapse mechanisms of the pore matrix. AE results also reveal the weakening effect of rock pore structure with CO₂ injection, which suggests a significant effect of CO₂ on failure mechanisms of the reservoir rock, with CO₂ saturation showing a significant influence on crack initiation and crack damage stages.

© 2015 Elsevier B.V. All rights reserved.

3.4.1. Introduction

Carbon capture and storage (CCS) is one of the best ways to reduce anthropogenic CO₂ emissions into the atmosphere. According to the United Nations (UN) statistical estimation, the

annual carbon dioxide (CO₂) emission in Australia is about 430,000 t per year, which represents 1.34% of the world's total CO₂ emissions [46]. In order to reduce greenhouse gas emissions, scientists have made various proposals. Of these, CO₂ sequestration in deep saline aquifers has attracted the attention of the scientific media and the general public due to its unique advantages. For instance, the CO₂ storage capacity of saline aquifers compared to other geological media has been estimated to be between 320 Gt CO₂ and 200,000 Gt CO₂, with a life-time of more than 100 years [3].

* Correspondence to: Deep Earth Energy Laboratory, Monash University, Building 60, Melbourne, Victoria 3800, Australia. pranav.ranjith@monash.edu

Generally, geo-sequestration of CO₂ in deep saline aquifers involves a number of steps, including CO₂ capture, transport and injection deep under the surface through wells. In many sequestration projects, the injection of CO₂ is the most important step, and needs to be carefully conducted and monitored for the long-term integrity of the sequestration project. The captured CO₂ is injected into the aquifer in a compressed form as a super-critical phase fluid (temperature $\geq 31.48^\circ\text{C}$, pressure $\geq 7.38\text{ MPa}$ [33]). The injected CO₂ is then trapped in the aquifer through a number of mechanisms including solubility trapping, residual trapping, mobility trapping and mineral trapping, with solubility trapping being the dominant trapping mechanism for rock mineral alteration, while mineral trapping makes a small contribution to rock mineral alteration [10] during CO₂ sequestration. Normally, saline aquifers consist of sedimentary rocks, mainly sandstone, and lie at depths between 800 and 2000 m. Most are highly saline, with salinity values varying between 100,000 (10% NaCl by weight) to 300,000 ppm (30% NaCl by weight) [42]. As a consequence, the interaction between highly saline aquifer pore fluid and super-critical carbon dioxide (scCO₂) creates significant changes in the chemical and mineralogical structures of the aquifer formation.

As shown in Fig. 1, depending on the degree of saturation and the saturation medium of the reservoir rock mass, there are three different saturated reaction zones in saline aquifers: fully CO₂-saturated, fully brine-saturated and mixed saturated [26,19,12]. The fully CO₂-saturated zone forms adjacent to the injection well due to forced brine migration and the fully brine-saturated zones are created in more remote areas due to the absence of excess CO₂. The mixed zone, which is characterized by both CO₂ and brine-saturated rocks, is formed in the region between. Therefore, it is clear that differently saturated rock masses may exist at the same time within the reservoir during CO₂ injection. However, due to the lack of understanding of this aspect, detrimental effects, such as back-migration of the injected CO₂ into the atmosphere, heaving in the ground surface, reservoir compaction and contamination of fresh water from the injected CO₂, may occur during the CO₂ sequestration process in saline aquifers. To date, little consideration has been given to the prediction of the effects of CO₂/water/rock and CO₂/brine/rock chemical interactions on rock properties under in situ conditions, which raises the importance of the appropriate evaluation of the chemical–mechanical responses of saline aquifers to CO₂ injection under different stress environments.

The aim of this study was to discover the effect of the interaction between CO₂/water/rock and CO₂/brine/rock systems on the mechanical properties of aquifer formations under the super-critical condition of CO₂. In addition, this study presents the findings of a laboratory investigation into the identification and characterization of CO₂-induced failure patterns and damage mechanisms of fully saturated reservoir rock under high concentrations of NaCl and CO₂ by integrating the use of acoustic emission (AE) monitoring and digital image correlation technology. Finally, X-ray diffraction (XRD), X-ray fluorescence (XRF) and scanning

electron microscopy (SEM) analyses were carried out to verify the results by correlating possible changes in chemical and mineral structures.

3.4.2. The CO₂-water/brine system and its influence on rock properties

Dissolution of CO₂ is the fundamental reaction for solubility trapping in CO₂ sequestration in deep saline aquifers. According to past studies, CO₂ readily reacts with water to form carbonic acid [22,36]. The reaction can be represented by the following chemical equation:



The solubility of CO₂ in fresh water mainly depends on the temperature and pressure, and is normally lower at higher temperatures and higher at elevated pressures [36]. According to Rosenbauer et al. [36], the maximum dissolution occurs at 50 °C and the dissolution constant decreases with increasing temperature above 50 °C. Koide et al. [22] suggested that cooler aquifers can store more CO₂, as the solubility of CO₂ increases with decreasing temperature.

The solubility reaction of CO₂ in brine is highly sensitive to temperature and pressure and also to the salt concentration of the brine (ionic strength). The influences of temperature and pressure on the solubility of CO₂ in brine have been extensively studied by a number of researchers [15,45,40,6]. The effect of NaCl concentration on the solubility of CO₂ has also been studied in detail by Lagneau et al. [24]. According to Lagneau et al. [24], the solubility of CO₂ in brine increases with pressure and decreases with temperature, while at constant pressure CO₂ dissolution decreases with increasing salinity due to the salting-out effect. In addition, Oshumi et al. [29] illustrated the rise in density of water with increasing CO₂ concentration by conducting experiments under deep-sea conditions. The geo-mechanical effects of short-term and long-term exposure of scCO₂ and brine on reservoir rock are still not completely understood. Normally, CO₂ injection does not create any significant mineralogical changes in the reservoir rock in the initial period of injection, and such changes occur slowly and increase only after around 200 years. Therefore, these changes are generally considered as a long-term effect of CO₂ injection into saline aquifers [32]. However, some recent studies have shown significant changes in reservoir rock's mineral structure in saline aquifers due to short-term exposure to CO₂ [41]. For example, Marbler et al. [26] found a clear variation in the mineralogical structure and the mechanical properties of sandstone samples obtained from the North German basin after short-term exposures (2–4 weeks) to scCO₂ and brine. According to Feng et al. [7], the characteristics of the aquifer fluid, including pH, ionic composition and ionic strength, significantly affect rock strength, crack initiation and propagation and finally its instability. Feucht and Logan [8] have shown a significant mechanical weakening in reservoir rock at low and high ionic strengths of the pore fluid and, interestingly, a mechanical strengthening effect under the intermediate ionic strength condition. This is not consistent with the findings of Shukla et al. [42], who showed a trend of reduction of reservoir strength at low ionic strengths of the host fluid (0–5% NaCl concentration) and an increasing trend of reservoir strength with increasing ionic strength for higher ionic strengths of the host fluid (greater than 5% NaCl concentration).

Generally, the long-term safety of the CO₂ sequestration process in saline aquifers is largely dependent on cap rock stability during CO₂ injection [47,38,44]. Laterally migrating saline water may create brine leakage out of the formation vertically upward

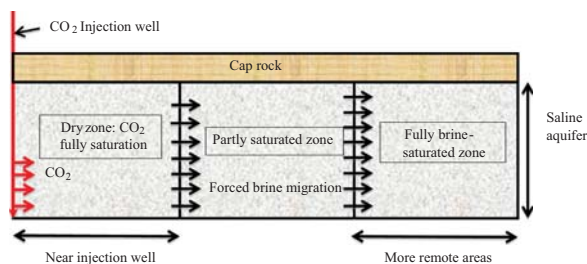


Fig. 1. Formation of differently saturated zones during injection of CO₂

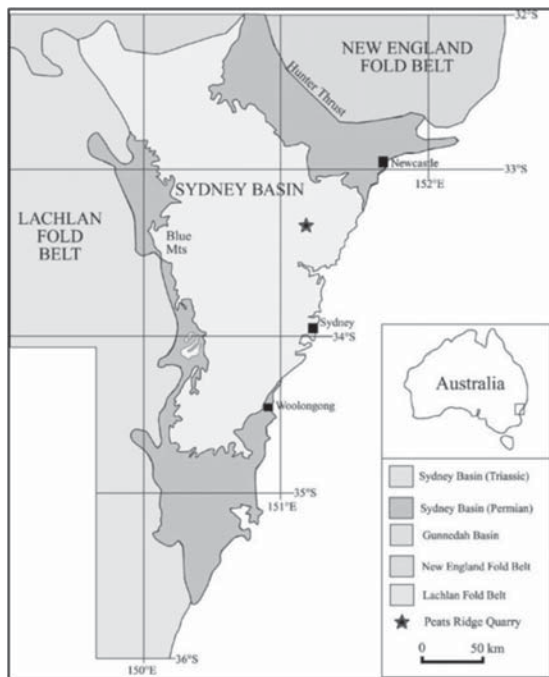


Fig. 2. Simplified geological map of the Sydney Basin, Australia [37].

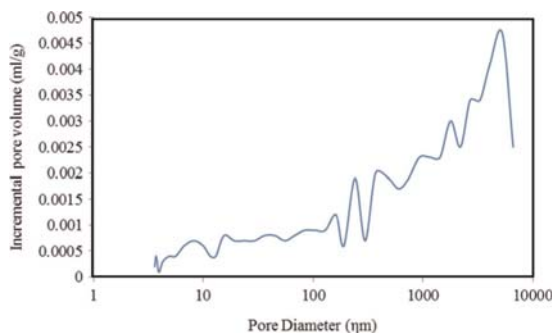


Fig. 3. MIP test results: relationship between pore diameter and incremental pore volume.

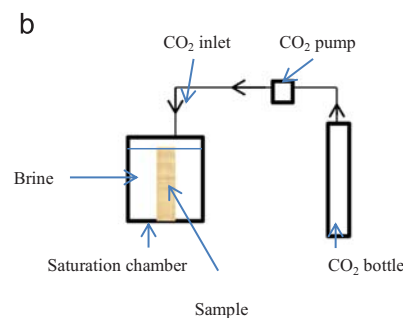
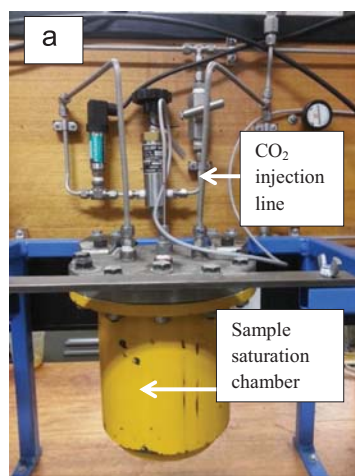


Fig. 4. (a) CO₂ rig used to achieve the partly-saturated condition in sandstones and (b) a schematic diagram of saturation rig.

and/or downward due to pressure variations among the formations, and eventually contaminate groundwater aquifers [2]. According to Sibson and Rowland [43] and Wibberley and Shimamoto [49], the existence of faults in cap rock and reservoir rock significantly enhances CO₂ leakage into the atmosphere and surrounding rock masses during the sequestration process in saline aquifers, and stress variations in fault zones lead to seismic or aseismic slippage in the brittle part of the crust. Rutqvist et al. [39] observed around 5 mm per year surface uplift in the cap rock near the injection well in the saline aquifer they studied. Although different pore fluid types (H₂O, argon and CO₂ as pore fluids) create different effects on the reservoir rock strength, water saturation creates the highest strength reduction (30–40% reduction compared to dry strength) in reservoir rock [18,16], and scCO₂ saturation creates the greatest shear modulus reduction (6–8% reduction compared to water-saturated samples at 15 MPa differential pressure) [41].

3.4.3. Experimental procedure

3.4.3.1. Sandstone samples

The sandstone samples were collected from the Hawkesbury sandstone unit in the Gosford quarry in the Sydney basin, Australia and belong to the early Triassic age [48]. Fig. 2 shows a simplified geological map of the Sydney basin. Hawkesbury sandstone has a grain size between 0.04 and 1.0 mm with a predominantly argillaceous matrix. The nature of the colour banding and the density of colour in Hawkesbury sandstone are decided by the concentration and distribution of iron oxides present in the sample mineralogy. According to XRD results, the mineral composition of this dry sandstone includes 85% quartz, 5% calcite, 1% siderite, 1% mica, 5% kaolinite, 2% anatase and 1% amphibole. The main cementing phases of the selected sandstone consist of quartz, calcite and kaolinite. According to Shukla et al. [42], the existence of clay minerals in the sandstone pore matrix enhances the rock strength.

3.4.3.2. Sample preparation

The sandstone blocks were first cored according to ASTM standards in the Deep Earth Energy Laboratory and both ends of each specimen were then carefully ground to produce flat parallel surfaces to ensure uniform load distribution. The 38 mm in diameter and 76 mm in length sandstone samples were then tested to obtain the required specific rock parameters: density, water

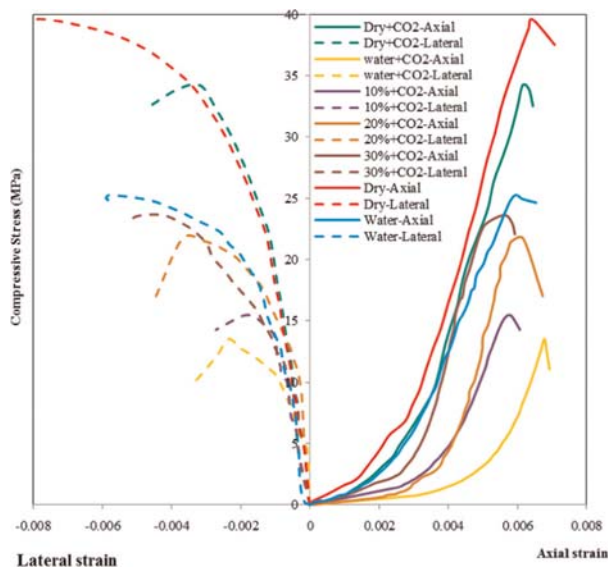


Fig. 5. Stress-strain curves for tested specimens.

absorption and porosity. The water absorption capacity of the tested sandstone was around 4.4% (by weight) and the porosity around 37.24% based on mercury intrusion porosimetry (MIP) tests. The relationship between the pore diameter of the sample and the incremental pore volume is shown in Fig. 3.

Two sets of samples were considered without scCO₂ saturation and with scCO₂ saturation, and both sets included dry and water- and brine-saturated (with different NaCl concentrations of 10%, 20% and 30% NaCl) reservoir rock samples. The experimental data relevant to the former samples, those without scCO₂-saturation, were obtained from [34] and only the latter type of samples, those with scCO₂ saturation, were tested in the present study.

In order to achieve the fully water- or brine-saturated condition in the former type of samples (without scCO₂ saturation), Rathnaweera and Ranjith [34] kept each sample in desiccators under vacuum. However, the preparation of the latter type of sample (with scCO₂ saturation) in the present study required a high pressure chamber to inject scCO₂ into the dry or brine-saturated or water-saturated samples and the following set-up was used for that purpose (see Fig. 4). Here, similar to [34], the samples were first vacuum-saturated in desiccators to produce fully brine- (with different NaCl concentrations of 10%, 20% and 30% NaCl) or water-saturated samples, and the saturated samples were then kept in the reaction chamber at 32 °C. The reaction chamber was then filled with brine or water (brine (with different NaCl concentrations of 10%, 20% and 30% NaCl) for brine-saturated samples and water for water-saturated samples) and CO₂ was finally injected into the sample at 8 MPa injection pressure and 32 °C for four months (Fig. 4(b)). In the case of the dry samples, samples were kept in the chamber without brine/water and CO₂ was injected into the dry samples for four months. Table 1 shows the summary of saturation mediums and the number of replicates used in the study.

3.4.3.3. Testing procedure

Thirty-nine unconfined compression tests were performed on the cylindrical sandstone samples at the Monash University Deep Earth Energy Laboratory to quantify the effect of scCO₂ saturation on reservoir rock, following the specifications outlined in the ASTM standards. A Shimadzu AG 9 compression machine with a

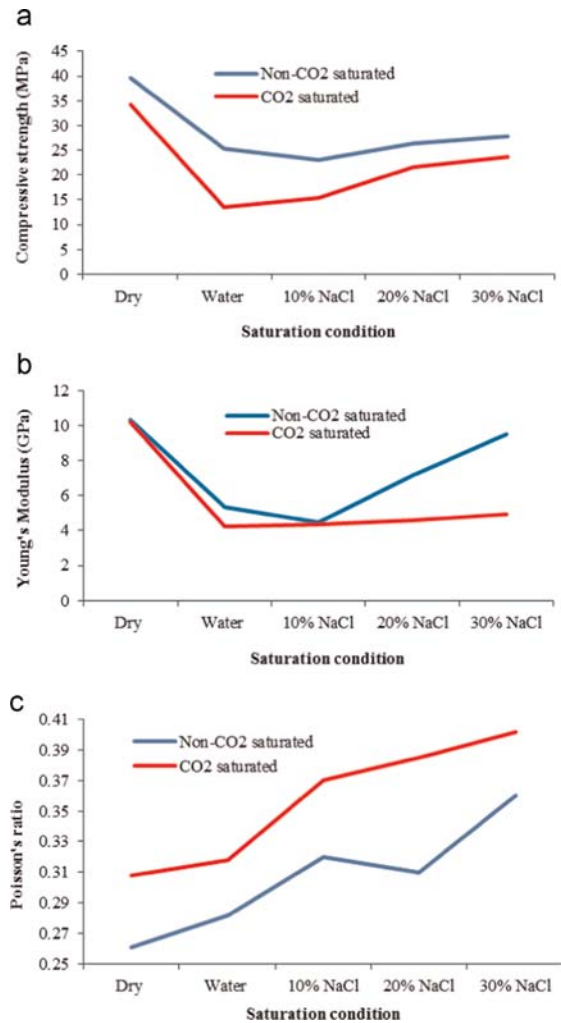


Fig. 6. Effects of CO₂ injection on reservoir rock (a) average unconfined compressive strength, (b) Young's modulus and (c) Poisson's ratio.

Table 1
Summary of saturation mediums and number of replicates used.

Saturation medium	Saturation conditions	Number of samples
Dry condition (without any saturation)	Room temperature	3
Water saturation [34]	Room temperature	4
CO ₂ saturation (dry condition)	8 MPa, 32° C	4
CO ₂ + Water saturation	8 MPa, 32° C	4
10% NaCl brine [34]	Room temperature	4
20% NaCl brine [34]	Room temperature	4
30% NaCl brine [34]	Room temperature	4
CO ₂ + brine with 10% NaCl	8 MPa, 32° C	4
CO ₂ + brine with 20% NaCl	8 MPa, 32° C	4
CO ₂ + brine with 30% NaCl	8 MPa, 32° C	4

maximum compression load capacity of 300 kN was used to conduct the uniaxial compression (UCS) tests and the load was applied at 0.1 mm/min rate (a 300 kN load was gradually applied by slowly dropping the load onto the sample at a 0.1 mm/min rate). The applied load was recorded using an advanced data acquisition system and the corresponding strains were recorded using digital

image correlation technology (a computerised system with a 3-D camera which captures both axial and lateral strains based on an image processing system), which was also used to analyse the images of strain distribution. The necessary basic corrections, including displacement correction and filter correction, were carried out to obtain better resolution during the loading stages. The observed deformations were then analysed using a non-contact optical 3-D metrology system to obtain average values for both axial and lateral displacements.

3.4.3.4. Acoustic emission (AE) methodology

The acoustic emission (AE) system available in Monash University's Deep Earth Energy Laboratory was used to identify the effect of scCO₂ saturation on the fracturing process of reservoir rock. The PCI (peripheral component interconnection) 2-channel data acquisition system was used as the AE system, which consists of a band-pass filter with a frequency range of 250–750 kHz and a nominal resonant frequency of 500 kHz. In each test, two sensors were attached to the middle part of the sample (10 mm below the top of the sample) on two opposite sides to achieve effective data acquisition. External amplifiers were used to amplify the low-frequency acoustic waves resulting from the crack fracturing process in the rock. The amplifiers were set to 60 dB to amplify the AE signals from the specimen during loading.

3.4.3.5. X-ray diffraction (XRD) methodology

In order to investigate the possible mineralogical changes which occur in reservoir rock with each saturation condition, X-ray diffraction (XRD) analysis was carried out. Powder XRD was used to analyse the samples and a combination of matrix flushing and reference intensity ratio (RIR)-derived constants were used in the quantification of the minerals identified in the samples. A rotation speed of 120 rpm and 1 s time/steps were used to collect the XRD traces using a 45 kV and 40 mA generator under Cu K α 1.5406 radiation.

3.4.3.6. Scanning electron microscopy (SEM) methodology

The possible micro-structural variations in the reservoir rock under each saturation condition were identified by conducting

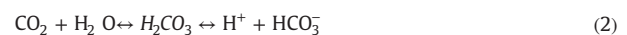
SEM analysis. A FEI Nova Nano SEM machine was used under low vacuum mode to capture the changes in sandstone microstructure by using two Bruker EDS detectors and in-lens detectors. The SEM analysis was conducted on a 0.3 mm thick sandstone slice taken from the sample prior to each experiment (after four months' saturation) under dry and wet conditions. Before the SEM analysis, two 3 nm thick titanium layers were applied on the sample to obtain clear images while avoiding the charging effect. Furthermore, a spot size of 3.5 and a magnification of 10,000 \times were used to analyse the microstructure of the sandstone specimens.

3.4.4. Results and discussion

The results obtained from this study enable some important conclusions to be drawn on the effect of scCO₂ saturation on the mechanical properties of silicate cemented reservoir rock in unconfined stress environments. The results are discussed under three categories: (1) rock mass mineral structure alterations with CO₂ injection, (2) geo-mechanical effects and (3) effect of scCO₂ saturation on the fracture formation pattern of the reservoir rock.

3.4.4.1. Rock mass mineral structure alterations with CO₂ injection

The mineralogical variation associated with CO₂-induced strength reduction in brine-saturated sandstone was investigated by performing XRD and SEM analyses, and considerable changes in the reservoir rock's mineralogical structure were observed in the scCO₂-rich water and brine-saturated samples compared with others. Kaszuba et al. [20] explained this using the fundamental reaction between CO₂ and the host fluid of the aquifer (Eq. (2)). According to these researchers, this is the most important reaction for solubility trapping during CO₂ storage in deep saline aquifers.



According to Eq. (2), once CO₂ is injected into saline aquifers it starts to react with the water phase and produces carbonic acid, which releases active H⁺ ions into the system, creating an acidic medium. As a consequence of the resultant free H⁺ ions,

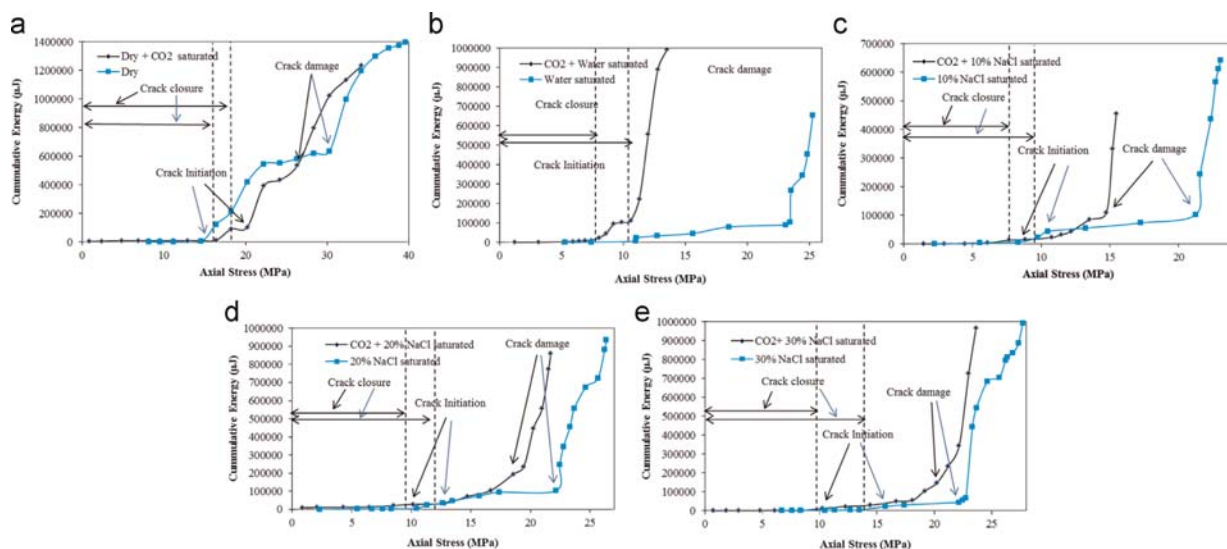


Fig. 7. Variation of cumulative AE counts with axial stress for (a) water-saturated specimen, (b) 10% NaCl-saturated specimen, (c) 20% NaCl-saturated specimen and (d) 30% NaCl-saturated specimen.

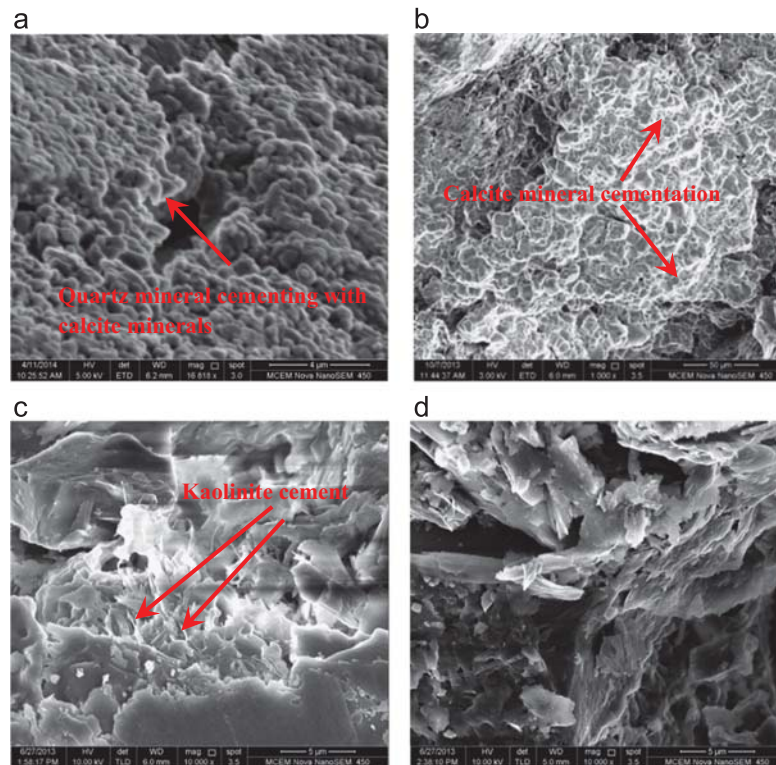
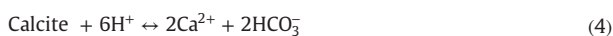


Fig. 8. SEM test results of dry sample without CO₂ (a) detail of quartz mineral cementation, (b) details of calcite mineral cementation and (c) and (d) details of kaolinite cement textures.

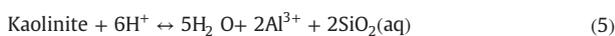
some mineral dissolution may occur during the exposure period, which subsequently alters the mineral structure of the reservoir rock. This mineralogical alteration mainly appears in the silicate and the carbonate cemented grain-to-grain contacts in the rock pore matrix. Some possible mineral dissolution reactions are given in Eqs. (3)–(8).



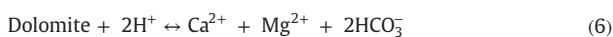
[35]



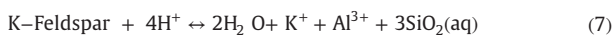
[35,31]



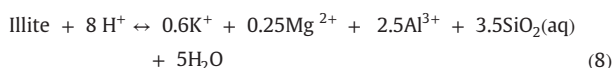
[35,21]



[35,31]



[35]



[35]

However, it should be noted that these are only one set of favoured dissolution reactions and, depending on the aquifer's environmental condition (ex. pH), other types of mineral reactions such as Ca²⁺ or Mg²⁺ dissolution from dolomite can occur. For example, Ketzner et al. [21] have clearly shown the preferentiality of

a low pH environment for carbonate dissolution reactions, and according to Omole and Osoba [28], higher CO₂ pressures move the carbonate dissolution reaction to the right, accelerating the dissolution, while lower pressures move it to the left, decelerating the dissolution (some calcite that was initially dissolved during the reaction can be re-precipitated if depressurization occurs). Wigand et al. [50] observed quartz dissolution and silicate reaction kinetic rates enhancement in high pressure–temperature environments. According to Ketzner et al. [21], siderite dissolution may also occur in this system, depending on the ionic concentration, and the dissolution of Fe²⁺-bearing minerals (e.g. pyrite and biotite) decelerate the siderite dissolution [21] and siderite re-precipitation can be initiated with increasing Fe²⁺/iron concentration under high salinity, pH, and temperature conditions [23]. However, if the system contains both calcite and siderite, this re-precipitation can occur as a calcite–siderite complex depending on the salinity, pH and Ca²⁺/Fe²⁺ ratio of the system [21].

Further, it should be noted that these reactions can reverse direction over time with the variation of environmental conditions, such as the pH and the thermodynamic equilibrium of the system. For example, calcite re-precipitation (reverse reaction) can initiate after some time of calcite dissolution (forward reaction) due to the resulting increased concentration of bicarbonate ions in the pore fluid [31], and the dissolution of feldspar and albite rock minerals–lead precipitation of quartz, calcite and kaolinite minerals [21]. Furthermore, increasing salinity, pH, and temperatures leads to the initiation of siderite re-precipitation [23].

Such reversibility can be clearly seen in the XRD results of the present study (refer to Table 5), where clear kaolinite, talc, and clay mineral precipitations occurred during the CO₂ saturation period. However, other rock minerals such as calcite re-precipitation were

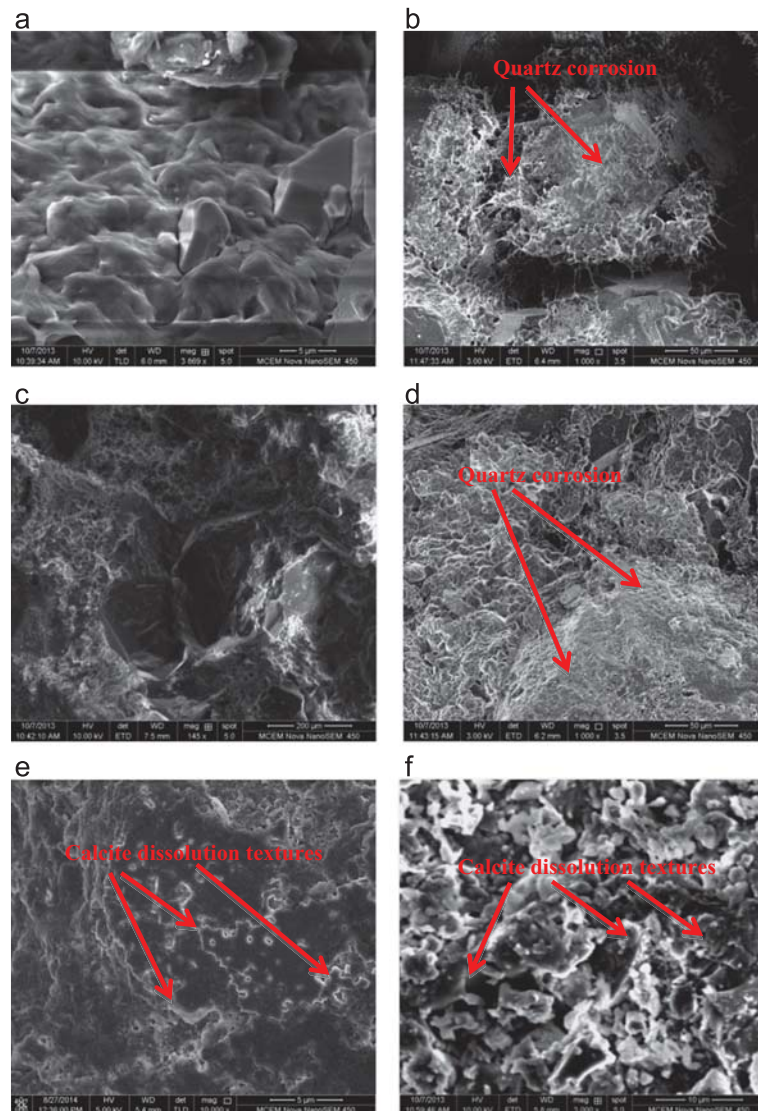


Fig. 9. SEM test results of CO₂-rich water-saturated sample (a) detail of detrital grain surface with randomly-oriented dissolution pits (b), (c) and (d) details of quartz mineral corrosion and (e) details of calcite cement dissolution textures.

not observed in the rock mass after CO₂ saturation, possibly because four months of CO₂ saturation under the pressure–temperature conditions studied here cannot create sufficient alterations in the reaction environment to initiate the reversibility of such mineral dissolution reactions.

According to Refs. [4,17,26], initial dissolution of silicate cemented minerals, including quartz, feldspar-bearing minerals and clay, significantly affects the grain-to-grain contacts in the reservoir rock and reduces the bond energy of the pore structure, subsequently reducing the strength of the reservoir rock. According to Marbler et al. [26], dissolution of pore filling calcite also weakens the pore structure by producing a secondary porosity system within the primary pores. The authors [4,27,17,26] discuss the dissolution effects of K-feldspars, clay minerals and carbonates with CO₂ injection into saline aquifers. According to these researchers, the alteration effect of clay minerals like smectite, illite, muscovite and kaolinite changes the accumulation of Mg with Si and Al in the pore fluid, which causes a significant reduction of the

reservoir's rock mass strength. However, the effect of long-term reactions (in the order of 10–1000 s of years), such as the dissolution of feldspars and clay minerals, cannot be experimentally investigated over short time-scales (weeks, months) and only short-term reactions [14], such as some carbonate dissolution (calcite and siderite etc.), were expected to occur during the laboratory experiments conducted in the present study.

The XRD and XRF results displayed in Tables 5 and 6 show a considerable amount of calcite dissolution (Eq. (4)) during the saturation period of CO₂, which was verified by performing SEM analyses and measuring the Ca²⁺ concentration variation (see Fig. 9 and Table 6). The XRF results illustrate that Ca²⁺ concentrations in CO₂-rich water and CO₂-rich 20% brine-saturated samples are around 421.77% and 364.52% higher than in dry samples, which confirms the occurrence of calcite dissolution during the CO₂/rock/water or CO₂/rock/brine interaction stage. In addition, SEM analysis clearly shows the dissolution textures of calcite minerals, which can be seen in Fig. 9 (e) and (f). Fig. 8(b) shows the calcite cementation textures of natural

Table 2

Mean values of uniaxial compressive strength (UCS), Young's modulus (E) and Poisson's ratio obtained from testing.

Specimen		Strength (MPa)	Average strength	Young's Modulus (GPa)	Average E	Poisson's ratio	Average Poisson's ratio
Dry [34]	Sample 1	38.95		11.24		0.25	
	Sample2	39.96	39.52	10.07	10.29	0.28	0.26
	Sample3	39.63	(SD=0.52)	10.04	(SD=0.680)	0.24	(SD=0.02)
	Sample1	25.66		4.89		0.32	
Water saturation [34]	Sample2	25.03	25.28	5.65	5.35	0.25	0.28
	Sample3	25.34	(SD=0.30)	4.98	(SD=0.45)	0.29	(SD=0.03)
	Sample4	25.04		5.77		0.27	
	Sample 1	33.66		9.93		0.30	
Dry + CO ₂	Sample 2	34.75	34.20	10.18	10.10	0.32	0.31
	Sample 3	34.21	(SD=0.55)	10.20	(SD=0.15)	0.32	(SD=0.01)
	Sample 1	14.24		4.25		0.32	
Water + CO ₂	Sample 2	13.27	13.54	4.52	4.23	0.33	0.32
	Sample 3	13.76	(SD=0.59)	3.82	(SD=0.29)	0.31	(SD=0.01)
	Sample 4	12.87		4.31		0.32	
	Sample1	22.62		4.02		0.32	
10% NaCl [34]	Sample2	23.22	23.05	4.23	4.44	0.31	0.32
	Sample3	23.07	(SD=0.28)	4.21	(SD=0.18)	0.33	(SD=0.01)
	Sample4	22.73		4.46		0.32	
	Sample1	26.08		7.24		0.31	
20% NaCl [34]	Sample2	25.93	26.35	7.67	7.18	0.32	0.31
	Sample3	26.48	(SD=0.43)	6.99	(SD=0.46)	0.31	(SD=0.01)
	Sample4	26.89		6.58		0.31	
	Sample1	27.43		9.16		0.35	
30% NaCl [34]	Sample2	28.61	27.72	9.45	9.50	0.36	0.36
	Sample3	27.89	(SD=0.68)	8.94	(SD=0.21)	0.37	(SD=0.01)
	Sample4	27.03		9.11		0.36	
	Sample1	16.13		4.01		0.37	
10% NaCl + CO ₂	Sample2	15.48	15.47	3.93	4.36	0.36	0.37
	Sample3	15.07	(SD=0.47)	4.54	(SD=0.48)	0.37	(SD=0.01)
	Sample4	15.21		4.96		0.37	
	Sample1	22.38		4.64		0.38	
20% NaCl + CO ₂	Sample2	21.04	21.70	4.57	4.56	0.39	0.39
	Sample3	21.88	(SD=0.56)	4.46	(SD=0.10)	0.41	(SD=0.01)
	Sample4	21.56		4.68		0.39	
	Sample1	23.93		4.86		0.41	
	Sample2	23.61	23.63	4.85	4.94	0.39	0.40
30% NaCl + CO ₂	Sample3	23.89	(SD=0.42)	4.94	(SD=0.12)	0.40	(SD=0.01)
	Sample4	23.03		5.11		0.40	

(SD=Standard deviation)

samples (dry condition without CO₂) and Fig. 9(e) and (f) shows the calcite cementation textures of scCO₂-rich water-saturated samples.

The SEM analysis of dry samples confirms that the grain-to-grain cementation of the tested samples mainly consists of quartz, calcite and kaolinite cements (see Fig. 8). However, the calcite and kaolinite minerals do not seem to sufficiently contribute to the rock strength, as these minerals exist in only small amounts compared to quartz minerals (see Table 5). Therefore, a significant effect due to calcite dissolution cannot be expected during the experiment. According to Fig. 9, there is significant corrosion in quartz crystals. Therefore, a significant effect due to quartz mineral corrosion can be expected during the experiment compared to dry samples (without scCO₂ saturation), as the presence of water or brine causes the mineral corrosion reactions to initiate (Eqs. (3)–(8)). The reduction of failure strength in CO₂/water/rock or CO₂/

brine/rock systems compared to non-CO₂-saturated systems also occurs for the same reason, since the rapid corrosion of quartz cement at grain contacts, in the presence of CO₂, causes the rock mass to weaken, even over a short time-scale. Therefore, the rock matrix collapses by losing the grain-to-grain bonds during the injection of CO₂, which may damage the cap rock sealing and therefore affect the long-term safety of CO₂ sequestration.

As mentioned earlier, according to the SEM analysis (Fig. 9), there is significant corrosion in quartz crystals and removal of siderite cement caused by scCO₂ exposure, and this may also reduce the CO₂-induced rock strength. In addition, secondary precipitation of kaolinite mineral was also shown in the XRD analyses of the CO₂-rich water-and CO₂-rich brine-saturated samples (Table 5). These processes affect the reduction of CO₂-saturation-caused strength in the aquifer rock mass.

Table 3
The saturation condition and its corresponding failure mechanism and strain distribution of tested specimens at failure.

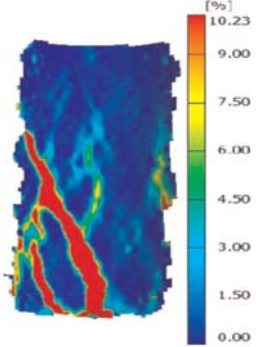
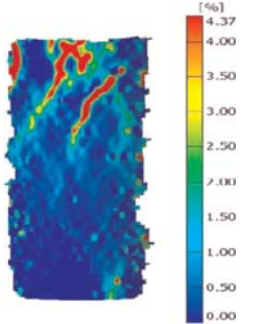
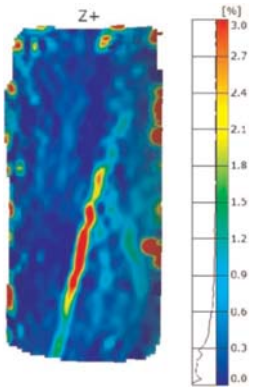
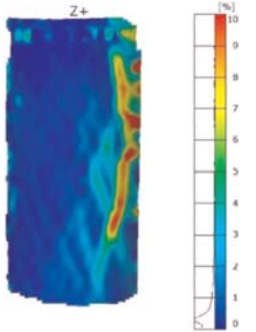
Saturation condition	Failure mechanism	Failed specimen	Major strain distribution before failure
Dry [34]	Shear failure		
CO ₂ saturation (dry condition)	Splitting		
Water saturation [34]	Shear failure		
CO ₂ +water saturation	Splitting		

Table 3 (continued)

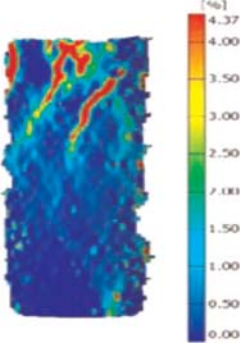
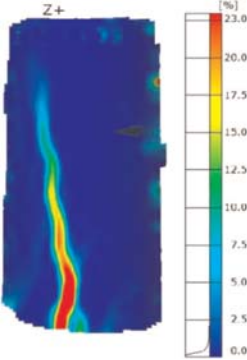
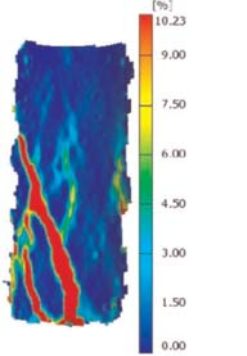
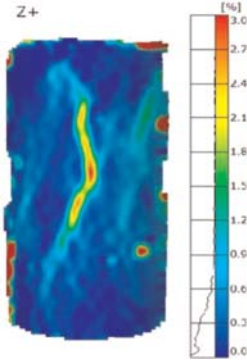
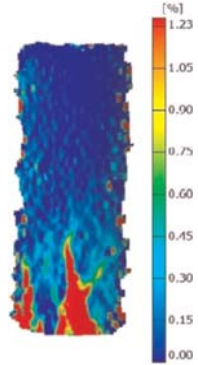
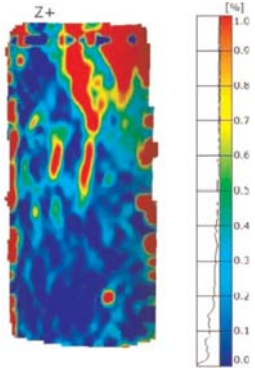
Saturation condition	Failure mechanism	Failed specimen	Major strain distribution before failure
10% NaCl saturated (without CO ₂) [34]	Splitting		
CO ₂ +brine with 10% NaCl	Splitting		
20% NaCl saturated (without CO ₂) [34]	Shear failure		
CO ₂ +brine with 20% NaCl	Splitting		

Table 3 (continued)

Saturation condition	Failure mechanism	Failed specimen	Major strain distribution before failure
30% NaCl saturated (without CO ₂) [34]	Splitting		
CO ₂ + brine with 30% NaCl	Splitting		

3.4.4.2. Geo-mechanical effects

The stress-strain relationship of a material provides fundamental information about its mechanical behaviour and is used in many engineering designs. Fig. 5 below shows the stress-strain curves of the specimens under different saturation conditions. The observed average failure strength, Young's modulus and Poisson's ratio values for each tested condition are given in Table 2. Table 2 clearly shows that the obtained failure strength, Young's modulus and Poisson's ratio for each replicate under each saturated condition are in good agreement, the standard deviations for failure strengths for each replicate being between 0.3 and 0.68. This suggests no significant effect of discontinuous features of sandstone due to careful selection of the specimens from a single sandstone block. However, for the purposes of discussion, the average values are considered. The failure strength, Young's modulus and Poisson's ratio values for each scCO₂-rich-saturated condition are compared with the non-CO₂-saturated conditions, including the dry, water-and brine-saturated strength values obtained from [34].

According to Table 2, the dry strength of the reservoir rock decreases from 39.52 MPa to 34.20 MPa with the saturation of scCO₂, and the reduction is about 13.46% compared to the dry strength of the specimen. The observed strength reduction in tested sandstone samples is mainly due to the super-critical CO₂ dissolution-induced mineralogical alteration in the rock matrix, and this was confirmed by performing SEM analysis on both non-scCO₂ and scCO₂-saturated dry sandstone samples (Figs. 8 and 9).

According to Figs. 8 and 9, a considerable amount of quartz mineral corrosion occurred due to scCO₂-saturation, which possibly reduces the strength of sandstone. This is consistent with the findings of Marbler et al. [26], who found a considerable mechanical alteration in dry silicate sandstone due to scCO₂ saturation.

Interestingly, around 46.44% reduction in failure strength was observed in the CO₂-rich water-saturated specimens compared to the non-CO₂-rich water-saturated specimens (Table 2). This significant strength reduction is due to the CO₂/water/rock chemical interaction and may lead to changes in the hydro-mechanical behaviour of reservoir rock via chemically-coupled mechanical effects. Dissolution of CO₂ in water produces carbonic acid (Eq. (2)), which may accelerate the chemical reactions between host rock and pore fluid, leading to the rapid dissolution of carbonates and the long-term dissolution of feldspars, clay minerals, micas and Fe-oxides during the long-term CO₂ injection process. According to Marbler et al. [26], the introduction of CO₂ into water-saturated silicate-cemented sandstone samples (the sandstone type used in this study) causes its ability to resist differential stresses to be reduced, and according to these researchers, this reduction is due to the surface corrosion of quartz crystals under scCO₂ exposure. In addition, partial dissolution of the clay mineral kaolinite in sandstone under scCO₂ exposure has been observed by Marbler et al. [26], and this is also believed to contribute to the observed CO₂ saturation-induced strength reduction in wet sandstone. The CO₂ creation of mechanical, micro-structural and AE energy alterations in wet sandstone has been well explained by

Table 4
Crack propagation stress thresholds values from AE analysis.

Specimen (saturation condition)	Crack initiation (MPa)	Crack initiation (% of peak)	Crack damage (MPa)	Crack damage (% of peak)
Dry	16.36	41.40	30.27	76.47
Dry + CO ₂	14.71	37.22	28.33	71.69
Water [34]	10.98	43.43	18.52	73.26
Water + CO ₂	7.43	29.39	9.22	36.47
10% NaCl [34]	9.75	42.30	21.23	92.10
10% NaCl + CO ₂	7.64	33.15	14.74	63.95
20% NaCl [34]	10.45	39.66	22.12	83.95
20% NaCl + CO ₂	10.15	38.52	19.56	72.64
30% NaCl [34]	13.73	49.53	22.45	80.99
30% NaCl + CO ₂	10.65	38.42	21.21	76.52

Table 5
XRD test results of dry sample, CO₂-rich water-saturated sample and CO₂-rich (10% NaCl by weight) brine-saturated samples.

Mineral ID	Dry sample	Mass percentage %		
		Dry + CO ₂	CO ₂ -rich water-saturated sample	CO ₂ -rich brine-saturated Sample (20% NaCl)
Alpha Quartz	85	81	77	80
Kaolinite	5	5	13	12
Calcite	4	4	0	0
Mica	1	2	2	2
Siderite	1	1	0	0
Gypsum	0	1	1	1
Halite	0	1	< 1	< 1
Zeolite	< 1	< 1	< 1	< 1
Clinocllore	< 1	1	1	< 1
Talc	0	1	2	1
Anatase	2	2	2	2
Dolomite	0	0	0	< 1
Amphibole	< 1	1	1	1
Serpentine	< 1	< 1	< 1	< 1

[25,14]. According to Le Guen et al. [25], there is a clear strength reduction in wet sandstone due to CO₂ absorption, and according to Hangx et al. [13], the injection of high-pressure CO₂ reduces the creep rate in wet quartz. The sandstone samples in this study contain more than 80% quartz and the strength reduction observed due to CO₂ saturation is therefore proven.

The pore water available in saline aquifers is often highly saline and the CO₂/brine/rock chemically-coupled mechanical behaviour is therefore critically important in the CO₂ sequestration process. In addition to the CO₂/brine/rock interaction, the effect of different salinity levels on CO₂-induced mechanical behaviour is also important in identifying suitable aquifer depths for effective CO₂ sequestration, since the degree of salinity generally increases with increasing depth. It is known that the dissolution of CO₂ in water is more significant than in brine [24]. Lagneau et al. [24] illustrated that, at constant pressure and temperature, CO₂ dissolution or solubility decreases with salinity as the salting-out effect takes over. Therefore, a considerably higher chemical reaction rate is to be expected between host rock and water compared to rock and brine. According to Table 2, the unconfined compressive strength for NaCl-rich CO₂-saturated samples varies with varying salinity levels in the pore fluid, where the strengths of 10%, 20% and 30% NaCl-saturated samples are 15.47, 21.70 and 23.63 MPa, respectively (Table 2). According to Rathnaweera and Ranjith [34], the average unconfined compressive strength values for 10%, 20% and 30% concentrations of NaCl-rich non-CO₂-saturated samples are 23.05, 26.35 and 27.72 MPa, respectively, and the strength values are much higher than the observed strength values in the present study given above (the

same sandstone type was used). This implies that the presence of CO₂ leads to higher strength gain with the increasing salinity level in the pore fluid. Dissolution of CO₂ in water or brine produces carbonic acid inside the sample pore structure [20], which leads to quartz corrosion in the reservoir rock [26], resulting in reduced rock mass strength. The expected reduced CO₂ dissolution with increasing salinity level in the pore fluid therefore results in lower carbonic acid production [30] and consequently lower strength reduction. According to Gledhill and Morse [11], increasing the ionic strength of the pore fluid causes increased calcite dissolution. This dissolution of calcite, being one of the cementing phases, strongly influences the rock mass strength, and according to these studies, the increasing of ionic strength (with increasing NaCl concentration in the pore fluid) causes higher degrees of strength reduction in the reservoir rock. However, the sandstone used in the present study has only a small amount of calcite minerals at 4% (silicate-cemented sandstone was tested). Therefore, the effect of calcite dissolution on strength reduction is much lower, and in spite of that, the effect of salinity level on CO₂ dissolution plays the major role.

The other important mechanical fact that exhibits the mechanical behaviour of reservoir rock is its elastic modulus (Young's modulus). According to Fig. 6 and Table 2, the presence of CO₂ has a negligible influence on the Young's modulus of the tested sandstone under dry conditions (without water saturation), where only 1.8% reduction is shown. This is because under dry conditions there is no CO₂ dilution in water, the major reaction of CO₂ in saline aquifers, and the only possible reaction is the CO₂-rock mineral interaction. That is minimal during the considered short time-scale and appears to be insufficient to create a significant influence on the Young modulus of the silicate-cemented sandstone. Moreover, CO₂-rich water-saturated samples show around 21.31% reduction in Young's modulus compared to non-CO₂-rich water-saturated samples. According to Marbler et al. [26], this may be due to the dissolution of rock minerals and the weakening of the grain structure of the rock by chemical alteration in CO₂-rich environments in the presence of water, which reduce the elastic properties of the reservoir rock. If the brine-saturated samples are considered, it is of interest that the reduction of brine saturation-induced Young's modulus greatly decreases with the increasing brine concentration in the pore fluid. The CO₂ saturation-induced Young's modulus reductions in 10%, 20% and 30% NaCl-saturated samples are around 1.8%, 57.45%, and 92.3% (compared to non-CO₂-saturated samples), respectively (Table 2), probably due to the salting-out effect in brine being reduced by CO₂ due to the brine-CO₂ interaction. According to Rathnaweera and Ranjith [34], increased NaCl concentration in brine causes a higher degree of NaCl crystallisation in the rock pore space, which enhances the rock mass Young's modulus (increasing the brine concentration from 10% to 30% creates a 113.96% Young's modulus increment in sandstone), and if this effect is reduced by CO₂, it is possible to expect a greater CO₂ saturation-induced Young's modulus

Table 6
XRF test results of dry sample, CO₂-rich water-saturated sample and CO₂-rich (10% NaCl by weight) brine-saturated samples.

Main elements	Sample description		
	Dry	CO ₂ rich water-saturated sample	CO ₂ rich brine-saturated sample (20% NaCl)
N	88.3	90.1	90.2
CaO	0.03	0.20	0.41
Al ₂ O ₃	4.36	5.61	5.54
MgO	0.05	0.05	0.04
Fe ₂ O ₃	0.33	0.51	0.37
K ₂ O	1.15	1.15	1.16
Na (ppm)	1213	1500	2300
Ca (ppm)	124	647	576

reduction for samples with higher percentages of NaCl.

The effect of CO₂ saturation on the Poisson's ratio of the reservoir rock was then considered, and around 19.23% increment in Poisson's ratio was found for CO₂-rich dry samples compared to non-CO₂ rich dry samples (Table 2). Moreover, the introduction of CO₂ into water-saturated samples also causes the Poisson's ratio to increase by 14.29%, and in the case of CO₂-rich brine-saturated samples, increasing the NaCl concentration from 10% to 30% causes the Poisson's ratio to be increased by 8.11%. Therefore, it is clear that the presence of CO₂ clearly enhances the Poisson's ratio of the reservoir rock under any saturation condition. This demonstrates the enhancement of the lateral expandability of reservoir rock with CO₂ injection, which is favourable for the safety of sequestration projects. According to Zhang and Bentley [51], rock's Poisson's ratio can be increased with the precipitation of clay minerals inside the rock pore space due to the high expandability of clay minerals. According to Table 5, there is a clear enhancement in clay mineral percentage in the tested rock samples (5–13% increment in kaolinite and 0–2% increment in talc) after the CO₂ saturation period and such clay mineral precipitations should contribute to the enhancement of the expandability and therefore Poisson's ratio of the formation rock mass [51]. On the other hand, CO₂ saturation has also caused a clear dissolution of quartz, a silica mineral, which is a well-defined brittle mineral available in rocks [19]. Reduction of such brittle minerals should also contribute to enhancement of the ductile properties or expandability of the formation. Overall, the combined influence of clay mineral precipitation and quartz dissolution has caused the enhancement of Poisson's ratio of the tested rock. Increasing the Poisson's ratio by any means demonstrates the enhancement of the lateral expandability of reservoir rock with CO₂ injection, which is favourable for the safety of CO₂ sequestration field projects.

The effect of different saturation conditions on reservoir rock failure mechanisms was then investigated using digital image correlation technology, and the results are shown in Table 3. As Table 3 shows, the injection of scCO₂ into the system produces splitting-type failure (without confinement or small confining pressures, sandstone will generally fail by axial splitting), which happens suddenly and quite violently through the material. In general, rock failure occurs through two main mechanisms: (1) axial splitting under no or negligible confinement, and (2) shearing along a weaker plane under confined conditions. According to Table 3, the tested sandstone exhibits shear failure under dry or water-saturated conditions, and the failure mechanism shifts to axial splitting failure in the presence of scCO₂. This observation confirms the weakening effect created by injecting CO₂ into reservoir rock, which is a highly negative influence on the long-term safety of CO₂ sequestration in deep saline aquifers. Interestingly, according to Table 3, brine saturation also seems to create an axial splitting type of failure in sandstone, which is contradictory to the observed strength gain observed with NaCl saturation. It is possible that, although there is an overall strength gain in sandstone due to crystallised NaCl in the pore space, crystallization-created pore expansion may squeeze pore walls, creating thinner, weaker zones. Therefore, with the load application, before shear failure is reached the samples fail along these weak zones. The failure in brine-saturated sandstone is therefore not really an axial splitting type of failure, but is due to the breakage of the weakened zones caused by NaCl crystallization in the pore space.

3.4.4.3. Effect of CO₂ saturation on the fracture formation pattern of the reservoir rock

AE analysis is a well-accepted method for analysing the implications of CO₂ on the stages of crack closure, crack initiation and crack damage. If the crack formation behaviour shown by the AE

system is described at the beginning of the load application, no significant AE energy release can be seen and the rock mass is at its crack closure state. Then, with the gradually increasing compressive load on the rock mass, stable crack propagation begins, which is indicated by the gradually increasing AE energy release. The further increase of the load causes unstable crack propagation in the rock mass, which is exhibited by the exponential increase in the AE energy release. This stage of the load application clearly creates significant damage to the rock mass and it eventually fails. Based on the results obtained, it is clear that rapid energy release can be seen near failure, and with failure it disappears. Therefore, AE results can also be used to predict the failure strength of reservoir rock. Fig. 7 shows the cumulative AE energy versus stress for each saturation condition, and the same figure was used to identify the stress thresholds of crack initiation and crack damage for different saturation conditions (refer to Table 4).

For the dry samples, according to Fig. 7 and Table 4, CO₂-rich dry samples show crack initiation and crack damage at 37.22% and 71.69% of dry failure strength, compared to 41.40% and 76.47% for non-CO₂-saturated dry samples. The wet condition was then considered and a similar pattern was observed, with CO₂-rich water-saturated samples showing crack initiation and crack damage at 29.39% and 36.47% of water-saturated failure strength, compared to 43.43% and 73.26% of those for non-CO₂-rich water-saturated samples. These results are probably due to scCO₂ saturation-induced mineralogical changes (mainly quartz mineral corrosion) and grain re-arrangement in the sandstone samples [5].

In addition, according to Table 4, crack initiation is delayed due to the presence of CO₂ in the dry condition and occurs earlier in the wet condition. This can be explained by the fundamental dissolution process of CO₂ in water. Dissolution of CO₂ in water or brine produces carbonic acid inside the sample pore structure [30], which leads to quartz corrosion in the reservoir rock [26], resulting in early crack initiation under reduced strength in the rock mass. This cannot occur under dry conditions and instead only the reactions between CO₂ and the rock minerals occur. Delays in crack initiation and crack damage stages were then observed in CO₂-rich brine-saturation specimens, while increasing the NaCl concentration from 10% to 30%. According to Table 4, under the 10% brine-rich CO₂-saturated condition, the crack initiation stress is 7.64 MPa, and the stress value increases up to 10.15 and 10.65 MPa under 20% and 30% brine-rich CO₂-saturated conditions, respectively. This is due to the crystallisation of NaCl in the pore structure, which strengthens the rock mass, and therefore delays crack initiation. This effect increases with increasing NaCl concentration due to the greater amounts of NaCl crystals under higher salinity conditions [34].

A similar trend can be seen for the crack damage stress of specimens, where under the 10% brine-rich CO₂-saturated condition, the crack damage stress is 14.74 MPa and the stress value increases up to 19.56 and 21.21 MPa under 20% and 30% brine-rich CO₂-saturated conditions, respectively. This is because the dissolution of CO₂ in brine decreases with increasing brine concentration. Therefore, the occurrence of carbonic acid reduces, while reducing the weakening effect of the acidic environment on the sandstone's mineral structure.

AE analysis assists in understanding the internal rock matrix responses to external loading, and importantly it exhibits how the rock mass weakening process is initiated and progresses with load application. According to the AE analysis conducted in the present study, CO₂ saturation causes early crack initiation and damage under any conditions (dry or wet (water/brine)), and it is therefore clear that internal structure weakening occurs with CO₂ saturation. However, this is not favourable for the long-term safety of CO₂ sequestration, and indicates the importance of careful attention in field CO₂ sequestration projects.

3.4.5. Conclusions

A comprehensive experimental study, including a series of uniaxial compressive strength tests and advanced chemical analyses (XRD and SEM), was conducted to evaluate the effect of super-critical CO₂ injection on the mechanical properties of Hawkesbury sandstone taken from a potential carbon capture and sequestration (CCS) site at Gosford. Some major conclusions can be drawn as follows:

Super-critical CO₂ injection causes mechanical weakening in the reservoir rock available at the potential CCS site, and the reduction is greatly dependent on the degree of saturation of the reservoir. For example, super-critical CO₂ saturation causes the uniaxial compressive strength and Young's modulus of dry and water-saturated sandstone from the site to be reduced by around 13.4%, and 46.44% and 1.85% and 20.93%, respectively. This mechanical property weakening is partially due to the CO₂-water-rock mineral interaction (dissolution of CO₂ in water produces carbonic acid inside the sample pore structure), which leads to quartz corrosion in the reservoir rock and partially to the CO₂-rock mineral interaction which creates rock mass mineral dissolution. Under dry conditions, there is no CO₂ dilution in water (the former causative fact), and the only possible reaction is the CO₂-rock mineral interaction, resulting in lower strength reduction.

The degree of salinity of the pore fluid also greatly influences the CO₂ adsorption-induced strength reduction in Hawkesbury sandstone. For example, super-critical CO₂ saturation causes around 32.89%, 17.65%, and 14.75% uniaxial compressive strength reductions and 1.8%, 57.45%, and 92.3% Young's modulus reductions in brine-saturated Hawkesbury sandstone with 10%, 20%, and 30% NaCl concentration brines, respectively. These reduced mechanical properties in Hawkesbury sandstone at increased brine concentration are possibly related to the injected CO₂ influencing the salting-out effect in brine-saturated sandstone. According to existing studies, increased NaCl concentration in brine causes a higher degree of NaCl crystallisation in the rock pore space, leading to enhanced rock mass Young's modulus with increasing brine concentration. If this effect is reduced by CO₂, it is possible to expect a greater CO₂ saturation-induced Young's modulus reduction for samples with higher percentages of NaCl.

The studied Hawkesbury sandstone is a silicate-cemented sandstone and mainly consists of quartz with only minor amounts of calcite and clay minerals. Therefore, although there is quartz corrosion caused by the carbonic acid made through the dissolution of CO₂ in brine, the dissolution of calcite and other minerals is minimal, resulting in less mechanical property alteration compared to widely available carbonate-cemented sandstone saline aquifers. Therefore, these types of silicate-cemented sandstone formations are more suitable for CO₂ sequestration in terms of safety. However, when considering the storage potential, the lack of calcite and other clay minerals leads to a lower contribution to the long-term mineral trapping process, and therefore, less CO₂ storage capacity.

However, this study could consider only the short-term interaction of CO₂-brine-rock mass. Therefore, to obtain a comprehensive understanding of this process, including the long-term strength reduction associated with the dissolution of feldspars and clay minerals, more tests conducted over long-term time-scales are suggested.

Acknowledgement

This research was supported under Australian Research Council's *Discovery Projects* funding scheme (project number DP120103003). The authors (Ranjith, Aref and Nassir) extend their appreciation to

the Deanship of Scientific Research at King Saud University, Saudi Arabia, for funding the work through the international research group project (IRG14-36).

3.4.6. References

- [1] L. Andre, P. Audigane, M. Azaroual, A. Nenjoy, Numerical modelling of fluid-rock chemical interactions at the supercritical CO₂-liquid interface during CO₂ injection into a carbonate reservoir, the Dogger aquifer (Paris basin, France), *Energy Convers. Manag.* 48 (2007) 1782–1797.
- [2] J.T. Birkholzer, Q. Zhou, C. Tsang, Large-scale impact of CO₂-storage in deep saline aquifers: a sensitive study on pressure response in stratified systems, *Int. J. Greenh. Gas Control* 3 (2009) 181–194.
- [3] R.G. Bruant, A.J. Guswa, M.A. Celia, C.A. Peters, Safe storage of CO₂ in deep saline aquifers, *Environ. Sci. Technol.* 36 (2002) 240A–245A.
- [4] E. Busenberg, C. Clemency, The dissolution kinetics of feldspars at 25 °C and 1 atm CO₂ partial pressure, *Geochim. Cosmochim. Acta* 40 (1) (1976) 41–49.
- [5] F.M. Chester, J.S. Chester, A.K. Kronenberg, A. Hajash, Subcritical creep compaction of quartz sand at diagenetic conditions: effect of water and grain size, *J. Geophys. Res.* 112 (2007) 634–646.
- [6] Z. Duan, R. Sun, C. Zhu, I. Chou, An improved model for the calculation of CO₂ solubility in aqueous solutions containing Na⁺, K⁺, Ca²⁺, Mg²⁺, Cl⁻, and SO₄²⁻, *Mar. Chem.* 98 (2) (2006) 131–139.
- [7] X.T. Feng, S. Chen, H. Zhou, Real-time computerized tomography (CT) experiments on sandstone damage evaluation during triaxial compression with chemical corrosion, *Int. J. Rock Mech. Min. Sci.* 41 (2004) 181–192.
- [8] L.J. Feucht, J.M. Logan, Effects of chemically active solutions on shearing behavior of a sandstone, *Tectonophysics* 175 (1990) 159–176.
- [9] I. Gaus, P. Audigane, L. Andre, J. Lions, N. Jacquemet, P. Durst, I. Czernichowski-Lauriol, M. Azaroual, Geochemical and solute transport modelling for CO₂ storage: what to expect from it? *Int. J. Greenh. Gas Control* 2 (2008) 605–625.
- [10] S.M.V. Gilfillan, S.L. Barbara, H. Greg, B. Dave, S. Scott, S. Martin, et al., Solubility trapping in formation water as dominant CO₂ sink in natural gas fields, *Nature* 458 (7238) (2009) 614–618.
- [11] D.K. Gledhill, J.W. Morse, Calcite solubility in Na-Ca-Mg-Cl brines, *Chem. Geol.* 233 (2006) 249–256.
- [12] D. Grgic, Influence of CO₂ on the long-term chemomechanical behaviour of an oolitic limestone, *J. Geophys. Res.* 116 (2012) 72–82.
- [13] S.J.T. Hangx, C.J. Spiers, C.J. Peach, Creep of simulated reservoir sands and coupled chemical-mechanical effects of CO₂ injection, *J. Geophys. Res.* 115 (2010) 92–105.
- [14] S. Hangx, A.V.D. Linden, F. Marcellis, A. Baucer, The effect of CO₂ on the mechanical properties of the captain sandstone geological storage of CO₂ at the Goldeneye field (UK), *Int. J. Greenh. Gas Control* 19 (2013) 609–616.
- [15] H.S. Harned, R. Davis, The ionization constant of carbonic acid in water and the solubility of carbon dioxide in water and aqueous salt solution from 0° to 50°, *J. Am. Chem. Soc.* 65 (1943) 2030–2037.
- [16] S. Hickman, R. Sibson, R. Bruhn, Introduction of special section: mechanical involvement of fluid in faulting, *J. Geophys. Res.: Solid Earth* 100 (1995) 12831–12840.
- [17] G.R. Holden Jr., R.A. Berner, Mechanism of feldspar weathering: experimental studies, *Geochim. Cosmochim. Acta* 43 (1979) 1161–1171.
- [18] A. Holl, E. Althaus, C. Lempp, O. Natau, The petrophysical behaviour of crustal rocks under the influence of fluids, *Tectonophysics* 275 (1997) 253–260.
- [19] D.M. Jarvie, R.J. Hill, T.E. Ruble, R.M. Pollastro, Unconventional shale-gas systems: the Mississippian Barnett Shale of north-central Texas as one model for thermogenic shale-gas assessment, *AAPG Bull.* 91 (4) (2007) 475–499.
- [20] J.P. Kaszuba, D.R. Janecky, M.G. Snow, Carbon dioxide reaction processes in a model brine aquifer at 200 °C and 200 bars: implications for geologic sequestration of carbon, *Appl. Geochem.* 18 (7) (2003) 1065–1080.
- [21] J.M. Ketzer, R. Iglesias, S. Einloft, J. Dullius, R. Ligabue, V.D. Lima, Water-rock-CO₂ interactions in saline aquifers aimed for carbon dioxide storage: experimental and numerical modelling studies for the Rio Bonito formation (Permian), southern Brazil, *Appl. Geochem.* 24 (2009) 760–767.
- [22] H. Koide, M. Takahashi, H. Tusukamoto, Self-trapping mechanisms of carbon dioxide in the aquifer disposal, *Energy Conserv. Manag.* 36 (1995) 505–508.
- [23] K.B. Krauskopf, D.K. Bird, Introduction to Geochemistry, third ed., McGraw-Hill, Inc., New York (1995), p. 647–670.
- [24] V. Lagneau, A. Pipat, H. Catalette, Reactive transport modelling of CO₂ sequestration in deep saline aquifers, *Oil Gas Sci. Technol. – Rev. 60* (2005) 231–247.
- [25] Y. Le Guen, F. Renard, R. Hellmann, E. Brosse, M. Collomber, D. Tisserand, J. P. Gratier, Enhanced deformation of limestone and sandstone in the presence of high PCO₂ fluids, *J. Geophys. Res.* 112 (2007) 5421–5432.
- [26] H. Marbler, K.P. Erickson, M. Schmidt, C. Lempp, H. Pollmann, Geomechanical and geochemical effects on sandstones caused by the reaction with supercritical CO₂: an experimental approach to in situ conditions in deep geological reservoirs, *Environ. Earth Sci.* 69 (2012) 1981–1998.
- [27] L. Marini, Geological sequestration of carbon dioxide: thermodynamics, kinetics, and reaction path modelling, *Dev. Geochem.* 11 (2007) 453–467.
- [28] O. Omole, J.S. Osoba, Carbon dioxide-dolomite rock interaction during CO₂ flooding process, *Pet. Soc. Can. Inst. Min. Metall.* 83 (1983) 17–34.
- [29] T. Oshumi, N. Nakashiki, K. Shitashima, K. Hiram, Density change of water

- due to dissolution of carbon dioxide and near-field behaviour of CO₂ from a source on deep-sea floor, *Energy* 33 (1992) 685–690.
- [30] T. Paces, Chemical characteristics and equilibration in natural water-felsic rock- CO₂ system, *Geochim. Cosmochim. Acta* 36 (1972) 217–240.
- [31] O.S. Pokrovsky, S.V. Golubev, J. Schott, A. Castillo, Calcite, dolomite and magnesite dissolution kinetics in aqueous solutions at acid to circumneutral pH, 25–150 C and 1–55 atm pCO₂: new constraints on CO₂ sequestration in sedimentary basins, *Chem. Geol.* 265 (1) (2009) 20–32.
- [32] P. Ranganathan, H.P. Van, E. Rudolph, J. Susanne, Zitha PZJ, Numerical modeling of CO₂ mineralisation during storage in deep saline aquifers, *Energy* 4 (2011) 4538–4545.
- [33] P. Ranjith, M. Perera, E. Khan, A study of safe CO₂ storage capacity in saline aquifers: a numerical study, *Int. J. Energy Res.* 37 (2013) 189–199.
- [34] T.D. Rathnaweera, P.G. Ranjith, Perera MSA, Salinity-dependent strength and stress-strain characteristics of reservoir rocks in deep saline aquifers: an experimental study, *Fuel* 122 (2014) 1–11.
- [35] C.A. Rochelle, I. Czernichowski-Lauriol, A.E. Milodowski, The Impact of Chemical Reactions on CO₂ Storage in Geological Formations: A Brief Review, 233, Special Publications, Geological Society, London (2004), p. 87–106.
- [36] R.J. Rosenbauer, T. Koksalan, L.P. James, Experimental investigation of CO₂-brine-rock interactions at elevated temperature and pressure: Implications for CO₂ sequestration in deep-saline aquifers, *Fuel* 86 (2005) 1581–1597.
- [37] B.R. Rust, B.G. Jones, The Hawkesbury sandstone south of Sydney, Australia: Triassic analogue for the deposit of a large, braided river, *J. Sedim. Petrol.* 57 (1987) 222–233.
- [38] J. Rutqvist, J.T. Birkholzer, F. Cappa, C.-F. Tsang, Estimating maximum sustainable injection pressure during geological sequestration of CO₂ using coupled fluid flow and geomechanical fault-slip analysis, *Energy* 48 (2007) 1798–1807.
- [39] J. Rutqvist, D.W. Vasco, L. Myer, Coupled reservoir-geomechanical analysis of CO₂ injection and ground deformations in In Salah, Algeria, *Int. J. Greenh. Gas* 4 (2) (2010) 225–230.
- [40] C. Schmidt, R.J. Bodnar, Synthetic fluid inclusions: XVI.PVTX properties in the system H₂O–NaCl–CO₂ at elevated temperatures, pressures and salinities, *Geochim. Cosmochim. Acta* 64 (2000) 3853–3869.
- [41] H. Schutt, M. Wigand, E. Spangenberg, Geophysical and geochemical effects of supercritical CO₂ on sandstones, *Int. J. Geophys.* 2 (2005) 767–786.
- [42] R. Shukla, P.G. Ranjith, S.K. Choi, A. Haque, M. Yellishetty, L. Hong, Mechanical behaviour of reservoir rock under brine saturation, *Rock Mech. Rock Eng.* 46 (1) (2012) 83–89.
- [43] R.H. Sibson, J.V. Rowland, Stress, fluid pressure and structural permeability in seismogenic crust, North Island, New Zealand, *Int. J. Geophys.* 154 (2003) 584–594.
- [44] J.E. Streit, R.R. Hillis, Estimating fault stability and sustainable fluid pressure for underground storage of CO₂ in porous rock, *Energy* 29 (2004) 1445–1456.
- [45] S. Takenouchi, G.C. Kennedy, The solubility of carbon dioxide in NaCl solutions at high temperature and pressure, *Am. J. Sci.* 263 (1965) 445–454.
- [46] United Nations Framework Convention on Climate Change, UNFCCC greenhouse gas inventory data, (2012) <http://unfccc.int/di/detailedbypartly/event.do?event=go>.
- [47] V. Vilarassa, S. Olivella, J. Carrera, Geomechanical stability of the caprock during CO₂ sequestration in deep saline aquifers, *Energy* 4 (2011) 5306–5313.
- [48] C.R. Ward, Sedimentation in the Narrabeen group, southern Sydney basin, New South Wales, *J. Geol. Soc. Aust.* 19 (1972) 393–409.
- [49] C.A.J. Wibberley, T. Shimamoto, Earthquake slip weakening and asperities explained by thermal pressurization, *Nature* 436 (2005) 689–692.
- [50] M. Wigand, J.W. Carey, H. Schutt, E. Spangenberg, J. Erzinger, Geochemical effects of CO₂ sequestration in sandstones under simulated in situ conditions of deep saline aquifers, *Appl. Geochem.* 23 (2008) 2735–2745.
- [51] J.J. Zhang, L.R. Bentley, Factors determining Poisson's ratio, *CREWES Res. Rep.* 17 (2005) 123–139.

3.5 The effect of interaction between injected CO₂, aquifer brine and reservoir rock on overall mechanical performance of the formation under in situ stress environments

Section 3.4 confirmed the influence of CO₂ on the mechanical behaviour of deep saline reservoir rock under uniaxial stress and according to Section 3.4, CO₂ injection causes the strength of reservoir rock to be considerably reduced. This reduction involves the dissolution of some rock minerals in the rock pore structure, which implies that mineralogical and geochemical rock alteration affects the rock mechanical properties by accelerating the collapse mechanisms of the reservoir pore structure. Eventually, this leads to changes in the effective stress field of the natural formation during long-term sequestration, creating poro-elastic compaction and sudden pore collapse in the reservoir formation. Therefore, a comprehensive knowledge relating to this aspect is required for in situ stress environments. Based on this requirement, the effect of interaction between injected CO₂, aquifer brine and reservoir rock on the overall mechanical performance of reservoir formations was investigated in this section of the study. The following submitted journal paper reports on this study.

Stress State and Stress Path Evaluation to Address Uncertainties in Reservoir Rock Failure in CO₂ sequestration in Deep Saline Aquifers: An Experimental Study of the Hawkesbury Sandstone Formation

T. D. Rathnaweera¹, P.G. Ranjith¹, M. S. A. Perera¹

¹Department of Civil Engineering, Monash University, Building 60, Melbourne, Victoria, 3800, Australia.

Abstract

Dissolution of injected CO₂ in aquifer pore fluid (high salinity brine) in deep saline aquifers during the sequestration process causes its chemico-mineral structure to be altered by the creation of complex chemically-coupled mechanical deformations. This is as yet poorly understood in the field and therefore has led to many critical issues, including fault re-activation, ground subsidence and CO₂ leakage. This authors conducted a series of triaxial strength tests on Hawkesbury sandstone under in-situ stress and temperature conditions to characterise the behaviour of reservoir rock upon exposure to super-critical CO₂ (scCO₂) to precisely identify this chemically-coupled mechanical behaviour of reservoir rock. Three different reservoir conditions were selected: dry (15% NaCl by weight), brine-saturated, (which represents the behaviour of natural formations prior to CO₂ injection), and brine+CO₂-reacted (which simulates the sequestered reservoir formation).

According to the findings, injection of CO₂ into brine-saturated reservoir rock mass may cause a considerable strength reduction, probably due to the rock's mineralogical alteration-induced mechanical weakening of grain contacts. This was confirmed by SEM analysis, according to which the mineral dissolution process upon exposure to scCO₂ is significant, and considerable quartz and calcite dissolution was noticed in the tested samples. Importantly, this rock mineral dissolution may alter the reservoir's natural pore geometry. This eventually affects the effective stress patterns acting on the rock matrix. A significant increase in effective stress coefficient was observed in the tested brine+CO₂-reacted sandstone samples (compared to brine-saturated and dry samples) upon CO₂/brine/rock mineral interaction, creating a pore pressure (compared to mean total stress) dominant mean effective stress field inside the formation. In addition, the slip tendency of brine+CO₂-reacted reservoir rock is increased with increasing injection pressure, revealing the fate of the resulting pore pressure-dominant effective stress field through the CO₂ injection process. The results were then incorporated to visualise the mechanical

behaviour of reservoir formations in the effective stress field through the development of a stress-induced model. This model can be used to predict the possibility of mechanical failure of reservoir rock upon CO₂ injection into saline aquifers.

Key words: Reservoir rock, stress-strain, brine, compaction, triaxial, mean effective stress, pore pressure

3.5.1 Introduction

CO₂ injection causes the existing effective stress field in deep saline aquifers to change during long-term CO₂ sequestration. This altered stress field may increase the stress carried by the load-bearing grain framework in the rock matrix, resulting in poro-elastic compaction and sudden collapse in the reservoir formation during the production process (Johnson et al., 1989). The CO₂ storage and monitoring processes in saline aquifers however remain little understood, particularly the physio-chemical reactions that occur in saline aquifers during the CO₂ storage process, which increase the risk of CO₂ leakage through the depleted reservoir formation after CO₂ injection. In-depth knowledge related to the mechanical behaviour of reservoir rock is therefore required to ensure the long-term integrity of the CO₂ sequestration process in saline aquifers.

Such in-depth knowledge cannot be gained without investigating the mechanical behaviour of natural aquifers (brine-saturated formations before injection) under in situ stress conditions. This has therefore been considered by several researchers (Shukla et al., 2012; Rathnaweera et al., 2014; Rathnaweera et al., 2015a; Rathnaweera et al., 2015b). Rathnaweera et al. (2014) investigated the mechanical behaviour of natural aquifers in the uniaxial stress environment, paying special attention to the salinity-dependent strength characteristics of reservoir rocks. However, the actual behaviour of aquifers cannot be understood by ignoring the effective stress effect. Therefore, the salinity-dependent strength variation of natural reservoir rock under confined stress condition was studied by Rathnaweera et al. (2015a). Later in 2015, Rathnaweera et al. (2015b) studied the changes in CO₂ sequestration process-induced mechanical properties in saline aquifer reservoir rocks. Since CO₂ sequestration in deep saline aquifers is a long-term process, there is long-term geochemical interaction among the brine/CO₂ and the reservoir rock minerals. Therefore, Rathnaweera et al. (2015a) studied the mechanical property alterations which occur in long-term brine/CO₂-reacted Hawkesbury sandstone in an unconfined environment to investigate the influence of brine/CO₂/rock interaction on the

mechanical behaviour of reservoir rock. This study revealed the significance of the brine/CO₂/rock interaction on reservoir rock strength. Although this study revealed the effect of brine/CO₂/rock mineral interaction on the mechanical behaviour of reservoir rock, comprehensive knowledge related to the CO₂-injection-induced mechanical behaviour of reservoir rock requires the mechanical response in a confined environment to reliably represent the real field situation, in which the aquifer is in an in-situ stress environment. The present study has therefore been conducted to fill this gap.

The authors conducted a comprehensive mechanical investigation including a series of triaxial strength tests on dry, brine- and brine/CO₂-reacted reservoir rock for a range of injection (0.25-16MPa) and confining (2.5-20MPa) pressures at a constant temperature of 35°C. The aim of the study was to investigate how the stress state and mechanical response of rock mass of natural saline aquifers vary with CO₂ sequestration. In order to visualize the stress state of each formation, based on the results of triaxial strength tests, the present study finally developed a stress model as a function of stress state and stress path.

3.5.2 Experimental procedure

3.5.2.1 Sample preparation

The Hawkesbury sandstone samples were collected from a potential carbon capture and storage (CCS) site in the Sydney basin. X-ray diffraction (XRD) mineralogical analysis of the dry samples confirmed that the mineral composition of the tested silicate cemented sandstone consists of 88% quartz, 8% calcite, 2% kaolinite, 1% muscovite, and <1% other clay minerals. Sample preparation and testing were performed in the Deep Earth Energy Research Laboratory (DEERL) of the Civil Engineering Department at Monash University, and the sample preparation was conducted according to the ISRM standard (ISRM, 1981). All samples were cored to 38 mm in diameter at the same orientation (perpendicular to stratification). Cored samples were then cut into 76mm high cylinders and both ends of the samples were carefully ground to produce smooth parallel faces. The prepared samples were then oven-dried for 48 hours at 35°C, before being kept for reaction in selected reaction mediums (brine and brine+CO₂).

3.5.2.2 Brine saturation process

In order to check the stress-strain behaviour of reservoir rock under natural conditions (before CO₂ injection), a brine solution with 15% NaCl concentration was used (% by weight) as the aquifer pore fluid. In this study NaCl was used to simulate reservoir salinity, because although saline aquifer brine is a mixture of ions (Na⁺, Mg²⁺, Ca²⁺, Cl⁻, HCO₃⁻ and SO₄²⁻ etc.), the NaCl percentage is much higher than that of other elements (70-90% of brine is composed of NaCl) (Ham 1959). Further, according to Bachu and Bennion (2008) and Shukla et al. (2012), the brine concentration in saline aquifers is in the range of 2×10⁴ (2% by weight) to 2×10⁵mg/l (25% by weight). Considering this range, 15% NaCl concentration was selected to cover the above salinity range, and 15% NaCl saturated samples represent the medium salinity level of aquifer pore fluid. The saturation was carried out under vacuum in desiccators (refer to Fig.3.2a) for 24 months to ensure maximum saturation, and the weights of the samples were measured regularly to ensure the steady-state full saturation condition until constant mass was reached.

3.5.2.3 Brine+CO₂ reaction

The brine+CO₂ reaction in sandstone represents saline aquifers that have been subjected to a CO₂ sequestration process. The reaction was carried out in a specially-designed reaction rig available in the DEERL (see Figs. 3.2b and 3.2c). Samples were first saturated in a 15% NaCl concentration of brine (% by weight) in desiccators under vacuum (0.2MPa suction pressure) and once the weights reached a steady state (full saturation), samples were removed from the desiccators and kept in reaction chambers to facilitate reaction with CO₂. Before placing the samples in the reaction chambers, the chambers were filled with the same concentration (15% NaCl) of brine and then the samples were inserted into the chambers. Gas injection was then carried out at an injection pressure of 10MPa and a temperature of 35°C (similar to the oven-drying temperature) for a period of two years. The reaction pressure and temperature were selected to maintain the super-critical CO₂ injection condition (CO₂ critical pressure and temperature are 31°C and 7.38MPa, respectively) (Perera et al., 2013; Span and Wagner, 1996).

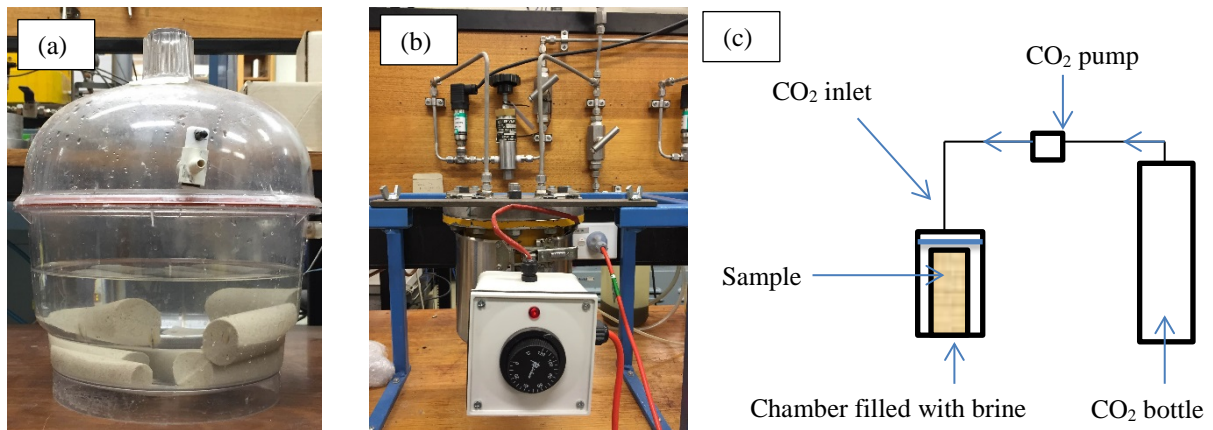


Figure 3.2. (a) The set-up of desiccators used for brine-saturated samples (b) the set-up of saturation chambers used for brine+CO₂-reacted samples and (c) schematic diagrams of CO₂ reaction chamber.

3.5.2.4 Design of triaxial tests

A series of undrained triaxial experiments was conducted on both wet (brine-and brine+CO₂-reacted) and dry samples. The wet samples were tested under six different confining pressures (2.5, 5, 7.5, 10, 15 and 20 MPa) and the dry samples were tested under four different, but lower, confining pressures (2.5, 5, 7.5 and 10MPa) at a temperature of 35°C. It should be noted that two different confinement ranges were used in the tests due to the high strength of the tested dry sandstone (around 40 MPa UCS strength). Due to the limitation of loading capacity in the triaxial load cell (maximum capacity of 160MPa), the maximum confining pressure under dry conditions was limited to 10MPa and the maximum confining pressure under wet conditions was 20MPa. Table 3.1 below shows the full set of CO₂ injection pressures selected. The injection pressures were selected considering the safety of the process and to prevent any fracturing. For this reason, the injection pressure was maintained at less than 90% of confining pressure to avoid both re-activation of joints and CO₂ leakage through the space between the membrane and the specimen. The complete arrangement of the triaxial cell is shown in Fig. 3.3. Prior to the triaxial tests, microstructural and mineralogical tests were performed for the varyingly saturated samples using SEM. In addition, XRD analyses were also conducted to identify the corresponding mineralogical variations (see Table 3.2 and Fig. 3.4).

For the triaxial testing, the saturated samples were placed inside the cell and the required confinement was applied using oil. After applying the confining pressure, a constant injection pressure was applied to the sample using a syringe pump while observing the downstream

pressure. When the downstream pressure development became constant (constant pore pressure inside the sample), the axial load was applied on the sample. During the load application, axial strain was measured using linear variable differential transducers and the lateral strain was measured using two strain gauges (clip gauges) attached around the sample. Two replicates were tested for each condition and after statistically evaluating the standard deviation of each data set, the average value was taken for analysis and discussion (refer to Table 3.3).

Table 3.1. The full set of selected CO₂ injection pressures.

Confining pressure (MPa)	Injection pressures (MPa)
2.5	0.25, 0.5, 1.0, 1.5
5.0	1, 2, 3, 4
7.5	2, 3, 4, 5
10.0	2, 4, 6, 8
15.0	2, 4, 10, 12
20.0	2, 8, 12, 16



Figure 3.3. The complete arrangement of the triaxial cell.

Table 3.2. XRD results of dry, brine-saturated and brine+CO₂-reacted samples.

Mineral	Dry	Brine-saturated	Brine+CO ₂ -reacted
Quartz	88	86	83
Calcite	8	7	3
Kaolinite	2	5	11
Muscovite	1	2	3

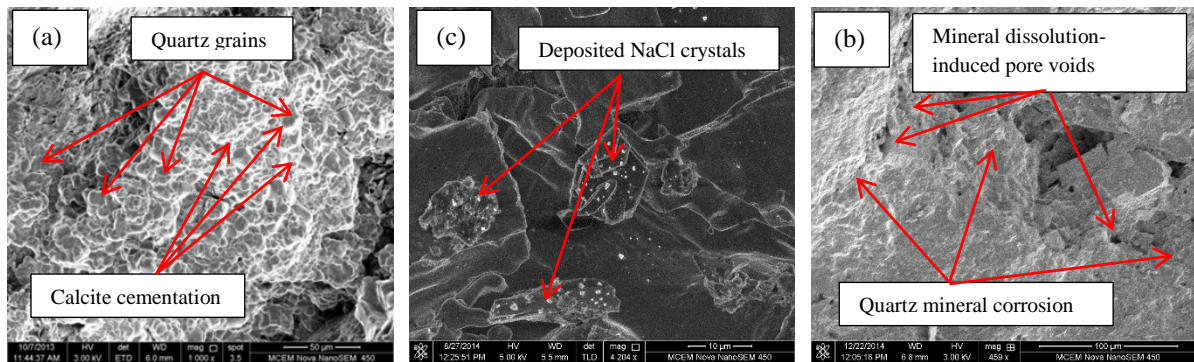
Figure 3.4. SEM images of (a) dry (b) brine-saturated and (c) brine+CO₂-reacted samples.

Table 3.3. The strength values of each specimen and their standard deviation.

Condition	Confining pressure (MPa)	Injection pressure (MPa)	Average failure Strength (MPa)	Standard deviation (MPa)
Dry	2.5	0.25	98.21	0.32
		0.75	95.3	1.01
		1.25	91.34	0.75
		1.5	88.71	0.24
	5.0	1	110.24	1.10
		2	106.31	0.54
		3	98.57	0.12
		4	88.63	0.43
	7.5	2	128.61	1.65
		3	120.96	0.95
		4	103.74	1.13
		6	91.31	0.77
	10	2	136.47	1.28
		4	124.12	2.16
6		110.02	0.74	
8		96.47	1.08	
Brine-saturated	5	1	64.35	1.12
		2	60.48	0.95
		3	54.19	0.78
		4	47.90	2.17
	10	2	91.94	1.37
		4	84.68	0.74
		6	76.45	1.45
		8	68.22	2.01
15	2	109.84	0.78	
	4	102.58	0.98	

		8	98.71	1.62
		12	94.35	1.38
		2	125.81	0.74
	20	8	122.42	1.18
		12	118.06	0.84
		16	113.71	1.73
		1	56.58	0.94
	5	2	52.85	1.48
		3	47.56	1.73
		4	41.96	0.95
		2	84.83	2.76
	10	4	80.53	3.25
		6	73.64	1.74
		8	65.02	0.75
Brine+CO ₂ -reacted		2	104.74	2.19
	15	4	99.47	2.96
		8	92.63	1.94
		12	88.94	0.94
		2	121.81	1.33
	20	8	118.62	1.07
		12	111.65	0.89
		16	109.23	1.48

3.5.3 Results and discussion

3.5.3.1 CO₂ injection-induced stress-strain characteristics in reservoir rocks

The stress-strain behaviour of reservoir rock under different reservoir conditions (natural and after CO₂ injection) is important for many applications, including reservoir and well-bore design related to CO₂ sequestration. The prediction of the stability and failure of reservoirs and injection wells, the estimation of the possibility of subsidence in over-depleted reservoirs, the optimization of drilling and well completion costs, the optimization of hydro-fracturing treatments and methods, and the evaluation of effective injection scenarios are the most important concerns in relation to the safety, efficiency and economic impacts of sequestration projects.

According to Scott (1985), the evaluation of elastic and non-elastic terms of a stressed body provides a general approach to the investigation of the mechanical behaviour of deformed material. Therefore, to investigate the mechanical behaviour of reservoir rocks under different reservoir conditions, a number of triaxial strength tests were conducted under undrained condition. Figs. 3.5-3.7 show the stress-strain behaviour of dry, brine-saturated and brine+CO₂-reacted samples under the tested conditions (confining pressure, injection pressure and temperature). As can be seen in these figures, the initial portion of the stress-strain curve displays non-linear behaviour with an upward curvature, which is probably due to the crack

closure process in the reservoir rock. This non-linear portion is then followed by a linear segment, along which is generally considered the elastic range (Friedman, 1975). With further increasing of stress, the behaviour again changes to non-linear-inelastic. According to past studies done on quartz-rich sandstone (Schutjens et al., 1995; Wong et al., 1997; Hettema et al., 2000), this latter inelastic deformation mechanism is mainly dominated by intergranular micro-crack-induced grain sliding and grain rotation and cement breakage (contact spalling) (Hettema et al., 2000). Generally, inelastic behaviour can be diagnosed by the onset of dilatancy, acoustic emission and permeability changes in the rock mass (Wong et al., 1997; Bouteca et al., 2000) and the onset of non-linear deformation in the laboratory is often identified by the yield stress (Schutjens et al., 2004). The behaviour of the elastic and inelastic deformations of each tested condition are discussed in Section 3.4.

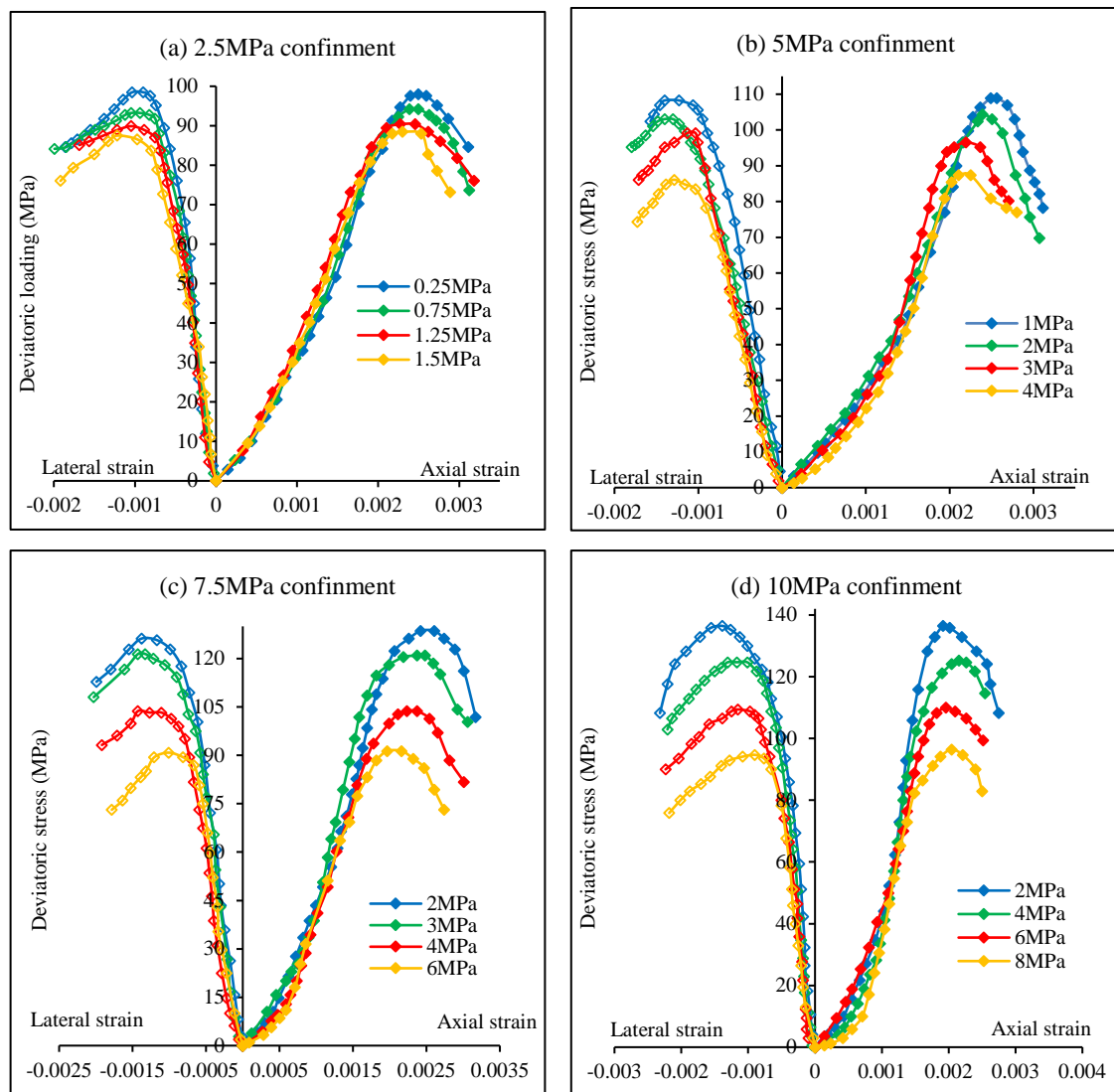


Figure 3.5. The stress-strain behaviour of dry samples under tested conditions.

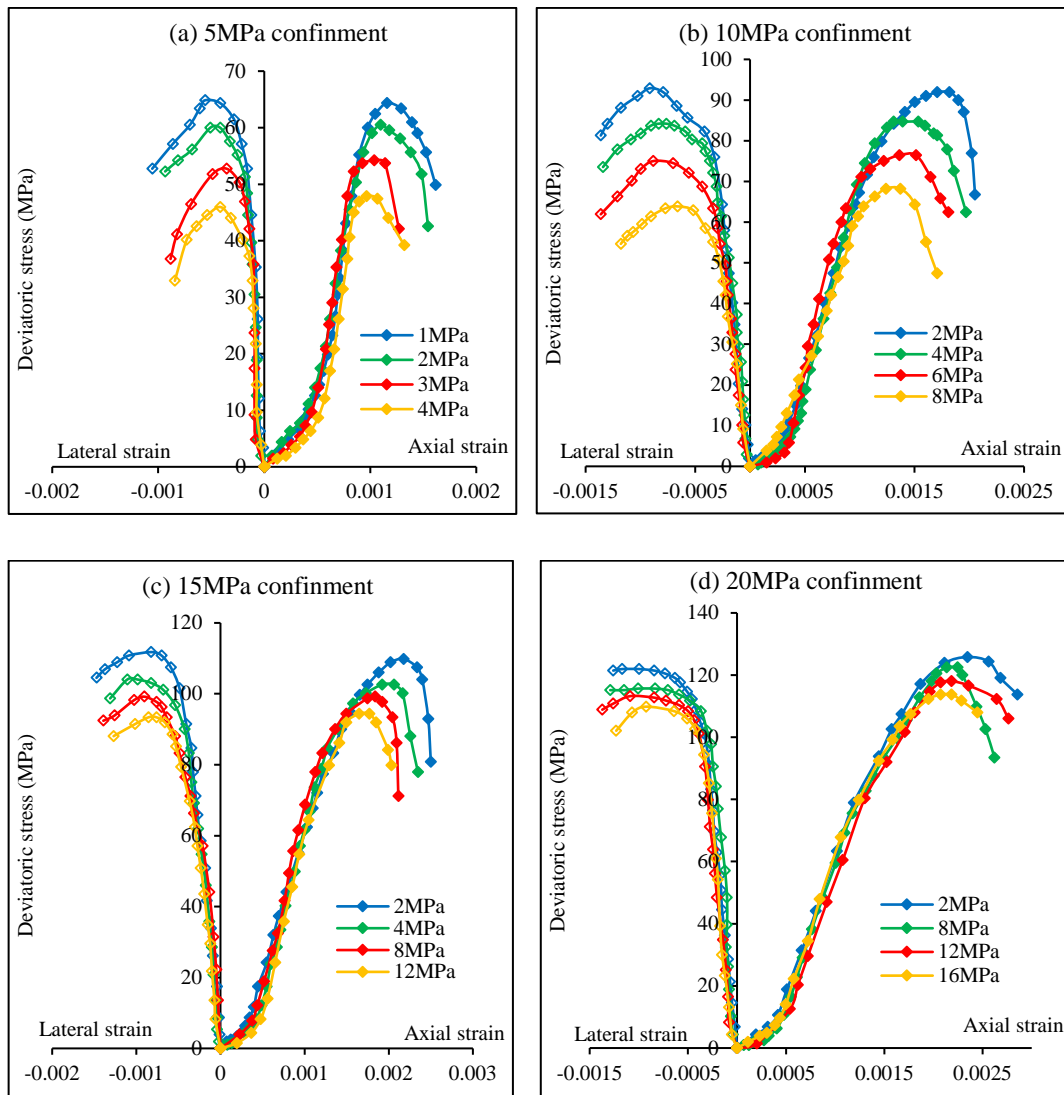
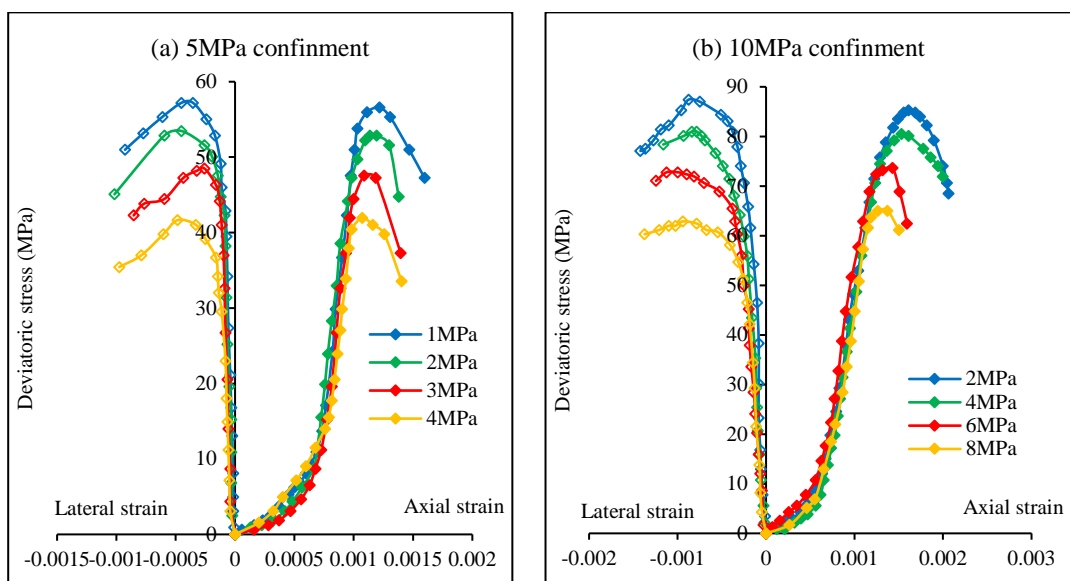


Figure 3.6. The stress-strain behaviour of brine-saturated samples under tested conditions.



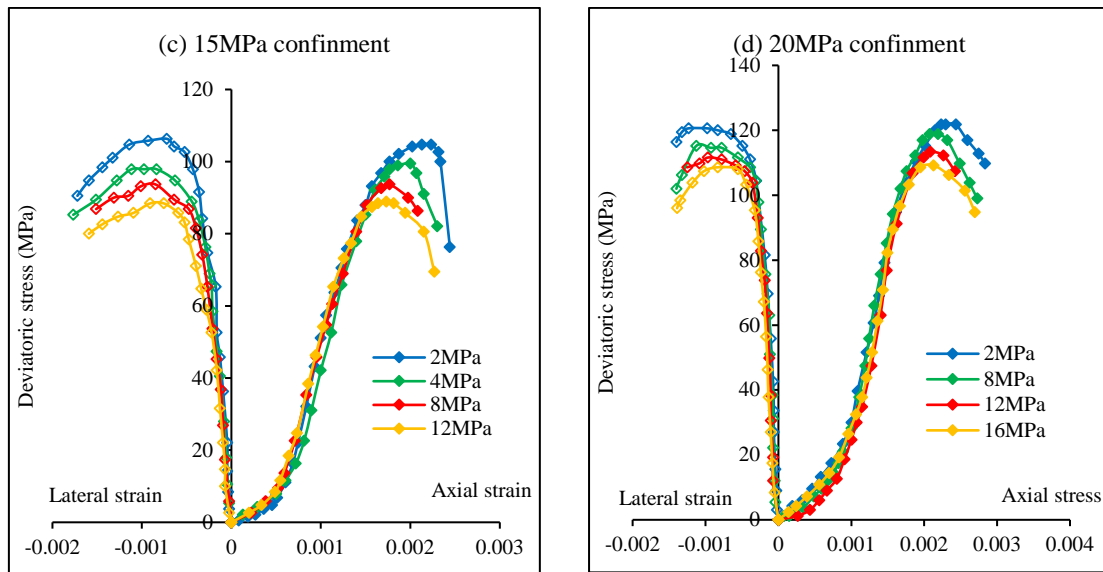
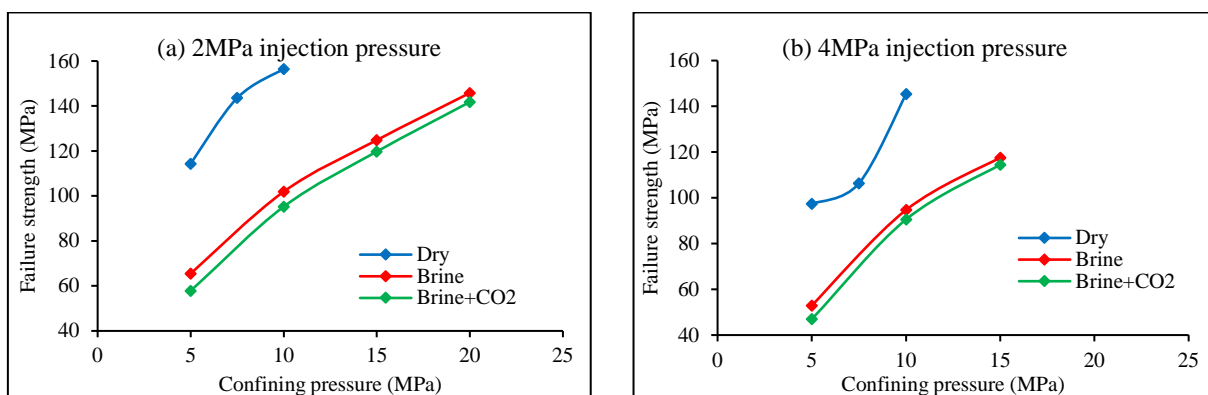


Figure 3.7. The stress-strain behaviour of brine+CO₂-reacted samples under tested conditions.

Figs. 3.8 and 3.9 show the variation of failure strength (peak strength) with confining and injection pressures, respectively. Interestingly, considerable strength reduction can be seen in the brine+CO₂-reacted samples compared with the dry and brine-saturated samples, as can be clearly seen in Figs. 3.7 and 3.8. This strength reduction can be explained by investigating the corresponding mineralogical rock alterations. According to Marbler et al. (2013), this brine-CO₂-rock minerals interaction-induced rock mineral dissolution causes a mechanical weakening in rock minerals' grain contacts and cement bounds. This is supported by the results of the SEM analysis shown in Fig. 3.4. This weakening of grain boundaries and cementing bonding phases in the rock mass reduces the failure strength of the reservoir rock by causing early failures compared to the dry and brine-saturated conditions.



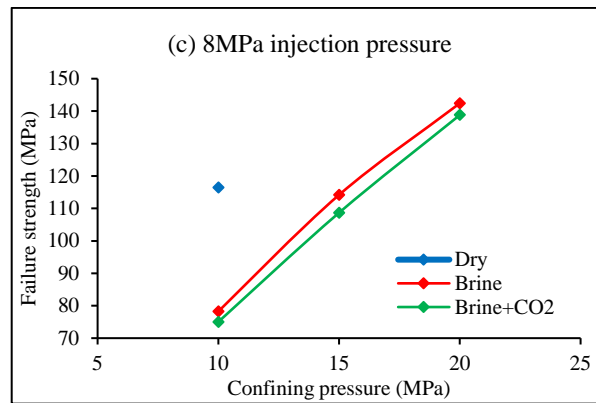


Figure 3.8. The variation of failure strength with respect to confining pressure for tested conditions.

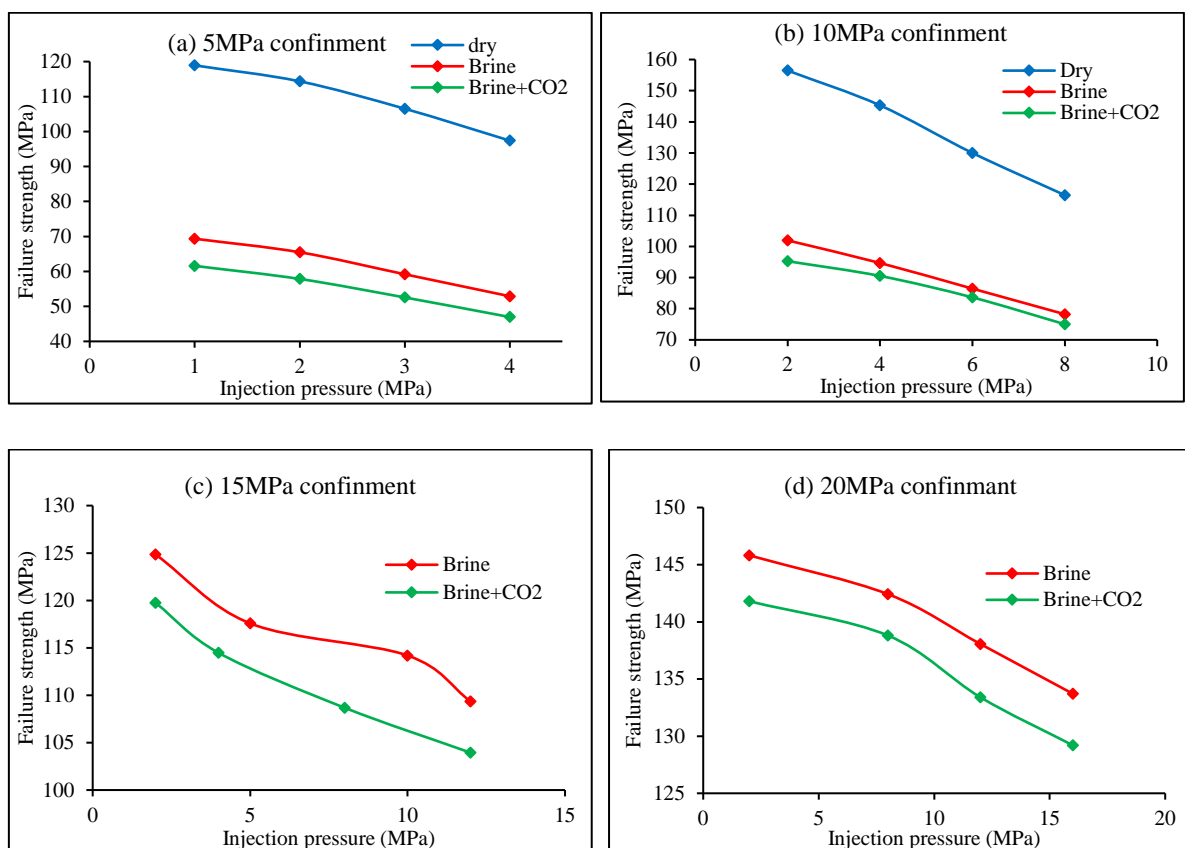


Figure 3.9. The variation of failure strength with different injection pressures for tested conditions.

If the influence of confining pressure on reservoir rock failure strength is considered, Fig. 3.8 shows the variation of reservoir rock strength with confining pressure. The figure shows a non-linear increase in failure strength with increasing confining pressure. It is well known that increased confining pressure or depth (increased effective stress) causes the natural fractures in

the reservoir rock to close, ultimately causing the reservoir rock strength to increase. To date, numerous studies have been conducted on the effect of confining pressure on rock deformation characteristics (Gowd and Rummel, 1980; Bernabe et al., 1994; Wong et al., 1997; Mavko et al., 1998; Streit and Hillis, 2004), and these studies have proposed various stress-dependent models to explain this behaviour (Schutjens et al., 2004).

According to Fig. 3.9, the failure strength of reservoir rock decreases with increasing injection pressure, and the observed strength reduction with increasing injection pressure is also related to the effective stress effect, which reduces with increasing injection pressure, creating a pore pressure increment inside the rock pore space. This enhancement in pore pressure causes natural fractures to open and creates new fractures in the rock mass, reducing its strength and shifting the Mohr circle towards the failure envelope (Fig. 3.10). Many past studies have shown that increasing the pore fluid pressure in reservoir rocks reduces their strength (Handin et al., 1963; Blanpied et al., 1992). Australia's GEODISC research program (Rigg et al., 2000; Bradshaw and Rigg, 2001), which was conducted to evaluate the in-situ stresses and sustainable CO₂ injection pressures for safe sub-surface CO₂ storage, provides ample evidence of this increased pore pressure effect.

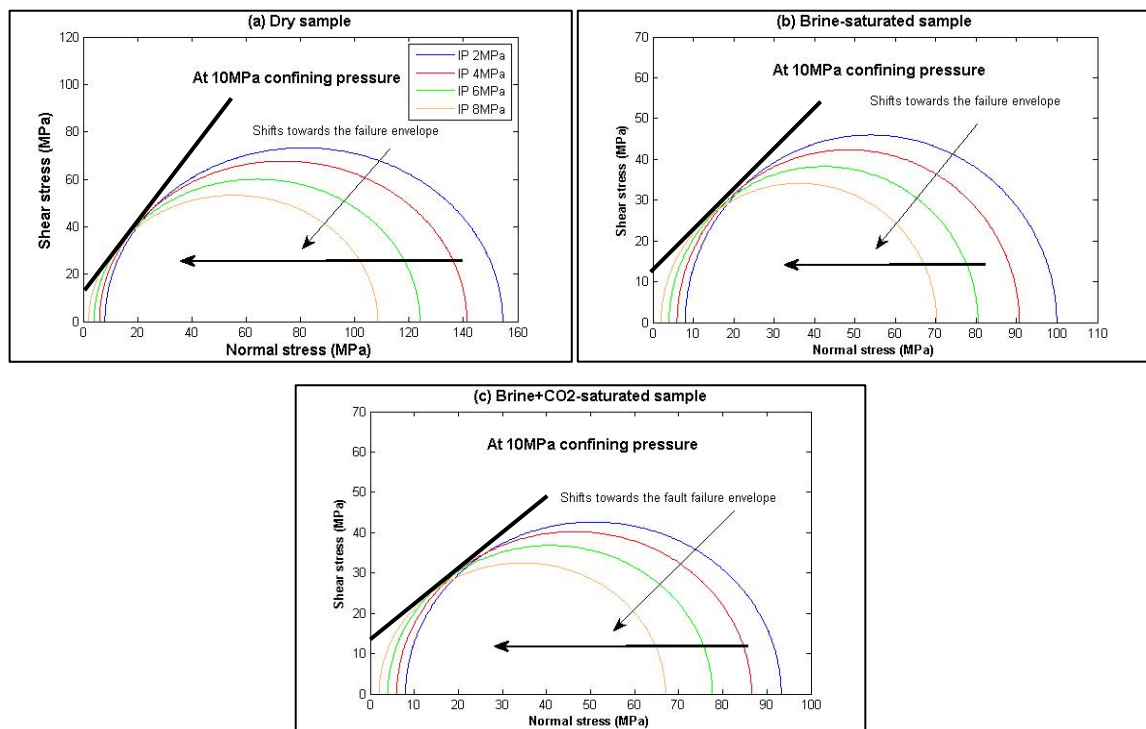


Figure 3.10. Effect of increasing injection pressure (2, 4, 6 and 8MPa) on stability of reservoir rock mass.

3.5.3.2 Change of effective stress behaviour in deep saline reservoir rock upon CO₂ injection

The experimental data were then used to determine the pore pressure sensitivity of depleted reservoir rock by evaluating the Biot effective stress coefficient for each tested condition (dry, brine and brine+CO₂-reacted). The concept proposed by Terzaghi (1936) was used here to evaluate the effective stress coefficient for failure strength. According to this concept, the pore pressure and maximum mean stress have opposite effects on the rock bulk volume and therefore on many rock mechanical properties, including pore volume compression, bulk volume compression, acoustic wave propagation and failure. Rock strength, or any other material property of rock, obeys an effective stress concept if it can be defined as a linear combination of total stress and pore pressure. It is now well accepted that there is no unique effective stress coefficient applicable to all the material properties of rocks, because different material properties respond differently to the total stress and pore pressure (Ghabezloo et al., 2009; Rathnaweera et al., 2015a). This implies the requirement to have different effective stress relationships for different material properties. Moreover, the CO₂ injection-induced mineralogical changes and the corresponding pore space modifications cause the effective stress space of natural reservoir formations to change during the sequestration process, which therefore should affect the effective stress relations. For this reason, the present study developed an effective stress relationship to describe the stress dependency of the rock deformation in saline aquifer rock mass subjected to CO₂ sequestration and used this relationship to find the appropriate effective stress coefficients and α (the Biot coefficient), for the tested conditions.

The stress dependency of reservoir rock strength, F , can be defined as follows:

$$F = F(\sigma_n, P_p) = F(\sigma'_n) \quad (3.1)$$

where σ_n is the mean total stress, P_p is the pore pressure and σ'_n is the mean effective stress acting on the rock mass.

Based on Terzaghi's (1936) force-balance argument, the mean effective stress acting on the reservoir rock mass can be written as:

$$\sigma'_n = \sigma_n - \alpha P_p = \frac{\sigma_1 + 2\sigma_3}{3} - \alpha P_p \quad (3.2)$$

Accordingly, the incremental variation of the failure stress (F) can be expressed as (derivation of $F(\sigma_n, P_p)$);

$$dF = \frac{\partial F}{\partial \sigma_n} d\sigma_n + \frac{\partial F}{\partial P_p} dP_p \quad (3.3)$$

Eq. 3.3 can then be re-arranged as follows:

$$dF = \frac{\partial F}{\partial \sigma_n} \left[d\sigma_n - \left(-\frac{\partial F / \partial P_p}{\partial F / \partial \sigma_n} \right) dP_p \right] \quad (3.4)$$

The stress dependency behaviour of F can then be defined as a function of the incremental variation of mean effective stress ($d\sigma'_n$):

$$dF = \frac{\partial F}{\partial \sigma_n} d\sigma'_n \quad (3.5)$$

$$d\sigma'_n = d\sigma_n - \alpha dP_p \quad (3.6)$$

A comparison of Eq. 3.4 with Eq. 3.5 shows the relationship between F and the mean effective stress and can be correlated using the effective stress coefficient (α) (Eq. 3.6), which is the effective stress coefficient corresponding to the failure stress of the reservoir rock, and can be expressed as follows:

$$\alpha = -\frac{\partial F / \partial P_p}{\partial F / \partial \sigma_n} \quad (3.7)$$

Therefore, the iso-lines of failure stress can be obtained by integrating the differential equation of $d\sigma'_n = 0$, which gives the expression for mean effective stress for the failure stress of reservoir rock. The linear relationship presented in Eq. 3.2 is the most commonly used expression for mean effective stress evaluation in rocks, and can be obtained by evaluating the iso-lines of $F(\sigma_n, P_p)$. Furthermore, the α coefficient in the effective stress law can be determined using the gradient of the iso-failure stress curves in the (σ_n, P_p) plane.

The obtained iso-failure stress curves based on the conducted triaxial strength tests are presented in Fig. 3.11. According to the results, the effective stress coefficient of dry samples decreases from 0.94 to 0.86 when brine (15% NaCl) is introduced into the rock pore space. The observed reduction in effective stress coefficient with brine saturation is probably due to the deposition of NaCl crystals in the rock pore space, which consequently reduces the pore volume

of the rock pore structure by clogging the pore voids with deposited NaCl crystals. The results reveal that the deposition of NaCl crystals in the rock pore space makes the reservoir pore structure insensitive to the internally-imposed pore pressure. This observation is consistent with Rathnaweera et al.'s (2015c) findings in their study of the effect of salinity level on the effective stress coefficient for effective permeability in reservoir rocks. According to their results, the effective stress coefficient decreases with increasing salinity level from 0 to 30% (NaCl concentration) and explained this reduction by conducting microstructural analysis. They found deposition of NaCl crystals in the pore space. Importantly, according to Fig. 3.11, the brine+CO₂-reacted sample shows the highest effective stress coefficient (1.13) compared to the dry and brine-saturated conditions, and the value is greater than unity. When the effective stress coefficient is greater than unity, pore pressure change has more influence on mean effective stress than mean normal stress. Therefore, the brine+CO₂ reaction appears to create pore pressure-dominant mean effective stress behaviour in reservoir rock, probably due to the mineralogical rock alteration-induced pore expansion. This pore expansion increases the pore volume of the pore structure, enhancing the influence of pore pressure on the effective stress field acting on the rock mass.

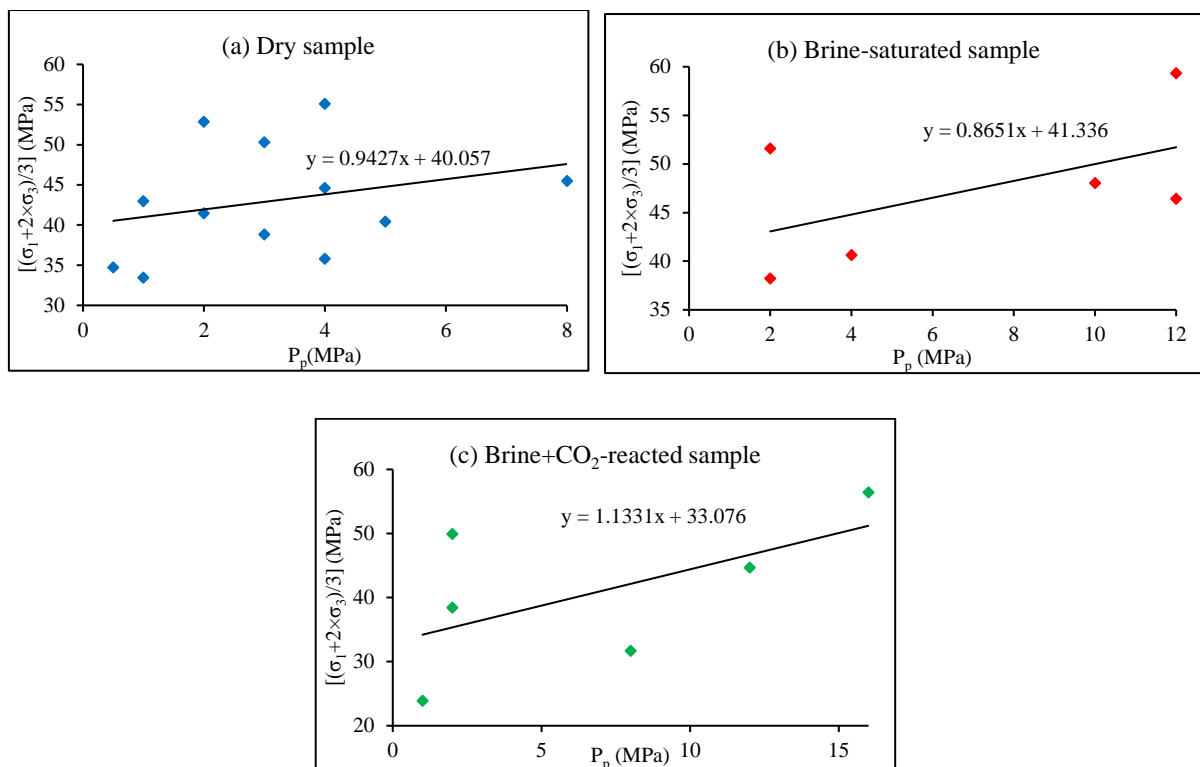


Figure 3.11. Iso-failure stress curves (a) dry samples (b) brine-saturated samples and (c) brine+CO₂-reacted samples.

3.5.3.3 Change of reservoir shear strength parameters under various stress environments

Since the stability of a saline aquifer is dependent on its shear strength, the alteration of shear strength parameters upon CO₂ injection was then considered under various reservoir and injection conditions by changing the injection pressure, confining pressure and saturation condition. The influence of injection pressure is considered first and the results are shown in Figs.3.12-3.14. Here, conventional Mohr circles have been drawn for the constant injection pressure condition, and two injection pressure conditions (2 and 4MPa) were selected for the dry condition, and three different injection pressures (2, 4, and 8MPa) were selected for the wet condition (both brine- and brine+CO₂-reacted). According to Figs. 3.12-3.14, Mohr-Coulomb failure lines deviate from linear to non-linear when the sample condition changes from dry to brine and dry to brine+CO₂-reacted. A more detailed view based on the analysis of shear strength parameters (cohesion and friction angle) shows that in dry rock, cohesion decreases and the friction angle increases with increasing injection pressure. However, this injection pressure influence on the shear strength parameters of brine- and brine+CO₂-reacted samples could not be predicted, due to the non-linear behaviour obtained under different injection pressure conditions.

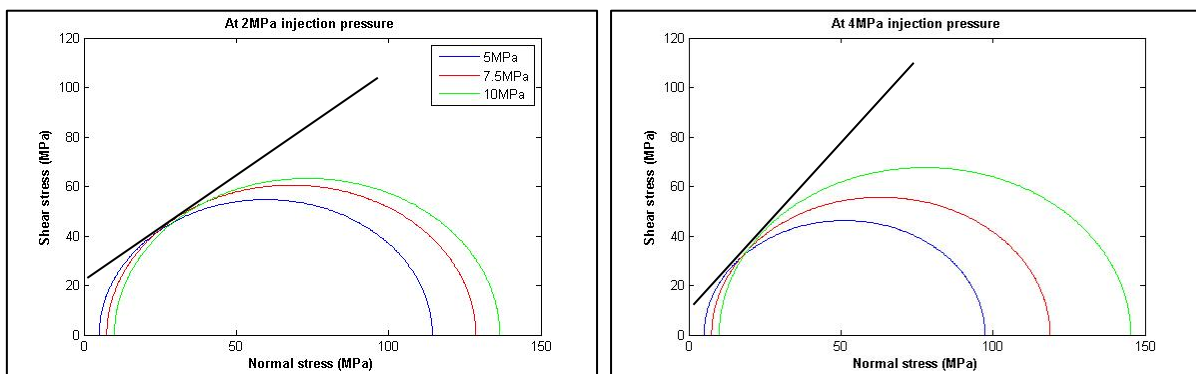


Figure 3.12. Mohr circle plots for dry reservoir rock samples under different confining pressure conditions.

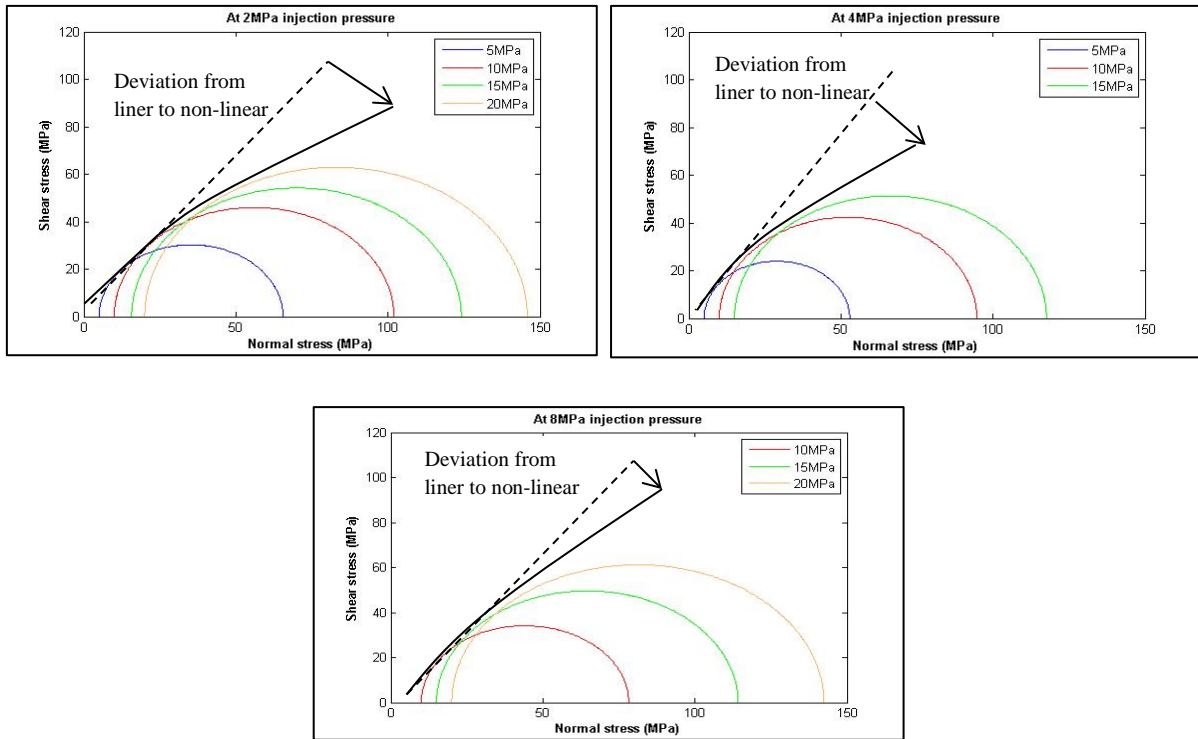


Figure 3.13. Mohr circle plots for brine-saturated reservoir rock samples under different confining pressure conditions.

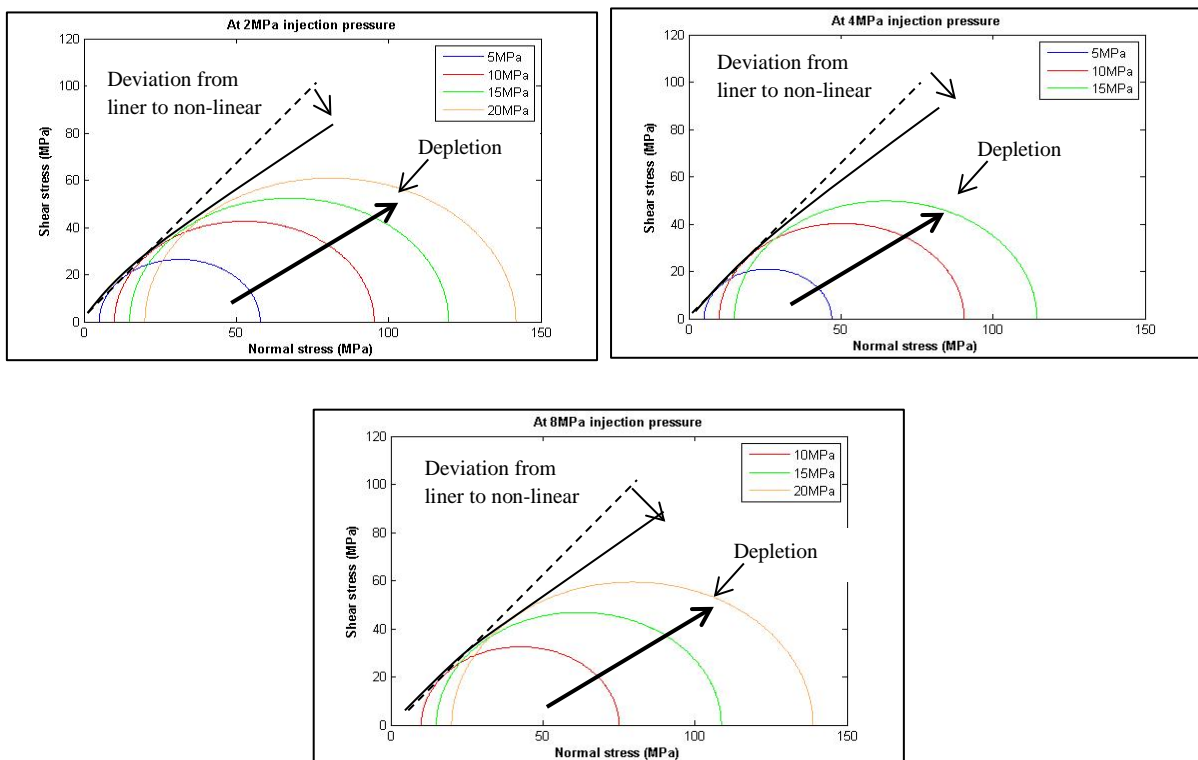


Figure 3.14. Mohr circle plots for brine+CO₂-reacted reservoir rock samples under different confining pressure conditions.

The influence of confining pressure on shear strength parameters (C and μ) was then evaluated by plotting the conventional Mohr-Coulomb failure circles under two circumstances. The effect of low confining pressures was first evaluated by plotting Mohr circles at 2.5, 5, 7.5 and 10MPa confining pressure conditions and the Mohr circles for each tested condition under constant confining pressure of 10MPa are shown in Fig. 3.10. According to Fig. 3.10, under constant low confining pressure, the failure envelopes of each tested condition display approximately linear behaviours with varying injection pressures and the corresponding friction angle decreases with the change of saturation condition from dry to wet condition. This is probably due to the water softening effect created by the brine in the rock pore space. Interestingly, the brine-saturated sample displays a greater friction angle than the brine+CO₂-reacted sample, exhibiting a CO₂ injection-induced friction angle reduction in the reservoir rock mass, which is probably due to the variation of NaCl crystals deposition in the rock pore space. This was confirmed by the significant NaCl crystal depositions observed in the brine-saturated sample compared to the brine+CO₂-reacted sample, where the friction between grain-to-grain contacts is increased with the deposition of NaCl crystals and CO₂ injection causes this NaCl crystalline process to slow down, enhancing the friction angle.

In relation to the variation of cohesion, cohesion appears to be enhanced with the brine saturation of reservoir rock sample, and interestingly, it is further enhanced by CO₂ injection. For example, the lowest cohesion can be seen in the dry sample and the highest cohesion can be seen in the brine+CO₂-reacted sample. The observed cohesion gain upon brine saturation is due to the enhanced rock mineral alteration due to brine and the injection of CO₂ further accelerates this reaction. The corresponding mineralogical changes can be clearly seen in the results of the XRD analysis (refer to Table 3.2). According to the table, brine+CO₂ and brine saturation enhance kaolinite precipitation, which eventually enhances the cohesiveness between grain contacts. Importantly, a significantly greater amount of kaolinite precipitation was observed in the brine+CO₂-reacted sample than the brine-saturated sample, which indicates the reason for the higher cohesion value observed for the brine+CO₂-reacted condition.

In relation to the effect of high confinement on shear strength parameters, as shown in Table 3.4, increasing the confinement causes the reservoir rock mass cohesion to be reduced and friction angle to be increased, regardless of saturation type, because the increased effective stress conditions under high confinements create more restriction for slippage. As shown in Figs. 3.15-3.16, in high confining stress environments, regardless of saturation type, the Mohr

circles lines obtained exhibit a non-linear variation with injection pressures, making it difficult to evaluate the shear strength parameters (Figs. 3.15 and 3.16).

Table 3.4. Results for cohesion and friction angle for each condition tested under constant confining pressure with different injection pressures.

Confining pressure (MPa)	Cohesion (MPa)			Friction angle (°)		
	Dry	Brine	Brine+CO ₂	Dry	Brine	Brine+CO ₂
2.5	13.14	14.87	15.01	39.41	35.76	33.81
5.0	12.78	14.51	14.88	39.88	36.10	34.03
7.5	11.51	13.43	13.89	40.53	36.98	34.81
10	10.13	12.47	13.41	41.21	37.41	35.16

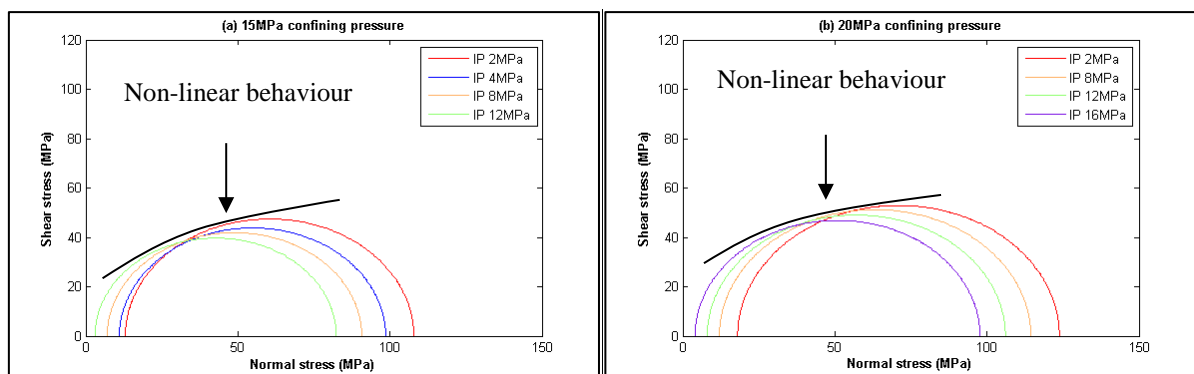


Figure 3.15. Mohr circle plots for brine-saturated samples under high confining pressure conditions.

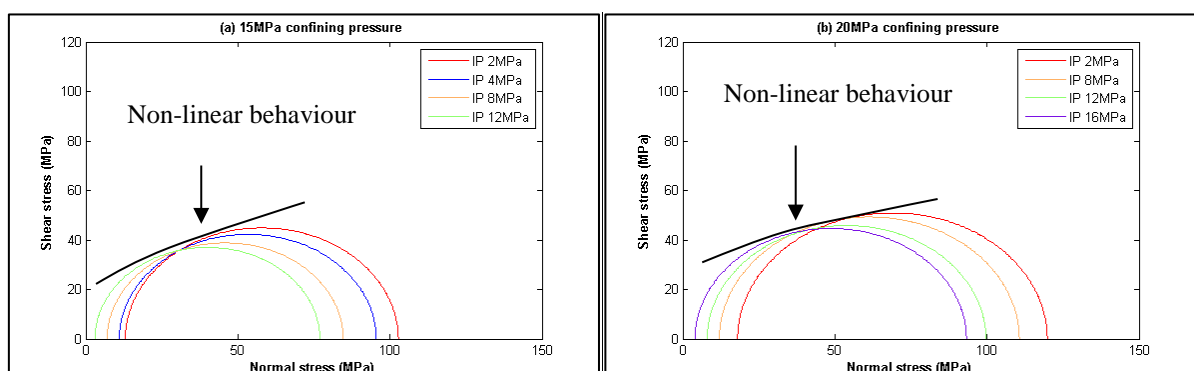


Figure 3.16. Mohr circle plots for brine+CO₂-reacted samples under high confining pressure conditions.

3.5.3.4 Evaluation of mechanical stability of reservoir rock using triaxial data

After evaluating the effective stress coefficient and shear strength parameters, the possible application of these data in estimating the mechanical stability of a given reservoir formation was investigated. The mechanical stability was first evaluated in terms of slip tendency and later, stress state and stress path analysis was carried out to identify the mechanical stability of reservoirs.

In the present study, the slip tendency (T_s), which is defined as the ratio of resolved shear stress to effective normal stress acting on failure plane ($\sigma_n - \alpha P_p$), was calculated based on Morris et al.'s (1996) findings :

$$T_s = \frac{\tau_r}{\sigma_n - \alpha P_p} = \frac{C + \mu[0.5(\sigma_1 + \sigma_3 - 2\alpha P_p) - 0.5(\sigma_1 - \sigma_3) \cos 2\theta]}{0.5(\sigma_1 + \sigma_3 - 2\alpha P_p) - 0.5(\sigma_1 - \sigma_3) \cos 2\theta} \quad (3.8)$$

where, τ_r is the shear stress that causes sliding, μ is the static friction coefficient, C is the inherent cohesion strength of the slip surface, σ_1 is the maximum principal stress, σ_3 is the minimum principal stress (confining pressure), θ is the angle between the shear plane and σ_1 and P_p is the pore pressure (CO₂ injection pressure).

For the calculation of slip tendency, the angle (θ) between shear plane and maximum principal stress axis was determined by resolving the stress field on the slip surface of each tested condition, as mentioned in Fig. 3.17. The calculated slip tendency data at 10MPa confining pressure for brine-saturated and brine+CO₂-reacted samples under different injection pressures are shown in Fig. 3.18. As Fig. 3.18 shows, slip tendency increases with increasing injection pressure for both conditions. Interestingly, with respect to the brine-saturated sample, slip tendency tends to occur easily in CO₂-reacted samples, because the brine+CO₂ interaction-associated weakening of the rock matrix and the dissolution of grain bonding can potentially activate fractures and cause slip on faults that exist in a reservoir formation (Sminchak et al., 2002). This shows the importance of detailed knowledge of stresses that act on reservoir rock mass to precisely estimate the sustainable injection pressures for selected saline aquifers to avoid the slipping effect. Such knowledge is also required to assess any possibility of seismic events during the CO₂ storage process.

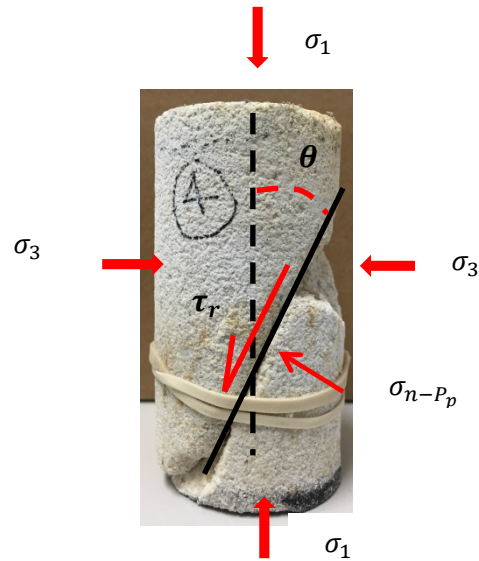


Figure 3.17. Stresses resolved on a slip surface of brine+CO₂-reacted sample.

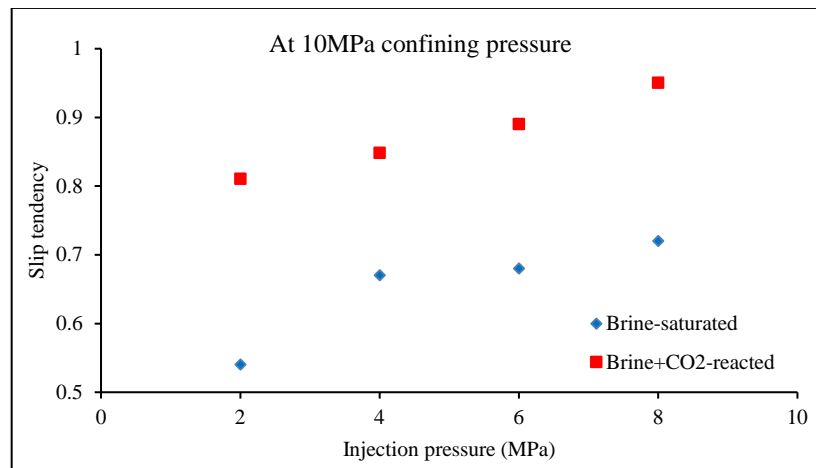


Figure 3.18. The calculated slip tendency data for brine+CO₂-reacted samples under different injection pressures.

After evaluating the slip tendency effect, triaxial data were used to develop a stress model which has the capability of giving the stress state of reservoir rock under any given injection and confining pressure conditions.

According to the stress-strain behaviour of reservoir rock, the effective stress development in a reservoir rock yields a combination of elastic and inelastic deformation mechanisms, which can be demonstrated by 2-D and 3-D stress space, as shown in Fig. 3.19. Based on a conceptual picture of 2-D and 3-D deformation mechanisms in P_{eff} (mean effective stress) and Q (effective principal stress) stress space, three different deformation domains can be identified:

(1) near-elastic (2) inelastic and (3) failure domains. Here, P_{eff} and Q are defined as Eqs. 9 and 10, respectively:

$$\sigma'_n (P_{eff}) = \frac{\sigma_1 + 2\sigma_3}{3} - \alpha P_p = \frac{I_1}{3} - \alpha P_p \quad (3.9)$$

$$Q = \sigma_1 - \sigma_3 = \sqrt{3}\sqrt{J_2} \quad (3.10)$$

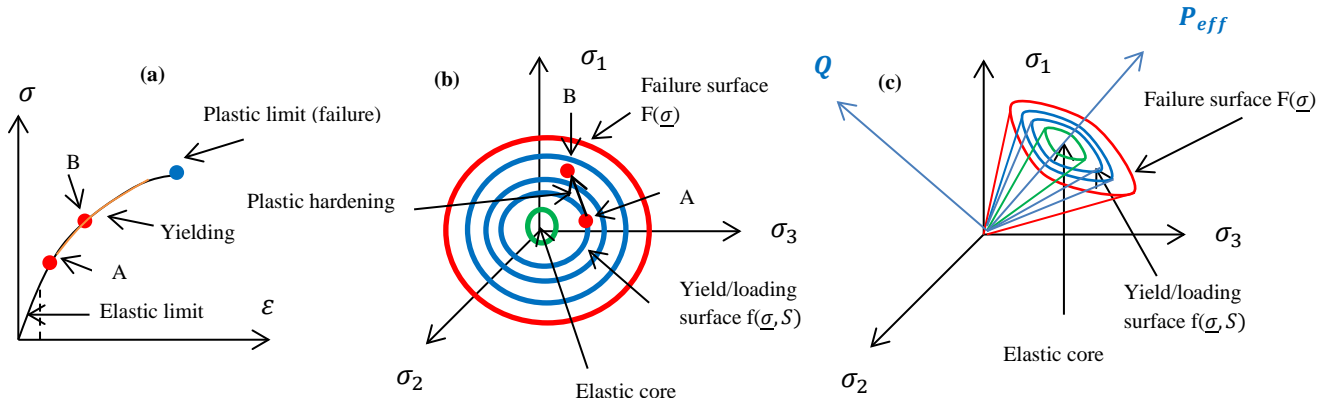
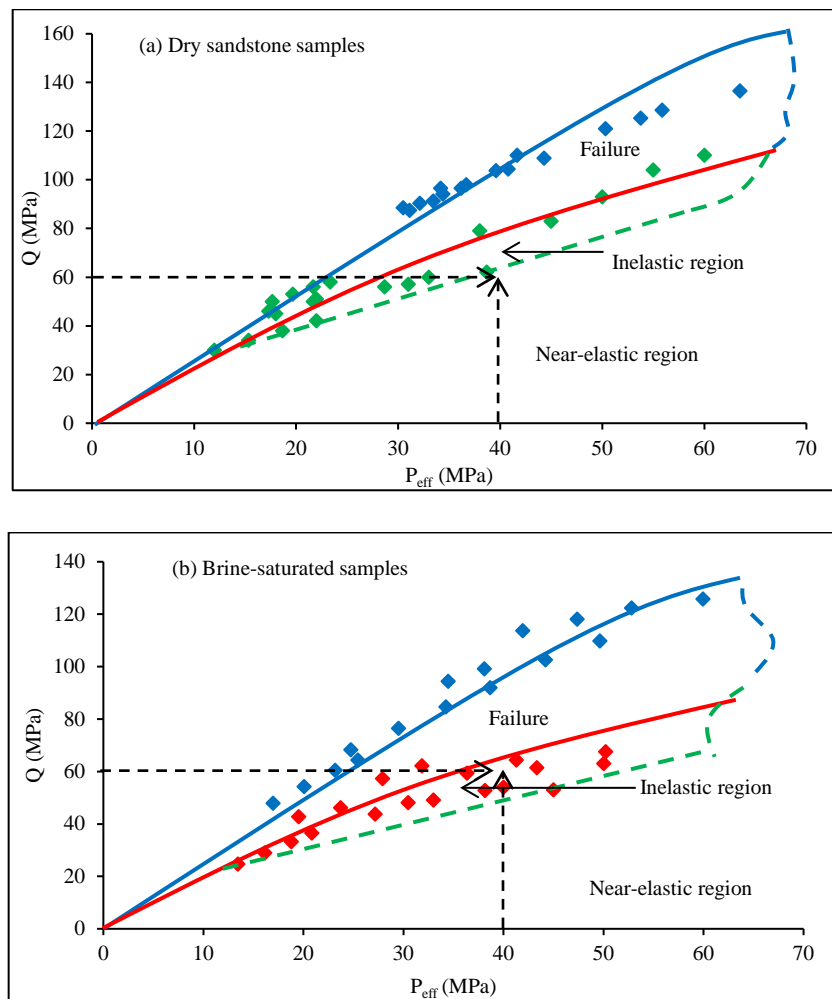


Figure 3.19. Conceptual picture of elastic and inelastic deformation mechanisms in 2-D and 3-D stress space

To date, similar studies have been carried out by a number of researchers (Bernabe et al., 1994; Wong and Baud, 1999; Schutjens et al., 2004), especially in quartz-rich sandstone. However, no study can be found on stress state variation due to CO_2 injection-induced rock mineral alteration in reservoir rock in deep saline sequestration. Therefore, this is considered in this section.

In order to evaluate the elastic and inelastic parts of the deformation, small unload/reload cyclic tests were carried out under each saturation condition. According to plasticity theory, reservoir rock can be assumed to behave elastically along stress excursions if the unload/reload cycle coincides with the stress-strain curve (Bernabe et al., 1994). Based on experimentally-observed unload/reload stress-strain behaviours, the corresponding yield point for each condition was defined. For the dry sample it occurs at around 80% of the peak strength and for the brine- and brine+ CO_2 -reacted samples it occurs at around 70% and 60% of the peak strength, respectively. The triaxial data for reservoir rock were then used to define the boundaries of the three deformation domains. Fig. 3.20 shows the proposed stress models for each tested condition (dry, brine-saturated and brine+ CO_2 -reacted reservoir rock). As mentioned earlier, each model has three domains: near-elastic, inelastic and failure, and each boundary condition was defined based on the model proposed by Schutjens et al. (2004). The top boundary of the failure domain

was defined by a polynomial function splined through the data corresponding to its failure. The bottom of the failure domain was also delineated by a polynomial function splined through the higher yield-stress data. The lower boundary of the inelastic domain was modelled using a straight line drawn through the lower yield-stress data. The near-elastic domain occurs under this lower boundary of the inelastic region. The major advantage of this stress model is that it can predict the mechanical stability for a given stress coordinate (injection and confining pressures) of a reservoir. For instance, if the stress state of a reservoir is assumed to be $P_{eff} = 40\text{MPa}$ and $Q = 60\text{MPa}$, according to the proposed model (Fig. 3.20), in the assumed effective stress environment, the dry reservoir rock sample deforms under the near-elastic domain while the brine-saturated reservoir rock (natural aquifer condition) sample deforms under the inelastic domain. Interestingly, under the same stress conditions, the brine+CO₂-reacted (depleted reservoir due to CO₂ injection) sample deforms under the failure domain, which indicates the instability of depleted reservoir rock compared to the other two conditions.



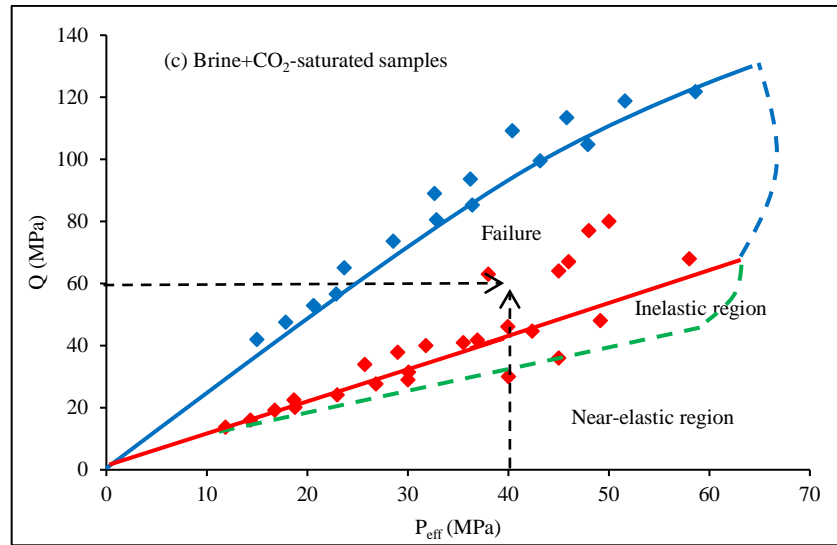


Figure 3.20. Reservoir compaction domains (a) dry sample (b) brine-saturated sample and (c) brine+CO₂-reacted sample.

In addition, stress path analysis was carried out to better understand the deformation process induced by CO₂ injection in reservoir rock. Generally, stress path analysis is one of the best methods to evaluate the mechanical deformation of reservoir rock, including deformation processes like fracturing, pore collapse with grain-size reduction, arching effects and grain crushing (Papamichos et al., 2000). The stress path coefficient (K) was defined as the ratio between changes in minimum effective principal stress to the change in maximum effective principal stress, which can be expressed as follows:

$$K = \frac{\Delta\sigma_3 - \alpha\Delta P_p}{\Delta P_{eff}} \quad (3.11)$$

According to Crawford et al. (1999), the stress path coefficient can be determined by the equivalent line slopes (η) of the P_{eff} versus Q stress plan.

$$\eta = \frac{\Delta Q}{\Delta P_{eff}} = \frac{3(1-K)}{1+2K} \quad (3.12)$$

Fig. 3.21a shows the equivalent line slopes (η) of the P_{eff} versus Q stress plan for each tested condition and Fig. 3.21b shows the variation of calculated K values for each saturation condition. The $K < 1$ is the general case for the reservoir depletion scenario and $K = 1$ represents the special case of reservoir depletion under isotropic stress conditions (constant total stress, $\Delta\sigma_1 = \Delta\sigma_3 = 0$) (Holt, 1999). Morita et al. (1992) evaluated the stress path coefficient of 12% (% by weight) NaCl-saturated Berea sandstone (with porosity ranging from 20-23%)

and found that the stress path coefficient is about 0.16. The calculated K values for depleted reservoir samples are consistent with the above findings, where the values lie below one, satisfying the condition of $K < 1$. The observed stress path characteristics indicate that the dry reservoir rock stress path changes upon exposure to both brine and injected CO_2 . Fig. 3.21b suggests that deformation along a stress path defined by $K = 0.05$ (brine+ CO_2 -reacted condition) and $K = 0.07$ (brine-saturated condition) will occur in the failure domain when compared to the stress path of dry reservoir rock ($K = 0.12$). Therefore, the value of K , corresponding to the dry reservoir rock sample, can be treated as a limit stress path for values larger than 0.12, deformation will occur entirely in the near-elastic domain. Furthermore, the variation of stress path coefficient with respect to confining pressure and injection pressure were also studied under the tested conditions (Fig. 3.22).

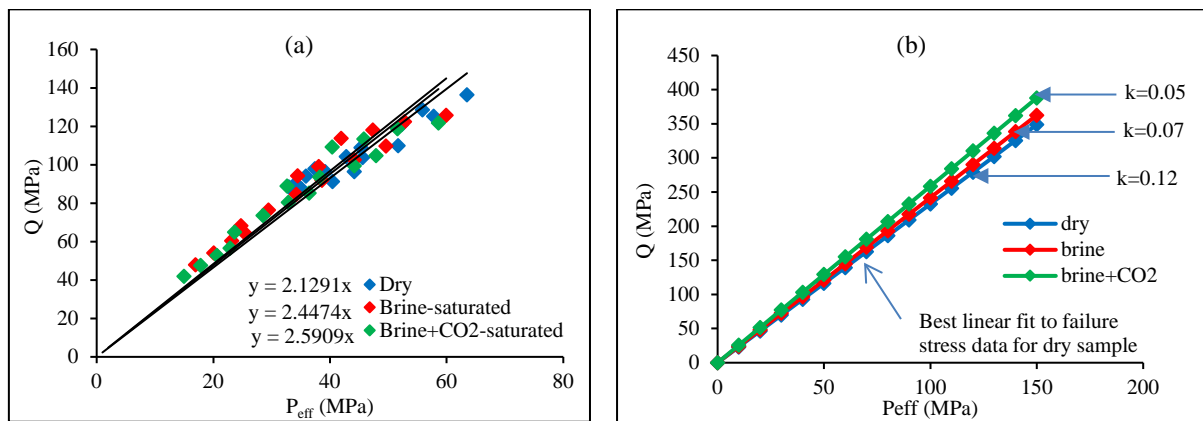


Figure 3.21. (a) Equivalent line slopes in the P_{eff} versus Q stress plane (b) Stress path coefficient for each tested condition.

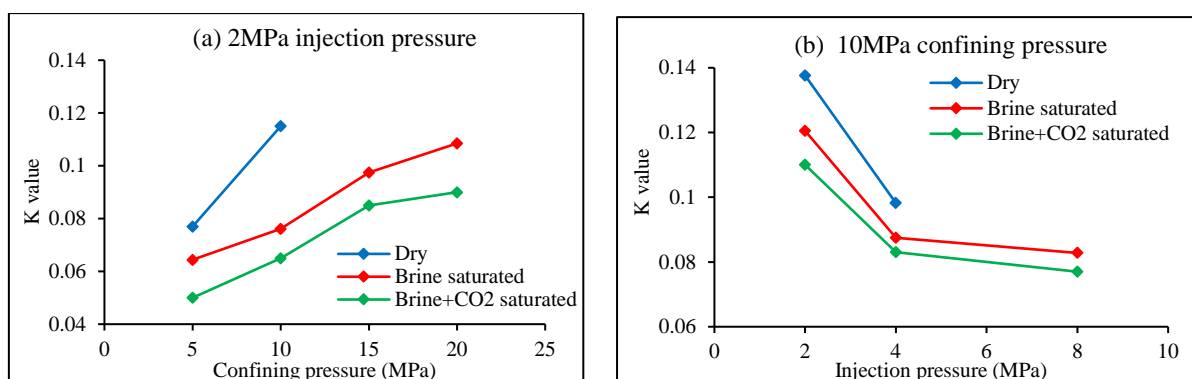


Figure 3.22. Variation of stress path coefficient with respect to (a) confining pressure and (b) injection pressure.

The influence of confining pressure on stress path was evaluated under constant injection pressure conditions. The stress path coefficient increases with increasing confining pressure, and this increment is probably due to the mobilised high effective stress field (under constant injection pressure) in the rock matrix. For example, in the dry sample, the stress path coefficient increases from 0.077 to 0.115 as the confining pressure increases from 5 to 10MPa under 2MPa constant injection pressure. Similar increasing trends were observed for the other two conditions. In the brine-saturated sample, the stress path coefficient increases from 0.0644 to 0.1085 with increasing confining pressure from 5 to 20MPa, and in the brine+CO₂-reacted sample, it increases from 0.05 to 0.09 with the increase of confining pressure from 5 to 20MPa under 2MPa injection pressure condition. However, contrary behaviour was observed with increasing injection pressure under constant confining pressure condition, and the stress path coefficient decreases with increasing injection pressure due to the reduction of effective stress acting on the rock matrix. For instance, in the dry sample, the stress path coefficient decreases from 0.138 to 0.098 as the injection pressure increases from 2 to 4MPa under 10MPa constant confining pressure. Similar increasing trends were observed for the other two conditions. In the brine-saturated sample, the stress path coefficient decreases from 0.12 to 0.083 with increasing injection pressure from 2 to 8MPa and in the brine+CO₂-reacted sample, it decreases from 0.11 to 0.077 with the increase of confining pressure from 2 to 8MPa under 10MPa confining pressure.

3.5.4 Conclusions

A series of triaxial strength tests was conducted on sandstone samples obtained from the Gosford (Sydney) basin to characterise the mechanical behaviour of reservoir rocks upon exposure to scCO₂. The following conclusions can be drawn:

- CO₂ injection into deep saline aquifers causes its rock mass to weaken, and the strength of the tested depleted sandstones (brine+CO₂-reacted) was noticeably reduced upon CO₂ injection.
- This mechanical weakening is mainly related to the alteration of the rock's mineralogical structure through brine/scCO₂ interaction, which mainly affects the cement among grain-to-grain contacts. SEM and XRD analyses showed significant quartz and calcite minerals dissolutions in brine+CO₂-reacted sandstone.
- The rock mineral dissolution alters the reservoir rock pore structure, resulting in an altered effective stress field acting on the reservoir rock mass. Eventually, this leads to early

reservoir rock failure. For instance, two years of reaction with scCO₂ at 15MPa confinement and 8MPa injection pressure caused the failure strength of brine-saturated sandstone to decrease from 114.19 to 108.68 MPa.

- Importantly, CO₂ injection may cause the creation of a pore-pressure dominant effective stress field inside the depleted reservoir formation. This was confirmed by the effective stress coefficients observed for the brine+CO₂-reacted and brine-saturated samples (1.13 and 0.87, respectively). This pore-dominant effective stress field may affect the maximum sustainable pore fluid pressure for CO₂ injection and therefore the long-term safety of the reservoir.
- CO₂ injection also causes the slip tendency in the reservoir rock mass to increase, which increases with increasing CO₂ injection pressure. This indicates the need for precise evaluation of the sustainable fluid pressure for the underground storage of CO₂ in deep saline aquifers.
- Finally, a stress model was developed based on the results, which shows the relationship between stress state and mechanical stability of reservoir rock and characterising the mechanical behaviour of reservoir rock in effective stress versus effective principal stress space. Such models will be useful for predicting the possible failure of reservoir formations upon CO₂ sequestration and enabling the conduct and maintenance of safe injection in deep saline sequestration.

3.5.5 References

1. Addis MA, Cauley MB, Kuyken C. Brent in-fill drilling programme: Lost circulation associated with drilling depleted reservoirs. SPE/IADC Drilling Conference, Amsterdam, 27 February-1 March, 2001.
2. Bachu S, Bennion B. Effects of in-situ conditions on relative permeability characteristics of CO₂-brine systems. *Environmental Geology* 2008; 54(8): 1707-1722.
3. Bernabe D, Fryer T, Shively RM. Experimental observations of the elastic and elastic behaviour of porous sandstones. *Journal of International Geophysics* 1994; 117: 403-418.
4. Blanpied ML, Lockner DA, Byerlee JD. An earthquake mechanism based on rapid sealing of faults. *Nature* 1992; 358: 574-586.
5. Bouteica MJ, Sarda JP, Vincke O. Constitutive law for permeability evolution of sandstones during depletion. SPE International Symposium on Formation Damage Control, Lafayette, Louisiana, 23-24 February, 2000.
6. Bradshaw J, Rigg A. The GEODISC program: research into geological sequestration of CO₂ in Australia. *Environmental Geoscience* 2001; 8(3): 166-76.
7. Chen WF, Han DJ. *Plasticity for structural engineers*, Springer, 1998.
8. Chilingarian GV, Donaldson EC, Yen FF. *Subsidence due to fluid withdrawal. Developments in petroleum science*, Elsevier Science, Amsterdam 41, 1995.
9. Crawford BR, Hutcheon R, Smart BGD, Yale DP. Coupled mechanical deformation and fluid flow in experimentally yielded granular reservoir materials. In 9th ISRM Congress. International Society for Rock Mechanics 1999.
10. Ewy RT. Wellbore-stability predictions by use of a modified Lade criterion. *SPE Drilling and Completion* 1999; 14(2): 85-91.
11. Fredrich JT, Arguello JG, Deitrick GL, De Rouffignac EP. Geomechanical modelling of reservoir compaction surface subsidence and casing damage at the Belridge Diatomite Field. *SPE Reservoir Evaluation and Engineering* 2000; 3(04): 348-359.
12. Freeze RA. Social decision making and land subsidence. *Land Subsidence Proceedings SISOLS*, L. Carbognin, G. Gambolati, and A.I. Johnson (eds.), Ravenna, Italy (September) 353, 2000.

13. Friedman M. Fracture in rock. *Geophysics and Space Physics* 1975; 13: 352-358.
14. Ghabezloo S, Sulem J, Guedon S, Martineau F. Effective stress law for the permeability of a limestone. *International Journal of Rock Mechanics and Mining Sciences* 2009; 46: 297-306.
15. Gowd TN, Rummel F. Effect of confining pressure on the fracture behaviour of a porous rock. *International Journal of Rock Mechanics and Mining science* 1980; 17: 225-229.
16. Grasso JR, Volant P, Fourmaitreaux D. Scaling of seismic response to hydrocarbon production: A tool to estimate both seismic hazard and reservoir behaviour over time,” paper presented at EUROCK, Delft, The Netherlands, 1994.
17. Handin J, Hager Jr RV, Friedman M, Feather JN. Experimental deformation of sedimentary rocks under confining pressure: pore pressure tests. *Bulleting American Association of Petroleum Geology* 1963; 47(5): 717-55.
18. Hellevang H, Declercq J, Aagaard P. Why is dawsonite absent in CO₂ charged reservoirs? *Oil and Gas Science and Technology* 2011; 66(1):119-135.
19. Hem JD. Study and interpretation of the chemical characteristics of natural water. U.S. Geology Survey and Water- Supply 1959; 54: 1473-1482.
20. Hettema MHH, Schutjens PMTM, Verboom BJM, Gussinklo HJ. Production-induced compaction of a sandstone reservoir: the strong influence of stress path. *SPE Reservoir Evaluation and Engineering* 2000; 3(04): 342-347.
21. Holt RM. Reservoir stress path: Evaluation of core and field data,” *Rock Mechanics for Industry*, Amadei, Kranz, Scott, and Smeallie (eds.), Balkema, Rotterdam, The Netherlands, 1999.
22. I.S.R.M. ISRM suggested methods: rock characterization, testing and monitoring. In: Brown ET, editor. London: Pergamon, 1981.
23. Jaeger CJ, Cook NGW, Zimmerman R. *Fundamentals of rock mechanics*. Wiley-Blackwell 2007; 488-523.
24. Johnson JP, Khctt DW, Siemens WT. Rock mechanics of the Ekofisk reservoir in the evaluation of subsidence. *Journal of Petroleum technology* 1989; 24: 717-722.
25. Marbler H, Erickson KP, Schmidt M, Lempp C, Pollmann H. Geomechanical and geochemical effects on sandstones caused by the reaction with supercritical CO₂: an

experimental approach to in situ conditions in deep geological reservoirs. *Environmental Earth Science* 2013; 69: 1981-1998.

26. Marini L. Geological sequestration of CO₂-Thermodynamic kinetics and reaction path modelling; 11: 453. Elsevier, Amsterdam. The Netherlands, 2007.

27. Mavko G, Mukerji T, Dvorkin J. The rock physics hand book. Cambridge University Press, 1998.

28. McLean M, Addis M. Wellbore stability: the effect of strength criteria on mud weight recommendations. In: Proceedings of the 65th annual technical conference and exhibition, Society of petroleum engineers, New Orleans, September 23–26, 1990.

29. Morita N, Gray SPE, SrouJI KE, Jogl P N. Rock property changes during reservoir compaction. SPEFE Transaction AIME 1992; 197: 293-306.

30. Morris A, Ferril DA, Henderson DB. Slip tendency analysis and fault reactivation. *Geology* 1996; 24(3): 275-288.

31. Papamichos E. Constitutive laws for geomaterials. *Oil and Gas Science and Technology* 1999; 54: 759-772.

32. Rathnaweera TD, Ranjith PG, Perera MSA. Salinity-dependent strength and stress–strain characteristics of reservoir rocks in deep saline aquifers: An experimental study. *Fuel* 2014a; 122: 1-11.

33. Rathnaweera TD, Ranjith PG, Perera MSA. Effect of salinity on effective CO₂ permeability in reservoir rock determined by pressure transient methods: an experimental study on Hawkesbury sandstone. *Rock Mechanics and Rock Engineering*; DOI 10.1007/s00603-014-0671-0, 2014b.

34. Rathnaweera TD, Ranjith PG, Perera MSA, Yang SQ. Determination of effective stress parameters for effective CO₂ permeability in deep saline aquifers: An experimental study. *Journal of Natural Gas Science and Engineering* 2015a; 24: 64-79.

35. Rhett DW, Teufel LW. Effect of reservoir stress path on compressibility and permeability of sandstones. SPE Annual Technical Conference and Exhibition, Washington, DC, 4-7 October, 1992.

36. Rigg A, Allison G, Bradshaw J, Ennis-King J, Gibson-Poole C, Hillis RR, et al. The search for sites for geological sequestration of CO₂ in Australia: a progress report on GEODISC. *Journal of Appea* 2000; 41: 711-25.
37. Ruistuen H, Teufel L, Rhett D. Influence of reservoir stress path on deformation and permeability of weakly cemented sandstone reservoirs. SPE Annual Technical Conference and Exhibition, Denver, 6-9 October, 1996.
38. Schutjens PMTM, Fens TW, Smits RMM. Experimental observations of the uniaxial compaction of quartz-rich reservoir rock at stresses up to 80 MPa. *Land Subsidence Proceedings of 5th International Symposium on Land Subsidence, Intl. Assn. of the Hydrological Sciences, The Hague (16-20 October), 1995; 389-412.*
39. Schutjens PMTM, Hanssen TH, Hettema MHH, Merour J, Bree PD, Coremans JWA, et al. Compaction-induced porosity/permeability reduction in sandstone reservoirs: Data and model for elasticity-dominated deformation. *SPE Reservoir Evaluation and Engineering* 2004; 7: 12-27.
40. Scott RF. Plasticity and constitutive relations in soil mechanics. *Journal of Geotechnical Engineering* 1985; 111: 563-605.
- 41 Shukla R, Ranjith PG, Choi SK, Haque A, Yellishetty M, Hong L. Mechanical behaviour of reservoir rock under brine saturation. *Rock Mechanics and Rock Engineering* 2012; 46(1): 83-9.
42. Sing M, Raj A, Bhawani S. Modified Mohr-Coulomb criterion for non-linear triaxial and polyaxial strength of intact rocks. *International Journal of Rock Mechanics and Mining Sciences* 2011; 48: 546-555.
43. Sminchak J, Gupta N, Byrer C, Bergman P. Issues related to seismic activity induced by the injection of CO₂ in deep saline aquifers. *Journal of Energy and Environment Research* 2002; 2(1): 32-46.
44. Span R, Wagner W. A new equation of state for carbon dioxide covering the fluid region from the triple-point temperature to 1100 K at pressures up to 800 MPa. *Journal of Physics and chemistry* 1996; 25, 1509-1596.
45. Streit JE, Hillis RR. Estimating fault stability and sustainable fluid pressures for underground storage of CO₂ in porous rock. *Energy* 2004; 29: 1445-1456.

46. Terzaghi K. The shearing resistance of saturated soils and the angle between the planes of shear. In: Proceedings of the First International Conference on Soil Mechanics; vol. 1. Cambridge: Harvard University, 1936: 54-6.
47. Wigand M, Carey JW, Schmitt H, Spangenberg E, Erzinger J. Geochemical effects of CO₂ geochemistry in sandstones under simulated in situ conditions of deep saline aquifers. *Applied Geochemistry* 2008; 23: 2735-2745.
48. Wong TF, David C, Zhu W. The transition from brittle faulting to cataclastic flow in porous sandstones: Mechanical deformation. *Journal of Geophysics* 1997; 102: 3009-3019.
49. Wong TF, Baud P. Mechanical compaction of porous sandstone. *Oil and Gas Science and Technology* 1999; 54: 785-797.

3.6 Summary of Chapter 3

The main objective of this chapter was to experimentally investigate the effect of CO₂ sequestration on the mechanical properties of deep saline reservoir rock. The results of uniaxial and triaxial strength tests conducted on reservoir rock have therefore been presented. The experimental series was started by evaluating the mechanical behaviour of natural formations under brine-saturated conditions and then CO₂ was injected into brine-saturated samples to investigate the influence of CO₂ on the mechanical properties of reservoir rock. For the triaxial strength tests, undrained experiments were performed using the newly-developed triaxial set-up (Section 3.1) on reservoir rock samples obtained from the Gosford site.

First, the natural aquifer's mechanical behaviour was characterised based on the salinity effect in both uniaxial and triaxial stress environments. According to the results of the salinity tests, the presence of NaCl in the pore fluid causes the reservoir rock mechanical properties to change. Uniaxial strength tests on brine-saturated samples confirmed a strength gain in reservoir rock compared to water-saturated samples, which was also shown by triaxial test results. The maximum strength gain was observed in samples saturated with higher percentages of NaCl (20 and 30%). According to SEM analysis, when the aquifer has a higher percentage of salinity, there is a significant number of NaCl deposits in the pore structure of the rock mass, and these deposits enhance the reservoir rock strength by reducing the number of voids. In addition, confining pressure also plays a considerable role in reservoir rock strength, and it causes the reservoir rock strength to increase. Next, the applicability of the conventional Mohr-Coulomb criterion to represent the stress state of brine-saturated reservoir rock was investigated. The results confirmed a considerable deviation of the measured triaxial data of brine-saturated Hawkesbury sandstone from the conventional Mohr-Coulomb failure criterion, especially at high confining pressures. In order to correct this deviation, the present study modified the conventional Mohr-Coulomb failure criterion, based on experimental data and a modified version is proposed. The proposed model was finally validated and its accuracy confirmed in predicting the stress-strain behaviour of reservoir rock in deep saline aquifers.

According to the results of CO₂-reacted samples, the interaction between injected CO₂, brine and reservoir rock causes the Hawkesbury sandstone strength to be reduced in CO₂ sequestration in deep saline aquifers. For instance, super-critical CO₂ reaction causes around 32.89%, 17.65% and 14.75% uniaxial compressive strength reductions and 1.8%, 57.45% and 92.3% Young's modulus reductions in brine-saturated Hawkesbury samples with 10%, 20%

and 30% NaCl concentration brines, respectively. According to the SEM, XRD and XRF results, considerable quartz mineral corrosion and dissolution of calcite and siderite minerals were observed during the interaction of CO₂, brine and reservoir rock. The dissolution of these minerals weakens the grain-cemented bonds, accelerating the failure mechanisms of the pore matrix. The last section of this chapter summarises the mechanical behaviour of CO₂-induced reservoir rock in a triaxial stress environment. The experimental results reveal mechanical weakening in reservoir rock upon exposure to CO₂.

CHAPTER 4

Experimental Investigation of the Effect of CO₂ Sequestration on Flow Behaviour of Deep Saline Reservoir Rock

Declaration

Four publications are included in Chapter 4 and the details of the publications are given below.

Chapter 4.1

Rathnaweera TD, Ranjith PG, Perera MSA. Effect of salinity on effective CO₂ permeability in reservoir rock determined by pressure transient methods: An experimental study on Hawkesbury sandstone. *Rock Mechanics and Rock Engineering* 2015; 48(5): 2093-2110.

Chapter 4.2

Rathnaweera TD, Ranjith PG, Perera MSA, Yang SQ. Determination of effective stress parameters for effective CO₂ permeability in deep saline aquifers: An experimental study. *Journal of Natural Gas Science and Engineering* 2015; 24: 64-79.

Chapter 4.3

Perera MSA, **Rathnaweera TD**, Ranjith PG, Wanniarachchi WAM, Nasvi MCA, Abdulagatov IM, Haque A. Laboratory measurement of deformation-induced hydro-mechanical properties of reservoir rock in deep saline aquifers: An experimental implication of CO₂ sequestration. *Marine and Petroleum Geology* 2016; 77: 640-652.

Chapter 4.4

Rathnaweera TD, Ranjith PG, Perera MSA. Experimental investigation of geochemical and mineralogical effects of CO₂ sequestration on flow characteristics of reservoir rock in deep saline aquifers. *Nature Scientific Reports* 2016; 6: 19362.

Declaration for Thesis Chapter 4.1

Declaration by candidate

Monash University

In the case of Chapter 4.1 the nature and extent of my contribution to the work was the following:

Nature of Contribution	Extent of contribution (%)
Initiation, key ideas, experimental work, analysis of data and writing up	85

The following co-authors contributed to the work. Co-authors who are students at Monash University must also indicate the extent of their contribution in percentage terms:

Name	Nature of contribution	Extent of contribution (%) for student co-authors only
Ranjith PG	Key ideas, reviewing and editing the manuscript	N/A
Perera MSA	Reviewing and editing the manuscript	N/A

The undersigned hereby certify that the above declaration correctly reflects the nature and extent of the candidate's and co-authors' contributions to this work*.

**Candidate's
Signature**

		Date 22/07/16
--	--	-------------------------

**Main
Supervisor's
Signature**

		Date 22/07/16
--	--	-------------------------

*Note: Where the responsible author is not the candidate's main supervisor, the main supervisor should consult with the responsible author to agree on the respective contributions of the authors.

Declaration for Thesis Chapter 4.2

Declaration by candidate

Monash University

In the case of Chapter 4.2 the nature and extent of my contribution to the work was the following:

Nature of Contribution	Extent of contribution (%)
Initiation, key ideas, experimental work, analysis of data and writing up	85

The following co-authors contributed to the work. Co-authors who are students at Monash University must also indicate the extent of their contribution in percentage terms:

Name	Nature of contribution	Extent of contribution (%) for student co-authors only
Ranjith PG	Key ideas, reviewing and editing the manuscript	N/A
Perera MSA	Reviewing and editing the manuscript	N/A
Yang SQ	Reviewing and editing the manuscript	N/A

The undersigned hereby certify that the above declaration correctly reflects the nature and extent of the candidate's and co-authors' contributions to this work*.

Candidate's Signature		Date 22/07/16
------------------------------	---	-------------------------

Main Supervisor's Signature		Date 22/07/16
------------------------------------	---	-------------------------

*Note: Where the responsible author is not the candidate's main supervisor, the main supervisor should consult with the responsible author to agree on the respective contributions of the authors.

Declaration for Thesis Chapter 4.3

Declaration by candidate

Monash University

In the case of Chapter 4.3 the nature and extent of my contribution to the work was the following:

Nature of Contribution	Extent of contribution (%)
Initiation, key ideas, experimental work, analysis of data and writing up	85

The following co-authors contributed to the work. Co-authors who are students at Monash University must also indicate the extent of their contribution in percentage terms:

Name	Nature of contribution	Extent of contribution (%) for student co-authors only
Perera MSA	Key ideas, reviewing and editing the manuscript	N/A
Ranjith PG	Reviewing and editing the manuscript	N/A
Waniarachchi WAM	Reviewing and editing the manuscript	N/A
Nasvi MCA	Reviewing and editing the manuscript	N/A
Abdulgatov IM	Reviewing and editing the manuscript	N/A
Haque A	Reviewing and editing the manuscript	N/A

The undersigned hereby certify that the above declaration correctly reflects the nature and extent of the candidate's and co-authors' contributions to this work*.

Candidate's
Signature

		Date 22/07/16
--	--	-------------------------

Main
Supervisor's
Signature

		Date 22/07/16
--	--	-------------------------

*Note: Where the responsible author is not the candidate's main supervisor, the main supervisor should consult with the responsible author to agree on the respective contributions of the authors.

Declaration for Thesis Chapter 4.4

Declaration by candidate

Monash University

In the case of Chapter 4.4 the nature and extent of my contribution to the work was the following:

Nature of Contribution	Extent of contribution (%)
Initiation, key ideas, experimental work, analysis of data and writing up	85

The following co-authors contributed to the work. Co-authors who are students at Monash University must also indicate the extent of their contribution in percentage terms:

Name	Nature of contribution	Extent of contribution (%) for student co-authors only
Ranjith PG	Key ideas, reviewing and editing the manuscript	N/A
Perera MSA	Reviewing and editing the manuscript	N/A

The undersigned hereby certify that the above declaration correctly reflects the nature and extent of the candidate's and co-authors' contributions to this work*.

**Candidate's
Signature**

		Date 22/07/16
--	--	-------------------------

**Main
Supervisor's
Signature**

		Date 22/07/16
--	--	-------------------------

*Note: Where the responsible author is not the candidate's main supervisor, the main supervisor should consult with the responsible author to agree on the respective contributions of the authors.

4 Experimental Investigation of the Effect of CO₂ Sequestration on Flow Behaviour of Deep Saline Reservoir Rock

4.1 Effect of salinity on effective CO₂ permeability in reservoir rock

According to Chapter 3, salinity has major mechanical effects in deep saline reservoir rock. The influence of salinity on reservoir permeability is also important in deep saline sequestration, since deep saline aquifers generally contain high salinity brine. Therefore, this section of the thesis deals with the influence of salinity on the permeability of Hawkesbury sandstone. The selected brine concentrations are 0, 10, 20, and 30% NaCl by weight. In addition, the influence of CO₂ injection pressure on effective CO₂ permeability is also investigated for a range of injection pressures (2, 4, 6, 8, 10 and 12) at a constant confining pressure condition. Moreover, effective permeability behaviour following sub- and super-critical CO₂ injection are identified. The following published journal paper reports on this part of the study.



Effect of Salinity on Effective CO₂ Permeability in Reservoir Rock Determined by Pressure Transient Methods: an Experimental Study on Hawkesbury Sandstone

T. D. Rathnaweera · P. G. Ranjith ·
M. S. A. Perera

Received: 30 June 2014 / Accepted: 24 October 2014 / Published online: 12 November 2014
© Springer-Verlag Wien 2014

Abstract The determination of effective carbon dioxide (CO₂) permeability in reservoir rock and its variation is of great interest in the process of CO₂ sequestration in deep saline aquifers, as CO₂ sequestration-induced permeability alternations appear to create major problems during the CO₂ injection process. The main objective of this study is to investigate the effect of salinity on the effective CO₂ permeability of reservoir rock under different injection pressures. A series of high-pressure tri-axial experiments was, therefore, performed to investigate the effect of salinity on effective CO₂ permeability in Hawkesbury sandstone under various brine concentrations. The selected brine concentrations were 0, 10, 20, and 30 % sodium chloride (NaCl) by weight and the experiments were conducted for a range of CO₂ injection pressures (2, 4, 6, 8, 10, and 12 MPa) at a constant confinement of 20 MPa and a temperature of 35 °C, respectively. According to the results, the degree of salinity of the aquifer's pore fluid plays a vital role in the effective CO₂ permeability variation which occurs with CO₂ injection, and the effective permeability decreases with increasing salinity in the range of 0–30 % of NaCl. Interestingly, in dry reservoir rock samples, the phase transition of the injection of CO₂ from gas to super-critical condition caused a sudden reduction of CO₂ permeability, related to the slip flow effect which occurs in gas CO₂. Transfer into vapor or super-critical CO₂ causes this slip flow to be largely reduced, reducing the reservoir permeability for CO₂ movement in dry reservoir rock samples. However, this behavior was not

observed for water- and brine-saturated samples, and an increasing trend of effective CO₂ permeability was observed with increasing injection pressure. A detailed chemical analysis was then conducted to understand the physical phenomenon causing the salinity effect on effective CO₂ permeability using scanning electron microscopy analyses. Such analyses explain the reason for the observed permeability variations by giving detailed images of the rock sample's microstructure. There were clear depositions of NaCl crystals in the rock's pore space, and the amount increased with increasing brine concentration.

Keywords CO₂ sequestration · Saline aquifers · Effective CO₂ permeability · Salinity · Effective stress

4.1.1. Introduction

According to existing studies, deep saline aquifers are the most effective geological formation for CO₂ geo-sequestration, and seams located at 800–2,000 m depths which are highly saline ($\approx 20,000$ and $250,000$ mg/l) are most preferable, (Bachu and Bennion 2008). However, both CO₂ injection and storage capacities in saline aquifers are largely dependent on its permeability. According to past studies, permeability of sedimentary rocks in saline aquifers may vary significantly, depending on the rock formation properties and its depth (Neuzil 1994; Wang 2000). Injection of CO₂ into a saline aquifer during the sequestration process initiates many complex geo-chemical reactions, which significantly affect aquifer permeability. Due to high pressure and temperature conditions in deep saline aquifers, CO₂ exists in its highly complex and chemically reactive super-critical state, which enhances the process complexity. As a result, the prediction of aquifer

T. D. Rathnaweera · P. G. Ranjith (✉) · M. S. A. Perera
Deep Earth Energy Laboratory, Department of Civil
Engineering, Monash University, Building 60, Melbourne,
VIC 3800, Australia

permeability during the sequestration process becomes a challenge. According to Hangx et al. (2013) and Mohan et al. (1999), CO₂ injection pressure induces creep and micro-cracking, diffusive mass transfer processes, long-term mineralogical alteration, growth of NaCl crystals in the formation pore structure and fine particle migration in the rock pore space. These are the main factors which alter the aquifer's permeability during the CO₂ sequestration process. Although, the combined effect decides the final permeability variation, in most cases permeability tends to reduce with long-term CO₂ injection (Pearce et al. 1996, White et al. 2003). It is possible that the permeability reducing measures (e.g., NaCl crystallization and mineral depositions mainly clay mineral precipitation) make a greater contribution than the enhancing measures (e.g., cracking and mineral dissolution). However, the fluctuation of reservoir permeability during CO₂ injection is by no means favorable, as it causes the aquifer's storage capacity to decrease (Ranjith et al. 2013) and CO₂ injectability into the reservoir to decline, which affect the effectiveness of the whole process. Therefore, high injection pressures are required to maintain the effectiveness of the process. According to Vilarrasa et al. (2010), over-pressured CO₂ injection can cause excessive compression or even tension in the formation, resulting in formation of cracks and fractures (Rutqvist and Tsang 2002), which create leakage pathways for the injected CO₂ to back-migrate into the atmosphere. In spite of these facts, increased pore pressure in the reservoir at higher injection pressures counteracts the overburden pressure that may even cause the ground surface to be uplifted (e.g., the Salah CO₂ storage project) (Arsyad et al. 2013). In addition, lateral movement of the CO₂ plume along the formed fractures can contaminate underground fresh-water aquifers, which is a crucial

environmental impact. Therefore, it is essential to have detailed knowledge of reservoir permeability and its variation during the sequestration process. The main objective of the present study was to obtain such knowledge through (1) a comprehensive literature review and (2) a well-planned experimental programme. Under the experimental programme, the effect of the salinity level of the aquifer on its effective CO₂ permeability was determined under in situ conditions by performing high-pressure tri-axial experiments on samples sourced from the Gosford Basin, Australia. Scanning electron microscopy (SEM) and chemical analysis were also conducted to identify the corresponding interior (mineralogical and micro-logical) structure variation in the aquifer.

4.1.2. Literature Review

4.1.2.1. Effect of Brine Concentration

Over the last decade, a number of experimental studies on CO₂-brine flow systems in various rocks have been performed using steady and unsteady state tri-axial tests and core-flooding techniques to evaluate the rock permeability variation with CO₂ injection under various test conditions, including different CO₂ injection pressures, temperatures, depths, and salinity levels. The effect of salinity level is the main concern of this study. Table 1 below shows the summary of experimental studies carried out to date on the effect of salinity on effective CO₂ permeability of sandstone. As Table 1 indicates, although understanding of the effect of pore fluid brine concentration on reservoir effective CO₂ permeability is of great interest in environmental engineering, geothermal exploration, and the petroleum

Table 1 Summary of studies on the salinity effects on the permeability of reservoir rocks

Reference	Sample	Used fluids	Confining pressure (bar)	Temperature (°C)	Permeability variation (%)
Aktan and Farouk (1975)	Berea sandstone	NaCl (2 %)	4.1–206	27–260	Decrease
	Boise sandstone	NaCl (2 %)	4.1–206	27–260	N. C
Sydansk (1981)	Berea sandstone fired at 450 °C	NaCl (3 %)	138	22–85	Decrease
Khilar (1981)	Berea sandstone	NaCl: H ₂ O		0; 30; 60	$k_{60} > k_{30} > k_0$
Miller and Ramey (1986)	Berea sandstone	NaCl (22 %)	34	21–93	N. C
		NaCl (2 %)	34	21–93	Decrease
Ochi and Vernoux (1998)	Berea sandstone	NaCl (0.01–0.5 M)	0–250	0–90	Decrease
Bachu and Bennion (2008)	Alberta basin Canada	CO ₂ /brine system	200–2,000	30–50	Decrease
Berg et al. (2013)	Berea sandstone	CO ₂ /brine system	100–300	45	N.C
Samuel et al. (2012)	Berea sandstone Mt. Simon sandstone	CO ₂ /brine system	400–1,000	50	Decrease

industry, to date few related studies are available (Ochi and Vernoux 1998; Kuhn et al. 1998; Bachu and Bennion 2008; Probst 2008; Berg et al. 2013; Ranjith et al. 2013).

Of these studies, that conducted by Probst (2008) found a decreasing trend of aquifer effective CO₂ permeability with increasing brine concentration, and the salt evaporation effect, called the “salting out effect”, was the factor suspected to cause a denser water phase that reduces CO₂ solubility in water. According to Julio (2001), this salting out effect may cause water density to be increased by up to around 20 %, and H₂O–CO₂ interaction may cause this value to be further increased by 2–3 %. Later, Ranjith et al. (2013) studied the effect of salinity on effective CO₂ permeability in saline aquifers with 100,000–160,000 ppm high salinity levels, and confirmed the effective CO₂ permeability reduction with increasing salinity. The estimated total CO₂ storage capacity reduction in their study due to this permeability reduction is up to around 1.8 %.

Although few studies are available related to the effect of brine concentration on effective CO₂ permeability in aquifers, many studies have been conducted on the effect on effective brine permeability (Baudracco and Tardy 1988; Mohan et al. 1999). Mohan et al. (1999) showed the effect of high ionic strength brines on the absolute permeability of smectitic sandstones, and a decreasing trend of effective brine permeability in sandstone with increasing brine concentration was observed. According to these researchers, the corresponding damage, which is the permeability reduction of the host rock due to contact with the foreign fluid, is irreversible (Mohan et al. 1999). According to Baudracco and Tardy (1988), a reservoir's effective brine permeability decreases with increasing brine concentration for a given cation, and 10 % reduction in permeability in specimens saturated in NaCl, 12 % in NaNO₃, 13 % in Na₂SiO₃, and 16 % in NaOH was observed by Omar (1990). This permeability variation creates permanent changes in the flocculation and deflocculation phases of colloidal clay in reservoir rocks (Baudracco and Tardy 1988). The different ionic concentrations creating variation in host fluid permeability have also been studied by Dahab et al. (1992) using three types of sandstones (Berea, Saudi, and Aramco) under a range of temperatures and pressures. These researchers concluded that the observed permeability reduction is related to both the degree of variation of the pore fluid's ionic concentration and the nature of the ions. Moreover, Juanes et al. (2006) presented a comprehensive discussion on the relative permeability characteristics of multi-phase systems related to CO₂ sequestration in deep saline aquifers, and demonstrated how the mechanism of relative permeability-induced capillary trapping can be exploited to improve the overall effectiveness of the injection process. According to past studies (Odeh 1959; Bennion and

Bachu 2005; Bachu and Bennion 2008), among the various factors for the effective CO₂ permeability of sandstone in CO₂-brine systems [injection and confining pressures, temperature, interfacial tension (IFT), viscosity ratio, capillary pressure, degree of saturation], IFT has a significant effect on the displacement characteristics of CO₂-brine systems during the CO₂ injection phase (Bachu and Bennion 2008). Bachu and Bennion (2008) conducted a comprehensive experimental study to investigate the effect of IFT between CO₂ and brine on the relative permeability characteristics of reservoir rock and found that effective CO₂ permeability decreases with increasing IFT. The IFT mainly depends on the pressure, temperature, and brine salinity, and it increases with increasing temperature and salinity and decreasing injection pressure (Yang et al. 2005; Chalbaud et al. 2006). According to Bennion and Bachu (2006c, 2010), the viscosity ratio between CO₂ and brine may also play a considerable role in governing the fluid movement through the CO₂-brine system, and increasing the viscosity contrast between CO₂ and brine causes more easy fluid movement.

Wegener and Harpole (2010) and Burton et al. (2009) showed the importance of correctly evaluating the effective CO₂ permeability in deep saline aquifers CO₂ to determine the potential injectivities and eventually to decide the number of injection wells required.

4.1.2.2. Existing Reservoir Permeability Evaluation Measures

Although the variation of reservoir rock permeability with effective stress is a well-established fact, the amount of change is highly variable (Jing et al. 1992; Chen et al. 2007). Davies and Davies (1999) introduced a novel model to evaluate the stress effect on reservoir permeability: see Eq. (1).

$$k = k_0 \exp \left[22.2 \left(\frac{\Phi}{\Phi_0} - 1 \right) \right] \quad (1)$$

$$\Phi = (\Phi_0 - \Phi_r) \exp(5 \times 10^{-8} \sigma'_M) + \Phi_r \quad (2)$$

where, k_0 is the zero stress permeability, Φ is the porosity and Φ_0 is porosity at zero stress, Φ_r is the residual porosity and σ'_M is the mean effective stress and can be defined as follows as a function of principle effective stresses:

$$\sigma'_M = \frac{1}{3} (\sigma'_1 + \sigma'_2 + \sigma'_3) \quad (3)$$

where, the principle effective stresses can be calculated using Biot's effective stress parameters (Biot 1941) as follows:

$$\sigma'_1 = \sigma_1 + \alpha P \quad (4)$$

$$\sigma'_2 = \sigma_2 + \alpha P \quad (5)$$

$$\sigma'_3 = \sigma_3 + \alpha P \quad (6)$$

where α is Biot's effective stress parameter and P is an average pore pressure, defined as follows:

$$P = S_1 P_1 + (1 - S_1) P_g \quad (7)$$

where S_1 is the degree of liquid saturation, P_1 is the liquid partial pressure, and P_g is the gas partial pressure in the pore fluid. According to Davies and Davies (1999), there can be a one order of magnitude reduction in permeability with the increase of effective stress from zero to 30 MPa. This developed relation was then successfully applied in a numerical simulation developed by Rutqvist and Tsang (2002) to examine the hydro-mechanical changes in reservoir rock due to geo-sequestration of CO_2 . The researchers observed proportionally changing aquifer and cap rock permeability values with the effective stress applied to the formation.

Understanding the theory behind fluid flow behavior in reservoir rocks is important to find appropriate solutions to the problems raised in the CO_2 geo-sequestration process in deep saline aquifers. Leverett (1940) developed such a basic theory, combining thermodynamic theories with basic physics, and performed the first experiments to correlate the basic effective factors: saturation, capillary pressure, IFT, and permeability. The capillary pressure function developed by Davies and Davies (1999) was then modified as follows:

$$P_c = P_{co}(S_1) \frac{\sqrt{\frac{k_0}{\Phi_0}}}{\sqrt{\frac{k}{\Phi}}} \quad (8)$$

where, k_0 is the zero stress permeability, Φ is the porosity, Φ_0 is porosity at zero stress, S_1 is the liquid saturation, P_c is the confining pressure, and P_{co} is the initial confining pressure. According to Eqs. (2) and (8), it is clear that the mean stress field greatly influences all the rock flow parameters in saline aquifers; porosity, permeability, and capillary pressure. Later, this phenomena was successfully used by researchers to find the long-term safety of the geo-sequestration process in saline aquifers (failure of the cap rock) by checking the critical pressure, which induces shear slip in pre-existing faults (Rutqvist and Tsang 2002).

Scheidegger (1958) proposed an equation to estimate the reservoir rock permeability for compressible gas flow under steady-state conditions (constant flow rate, Q and a constant hydraulic gradient) as follows:

$$k = \frac{2Q\mu_g L P_d}{A(P_u^2 - P_d^2)} \quad (9)$$

where k denotes the permeability, μ_g represents the viscosity coefficient of the gas, L and A are the length and cross-sectional area of the core sample, and P_u and P_d are the pore air pressure and atmospheric pressure. Later, Dong et al. (2010) used this permeability function to evaluate the stress-dependent permeability and porosity of sedimentary rocks and showed that the intrinsic permeability is independent of the pore fluid. These researchers proposed that rock permeability for gas or water flow should be identical. However, many laboratory experiments have exhibited a greater difference between gas and liquid permeability through porous rocks, where permeability to gas is higher than that to water (Tanikawa and Shimamoto 2009; Faulkner and Rutter 2000). This implies the importance of correctly identifying the difference between gas and water permeability behavior in rocks, especially when considering gas-fluid two-phase systems.

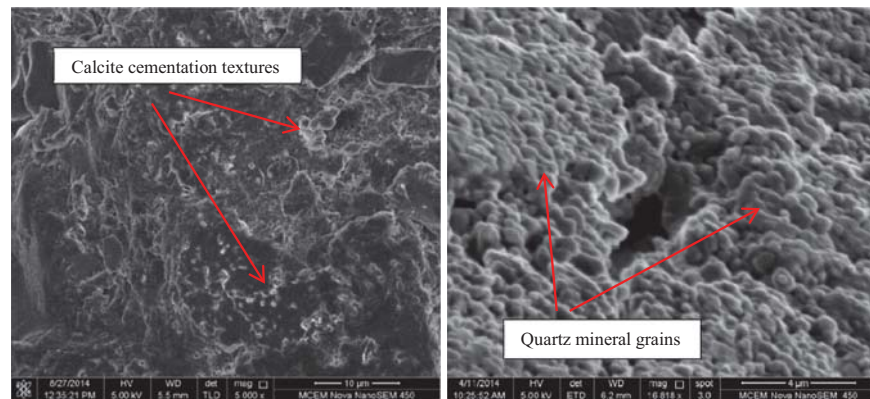
4.1.2.3. Klinkenberg Effect for Gas Permeability Measurement

The Klinkenberg effect is one of the best ways to explain the difference between gas and water permeability in porous media. Klinkenberg (1941) discovered that permeability to gas is relatively higher than that to water and explained the reason by introducing a new phenomenon called the "slip flow" effect. The slip flow is the additional flux which occurs due to the collision of gas molecules and solid walls, when a pore radius approaches the mean free path of gas molecules. This significantly enhances the flow rate and is called the Klinkenberg effect (Eq. 10). This phenomenon explains the difference between intrinsic permeability and apparent permeability in porous media, where intrinsic permeability is independent of fluid properties but apparent permeability is a function of both medium and fluid properties. Therefore, although the intrinsic permeability measured for any gas as liquid movement in porous media is the same, apparent permeability may vary with the fluid type. The relationship between the intrinsic and apparent permeability can be given as follows:

$$K_a = \frac{k_i \rho g}{\eta} \quad (9)$$

where, k_i is apparent permeability (m/s), k_i is intrinsic permeability (m^2), η is viscosity of fluid (Pa.s), ρ is fluid density (kg/m^3), and g is gravitational acceleration (m^2/s).

$$k_a = k_i \left(1 + \frac{4cl}{r} \right) = k_i \left(1 + \frac{cKT}{\pi\sqrt{2}r^3P} \right) = k_i \left(1 + \frac{b}{P} \right) \quad (10)$$

Fig. 1 SEM images of studied sandstone topography

$$b = \frac{cKT}{\pi\sqrt{2}r^3} \quad (11)$$

$$l = \frac{KT}{4P\pi\sqrt{2}r^2} \quad (12)$$

where k_a is the apparent permeability, k_i is the intrinsic permeability, l is the length of the mean free path of the gas molecules, r is the Boltzmann's constant, T is the temperature, c is a constant, P is the pore pressure, and b is the Klinkenberg slip factor. Later, Tanikawa and Shimamoto (2009) measured the permeability of sedimentary rocks taken from the Western Foothills of Taiwan, using nitrogen gas and distilled water as pore fluids under various effective pressure conditions. These researchers observed significantly higher gas permeability values compared to water permeability, and the discrepancy was mainly due to the Klinkenberg effect. They also took an important further step to check the effect of pore pressure on this Klinkenberg effect, and found that although the permeability to gas linearly increases with decreasing pore pressure, water permeability does not have such a linear relationship.

4.1.3. Experimental Program

4.1.3.1. Sample Preparation

The Hawkesbury sandstone samples were collected from the Gosford quarry in the Sydney basin, Australia and belong to the early Triassic age (Ward 1972). The tested sandstone has a grain size between 0.04 and 1.0 mm with a predominantly argillaceous matrix. The XRD results illustrate that the mineral composition of this dry sandstone includes 85 % quartz, 5 % calcite, 1 % siderite, 1 % mica, 5 % kaolinite, 2 % anatase, and 1 % amphibole, and the main cementing phases consist of quartz, calcite, and kaolinite. Figure 1 below shows the topography of a typical

sandstone sample that clearly shows the existing quartz grain and the calcite and kaolinite cementing phase.

The Hawkesbury sandstone samples were cored into 76 mm long and 38 mm diameter cylindrical samples in the Deep Earth Energy Laboratory at Monash University. The top and bottom ends of the samples were then carefully ground to ensure uniform gas injection during the experiments. The prepared samples were oven-dried at 35 °C for 48 h to remove the water added into the pore space during the coring process (during the coring, constant water flow was used to soften the sandstone blocks). All the samples were then saturated using water and brine, with the exception of the two dry samples (at 35 °C), which were used to determine the CO₂ permeability under dry conditions. Two distilled water-saturated samples were used as control samples and the remaining samples were subjected to brine saturation, under three different NaCl concentrations, 10, 20, and 30 % (by weight), to investigate the effect of salinity level on CO₂ injection. Saturation was performed inside desiccators under vacuum for 6 months to achieve full saturation and two replicates were tested for each saturation condition.

4.1.3.2. The Tri-Axial Apparatus and Experimental Procedure

Permeability tests were performed using the high-pressure tri-axial rig available in the Deep Earth Energy Laboratory at Monash University. The setup (see Fig. 3a) can deliver injection pressures up to 50 MPa, confining pressures up to 70 MPa, axial loads up to 100 kN and temperatures up to 70 °C. The schematic diagram of the experimental setup is shown in Fig. 2, and a detailed description of this setup can be found in Ranjith and Perera (2011). Before placing the sample in the tri-axial cell, it was covered by a 2 mm thick and 37.5 mm internal diameter nitrile membrane to prevent oil leakage into the sample and CO₂ leakage into the oil.

Fig. 2 Schematic diagram of the experimental setup

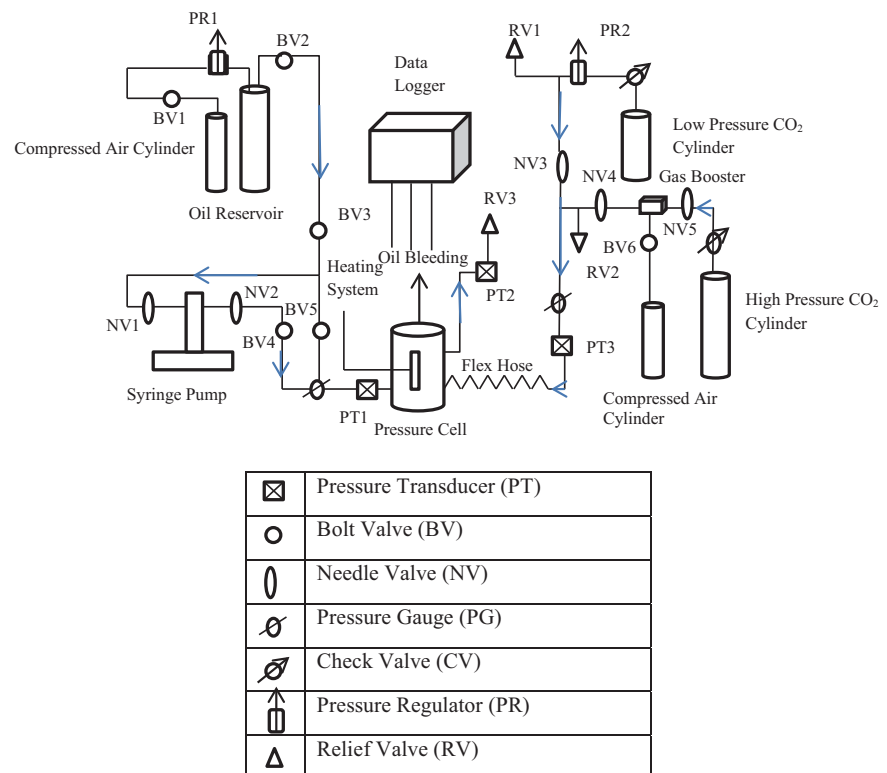
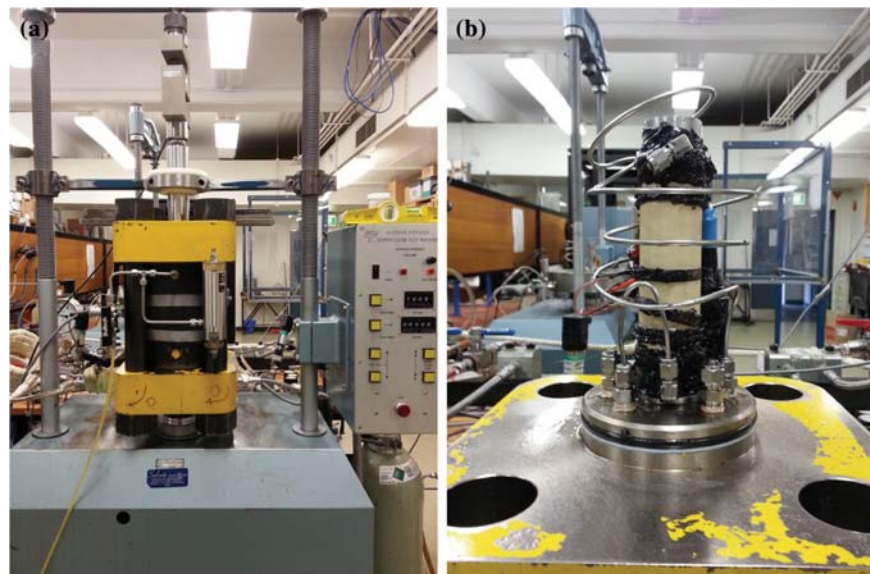


Fig. 3 **a** The high-pressure tri-axial setup, **b** the sample after applying the silicon



The prepared sample was then placed in the tri-axial pressure cell and silicon sealing was applied over the boundaries between the top edge of the membrane and the top platen and bottom edge of the membrane and the bottom platen to minimize leakage (Fig. 3b).

After placing the sample, the cell was filled with oil and the required confining pressure was applied using a syringe pump with 50 MPa capacity. 20 MPa was selected as the confining pressure for the present study to represent the in situ stress condition at 1 km depth, assuming the density

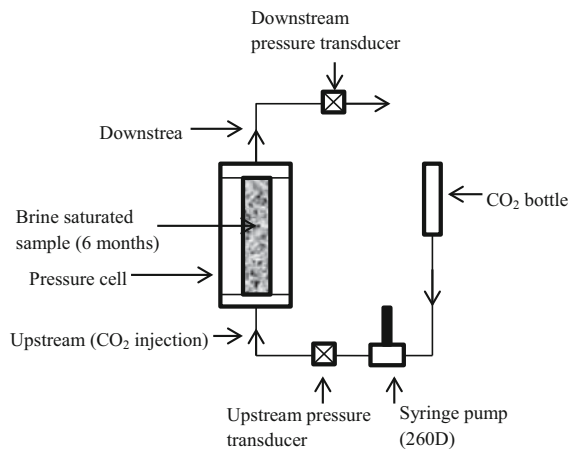


Fig. 4 Schematic diagram of CO₂ injection procedure

of sandstone is 2,000 kg/m³. When the desired confinement was reached the test temperature was set to 35 °C and the sample was allowed to heat for 24 h. CO₂ injection was conducted for both sub-critical and super-critical conditions.

After obtaining the required confinement, CO₂ was injected into the sample at constant injection pressure using a syringe pump (capacity of 260 D) and the downstream pressure development was recorded for the effective permeability calculation. The pressure values of the sample inlet and outlet were monitored using pressure transducers mounted across the upstream and downstream of the system. Figure 4 below shows the schematic diagram of the CO₂ injection procedure. The permeability tests were conducted under undrained conditions and the permeability calculation was done using the measured downstream pressure development curve and pressure transient approach was used. Each permeability test was completed within around 8 min and the system temperature was maintained at a constant 35 °C during each experiment. The overall test conditions are shown in Table 2.

As shown in Table 2, CO₂ was first injected into the water-saturated samples at 2 MPa constant injection pressure and the corresponding downstream pressure development was recorded for effective permeability

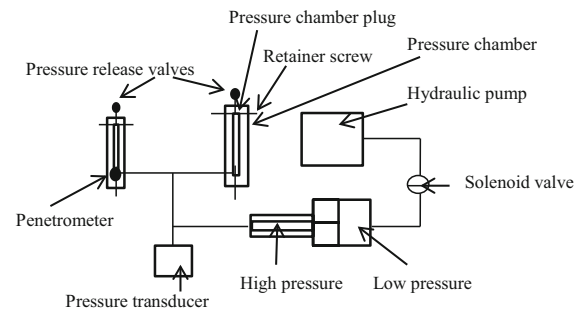


Fig. 5 Schematic diagram of high-pressure instrument used for MIP tests

calculation under this injection condition. After the downstream reached a steady-state pressure condition, downstream was opened and the downstream pressure was released before the subsequent injection. CO₂ was then injected at 4 MPa higher (constant) injection pressure, following the same procedure. The same procedure was repeated for 6, 8, 10, and 12 MPa injection pressures for the water-saturated samples. After testing the water-saturated samples, brine-saturated samples were tested in a similar way, and 10, 20, and 30 % NaCl brine-saturated samples were tested for the same injection pressures. Here, the injection pressures were selected considering the safety of the process (to prevent hydrofracturing), and the injection pressure was not allowed to exceed 90 % of the confining pressure to prevent the re-activation of joints or CO₂ leakage through the membrane and the specimens.

4.1.3.3. Porosity Measurement of Tested Samples

The porosity of the rock mass indicates its available pore space and is therefore important in fluid flow movement analysis. The porosity of the sandstone tested under each saturated condition was determined using mercury intrusion porosimetry (MIP) tests (Cnudde et al. 2009; Molina et al. 2011). The test was conducted in scanning mode and a continuously increasing pressure was applied to obtain the extrusion curve (Fig. 6), which was used to predict the sample's porosity. Figure 5 shows the schematic diagram

Table 2 Summary of tested saturation conditions and injection pressures

Saturation mediums	Number of replicates	Injection pressures (MPa)					
		2	4	6	8	10	12
Water saturated	2	2	4	6	8	10	12
10 % NaCl brine saturated	2	2	4	6	8	10	12
20 % NaCl brine saturated	2	2	4	6	8	10	12
30 % NaCl brine saturated	2	2	4	6	8	10	12

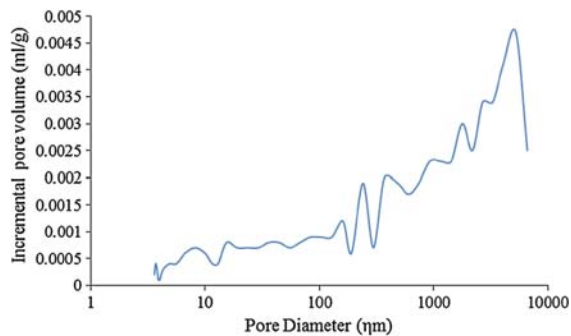


Fig. 6 Cumulative intrusion versus pore diameter curve derived by scanning (dry sample)

of the high-pressure instrument with a maximum pressure of 60,000 psi. The pressure was gradually increased from 1.6 psi to 60,000 psi in 117 steps, to measure the sample's pore volume, if the sample pore apertures ranged from ~ 140 to ~ 0.0036 microns in diameter.

To briefly describe the test procedure, the rock sample is first placed in the penetrometer, which holds a known amount of mercury at the beginning of the test. The penetrometer is initially filled with mercury at a pre-set filling pressure, and is then subjected to several pressure reduction steps, up to around 26 psi. It is then transferred to a high-pressure cell to complete the mercury injection at 60,000 psi pressure. During the high-pressure phase, the penetrometer is immersed in an oil bath (pressure transfer fluid) inside a steel pressure vessel. Increased oil pressure in the vessel causes the mercury to push into the sample and the position of the mercury meniscus in the penetrometer stem is read by capacitance. The data from the penetrometer, the low pressure, and high-pressure modes and the intrusion conditions used for the present study are shown in Table 3. The derived cumulative intrusion versus pore diameter curve using scanning mode, for the dry sample, is shown in Fig. 6.

4.1.4. Results and Discussion

In this study, water- and brine-saturated samples were selected to inject CO_2 under undrained conditions, assuming that injected CO_2 behaves as a laminar flow. This was confirmed by plotting the variation of CO_2 flow rate with the injection pressure (Fig. 7). According to Fig. 7, the CO_2 flow rate shows a linear relationship with injection pressure, which explains the applicability of Darcy's equation to find the effective CO_2 permeability in the rock samples under the conditions considered in this study.

Table 3 Summary of penetrometer, low pressure, high-pressure modes, and summary of intrusion data

Penetrometer:

Pen. constant: 10.683 $\mu\text{l/pF}$
 Pen. weight: 63.4358 g Rec.
 Stem volume: 0.3920 ml
 Max. head pressure: 4.4500 psia
 Pen. volume: 5.9723 ml
 Contact angle: 130.000°
 Adv. contact angle: 130.000°
 Hg surface tension: 485.000 dynes/cm
 Hg density: 13.5335 g/ml

Low pressure:

Evacuation pressure: 50.000 μmHg
 Evacuation time: 30 min
 Mercury filling pressure: 0.62 psia
 Equilibration time: 10 s
 Maximum intrusion volume: 100.000 ml/g

High pressure:

Equilibration time: 10 s
 Maximum intrusion volume: 100.000 ml/g
 No blank correction

Intrusion data summary

Total intrusion volume = 0.1717 ml/g
 Total pore area = 127.370 m^2/g
 Median pore diameter (volume) = 3.7 nm
 Median pore diameter (area) = 3.8 nm
 Average pore diameter ($4 V/A$) = 5.4 nm
 Bulk density = 2.1684 g/ml
 Apparent (skeletal) density = 3.4551 g/ml
 Stem volume used = 71 %

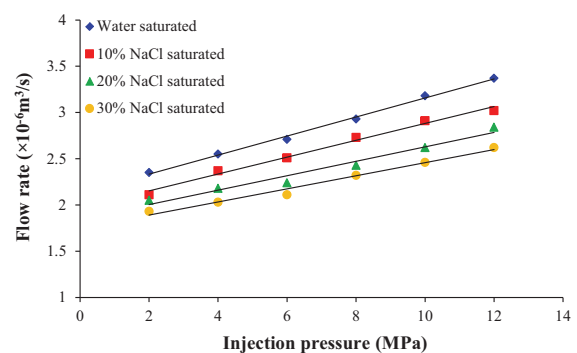
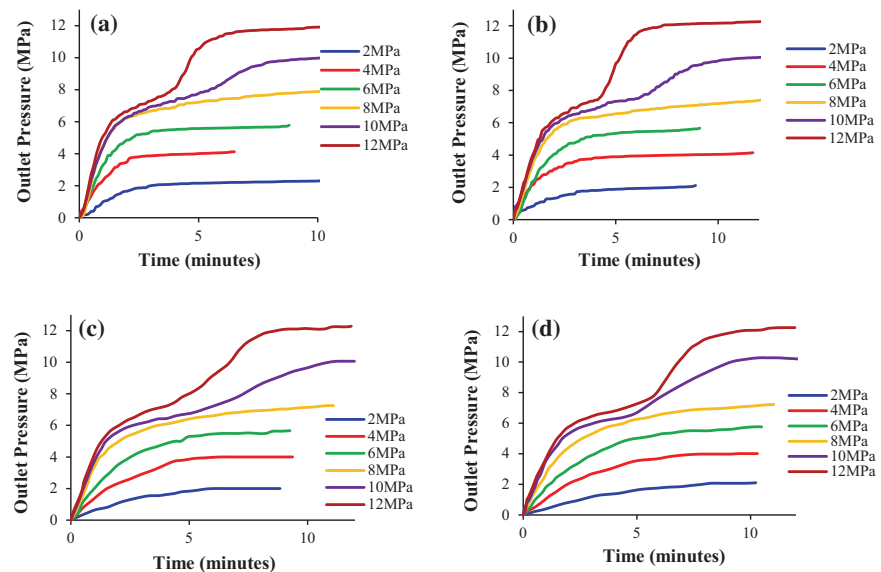


Fig. 7 Observed variation of flow rate with injection pressure for each saturation condition (confining pressure = 20 MPa)

The observed downstream pressure developments for each saturation condition are shown in Fig. 8. It is worth mentioning that the time required for outlet pressure to reach

Fig. 8 Observed downstream pressure developments for each saturation condition **a** water, **b** 10 % NaCl, **c** 20 % NaCl, and **d** 30 % NaCl-saturated samples



equilibrium increases with increasing salinity in the pore fluid. For example, at 12 MPa injection pressure, water-saturated samples took approximately 5 min to reach equilibrium, which then took nearly 6–8 min with the increase of salinity from 10 to 30 %. Interestingly, according to Fig. 8, there is a different downstream pressure development trend for higher CO₂ injection pressures (>8 MPa) compared to low pressures. This is mainly due to the higher pushing force created by the higher advective flux made by the higher injection pressure (the rate of the advective flux proportionally increases with the pressure gap between the upstream and downstream). This force causes inter-granular bonds to be weak, and this weakening effect gradually increases with time due to the continuously applied pushing force by the injection pressure creating advective flux. Eventually, the loosened bonds start to break at one stage of the injection, at which point a considerable amount of fine aggregates will be separated from the rock matrix and released to the downstream. This causes a sudden increase in rock mass pore space and eventually reduced tortuosity in the rock mass, resulting in quicker CO₂ mass flow rate toward downstream, resulting in the observed sudden downstream pressure development. In addition, according to Shukla (2011), the previously explained pushing force at high injection pressures causes CO₂ molecules to travel along preferential flow paths at the beginning of the injection as the pressure gap is higher at the beginning, resulting in the observed primary pressure development. This is believed to occur before the saturation of the whole rock mass. However, once the rock mass is totally saturated, this effect of preferential flow path will be replaced as now CO₂ movement can occur through the whole pore space of the rock mass. This effect may also partially contribute to the observed unique

pressure development trend at higher injection pressures. The temporal change in pressure was then used to calculate the gas flow rate through the reservoir rock using the following equation for a selected time period (Siriwardane et al. 2009; Perera et al. 2011).

$$Q = \left(\frac{dP}{dt} \right) \beta V \quad (13)$$

where, Q is the downstream flow rate, $\frac{dP}{dt}$ is the pressure gradient developed downstream, V is the downstream volume and β is the adiabatic compressibility of the pore fluid. The CO₂ permeability of the reservoir rock for each condition was then calculated using the Darcy equation (Monlouis-Bonnaire et al. 2004; Jasinge et al. 2011; Perera et al. 2011).

$$k = \frac{2QP_0\mu L}{A(P_i^2 - P_0^2)} \quad (14)$$

where Q , μ , P_0 , P_i , A , L , and k are the downstream flow rate, the viscosity of the pore fluid, the downstream pressure, the upstream pressure, the sample cross-sectional area, the sample length, and the initial permeability of the sample. The adiabatic compressibility and viscosity of CO₂ depend on the pressure and temperature values (Fenghou et al. 1998). Therefore, the REFPROP database was used to calculate the adiabatic compressibility and the viscosity of the CO₂ employed during the test (Table 4).

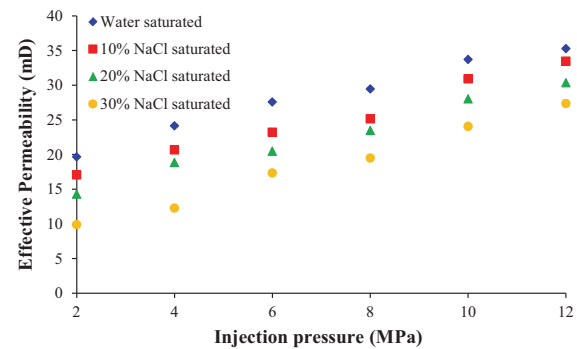
4.1.4.1. Effect of Salinity on Effective CO₂ Permeability

The degree of salinity is one of the critical considerations in deep saline sequestration studies, and it is found to

Table 4 Adiabatic compressibility and viscosity values obtained from REFPROP at different mean injection pressures

Temperature	Average injection pressure (MPa)	Adiabatic compressibility (MPa^{-1})	Viscosity (μMPas)
35 °C	0.25	2.867	1.56E-11
	1.15	0.67968	1.57E-11
	2	0.41451	1.58E-11
	2.25	0.34991	1.59E-11
	2.75	0.28657	1.6E-11
	3	0.36275	1.6E-11
	3.65	0.21588	1.63E-11
	4.7	0.16685	1.68E-11
	6.5	0.11624	1.85E-11

increase with increasing depth of the aquifer. It is therefore important to understand the effect of salinity on both the mechanical and permeability characteristics of reservoir rock to identify the most preferable aquifers for sequestration before initiating the process. Therefore, based on the experimental results, the effect of salinity on the effective CO_2 permeability of Hawkesbury sandstone is discussed in this section. According to past studies (Odeh 1959; Bennion and Bachu 2005; Bachu and Bennion 2008), among the various factors for the effective CO_2 permeability of sandstone in CO_2 -brine systems (injection and confining pressures, temperature, IFT, viscosity ratio, capillary pressure, and degree of saturation), IFT has a significant effect on the displacement characteristics of CO_2 -brine systems during the CO_2 injection phase (Bachu and Bennion 2008). Bachu and Bennion (2008) conducted a comprehensive experimental study to investigate the effect of IFT between CO_2 and brine on the effective permeability characteristics of reservoir rock, and found that the effective CO_2 permeability decreases with increasing IFT. This IFT mainly depends on the pressure, temperature, and brine salinity, and it increases with increasing temperature and salinity and decreasing injection pressure (Yang et al. 2005; Chalbaud et al. 2006). According to Bennion and Bachu (2006c), the viscosity ratio between CO_2 and brine may also play a considerable role in governing fluid movement through the CO_2 -brine system, and increasing the viscosity contrast between CO_2 and brine causes more easy CO_2 movement. Figure 9 below shows the relationship between CO_2 injection pressure and effective CO_2 permeability of the rock samples tested under different salinity conditions. Here, water-saturated samples were used as benchmarks to identify the pure brine effect on the effective CO_2 permeability of reservoir rock. According to Figs. 9 and 10, it is clear that the effective CO_2 permeability of reservoir rock increases with increasing injection pressure and decreasing NaCl

**Fig. 9** Relationship between CO_2 injection pressure and the effective CO_2 permeability of reservoir rock under different salinity conditions (confining pressure = 20 MPa)

concentration of the pore fluid, and the effective CO_2 permeability values for 10 % NaCl-saturated samples at 2, 4, 6, 8, 10, and 12 MPa injection pressures are 17.046, 20.662, 23.218, 25.148, 30.919, and 33.465 mD, respectively. Therefore, effective CO_2 permeability in 10 % NaCl-saturated samples increases by around 96.32 % when the injection pressure is increased from 2 to 12 MPa. Similar trends were observed for both 20 and 30 % NaCl-saturated samples, where effective CO_2 permeability increases from 14.27 to 30.35 mD in 20 % NaCl-saturated samples and from 9.88 to 27.35 mD in 30 % NaCl-saturated samples with 2 to 12 MPa CO_2 injection pressure increments (Table 5). The observed effective CO_2 permeability increments with increasing injection pressures mainly relate to the effective stress effect, where increased injection pressure causes the rock mass pore pressure to increase, resulting in reduced effective stress. Effective stress is the parameter which exhibits the effect of external stress on any rock mass, and its reduction causes the rock mass to expand by increasing its pore space. This eventually reduces the rock mass tortuosity for CO_2 movement, resulting in enhanced permeability in the rock mass. Apart from this, increasing injection pressure creates higher advective flux through the rock mass, and the higher pushing force created by this flux enhances the force applied on inter-aggregate bonds and eventually extracts fine particles from the rock mass. This also influences the permeability enhancement, because fine particles always obstruct the fluid flow path in the rock mass by creating a closer packing arrangement between aggregates. The removal of at least some of them should create better flow paths for CO_2 movement, resulting in enhanced permeability in the rock mass. Moreover, according to Yang et al. (2005), IFT between CO_2 and brine strongly depends on injection pressure, and it decreases with increasing injection pressure, resulting in increased effective CO_2

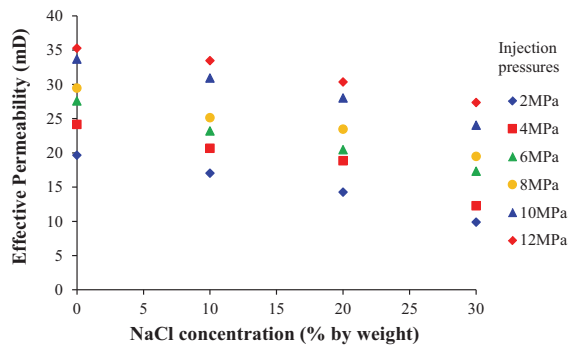


Fig. 10 Relationship between salinity and the CO₂ permeability of reservoir rock under different CO₂ injection pressures (confining pressure = 20 MPa)

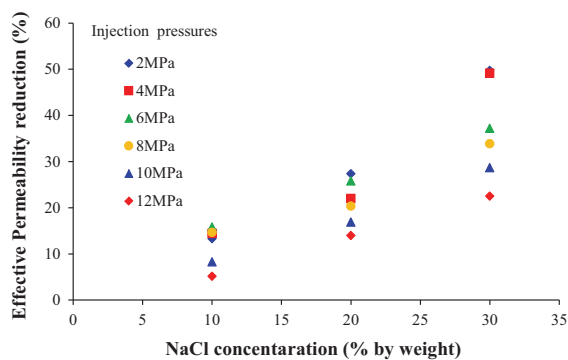


Fig. 11 Relationship between salinity and the reduction of effective CO₂ permeability compared to water saturation (confining pressure = 20 MPa)

permeability as IFT always creates a negative influence on the CO₂ migration through the rock mass. If the salinity effect on effective CO₂ permeability is considered, as can be seen in Fig. 10, effective CO₂ permeability exhibits a decreasing trend with increasing salinity at each injection pressure. Figure 11 and Table 5 below show the observed reduction in effective CO₂ permeability compared to water-saturated values. According to these results, at 2 MPa injection pressure, significant reductions of 13.28, 27.38, and 49.74 % in effective CO₂ permeability were observed in 10, 20, and 30 % NaCl-saturated samples compared to water-saturated samples. However, there was a clear reduction in permeability with increasing injection pressures from 2 to 12 MPa, with around 5.16, 13.99, and 22.49 % reductions in permeability being observed in 10, 20, and 30 % NaCl-saturated samples at 12 MPa injection pressure compared to water-saturated samples. The permeability reductions are clearly significant at low injection pressures compared to high injection pressures for each

Table 5 Summary of calculated permeability values and permeability reduction compared to water-saturated specimens

Saturation medium	Injection pressures	CO ₂ permeability (mD)	Permeability reduction (%) compared to water saturation
Water	2	19.657	
	4	24.147	
	6	27.581	
	8	29.459	
	10	33.71	
	12	35.284	
10 %	2	17.046	13.28
	4	20.662	14.42
	6	23.218	15.82
	8	25.148	14.63
	10	30.919	8.27
	12	33.465	5.15
20 %	2	14.274	27.38
	4	18.838	21.98
	6	20.462	25.81
	8	23.465	20.34
	10	28.02	16.88
	12	30.346	13.99
30 %	2	9.879	49.74
	4	12.273	49.17
	6	17.318	37.21
	8	19.479	33.87
	10	24.040	28.68
	12	27.350	22.48

tested condition due to the high effective stress applied on the rock mass at low injection pressure. According to Yang et al. (2005) and Chalbaud et al. (2006), IFT between CO₂ and brine depends on pore fluid salinity, and IFT increases with increasing salinity, resulting in reduced effective CO₂ permeability in the system. In addition, according to Bennion and Bachu (2006c), the viscosity ratio between the two fluids may also play a considerable role in governing the fluid movement behavior in the CO₂-brine system, where the fluid movement through the pore space becomes much easier (increases) at increased viscosity contrast between CO₂ and brine. Increasing the salinity causes the brine viscosity to increase, which therefore, enhances the viscosity gap between the CO₂ and brine. According to the explanation of Bennion and Bachu (2006c), this should create a positive influence on the CO₂ movement in brine or effective CO₂ permeability in brine that is in contrast to the observed permeability reduction at increased NaCl concentration in brine. However, according to Bachu and Bennion (2008), the effect of the viscosity ratio between brine and CO₂ is less significant compared to the effect of

IFT between brine and CO₂ on the effective permeability of reservoir rock. This explains the decreased effective CO₂ permeability at higher salinity conditions. In addition, there is a possibility of NaCl crystallization in the rock pore space during long-term brine saturation conditions, which is a further possible reason for the effective CO₂ permeability reduction observed with increasing salinity in the pore fluid. It should be noted that here each sample was saturated in brine with various concentrations (0, 10, 20, and 30) for 6 months before starting the permeability tests, and interaction between the brine and rock mass during such long time period causes the NaCl in brine to be crystallized in the rock mass pore space and increasing the NaCl concentration in the pore fluid offers more opportunity for the crystallization process. Effective permeability reduction with increasing NaCl concentration has been seen by other researchers (Shukla et al. 2012; Rathnaweera et al. 2014) and according to them, NaCl crystals are deposited in the rock pore structure as a result of long-term exposure of rock mass to highly saline brine.

In addition to this permeability analysis (pressure transient method), data on porosity from the MIP tests were also used to evaluate the effective CO₂ permeability in brine-saturated reservoir rock samples (Eq. 1). This analysis can be used to confirm the accuracy of the experimental results and also to confirm the influence of the suspected pore structure variation on rock sample permeability under various injection conditions, including injection pressure, effective confining pressure, and NaCl concentration in the pore fluid. To perform the MIP test, a small portion of sandstone was extracted from the sample, after finishing the permeability testing under each test condition (different injection and confining pressures and salinity), and the effects of effective confining pressure and degree of salinity on the sandstone sample's porosity were investigated. The porosity values were then used to determine the effective CO₂ permeability of sandstone under the tested condition and this value was compared with the values obtained from the experiments. According to the comparison, the values obtained from the two methods are mostly similar, with a standard deviation around 0.032, which confirms the accuracy of the experimental results.

Figure 12 shows porosity variation with injection pressure for each brine saturation condition. According to the figure, porosity increases with increasing injection pressure (from 2 to 12 MPa), probably due to the reduction of effective confining pressure with injection pressure increment, which eventually expands the pore space of the rock sample. In addition, Fig. 12 shows a trend of reduction of reservoir rock porosity with increasing NaCl concentration in the pore fluid (from 10 to 30 %), regardless of injection pressure. This is believed to be related to the NaCl

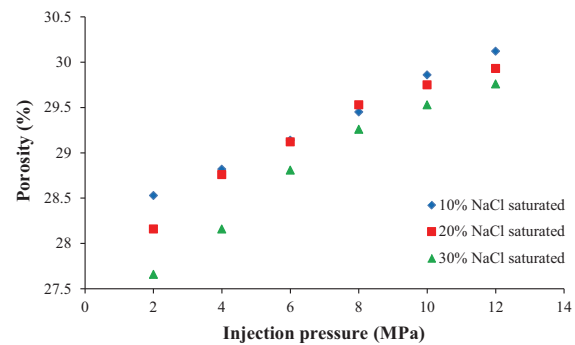


Fig. 12 Relationship between porosity and the injection pressure in 10, 20, and 30 % concentration of NaCl-saturated samples (confining pressure = 20 MPa)

crystallization process in the rock mass pore space. The occupation of the existing pore space by the NaCl crystals causes the pore space to be reduced. Increasing the NaCl concentration in the pore fluid offers more opportunity for the NaCl crystallization process, resulting in reduced porosity at higher NaCl concentrations in the pore fluid. This NaCl crystallization process-induced porosity reduction was then confirmed by performing SEM analyses (Fig. 13) on variably saturated rock samples (at different NaCl concentrations of 10, 20, and 30 % NaCl). These findings are fairly consistent with the findings on the experimental permeability data and, therefore, prove the validity of the pore structure variation argument to describe the influence of injection and confining pressures and NaCl concentration in the pore fluid on reservoir effective permeability.

Figure 14 shows the comparison of results for effective CO₂ permeability values from this method and the previously mentioned pressure transient analysis. According to the results, both methods are in good agreement in evaluating effective CO₂ permeability in brine-saturated reservoir rock samples.

Considering these findings, SEM and chemical analysis were then performed to identify the physical phenomena behind this observed permeability reduction with increasing salinity. The results are discussed in Sect. 4.4.

4.1.4.2. Influence of Effective Stress on Effective CO₂ Permeability in Brine-Saturated Sandstone

According to past studies, it is clear that permeability is dependent on effective stress, and permeability decreases as effective hydrostatic pressure is increased (Keaney et al. 2004). Effective pressure can be defined as $P_{\text{eff}} = P_{\text{con}} - P_{\text{flu}}$, where P_{eff} is the effective confining pressure, P_{con} is the confining pressure, and P_{flu} is the fluid pressure.

Fig. 13 SEM images of NaCl crystals deposited in the rock pore space during 6 months saturation

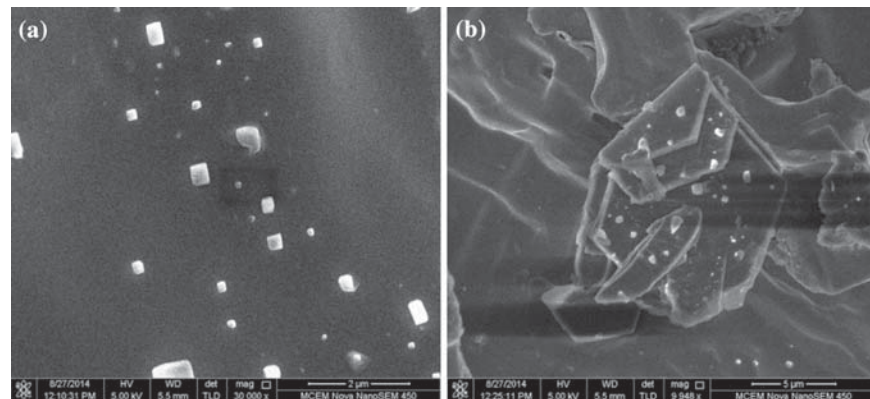


Figure 15 shows the effective CO₂ permeability of the sandstone samples as a function of effective confining pressure for different saturation conditions. According to Fig. 15, it is clear that effective CO₂ permeability decreases as the effective confining pressure is increased from 8 to 18 MPa for all the saturation conditions. In water-saturated specimens, a reduction of 36.92 % in effective CO₂ permeability was observed by increasing the effective confining pressure from 8 to 18 MPa. Furthermore, reductions of 49.12, 60.92, and 69.92 % in effective CO₂ permeability were observed as the effective confining pressure was increased from 8 to 18 MPa in 10, 20, and 30 % NaCl-saturated samples, respectively. This observed reduction in effective CO₂ permeability (see Fig. 15) is due to the shrinkage of the rock mass caused by increased effective confining stress, which consequently reduces the effective fluid pathway connectivity in the pore structure. Moreover, the observed reduction in effective confining pressure with increasing CO₂ injection pressure causes the effective CO₂ permeability to be increased in water- and brine-saturated samples. The shrinkage effect reduces with decreasing effective confining pressure in the rock pore structure and consequently increases the effective pore space for CO₂ migration along the sample. This may be the reason for the effective CO₂ permeability increments observed with increasing injection pressures in water- and brine-saturated samples. In addition, fine particle migration (particle rearrangement) increases with increasing injection pressure, which also enhances the free path of gas flow and consequently increases the effective CO₂ permeability of reservoir rock. Moreover, according to Yang et al. (2005), IFT between CO₂ and brine strongly depends on injection pressure, and it decreases with increasing injection pressure, resulting in increased effective CO₂ permeability, as IFT always creates a negative influence on the CO₂ migration through the rock mass.

In addition, for a certain effective confining pressure, effective CO₂ permeability decreases with increasing

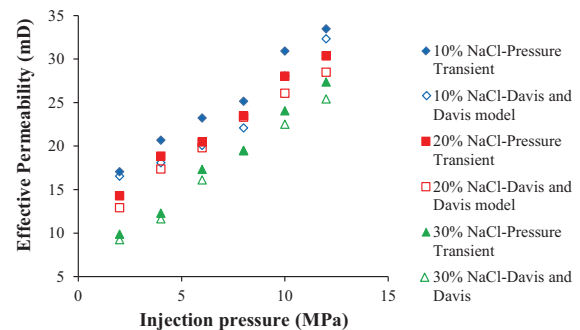


Fig. 14 Comparison between pressure transient permeability evaluation and Davies and Davies (1999) permeability model (confining pressure = 20 MPa)

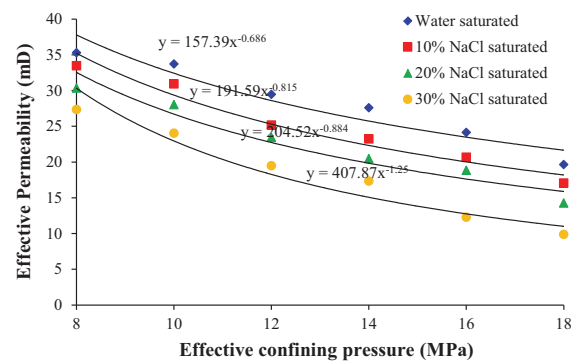


Fig. 15 Effective CO₂ permeability as a function of effective confining pressure for different saturation conditions compared to water saturation

salinity in the pore fluid from 0 to 30 % NaCl, which may be related to the crystallization process of NaCl in the pore structure, where deposited crystals reduce the free flow paths for CO₂. Increasing salinity causes this crystal growth to be enhanced.

4.1.4.3. The Klinkenberg Effect

The variation of effective CO₂ permeability in reservoir rock under dry (CO₂ permeability), water-, 10, 20, and 30 % brine-saturated conditions with different injection pressures is shown in Fig. 16. As Fig. 16 shows, CO₂ permeability in dry reservoir rock reduces with increasing injection pressure, and a similar trend has been observed by Nasvi et al. (2013) for dry geo-polymer samples. In contrast, an increasing trend of effective CO₂ permeability with increased injection pressure can be seen in wet samples (water-saturated and brine-saturated). These opposite permeability behaviors of CO₂ in dry and wet sandstones may be related to Klinkenberg effect (Abbas et al. 1999; Loosveldt et al. 2002; Picandet et al. 2009). According to existing studies, gas permeability through porous rocks reduces with increasing injection pressure due to Klinkenberg effect (Abbas et al. 1999; Loosveldt et al. 2002; Picandet et al. 2009). As described in Sect. 2.3, the permeability of any porous medium to gas is relatively higher

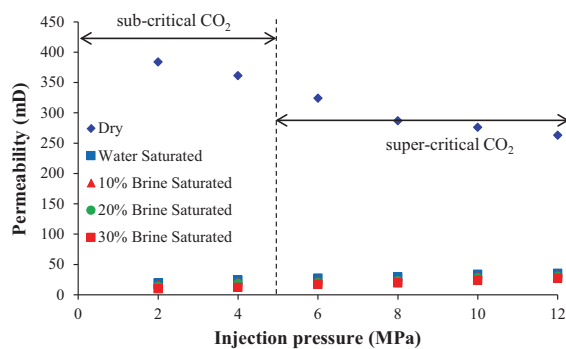


Fig. 16 Variation of effective CO₂ permeability in reservoir rock under dry, water, 10, 20, and 30 % brine-saturated conditions at different injection pressures (confining pressure = 20 MPa)

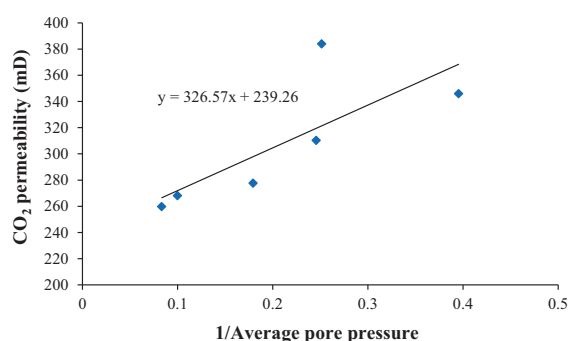


Fig. 17 Variation of CO₂ permeability in dry sample against the inverse of the average pore pressure (confining pressure = 20 MPa)

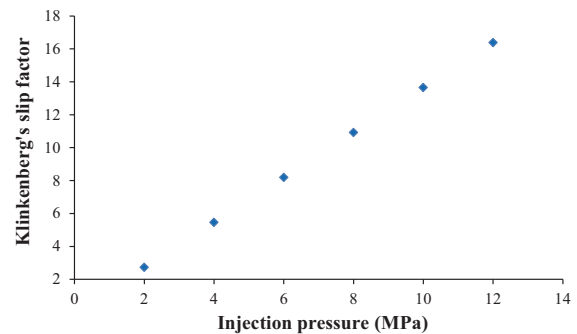


Fig. 18 Relationship between Klinkenberg slip factor and the injection pressure (confining pressure = 20 MPa)

than water due to the slip flow effect, which leads to the creation of an additional flux, and consequently increases the flow rate (Tanikawa and Shimamoto 2009). This explains the observed permeability behavior in the dry samples, which show a reduction of effective CO₂ permeability from 383.9 to 330.23 mD with the increase of injection pressure from 2 to 6 MPa (13.98 % reduction of CO₂ permeability). Interestingly, more significant CO₂ permeability reduction is seen with the phase transition of the CO₂ from gas to super-critical state (6 MPa to 8 MPa at 35 °C), which is around a 21.99 % reduction, possibly due to the reduced slip flow effect at the super-critical state of CO₂. A further increase of CO₂ pressure (8 to 10 MPa) causes only a small permeability reduction (3.85 %). This is because the CO₂ is now in its super-critical condition and, therefore, further increase of pressure while keeping the temperature constant does not change its phase. Therefore, a minor slip flow effect can be expected.

If the permeability of the wet samples (water- and brine-saturated) is now considered, as a consequence of water/brine saturation, the frequency of collisions between the solid wall and mean gas molecules is decreased due to the friction between water and gas phases, resulting in a reduced slip flow effect. Therefore, the observed permeability reduction trend is mainly related to the pressure-dependent brine/water migration phenomenon, where the migration process increases with increasing injection pressure (due to reduced effective stress), resulting in increased rock permeability. In addition, a small amount of injected CO₂ may also dissolve in brine/water, depending on the CO₂ concentration. Overall, it can be said that the gas and super-critical effective CO₂ permeability values of water/brine-saturated samples do not differ greatly from those of dry samples.

In addition, the CO₂ permeability data of dry samples were used to determine the Klinkenberg slip factor. The CO₂ permeability data were plotted against the inverse of the average pore pressure, and the average pore pressure

Table 6 Amount of NaCl deposition from chemical analysis

	Water	10 % NaCl saturated	20 % NaCl saturated	30 % NaCl saturated
Amount of NaCl (ppm)	731	18,251	41,433	61,712

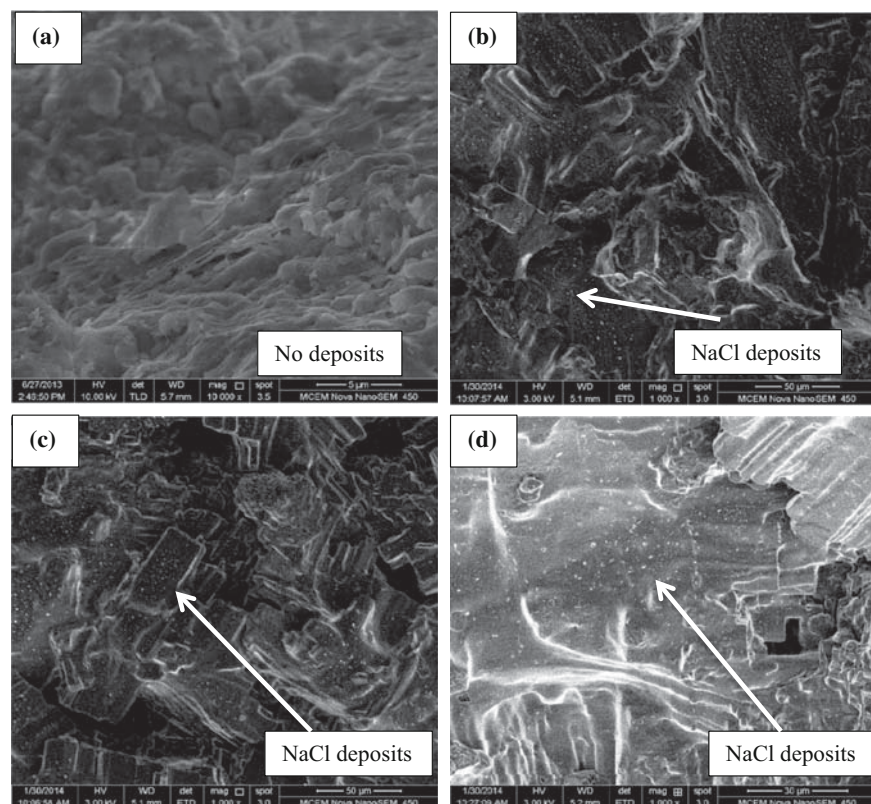
was calculated by finding the average of the inlet and outlet CO₂ injection pressures (Fig. 17). According to the test results, the CO₂ permeability increases linearly as the inverse of pore pressure increased. Interestingly, the Klinkenberg slip factor for dry Hawkesbury sandstone varies from 2.7 to 16.4 with increasing injection pressure from 2 to 12 MPa (Fig. 18).

4.1.4.4. The Corresponding Variations in the Rock Mineral Structure

To identify the variations observed in effective CO₂ permeability in reservoir rocks, a complete micro-structural analysis using SEM was performed (Fig. 19). The SEM analysis was conducted on a 0.3 mm thick sandstone slice taken from the sample prior to each experiment (after 6 months' saturation) under wet conditions. The slice was

then double-coated using Pt (3 mm platinum coating) to remove the charging effect during the image processing (scanning) stage. To obtain clear images of the sandstone topography, the voltage and spot size were selected to be 5.0 kV and 2.0–3.5, respectively. According to Fig. 19, there are significant depositions of NaCl crystals in the tested sandstones, which have been saturated in brine with 20 and 30 % NaCl concentrations, and only a minor deposition of NaCl crystals in sandstone saturated in brine with 10 % NaCl. This NaCl crystallization process occurred during the long-term saturation (6 months) of sandstone in brine. Although the amount of NaCl crystallized might not be exactly similar to the real field situation (crystallization occurs under high pressure and temperature conditions in the field), the trend is believed to be similar. A detailed chemical analysis was then conducted to identify the amount of NaCl deposition in the rock pore space under each brine saturation condition (water, 10, 20, and 30 % NaCl concentrations). This was achieved by stirring a weighted quantity of sample in de-mineralized water, filtering this water and analyzing the solution for Na and Cl. The analysis was conducted on a small sandstone slice taken from each tested sample prior to conducting the permeability experiments (after 6 months saturation in

Fig. 19 SEM analysis results of **a** water, **b** 10 % NaCl, **c** 20 % NaCl, and **d** 30 % NaCl-saturated specimens



water, 10, 20, and 30 % NaCl concentrations). According to the analysis (Table 6), the NaCl concentration in water-saturated samples, 731 ppm, increases up to 18,251, 41,433, and 61,712 ppm due to the presence of 10, 20, and 30 % NaCl (brines), which confirms the increment of salt deposition in rock mass with increasing NaCl concentration. Although the result is not precise, as there are many soluble compounds present in the sample and Na is ubiquitous, the trend should be correct. Therefore, this analysis is believed to be a good indication of the effect of NaCl concentration in brine on the NaCl crystallization process in sandstone.

According to the permeability analysis, 10, 20, and 30 % of NaCl saturation caused the reservoir rock's permeability to be reduced by 5, 15, and 22 % at low effective confining pressures (pressure range of 8–10 MPa) and 13, 27, and 50 % at high effective confining pressures (pressure range of 16–18 MPa), respectively, compared to water-saturated samples. This permeability reduction in the rock specimens appears to be clearly related to the NaCl crystallization process in the rock pore spaces, where the crystals deposited in the rock pore space block the free flow CO₂ paths, resulting in reduction of effective CO₂ permeability.

4.1.5 Conclusions

carbon dioxide sequestration in deep saline aquifers is a promising solution to reducing the anthropogenic emissions of CO₂ into the atmosphere. However, the permeability variation with effective stress and salinity add many complications to the sequestration process. A compressive study was, therefore, conducted to identify the effect of salinity on aquifer effective CO₂ permeability for a range of salinities (0, 10, 20, and 30 % NaCl) using a series of high-pressure tri-axial permeability tests. The following major conclusions can be drawn:

- The presence of NaCl in pore fluid causes the reservoir rock's permeability to be reduced and this effect increases with increasing NaCl saturation in the pore fluid. For example, at low injection pressures (2–6 MPa), 13, 27, and 50 % effective permeability reductions were observed in 10, 20, and 30 % brine-saturated specimens compared to water-saturated specimens. At high injection pressures (10–12 MPa), 5, 14, and 23 % effective permeability reductions were observed in 10, 20, and 30 % brine-saturated specimens compared to water-saturated samples.
- According to a comprehensive chemical analysis, when the pore fluid has a higher degree of salinity, there are considerable numbers of NaCl crystals in the pore

structure, which reduces the reservoir effective permeability by obstructing the flow paths.

- Effective CO₂ permeability of reservoir rock increases with increasing injection pressure in wet (water/brine-saturated) samples for a given confining pressure, due to the effective stress reduction.
- In contrast, CO₂ permeability reduces with increased injection pressure for dry samples, due to Klinkenberg effect.

4.1.6. References

- Abbas A, Carcasses M, Ollivier JP (1999) Gas permeability of concrete in relation to its degree of saturation. *Mater Struct* 32:3–8
- Aktan T, Farouk ASM (1975) Effect of cyclic and in situ heating on the absolute permeabilities, elastic constants and electrical resistivities of rocks. Presented at the 50th Annual Fall Meeting of the SPE of AIME, Dallas, TX SPE, 5633:1–10
- Arsyad A, Mitani Y, Babadagli T (2013) Comparative assessment of potential ground uplift induced by injection of CO₂ into Ainoura, and Berea sandstone formations. *Procedia Earth Planet Sci* 6:278–286
- Bachu S, Bennion B (2008) Effects of in situ conditions on relative permeability characteristics of CO₂-brine systems. *Environ Geol* 54(8):1707–1722
- Baudracco J, Tardy Y (1988) Dispersion and flocculation of clays in unconsolidated sandstone reservoirs subjected to percolation with NaCl and CaCl₂ solutions at different temperatures. *Appl Clay Sci* 3(4):347–360
- Bennion B, Bachu S. (2005). Relative permeability characteristics for CO₂ displacing water in a variety of potential sequestration zones in the Western Canada Sedimentary Basin. Paper SPE 95547, p 15, presented at the 2005 SPE Technical Conference and Exhibition, Dallas, TX, 9–12 October 2005 PAGES?
- Bennion B, Bachu S (2006c) Dependence on temperature, pressure and salinity of the IFT and relative permeability displacement characteristics of CO₂ injected in deep saline aquifers. Paper SPE 102138, p 10, presented at the 2006 SPE technical conference and exhibition, San Antonio, TX, 24–27 September : 120–133
- Bennion DB, Bachu S (2010) Drainage and imbibition CO₂/brine relative permeability curves at reservoir conditions for carbonate formations, in SPE Annual technical conference and exhibition, SPE 134028, pp 1–18, Society of Petroleum Engineers, Florence, Italy
- Berg S, Oedai S, Ott H (2013) Displacement and mass transfer between saturated and unsaturated CO₂-brine systems in sandstone. *Int J Greenh Gas Control* 12:478–492
- Biot MA (1941) General theory of three-dimensional consolidation. *J Appl Phys* 12(2):155–164
- Burton M, Kumar N, Bryant SL (2009) CO₂ injectivity into brine aquifers: why relative permeability matters as much as absolute permeability. *Energy Procedia* 1(1):3091–3098
- Chalraud C, Robin M, Egermann P (2006) Interfacial tension of CO₂/brine systems at reservoirs conditions. In: Gale J, Rokke N, Zweigel P, Swenson H (eds) Proceedings of the 8th International Conference on Greenhouse Gas Control Technology, Elsevier, Amsterdam CD ROM
- Chen Y, Zhou C, Sheng Y (2007) Formulation of strain-dependent hydraulic conductivity for a fractured rock mass. *Int J Rock Mech Min Sci* 44(7):981–996

- Cnudde V, Cwirzen A, Masschaele B, Jacobs PJS (2009) Porosity and microstructural characterization of building stones and concretes. *Eng Geol* 103(3–4):76–83
- Dahab AE, El Omar, Gassier MM, Kariem HA (1992) Formation damage effects due to salinity, temperature and pressure in sandstone reservoirs as indicated by relative permeability measurements. *J Petrol Sci Eng* 6(4):403–412
- Davies JP, Davies DK (1999) Stress-dependent permeability: characterization and modeling. *Soc Pet Eng (SPE)*, Houston
- Dong JJ, Hsu JY, Wu WJ, Shimamoto T, Hung JH, Yeh EC et al (2010) Stress-dependence of the permeability and porosity of sandstone and shale from TCDP Hole-A. *Int J Rock Mech Min Sci* 47(7):1141–1157
- Faulkner D, Rutter E (2000) Comparisons of water and argon permeability in natural clay-bearing fault gouge under high pressure at 20 °C. *J Geophys Res Solid Earth* (1978–2012) 105(B7):16415–16426
- Fenghou A, Wakeham WA, Vesovic V (1998) The viscosity of carbon dioxide. *J Phys-Chem Ref Data* 27:31–44
- Hangx S, Van der Linden A, Marcellis F, Bauer A (2013) The effect of CO₂ on the mechanical properties of the Captain Sandstone: geological storage of CO₂ at the Goldeneye field (UK). *Int J Greenh Gas Control* 2011:5–17
- Jasinge D, Ranjith PG, Choi SK (2011) Effects of effective stress changes on permeability of Latrobe Valley brown coal. *Fuel* 90(3):1292e 300
- Jing XD, Archer JS, Daltaban TS (1992) Laboratory study of the electrical and hydraulic properties of rocks under simulated reservoir conditions. *Mar Pet Geol* 9(2):115–127
- Juanes R, Spiteri EJ, Orr FM, Blunt MJ (2006) Impact of relative permeability hysteresis on geological CO₂ storage. *Water Resour Res* 42(12):32–41
- Julio GE (2001) Density of aqueous solutions of CO₂. Lawrence Berkeley National Laboratory. <http://escholarship.org/uc/item/6dn022hb>
- Keaney GM, Meredith P, Murrell S, Barker J (2004) Determination of the effective stress laws for permeability and specific storage in low porosity sandstone. Gulf Rocks 2004, the 6th North America rock mechanics Symposium (NARMS), 5–9 June, Texas, Houston, pp 24–36
- Khilar KC (1981) Water sensitivity of sandstone. Ph.D thesis, University of Michigan
- Klinkenberg L (1941) The permeability of porous media to liquids and gases. *Drilling and production practice*. American Petroleum Institute, New York, pp 21–34
- Kuhn M, Vernoux JF, Kellner T, Isenbeck-Schroter M, Schulz HD (1998) Onsite experimental simulation of brine injection into a clastic reservoir as applied to geothermal exploitation in Germany. *Appl Geochem* 13:477–490
- Leverett M (1940) Capillary behavior in porous solids. *Trans. Am. Inst. Pet Transp* 12:123–134
- Loosveldt H, Lafhaj Z, Skoczylas F (2002) Experimental study of gas and liquid permeability of a mortar. *Cem Concr Res* 32:1357–1363
- Miller MA, Ramey HJ (1986) Effect of temperature on oil/water relative permeability of unconsolidated sands. *J Pet Eng* 34:1945–1955
- Mohan KK, Reed MG, Fogler HS (1999) Formation damage in smectic sandstones by high ionic strength brines. *Colloids and surfaces A: physical and Chemical Engineering*. Aspects 154:249–257
- Molina E, Cultrone G, Sebastian E, Alonso FJ, Carrizo L, Gisbert J, Buj O (2011) The pore system of sedimentary rocks as a key factor in the durability of building materials. *Eng Geol* 118(3–4):110–121
- Monlouis-Bonnaire JP, Verdier J, Perrin B (2004) Prediction of the relative permeability to gas flow of cement-based materials. *Cement and Concrete Research* 34:737–744
- Nasvi MCM, Ranjith PG, Sanjayan J (2013) The permeability of geopolymer at down-hole stress conditions: application for carbon dioxide sequestration Wells. *Appl Energy* 102:1391–1398
- Neuzil CE (1994) How permeable are clays and shales? *Water Resour Res* 30(2):145–150
- Ochi J, Vernoux JF (1998) Permeability decrease in sandstone reservoirs by fluid injection: hydrodynamic and chemical effects. *J Hydrol* 208:237–248
- Odeh AS (1959) Effect of viscosity ratio on relative permeability. *Pet Transp AIME* 216:346–353
- Omar A (1990) Effect of brine composition and clay content on the permeability damage of sandstone cores. *J Pet Sci Eng* 4(3):245–256
- Pearce JM, Holloway S, Wacker H, Nelis MK, Rochelle C, Bateman K (1996) Natural occurrences as analogues for the geological disposal of carbon dioxide. *Energy Convers Manag* 37(6–8):1123–1128
- Perera MSA, Ranjith PG, Airey D, Choi SK (2011) Sub-critical and super-critical carbon dioxide flow behaviour in naturally fractured black coal: an experimental study. *J Fuel*. doi:10.1016/j.fuel.2011.05.016
- Picandet V, Khelidj A, Bellegou H (2009) Crack effects on gas and water permeability of concretes. *Cem Concr Res* 39:537–547
- Probst P (2008) Numerical simulations of CO₂ injection into saline aquifers: estimation of storage capacity and arrival times using multiple realizations of heterogeneous permeability fields. Master thesis, University of Stuttgart, German
- Ranjith PG, Perera MSA (2011) A new triaxial apparatus to study the mechanical and fluid flow aspects of carbon dioxide sequestration in geological formations. *Fuel* 90:2751–2759
- Ranjith PG, Perera MSA, Khan E (2013) A study of safe CO₂ storage capacity in saline aquifers: a numerical study. *Int J Energy Res* 37:189–199
- Rathnaweera TD, Ranjith PG, Perera MSA (2014) Salinity-dependent strength and stress-strain characteristics of reservoir rocks in deep saline aquifers: an experimental study. *Fuel* 122:1–11
- Rutqvist J, Tsang CF (2002) A study of caprock hydro-mechanical changes associated with CO₂-injection into a brine formation. *Environ Geol* 42:296–305
- Samuel CMK, Ronny P, Zuo L, Benson SM (2012) Relative permeability and trapping of CO₂ and water in sandstone rocks at reservoir conditions. *Water Resour Res* 48:w02532. doi:10.1029/2011wr010859
- Scheidegger AE (1958) The physics of flow through porous media. *Soil Sci* 86(6):355–342
- Shukla R (2011) Study of reservoir rock and caprock integrity in geo-sequestration of carbon dioxide. Ph. D. thesis. Monash University, Australia
- Shukla R, Ranjith PG, Choi SK, Haque A, Yellishetty M, Hong L (2012) Mechanical behaviour of reservoir rock under brine saturation. *Rock Mech Rock Eng* 46(1):83–89
- Siriwardane HJ, Gondle RK, Smith DH (2009) Influence of carbon dioxide on coal permeability determined by pressure transient methods. *Int J Coal Geol* 77(1):109–118
- Sydansk RD (1981) Discussion of the effect of temperature and confining pressure on single-phase flow in consolidated rocks. *J Pet Eng* 32:1329–1330
- Tanikawa W, Shimamoto T (2009) Comparison of Klinkenberg-corrected gas permeability and water permeability in sedimentary rocks. *Int J Rock Mech Min Sci* 46(2):229–238
- Vilarrasa V, Olivella S, Carrera J (2010) Geomechanical stability of the caprock during CO₂ sequestration in deep saline aquifers. *Energy* 4:5306–5313
- Wang HF (2000) Theory of linear poroelasticity: with applications to geomechanics and hydrogeology. Princeton University Press, Princeton

- Ward CR (1972) Sedimentation in the Narrabeen Group, southern Sydney basin, New South Wales. *J Geol Soc Australia* 19(3):393–409
- Wegener DC, Harpole KJ (2010) Determination of relative permeability and trapped gas saturation for predictions of WAG performance in the South Cowden CO₂ flood, in SPE/DOE tenth symposium on improved oil recovery, SPE 35429, Society of Petroleum Engineers, Tulsa, Oklahoma, pp 1–13
- White CU, Strazisar BR, Granite EJ, Hoffman JS, Pennline HW (2003) Separation and capture of CO₂ from large stationary sources and sequestration in geological formations—coalbeds and deep saline aquifers. *J Air Waste Manag Assoc* 53(6):645–715. doi:[10.1080/10473289.2003.10466206](https://doi.org/10.1080/10473289.2003.10466206)
- Yang D, Tontiwachwuthikul P, Gu Y (2005) Interfacial tensions of the crude oil + reservoir brine + CO₂ systems at pressures up to 31 MPA and temperatures of 27°C and 58°C. *J Chem Eng Data* 50:1242–1249

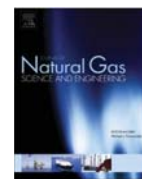
4.2 The effect of salinity on effective stress parameters for effective CO₂ permeability in deep saline aquifers

A thorough understanding of CO₂ permeability and its variation with varying effective stress conditions is important for deep saline sequestration, as it greatly affects the effectiveness and safety of the entire process. For example, reduced permeability causes the CO₂ injection rate to be reduced, making the overall sequestration process inefficient. According to Section 4.1, it is now clear that the long-term interaction of reservoir rock with high salinity brine causes the effective CO₂ permeability to be reduced in deep saline aquifers. In addition, enhanced effective stress causes reservoir rock permeability to be reduced, resulting in reduced production rates. Evaluation of the effect of effective stress laws on the permeability and the effective stress coefficient of CO₂/brine/rock systems is therefore important. In order to understand the effect of different salinity levels on effective stress coefficients for effective CO₂ permeability in deep saline reservoir rock, a series of high-pressure undrained triaxial permeability tests was conducted, and the results of this study are reported in a published journal paper entitled “*Determination of effective stress parameters for effective CO₂ permeability in deep saline aquifers: An experimental study*”.



Contents lists available at ScienceDirect

Journal of Natural Gas Science and Engineering

journal homepage: www.elsevier.com/locate/jngse

Determination of effective stress parameters for effective CO₂ permeability in deep saline aquifers: An experimental study

T.D. Rathnaweera^a, P.G. Ranjith^{a,*}, M.S.A. Perera^a, S.Q. Yang^b^a Deep Earth Energy Laboratory, Department of Civil Engineering, Monash University, Building 60, Victoria, 3800, Australia^b State Key Laboratory for Geomechanics and Deep Underground Engineering, China University of Mining and Technology, Xuzhou, 221116, China

ARTICLE INFO

Article history:

Received 2 October 2014

Received in revised form

11 February 2015

Accepted 11 February 2015

Available online 21 March 2015

Keywords:

CO₂ sequestration

Saline aquifers

Permeability

Effective stress parameters

ABSTRACT

Global warming has been a major threat to the world for many decades, and CO₂ geo-sequestration in deep saline aquifers has recently been identified as an effective solution due to its ability to greatly mitigate anthropogenic CO₂ emissions to the atmosphere. However, CO₂ sequestration-induced chemical and mineralogical reactions affect the hydro-mechanical characteristics of natural formations, resulting in limited injectability to aquifers. A detailed knowledge of the hydro-mechanical behaviour of natural formations is therefore important to enhance the safety and effectiveness of the CO₂ storage process. Such understanding can only be gained on the basis of in-depth knowledge of the applied effective stresses on the formations. The aim of this study was therefore to understand the effect of reservoir salinity level on the effective stress parameters of deep saline aquifer rock under various in-situ conditions, including salinity levels ranging from 0 to 30% (NaCl concentration by weight) and confining pressures ranging 20–35 MPa. Tri-axial permeability tests were conducted for a range of injection pressures (1–12 MPa) under different confining pressures (20, 25, 30 and 35 MPa) at 35 °C constant temperature. Comprehensive SEM (scanning electron microscopy) and acoustic emission analyses were also conducted to clarify the observed results.

According to the results, the effective stress coefficient (α) for CO₂ permeability decreases with increasing aquifer salinity level, and increasing salinity level from 0 to 30% causes the effective stress coefficient to be reduced by 31%. Moreover, the Skempton coefficient (B) increases with increasing salinity level from 0 to 30% and the increment is about 18%. Interestingly, the poro-elastic coupling parameter (αB) decreases from 0.89 to 0.72 as the salinity level increases from 0 to 30% and the reduction is about 19%. The SEM analysis conducted on tested samples confirmed the deposition of NaCl crystals in rock pore space during the saturation period of one year, and these observed variations in effective stress parameters are probably due to the NaCl crystal deposition in the rock pore space. This significantly alters the rock porosity and pore geometry, causing the simple effective stress law for CO₂ permeability to be inapplicable to saline aquifers.

© 2015 Elsevier B.V. All rights reserved.

4.2.1. Introduction

The evaluation of rock permeability and its variation with varying effective stress is important in many engineering applications, including mining engineering, petroleum engineering and CO₂ storage projects in deep sub-surface geological reservoirs, as it greatly affects the effectiveness and safety of these projects. For example, reduced pore pressure causes the permeability of oil/gas fields to be reduced, resulting in reduced production rates

(Ghabezloo et al., 2009; Rempel and Rice, 2006; Sulem et al., 2007). Therefore, this implies the importance of having a clear understanding of the effect of effective stress laws on permeability for many geo-physics and geo-engineering applications. The CO₂ geo-sequestration process in deep saline aquifers is one such application, which has been recently identified as one of the most promising means of reducing anthropogenic CO₂ emissions in the world (Bruant et al., 2002). Generally, the preferable aquifers for this purpose are 800–2000 m deep sedimentary rocks, mainly sandstone, most of which are highly saline (salinity percentages may vary from 5% to more than 25% (NaCl by weight) depending on the depth (Shukla et al., 2012)). However, to date, little consideration

* Corresponding author.

P.G. Ranjith).

has been given to understanding the influence of effective stress on reservoir rock properties of deep saline aquifers, especially under in situ conditions. Evaluation of the effective stress coefficients for CO₂/water/rock and CO₂/brine/rock systems plays a vital role in offering accurate input parameters for long-term numerical models, which are used to simulate the sequestration process in deep saline aquifers. It is therefore important to conduct an appropriate evaluation of the hydro-mechanical responses of saline aquifers to CO₂ injection under various effective stress environments.

The aim of this study was therefore to conduct a comprehensive set of experiments to evaluate the effective stress parameters for reservoir rock permeability in deep saline aquifers and to identify the influence of reservoir salinity level on them. A series of undrained tri-axial permeability tests was therefore performed on water- and brine-saturated reservoir rock samples under different confining and pore pressures, and a series of scanning electron microscopy (SEM) analyses was also carried out to clarify the corresponding chemico-physico microstructural variation of the reservoir rock.

4.2.1.1. The concept of effective stress law for permeability of reservoir rock

The concept of “effective stress” has long been used in rock mechanics. The concept was first introduced by Terzaghi (1936), who defined it as the difference between the confining pressure and the pore pressure, based on a simple force-balance argument (Eq. (1)):

$$P_d = P_c - P_p \quad (1)$$

This proposed concept reveals that the pore pressure and confining pressure tend to have opposite effects on the volume and therefore on many petro-physical properties, including permeability, storage capacity, electrical resistivity, and mechanical properties, such as pore volume compression, bulk volume compression, acoustic wave propagation, and failure. Terzaghi (1936) proposed this equation (Eq. (1)) based on an experimental study conducted to evaluate the application of effective stress on the permeability of reservoir rock in deep saline aquifers. Permeability, or any material property of rock, follows an effective stress law if it can be defined as a linear combination of total stress and the pore pressure. However, since different material properties depend on total stress and pore pressure in different ways, there is no unique effective stress to represent all the material properties of rocks (Ghabezloo et al., 2009). This implies the requirement of different effective stress relationships for different material properties. According to past studies (Zimmerman, 1991; Berryman, 1992; Keaney et al., 2004; Ghabezloo et al., 2009), effective stress can be simply used as a single variable to express the stress dependency of many material properties, and the stress dependency of reservoir rock permeability, k , can be defined as follows:

$$k = k(P_c, P_p) = k(P_d) \quad (2)$$

As can be seen from Eq. (2), the development of such a relationship reduces the number of independent variables from two to one. If the incremental variation of the permeability (k) is considered (derivation of $k(P_c, P_p)$):

$$dk = \frac{\partial k}{\partial P_c} dP_c + \frac{\partial k}{\partial P_p} dP_p \quad (3)$$

Eq. (3) can then be re-arranged as follows:

$$dk = \frac{\partial k}{\partial P_c} \left[dP_c - \left(-\frac{\partial k / \partial P_p}{\partial k / \partial P_c} \right) dP_p \right] \quad (4)$$

The stress dependency behaviour of k can then be defined as a function of the incremental variation of effective pressure (dP_d):

$$dk = \frac{\partial k}{\partial P_c} dP_d \quad (5)$$

$$dP_d = dP_c - \alpha dP_p \quad (6)$$

Comparison of Eq. (4) with Eq. (5) shows the relationship between k and the differential pressure (effective stress), and can be correlated using coefficient α (Eq. (6)), which is the effective stress coefficient corresponding to the permeability of the reservoir rock, and can be presented as follows:

$$\alpha = -\frac{\partial k / \partial P_p}{\partial k / \partial P_c} \quad (7)$$

Thus, the iso-lines of permeability can be obtained by integrating the differential equation of $P_d = 0$, which gives the expression for effective stress for the permeability of reservoir rock. The linear relationship presented in Eq. (8) is the most commonly used expression for effective stress evaluation in rocks, which can be obtained by evaluating the iso-lines of $k(P_c, P_p)$. Furthermore, the α coefficient in the effective stress law can be determined using the gradient of the iso-permeability curves in the (P_c, P_p) plane.

$$P_d = P_c - \alpha P_p \quad (8)$$

4.2.2. Relevant literature

To date, many approaches have been taken to identify the applicability of effective stress law to the permeability of many materials, including sedimentary (sandstone) and crystalline rocks (limestone, granite) (Zoback, 1975; Zoback and Byerlee, 1975; Walls and Nur, 1979; Nur et al., 1980; Walls, 1982; Zimmerman, 1991; Berryman, 1992; Al-Wardy, 2003; Keaney et al., 2004; Ghabezloo et al., 2009). However, there are still limited experimental data available on this aspect for permeability of reservoir rocks in deep saline aquifers, especially during the CO₂ geo-sequestration process. This results in a poor understanding of the effect of CO₂ geo-sequestration in deep saline aquifers (fully brine-saturated sandstones) on their stress-dependent behaviour.

Keaney et al. (2004) conducted hydrostatic compression experiments to investigate the influence of effective pressure on both the permeability and specific storage capacity of water-saturated Tennessee sandstone and observed reduction trends of both with increasing effective pressure. They determined the effective stress coefficient, α , for both properties by developing iso-permeability and iso-specific storage lines in the (P_c, P_p) plane. According to the plots, the α values for both permeability and specific storage were not constant over the considered effective pressure range, and the α for permeability varied from 1.1 to 0.5 and for specific storage from 1.1 to 0.8 at low and high effective pressures, respectively. These observed changes in effective stress coefficient α with the effective pressure were then interpreted to examine how the volume and shape of flow paths change with effective pressure. A similar experiment was performed by Bernabe (1987) on Chelmsford and Barre granites to determine the effect of the effective

stress law on their permeability characteristics and these researchers observed a reducing trend of effective stress coefficient, α , for permeability with increasing confining pressure in both Chelmsford and Barre granites, where α for permeability varied between 0.6 and 0.7 with changing confining pressure. However, there was no noticeable orientation effect (different coring directions; perpendicular to rift plane, perpendicular to grain plane and perpendicular to hard way plane). The experiments were conducted on water-saturated samples and both loading and unloading behaviours in Barre granite and only loading behaviour in Chelmsford granite were observed. The values obtained for loading showed a significant deviation from the unloading values, which were around 0.55 and 1.1 for loading and unloading, respectively for the Barre granite samples. According to these researchers, this relates to the anisotropy effect and the hysteresis and stress history effect of granite samples.

Ghabezloo et al. (2009) also carried out a series of constant-head permeability tests in a tri-axial cell to evaluate the effect of effective stress law on the permeability of water-saturated limestone under isotropic loading. These researchers found a linearly-increasing permeability-effective stress coefficient, α , with increasing differential pressure, and observed that the α values for permeability reduced from 2.4 to 0.9 with reducing effective pressure. Based on the data, they proposed the following relationship between the effective stress coefficient and the differential pressure (Eq. (9)):

$$\alpha = 0.89 + 0.17P_d \quad (9)$$

Although the effect of clay on permeability is well known, only minor consideration has been given to understanding the applicability of the effective stress law on the permeability characteristics of clay-rich sandstone (Zoback and Byerlee, 1975; Walls and Nur, 1979; Berryman, 1992), which is important in many engineering applications such as CO₂ geosequestration. Although it is well known that the effective stress coefficient, α , does not go beyond unity when the main cementing phase has only a single mineral (Berryman, 1992), according to Zoback and Byerlee (1975), it may be as high as 3–4 for clay-rich sandstone, and according to Walls and Nur (1979), it may reach the very high value of 7. To explain this unique behaviour of sandstone with clay particles, Zoback and Byerlee (1975) proposed a model taking into consideration the quartz and pores in clay layers. According to the model, the effective stress coefficient becomes more than unity when the inner layer is more compliant than the outer layer. This is because such a system is more sensitive to changes in pore pressure compared to confining pressure, and it therefore offers higher α values (>1). Al-Wardy and Zimmerman (2004) evaluated the effect of the effective stress law for clay-rich Stainton sandstone by performing permeability tests under a hydrostatic stress environment. They found an increasing α trend with increasing clay content, and according to them, the rate of increase largely depends on the rock-

clay stiffness ratio. Table 1 shows how the effective stress coefficient, α , varies with the clay fraction for different types of sandstones.

However, as mentioned earlier, the understanding of CO₂ sequestration-induced permeability variation in deep saline aquifers, and the effect and applicability of effective stress law on it, remain limited. Moreover, to date there is no adequate data set related to the influence of effective stress parameters for CO₂ permeability on reservoir rock stress behaviour under brine-saturated conditions (saline water), which is the most common condition in saline aquifer reservoir rocks. Therefore, the aim of this paper is to provide a comprehensive understanding of the influence of effective stress parameters for CO₂ permeability on the stress-dependent behaviour of deep saline aquifer reservoir rocks, giving special attention to how the coefficient, α , varies with reservoir salinity levels during the CO₂ storage process.

4.2.3. Experimental methodology

4.2.3.1. Rock samples

Hawkesbury sandstone belonging to the early Triassic age (Ward, 1972) was collected from the Gosford basin in New South Wales, Australia. Based on microscopic observations, the sandstone samples can be considered as rather homogeneous, as the grain size varied between 0.01 and 1.0 mm within a predominantly argillaceous matrix. This sandstone mainly consists of quartz, calcite and kaolinite, and according to the X-ray diffraction test (XRD) results, the mineral composition of the sandstone is 85% quartz, 5% calcite, 5% kaolinite, 2% anatase, 1% siderite, 1% mica and 1% amphibole. Fig. 1(a) and (b) show the details of the microstructure observed from SEM (scanning electron microscopy) analysis and the results of computed tomography (CT) scanning, respectively. Fig. 1(a) displays the randomly-oriented pore voids within the width of 124 μ m in the main cementing phase of the sandstone pore structure, and Fig. 1(b) provides a detailed picture of how the pore network is oriented (black patches indicate the voids) in the pore space. As shown in Fig. 1(b), a discontinuous pore network can be seen along the sample height and this can significantly alter the permeability of reservoir rock.

4.2.3.2. Sample preparation

The collected sandstone blocks were cored in the Deep Earth Energy Research Laboratory (DEERL) at Monash University according to the ASTM standards. A sample diameter of 38 mm was selected and the cored samples were then cut into cylinders 76 mm high. The two ends of the specimens were then carefully ground to create smooth faces, and the prepared specimens were then oven-dried for 24 h before being set aside for saturation.

For the present study, brine and water saturation mediums were selected as the test conditions and the water saturation was selected as the control test and compared with brine-saturated samples to check the pure brine saturation effect on CO₂ permeability. Moreover, three different NaCl concentrations were selected (10, 20 and 30% (by weight)) in order to simulate deep saline aquifer salinity conditions and to determine the influence of salinity on the effective stress parameters. The intention of this study was to check the effect of different CO₂ injection conditions on the permeability of saline aquifers. In order to have an appropriate representative of brine-saturated saline aquifers, brine-saturated sandstone samples were used. In natural saline aquifers, the aquifer rock mass is in contact with brine over a long time and such long-term brine saturation creates considerable mineralization in the rock matrix and allows a significant amount of

Table 1
The variation of the effective stress coefficient as a function of clay fraction for different sandstones.

Rock type	Clay fraction	Porosity	Effective stress coefficient	Reference
St. Peter	0.01	0.2	1.2	Walls and Nur (1979)
Massilion	0.05	0.23	3.2	Walls and Nur (1979)
Massilion	0.06	0.24	3.5	Zoback (1975)
Berea	0.08	0.2	3.3	Walls and Nur (1979)
Stainton	0.08	0.16	5.4	Al-Wardy and Zimmerman (2004)
Bandera	0.2	0.16	7.1	Walls and Nur (1979)

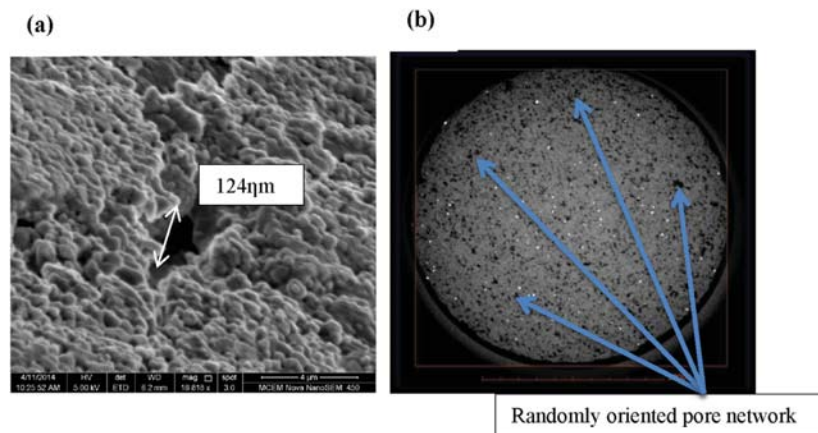


Fig. 1. (a) The details of the microstructure observed from the SEM analysis and (b) the variation of the pore network.

crystallized NaCl in the pore space. Such modification to pore structure is created only after long-term exposure of the rock matrix to brine. In order to simulate this reservoir condition, a one-year saturation period was utilised to offer maximum possible time for the saturation. For this purpose, vacuum saturation was utilized, as it is not possible to use a high-pressure saturation chamber or a tri-axial apparatus for such a long time, in particular when a total of 20 samples were to be tested, as was the case here. However, rather than only immersal in brine/water, the use of a vacuum chamber offers a more effective saturation process by removing the air inside the pore space and facilitating brine saturation. Full saturation was guaranteed by measuring the weight of the sample during saturation at regular intervals until the constant weight was reached (after around two days). Since our intention was to offer more time for the samples to be in contact with brine, even after the samples reached full saturation, they were kept in the vacuum chamber for one year.

4.2.3.3. Permeability tests

Permeability tests were then performed under undrained tri-axial conditions using the high-pressure tri-axial set-up available in the DEERL (a detailed description of this apparatus can be found in Perera et al. (2011) and a detailed description of sample assembly can be found in Rathnaweera et al. (2014b)). After assembling the sample in the cell, the permeability tests were carried out with different combinations of injection and confining pressures. After applying the confining pressure, the constant injection pressures were applied to the sample using a syringe pump (capacity of 260D) and subsequently, the downstream pressure development was observed.

The test series was initiated with CO₂ injection into water-saturated samples at 1 MPa injection pressure under 20 MPa confining pressure. Once the downstream pressure development became constant, the inlet was closed and the downstream pressure released to remove the injected CO₂ from the sample. The pressure was released at 0.02 MPa/min, a very slow rate to avoid any possible damage to the sample by the CO₂ volumetric expansion incorporated with the pressure change. This step was repeated for each injection pressure and after all the injected CO₂ was removed from the sample (once the downstream pressure reached the atmospheric pressure), the next injection pressure was applied. The injection pressures were 1–12 MPa in steps of 1.0 MPa. Once the test series was completed for 20 MPa confining pressure, the

same procedure was repeated on another three water-saturated samples for 25, 30 and 35 MPa confining pressures. The brine saturation condition was then considered, under which brine-saturated samples with 10, 20 and 30% NaCl concentrations were tested under the same conditions.

The tested sandstone samples were highly porous (30% value from MIP (mercury intrusion porosimetry) test) and therefore, quickly reached the steady-state condition. In order to check the time taken to achieve the steady-state condition of the CO₂ flow in the sample, single tri-axial drained testing was conducted. According to the results, the downstream flow rate became constant (steady state) within 3 min for 1 MPa injection pressure at 20 MPa confinement (the highest effective stress condition considered). Therefore, each undrained permeability test was completed within 10 min and the corresponding downstream pressure development was recorded. Eq. (10) (the well-known Darcy equation (Monlouis-Bonnaire et al., 2004, Jayasinge et al., 2011, Perera et al., 2011)) was then used to calculate the CO₂ permeability through the tested sandstone sample after 4 min of injection, at which the sample should be at the steady state due to its high porosity condition and according to the above-mentioned drained tri-axial test results.

$$k = \frac{2QP_0\mu L}{A(P_i^2 - P_0^2)} \quad (10)$$

where,

$$Q = \left(\frac{dP}{dt}\right)\beta V \quad (11)$$

Here, Q is CO₂ flow rate coming from the sample to downstream at a particular time (4 min after the injection), dP/dt , β , μ and P_0 are the gradient of the downstream pressure with time curve at the considered time (4 min after the injection), the adiabatic compressibility of the CO₂ accumulated in the downstream at the considered time (4 min after the injection), and the dynamic viscosity of the CO₂ at mean pore pressure at the considered time (4 min after the injection), and P_0 is the downstream pressure at the considered time (4 min after the injection), V is the downstream volume, P_i is the CO₂ injection pressure, L is the sample length along the flow direction and A is the sample's cross-section area.

In order to apply the Darcy equation, a 10 s small time step (dt shown in Fig. 2(a)) in the curve after 4 min of injection (once the sample came to steady state) was considered and then the CO₂ fluid

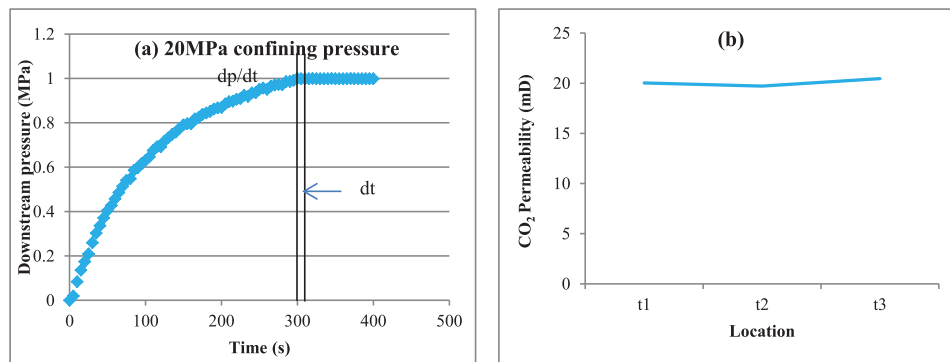


Fig. 2. The (a) downstream pressure development and (b) the calculated CO₂ permeability at 4, 5 and 6 min after the injections for 1 MPa injection pressure and 20 MPa confining pressure condition.

flow rate coming from the sample into downstream at that particular time was checked using Eq. (11) (Perera et al., 2011), given the condition that downstream CO₂ compressibility changes with the pressure development occurred in the fixed downstream volume. The Darcy equation (Eq. (10)) was then used to calculate the CO₂ permeability through the sample at that particular time (4 min after the injection). The adiabatic compressibility (β) and dynamic viscosity (μ) of CO₂ depend on the mean pressure and temperature of the CO₂ at downstream volume and inside the sample respectively, during the considered time and therefore, the precise REFPROP database was used to calculate them (Fenghou et al., 1998).

During the tri-axial test, CO₂ was first injected at 1 MPa injection pressure under drained conditions until all the brine was flushed out and CO₂ flow reached the steady state inside the sample. This was confirmed by measuring the removed brine weight and the CO₂ flow rate. Once the CO₂ flow rate became constant (steady-state flow rate), the sample was assumed to be fully saturated with CO₂. The permeability calculation for the single-phase condition (Eqs. (10)–(11)) is therefore correct. The undrained permeability test for the same testing condition was then performed by closing the downstream and recording the downstream pressure development. Eqs.(10)–(11) were then used to calculate the sample permeability after 4 min of injection. Likewise, the CO₂ permeability of the sample was calculated for three different times after the injection by considering the same 10-s time interval to check the accuracy of the process. As shown in Fig. 2(b) (t1, t2 and t3 equal 4, 5 and 6 min after the injections), the calculated permeability values at different times exhibited almost similar values, proving the accuracy of the method employed.

4.2.4. Results and discussion

The variations of effective CO₂ permeability in sandstone with injection and confining pressures were first determined, and the applicability of the effective stress law and the effective stress coefficients were then determined for each saturation condition. As mentioned earlier, the prepared water-saturated samples were used as control specimens for the test to identify the effect of salinity on effective CO₂ permeability. The results are discussed under six categories: (Al-Wardy, 2003) effect of injection pressure on effective CO₂ permeability of Hawkesbury sandstone under brine saturation, (Al-Wardy and Zimmerman, 2004) effect of confining pressure on effective CO₂ permeability of Hawkesbury sandstone under brine saturation (Bernabe et al., 1982) importance of evaluating effective stress coefficient for the CO₂ sequestration

process in deep saline aquifers (Bernabe, 1987) the corresponding variation of the effective stress coefficient for permeability of Hawkesbury sandstone under brine saturation and (Berryman, 1992) the corresponding variations in rock mass mechanical properties and seismic behaviour (Biot, 1962) effect of effective pressure on effective CO₂ permeability of Hawkesbury sandstone under aquifer conditions.

4.2.4.1. Effect of injection pressure on effective CO₂ permeability of brine-saturated Hawkesbury sandstone

The role of injection pressure on effective CO₂ permeability in Hawkesbury sandstone is plotted in Fig. 3 and each sub-figure demonstrates the variation of effective CO₂ permeability with different aquifer salinity conditions, including water saturation. According to the results, the effective CO₂ permeability of reservoir rock increases with increasing injection pressure, and the observed effective CO₂ permeability increments with increasing injection pressures mainly relate to the effective stress effect in the rock pore space. The pore pressure inside the rock mass increases due to this increased injection pressure, resulting in reduced effective stress, and this effective stress reduction causes the rock mass to expand by increasing its pore space. This eventually reduces the rock mass tortuosity for CO₂ movement, resulting in enhanced permeability in the rock mass. In addition, increasing injection pressure produces higher advective flux along the rock mass, and the higher pushing force created by this flux enhances the force applied on inter-aggregate bonds and eventually extracts fine particles from the rock mass. However, in these experiments pressure was released at a very slow rate and did not disturb the sample. Therefore, this fine migration is mainly related to the injection pressure. With the injection of CO₂, a large pressure gap is created inside the sample pore space, which creates a pushing force towards the rock matrix, that causes some loosely-bonded fine particles and crystallized NaCl to break off from the rock matrix. With the increasing injection pressure, more fine particle movement occurs by both methods. This implies that, after injecting one pressure condition, the sample pore structure changes somewhat due to this fine migration. However, in this test series care was taken to conduct the tests in ascending order, and injection pressure was always gradually increased from low pressure to high pressure. Therefore, even though sample porosity was increased by a lower injection pressure condition with fine migration, the next higher injection pressure applied caused further fine migration with higher pushing force and therefore, the effect of the injection pressure trend was not greatly changed. This also affects the

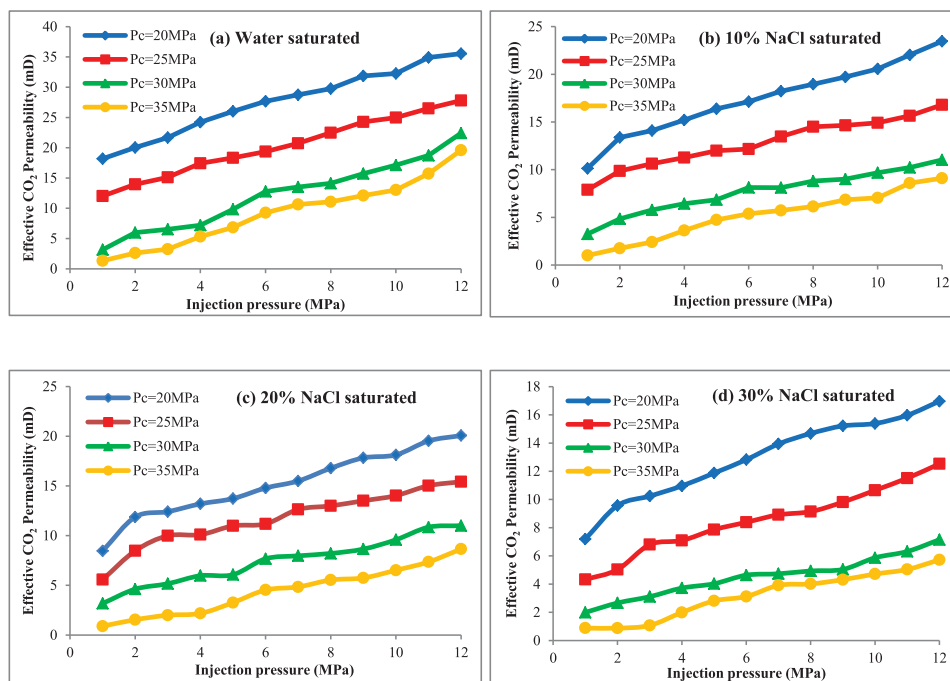


Fig. 3. The role of injection pressure on effective CO₂ permeability in Hawkesbury sandstone.

permeability enhancement, because fine particles always block the fluid flow path in the rock mass by creating a closer packing arrangement between aggregates. The removal of these fine particles should create better flow paths for CO₂ movement, resulting in enhanced permeability in the rock mass. In addition, Klinkenberg's slip flow effect also influences CO₂ permeability in porous rock, where the slip flow ability is mainly dependent on the compressibility and viscosity of the pore fluid and the pore structure of the medium (Tanikawa and Shimamoto, 2009). Increasing the pressure causes the CO₂ viscosity to be enhanced (Guo et al., 1997) and compressibility to be reduced (Garcia, 2003), which eventually reduces slip flow ability through the rock matrix and permeability. However, according to Fig. 3, Klinkenberg's slip flow effect on the permeability of the tested sandstone is not significant, probably due to the high porosity of the sandstone. For example, under 20 MPa confining pressure, increasing the injection pressure from 1 to 12 MPa caused the effective CO₂ permeability of 0 (water-), 10, 20, and 30% NaCl-saturated samples to increase from 18.19 to 35.54 mD, 10.13 to 23.45 mD, 8.46 to 20.07 mD, and 7.19 to 16.96 mD, respectively. Similar increasing trends can be seen in other confining pressure conditions tested.

However, effective CO₂ permeability appears to decrease with increasing salinity of the pore fluid. For example, at 2 MPa injection pressure, effective CO₂ permeability decreases from 20.035 to 13.374 mD and 11.875 to 9.567 mD with the increment of NaCl concentration from 0 to 10% and 20 to 30% at 20 MPa confining pressure, respectively. Similar trends were observed under 25, 30 and 35 MPa confining pressures for all the injection pressures. For example, at 35 MPa confining pressure and 2 MPa injection pressure, effective CO₂ permeability decreases from 2.62 to 1.76 mD and 1.54 to 0.88 mD with increasing NaCl concentration from 0 to 10% and 20 to 30%, respectively. In order to understand the observed effective CO₂ permeability reduction with increasing salinity, a microstructural analysis was performed, which exhibited considerable deposition of NaCl crystals in the pore structure during the

saturation period of one year. This may obstruct the pore structure and consequently reduce the effective pore space for CO₂ movement, resulting in reduced effective CO₂ permeability, and the reduction is enhanced with increasing salinity level in the pore fluid. To date, two studies have shown this clogging of free flow paths due to the deposition of NaCl crystals (Shukla et al., 2012; Rathnaweera et al., 2014a,b). SEM analysis was also performed to support this argument and the images are shown in Fig. 8. Fig. 8(b) and (c) clearly show the deposition of NaCl crystals with a width of about 2–5 μm.

Fig. 4(a) shows the variation of acoustic energy (AE) emissions during the application of injection pressures at 20 MPa confining pressure for each saturation condition. According to Fig. 4(a), AE energy release increases from 224.5 to 925.1 μJ with the increase of injection pressure from 1 to 12 MPa in water-saturated samples, and from 311 to 1328.1 μJ, 911 to 2028.1 μJ and 1757 to 2874.1 μJ in 10, 20 and 30% NaCl-saturated samples, respectively. In addition, it is clear that the AE energy increases from 224.5 to 1757 μJ with increasing NaCl concentration from 0 to 30% at 1 MPa injection pressure, and similar increasing trends were seen for other injection pressures. These results clearly show that the AE release increases with increasing injection pressure for each saturation condition, probably due to the expansion of the rock pore space with the decreasing effective stress. Moreover, the results reveal that the AE energy release increases with increasing salinity level in the pore fluid, probably due to the increment of electron conductivity with the increasing salinity level, which increases the transferability of the acoustic pulse from the pore voids to the AE sensors. In addition, the movement of crystallised NaCl particles may also contribute to the production of more acoustic pulses with increasing injection pressure, which is an important consideration in this study. Fig. 8(b) and (c) show how NaCl crystals are deposited around the pore voids of the reservoir rock and how this contributes to reducing the effective pore space of the reservoir rock.

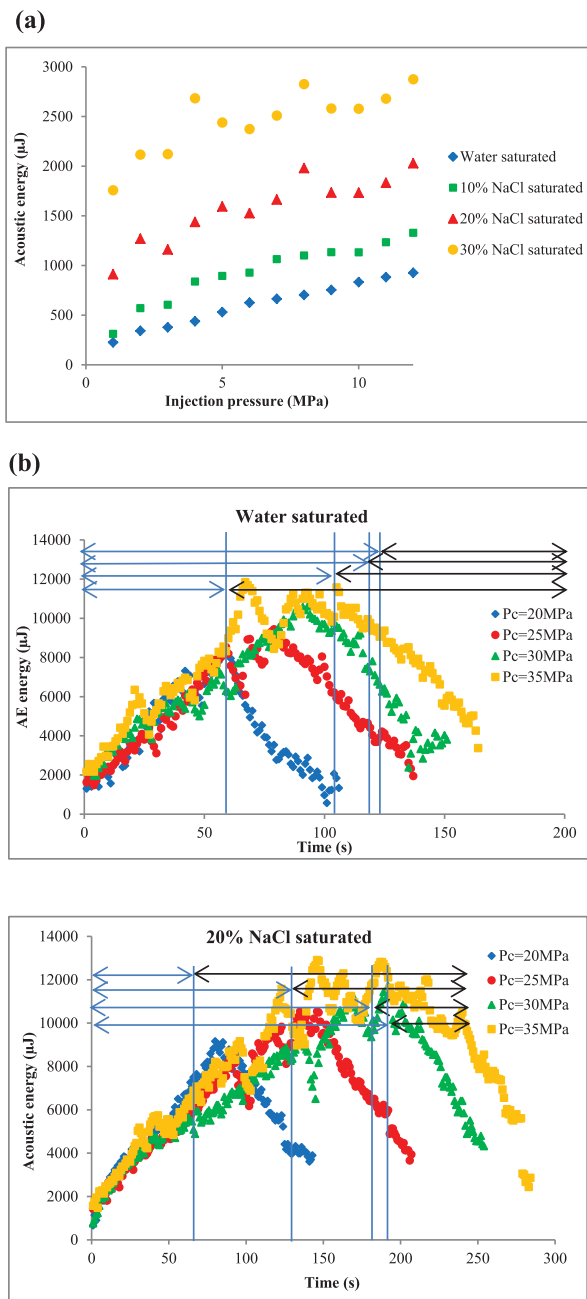


Fig. 4. The variation of acoustic energy (a) during the application of injection pressures under 20 MPa confining pressure (b) with confining pressure for water and 20% concentration of NaCl-saturated samples (Blue arrows = effect of confining pressure, black arrows = effect of injection pressure). (For interpretation of the references to colour in this figure legend, the reader is referred to the web version of this article.)

4.2.4.2. Effect of confining pressure on effective CO₂ permeability of brine-saturated Hawkesbury sandstone

The confining pressure effect on the effective CO₂ permeability of variably saturated (water, 10%, 20% and 30% NaCl) Hawkesbury sandstone was then considered. According to Fig. 6, the CO₂ permeability of reservoir rock reduces with increasing confining

pressure for each injection pressure and saturation condition. It is well known that increased confining pressure (depth) causes the natural fractures in sandstone to close, resulting in reduction of rock permeability. To date, numerous studies have been conducted on the effect of confining pressure on rock permeability (David et al., 1994; Heikamp and Nover, 2003; Lion and Skoczylas, 2004; Ghabezloo et al., 2009; Tanikawa and Shimamoto, 2009), and these studies have proposed various stress-dependent models to explain this behaviour (Brace et al., 1965, 1968; Walsh, 1965).

According to past studies, this observed decreasing non-linear trend of effective CO₂ permeability in sedimentary and crystalline rocks under increasing confining pressure can be attributed to the effective stress-induced anisotropic tortuosity. Physically, the tortuosity of a porous medium is defined as the ratio of the actual distance Δl travelled by the species per unit length Δx of the medium (see Fig. 5(a1)). The anisotropic tortuosity of the pore structure is important, because the diffusivity and permeability decreases with increasing tortuosity of the system (Nakashima and Kamiya, 2007). The pore size and the grain arrangement of the pore space are also important for effective permeability, because the tortuosity of the porous rock strongly depends on the pore size and the grain arrangement. Generally, the effective stress on the rock mass increases with increasing confining pressure under constant injection pressure conditions and its increment causes the rock mass to shrink by reducing its pore space. Consequently, this shrinkage effect of the pore space will increase the actual distance Δl_1 (see Fig. 5(a2)) travelled by the species per unit length Δx_1 of the medium, and this eventually increases the rock mass tortuosity for CO₂ movement, resulting in reduced effective CO₂ permeability in the rock mass.

Moreover, the concept of geometrical aspect ratio has been widely used by many researchers (Walsh, 1965; Witherspoon et al., 1982; Bernabe et al., 1982) to explain the effect of increasing confining pressure on the permeability characteristics of porous rock. This can be explained by using simple models of elliptic cracks: two-dimensional models and three-dimensional models. These models illustrate the effect of confining pressure based on the geometrical aspect ratio of the pore matrix (Walsh, 1965; Bernabe et al., 1982). The aspect ratio gives a relationship between the effective length and width of existing cracks/faults and pore voids in rock mass, where cracks/faults have a lower aspect ratio compared to pore voids (Bernabe et al., 1982). Witherspoon et al. (1982) proposed a model for crack closure to explain this confining pressure effect by observing the behaviour of effective crack length during the process of application of confining pressure. According to these researchers, effective crack length can be defined as the average distance between two interconnected crack walls, as shown in Fig. 5 (Fig. 5(b1) by L_1 and Fig. 5(b2) by L_2). The results reveal that effective crack length reduces and the effective aspect ratio increases with increasing confining pressure due to crack closure. As can be seen in Fig. 5(b), a single crack may progressively transform into an array of relatively high aspect ratio voids ($W_2/L_2 > W_1/L_1$, where W_1 and W_2 are crack widths) with the increase of confining pressure, and such voids are more resistant to confining pressure than single cracks (Bernabe, 1987). Therefore, at relatively high confining pressures, the porous network is dominated by both existing and newly-formed relatively high aspect ratio cracks, resulting in the closure of cracks and grain boundaries. This leads to the reduction in the free flow paths, which decreases the rock mass permeability. Bernabe (1987) studied the effective stress coefficient of permeability of Chelmsford granite and observed a reduction of permeability with increasing confining pressure. He provided a similar explanation: low aspect ratio cracks transform into arrays of relatively high aspect ratio voids due to the rugosity of the crack walls at high confinements.

According to David et al. (1994), permeability and depth

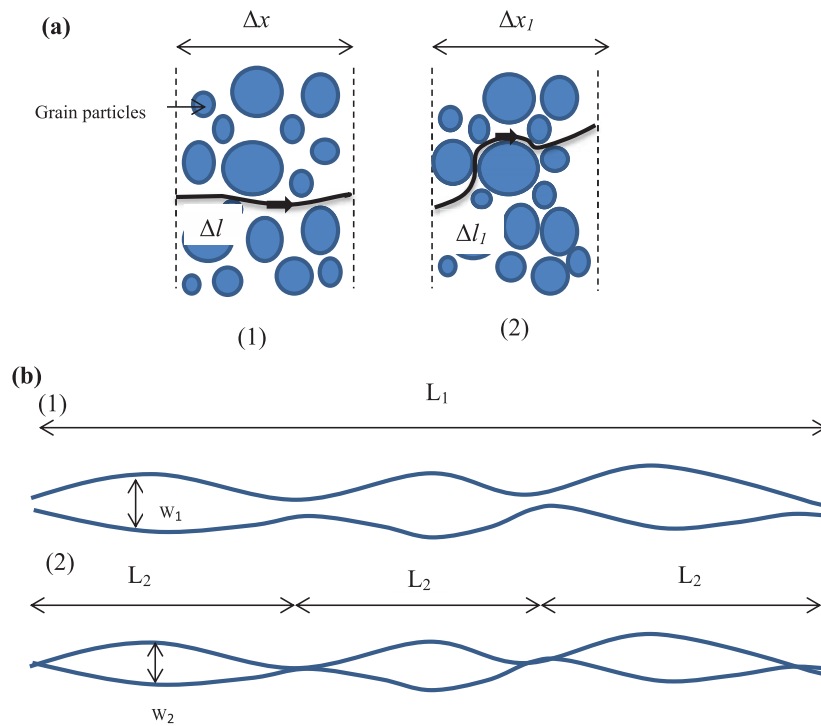


Fig. 5. (a) The effect of effective stress on anisotropic tortuosity of the porous medium (b) model of crack closure to explain the effect of confining pressure on permeability of rocks (Bernabe, 1987).

(effective confining pressure) exhibit an exponential relationship as follows:

$$k = k_0 \exp[-\gamma(P_d - P_0)] \quad (12)$$

Shi and Wang (1986) proposed a power law function, which is more suitable to describe the confining pressure effect on permeability. The proposed power law relationship can be given as follows:

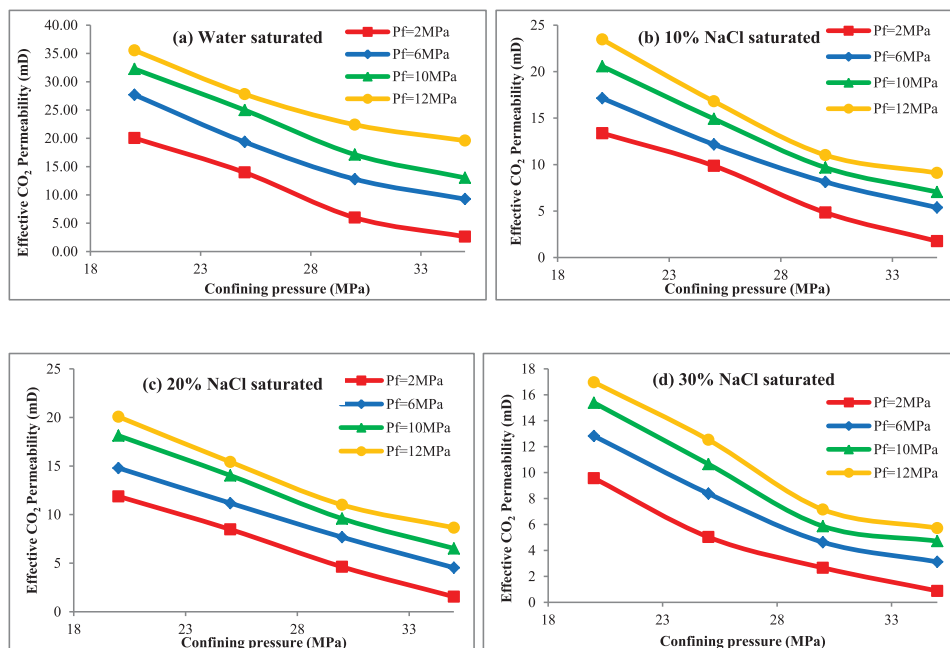


Fig. 6. The variation of effective CO₂ permeability of Hawkesbury sandstone at different confining pressures for water-, 10%, 20% and 30% NaCl-saturated samples.

$$k = k_0 \left(\frac{P_d}{P_0} \right)^{-u} \quad (13)$$

In the present study, the behaviour of CO₂ permeability with increasing confining pressure at various aquifer salinity levels was also determined, to understand the CO₂ sequestration-induced permeability variation in deep saline aquifers. As mentioned earlier, CO₂ permeability decreased with increasing salinity at each confining pressure. For instance, at 2 MPa injection pressure, CO₂ permeability in water-saturated, 10, 20 and 30% NaCl samples reduced from 20.04 to 2.62 mD, 13.37 to 2.41 mD, from 11.88 to 1.54 mD and from 9.57 to 0.88 mD, respectively when the confining pressure was increased from 20 to 35 MPa.

Fig. 7 shows how the confining pressure variation affects the CO₂ permeability in sandstone. The Y axis shows the CO₂ permeability reduction percentage when the confining pressure is increased from 20 to 35 MPa for a range of injection pressures (1–12 MPa) and brine concentrations (0, 10, 20 and 30% NaCl). According to Fig. 7, it is clear that increasing the injection pressure from 1 to 12 MPa causes the CO₂ permeability reduction to be reduced, and a 90–80% reduction can be seen at the low injection pressure range, and 50–40% reduction can be seen at the high injection pressures. The physical phenomenon causing this was then examined by conducting an AE analysis (Fig. 8). According to the results, there is a rapid energy release at the beginning of the confining pressure application, which eventually diminishes over time. This rapid energy release is due to the crack closure process of the reservoir rock resulting from the confining pressure application and further emission is due to the minor dilation of pores during the injection pressure increment.

4.2.4.3. Importance of evaluating effective stress coefficient for the CO₂ sequestration process in deep saline aquifers

Currently, the links between the hydraulic and mechanical phenomena and between the thermal and mechanical phenomena can be considered as two major drawbacks to CO₂ geo-sequestration in deep saline aquifers. For example, the increased CO₂ injection pressure (pore pressure) during the sequestration process may increase mechanical stresses and strains in the rock mass, and this alteration will then in turn influence the flow field (permeability characteristics). This clearly exhibits the coupled hydro-mechanical behaviour in reservoir rocks during the sequestration process, and the evaluation of the effective stress coefficient plays a vital role in this coupling (Zimmerman, 2000). According to Wang (1993), the relationship between pore fluid and macroscopic deformation can be identified using the dimensionless parameter αB , which is the product of the effective stress coefficient

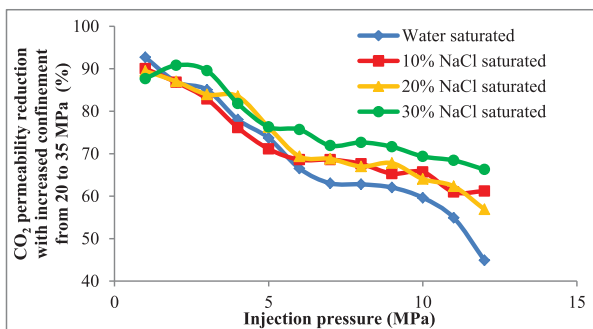


Fig. 7. The effect of confining pressure on CO₂ permeability in tested sandstone.

(Keaney et al., 2004; Zimmerman, 2000) and the Skempton coefficient (B). The effect of pore pressure on mechanical deformation can be explained using Eq. (14), the relationship developed for total bulk volumetric strain (ε_b),

$$\varepsilon_b = \frac{1}{M} (P_c - \alpha P_p) \quad (14)$$

As seen in Eq. (14), if α (effective stress coefficient) reaches zero, pore pressure would have no effect on mechanical deformation. According to Zimmerman et al. (1986) and Norris (1989), to satisfy the poro-elastic coupling in fluid rich porous media, α (effective stress coefficient) must always satisfy the following condition:

$$\frac{3\phi}{2 + \phi} \leq \alpha \leq 1 \quad (15)$$

For instance, according to Eq. (15), a reservoir rock with 10% porosity should have an effective stress coefficient of at least 0.14 to use the above hydro-mechanical coupling Eq. (14). This implies that there is a direct relationship between the rock pore structure and the effective stress coefficient. This is because cracks and voids in the pore structure render a rock highly compressible, and consequently increase α with increasing bulk compressibility, as seen in Eq. (16) (Zimmerman, 2000):

$$\alpha = 1 - \frac{C_m}{C_{bc}} \quad (16)$$

As mentioned earlier, the determination of the effective stress coefficient is important for hydro-mechanical coupling in poro-elastic media, and this poro-elastic coupling parameter can be determined by obtaining the product of the effective stress coefficient and the Skempton coefficient. The Skempton coefficient can be derived based on the equation of fluid content increment ($d\zeta$) in the undrained process (Skempton, 1954), where the increment must be zero due to the undrained process. The above relationship can be written as Eq. (17) below:

$$d\zeta = -\phi [C_{pc} dP_c - (C_{pp} + C_f) dP_p] = 0 \quad (17)$$

where C_{pc} and C_{pp} are the two porous compressibilities, which can be defined as follows:

$$C_{pc} = \frac{-1}{V_p} \left(\frac{\partial V_p}{\partial P_c} \right)_{P_p} \quad (18)$$

$$C_{pp} = \frac{1}{V_p} \left(\frac{\partial V_p}{\partial P_p} \right)_{P_c} \quad (19)$$

Taking $d\zeta = 0$ yields the Skempton coefficient in the form

$$B = \left(\frac{dP_p}{dP_c} \right)_{d\zeta=0} = \frac{C_{pc}}{C_{pp} + C_f} \quad (20)$$

Considering the various relationships between the porous rock compressibilities, Eq. (17) can be rearranged as

$$d\zeta = -\frac{\alpha}{M} \left[dP_c - \frac{1}{B} dP_p \right] \quad (21)$$

Eq. (21) shows that $1/B$ is the effective stress coefficient for the excess fluid content (ζ). Considering the unstressed state (where $\zeta = 0$), Eq. (Lion and Skoczylas, 2004) can be integrated, yielding

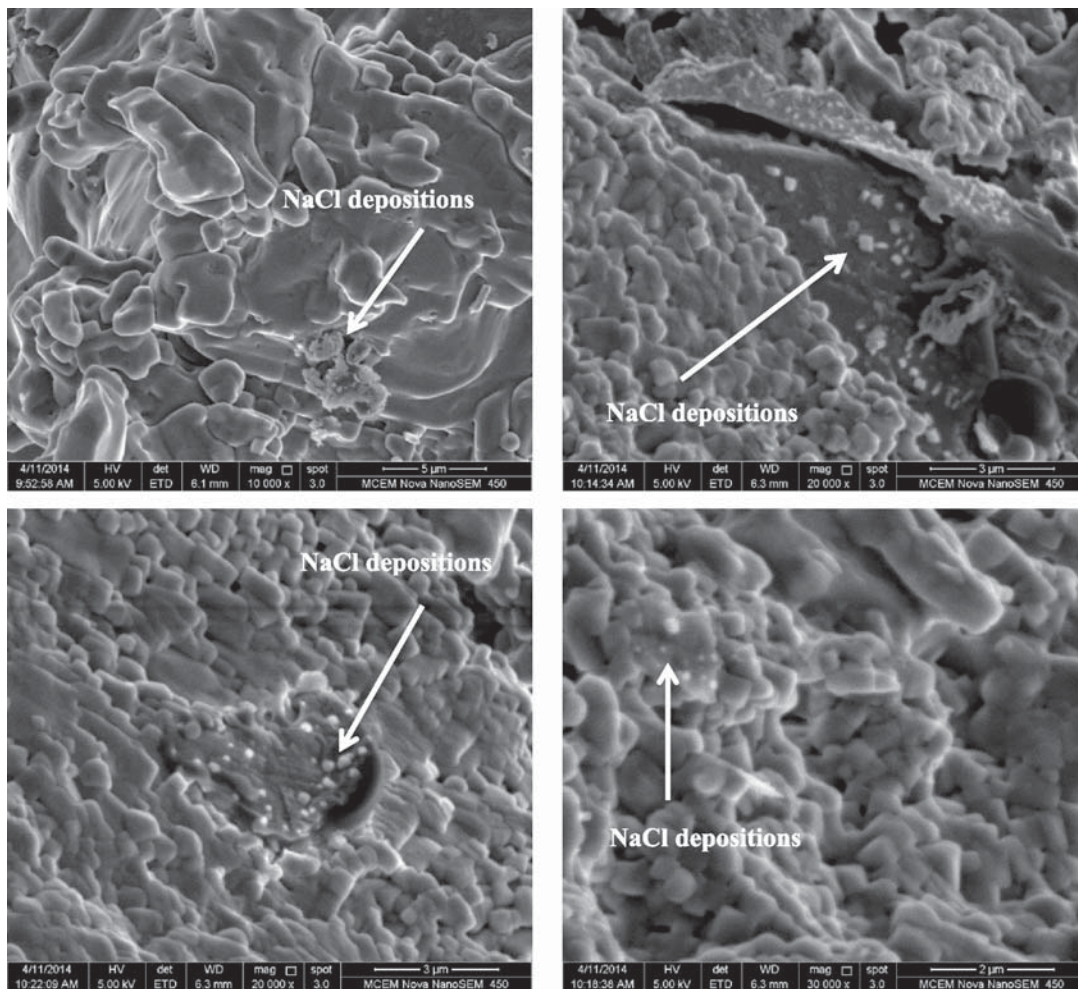


Fig. 8. SEM images of studied sandstone under brine-saturated conditions which show the deposition of NaCl crystals during the saturation period.

$$\zeta = -\frac{\alpha}{M} \left[P_c - \frac{1}{B} P_p \right] \quad (22)$$

Finally, combining Eqs. (14) and (22) gives

$$\varepsilon_b = \frac{(1 - \alpha B)}{M} P_c - B\zeta \quad (23)$$

The corresponding bulk modulus values (M) were calculated using Eq. (Nur et al., 1980) (Rathnaweera et al., 2014a), where the required parameters (E and γ values) for each saturated condition were obtained from Rathnaweera et al. (2014a), who conducted a series of strength tests using the same type of sandstone under the same saturation conditions.

$$M = \frac{E}{3(1 - 2\gamma)} \quad (24)$$

Therefore, if the effective stress coefficient is known, it is possible to gain a detailed knowledge of how rock pore space and deformation vary with time.

4.2.4.4. Variation of effective stress coefficient for permeability of brine-saturated Hawkesbury sandstone with pressures

The effective stress law for permeability states that the pore pressure (P_p) should be changed by $\Delta P_p/\alpha$ amount, when the confining pressure (P_c) changes by ΔP_c to maintain a constant permeability in any medium (Bernabe, 1987; Keaney et al., 2004). Variation of the effective stress coefficient, α , under various pressures and saturated conditions was therefore considered in the next stage of the study by obtaining the slopes of the constant permeability curves in the P_p , P_c plane. Fig. 9 shows the iso-permeability curves for the saturation conditions studied. According to the results, increasing the salinity in the aquifer pore fluid from 0 to 30% (concentration of NaCl) causes the α for permeability to be decreased. The variation of average effective stress coefficient for permeability with increasing salinity is shown in Fig. 10 (variation can be approximated by using the power law function with a 99% confidence band). According to Fig. 10, the effective stress coefficient decreases from 1.11 to 0.89 and 0.82 to 0.77 when the NaCl concentration increases from 0 to 10% and 20 to 30%, respectively. Importantly, the water-saturated sample shows the highest effective stress coefficient compared to other saturation conditions, and

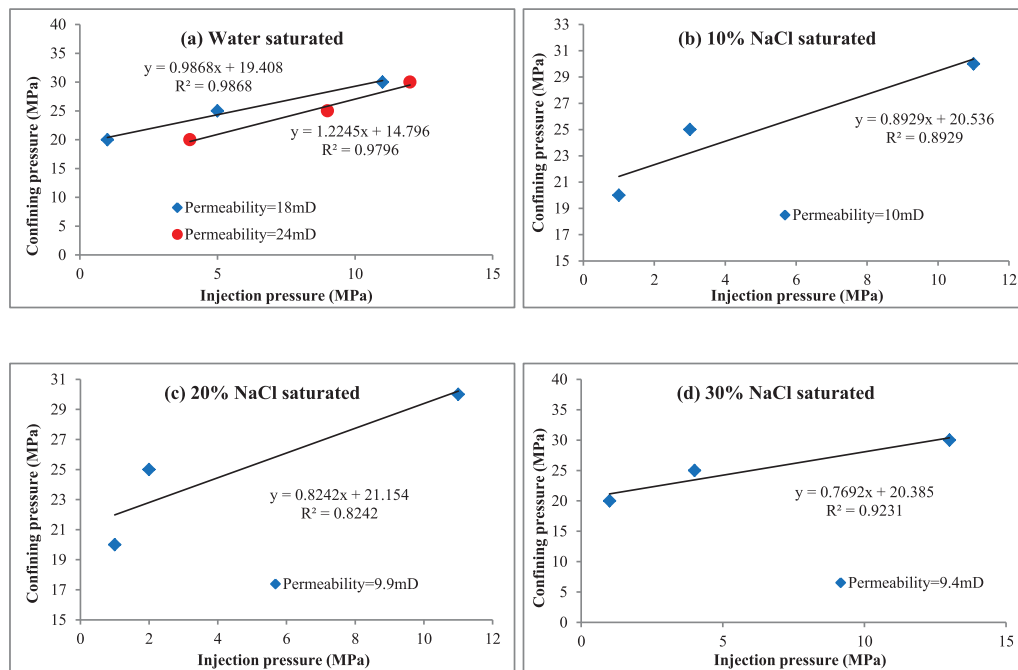


Fig. 9. The obtained iso-permeability curves for the studied saturation conditions.

the value is greater than unity. According to Equation (8), when the effective stress coefficient is greater than unity, pore pressure change has more influence on effective stress than confining pressure. Therefore, water saturation appears to create pore pressure-dominant effective stress behaviour in sandstone, probably due to the pore expansion process associated with the softening which occurs with water saturation. This pore expansion increases the pore volume of the pore structure, and consequently increases the sensitivity to pore pressure. In contrast, increasing the salinity seems to increase the influence of confining pressure on the effective stress. This is because the deposition of NaCl crystals reduces the pore volume of the rock pore structure and the crystals are crushed by the confinement. Therefore, increased confinement causes this crushing effect to be enhanced. These results reveal that the deposition of NaCl crystals with increasing NaCl concentration in aquifer pore fluid makes the pore structure of reservoir rock less

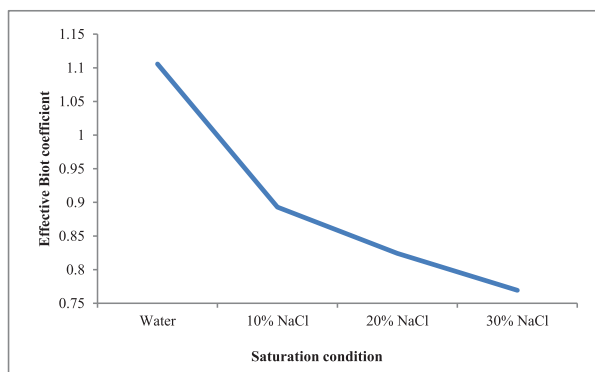


Fig. 10. The variation of obtained average effective stress coefficient for permeability with respect to increasing salinity.

insensitive to the internally-imposed pore pressure. This shows the non-linear behaviour of effective CO_2 permeability related to a given pore pressure and confining pressure, which reflects the unequal role of confining pressure and pore pressure in the deformation of reservoir rock pore networks in various stress environments.

The reduction of effective stress coefficient with increasing salinity can also be explained using Eq. (16). The chemical process (precipitation/dissolution) occurring during the one-year saturation process and the NaCl crystals deposited in the rock pore space reduce the rock porosity and consequently reduce the rock compressibility and the effective stress coefficient in brine-saturated samples. The results of the present study reveal some important evidence related to the influence of rock mineral precipitation and NaCl crystals on rock porosity. The XRD results of 10% brine saturated samples confirmed the precipitation of some clay minerals (kaolinite increases from 2 to 7%) and dissolution of quartz minerals (decrease from 85% to 81.6%) in the rock pore structure during the one-year saturation process. The combined effect of clay mineral precipitation and NaCl crystal deposition in the rock pore space leads to reduced rock porosity and the corrosion of quartz minerals leads to enhanced rock porosity. The net influence of these contradictory processes decides the final effective porosity of the brine-saturated samples. This was cross-checked by calculating the number of NaCl crystals deposited in the rock pore structure based on porosity results (MIP analysis). According to the mass values, 5.15, 6.05 and 8.52 g of NaCl was deposited in the rock mass pore space during the one-year saturation period under 10%, 20% and 30% NaCl saturations, and the values are much lower than the amount of NaCl which existed in the brine injected into the rock samples. According to that calculation, a significant portion of NaCl has been pushed out from the pore space with the effluent brine and only a small amount of NaCl has been crystallised in the pore space. This observation exhibits the more significant pore structure

modification made by the quoted corrosion and mineral depositions during the one-year saturation period compared to the NaCl crystallization in the pore space.

The reason for the observed largest effective stress coefficient in the water-saturated sample compared to various NaCl-saturated samples (10, 20 and 30% concentrations of NaCl-saturated samples) can also be justified using the above argument. Water saturation causes existing and newly-formed pores in reservoir rock to open, and this porosity increment causes the rock compressibility to increase. This in turn increases the sensitivity to pore pressure by creating a greater effective stress coefficient compared to brine-saturated samples (refer to Eq. (16)). A series of MIP tests was conducted to measure rock porosity under various saturation conditions (a detailed description of the MIP porosity measurement method and process can be found in Rathnaweera et al., 2014b) and according to the results, rock porosity decreases with increasing NaCl concentration such that the addition of 10, 20 and 30% NaCl to the saturation fluid causes the rock porosity to be reduced to 0.291, 0.287 and 0.276, respectively. This is because the brine concentration in the pore fluid affects mineral reaction rates in the pore structure, and the reaction rates are expected to be reduced with the NaCl concentration in the pore fluid due to the NaCl creating pore barriers. It is therefore clear that, when the pore fluid has a higher salinity level, the porosity reduction due to NaCl crystals is significant compared to the mineral precipitation and dissolution effects. In order to check this, after each permeability test, the samples, which had no water/brine inside due to initial flushing out, were removed from the cell and the MIP tests were performed to estimate the remaining porosity in the samples. Although the tests could not be used to find the pure influence of the NaCl as the pore structure of these samples had already been altered by the injection and confining pressures, such tests do provide overall knowledge of the NaCl crystallization-created pore space modification and the influence of NaCl concentration in the pore fluid on it. An 8% porosity increment was observed in the originally water-saturated samples (0% NaCl) compared to dry samples. Such a large porosity increment in water-saturated samples in the absence of NaCl probably occurred mainly due to the dissolution of sandstone minerals such as quartz during the one-year saturation process and their eventual flushing out together with the fragmented sandstone around the dissolution spots with the effluent fluid. The XRD analysis confirmed the corrosion of quartz minerals in the rock pore space and according to the XRD results the initial quartz composition decreases from 85% to 79.26% with water saturation. Due to this dissolution process, the rock pore structure re-arranges and consequently changes the porosity from its initial condition. However, it should be noted that there was no water in the water-saturated sample during the porosity measurement, as the sample was taken after testing. Therefore, a water-saturated sample means a sample that had originally been water-saturated before the permeability tests.

4.2.4.5. The corresponding variations in rock mass mechanical properties and seismic behaviour

The injection of CO₂ into saline aquifers during CO₂ sequestration has a significant influence on the long-term safety of the process. This fluid flow creates mechanical property variations in the rock mass, and this matter was therefore then considered on the basis of the variation of effective stress coefficient under various injection conditions. Fluid flow-induced bulk strain data were recorded for each testing condition and these were then plotted against confining pressure and the gradients were used to evaluate the corresponding Skempton coefficients (Eq. (23)). Fig. 11 below shows the relationships between bulk strain and the confining

pressure for three different pore pressures for water- and brine-saturated samples. According to the results shown in Table 2, the Skempton coefficient increases with increasing NaCl concentration in the pore fluid (from 0 to 30%). However, the corresponding poro-elastic coupling parameter, αB , reduces with the salinity percentage enhancement in the flowing fluid due to the reduction of the effective stress coefficient, α . According to Zimmerman (2000), the fluid flow-coupled mechanical property variation in the rock mass can be ignored under the condition $\alpha B \ll 1$. However, according to Table 2, the coupling parameters (αB) obtained in the present study lie in the range of 0.71–0.89, and the coupled mechanical property variations therefore cannot be ignored. This indicates that the injection of CO₂ into brine-saturated reservoir rock can create considerable hydro-mechanical deformations in natural rock formations during and after the injection process, which may lead to catastrophic mechanical failures (Rutqvist and Tsang, 2002; Villarasa et al., 2010). CO₂ injected into a deep sedimentary rock moves vertically due to buoyancy forces and horizontally due to differential pressure. Therefore, over-pressured CO₂ injection may cause excessive compression or tension in the formation (Villarasa et al., 2010), creating cracks and fractures (Rutqvist and Tsang, 2002), which may create pathways for CO₂ leakage into the atmosphere and surrounding clean water aquifers. Therefore, it is highly important to pay attention to this in CO₂ sequestration field projects.

Another important disaster that can be triggered by the CO₂ sequestration process is CO₂ injection-induced seismic activities, which may extend up to devastating earthquakes. Generally, CO₂ injection-induced seismic activities occur along existing fractured rocks or reactivated jointed rocks due to high injection pressures. Density-driven stress conditions created by super-critical CO₂ movement may also lead to seismic activity. According to past studies (Gupta et al., 2001), to date most seismic events have occurred due to high CO₂ injection pressures through wells, and existing reports related to earthquakes reveal that such injections caused moderate earthquakes (Richter magnitudes of 5.1 and 5.2) in Denver, Colorado, in 1966 (Sminchak and Gupta, 2002). The injection pressure pressurizes the fluid in faults during the injection period and frictional resistance along the faults reduces due to the low shear strength of the fluid. This leads to the creation of fault slips, which may cause seismic events. Moreover, processes including hydraulic fracturing, transfer of stresses to weaker faults, contraction of rocks due to the fluid extraction process, mineral precipitation along faults, subsidence due to rock saturation and density-driven stress loading can also trigger seismic activity during the CO₂ injection process.

Hydraulic diffusivity (D) is an important parameter in this respect, and can be used to estimate the seismicity-based permeability variation in reservoirs (Shapiro et al., 1997). According to Biot (1962) and Shapiro et al. (1997), hydraulic diffusivity can be estimated as follows (Eq. (25)), using the linear dynamics of poro-elastic theory:

$$D = \frac{Nk}{\eta} \quad (25)$$

where N is a poro-elastic modulus defined as follows:

$$N = \frac{JP_d}{H} \quad (26)$$

$$J = \left(\frac{\phi}{M_f} + (\alpha - \phi)/M_g \right)^{-1} \quad (27)$$

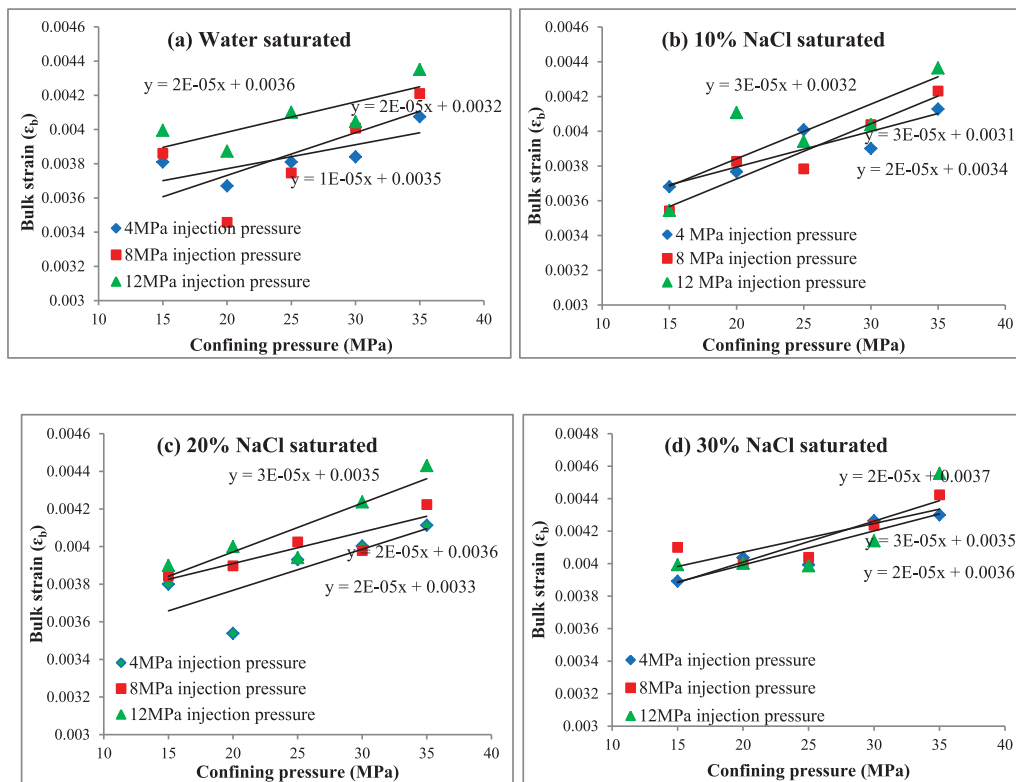


Fig. 11. The obtained relationships between bulk strain and the confining pressure under three different pore pressures for water- and brine-saturated samples.

Table 2
Obtained poro-elastic parameters for different saturation conditions.

Saturation condition	ϕ	K (GPa)	α	B	αB
Water	0.314	6.87	1.11	0.80	0.89
10% NaCl	0.291	7.12	0.89	0.91	0.81
20% NaCl	0.287	8.34	0.82	0.93	0.76
30% NaCl	0.276	9.91	0.77	0.94	0.72

$$H = P_d + \alpha^2 J \quad (28)$$

$$P_d = M_d + 4/3 \mu_d \quad (29)$$

According to Eqs. (25)–(29), the effective stress coefficient can be used to predict poro-elastic modulus and hydraulic diffusivity in rock mass. This is one of the main advantages of the effective stress coefficient, because the correct hydraulic diffusivity value, D , can be used to evaluate the pore pressure perturbation (ΔP) required to trigger micro-seismicity and therefore find the safe limit for the pore pressure change with gas injection, ΔP . The relationship between hydraulic diffusivity and pore pressure perturbation can be written as follows (Biot, 1962):

$$\frac{\partial p}{\partial t} = D \Delta^2 P \quad (30)$$

Fig. 12 below shows how the hydraulic diffusivity changes with respect to injection pressure and different saturation conditions. According to the results, it is clear that hydraulic diffusivity increases with increasing injection pressure, and interestingly, the diffusivity decreases with increasing NaCl concentration in the pore

fluid. For example, at 8 MPa injection pressure, the hydraulic diffusivity decreases from 2.88×10^{-5} to $2.03 \times 10^{-5} \text{ m}^2/\text{s}$ with the initial increment of the NaCl concentration from 0 to 10%, and a further reduction was observed in hydraulic diffusivity with increasing NaCl concentration from 20 to 30%. Moreover, at low injection pressures (up to 6 MPa), there is no significant variation in hydraulic diffusivity. However, at high injection pressures ($>6 \text{ MPa}$), the variation is significant compared to that at low injection pressures. In contrast, it can be said that the potential injection-induced seismicity in CO_2 sequestration in deep saline aquifers decreases with increasing NaCl concentration in the pore

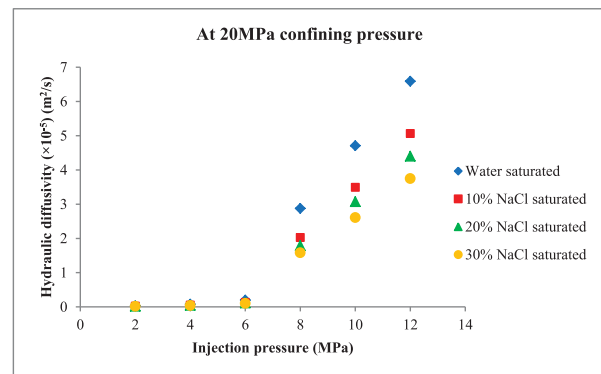


Fig. 12. The variation of hydraulic diffusivity with respect to the injection pressure for different saturation mediums.

fluid.

Therefore, the estimation of the effective stress coefficient can be used to predict other important parameters, such as the Skempton coefficient and poro-elastic coupling parameters, mechanical properties like poro-elastic modulus, CO₂ injection-induced seismicity and safe injection pressures (critical injection pressures) into aquifers. All of these facts clearly exhibit the importance of estimating the effective stress coefficient in deep saline aquifer CO₂ sequestration.

4.2.4.6. Effect of effective confining pressure on effective CO₂ permeability of brine-saturated Hawkesbury sandstone

The term 'effective confining pressure' is generally defined as the difference between the confining and pore pressure in rock mass. This is especially important in identifying the external stress application on the rock mass, and an increase of external stress will basically reduce the pore space. The dependency of the effective CO₂ permeability of reservoir rock on simple effective confining pressure was therefore checked using the determined effective stress coefficients and the results are discussed in this section. Fig. 13 shows how effective CO₂ permeability varies with effective confining pressure for brine-saturated Hawkesbury sandstone. According to Fig. 13, effective CO₂ permeability exhibits a linearly reducing trend with increasing effective confining pressure, regardless of saturation condition. According to the existing studies, this is mainly due to the easy closure of low aspect ratio voids at high confinements. Those low aspect ratio voids control the tortuosity of fluid movement in the rock matrix and therefore, change the permeability (Keaney et al., 2004, Ghabezloo et al., 2009). As mentioned earlier, these low aspect ratio voids are more sensitive to pressure changes than high aspect ratio voids, which are more resistant to pressure changes (Bernabe, 1987; Keaney et al., 2004, Ghabezloo et al., 2009).

The present study investigates the effect of effective confining pressure on effective CO₂ permeability in a wider pressure range, 6.5–34.5 MPa, which has not been covered in previous studies. According to the results, increasing the effective confining pressure from 6.5 to 34.5 MPa causes the effective CO₂ permeability to be reduced from 35.54 to 1.33 mD, from 23.45 to 1.01 mD, from 20.07 to 0.89 mD and from 16.96 to 0.87 mD for water-saturated, and 10, 20 and 30% NaCl-saturated samples, respectively, which are greater reductions for each saturation condition. However, the results exhibit a higher effective confining stress effect on sandstone permeability at lower saline percentages, probably because the formed NaCl crystals cause the effective confining pressure effect to be reduced by filling the pore space. This reduced effective CO₂

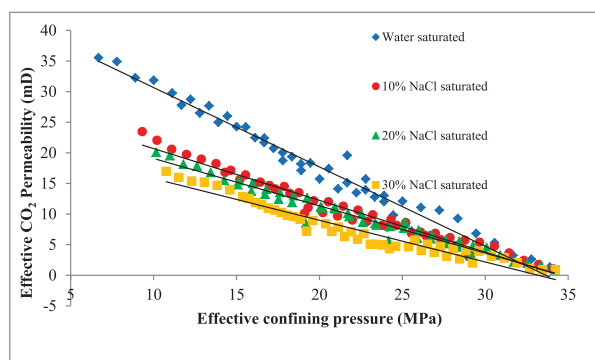


Fig. 13. The variation of effective CO₂ permeability with effective confining pressure.

permeability in reservoir rock with increasing effective confining pressure is not a favourable fact for CO₂ injectability into the aquifer during the CO₂ sequestration process, given the fact that the most preferable and safest reservoirs for CO₂ sequestration exist in deeper locations. Therefore, this observation indicates the importance of having clear knowledge of the effective stress changes in aquifer formations for efficient CO₂ storage field projects.

4.2.5. Conclusions

CO₂ geo-sequestration in deep saline aquifers is a well-accepted measure to address the issue of global warming, as it can greatly reduce anthropogenic CO₂ emissions into the atmosphere. However, the lack of understanding of the hydro-mechanical variations which occur in aquifers with long-term chemical and mineralogical changes in the reservoir rock due to the sequestration process creates many complications for the CO₂ storage process. Such understanding can only be gained by having a thorough knowledge of the applied effective stresses on the formation. This study therefore aimed to understand the effect of effective stress on the permeability of deep saline aquifer rock under various conditions, including salinity levels from 0 to 30% NaCl concentration by weight. The results were verified by conducting a comprehensive microstructural analysis using SEM. The results enable the following major conclusions to be drawn:

- The effective CO₂ permeability of reservoir rock significantly decreases with increasing confining pressures, and increasing the confining pressure from 20 to 35 MPa at 10 MPa injection pressure caused 59.64%, 63.70%, 64.04% and 69.35% permeability reductions in the water, 10, 20 and 30% saline samples, respectively. This reduction is mainly due to the closure of some internal fractures under increased effective stress applied to them that blocks the inter-connected pathways available in rock mass for fluid movement. This was confirmed by the enhanced acoustic emission counts with increasing confinement from 20 to 35 MPa.
- Interestingly, the effective CO₂ permeability reduction observed with increased confinement increases with increasing salinity level in the pore fluid from 0 to 30%. A high degree of salinity in the pore fluid leads to enhanced NaCl crystal depositions in the pore space. Therefore, crushing these greater NaCl depositions at higher confinements causes greater reduction in rock mass permeability, as these crushed depositions obstruct the connected pathways available for CO₂ movement. On the other hand, there are negative and positive influences on rock mass pore space and eventually permeability created by the precipitated and dissolved rock mass minerals during the saturation period. However, these reaction rates are expected to be reduced with the NaCl concentration in the pore fluid due to the NaCl creating pore barriers. Therefore, when the pore fluid has a higher salinity level, the porosity and eventually permeability reductions occurring due to NaCl crystals are significant compared to the mineral precipitation and dissolution effects, which therefore leads to enhanced permeability reductions at high confinements.
- The effective CO₂ permeability of reservoir rock increases with increasing injection pressure at any confinement due to the opening of existing pores and the corresponding new pathways for CO₂ movement.
- The significant alterations created in saline aquifer rock porosity and pore geometry by mineralogical reactions, NaCl deposition, and confining and pore pressures cause the simple effective stress law for permeability, $P_d = P_c - P_p$, to be inapplicable to saline aquifers.

- The effective stress coefficient for saline aquifer permeability decreases with increasing aquifer salinity levels, and the increasing salinity level in the pore fluid from 0 to 30% caused the effective stress coefficient for the permeability of the brine-saturated sandstone to be reduced from 1.11 to 0.77. This implies that the salinity level in the pore fluid plays a major role in determining the effective stress coefficient in deep saline aquifers.

4.2.6. References

- Al-Wardy, W., 2003. Analytical and Experimental Study of the Poro-elastic Behaviour of Clean and Clay-rich Sandstones. PhD thesis. Imperial College, London.
- Al-Wardy, W., Zimmerman, R.W., 2004. Effective stress law for the permeability of clay-rich sandstone. *J. Geophys. Res.* 109, 231–245.
- Bernabe, Y., 1987. The effective pressure law for permeability during pore pressure and confining pressure cycling of several crystalline rocks. *J. Geophys. Res.* 92, 649–657.
- Bernabe, Y., Brace, W.F., Evans, B., 1982. Permeability, porosity and pore geometry of hot pressed calcite. *Mech. Mater.* 1, 173–181.
- Berryman, J.G., 1992. Effective stress for transport properties of in-homogeneous porous rock. *J. Geophys. Res.* 97, 17409–17424.
- Biot, M.A., 1962. Mechanics of deformation and acoustic propagation in porous media. *J. Appl. Phys.* 33, 1482–1498.
- Brace, W.F., Orange, A.S., Madden, T.R., 1965. The effect of pressure on the electrical resistivity of water-saturated crystalline rocks. *J. Geophys. Res.* 70, 5669–5678.
- Brace, W.F., Walsh, J.B., Frango, V.T., 1968. Permeability of granite under high pressure. *J. Geophys. Res.* 73, 2225–2236.
- Bruant, R.G., Guswa, A.J., Celia, M.A., Peters, C.A., 2002. Safe storage of CO₂ in deep saline aquifers. *Environ. Sci. Technol.* 36, 240A–245A.
- David, C., Wong, T.F., Zhu, W., Zhang, J., 1994. Laboratory measurement of compaction-induced permeability change in porous rocks: implication for the generation and maintenance of pore pressure excess in the crust. *Pure Appl. Geophys.* 143, 425–456.
- Fenghou, A., Wakeham, W.A., Vesovic, V., 1998. The viscosity of carbon dioxide. *J. Phys. Chem. Ref. Data* 27, 31–44.
- Garcia, J.E., 2003. Fluid Dynamics of Carbon Dioxide Disposal into Saline Aquifers. PhD thesis. University of California, Berkeley.
- Ghabezloo, S., Sulem, J., Guedon, S., Martineau, F., 2009. Effective stress law for the permeability of a limestone. *Int. J. Rock Mech. Min. Sci.* 46, 297–306.
- Guo, X.Q., Wang, L.S., Rong, S.X., Guo, T.M., 1997. Viscosity model based on equations of state for hydrocarbon liquids and gases. *J. Fluid Phase Equilib.* 139, 405–421.
- Gupta, N., Wang, P., Sass, B., Bergman, P., Byrre, C., 2001. Regional and site-specific hydrogeologic constraints on CO₂ sequestration in the Mid-western United States saline formations. In: *Proceedings of 5th International Conference on Greenhouse Gas Control Technologies*, Cairns, Australia, August 14–16, pp. 123–132.
- Heikamp, S., Nover, G., 2003. An integrated study on physical properties of a KTB gneiss sample and marble from Portugal: pressure dependence of the permeability and frequency dependence of the complex electrical impedance. *Pure Appl. Geophys.* 160, 929–936.
- Jayasinge, D., Ranjith, P.G., Choi, S.K., 2011. Effects of effective stress changes on permeability of Latrobe Valley brown coal. *Fuel* 90 (3), 1292–1300.
- Keaney, G.M., Meredith, P., Murrell, S., Barker, J., 2004. Determination of the effective stress laws for permeability and specific storage in low porosity sandstone. In: *Gulf Rocks 2004, the 6th North America Rock Mechanics Symposium (NARMS)*, pp. 27–37.
- Lion, M., Skoczylas, F., 2004. Determination of the main hydraulic and poro-elastic properties of a limestone from Bourgogne France. *Int. J. Rock Mech. Min. Sci.* 41, 915–925.
- Monlouis-Bonnaire, J.P., Verdier, J., Perrin, B., 2004. Prediction of the relative permeability to gas flow of cement-based materials. *Cem. Concr. Res.* 34, 737–744.
- Nakashima, Y., Kamiya, S., 2007. Mathematical programs for the analysis of three-dimensional pore connectivity and anisotropic tortuosity of porous rocks using X-ray computed tomography image data. *J. Nucl. Sci. Technol.* 44, 1233–1247.
- Norris, A., 1989. Stoneley-wave attenuation and dispersion in permeable formations. *Geophysics* 54, 330–341.
- Nur, A.M., Walls, J.D., Winkler, K., De Vilbiss, J., 1980. Effects of fluid saturation on waves in porous rock and relation to hydraulic permeability. *J. Pet. Sci. Eng.* 20, 450–458.
- Perera, M.S.A., Ranjith, P.G., Airey, D.W., Choi, S.K., 2011. Sub- and super-critical carbon dioxide flow behaviour in naturally fractured black coal: an experimental study. *Fuel* 90, 3390–3397.
- Rathnaweera, T.D., Ranjith, P.G., Perera, M.S.A., 2014a. Salinity-dependent strength and stress-strain characteristics of reservoir rocks in deep saline aquifers: an experimental study. *Fuel* 122, 1–11.
- Rathnaweera, T.D., Ranjith, P.G., Perera, M.S.A., 2014b. Effect of salinity on effective CO₂ permeability in reservoir rock determined by pressure transient methods: an experimental study on Hawkesbury Sandstone. *Rock mechanics and rock engineering*. *Rock Mech. Rock Eng.* <http://dx.doi.org/10.1007/s00603-014-0671-0>.
- Rempel, A.W., Rice, J.R., 2006. Thermal pressurization and onset of melting in fault zones. *J. Geophys. Res.* 111, 93–114.
- Rutqvist, J., Tsang, C.F., 2002. A study of caprock hydromechanical changes with CO₂ injection into a brine formation. *Environ. Geol.* 42, 296–305.
- Shapiro, S., Huenges, E., Borm, G., 1997. Estimating the crust permeability from fluid-injection-induced seismic emission at the KTB site. *Int. J. Geophys.* 131, 15–18.
- Shi, T., Wang, C.Y., 1986. Pore pressure generation in sedimentary basins: overloading versus aquathermal. *J. Geophys. Res.* 91 (B2), 2153–2162.
- Shukla, R., Ranjith, P.G., Choi, S.K., Haque, A., Yellishetty, M., Hong, L., 2012. Mechanical behaviour of reservoir rock under brine saturation. *Rock Mech. Rock Eng.* 46 (1), 83–89.
- Skempton, A.W., 1954. The pore pressure coefficients A and B. *Geotechnique* 4, 143–150.
- Sminchak, J., Gupta, N., 2002. Issues related to seismic activity induced by the injection of CO₂ in deep saline aquifers. *J. Energy Environ. Res.* 2, 32–46.
- Sulem, J., Lazar, P., Vardoulakis, I., 2007. Thermo-poro-mechanical properties of clayey gouge and application to rapid fault shearing. *Int. J. Numer. Anal. Methods Geomechanics* 31 (3), 523–540.
- Tanikawa, W., Shimamoto, T., 2009. Comparison of Klinkenberg-corrected gas permeability and water permeability in sedimentary rocks. *Int. J. Rock Mech. Min. Sci.* 46, 229–238.
- Terzaghi, K., 1936. The shearing resistance of saturated soils and the angle between the planes of shear. In: *Proceedings of the First International Conference on Soil Mechanics*, vol. 1. Harvard University, Cambridge, pp. 54–56.
- Vilarrasa, V., Bolster, D., Olivella, S., Carrera, J., 2010. Coupled hydromechanical modeling of CO₂ sequestration in deep saline aquifers. *Int. J. Greenh. Gas Control* 4, 910–919.
- Walls, J.D., 1982. Effects on Pore Pressure, Confining Pressure and Partial Saturation on Permeability of Sandstones. PhD thesis. Stanford University.
- Walls, J.D., Nur, A., 1979. Pore-pressure and confining pressure dependence of permeability in sandstone. In: *Proceedings of the Seventh Formation Evaluation Symposium of the Canada Well Logging Society*, Alberta, pp. 1–8.
- Walsh, J.B., 1965. The effect of cracks on the compressibility of rock. *J. Geophys. Res.* 70, 381–389.
- Wang, H.F., 1993. Quasi-static poroelastic parameters in rock and their geophysical applications. *Pure Appl. Geophys.* 141, 269–286.
- Ward, C.R., 1972. Sedimentation in the Narrabeen group, southern Sydney basin, New South Wales. *J. Geol. Soc. Aust.* 19 (3), 393–409.
- Witherspoon, P.A., Tsang, Y.W., Long, J.C.S., Nooriphad, J., 1982. New approaches to problems of fluid flow in fractured rock masses. In: *Proceedings of the 22nd US Symposium on Rock Mechanics*. MIT, Cambridge, pp. 14–19.
- Zimmerman, R.W., 1991. Compressibility of Sandstones. Elsevier, Amsterdam.
- Zimmerman, R.W., 2000. Coupling in poroelasticity and thermoelasticity. *Int. J. Rock Mech. Min. Sci.* 37, 79–87.
- Zimmerman, R.W., Somerton, W.H., King, M.S., 1986. Compressibility of porous rocks. *J. Geophys. Res.* 91, 765–777.
- Zoback, M.D., 1975. High Pressure Deformation and Fluid Flow in Sandstone, Granite, and Granular Materials. PhD thesis. Stanford University.
- Zoback, M.D., Byerlee, J.D., 1975. Permeability and effective stress. *Pet. Geol.* 59, 154–158.

4.2.7. Nomenclature

- P_d : differential pressure
 P_c : confining pressure
 P_p : pore pressure
 k : permeability
 α : effective stress coefficient
 Q : CO₂ flow rate
 dP/dt : downstream pressure gradient
 V : downstream volume
 β : adiabatic compressibility
 μ : CO₂ viscosity
 P_d : downstream pressure
 P_i : upstream pressure
 A : sample cross-sectional area
 L : sample length
 k_0 : permeability under atmospheric pressure
 P_0 : atmospheric pressure
 γ : material constant
 u_i : material constant
 B : the Skempton coefficient
 αB : poro-elastic coupling parameter
 ϵ_b : bulk volumetric strain
 M : bulk modulus
 ϕ : porosity
 C_m : compressibility of the rock matrix
 C_{bc} : bulk compressibility
 ζ : excess fluid content
 $d\zeta$: fluid content increment

C_f : compressibility of the pore fluid
 V_p : pore volume
 η : pore-fluid dynamic viscosity
 N : poro-elastic modulus
 D : hydraulic diffusivity
 M_f : bulk modulus of fluid

M_d : bulk modulus of dry condition
 M_g : bulk modulus of grain material (rock matrix)
 μ_d : shear modulus of the frame
 ΔP : pore pressure perturbation
 E : Young's modulus
 γ : Poisson's ratio

4.3 Overburden stress effect on flow behaviour of deep saline reservoir rock

Although many experimental studies have been conducted on the flow behaviour of porous rock masses, very few studies have been conducted on the overburden stress effect, and no data are available on this aspect in deep saline reservoir rock. In deep saline sequestration, overburden stress may naturally vary due to many factors such as landslides, sandstorms and man-made activities such as building construction. Extensive loading may create harmful impacts on natural formations, including micro-cracking due to local stress concentrations, frictional sliding on pre-existing micro-cracks, and even failure due to newly-formed micro- and macro-cracks. The determination of deformation-induced hydro-mechanical properties in deep saline aquifers caused by CO₂ sequestration is therefore very important, because unexpected permeability enhancements and formation strength reductions may lead to devastating catastrophes. The aim of this section is to identify the influence of overburden load variations on the long-term integrity of CO₂ storage in deep saline aquifers. The following published journal paper reports on this part of the study program.



Research paper

Laboratory measurement of deformation-induced hydro-mechanical properties of reservoir rock in deep saline aquifers: An experimental study of Hawkesbury formation



M.S.A. Perera^a, T.D. Rathnaweera^a, P.G. Ranjith^{a,*}, W.A.M. Wanniarachchi^a,
M.C.A. Nasvi^b, I.M. Abdulagatov^c, A. Haque^a

^a Deep Earth Energy Laboratory, Department of Civil Engineering, Monash University, Building 60, Victoria 3800, Australia

^b Department of Civil Engineering, Faculty of Engineering, University of Peradeniya, Sri Lanka

^c Institute Geothermal Research Institute of the Russian Academy of Sciences, Machachkala, Dagestan, Russia

ARTICLE INFO

Article history:

Received 5 August 2015

Received in revised form

10 July 2016

Accepted 12 July 2016

Available online 14 July 2016

Keywords:

CO₂ sequestration

Brine

Critical stress

Permeability

Saline aquifers

CCS

Reservoir

ABSTRACT

The long-term integrity of CO₂ storage in deep saline aquifers has become uncertain due to the unsteady character of surrounding factors, and the time-dependent nature of the aquifer's overburden load (the vertical stress imposed on the aquifer by the weight of overlying materials (rock/soil layers), which may vary over time as a result of natural incidents such as landslides and earthquakes) is critical. The aim of this study is to identify the influence of overburden load variations on the long-term integrity of the CO₂ storage process in deep saline aquifers. High-pressure tri-axial strength and permeability tests, along with acoustic emission (AE) and scanning electron microscopy (SEM) analyses, were conducted on Hawkesbury sandstone obtained from the Gosford basin.

According to the results, the injection of CO₂ into the Hawkesbury formation may dissolve aquifer rock minerals, enhancing aquifer flow performance and reducing aquifer strength. Increasing the stress applied on the aquifer causes aquifer flow ability to reduce to some extent due to pore matrix compaction. Further increase of the overburden pressure may accelerate the aquifer's flow performance due to dilation-induced pore opening. This permeability transition point occurs earlier at greater CO₂ injection pressures and overlaps with the crack formation point of the aquifer rock mass. Therefore, weakening of the rock mass after the transition point can be expected. Importantly, this permeability transition point occurs at lower overburden loads after longer interaction of CO₂ with the saline aquifer. This exhibits the long-term risk associated with CO₂ sequestration in saline aquifers. Permeability enhancement after the transition point may also produce environmental disasters, such as sudden leakages of injected CO₂ from the reservoir to surrounding fresh water aquifers (Evans et al. 2004; Little and Robert 2010), exceeding the specific rates proposed by many regulatory frameworks. Therefore, it is essential to study the long-term integrity of the sequestration process in order to develop a regulatory structure to meet the demands of deep saline sequestration projects.

© 2016 Published by Elsevier Ltd.

4.3.1 Introduction

An understanding of the hydro-mechanical response of geological materials like rocks to natural loading is imperative in many geo-engineering and petroleum industry-based applications, where extensive loading may create harmful impacts on natural formations, including micro-cracking due to local stress

concentrations, frictional sliding on pre-existing micro-cracks, and even failure due to newly-formed micro- and macro-cracks. The evaluation of deformation-induced changes in hydro-mechanical properties in deep saline aquifers caused by CO₂ geo-sequestration is very important, because unexpected permeability enhancements and formation strength reductions may cause many issues, including back-migration of the injected CO₂ into the atmosphere, contamination of freshwater aquifers (Brasier and Kobelski, 1996; Evans et al., 2004; Little and Robert, 2010), surface uplifting, unpredictable leakages, and seismic activities (Wilson

* Corresponding author.

et al., 2003; Ranjith et al., 2013). Some of these issues (e.g. contamination of freshwater aquifers and back-migration of the injected CO₂ into the atmosphere) may even create devastating catastrophes when they exceed critical limits, such as leakage of CO₂ into the atmosphere and surrounding aquifers at significantly high rates with the creation of major cracks in the formation caused by the injecting CO₂ (Bruant et al., 2002; Wilson et al., 2003).

A number of studies have been carried out to date on the deformation-induced fracturing process and its impacts for various underground reservoir materials, including rock salt, shale, siltstone and mudstone (Kachanov 1982; Steif, 1984; Stormont and Daemen, 1992; David et al., 1994; Schulze et al., 2001; Cappa and Rutqvist, 2011; De Silva and Ranjith, 2012; Wang et al., 2013). However, the deformation-induced hydro-mechanical behaviour of reservoir rocks in deep saline aquifers resulting from CO₂ sequestration has not been studied, and the chemico-mineralogical interactions between the injected CO₂, brine and reservoir rock make the problem extremely complex. It is now well accepted that CO₂/brine/rock interaction-induced mineralogical changes (Marbler et al., 2013; Rathnaweera et al., 2015, 2016) can alter the flow-mechanical properties in reservoir rocks. The coupling between these changes and existing overburden pressures will therefore create more complicated situations during the sequestration process. Moreover, in a developed reservoir, differential depletion of lithostatic layers with various permeabilities and the movement of fluid contacts can change the overburden pressure profile. Failure to manage and control these overburden pressure effects can cause serious equipment damage and injury or loss of life. It is therefore necessary to conduct comprehensive research studies to fully understand the hydro-mechanical behaviour of reservoir rock under different overburden pressure conditions during the CO₂ sequestration process.

To date, a number of studies have been conducted to identify the flow pattern alterations and fracture formations in reservoir rocks with deformation. For example, Stormont and Daemen (1992) carried out gas permeability and porosity measurements to characterise deformation-induced permeability and damage in rock salt. According to these researchers, the gas permeability of rock salt can increase by more than five orders of magnitude from its natural state with increasing deviatoric load applied on it. They also proposed a flow model based on the equivalent channel concept, and the model results were found to be consistent with the laboratory data. Similar trends in rock salt behaviour upon the application of deviatoric loading during conventional tri-axial compression testing have been shown by Lai (1971), Donath et al. (1987), Peach et al. (1987), David et al. (1994) and Peach and Spiers (1996). The experiment performed by Peach et al. (1987) under 5 MPa confining pressure revealed that gas permeability can be increased by more than four orders of magnitude by increasing axial strain by 10%. Donath et al. (1987) observed more than two orders of magnitude increment in brine permeability in Domal rock salt upon 5% axial strain increment under 6 MPa confining pressure. The permeability alterations of Domal rock salt upon axial deformation shown by Lai (1971) are higher than those in the above studies, and the discrepancy is believed to be due to the different pore arrangements. The development of damage and permeability in deforming rock salt has been studied by Schulze et al. (2001), who performed strength and creep tests using a Karman-type pressure apparatus coupled with ultrasonic wave velocities. This study further discussed the behaviour of rock salt under both non-dilatancy and dilatancy domains based on the analysis of acoustic emission (AE) counts, volumetric strain, permeability, and ultrasonic wave velocities. Peach and Spiers (1996) performed dilatometric tri-axial tests to investigate the influence of crystal plastic deformation on the dilatancy and

permeability of synthetic rock salt and observed a rapid permeability increment (from 10⁻²¹ to 10⁻¹⁶ m²) at 0.1–0.2 vol% dilatancy. This shows that even a minor dilatancy (<0.2 vol%) occurring during plastic deformation of rock salt may lead to huge permeability enhancements and extreme formation instability.

Flow and crack linkage models are able to articulate such rapid permeability developments in reservoir rocks upon deformation (Peach, 1991; Stormont and Daemen, 1992). The flow model developed by Stormont and Daemen (1992), based on the equivalent channel concept (the channels represent the pore structure of the rock mass), aimed to evaluate the deformation-induced permeability characteristics of rock salt. The concept was originally proposed by Wyllie and Rose (1950) and was subsequently re-derived and analysed by Paterson (1983) and Walsh and Brace (1984). The equivalent channel model describes the permeability characteristics as a function of the tortuosity (t^2), porosity (ϕ) and hydraulic radius of the equivalent channel (m) (see Eq. (8)). Stormont and Daemen (1992) used a frictional sliding crack model to understand the variations of permeability characteristics which occur as a result of micro-cracking initiation and propagation. This frictional sliding crack model considers the loading history of the sample to predict the stresses during the initial and secondary cracking stages, and to evaluate the secondary crack length during load application. A different crack model for sliding cracks initially oriented at an angle of $1/2 \tan^{-1}(1/\mu)$ with respect to the maximum principal stress has been proposed by Jaeger and Cook (1979):

$$\sigma_1 = \frac{2S + \sigma_3 \left[\sqrt{(\mu^2 + 1)} + \mu \right]}{\sqrt{\mu^2 + 1} - \mu} \quad (1)$$

where, S is the intrinsic shear strength, σ_1 is the axial stress, σ_3 is the confining stress and μ is the coefficient of static friction.

After the initial crack formation, secondary cracks generally initiate when the induced tensile stress (hoop stress) through compression exceeds the strength of the rock near the micro-flow tip (Stormont and Daemen, 1992). The angles of secondary cracks (β) with respect to the maximum principal stress, that slide along a particular stress direction can be given as follows (Brady, 1969):

$$\beta = \frac{1}{2} \left[\tan^{-1} \left(\frac{1}{\mu} \right) \pm \cos^{-1} \left(\frac{2S + \mu(\sigma_1 + \sigma_3)}{\sqrt{(1 + \mu^2)} (\sigma_1 - \sigma_3)} \right) \right] \quad (2)$$

Kachanov (1982) modified Eq. (1) by replacing $2S$ by $2K_{IC}/\phi(\sqrt{2/\pi l}) + 2S$ to capture the secondary crack initiation in the model (Eq. (3)), and the length of this secondary crack can be estimated based on Steif's (1984) findings. The deformation-induced flow paths predicted by this model are initially developed along the weaker grain boundaries and then along the secondary cracks upon continuous loading until the failure of the rock mass (Stormont and Daemen, 1992).

$$\sigma_1 = \frac{2K_{IC}/\phi(\sqrt{2/\pi l}) + 2S + \sigma_3 \left[\sqrt{(\mu^2 + 1)} + \mu \right]}{\sqrt{\mu^2 + 1} - \mu} \quad (3)$$

where ϕ is a constant, K_{IC} is the mode I critical stress intensity factor and l is the secondary sliding crack length. Fig. 1 gives the schematic illustration of the Eq. (3), and shows how a secondary crack originates from a primary crack (original crack) in an axial loading environment.

Peach and Spiers (1996) studied the influence of crystal plastic deformation on dilatancy and permeability developments in synthetic rock salt under low pressure and temperature conditions by

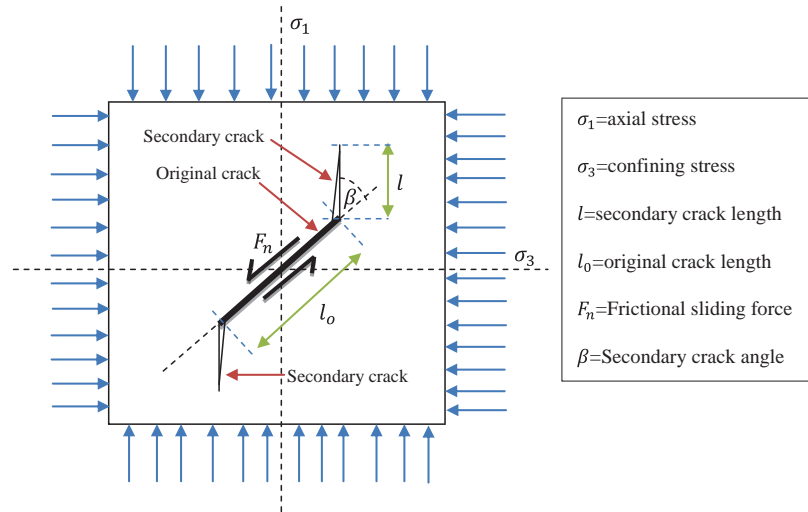


Fig. 1. Schematic representation of secondary crack growth from original crack in an axial loading environment.

developing a microphysical model based on percolation theory. This percolation theory has widely been used in material physics (Sahimi, 1994), and to simulate permeability in fractured rocks with macro-scale cracks (Indraratna et al., 2000). The number of fractures and the length/height/spacing of cracks within the rock matrix influence permeability (Germanovich and Astakhov, 2004; Jin et al., 2010). According to percolation theory, permeability in terms of crack geometry and dilatancy can be written as Eq. (4), and the corresponding crack widths and radius depend on the dilatancy characteristics of the rock (Peach and Spiers, 1996):

$$k = \frac{2}{15} \theta \alpha D w^2 \left[1 - 4 \left(\left(\frac{8\delta\alpha}{\pi D} - \frac{3}{4} \right)^{\frac{1}{2}} - \frac{1}{2} \right)^3 + 3 \left(\left(\frac{8\delta\alpha}{\pi D} - \frac{3}{4} \right)^{\frac{1}{2}} - \frac{1}{2} \right)^4 \right] \quad (4)$$

where k is the permeability, θ is the hydraulic aperture, α is the volumetric shape factor, D is the dilatancy, δ is the aspect ratio and w is the mean crack half width.

Although such studies play vital roles in assessing the repository performance of many petroleum and mining engineering applications, including radioactive waste disposal and CO₂ storage in deep geological formations, related studies on CO₂ sequestration in deep saline aquifers are still difficult to find. A comprehensive evaluation of the hydro-mechanical behaviour of reservoir rock during CO₂ sequestration considering the potential effects of mineralogical changes under in-situ overburden stresses is therefore required. The present study aims to evaluate the deformation-induced permeability and dilation characteristics of the Hawkesbury sandstone formation and the potential damage to the rock mass upon CO₂ injection, paying particular attention to CO₂ injection-induced crack propagation in the rock mass.

4.3.2 Sample preparation and saturation

The sandstone samples were collected from a potential carbon capture and storage (CCS) site located in the Gosford basin, Sydney. The Gosford sandstone formation belongs to the early Triassic period and is commonly called the Hawkesbury sandstone

formation. The main mineral composition of the sandstone is 90% quartz, 5% calcite, 2% kaolinite, 1% siderite, 1% muscovite and 1% other clay minerals such as illite and smectite (refer to Table 1). Therefore, it is clear that the sandstone belongs to the silicate-cemented group with a high percentage of quartz mineral in the rock cement. Furthermore, the reservoir rock samples are unlayered, white-grey coloured and medium-to fine-grained.

Homogeneous sandstone blocks without any macroscopic cracks were first carefully selected based on visual inspection. The collected sandstone blocks were cored to 38 mm diameter and 76 mm high cylinders in the Deep Earth Energy Research Laboratory (DEERL) at Monash University following ASTM standards. After coring, the two ends of the samples were carefully ground to create smooth faces, and then oven-dried for 48 h at 35 °C (a low temperature was selected to avoid temperature cracks) before being set aside for saturation. In addition to visual inspection, computed tomography (CT) scanning was used to check the micro-level homogeneity (Fig. 2). According to the results of CT scanning, it is quite reasonable to assume a homogeneous pore arrangement in and among the tested samples without any considerable micro-cracks.

For the present study, two saturation conditions were selected: 1) brine-saturated without CO₂ injection, and 2) brine-saturated with CO₂ injection (brine+CO₂). The pH of the prepared brine solution was measured using a calibrated pH meter and found to be equal to 7.1. Here, the brine-saturated samples without CO₂ injection represent the natural aquifer formation prior to CO₂ injection, and the brine+CO₂-saturated samples represent the resulting aquifer condition after completion of CO₂ injection. Fig. 3 shows the set-up of the saturation process: (a) brine-saturation using desiccators (b) brine+CO₂ saturation using a saturation chamber. For the

Table 1
Results of XRD analysis.

Rock minerals	Dry (%)	Brine-saturated (%)	Brine+CO ₂ -saturated (%)
Quartz	90	87	80
Calcite	5	4	1
Kaolinite	2	6	15
Siderite	1	1	–
Muscovite	1	1	–
Other clay minerals	1	1	4

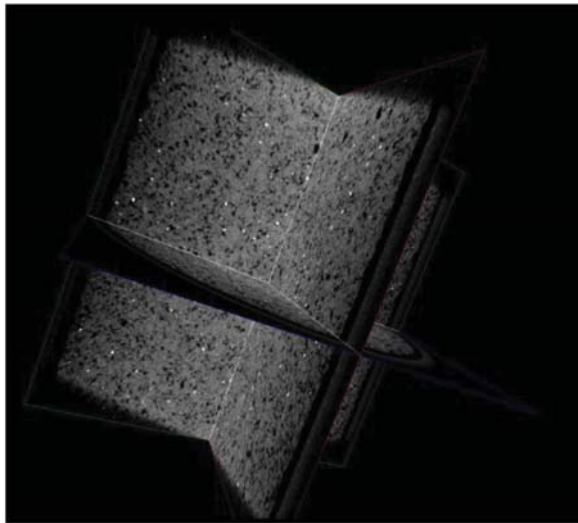


Fig. 2. Results of CT scanning along the sample length.

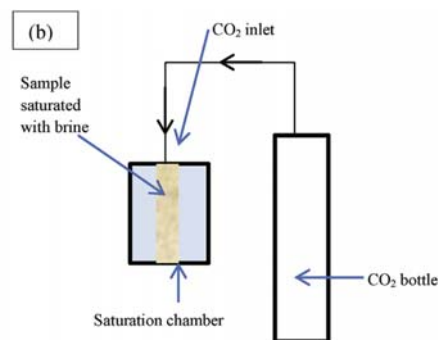
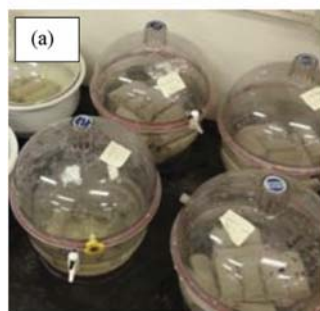


Fig. 3. Saturation process (a) brine-saturation using desiccators (b) brine+CO₂ saturation using saturation chamber.

brine saturation condition, samples were kept in desiccators under vacuum for two years (Fig. 3(a)) and to achieve the brine+CO₂ saturation condition, samples were kept in saturation chambers for two years (Fig. 3(b)). The CO₂ saturation was conducted under 10 MPa injection pressure at 35 °C. Since the selected temperature and pressure conditions exceed the critical boundaries of CO₂ (7.35 MPa and 31.8 °C), CO₂ saturation was done under super-critical conditions, as generally occurs in the field.

4.3.2.1 Experimental procedure

4.3.2.1.1 High-pressure tri-axial strength and permeability tests

A number of high-pressure tri-axial strength and permeability tests were conducted on prepared samples under undrained conditions, maintaining a constant temperature of 35 °C. Two replicates were selected for each condition and the tri-axial strength results are shown in Table 2. A multivariate multiple regression method was used to estimate the statistical significance of the data. The results suggest that the relationship between tri-axial strength and saturation condition (dry, brine-and brine+CO₂-saturated) ($F = 58.21$, $p = 0.0001$) and the relationship between tri-axial strength and the pore pressure ($F = 53.72$, $p = 0.0001$) are statistically significant for all the tested conditions (where, F is the critical one-tail parameter and p is the one-tail parameter in the F -test).

Detailed information regarding the high-pressure tri-axial set-up and the sample assembly procedure can be found in Rathnaweera et al. (2014b). The test series was initiated by removing the saturated brine in the pore space after two years of saturation by injecting CO₂ at 1 MPa injection pressure under 10 MPa confinement. This brine flushing-out process was conducted under drained conditions and the corresponding flushed-out brine mass was measured downstream until it gave a constant value, representing no further flow of brine in the sample.

The tests were performed under a constant confining pressure of 10 MPa, and to determine the CO₂ permeability CO₂ was injected at 2–6 MPa with 1 MPa increments (sub-critical phase condition). First, brine+CO₂-saturated samples were tested to evaluate the corresponding deformation-induced permeability characteristics under different CO₂ injecting pressures. 2 MPa CO₂ injection pressure was first applied to the sample without applying any deviatoric load, and the corresponding downstream pressure development was recorded (deviatoric stress, $\sigma'_1 = 0$). After the downstream pressure reached a constant value (approximately equal to the injection pressure), CO₂ injection was stopped and the developed pore pressure inside the sample was removed by

opening the downstream at an extremely slow rate (0.1 MPa/min) to avoid sample damage due to the sudden volumetric expansion of the rock matrix. The axial stress was then increased to produce a deviatoric load on the sample. The axial stress was increased by 5 MPa increments from 10 MPa to failure and the corresponding permeability values were evaluated at 5 MPa increments. The axial load was applied at 0.75 mm/min and the corresponding acoustic emission (AE) energy counts, axial and lateral strains were recorded. After the completion of 2 MPa injection pressure, the same procedure was repeated for the other injection pressures to evaluate the deformation-induced permeability variation under different pore pressure conditions. Once the brine+CO₂-saturated samples had been tested, the same test procedure was repeated on brine-saturated samples (without gas saturation) to understand the behaviour of natural saline aquifers with overburden stress variation. A comprehensive mineralogical analysis was finally carried out using SEM analysis to understand the possible rock alterations during long-term saturation.

4.3.2.1.2 Acoustic emission (AE) methodology

The tri-axial tests (of both strength and permeability tests) were conducted, simultaneously recording the acoustic signals to identify crack formation and propagation during the fluid migration and load application, and a peripheral component interconnection (PCI) 2-channel data acquisition system was used to acquire AE signals in

Table 2
Mean values of tri-axial strength tests.

Specimen	UCS (MPa)	Tri-axial strength (MPa)						Tri-axial mean strength (MPa)				
		CO ₂ pore pressure (MPa)						CO ₂ pore pressure (MPa)				
		2	3	4	5	6	2	3	4	5	6	
Dry	1	39.52	138.77	136.37	131.12	129.49	126.76	138.04	135.31	130.17	128.45	126.28
	2	40.21	137.31	134.25	129.22	127.41	125.8					
Brine-saturated	1	26.12	116.75	112.83	109.61	108.71	104.88	116.44	113.01	110.21	108.47	105.35
	2	25.74	116.13	113.19	110.81	108.23	105.82					
Brine+CO ₂ -saturated	1	19.31	105.15	104.53	102.19	100.94	100.48	105.50	104.13	102.60	101.07	100.65
	2	20.83	105.85	103.73	103.01	101.20	100.82					

* 1 and 2 represent sample 1 and sample 2.

all the experiments. The set-up consists of a band-pass filter with a frequency range of 200–750 kHz and a nominal resonant frequency of 500 kHz. The hardware includes six sensors and external amplifiers. Here, the AE system was coupled with tri-axial tests by attaching the six AE sensors on either side of the pressure cell to acquire the cracking data during the test. Both loading and AE data acquisition were simultaneously initiated to identify the cracking behaviour in the sample under each stress condition. The amplifiers were used to amplify the low-frequency acoustic waves resulting from the crack fracturing process in the rock and were set to 60 dB to amplify the AE signals.

4.3.2.2 Data processing and permeability calculation

During each gas injection, the upstream pressure was maintained at a constant injection pressure and downstream pressure development over time was recorded until pressure equilibrium was reached (when the upstream and downstream pressure were equal). Fig. 4 shows an example of the pattern of recorded downstream pressure development.

The recorded downstream pressure development curves were then used to calculate the CO₂ permeability of the sample under each injection condition, using the pressure decay approach proposed by Brace et al. (1968). The pressure decay curve used in this approach is shown in Eq. (5) (Peach and Spiers, 1996):

$$\Delta P(t) = \Delta P_0 e^{-mt} \quad (5)$$

where, ΔP_0 is the stress applied to the sample, t is the time, $\Delta P(t)$ is the differential pressure of upstream and downstream, and m is a decay time constant which can be determined by plotting the decay curve in terms of $\ln[\Delta P(t)]$ versus time. The obtained pressure decay curves are shown in Fig. 5. These curves yield a straight line and the corresponding gradient of each curve gives the values of m for the considered test condition. After obtaining the m values for each condition, the permeability (k) can be calculated using Eq. (6) (Sutherland and Cave, 1980):

$$k = mvC \left(\frac{L}{A} \right) \times \left[\frac{V_1 V_2}{V_1 + V_2} \right] \quad (6)$$

where, V_1 , V_2 are the upstream and downstream volumes, L is the sample length, A is the cross-section area of the sample, v is the CO₂ viscosity at temperature and mean pore pressure, and C is the compressibility of CO₂, which is calculated using the REFROPE database (Rathaweera et al., 2014b).

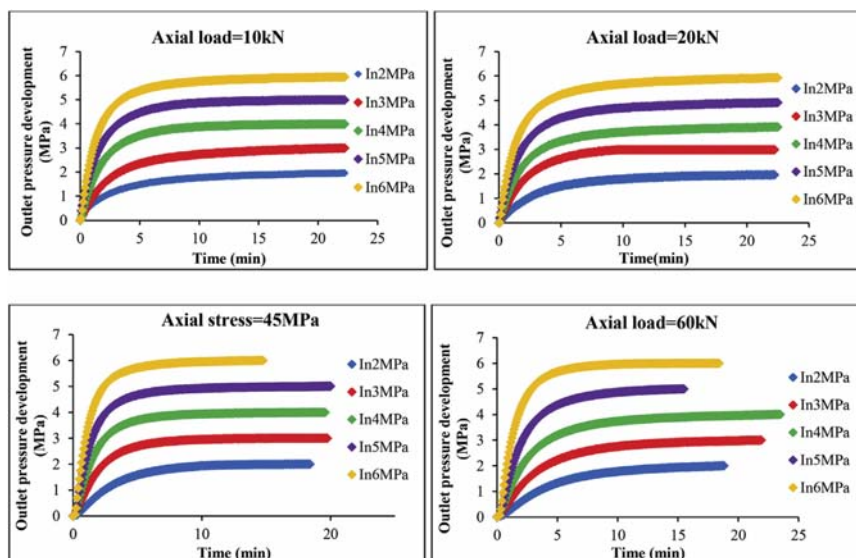


Fig. 4. Corresponding downstream pressure development curves of brine+CO₂-saturated samples.

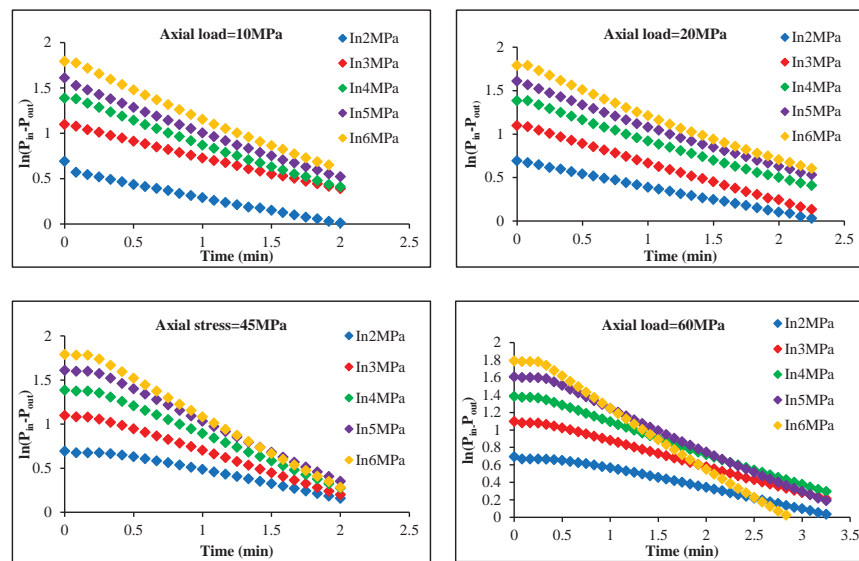


Fig. 5. Pressure decay curves for brine+CO₂-saturated samples.

4.3.3 Results and discussion

4.3.3.1 Stress-strain behaviour

The stress-strain behaviours of brine- (without CO₂ saturation) and brine+CO₂-saturated samples were first investigated to understand the possible impact of CO₂ injection on natural saline aquifers. Fig. 6 shows the stress-strain responses of Hawkesbury sandstone under two saturation conditions. These data were obtained from tri-axial undrained strength tests conducted at 10 MPa confining pressure and 35 °C temperature.

According to Fig. 6, regardless of saturation condition (brine or brine+CO₂), the axial strain of the tested sandstone starts to increase after the post-peak, reflecting a strain softening process at the later stage of load application. The lateral strain also increases with load application, revealing the dilatant behaviour of the tested sandstone. Investigation of the failure patterns of samples under each saturation condition revealed that all the samples tended to fail along a shear plane with load application, regardless of

saturation type (see Fig. 7). A similar failure pattern has been observed by Rathnaweera et al. (2015) for brine-saturated sandstone samples tested under tri-axial stress conditions. However, Rathnaweera et al. (2015) also observed a strain localisation process in brine-saturated samples during the later stage of load application, and such strain localisation was not exhibited in the present study. This difference is probably due to the differences in mineralogical alteration of the sandstones in the two studies related to the different saturation periods (Rathnaweera et al. (2015) used a saturation period of 1.5 years instead of 2 years), different saturation mediums (Rathnaweera et al. (2015) used 10, 20 and 30% NaCl concentrations of brine and this study used 15% NaCl concentration of brine) and different sandstone types (Rathnaweera et al. (2015) used 80% quartz-cemented sandstone and this study used 90% quartz-cemented sandstone).

Preferable saline aquifers for CO₂ sequestration normally have a high percentage of salinity in their pore fluid of around 2×10^4 (2% by weight) to 2×10^5 mg/l (25% by weight) (Bachu and Bennion, 2008). Therefore, the sandstone samples saturated with brine

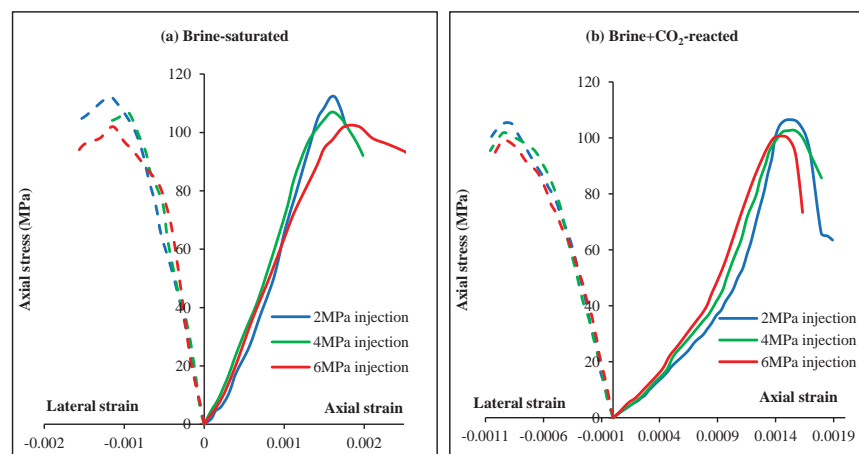


Fig. 6. Stress-strain behaviour of samples under tested conditions.

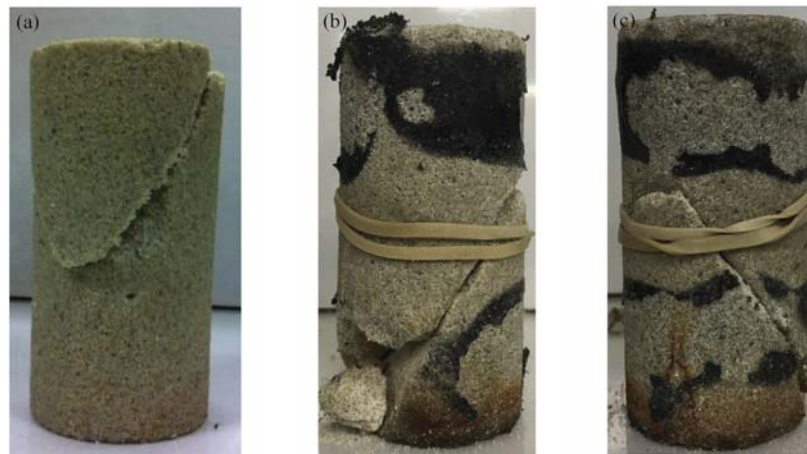


Fig. 7. Failure patterns for each saturated condition (a) brine-saturated sample (b) and (c) brine+CO₂-saturated samples under 2 MPa and 6 MPa injection pressures, respectively.

with 15% NaCl concentration (% by weight) can be considered as natural aquifer formation conditions (average salinity), and the strength results for the brine+CO₂-saturated samples can be used to understand the influence of CO₂ injection on the hydro-mechanical properties of natural formations. According to the results, under 10 MPa confining pressure, brine-saturated samples with CO₂ injection pressures of 2, 3, 4, 5 and 6 MPa fail at axial stresses (σ_1) of 116.44, 113.01, 110.21, 108.47 and 105.35 MPa, respectively.

To identify the effect of CO₂ injection in deep saline formations, brine+CO₂-saturated samples were then tested under the same conditions (the same confining pressure, injection pressures and temperature). Fig. 6(b) shows the stress-strain behaviour of brine+CO₂-saturated samples under different CO₂ injection pressures. According to the figure, under 10 MPa confining pressure, the brine+CO₂-saturated samples with 2, 3, 4, 5 and 6 MPa CO₂ injection pressures fail at axial stresses (σ_1) of 105.5, 104.13, 102.6, 101.07 and 100.65 MPa, respectively. Based on the above values and Fig. 6 (a) and (b), it can be stated that, regardless of saturation condition, the formation tri-axial strength decreases with increasing injection pressure from 2 to 6 MPa, due to the enhanced pore opening process of the rock matrix. The results of the geo-mechanical investigations conducted by Marbler et al. (2013) on silicate-cemented sandstone (Bunter sandstone) revealed some important evidence related to the CO₂ injection-induced mechanical property changes in reservoir rock, which clearly show a reduction of strength of brine-saturated sandstone samples on the introduction of CO₂. At 6 MPa effective confining pressure, a brine-saturated sample showed a 45 MPa deviatoric stress compared to the 30 MPa deviatoric stress given by a brine+CO₂ saturated sample (a reduction of about 34%). They also found a significant reduction in compressive strength (UCS) and cohesion of the tested brine-saturated sample after exposure to CO₂. This is consistent with the findings of the present study, which shows a 116.44 to 105.5 MPa (about 10%) failure strength reduction after exposure to CO₂ (injected at 2 MPa injection pressure) in brine-saturated samples, and similar strength reductions for other CO₂ injection pressures. This strength reduction with CO₂ injection shows the significant impact of injected CO₂ on the mechanical properties of reservoir rock during CO₂ sequestration. Such CO₂ injection-induced strength reductions are believed to be related to the CO₂ saturation-induced mineralogical changes which occur in the reservoir rock's pore structure. The effect of these mineralogical and geo-chemical changes on the mechanical behaviour of

reservoir rocks can be effectively identified using mechanical modelling coupled with mineralogical and geochemical rock alterations. To clearly identify the reason for the observed CO₂ injection-induced mineralogical rock changes, scanning electron microscopy (SEM) and X-ray diffraction (XRD) analyses were conducted on both brine-saturated samples under CO₂ treated and untreated conditions. Table 1 and Fig. 8 show the XRD and SEM results, respectively.

Previous studies clearly showed the possibility of the changing of rock strength with carbonation reactions and mineral formation during the CO₂ sequestration process (Marini, 2007; Marbler et al., 2013), and Marini (2007) found a 26.5% increment in solid phase in the pore fluid due to albite reaction and 35.4% due to anorthite reaction. These mineral dissolutions clearly influence the rock pore structure and lead to weakening of the grain bonds (Marbler et al., 2013). The present study observed a significant corrosion of quartz minerals in CO₂-treated samples compared to untreated samples. Moreover, some possible initial calcite mineral dissolution textures were found from SEM analysis in CO₂-treated samples compared to untreated samples. This is further confirmed by the XRD results (Table 1), according to which the initial composition of quartz and calcite mineral decreases from 90% to 80% and from 5% to 1% upon interaction with CO₂. The general reaction mechanism of quartz and calcite are given below:



These progressive alterations of quartz and carbonate minerals in the rock matrix probably weaken the grain bonds, and consequently reduce the failure strength of the rock mass, because the rock strength of silicate-cemented sandstone is mainly supported by grain-to-grain contacts. Furthermore, the corrosion reactions of primary and secondary silicate mineral rims around the quartz and calcite grains also contribute to the reduction of the grain-to-grain contacts in grain-supported parts of the reservoir rock. In addition, according to Marbler et al. (2013), the fate of clay mineral dissolution in the rock cement also reduces the strength in clay mineral-supported parts of the rock matrix. According to Lombard et al. (2010), increasing dissolution and weakening of the grain boundaries of the rock structure by mineralogical alteration also cause the reduction of the elastic deformation properties of sandstone.

A comprehensive knowledge of the influence of the interaction

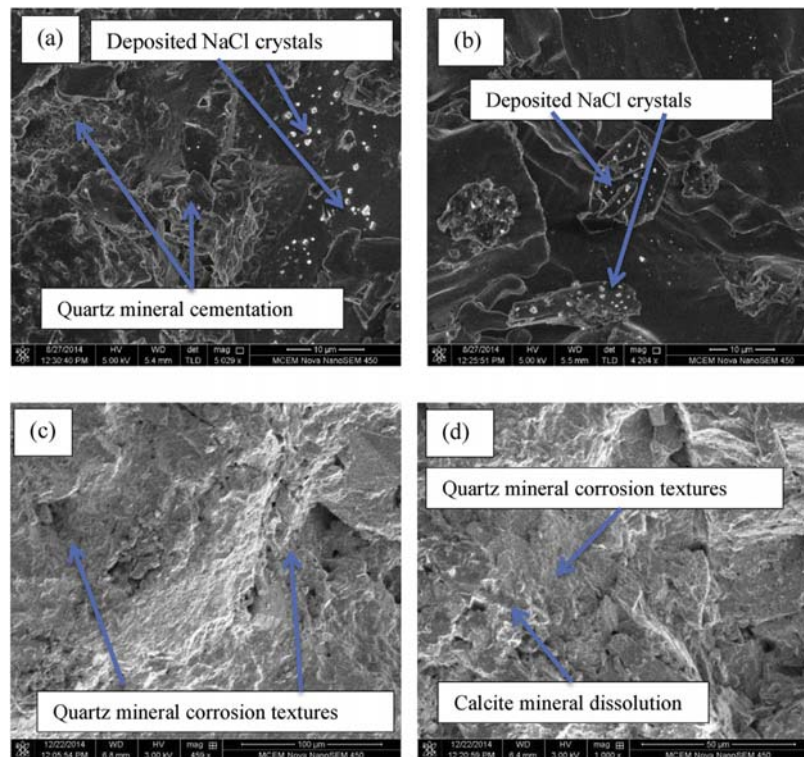


Fig. 8. Results of SEM analysis (a), (b) brine-saturated samples (without CO₂ treatment) and (c), (d) brine+CO₂-saturated samples.

of CO₂/brine/rock minerals on the rock mass deformation characteristics (e.g. Young's modulus, Poisson's ratio and toughness index) is therefore necessary to precisely identify the influence of geochemical reactions on aquifer rock mass mechanical properties. According to Table 3, with the introduction of CO₂ into the system, the Young's modulus of the reservoir rock starts to reduce, and the initial Young's modulus of dry reservoir rock of 9.58 GPa is reduced up to around 5.12 GPa with the saturation of the rock mass through brine and is further reduced up to around 4.44 GPa upon interaction with CO₂. This reduction of elastic modulus confirms the influence of geochemical interactions on reservoir rock mass ductility, which appears to be enhanced by these interactions. However, this is not favourable for the fracturing process. Apart from the deformability or enhancement of ductility, the geochemical reactions caused by CO₂/brine/rock mineral interactions also affect the fracturing properties of the reservoir rock, which was confirmed by the associated toughness index reduction observed in the reservoir rock. Compared to the dry and brine-saturated samples, the toughness index of the CO₂+brine-saturated samples decreased from 11.35 MPa to 2.66 MPa, respectively. This shows the weakening of the rock mass upon injection of CO₂. This is positive for the fracturing process, although it adds an additional risk to the safety of the fracturing process. A closer

consideration of the Poisson's ratio gives evidence for this. According to the test results, the Poisson's ratios of dry and brine-saturated samples increase by around 38.46% and 15.38% upon interaction with CO₂ (CO₂+brine-saturated sample). This Poisson's ratio enhancement may occur with the precipitation of expandable rock mineral in the pore space, and a considerable increase in the Poisson's ratio of reservoir rock due to the deposition of clay minerals in the pore space has been reported by Zhang and Bentley (2005). This was further confirmed by the XRD analysis, according to which there is clearly a greater amount of clay minerals in the tested CO₂+brine-saturated sample (13% increment in kaolinite and 3% increment in other clay minerals) compared to dry samples.

It is also necessary to determine how the CO₂/brine/rock mineral interaction affects the reservoir rock mass flow performance. The alteration of rock mass porosity is a good tool in this regard, as it links chemical reactions, fluid flow and transport and mechanical deformation of the reservoir rock. A comprehensive porosity evaluation was therefore carried out using mercury intrusion porosimetry (MIP) to determine the effect of CO₂ injection on reservoir porosity (see Table 4). According to the results, the average porosity of the brine-saturated sample (representing the natural reservoir conditions) is increased from around 0.27 to 0.34 with the introduction of CO₂ into the reservoir system (CO₂+brine-saturated

Table 3
Summary of Young's modulus, Poisson's ratio and toughness index obtained from testing.

Condition	In unconfined stress environment		
	Young's modulus (GPa)	Poisson's ratio	Toughness index (MPa)
Dry	9.58	0.26	15.18
Brine-saturated	5.12	0.30	6.49
Brine+CO ₂ -saturated	4.44	0.36	3.83

Table 4
Results of MIP analysis.

Condition	Porosity (MIP)
Dry	0.31
Brine-saturated	0.27
Brine+CO ₂ -saturated	0.34

samples). This enhancement in reservoir rock porosity has a significant influence on the effectiveness of the CO₂ sequestration process, because it accelerates the rate of CO₂ movement through the reservoir, which in turn increases the risk of CO₂ leakage from the aquifer to surrounding groundwater aquifers (Arsyad et al., 2013).

Overall, it is clear that CO₂ injection-induced mineralogical and chemical changes in the rock matrix alter the pore arrangement and mineral grain boundaries, which consequently affects the mechanical integrity of the reservoir formation.

4.3.3.2 Deformation-induced permeability variation

After confirming the consistency of the tri-axial strength tests of the prepared samples with existing findings, another set of sandstone samples (brine- and brine+CO₂-saturated) was tested under tri-axial stress conditions to evaluate the changes in deformation-induced permeability characteristics in reservoir rock. The permeability variation of the sample with increasing axial load was checked by calculating the sample's permeability at each 10 MPa axial load increment, and the test was repeated for all the CO₂ injection pressures. The variations of CO₂ permeability with axial stress and strain are given in Fig. 9 (a) and (b), respectively. The variation in CO₂ permeability with axial load increment is consistent at all the CO₂ injection pressures, and at each injection pressure, CO₂ permeability initially decreases with increasing axial load and then starts to rapidly increase until the rock mass fails. For example, at 2 MPa injection pressure, CO₂ permeability decreases from 91.34 to 53.41 mD with initial increment of the axial load from 0 to 75 MPa, and then starts to increase at 77.83 MPa axial load with an accumulated axial strain of 0.00128 and increases up to 188.31 mD (at failure) in brine-saturated samples. Under the same injection conditions, brine+CO₂-saturated sample permeability reduces from 91.34 to 53.41 mD during initial load increment and starts to increase at 74.78 MPa and fails at a 231.21 mD permeability value. Similar permeability variation trends were observed for all other injection pressures. Interestingly, the observed permeability transition point (where the permeability decreasing trend changes to an increasing trend under loading) occurs under lower axial stress at higher injection pressures compared to low injection pressures. The critical axial stress at a transition point under 2 MPa

occurs at 77.83 MPa and it changes to 65.72 MPa with the injection pressure of 6 MPa in brine-saturated samples. Under the same conditions, the brine+CO₂-saturated samples show a permeability transition point of 74.78 MPa (critical axial stress) at 2 MPa injection pressure and that point reduces to 61.21 MPa with the injection pressure of 6 MPa. This critical axial stress reduction with increasing injection pressure is probably due to the pore pressure-induced enhanced weakening of the reservoir pore structure. These contradictory variations of sandstone permeability (decreasing and then increasing) with loading are due to compaction-induced and dilation-induced influences, and the initial reduction in CO₂ permeability is mainly due to compaction-induced pore structure closure, while the following increments in CO₂ permeability are due to dilation-induced pore opening in the reservoir pore matrix.

Fig. 10 shows the variation in deformation-induced CO₂ permeability for brine and brine+CO₂-saturated samples under 2 MPa injection pressure conditions. Both saturation conditions show similar trends with increasing axial stress, as discussed above. However, the critical axial stress that reverses the permeability trend in brine-saturated samples displays much higher values compared to those obtained for brine+CO₂-saturated samples under the same conditions. For example, at 2 MPa injection pressure, the value is 82.06 MPa for the brine-saturated samples and 77.83 MPa for the brine+CO₂-saturated samples. This implies that the introduction of CO₂ into brine-saturated samples causes the crushing point to occur earlier due to the CO₂-created strength reduction in the rock mass. The brine-saturated samples show lower permeability values under any stress condition compared to brine+CO₂-saturated samples. For instance, at 2 MPa injection pressure, the permeability of brine-saturated samples is 81.51 mD

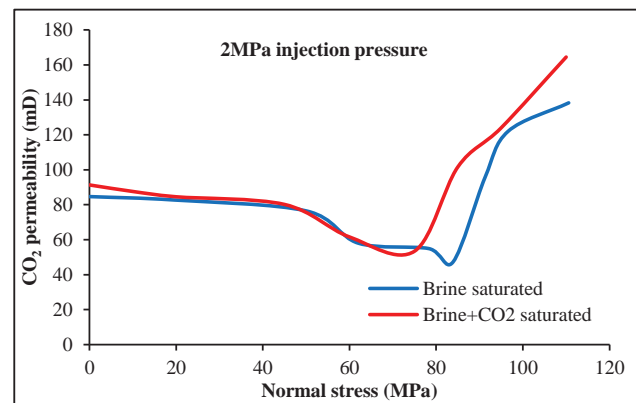


Fig. 10. Deformation-induced permeability variation for brine and brine+CO₂-saturated samples under 2 MPa injection pressure.

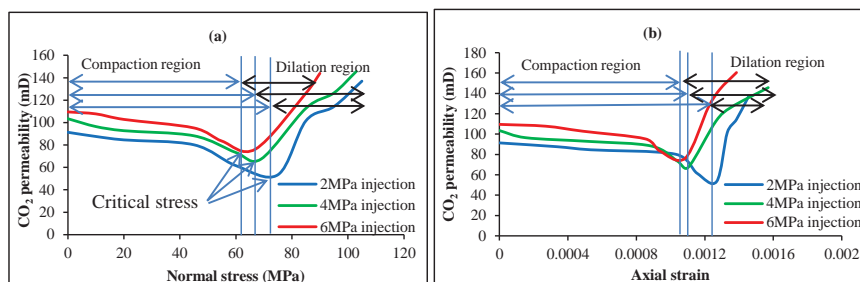


Fig. 9. Permeability variation for brine+CO₂-saturated samples under test conditions (a) variation of CO₂ permeability with respect to the normal stress and (b) variation of CO₂ permeability with respect to the axial strain.

and that of brine+CO₂-saturated samples is 91.34mD. This is due to the CO₂ injection-induced chemical and mineralogical reactions creating greater grain structure weakening, which in turn creates more fractures and enhances the pore space.

4.3.3.3 Further investigation of the influence of rock mass damage development (dilatancy) on its permeability

When reservoir rock is mechanically loaded, it shows two different behaviours, represented by two stress-dependent domains. The two domains are the compaction domain (non-dilatancy domain) and the dilatancy domain, and these two are separated by the dilatancy boundary. During deviatoric loading, the samples tend to dilate as a result of the formation of micro-cracks, and this dilatancy behaviour can be characterised in terms of changes in inelastic volumetric strain. In the present study, the axial (and lateral (ϵ_l)) strains are defined as positive for compression and negative for expansion. Assuming a small strain, volumetric strain (ϵ_v) can be calculated using Eq. (9) proposed by Jaeger and Cook (1979):

$$\epsilon_v = \epsilon_a + 2\epsilon_l \quad (9)$$

Fig. 11 shows the variation in volumetric strain with respect to the accumulated axial strain in brine and brine+CO₂-saturated samples during tri-axial loading. According to Fig. 11, it is clear that the volumetric strain initially changes positively (+signs) with deviatoric loading, and this response is dominated by non-linear compaction. Eventually, the sample begins to dilate and the volumetric strain reverses towards the dilation region (-sign). As Fig. 12 shows, dilation characteristics are more significant in brine+CO₂-saturated samples than in brine-saturated samples, probably due to the mineralogical alteration-induced mechanical weakening in brine+CO₂-saturated samples compared to brine-saturated samples. The critical stress threshold values confirm the above argument, as the brine-saturated samples display much stronger critical stress values than the brine+CO₂-saturated samples. For instance, at 2 MPa injection pressure, brine-saturated samples display 84.37 MPa critical stress and brine+CO₂-saturated samples show 76.48 MPa. The reduction of the critical stress value confirms the weakening induced by CO₂ injection in reservoir rock.

To clearly identify the rock mass dilatancy-induced flow property alterations with load application, a comprehensive study including acoustic emission (AE) analysis and SEM analysis was conducted. The acoustic energy-releasing characteristics of reservoir rock provide important evidence regarding their deformation-induced fracturing behaviour (Eberhardt et al., 1999; Alkan et al., 2007; Ranjith et al., 2010; Perera and Ranjith, 2013) during load application, including crack closure, crack initiation and unstable crack propagation (Ranjith et al., 2004; Perera et al., 2011; Rathnaweera et al., 2014a; Vishal et al., 2015). Fig. 13 below

shows the results of AE analysis and the corresponding permeability variations of brine+CO₂-saturated samples under different injection pressures. These values were then compared with the brine-saturated results to identify the influence of CO₂ introduction into brine-saturated reservoir rock (Table 5). According to Fig. 13, reservoir rock initially experiences compaction with deformation due to crack closure, grain re-arrangement, and pore collapse, which reduces the CO₂ permeability due to the reduction of free-flow paths for CO₂ movement. David et al. (1994) studied the compaction-induced permeability changes in sandstone and found that the permeability reduction occurs due to compaction-induced grain rearrangement and grain translation. These researchers evaluated the critical pressure (P_{cr}) corresponding to the onset of grain crushing and pore collapse (Brace, 1978). After the pore closure period, crack initiation occurs in the rock mass (Fig. 13), and this initiation point can be identified using cumulative AE energy data (a sudden increase of cumulative AE energy emissions can be seen at that point). Interestingly, the deformation-induced permeability behaviour seems to be consistent with the crack propagation behaviour of the rock mass (Fig. 13). According to Table 5, the critical stress at the permeability transition point nearly coincides with the crack initiation stress of the cumulative AE energy curve. This confirms the occurrence of a dilatant domain characterised by micro- and macro-cracking. As mentioned earlier, this crack initiation point (the point at which the transition from non-dilatant to dilatant deformation occurs) can also be defined as the dilatancy boundary (Schulze et al., 2001), and the loading in the dilatant domain enhances crack generation and propagation. The observed transition of CO₂ permeability with applied deviatoric loading occurred at this dilatancy boundary, and this transition process of CO₂ permeability with loading is mainly dominated by reservoir rock dilation.

In relation to the crack formation behaviour shown by the AE system, at the beginning of the load application no significant AE energy release can be seen and therefore the rock mass is in its crack closure state. Then, with the gradually increasing compressive load on the rock mass, stable crack propagation begins, which is indicated by the gradually increasing AE energy release. The starting point of the stable crack propagation is called the crack initiation point. Further increase of the load after gradual crack propagation causes unstable crack propagation to be initiated in the rock mass, when AE energy release occurs in an exponentially increasing manner. This unstable crack propagation stage of the load application clearly causes significant damage to the rock mass, leading to its failure. The present study used this concept to identify the crack formation behaviour of reservoir rock in saline aquifers. The influence of CO₂ injection on crack initiation was then investigated by comparing the results of brine+CO₂-saturated samples with those for brine-saturated samples. As Table 5 shows, under the same injection pressure, the crack initiation threshold value in

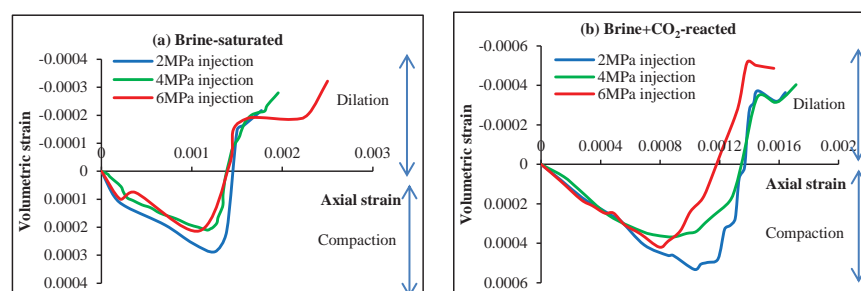


Fig. 11. Volumetric strain versus axial strain variation for (a) brine-saturated and (b) brine+CO₂-saturated samples.

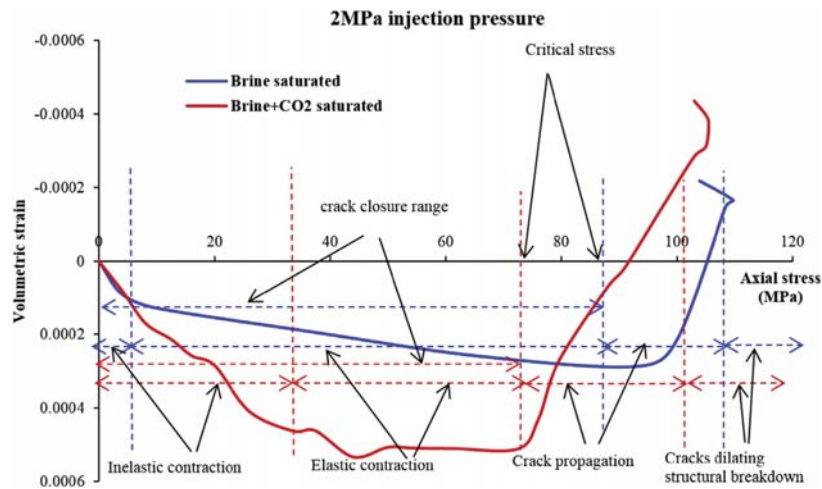


Fig. 12. Volumetric strain versus axial stress curves for brine- and brine+CO₂-saturated samples at 2 MPa injection pressure.

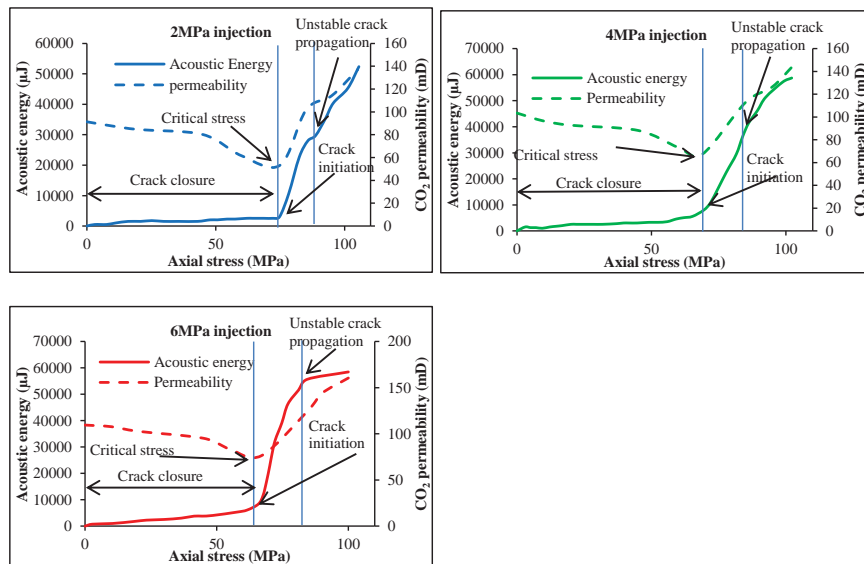


Fig. 13. Results of AE analysis and corresponding permeability variations obtained from tri-axial permeability tests for brine+CO₂-saturated samples under different injection pressures.

Table 5

Comparison of AE results and critical stress obtained from permeability analysis in brine-saturated samples and brine+CO₂ saturated samples.

Injection pressure (MPa)	Brine-saturated samples		Brine+CO ₂ saturated samples	
	Critical stress (MPa)	Crack initiation stress (MPa)	Critical stress (MPa)	Crack initiation stress (MPa)
2	82.06	84.03	77.83	78.01
4	76.47	77.46	69.04	73.83
6	71.81	72.19	61.72	62.69

natural formations (brine-saturated samples) decreases with the introduction of CO₂, indicating the early occurrence of cracks. For example, at 2 MPa injection pressure, samples saturated with brine exhibit a crack initiation value of 84.03 MPa, and this decreases to 78.01 MPa with the saturation of CO₂. As mentioned earlier, this easy crack initiation with CO₂ introduction into the reservoir rock mass is due to mineralogical weakening in the rock pore space (for example, the dissolution of quartz cement and calcite cement in the

reservoir pore structure).

Fig. 14 shows the results of the SEM analysis of brine and brine+CO₂-saturated samples at 85 MPa axial stress under 2 MPa injection pressure. According to Fig. 14, a significantly greater rock pore structure alteration occurs with the introduction of CO₂ into the reservoir rock mass, mainly due to quartz mineral corrosion. Although quartz mineral corrosion can also occur in brine-saturated samples due to the corrosive nature of the brine

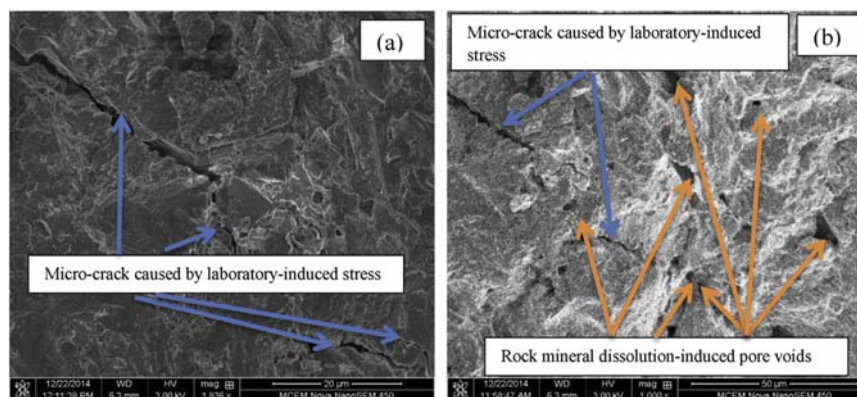


Fig. 14. SEM analysis results of (a) brine-saturated and (b) brine+CO₂-saturated samples at 85 MPa axial stress under 2 MPa injection pressure conditions.

solution, the interaction between brine and CO₂ appears to greatly enhance the process at this stage. Based on the observation of the SEM images, most of the cracks caused by laboratory-induced stress are long, relatively straight and narrow, with sharp ends, as shown in Fig. 14.

The present study illustrates the mechanical weakening in reservoir rocks with the long-term interaction with CO₂ and the corresponding enhancement of permeability characteristics, mainly due to mineralogical reaction-induced pore rearrangements in the silicate-cemented reservoir rock. These findings exhibit the influence of CO₂ injection on the coupled hydro-mechanical properties of reservoir rocks, which is important for field CO₂ sequestration in saline aquifers, because the crack-induced transport properties of the reservoir are responsible for the integrity of the sequestration process. In particular, the effect of dilatancy characteristics on the mechanical and hydraulic properties of reservoir rock must be known for the design of safe sequestration reservoirs and for the assessment of the long-term integrity of reservoir rock, including the assessment of the existing regulatory environment for safe sequestration.

The other important issue when considering the effectiveness of CO₂ sequestration in deep saline aquifers is the reservoir's permeability anisotropy induced by overburden load (axial load) and chemical reactions. According to Clennell et al. (1999), increasing overburden load may cause the particle orientation and pore size distribution in the rock mass to be significantly changed, and a reduction of flow path tortuosity parallel to the particle alignment direction and increment of it normal to the particle alignment direction occur during the initial stage of load application. This leads to the creation of anisotropic permeability within the reservoir rock at the early stage of the loading, where the horizontal permeability of reservoir rock is generally greater than the vertical permeability (Clennell et al., 1999). However, with gradual increasing of axial load, the reservoir rock tends to dilate and form macro-cracks, changing the final permeability profile of the rock sample. In respect of the influence of chemical reactions on permeability anisotropy, the intensity of each rock mineral reaction has a significant effect on the orientation of grain boundaries, pores and cementation in the rock matrix, which in turn affect the movement of CO₂ through the reservoir formation (Pruess et al., 2001; Rathnaweera et al., 2016). Rock mineral reactions with CO₂ may have different intensities in vertical and horizontal planes due to their inhomogeneous spreading pattern in the rock formation, which may cause anisotropic permeability during the CO₂ sequestration process. Such anisotropic permeability behaviour in reservoir rock significantly affects the CO₂ injectivity and CO₂ plume

movement (Pruess et al., 2001), and is therefore particularly important for CO₂ sequestration in deep saline aquifers. However, this possible permeability anisotropy behaviour could not be studied in the present study, because it was quite difficult to obtain a deep internal view into the samples under test during the load application with the existing laboratory facilities.

4.3.4 Conclusion

A number of tri-axial strength and permeability tests were conducted to identify the deformation-induced flow characteristics of reservoir rock (Hawkesbury quartz-cemented sandstone) in deep saline aquifers during CO₂ sequestration, giving special attention to the effect of overburden pressure variations on the flow behaviour of the CO₂ sequestration process. The following conclusions can be drawn based on the Hawkesbury formation:

- CO₂ injection-induced CO₂-brine-rock mineral geochemical reactions may cause some rock minerals such as quartz and calcite to significantly dissolve. This may have a major influence on reservoir rock formations such as quartz-cemented sandstone, because the grain-to-grain contacts in these reservoir rock formations are mainly made with minerals like quartz.
- This mineral dissolution enhances the formation rock mass flow performance through pore space expansion and weakens its mechanical properties through the dissolution of grain-to-grain bonding, and the influence is increased with increasing CO₂ injection pressure. For example, 10, 8, 7, 7 and 5% strength reductions were observed in brine-saturated (quartz-cemented) Hawkesbury rock samples when the injection pressures increased from 2 to 6 MPa under 10 MPa confinement.
- Increasing the overburden pressure acting on the reservoir rock mass negatively affects the Hawkesbury reservoir flow performance to some extent. Thereafter, further increasing the overburden pressure may cause the flow performance to be enhanced, the transition point being dependent on the CO₂ injection pressure. This initial reduction in CO₂ permeability is mainly due to compaction-induced pore structure closure. The following increments in CO₂ permeability are due to dilation-induced pore opening in the reservoir pore matrix, and this pore opening occurs more easily at higher injection pressures. For example, at 2 MPa injection pressure under 10 MPa confinement, CO₂ permeability decreases from 91.34 to 53.41 mD with increasing axial load from 0 to 75 MPa. With further increase of load up to around 77.83 MPa, permeability starts to increase and continues to increase up to 188.31 mD (at

failure), and this transient stage occurs at 65.72 MPa at 6 MPa injection pressure. However, dilation-induced pore opening may create sudden leakages, exceeding the acceptable rates proposed by many regulatory frameworks of injected CO₂ from the reservoir, causing pollution of surrounding freshwater aquifers.

- The stress at the permeability transition point overlaps with the crack initiation stress of the Hawkesbury rock mass. This observation confirms the crack-formation governing dilatant behaviour of the rock that is related to the weakening of the rock mass. This effect is significantly enhanced by the long-term interaction of the reservoir rock with CO₂.
- Therefore, excessive overburden pressure on saline aquifers subjected to CO₂ sequestration may cause reservoir rock mass weakening, and the creation of reservoir subsidence. However, these observations may significantly change from reservoir to reservoir due to the different mineral compositions of reservoir rocks, and cannot be generalised without considering the effect of different mineral compositions on the CO₂ sequestration process. Therefore, further research on this aspect is needed before firm conclusions can be drawn.

4.3.5 References

- Alkan, H., Cinar, Y., Pusch, G., 2007. Rock salt dilatancy boundary from combined acoustic emission and triaxial compression tests. *Int. J. Rock Mech. Min. Sci.* 44 (1), 108–119.
- Arsgoud, M.P., Y. Babayagi, T., 2013. Comparative assessment of potential gas and oil fields induced by injection of CO₂ into a reservoir and surrounding formations. *Earth Planet. Sci.* 6, 278–286.
- Bachu, S., Bennion, B., 2008. Effects of in-situ conditions on relative permeability characteristics of CO₂-brine systems. *Environ. Geol.* 54 (8), 1707–1722.
- Brace, W., Walsh, J.B., Frangos, W.T., 1968. Permeability of granite under high pressure. *J. Geophys. Res.* 73 (6), 2225–2236.
- Brace, W.F., 1978. A note on permeability changes in geologic material due to stress. *Pure Appl. Geophys* 116 (4–5), 627–633.
- Brady, B.T., 1969. A statistical theory of brittle fracture for rock material, part I—brittle failure under homogeneous axisymmetric states of stress. *Int. J. Rock Mech. Min. Sci.* 6, 21–42.
- Brasier, F.M., Kobelski, B.J., 1996. In: Apps, J.A., Tsang, C.-F. (Eds.), *Injection of Industrial Wastes in the United States*. Academic Press, San Diego, CA.
- Bruant, R., Guswa, A., Celia, M., Peters, C., 2002. Safe storage of CO₂ in deep saline aquifers. *Environ. Sci. Technology—Washington D.C.* 36 (11), 240A–245A.
- Cappa, F., Rutqvist, J., 2011. Modeling of coupled deformation and permeability evolution during fault reactivation induced by deep underground injection of CO₂. *Int. J. Greenh. Gas Control* 5 (2), 336–346.
- Clennell, M.B., Dewhurst, D.N., Brown, K.M., Westbrook, G.K., 1999. Permeability anisotropy of consolidated clays. *Geol. Soc. Lond. Spec. Publ.* 158 (1), 79–96.
- David, C., Wong, T.F., Zhu, W., Zhang, J., 1994. Laboratory measurement of compaction-induced permeability change in porous rocks: Implication for the generation and maintenance of pore pressure excess in the crust. *Pure Appl. Geophys.* 143, 425–456.
- De Silva, P.N.K., Ranjith, P.G., 2012. A study of methodologies for CO₂ storage capacity estimation of saline aquifers. *Fuel* 93 (1), 13–27.
- Donath, F.A., Holder, J.T., Fruth, L.S., 1987. Coupled tri-axial testing of rock salt specimens. In: Tsang, C.-F. (Ed.), *Coupled Processes Associated with Nuclear Waste Repositories*. Academic Press, London, pp. 627–636.
- Eberhardt, E., Stimpson, B., Stead, D., 1999. Effects of grain size on the initiation and propagation thresholds of stress-induced brittle fractures. *Rock Mech. Rock Eng.* 32 (2), 81–99.
- Evans, J.P., Heath, J., Shipton, Z.K., Kolesar, P.T., Dockrill, B., Williams, A., et al., 2004. Natural leaking CO₂-charged systems as analogs for geologic sequestration sites. In: *Third Annual Conference on Carbon Capture and Sequestration*, Alexandria, VA.
- Germanovich, L.N., Astakhov, D.K., 2004. Stress-dependent permeability and fluid flow through parallel joints. *J. Geophys. Res. Solid Earth* 109, B09203.
- Indraratna, B., Ranjith, P.G., Gale, W., 2000. Single phase water flow through rock fractures. *J. Geotechn. Geol. Eng.* 17, 211–240.
- Jaeger, J.C., Cook, N.G.W., 1979. *Fundamentals of Rock Mechanics*, third ed. Chapman & Hall, London.
- Jin, Z.H., Johnson, S.E., Fan, Z.Q., 2010. Subcritical propagation and coalescence of oil-filled cracks: getting the oil out of low-permeability source rocks. *Geophys. Res. Lett.* 37, L01305.
- Kachanov, M.L., 1982. A microcrack model of rock inelasticity part I: frictional sliding on microcracks. *Mech. Mater.* 1 (1), 19–27.
- Lai, C.S., 1971. *Fluid Flow through Rock Salt under Various Stress States*. Ph.D. Thesis. Michigan State University, Ann Arbor.
- Little, M.G., Robert, B.J., 2010. Potential impacts of leakage from deep CO₂ geo-sequestration on overlying freshwater aquifers. *Environ. Sci. Technol.* 44 (23), 9225–9232.
- Lombard, J.M., Azaroual, M., Pironon, J., Broseta, D., Egermann, P., Murnier, G., Mouronval, G., 2010. CO₂ injectivity in geological storages: an overview of program and results of the geocarbon-injectivity project. *Oil Gas Sci. Technol. Rev. IFP* 65 (4), 533–539.
- Marbler, H., Erickson, K.P., Schmidt, M., Lempp, C., Pöllmann, H., 2013. Geo-mechanical and geochemical effects on sandstones caused by the reaction with supercritical CO₂: an experimental approach to in situ conditions in deep geological reservoirs. *Environ. Earth Sci.* 69 (6), 1981–1998.
- Marini, L., 2007. Geological sequestration of carbon dioxide—thermodynamics, kinetics, and reaction path modelling. *Dev. Geochem.* 11, 453–468.
- Paterson, M.S., 1983. The equivalent channel model for permeability and resistivity in fluid-saturated rock: a re-appraisal. *Mech. Mater.* 2, 345–352.
- Peach, C.J., 1991. Influence of Deformation on the Fluid Transport Properties of Salt Rocks. *Geol. Ultraiectina*, 77. Ph.D. Thesis. Universiteit Utrecht.
- Peach, C.J., Spiers, C.J., 1996. Influence of crystal plastic deformation on dilatancy and permeability development in synthetic salt rock. *Tectonophysics* 256 (1), 101–128.
- Peach, C.J., Spiers, C.J., Tankink, A.J., Zwart, H.J., 1987. *Fluid and Ionic Transport Properties of Deformed Salt Rock*. Commission of the European Communities, Luxembourg, pp. 143–154.
- Perera, M.S.A., Ranjith, P.G., 2013. Effects of gaseous and super-critical carbon dioxide saturation on the mechanical properties of bituminous coal from the southern Sydney basin. *Appl. Energy* 231, 73–81.
- Perera, M.S.A., Ranjith, P.G., Mironov, P., 2011. Effects of saturation medium and pressure on strength parameters of Latrobe Valley brown coal: carbon dioxide, water and nitrogen saturations. *Energy* 36 (12), 6941–6947.
- Pruess, K., Tianfu, X., John, A., Julio, G., 2001. Numerical modelling of aquifer disposal of CO₂. In: *SPE/EPA/DOE Exploration and Production Environmental Conference*. Society of Petroleum Engineers, pp. 23–34.
- Ranjith, P.G., Fourar, M., Pong, S.F., Chian, W., Haque, A., 2004. Characterisation of fractured rocks under uniaxial loading states. *Int. J. Rock Mech. Min. Sci.* 41, 43–48.
- Ranjith, P.G., Jasinge, D., Choi, S.K., Mehic, M., Shannon, B., 2010. The effect of CO₂ saturation on mechanical properties of Australian black coal using acoustic emission. *Fuel* 89 (8), 2110–2117.
- Ranjith, P.G., Perera, M.S.A., Khan, E., 2013. A study of safe CO₂ storage capacity in saline aquifers: a numerical study. *Int. J. Energy Res.* 37 (3), 189–199.
- Rathnaweera, T.D., Ranjith, P.G., Perera, M.S.A., 2014a. Salinity-dependent strength and stress–strain characteristics of reservoir rocks in deep saline aquifers: an experimental study. *Fuel* 122, 1–11.
- Rathnaweera, T.D., Ranjith, P.G., Perera, M.S.A., 2014b. Effect of salinity on effective CO₂ permeability in reservoir rock determined by pressure transient methods: an experimental study on Hawkesbury sandstone. *Rock Mech. Rock Eng.* 123, 1–18.
- Rathnaweera, T.D., Ranjith, P.G., Perera, M.S.A., Lashin, A., Arifi Al, N., 2015. Non-linear stress–strain behaviour of reservoir rock under brine saturation: an experimental study. *Measurements* 71, 56–72.
- Rathnaweera, T.D., Ranjith, P.G., Perera, M.S.A., 2016. Experimental investigation of geochemical and mineralogical effects of CO₂ sequestration on flow characteristics of reservoir rock in deep saline aquifers. *Nat. Sci. Rep.* 6.
- Sahimi, M., 1994. *Applications of Percolation Theory*. Taylor and Francis, London.
- Schulze, O., Popp, T., Kern, H., 2001. Development of damage and permeability in deforming rock salt. *Eng. Geol.* 61 (2), 163–180.
- Steif, P.S., 1984. Crack extension under compressive loading. *Eng. Fract. Mech.* 20 (3), 463–473.
- Stormont, J.C., Daemen, J.J.K., 1992. Laboratory study of gas permeability changes in rock salt during deformation. *Int. J. Rock Mech. Min. Sci. Geomech.* 29 (4), 325–342.
- Sutherland, H.J., Cave, S.P., 1980. Argon gas permeability of New Mexico rock salt under hydrostatic compression. *Int. J. Rock Mech. Min. Sci. Geomech.* 17, 281–288.
- Vishal, V., Ranjith, P.G., Singh, T.N., 2015. An experimental investigation on behaviour of coal under fluid saturation, using acoustic emission. *J. Nat. Gas Sci. Eng.* 22, 428–436.
- Walsh, J.B., Brace, W.F., 1984. The effect of pressure on porosity and transport properties of rock. *J. Geophys.* 89, 9425–9431.
- Wang, J.G., Liu, J., Kabir, A., 2013. Combined effects of directional compaction, non-Darcy flow and anisotropic swelling on coal seam gas extraction. *Int. J. Coal Geol.* 109, 1–14.
- Wilson, E.J., Johnson, T.L., Keith, D.W., 2003. Regulating the ultimate sink: managing the risks of geologic CO₂ storage. *Environ. Sci. Technol.* 37 (16), 3476–3483.
- Wyllie, M.R.J., Rose, W.D., 1950. Some theoretical considerations related to the quantitative evaluation of the physical characteristics of reservoir rock from electrical log data. *Trans. Am. Soc. Mech. Eng.* 189, 105–1118.
- Zhang, J.J., Bentley, R.L., 2005. Factors determining Poisson's ratio. *CREWES Res. Rep.* 17, 123–139.

4.4 CO₂-induced flow behaviour of reservoir rock under reservoir conditions

Interactions between injected CO₂, brine and reservoir rock during CO₂ sequestration in deep saline aquifers change their natural chemical and mineral structures, ultimately affecting CO₂ flow performance. Recently, an effort has been made to bring these experimentally-based mineralogical rock alteration studies into a platform where they can be used by practising engineers. However, little attention has been given to the identification of the combined geochemical, mineralogical and permeability effects. The impact on flow in deep saline aquifers can only be understood by the combined investigation of these three effects (geochemical, mineralogical and permeability). Therefore, the effect of CO₂ sequestration on reservoir rock chemical, mineralogical and permeability characteristics and their combined effect are considered in this section. The following published journal paper reports on this part of the thesis.

SCIENTIFIC REPORTS

OPEN

Experimental investigation of geochemical and mineralogical effects of CO₂ sequestration on flow characteristics of reservoir rock in deep saline aquifers

Received: 28 September 2015

Accepted: 11 December 2015

Published: 20 January 2016

T. D. Rathnaweera, P. G. Ranjith & M. S. A. Perera

Interactions between injected CO₂, brine, and rock during CO₂ sequestration in deep saline aquifers alter their natural hydro-mechanical properties, affecting the safety, and efficiency of the sequestration process. This study aims to identify such interaction-induced mineralogical changes in aquifers, and in particular their impact on the reservoir rock's flow characteristics. Sandstone samples were first exposed for 1.5 years to a mixture of brine and super-critical CO₂ (scCO₂), then tested to determine their altered geochemical and mineralogical properties. Changes caused uniquely by CO₂ were identified by comparison with samples exposed over a similar period to either plain brine or brine saturated with N₂. The results show that long-term reaction with CO₂ causes a significant pH drop in the saline pore fluid, clearly due to carbonic acid (as dissolved CO₂) in the brine. Free H⁺ ions released into the pore fluid alter the mineralogical structure of the rock formation, through the dissolution of minerals such as calcite, siderite, barite, and quartz. Long-term CO₂ injection also creates a significant CO₂ drying-out effect and crystals of salt (NaCl) precipitate in the system, further changing the pore structure. Such mineralogical alterations significantly affect the saline aquifer's permeability, with important practical consequences for the sequestration process.

Due to their wide availability, deep saline aquifers show great promise for the sequestration of carbon dioxide (CO₂), and therefore the effective mitigation of anthropogenic emission of CO₂ into the atmosphere^{1,2}. However, this sequestration brings long-term interactions between CO₂, rock, and pore fluid (brine), causing unpredictable hydro-mechanical behaviour in the reservoir rock and uncertain long-term stability. In particular, changes in rock permeability critically affect the safety and efficiency of the sequestration process. Unexpected increases in reservoir permeability may cause sudden leakages, harmful to the environment and to human communities; they may also strengthen gradual migration of the CO₂ plume, allowing it to reach poorly characterized areas that are at even greater risk of leakage. Such considerations have made the effects on reservoir rock permeability a topic of great research interest³⁻⁷, but most studies have focused only on the mineralogical and geochemical consequences⁸⁻¹⁰, with little attention to how reservoir flow is influenced. The impact on flow in deep saline aquifers can only be appreciated by the combined investigation of geochemical and permeability changes with CO₂ sequestration.

A small number of experimental studies have set out to identify the combined geochemical and permeability effects^{11,12}, but their reach is limited. For example, Shiraki and Dunn¹¹ conducted a hydro-chemical laboratory experiment on dolomite- and anhydrite-cemented Tensleep sandstone saturated with a mixture of CO₂ and brine for nearly one week, to understand the influence on permeability. They found a reduction in permeability after one week of saturation, arising from the formation of kaolinite in pore throats and other mineral reactions such as the dissolution of dolomite and K-feldspar. Muller *et al.*⁶ performed a combined hydro-chemical experiment on Berea sandstone by flushing NaCl saturated cores with dry CO₂, and found a reduction in permeability due to the precipitation of halite minerals. Experiments on calcite- and dolomite-cemented sandstone by Ross *et al.*¹²

Department of Civil Engineering, Monash University, Building 60, Victoria 3800, Australia. Correspondence and requests for materials should be addressed to P.G.R. (email: ranjith.pg@monash.edu)

Lithology	Carbonate (CS) cemented sandstone
Formation	Early Triassic "Hawkesbury sandstone"
Macroscopic description	Colour: White-grey-brownish, medium to fine grained
Mineralogy (XRD)	60% quartz, 26% calcite, 6% kaolinite, 5% barite, 1% siderite, 1% muscovite, 1% other clay minerals
Structure	un-layered, inter-granular pore space
Cementation	Well cemented, sub-granular quartz rim with calcite fillings
Geochemistry (XRF, wt.%)	57.1 SiO ₂ , 27.4 CaO, 4.3 Al ₂ O ₃ , 1.1 MgO, 5.4 Fe ₂ O ₃ , 3.3 K ₂ O
Effective porosity (MIP)	29.4%
Permeability (mD)	94.32
Compressive strength (MPa)	48–52
Water absorption (%)	2.71

Table 1. Mineralogical, chemical and geo-mechanical characteristics of the reservoir rock.

showed a permeability increase in the reservoir formation from the dissolution of carbonate minerals; they report this increase as being due to enhanced pore space modification, associated with the dissolution of carbonate cement bonds. However, all these experiments were limited to short-term effects (2–4 weeks), revealing nothing about flow under long-term CO₂ exposure. This is a serious gap in our knowledge. In the long term, carbonic acid from CO₂ in brine reacts with many minerals in the formation, such as calcite, siderite, dolomite, quartz, barite, muscovite, feldspar, and clay minerals^{3,6–8,12–15}. These reactions dissolve rock cementation, weakening grain bonds and altering flow characteristics in ways that compromise the efficiency and safety of the whole sequestration exercise. In fact, any correct identification of alterations from injected CO₂ demands a rigorous and systematic comparison, with a bench study of inert gas injected into reservoir rock under the same conditions. That comparison would eliminate the effects on rock pore structure from gas injection generally, such as pore expansion and shrinkage. However, no such comparison has been undertaken in previous combined geochemical and permeability studies.

The present investigation is driven by that demand. It is a comprehensive, combined experimental study of chemical, mineralogical, and permeability alterations in saline aquifers from reactions in long-term CO₂ sequestration, over a realistic duration of 1.5 years. The study aims especially to provide the parameters needed for reservoir modelling of CO₂ sequestration. By allowing sufficient time for interactions to run their course, mineral reactions can emerge that are never seen in short-term saturation. The investigation will therefore be highly relevant to our understanding of actual flow properties in reservoir rock under sequestration conditions. The selected conditions for CO₂ reactions, i.e. a pressure of 10 MPa and a temperature of 40 °C, represent real field behaviour with CO₂ in its super-critical state. Permeability tests were included for a wide range of injection pressures (2–6 MPa) and confining pressures (10–30 MPa) to simulate field conditions accurately. This innovation enables the first-ever evaluation of the effective stress fields induced by rock mineral alterations. Care has been taken to isolate the pure CO₂ reaction effects on chemical, mineralogical, and flow behaviour in reservoir rock, by comparing them with alterations brought on by nitrogen (N₂), which is chemically inert for the present purposes.

Methods

Sample description. Brine-saturated Hawkesbury sandstone samples were used to represent the saline aquifer formation, and their possible geochemical and mineralogical alterations upon CO₂ injection were investigated. The sandstone samples were collected from the potential Gosford site for carbon capture and storage (CCS) in the Sydney basin, a formation belonging to the early Triassic period. Their composition is mainly quartz, calcite, and kaolinite, according to X-ray diffraction (XRD) analysis (by weight, around 60% quartz, 26% calcite, 6% kaolinite, 5% barite, 1% siderite, 1% muscovite, and 1% other clay minerals such as illite and smectite). It may be considered a carbonate-cemented sandstone formation, as it contains high percentages of calcite minerals in the pore structure.

Most current field-scale CO₂ sequestration projects have used saline aquifers with sandstone host rocks, because preferable saline aquifers for CO₂ sequestration require adequate permeability and porosity values for successful CO₂ injection and storage. Among the possible sandstone formations, carbonate-cemented sandstone formations with more than 20% carbonate minerals have more preferable characteristics for CO₂ sequestration, due to their potential to trap greater amounts of CO₂ through carbonate reactions⁷. This was the main reason for using Hawkesbury sandstone in this study, since Hawkesbury sandstone has a high percentage of calcite minerals (26%) and many favourable characteristics for CO₂ storage process in terms of its hydro-mechanical and mineralogical properties. A comprehensive description of the mineralogical, chemical and geo-mechanical information of Hawkesbury sandstone is given in Table 1.

The Hawkesbury formation consists of an un-layered, white-grey coloured, and medium-to fine-grained rock mass that exhibits a mostly inhomogeneous structure. Therefore, great care was taken to obtain homogeneous

samples from this formation, and only core specimens without visible discontinuities were selected for the experiment.

Sample preparation and reaction process. Hawkesbury sandstone blocks were collected and cored according to the ISRM standards in the Deep Earth Energy Laboratory (DEEL), at Monash University. The sample diameter was selected to be 38 mm and the cored samples were cut into 76 mm-long cylinders. The two ends of the samples were carefully ground to create smooth parallel faces, and the prepared specimens were oven-dried for 24 hours under 40 °C (a low temperature was selected to avoid possible thermal cracking) before beginning the reaction process.

Three different reaction conditions were selected: pure-brine-reacted (without any gas injection), brine+CO₂-reacted, and brine+N₂-reacted. Samples were first saturated with brine at a 20% NaCl concentration (% by weight) in desiccators under vacuum (0.2 MPa suction pressure). The samples were weighed at regular intervals during the saturation process, and when full saturation was reached, 15 samples were left inside the desiccator without applying vacuum for 1.5 years, to allow time for interaction. Later, this set was used as pure brine-reacted samples for both chemical and permeability measurements. The remaining 15 samples were removed from the desiccators and kept in reaction chambers to achieve CO₂- and N₂-reacted conditions. Before brine-reacted samples were placed in them the reaction chambers were filled with brine of the same concentration (20%), and samples were then inserted to facilitate the CO₂ and N₂ reactions. Two separate chambers were used for CO₂ and N₂ injection, and both gases were injected at 10 MPa pressure at 40 °C for 1.5 years to obtain CO₂+brine- and N₂+brine-reacted sandstone samples.

In the present study, a reaction period of 1.5 years was investigated, based on the time required to complete the reaction of existing major rock minerals (quartz, calcite and kaolinite) with CO₂ and brine to identify the ultimate alterations of these major rock minerals upon CO₂ interaction and the corresponding aquifer flow response. It is known that different rock minerals need different timescales and degrees of disequilibrium to complete their reaction with CO₂ and brine¹⁶. The time required to create the equilibrium of the resulting buffer solution (due to initial dissolution of CO₂ in brine) is within 1 to 2 years of interaction under reservoir conditions¹⁷. If the time required for mineral dissolution is considered, according to Knauss and Wolery¹⁸ and Davis *et al.*¹⁹, the initiation of the quartz reaction with CO₂ and brine requires a considerable geological time, which is certainly more than 1 year and kaolinite mineral also requires a considerable geological time-frame to initiate the early reaction. Therefore, conducting short-term experiments fails to identify such reaction-creating influence. As a result, considering the time-frame available for the study, 1.5 years was selected as being a reasonable time for the CO₂/brine/rock mineral interaction in this study. However, even using a 1.5-year time period, it is not possible to capture all the possible rock minerals alterations that occur with CO₂ and brine interaction (e.g. precipitation of feldspar and secondary precipitation of calcite and quartz). Therefore, only the dominant reactions, such as the initial dissolution of quartz, calcite, kaolinite, barite, and siderite and the salt drying-out effect were considered in this study. However, it should be noted that the reaction of some rock minerals with CO₂ and brine can occur within a very short time period. For example, carbonate mineral reactions, including calcite, magnesite and siderite, may occur within 2–4 weeks of interaction with CO₂ and brine^{6–8} and therefore can be captured in even short-term experiments.

Permeability tests. A series of high-pressure tri-axial permeability tests was conducted on the prepared variously- reacted sandstone samples (pure brine, brine+CO₂, brine+N₂), under undrained conditions. For the present study, three replicates were used in each test condition and permeability evaluation was performed taking its mean value (with standard deviation 1–3%). Details of the high-pressure tri-axial set-up and the sample assembly procedure can be found in Rathnaweera *et al.*²⁰. The permeability tests were performed by injecting CO₂ into the various prepared sandstone samples, and the corresponding downstream pressure developments were recorded to find the CO₂ permeability under each test condition using the pressure decay approach. Each sample was first kept inside the high-pressure cell; after assembly, the required confinement was applied under constant temperature and gas injection was initiated while recording the downstream pressure development. A high-precision syringe pump was used to inject CO₂ into the sample at constant injection pressure (2–6 MPa) under the required confinement (between 10 and 30 confining pressures were considered, to simulate the reservoir depth effect).

Just before the permeability tests, the reacted sample was removed from the reaction chamber and inserted into the tri-axial cell. The brine inside the samples was removed by injecting CO₂ at 1 MPa injection pressure under 10 MPa confining pressure, and the corresponding flush-out brine weight was measured over time using an accurate balance. This process was performed until brine removal ceased (at which time the measured weight value becomes constant). After confirming that there was no mobile brine inside the sample (there would be brine held in place by capillary forces), the normal permeability tests were initiated for single-phase CO₂ flow behaviour inside the sample. Here, the purpose of continuing the three kinds of reactions for 1.5 years was to provide sufficient time to initiate CO₂/brine/rock mineral interactions and for the sample pore structure to be changed accordingly. Permeability tests on these altered samples gave an opportunity to see how the sample flow characteristics had changed following these interactions.

Permeability tests were initiated using brine-reacted samples after removing their mobile brine. CO₂ was injected at 2 MPa injection pressure under 10 MPa confining pressure, and the downstream pressure development was recorded. Once it became constant, the developed pressure was released by opening the downstream valve at the extremely slow rate of 0.02 MPa/s to avoid any damage to the sample's pore structure. After this release, the downstream valve was closed and the experiment proceeded to the second stage of CO₂ injection (at 3 MPa) under the same confining pressure, and similar permeability tests were performed for a series of injection pressures (3, 4, 5, and 6 MPa). Once the permeability tests were completed with confining pressure set to

ICP-MS	
Plasma conditions	
Rf frequency	28 MHz
Rf power	1.5 kW
Gas flow rate	
Carrier gas	Ar 1.01 min ⁻¹
Auxiliary gas	Ar 1.01 min ⁻¹
Coolant gas	Ar 16.0 min ⁻¹
Sampling conditions	
Sampling depth	10 mm from work coil
Sampling cone	Copper, 1.0 mm orifice diameter
Skimmer cone	Copper, 0.35 mm orifice diameter
Nebulizer	Glass concentric type
Sample uptake rate	0.7 ml/min
ICP-AES	
Plasma conditions	
Rf frequency	27 MHz
Rf power	1.0 kW
Gas flow rate	
Carrier gas	Ar 0.5 min ⁻¹
Auxiliary gas	Ar 1.01 min ⁻¹
Coolant gas	Ar 20.0 min ⁻¹
Sampling condition	
Nebulizer	Cross-flow type
Sample uptake rate	1.2 ml/min
Spectrometer conditions	
Polychromator	Paschen-range mounting
Focal length	75 mm
Grating	2500 grooves mm ⁻¹
Entrance slit width	25 μm
Exit slit width	50 μm

Table 2. Operating conditions for ICP-MS and ICP-AES tests.

10 MPa, it was increased to the next level (first to 15 MPa confining pressure; then to 20, 25, and 30 MPa) and the permeability tests were conducted for the same injection pressures. All the brine-reacted, brine+CO₂- and brine+N₂-reacted samples were similarly tested, having first removed the mobile brine, for the same series of injection and confining pressure conditions.

Chemical and mineralogical analysis. *Inductively-coupled plasma mass spectroscopy (ICP-MS) and inductively-coupled plasma atomic emission spectroscopy (ICP-AES).* ICP-MS and ICP-AES, two advanced analytical techniques for elemental determinations, were used in this study to examine the trace and ultra-trace elements²¹ of the brine samples taken from the reaction chambers and desiccators after the 1.5-year reaction period. The main purpose of these chemical analyses was to identify changes in pore fluid properties due to CO₂/brine/rock mineral interactions. Table 2 shows the operating conditions for the ICP-MS and ICP-AES tests. A model SPQ 8000A instrument coupled with a quadrupole-type spectrometer was used for the ICP-MS tests, and a model plasma atom comp MK11 instrument was used for the ICP-AES tests.

Scanning electron microscopy (SEM) analysis. A detailed SEM analysis was also conducted to identify mineralogical changes in reservoir rock pore structures after three kinds of interaction. Samples reacted with brine+CO₂ and brine+N₂ were collected from the reaction chambers, and pure-brine-reacted samples were taken from the desiccator. SEM analysis was also performed on natural samples to identify the natural condition of the rock microstructure and compare it with the saturated samples' microstructures. A rock slice around 1 mm thick was prepared for each condition and a 3 μm titanium coating was applied before SEM testing, to avoid a charging effect during the image-scanning process. Tests were carried out under wet conditions for brine+CO₂-, brine+N₂-, and pure-brine-reacted samples, and dry conditions for natural samples. An FEI Nova Nano SEM machine coupled with two Bruker EDS and in-lens detectors was used in low-vacuum mode to capture changes in the sandstone microstructure. Furthermore, a spot size of 3.5 and a magnification of 10,000× were used to analyse the microstructure of the sandstone specimens under each reaction condition.

Results

Interacting brine, CO₂, and rock produced mineralogical and geochemical alterations. Three differently-reacted pore fluid conditions brine/rock (plain brine, without gas), brine/CO₂/rock, and brine/N₂/

Condition	pH	Na	K	Ca	Mg	Cl	Br	Si	Al	Fe	Mn	Ba
Initial brine	7.41	191433	2611	100.1	481	188311	1.43	0.11	—	—	—	1.11
Brine from desiccator after 1.5yrs	7.26	198304	3581	482.7	571	193110	1.50	874.11	—	—	—	13.26
Brine reacted with N ₂ after 1.5yrs	7.33	195917	3191	440.3	568	194215	1.42	815.31	—	—	—	12.21
Brine reacted with CO ₂ after 1.5yrs	4.81	277863	5868	3237	741	254782	1.63	4118	111	23.41	1.04	824.11

Table 3. Chemical analysis of pure brine and brine taken from the reaction chambers and desiccator (concentration in mg/l).

rock were analysed using ICP-MS, ICP-AES, and SEM techniques, and a plain unreacted brine sample was also tested as a control. The brine solution under each condition represented actual pore fluid in a saline aquifer. Dissolved Si^{4+} , Ca^{2+} , Mg^{2+} , Na^+ , K^+ , Br^- , Cl^- and Ba^{2+} were determined using the ICP-AES method, and Al^{3+} , Fe^{2+} , and Mn^{2+} using the ICP-MS method. Results of the desiccator and the chamber analyses are reported in Table 3. As the table shows, there is a significant pH drop in the brine+CO₂-reacted solution of around 49% (7.41 to 4.81) after long-term CO₂ injection, but no such drop in the brine+N₂-reacted solution. The observed pH reduction is therefore believed to be from the dissolution of injected scCO₂ in brine, resulting in the creation of an acidic medium: carbonic acid in the pore fluid, as shown in Eq. [1].



As expected, this pH reduction occurred only in the brine+CO₂-reacted solution, confirming the comparatively reactive nature of injected CO₂. Past studies have emphasized the relevance of this CO₂ dissolution in brine for the storage of injected CO₂ to solubility trapping in deep saline aquifers²². However, this dissolution process is not only important for solubility trapping; it also greatly affects the mineral-trapping process, because free H⁺ ions released into the pore fluid may react with minerals in the formation, dissolving them and eventually changing the composition and structure of the reservoir rock. Since such alterations mainly occur in silicate- and carbonate-cemented grain-to-grain contacts, they are more evident in formations where these minerals predominate. Studies have shown that carbonate-cemented sandstone in deep saline reservoirs yields the required geological conditions for CO₂ sequestration, and more than 60% of petroleum reservoirs are carbonate reservoirs²³.

ICP-AES and ICP-MS chemical analyses revealed the leachability of some minerals, when ions move from the sample into aquifer pore fluid as a result of these dissolution reactions. As mentioned previously, calcite dissolution is one of the most important dissolution reactions that occur during sequestration. Generally, the increment of Ca²⁺ ion concentration in the pore fluid (compared to its initial stage) provides basic identifying evidence for the calcite mineral dissolution process, which can be further investigated by microstructural analysis using SEM.

According to the ICP-AES analysis, significant quantities of Ca²⁺ ions leached into the pore fluid from the samples reacted with brine+CO₂, compared to either pure brine or brine+N₂. The initial concentration of Ca²⁺ ions in pure brine was 100.1 mg/l. This increased to around 482.7 mg/l after introducing the sandstone sample into the brine, up to around 440.3 mg/l after introducing N₂+sandstone, and up to around 3237 mg/l after introducing CO₂+sandstone. The presence of CO₂-releasing H⁺ clearly accelerates calcite dissolution. SEM analysis confirmed this much greater effect, showing a significant calcite dissolution texture in brine+CO₂-reacted samples compared to the other samples. Figure 1(a,b) show the mineral structure of a natural sample, and Fig. 1(g–j) show the mineral structure of brine+CO₂-reacted samples. The SEM image of a natural sample (Fig. 1(a,b)) shows the initial calcite mineral texture in the reservoir rock mass pore structure before significant changes caused by the CO₂ interaction (Fig. 1(g–j)). The SEM images of brine+CO₂-reacted samples (Fig. 1(g–j)) exhibit the dissolution textures of calcite minerals, with a relatively rough surface after CO₂-brine-rock interaction compared to a smooth surface in the natural sample. According to Marbler *et al.*⁷ and Gledhill and Morse²³, the dissolution of calcite in carbonate-cemented reservoir rocks significantly alters the arrangement of pores. It also helps create secondary pores by changing the effective stress and flow characteristics of the formation, and the combined effect is permeability enhancement in the reservoir and caprock. Although this heightened permeability increases CO₂ injectability into the reservoir and improves the aquifer's storage capacity, the increase in reservoir permeability brings a greater risk of CO₂ back-migration into the atmosphere.

Moreover, the ICP-MS results for brine+CO₂-saturated samples also showed some enrichment patterns in Al³⁺, Fe²⁺, and Mn²⁺ ions (see Table 3) compared to those in pure brine; and these patterns were not observed in samples reacted with pure brine or brine+N₂. The accumulated ions in brine+CO₂-reacted pore fluids are due solely to CO₂. The increased Fe²⁺ concentration is believed to be related to the dissolution of siderite minerals from the rock mass, and the increase in Al³⁺ and Mn²⁺ ions is probably from dissolution of clay minerals such as smectite, illite, kaolinite, and muscovite.

Apart from these mineral dissolutions, topographic SEM images of brine+CO₂-reacted samples (Fig. 1(h)) display tiny rectangular etching caverns and pits inside the pore structure, which do not appear in the other samples. These are thought to come from barite minerals dissolved from the rock mass due to CO₂ exposure, again confirming the effect of long-term injection of CO₂ on reservoir mineral structure.

Significant quartz mineral corrosion was also found, in the chemical analyses. Si⁴⁺ concentration in the pore fluid was considerably increased after the introduction of CO₂, most likely from dissolution of quartz in the rock

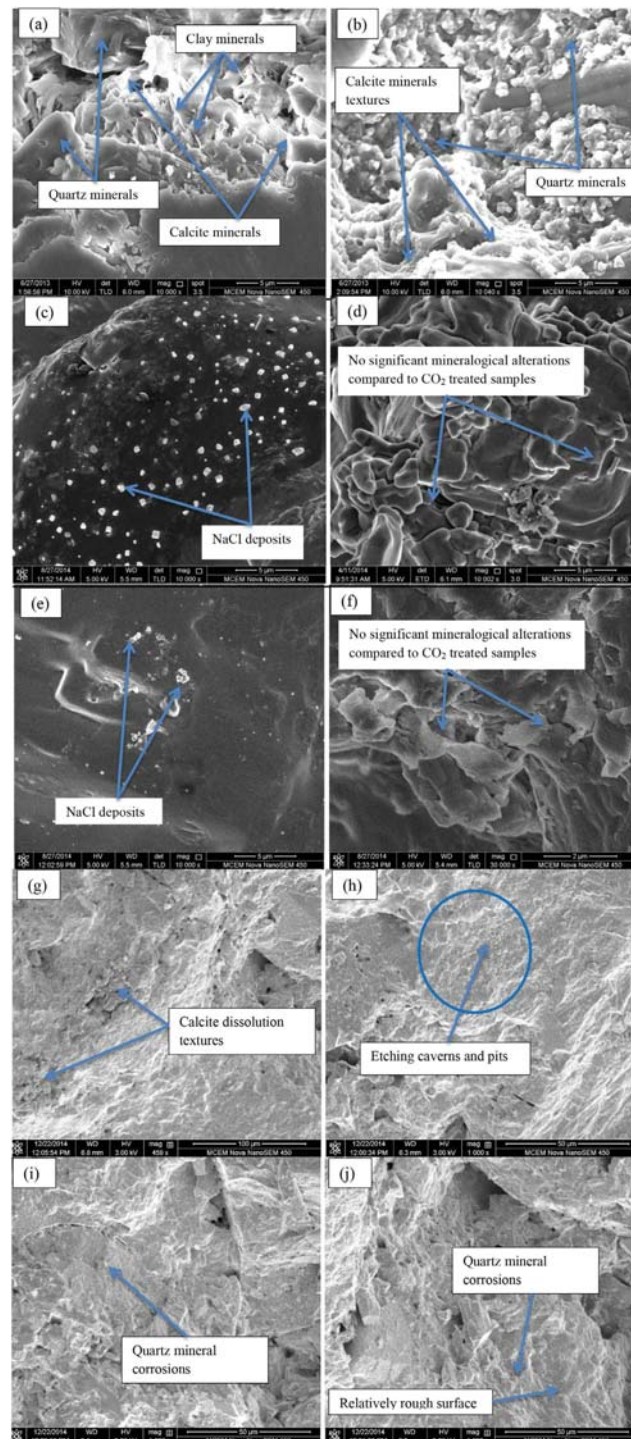


Figure 1. Results of SEM analysis (a,b) natural sample (c,d) brine (without gas reaction) (e,f) brine+N₂-reacted samples and (g–j) brine+CO₂-reacted sample.

mass. According to the ICP-AES analysis, the Si^{4+} ion concentration increased from 0.11 to 4118 mg/l with CO₂ reaction and to 815.31 mg/l with N₂ reaction. This quartz corrosion in the vicinity of CO₂ is also confirmed by the



Calcite mineral dissolution at surface

Figure 2. Results of visual inspection of the brine+CO₂-reacted sample; deposits of NaCl crystals (salt precipitation) and calcite dissolution textures at the outer surface of the sample.

SEM images of the brine+CO₂-reacted samples (see Fig. 1(i,j)), consistent with the findings of Kaszuba *et al.*²², who found similar patterns in quartz minerals with CO₂ introduced into brine-saturated sandstone. Marbler *et al.*⁷ provide valuable explanations of how quartz corrosion affects the structure of rock pores: the dissolution of primary and secondary silicate mineral rims around the quartz-cemented grains reduces the strength of quartz grain-grain contacts, significantly changing the rock mass pore structure. The small quartz mineral dissolution observed in brine+N₂- and pure-brine-reacted samples (both negligible compared to the brine+CO₂-reacted sample) is attributed to a slight corrosive effect of brine solution itself.

Apart from mineral dissolution, chemical analyses uncovered a significant CO₂ dry-out effect and NaCl crystal precipitation in the rock mass pore system in brine+CO₂-reacted samples. This is consistent with the findings of Pruess and Muller²⁴, who explained that the injection of CO₂ into saline aquifers causes formation dry-out and salt precipitation near the injection well, reducing porosity, permeability, and injectivity in the formation. When scCO₂ is injected into a saline aquifer, water evaporates into the scCO₂-phase, leaving the remaining brine with a higher salt concentration. If this concentration is greater than the solubility of salt under the prevailing pressure and temperature conditions, salt will precipitate; so salt precipitation is clearly associated an increase in salinity (Na⁺ concentration). According to the ICP-AES results, Na⁺ in the initial brine sample increases from 191,433 to 277,863 mg/l with CO₂ injection, thought to be related to salt precipitation. This was confirmed by SEM analysis, according to which the brine+CO₂-reacted samples display some NaCl crystal depositions inside the rock pore structure. Visual inspection of the brine+CO₂-reacted samples confirmed displacement of brine from the sample by injected CO₂ and there were consequent deposits of NaCl crystals at the outer surface of the samples (see Fig. 2). Interestingly, the SEM results for samples reacted with either plain brine or brine+N₂ also showed a small amount of NaCl deposition inside the pore structure (see Fig. 1(e)). According to the ICP-AES analysis, Na⁺ concentration from 191,433 to 198,304 mg/l for plain brine samples and from 191,433 to 195,917 mg/l for brine+N₂ reacted samples. The Na⁺ concentration increase in plain-brine-reacted samples is therefore greater than in brine+N₂-reacted samples, and considerably less than in brine+CO₂-reacted samples. In addition to Na⁺, slight increments in K⁺ and Mg²⁺ content (compared to the initial brine solution) were observed in all the reaction conditions, presumably related to salt precipitation from the pore fluid. The K⁺ and Mg²⁺ content increments are more significant in brine+CO₂-reacted samples than in all other samples (Table 3), probably due to the greater salt precipitation from the CO₂ dry-out effect.

According to Table 3, it is clear that significant rock mineral alterations are caused by CO₂ injection, leading to changes in the chemical and mineral structure of the rock mass. To facilitate further understanding of this CO₂-related dissolution process, the amounts of dissolved rock minerals were calculated as percentages of the initial compositions of each rock mineral in natural samples. Table 4 displays the calculated percentage values of each dissolved rock compound. According to Table 4, 8.15%, 1.11%, and 1.21% of calcite was dissolved in brine+CO₂, brine+N₂, and plain-brine-reacted samples respectively, compared to an initial measure of 39.73 g (26% of total rock mass). Moreover, 4.49%, 0.88%, and 0.95% of quartz was dissolved in brine+CO₂, brine+N₂ and brine-reacted samples respectively, compared to an initial measure of 91.68 g (60% of total rock mass). As Table 4 shows, significant dissolution of barite mineral occurred in brine+CO₂-reacted samples (10.79%) compared to the other two saturation conditions, with 0.16% and 0.17% of its initial barite mineral composition

Rock mineral	Dissolved % with respect to initial composition		
	Pure brine (without gas)	Brine+N ₂	Brine+CO ₂
Quartz	0.95	0.88	4.49
Calcite	1.21	1.11	8.15
Barite	0.17	0.16	10.79
Siderite	—	—	1.53

Table 4. Percentage of dissolved rock minerals in the three conditions with respect to natural mineral composition.

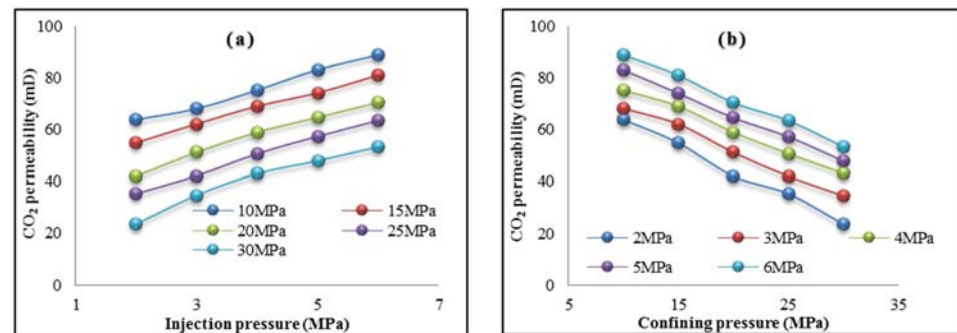


Figure 3. CO₂ permeability variation in brine+CO₂-reacted sample (a) with injection pressures and (b) with confining pressures.

being dissolved in brine+N₂ and brine-reacted samples respectively. The calculated dissolved mineral percentage values based on the initial composition indicate significant effects of CO₂ saturation on the structure of reservoir rock minerals compared to the other two tested conditions. Table 4 also reveals that this CO₂ injection-induced mineral alteration process (mineral trapping) is truly a long-term phenomenon; it dissolved only between 4% and 10% of the total mineral composition over 1.5 years of reaction in the present study. Significantly more dissolution can be expected over the large time-scales (more than 100 years) that are relevant in practice. This argument is consistent with previous research by Ranganathan *et al.*²⁵.

Flow characteristics affected by rock alteration in reservoir formations. Variation of flow characteristics in reservoir formations during and after CO₂ injection is one of the critical challenges for CO₂ sequestration in saline aquifers. Alterations in the permeability and porosity of formations during long-term injection consequent upon interactions of minerals, brine, and CO₂ have been widely reported in field-scale studies^{13,14}. The corresponding permeability of the sample under each injection condition was determined using the pressure decay approach^{26,27}. According to Pan *et al.*²⁷, pressure decay curves can be modelled as Eq. [2]:

$$\frac{(P_{in} - P_{out})}{(P_{in,0} - P_{out,0})} = e^{-\alpha t}, \quad (2)$$

where $P_{in} - P_{out}$ is the pressure difference between the gas inlet and outlet measured by a differential pressure transducer, $P_{in,0} - P_{out,0}$ is the initial pressure difference between gas inlet and outlet, t is the time and α is as given in Eq. [3]:

$$\alpha = \frac{k}{\mu\beta L^2} V_s \left(\frac{1}{V_{in}} + \frac{1}{V_{out}} \right), \quad (3)$$

where k is the permeability, μ is the flowing gas viscosity, β is the gas compressibility, L is the sample length, V_s is the sample volume, and V_{in} and V_{out} are the volume of the gas inlet and outlet plumbing systems. The effect on CO₂ permeability of pore structure modifications created by brine-CO₂ interactions in the tested sandstone was investigated for five injection pressures (from 2 to 6 MPa) under five confining pressures (from 10 to 30 MPa), at 40 °C. Figure 3 shows the calculated CO₂ permeability values; the CO₂ injection pressure's influence on permeability is shown in Fig. 3(a), and the confining pressure's influence on permeability is shown in Fig. 3(b).

As expected, sample permeability increases with increased injection pressure and reduced confining pressure, both of which are mainly related to the effective stress, which is lowered by increasing the injection pressure or by reducing the confining pressure applied to the sample^{2,20}. For instance, increasing injection pressure from 2 to 6 MPa under 20 MPa confining pressure raises the sample permeability by around 67%, and increasing the confining pressure from 10 to 30 MPa lowers it by around 43%.

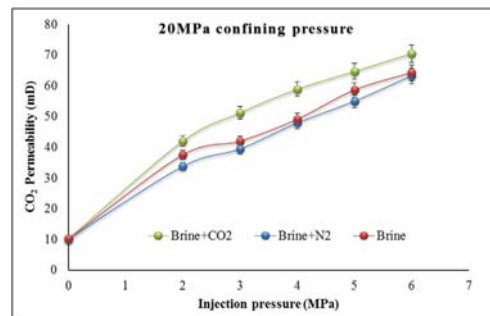


Figure 4. Permeability variations for each reacted condition under 20MPa confining pressure.

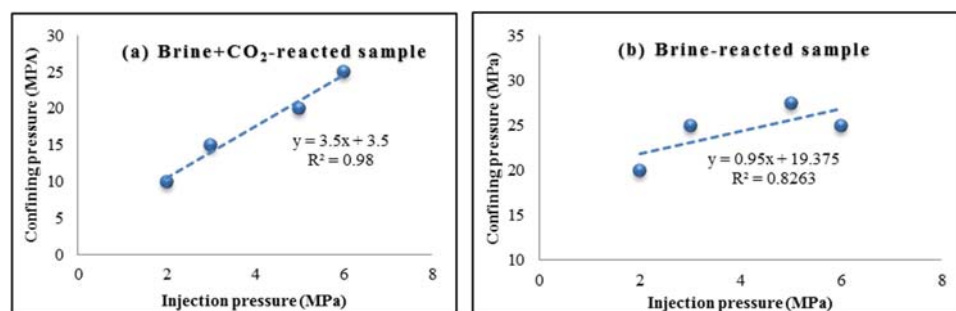


Figure 5. Variation in effective stress coefficient for samples: (a) brine+CO₂-reacted; and (b) pure brine-reacted.

The main purpose of this study, however, was to identify the effect on sample permeability of interactions between minerals, brine, and CO₂ in rock. Therefore, CO₂ permeability values for brine+CO₂-reacted samples were compared with CO₂ permeability through brine+N₂ and brine-only samples. Figure 4 shows the calculated CO₂ permeability values under 20 MPa confining pressure for each saturation condition. According to the figure, rock minerals-brine-CO₂ interaction has a significant effect on CO₂ permeability in the reservoir rock samples, and CO₂ permeability through brine+CO₂-reacted samples is clearly higher than through brine+N₂ and brine-only samples. For example, at 4 MPa injection pressure and 20 MPa confining pressure, CO₂ permeability through brine+CO₂-reacted samples is around 17% and 19% higher than through brine-only and brine+N₂ samples, respectively. The permeability enhancement in the brine+CO₂ samples clearly reveals the effect of injected CO₂/brine/rock interactions on the flow characteristics of deep saline aquifers and its influence on rock mineralogical alterations.

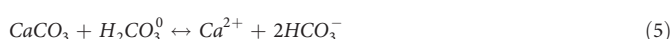
Permeability was found to be essentially the same through the brine+N₂-reacted samples and the plain-brine-reacted samples, confirming the negligible influence of N₂ saturation on sample flow characteristics. This is because, since non-reactive N₂ causes no mineralogical or chemical reaction in the sample during saturation, its pore structure is not noticeably altered, even over 1.5 years. This is further confirmed by the results of the SEM and ICP analyses. Sandstone permeability enhancement with CO₂ injection must therefore be seen as related to the reactions between rock minerals and carbonic acid produced by the interaction of CO₂ and brine. This conclusion is reinforced by the results of ICP-AES analysis, where the collected chamber pore fluid showed significant silicate and calcite mineral dissolution from the sandstone sample, and also by the SEM images, which clearly exhibit alterations in rock cement from CO₂ reactions. The dissolution of pore-filling calcite and calcite coatings of detrital minerals changes the pore structure and consequently the porosity of the reservoir rock, eventually creating new pathways for CO₂ migration and enhancing the permeability characteristics of the reservoir formation.

Weakening of the rock mass mineral grains with CO₂ injection-induced chemical and mineralogical changes also affects the effective stress patterns acting on the pore space system. It was therefore important to assess the impact of the effective stress field on permeability during brine/rock/CO₂ interaction and the variation of the effective stress coefficient for permeability under various conditions. The effective stress coefficient for the variation of permeability can be obtained from iso-permeability lines drawn as a function of pore pressure and confining pressure, and the slope of each curve gives the effective stress coefficient²⁸. Figure 5 shows the iso-permeability lines for the brine+CO₂ and brine-only samples, which give respectively 3.5 and 0.95 effective stress coefficients. The introduction of CO₂ into brine-saturated rock samples has therefore significantly raised the effective stress coefficient. Such observations indicate the importance of precisely understanding the possible consequences of rock hydro-mechanical changes as a result of mineralogical changes during the CO₂ injection process for any CO₂ sequestration field project.

Discussion

Although the laboratory experimental results provide crucial evidence related to mineralogical rock alterations in deep saline aquifers, modelling of reservoir simulations, coupled with both geochemical and geophysical behaviours, are also important to understand the reaction mechanisms of rock minerals upon exposure to CO₂/brine during real field time-frames due to the practical difficulties of laboratory conditions, particularly time limitations. However, the precise simulation of such mechanisms requires correct identification of potential reaction mechanisms and their behaviour over the time of CO₂/brine interaction and their variation with surrounding factors (CO₂ partial pressure, reservoir temperature and pH). To date, most related laboratory experiments have been conducted over short-term time durations, and they have therefore failed to capture long-term reaction mechanisms.

Among the various possible reaction mechanisms, if the possible short-term mechanisms are first considered, calcite dissolution is predominant. According to the existing findings, the calcite dissolution process mainly involves three simultaneous reaction mechanisms, as given below²⁹;



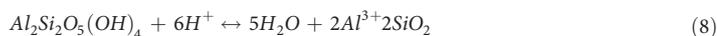
These reactions are dependent on the CO₂ partial pressure, reservoir temperature and pH, and the calcite dissolution rate increases with increasing CO₂ partial pressure and decreasing pore fluid pH²⁹, and varies with reservoir temperature³⁰ and foreign ions (e.g. orthophosphate)³¹. The short-term experimental study conducted by Wigand *et al.*¹⁷ found an enhancement of calcite dissolution over time (after five days of CO₂ interaction) with associated reduction of pH and the reduction of the calcite reaction rate after a certain time (two months) with the initiated pH increment. In this present study it was not possible to calculate the calcite dissolution rate over time. However, the long-term interaction of CO₂/brine/rock caused a significant calcite dissolution, as evidenced by the observed 100.1 mg/l to 3237 mg/l Ca²⁺ concentration increment in the pore fluid. Since CO₂ geological sequestration is conducted over long time-scales in the field, according to this study, there is a greater possibility of enhancing the calcite dissolution rate with the CO₂/brine interaction.

In relation to possible long-term reactions, the quartz mineral reaction dominates the mineral trapping process of CO₂ in deep saline aquifers, as the reservoir rocks are generally abundant in quartz minerals. The general reaction mechanism of quartz is given below:



According to existing studies, the quartz dissolution rate reduces with increasing pore fluid pH and increases with the presence of cations in the pore fluid (e.g. sodium, calcium and magnesium)^{18,32,33}. However, since this quartz dissolution process takes extensive time to initiate, this cannot be identified in short-term laboratory experiments. For example, the short-term experimental work conducted by Wigand *et al.*¹⁷ did not find any quartz dissolution in their experiments. However, the long-term experiments conducted in the present study revealed that the interaction of quartz with CO₂ and brine causes significant quartz dissolution, as evidenced by the observed 0.11 to 4118 mg/l Si⁴⁺ ion concentration in the pore fluid after 1.5 years of interaction.

Apart from the quartz dissolution, kaolinite dissolution is also a dominant long-term reaction mechanism that occur during CO₂ sequestration in saline aquifers, which mainly affects the reservoir rock mass pore structure by altering grain-to-grain contacts. The basic kaolinite dissolution reaction mechanism in acidic systems is given below:



According to the research, the rate of kaolinite dissolution increases with increasing reservoir temperature and pH of the aquifer pore fluid³⁴ and varies with the available Al³⁺ and SiO⁻ complexes³⁴. According to the study conducted by Gunter *et al.*³⁵, the final influence of CO₂/brine interaction on this kaolinite reaction is hard to determine, as the dissolution of Ca⁻ feldspar can re-precipitate kaolinite minerals during the sequestration process. However, 1.5 years of long-term interaction of kaolinite/brine/CO₂ in this study clearly caused a significant dissolution of kaolinite mineral, as evidenced by the observed increase of Al³⁺ ion concentration in the pore fluid after 1.5 years of interaction. This may have been influenced by the fact that the sandstone samples in this study do not contain feldspar minerals.

In general, the incorporation of laboratory data with field simulations has become one of the major challenges in predicting the long-term fate of mineral reactivity in reservoirs. This is because, reservoir rock mineral dissolution and precipitation may alter the reaction mechanisms over time, which progressively modifies the existing flow pathways for CO₂ movement. Therefore, it is important to consider these processes, including the coupling between reaction kinetics and mass transport processes when modelling reservoir-scale simulations. Long-term laboratory experiments therefore offer more promising data for the numerical simulation of CO₂ sequestration.

The effective implementation of CO₂ sequestration in deep saline aquifers requires significant development in the scientific understanding of mineral reaction-induced reservoir flow property alterations and the corresponding influence on the safety of the process in terms of the effect on caprock integrity and the corresponding possibility of CO₂ leakage. According to the findings of this study, the significant rock mass mineralogical and pore

structures alterations caused by around 1.5 years of long-term CO₂ interaction with the reservoir may cause its permeability to be enhanced by around 10%. According to Rochelle *et al.*³⁶, even such a small alteration in reservoir rock permeability may have a significant effect on the effectiveness of the sequestration process. According to the field-scale observations of Arsyad *et al.*³⁷, CO₂ sequestration created permeability enhancements in Ainoura and Berea sandstone formations, leading to easy movement for CO₂ plumes to migrate into upper cap rock layers, generating high risk of CO₂ leakage from the aquifer to surrounding groundwater zones. According to these researchers, enhanced reservoir permeability during the CO₂ sequestration process in saline aquifers may cause pore pressure enhancement in the aquifer and consequently affect the caprock, creating a negative impact on caprock stability. This is because, if pressure reaches the overburden pressure of the caprock, it may fail, creating hydraulic fractures that will cause CO₂ leakage into the surrounding aquifers and the atmosphere.

Apart from this, the moving CO₂ from the aquifer to caprock start to dissolve rock minerals in the caprock¹⁷. Generally, in deep saline sequestration, mudstone is widely found as a caprock sealing³⁸, and contains considerable amounts of clay minerals, quartz and feldspar³⁹. Therefore, the presence of these rock minerals has the potential to cause reactions with the dissolved CO₂ in brine, creating major changes in the caprock structure. Rutqvist and Tasang³⁹ confirmed the possibility of reacting these caprock minerals with dissolved CO₂ in brine and showed that supercritical CO₂ can react with the organic contents of the caprock including clay minerals and cause considerable changes in the permeability and porosity of the caprock. Moreover, Rochelle *et al.*⁴⁰ also stated that dissolved CO₂ in brine can react with the overlying caprock, thus reducing the caprock's sealing properties. Such caprock mineral alterations lead to the formation of new flow pathways along the caprock, creating a leakage risk from the aquifer to surrounding fresh water aquifers and ultimately back-migration into the atmosphere. This is a serious issue and negatively affects the potential implementation of CO₂ sequestration in deep saline aquifers.

Conclusions

CO₂ injection into a deep saline aquifer during the sequestration process causes its hydro-mechanical properties to be significantly altered, and the purpose of this study is to identify how CO₂ sequestration affects the mineralogical structure and alters the aquifer's flow response. According to the results of permeability tests on brine-saturated sandstone samples obtained from the Sydney basin, the following conclusions can be drawn:

- Long-term CO₂ reaction causes a carbonic acid to form in the aquifer, which causes a significant pH drop in the pore fluid, the observed drop in this study being around 49% after a 1.5 years.
- Importantly, a huge free H⁺ ions release occurs during this acid formation process, which has a significant influence on the aquifer's mineralogical structure. The 1.5 years of CO₂ + brine reaction in this study caused a significant dissolution of some rock minerals, including Ca²⁺, Al³⁺, Fe²⁺, quartz and barite minerals. Of the, Ca²⁺ and quartz dissolutions were prominent, and caused the pore fluid Ca²⁺ concentration to increase from 100.1 mg/l to 3237 mg/l and the pore fluid Si⁴⁺ ion concentration to increase from 0.11 to 4118 mg/l.
- Long-term CO₂ reaction also creates a significant CO₂ drying-out effect and NaCl crystallization (salt) in the aquifer's rock pore space by altering the pore structure. The tests showed a 191,433 to 277,863 mg/l increment in Na⁺ concentration and also considerable enhancements of K⁺ and Mg²⁺ in the pore fluid after the CO₂ reaction.
- Such significant rock mass mineralogical structure alterations certainly affect the aquifer's flow characteristics, and aquifer permeability is enhanced by the long-term CO₂ reaction in this study. For example, CO₂ permeability at 4 MPa injection pressure and 20 MPa confining pressure increased by around 17% with CO₂ saturation.
- The pore structure changes caused by the CO₂ reaction also affect the effective stress response of the aquifer rock mass, and a significant rise in effective stress coefficient from around 0.95 to 3.5 was observed in this study.

References

1. Holloway, S., Rochelle, C. A. & Pearce, J. M. Geological sequestration of carbon dioxide: implications for the coal industry. *T. I. Min. Metall.* **108**, 19–28 (1999).
2. Bachu, S. Sequestration of CO₂ in geological media: criteria and approach for site selection in response to climate change. *Energy Convers. Manage.* **41**, 953–970 (2000).
3. Moore, J., Adams, M., Allis, R., Lutz, S. & Rauzi, S. Mineralogical and geochemical consequences of the long-term presence of CO₂ in natural reservoirs: an example from the Springerville-St. Johns field, Arizona and New Mexico, USA. *Chem. Geol.* **217**, 183–186 (2005).
4. White, S. P. *et al.* Simulation of reactive transport of injected CO₂ on the Colorado Plateau, Utah, USA. *Chem. Geol.* **217**, 387–405 (2005).
5. Xu, T., Apps, J. & Pruess, K. Mineral sequestration of a sandstone-shale system. *Chem. Geol.* **217**, 295–318 (2005).
6. Muller, N., Qi, R., Mackie, E., Pruess, K. & Blunt, M. CO₂ injection impairment due to halite precipitation. *Energy* **112**, 3507–3514 (2009).
7. Marbler, H., Erickson, K. P., Schmidt, M., Lempp, C. & Pollmann, H. Geomechanical and geochemical effects on sandstones caused by the reaction with supercritical CO₂: an experimental approach to *in situ* conditions in deep geological reservoirs. *Environ. Earth Sci.* **69**, 1981–1998 (2013).
8. Chou, L., Garrels, R. M. & Wollast, R. Comparative study of the kinetics and mechanisms of dissolution of carbonate minerals. *Chem. Geol.* **78**, 269–282 (1989).
9. Palandri, J. L. & Kharaka, Y. K. Ferric iron-bearing sediments as a mineral trap for CO₂ sequestration: iron reduction using sulfur-bearing waste gas. *Chem. Geol.* **217**, 351–364 (2005).
10. Pokrovsky, O. S., Golubev, S. V. & Schott, J. Dissolution kinetics of calcite, dolomite and magnesite at 25 °C and 0 to 50 atm pCO₂. *Chem. Geol.* **217**, 239–255 (2005).
11. Shiraki, R. & Dunn, T. L. Experimental study on water-rock interactions during CO₂ flooding in the Tensleep Formation, Wyoming, USA. *Appl. Geochem.* **15**, 265–279 (2000).

12. Ross, G. D., Todd, A. C. & Tweedie, J. A. The effect of CO₂ flooding on the permeability of reservoir rocks. *Dev. Petrol. Sci.* **13**, 351–366 (1981).
13. Gaus, I. *et al.* Geochemical modelling and solute transport modelling for CO₂ storage, what to expect from it? *Int. J. Greenhouse Gas Cont.* **2**, 605–625 (2008).
14. Gilfillan, S. M. V. *et al.* Solubility trapping in formation water as dominant CO₂ sink in natural gas fields. *Nature* **458**, 614–618 (2009).
15. Gautelier, M., Oelkers, E. H. & Schott, J. An experimental study of dolomite dissolution rates as a function of pH from –0.5 to 5 and temperatures from 25 to 80 °C. *Chem. Geol.* **157**, 13–26 (1999).
16. Riaz, A., Hesse, M., Tchelepi, H. A. & Orr, F. M. Onset of convection in a gravitationally unstable diffusive boundary layer in porous media. *J. Fluid Mech.* **111**, 548–587 (2006).
17. Wigand, M., Carey, J. W., Schütt, H., Spangenberg, E. & Erzinger, J. Geochemical effects of CO₂ sequestration in sandstones under simulated *in situ* conditions of deep saline aquifers. *Appl. Geochem.* **23**(9), 2735–2745 (2008).
18. Knauss, K. G. & Wolery, T. J. The dissolution kinetics of quartz as a function of pH and time at 70 °C. *Geochim. Cosmochim. Ac.* **52**(1), 43–53 (1988).
19. Davis, M. C., Wesolowski, D. J., Rosenqvist, J., Brantley, S. L. & Mueller, K. T. Solubility and near-equilibrium dissolution rates of quartz in dilute NaCl solutions at 398–473 K under alkaline conditions. *Geochim. Cosmochim. Ac.* **75**(2), 401–415 (2011).
20. Rathnaweera, T. D., Ranjith, P. G. & Perera, M. S. A. Effect of salinity on effective CO₂ permeability in reservoir rock determined by pressure transient methods: An experimental study on Hawkesbury sandstone. *Rock Mech. Rock Eng.* **48**, 2093–2110 (2015).
21. Seyfried, W. E., Janecky, D. R. & Berndt, M. E. Rocking Autoclaves For Hydrothermal Experiments, II. *The Flexible Reaction-Cell System*. (eds. Ulmer, G. C. & Barnes, H. L.), 216–239 (John Wiley & Sons, 1987).
22. Kaszuba, J. P., Janecky, D. R. & Snow, M. G. Carbon dioxide reaction processes in a model brine aquifer at 200 °C and 200 bars: implications for geologic sequestration of carbon. *Appl. Geochem.* **18**(7), 1065–1080 (2003).
23. Gledhill, D. K. & Morse, J. W. Calcite dissolution kinetics in Na-Ca-Mg-Cl brines. *Geochim. Cosmochim. Ac.* **70**, 5802–5813 (2006).
24. Pruess, K. & Muller, N. Formation dry-out from CO₂ injection into saline aquifers: Effects of solids precipitation and their mitigation. *Water Resour. Res.* **45**, 3402–3412 (2009).
25. Ranganathan, P., Van, H. P., Rudolph, E., Susanne, J. & Zitha, P. Z. J. Numerical modeling of CO₂ mineralisation during storage in deep saline aquifers. *Energy* **4**, 4538–4545 (2011).
26. Brace, W. F., Walsh, J. B. & Frangos, W. T. Permeability of granite under high pressure. *J. Geophys. Res.* **73**(6), 2225–2236 (1968).
27. Pan, Z., Connell, L. D. & Camilleri, M. Laboratory characterisation of coal reservoir permeability for primary and enhanced coalbed methane recovery. *Int. J. Coal Geol.* **82**, 252–261 (2010).
28. Rathnaweera, T. D., Ranjith, P. G., Perera, M. S. A. & Yang, S. Q. Determination of effective stress parameters for effective CO₂ permeability in deep saline aquifers: An experimental study. *J. Natural Gas Sci. Eng.* **24**, 64–79 (2015).
29. Plummer, L. N., Wigley, T. M. L. & Parkhurst, D. L. The kinetics of calcite dissolution in CO₂-water systems at 5 degrees to 60 degrees C and 0.0 to 1.0 atm CO₂. *American J. Sci.* **278**(2), 179–216 (1978).
30. Pokrovsky, O. S., Golubev, S. V. & Jordan, G. Effect of organic and inorganic ligands on calcite and magnesite dissolution rates at 60 C and 30 atm pCO₂. *Chem. Geol.* **265**(1), 33–43 (2008).
31. Berner, R. A. & Morse, J. W. Dissolution kinetics of calcium carbonate in sea water; IV, Theory of calcite dissolution. *American J. Sci.* **274**(2), 108–134 (1974).
32. Sardini, P., Ledesert, B. & Touchard, G. Quantification of microscopic porous networks by image analysis and measurements of permeability in the Soultz-sous-Forêts granite (Alsace, France). *Fluid Flow Transport Rocks*, **24**, 171–189 (1995).
33. Dove, P. M. & Crerar, D. A. Kinetics of quartz dissolution in electrolyte solutions using a hydrothermal mixed flow reactor. *Geochim. Cosmochim. Ac.* **54**(4), 955–969 (1990).
34. Huertas, F. J., Chou, L. & Wollast, R. Mechanism of kaolinite dissolution at room temperature and pressure Part II: Kinetic study. *Geochim. Cosmochim. Ac.* **63**(19), 3261–3275 (1999).
35. Gunter, W. D., Perkins, E. H. & McCann, T. J. Aquifer disposal of CO₂-rich gases: reaction design for added capacity. *Energy Convers. Mgmt.* **34**(9), 941–948 (1993).
36. Rochelle, C. A., Czernichowski-Lauriol, I. & Milodowski, A. E. The impact of chemical reactions on CO₂ storage in geological formations: a brief review. *Geological Society, London, Special Publications*. **233**(1), 87–106 (2004).
37. Arsyad, A., Mitani, Y. & Babadagli, T. Comparative assessment of potential ground uplift induced by injection of CO₂ into Ainoura, and Berea sandstone formations. *Earth Planet. Sci.* **6**, 278–286 (2013).
38. Kharaka, Y. K. *et al.* Potential environmental issues of CO₂ storage in deep saline aquifers: geochemical results from the Frio-I Brine Pilot test, Texas, USA. *Appl. Geochem.* **24**(6), 1106–1112 (2009).
39. Rutqvist, J. & Tsang, C. F. A. study of caprock hydromechanical changes associated with CO₂-injection into a brine formation. *Enviro. Geol.* **42**, 296–305 (2002).
40. Rochelle, C., Pearce, J. & Holloway, S. The under-ground sequestration of carbon dioxide: containment by chemical reactions in the deep geosphere. In: Metcalfe, R., Rochelle, C. (Eds.), *Chemical Containment of Waste in the Geosphere, special publication, The Geological Society of London*. **157**, 117–129 (1999).

Acknowledgements

This research was supported under Australian Research Council's Discovery Projects funding scheme (project number DP120103003). The authors extend their appreciation to the Deanship of Scientific Research at King Saud University, Saudi Arabia, for funding the work through the international research group project IRG14-36.

Author Contributions

The studies were designed and analysed by all authors. R.P.G. planned the experiments and wrote the introduction section. T.D.R. carried out the chemical and microstructural analyses and wrote the chemical and microstructural part of the paper. M.S.A.P. provided permeability measurements and wrote the flow behaviour section.

Additional Information

Competing financial interests: The authors declare no competing financial interests.

How to cite this article: Rathnaweera, T. D. *et al.* Experimental investigation of geochemical and mineralogical effects of CO₂ sequestration on flow characteristics of reservoir rock in deep saline aquifers. *Sci. Rep.* **6**, 19362; doi: 10.1038/srep19362 (2016).



This work is licensed under a Creative Commons Attribution 4.0 International License. The images or other third party material in this article are included in the article's Creative Commons license, unless indicated otherwise in the credit line; if the material is not included under the Creative Commons license, users will need to obtain permission from the license holder to reproduce the material. To view a copy of this license, visit <http://creativecommons.org/licenses/by/4.0/>

4.5 Summary of Chapter 4

The main objective of this chapter was to experimentally investigate the effect of CO₂ sequestration on the flow characteristics of reservoir rock in deep saline aquifers. The results of permeability, microstructural, chemical and mineralogical tests have therefore been presented.

According to the results of the permeability tests, the effective CO₂ permeability of reservoir rock is highly dependent on aquifer salinity, CO₂ injection pressure, confining pressure and effective pressure. Effective CO₂ permeability decreases with increasing salinity in the aquifer, and therefore, needs to be carefully considered when selecting a suitable aquifer for sequestration. For example, at sub-critical CO₂ injection pressures (2-6MPa), effective CO₂ permeability reductions of 13, 27 and 50% were observed in 10, 20, and 30% brine-saturated specimens compared to water-saturated specimens. At super-critical CO₂ injection pressures (10-12MPa), 5, 14, and 23% effective permeability reductions were observed in 10, 20, and 30% brine-saturated specimens compared to water-saturated specimens. According to SEM analysis, when the aquifer has a high salinity condition, there are considerable numbers of NaCl crystals in the rock pore space and these crystals block the free flow pathways for CO₂ movement, causing reduced permeability. The other important factor when considering flow behaviour is the effective stress. According to Section 4.2, it is clear that the effective CO₂ permeability of the reservoir rock decreases with the increase of effective stress. This reduction is mainly due to the closure of the effective pore area for fluid movement under enhanced effective stress conditions.

According to the results of the combined geochemical, mineralogical and permeability tests, interaction between injected CO₂, brine and rock causes significant alterations in the chemical and mineral structures of the aquifer due to dissolution and precipitation of some rock minerals. SEM, ICP-AES and ICP-MS analyses confirm the considerable dissolution of calcite, quartz, siderite and barite minerals in the rock pore structure of Hawkesbury sandstone. According to the findings of this study, the significant rock mass mineralogical and pore structure alterations caused by around 1.5 years of long-term CO₂ interaction with the reservoir may cause its permeability to be enhanced by around 10%. The significant alterations created in deep saline aquifer rock permeability, porosity and pore geometry by mineralogical rock alteration, NaCl deposition and salt drying-out effect cause the simple effective stress law for effective permeability to be inapplicable to deep saline aquifers.

CHAPTER 5

Experimental Investigation of Chemical, Mineralogical and Mechanical Stability of Different Sandstone Formations under Deep Saline Sequestration Environment

5 Experimental Investigation of Chemical, Mineralogical and Mechanical Stability of Different Sandstone Formations under Deep Saline Sequestration Environment

5.1 Influence of reservoir mineralogy on deep saline storage process

To predict the long-term behaviour of CO₂ plume, it is useful to first understand some of the fundamental behaviours of reservoir properties, including chemical, mineralogical and hydro-mechanical properties that are typical of any deep saline aquifer. Generally, most preferable deep saline aquifers are either carbonate- or silicate-cemented sandstone formations. Due to this mineralogical difference, it is expected that these two saline aquifer formations display separate chemical, mineralogical and hydro-mechanical behaviours during the CO₂ sequestration process. Therefore, in this chapter of the thesis, a comprehensive chemical, mineralogical and mechanical study conducted to distinguish the two different behaviours of silicate- and carbonate-cemented sandstone formations is presented. Silicate- and carbonate-cemented sandstones obtained from the Gosford formation are considered for the experimental work. The following submitted journal paper reports the results of this section of the thesis.

An Experimental Investigation of Coupled Chemico-mineralogical and Mechanical Changes in Varyingly-cemented Sandstones upon CO₂ Injection in Deep Saline Aquifer Environments

T. D. Rathnaweera¹, P.G. Ranjith¹, M. S. A. Perera¹

¹Department of Civil Engineering, Monash University, Building 60, Melbourne, Victoria, 3800, Australia.

Abstract

Although CO₂ storage in deep saline aquifers is now accepted as a potential atmospheric CO₂ mitigation option, the chemico-mineralogical property alterations in the aquifer formation associated with the CO₂/brine/rock mineral interactions, the corresponding influence on formation hydro-mechanical properties and the effect of rock mineral structure are not yet fully understood. This study was therefore conducted to obtain a comprehensive understanding of the effect of long-term CO₂ exposure on the chemico-mineralogical structure and corresponding strength characteristics in saline aquifer rock formations using silicate cement (SS) and carbonate cement (CS) Hawkesbury sandstone samples collected from the Sydney basin. Sandstone samples were first reacted with brine+CO₂ under different injection pressures (both sub-critical (4, 6 MPa) and super-critical (8, 10 MPa)) under a constant temperature of 35°C. A comprehensive chemico-mineralogical analysis (ICP-AES and XRD) was first conducted on both the rock mass pore fluid and the rock matrix over the saturation period of one year, giving special attention the alteration of dominant rock minerals (quartz, calcite and kaolinite). The overall influence after 12 months of saturation with brine and CO₂ on the strength characteristics of the two types of sandstones (SS and CS) was then investigated and correlated to the chemico-mineralogical reaction, in order to understand the coupled process.

According to the test results, compared to the silicate cement-dominant mineral structure (SS), the presence of a carbonate cement-dominant mineral structure (CS) in the aquifer rock formation creates more significant alterations in the formation's chemico-mineralogical structure upon CO₂ injection. This is because calcite mineral reactions occur at much greater rates compared to quartz mineral reactions in the CO₂ exposed environment. In addition, although some minor precipitation of kaolinite minerals may also occur upon CO₂ injection, the effect may not be significant. Overall, rock mineral changes in deep saline aquifers upon CO₂ injection have a significant influence on the strength characteristics of the reservoir rock

mass, depending on the aquifer mineral structure, and CS formations are subject to much greater strength property changes upon exposure to CO₂ than SS formations. Interestingly, CO₂ injection causes a strength gain in SS sandstone and a strength reduction in CS sandstone. The occurrence of these mechanical property alterations in aquifer rock formations are also dependent on the CO₂ injection pressure and phase, and increasing the injecting CO₂ pressure significantly enhances the changes, due to highly acidic environment created by the enhanced CO₂ solubility process. Changing the CO₂ phase from sub- to super-critical condition also accelerates the reaction mechanisms, due to the greater chemical potential of super-critical CO₂. However, overall SS sandstone exhibits more stable chemical-mineralogical and mechanical characteristics upon CO₂ injection than CS sandstone, and exhibits more suitable characteristics for CO₂ sequestration.

Keywords: Chemical, mineralogical, mechanical, sequestration, carbonate, silicate

5.1.1 Introduction

Over the past century, the emission of anthropogenic CO₂ into the Earth's atmosphere has significantly increased with the expansion of the industrial sector (Leung et al., 2014). In order to overcome this crucial issue of ever-increasing atmospheric CO₂ levels, many mitigation options have been considered. CO₂ geo-sequestration in deep saline aquifers has recently attracted the attention of many researchers, due to its many unique advantages (White et al., 2003; Perera et al., 2013). However, sequestration of this ever-increasing anthropogenic CO₂ needs suitable deep underground reservoir formations with huge CO₂ storage capability and safety. To satisfy these two requirements, a host formation with adequate strength, permeability and porosity is required (Rochelle et al., 2004), and carbonate-, or silicate-cemented formations have been identified as potential reservoir rock formations (Perkins and Gunter, 1995; Marbler et al., 2013). It is therefore important to have a comprehensive knowledge of the CO₂ storage process in these particular types of geological reservoir rock, which requires a precise identification of their geochemical-mechanical behaviour upon CO₂ injection. Although a few studies have been conducted to distinguish the geochemical behaviour of these two formations (Law and Bachu, 1996; Gunter et al., 2000; Marbler et al., 2013), the long-term influence of CO₂/brine/rock interactions on the coupled geochemico-mechanical behaviour of these two formations with CO₂ sequestration has not been considered to date.

The aim of the present study therefore is to conduct a comprehensive experimental investigation to understand the unique behaviours of silicate- and carbonate-cemented sandstone formations upon long-term CO₂ sequestration, in terms of their chemical, mineralogical and mechanical responses after a one-year reaction period. Such a long time for the CO₂/brine/rock interaction gives sufficient time for the initiation of many long-term mineral reactions that cannot be seen under short-term saturation conditions. The estimation of reservoir mechanical properties after such a long saturation period would therefore be very applicable to the actual mechanical behaviour in these reservoir rock formations upon CO₂ sequestration. To investigate and distinguish the suitability of silicate- and carbonate-cemented sandstone formations for deep saline sequestration, the present study selected two mineralogically different Hawkesbury sandstone samples, obtained from the Sydney basin at Gosford. For the purposes of the study, a range of CO₂ reaction pressures (4, 6, 8 and 10MPa) at 35°C temperature was selected to conduct the investigation under both sub- and super-critical conditions of CO₂. For the first time, this study distinguishes the long-term mechanical behaviour of both silicate- and carbonate-cemented reservoir rocks upon CO₂/brine/rock interactions under various CO₂ injection pressures.

5.1.2 Experimental procedure

5.1.2.1 Sample description

The tested samples were collected from the Gosford formation in the Sydney Basin, which is known as the Hawkesbury sandstone formation. Fig. 5.1 shows the location of the Gosford formation in the Sydney Basin (Ward, 1972; Rathnaweera et al., 2015b). The Gosford formation has a fluvial origin and belongs to the early-Triassic age (McDonnell, 1973). The Triassic rocks in the Sydney Basin can be subdivided into the Narrabeen Group, the Hawkesbury Sandstone, and the Wianamatta Group, in ascending stratigraphic order (Conolly, 1969). Most of the sandstones in the Gosford formation are fine- to medium-grained.

The present study used two different sandstone types: silicate- and carbonate-cemented, which are very different in their lithology, mineralogy and texture. Specimen type 1 is silicate-cemented sandstone and is named “SS-type” sandstone here. This particular type of sandstone consists of almost equal amounts of matrix and quartz minerals, with minor amounts of kaolinite and calcite. According to x-ray diffraction (XRD) analysis, the SS-type consists of 90% quartz, 7% calcite, 1% kaolinite, 1% muscovite and <1% other clay minerals, such as illite and

smectite (% by weight). Specimen type 2 is carbonate-cemented sandstone and is named ‘‘CS-type’’, sandstone here. CS-type sandstone is basically composed of quartz with major amounts of calcite, kaolinite, siderite and barite, with 64% being quartz and about 30 % calcite. Before being processed in geochemical and geo-mechanical tests, the sandstone samples were carefully mineralogically, geochemically and petro-physically characterised (Table 5.1).

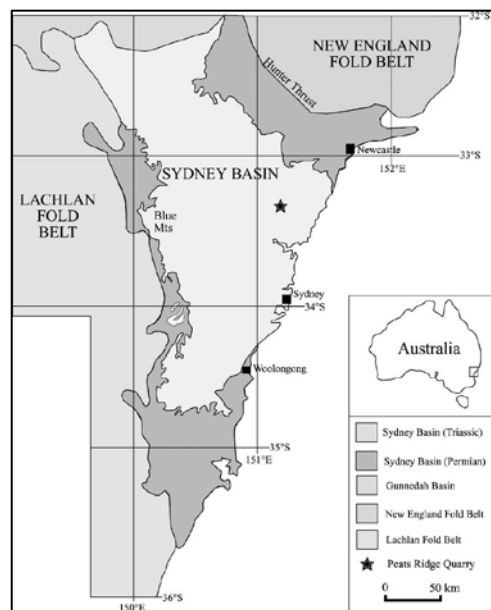


Figure 5.1. Map showing distribution of Hawkesbury Sandstone formation in Sydney Basin (Ward, 1972; Rathnaweera et al., 2015b).

Table 5.1. Mineralogical, chemical and geo-mechanical characteristics of the SS and CS reservoir rocks.

Lithology	Silicate (SS) cemented sandstone	Carbonate (CS) cemented sandstone
Formation	Early Triassic ‘‘Hawkesbury sandstone’’	Early Triassic ‘‘Hawkesbury sandstone’’
Macroscopic description	Colour: white-grey, medium- to fine-grained	Colour: White-grey-brownish, medium- to fine- grained
Mineralogy (XRD)	90% quartz, 7% calcite, 1% kaolinite, 1% muscovite, <1% other clay minerals	64% quartz, 30% calcite, 2% kaolinite, 1% barite, 1% siderite, 1% muscovite, <1% other clay minerals
Structure	Inhomogeneous, un-layered, inter-granular pore space	Inhomogeneous, un-layered, inter-granular pore space
Cementation	Poorly cemented, angular to sub-rounded quartz grains	Well cemented, sub-granular quartz rim with calcite fillings

Geochemistry (XRF, wt. %)	88.2 SiO ₂ , 4.2 CaO, 2.3 Al ₂ O ₃ , 0.8 MgO, 0.2 Fe ₂ O ₃ , 2.8 K ₂ O	57.1 SiO ₂ , 27.4 CaO, 4.3 Al ₂ O ₃ , 1.1 MgO, 5.4 Fe ₂ O ₃ , 3.3 K ₂ O
Effective porosity (MIP)	29.3%	28.4%
Permeability (mD)	103.28	94.32
Compressive strength (MPa)	54-57	48-52
Water absorption (%)	3.4	2.71

5.1.2.2 Sample preparation and reaction processes

Cylindrical sandstone samples 38mm in diameter and 76mm in length were prepared and used for both geochemical and geo-mechanical experiments. Before the geochemical tests, the samples were reacted with 15% NaCl concentrated brine and CO₂ to simulate the CO₂ sequestration process. In order to resemble the actual field conditions of the aquifers, the NaCl concentration in the pore fluid was selected as 15% by weight, which represents the average salinity condition of a typical aquifer (Bachu and Bennion, 2008; Rathnaweera et al., 2015a), and the pore water chemistry of the prepared synthetic brine is shown in Table 5.2. The laboratory experiments comprised chemical, mineralogical and mechanical experiments, in which the rock samples were reacted with prepared brine and CO₂ at different injection pressures (4, 6, 8, and 10MPa) at 35 °C for a period of 12 months to simulate the CO₂ sequestration environment for the rock masses under test. Fig. 5.2a shows a schematic diagram of the reaction chambers available in the Deep Earth Energy Research Laboratory (DEERL) at Monash University.

Table 5.2. Chemical composition of prepared brine solution (concentration in mg/l).

	Concentration (mg/l)
pH	6.88
Na	149,875
Ca	16.45
K	14.63
Fe	0.76
Al	1.32
Si	1.34
Ba	2.43
Cl ⁻	149,954
HCO ₃ ⁻	0.00
Br ⁻	1.35

Pore fluid samples were taken from the reaction chambers at 1, 2, 3, 4, 6, 8, 10 and 12 months to characterise the chemical equilibrium and reaction kinetics of the rock minerals. The final mineralogical compositions of the reacted samples were evaluated by performing XRD analysis on fully (12 months) reacted samples. The collected chamber pore fluids were analysed for both major and some minor cations (Si, Ca, Al, Ba, Fe) using (inductively- coupled plasma atomic emission spectroscopy (ICP-AES) and the pH was measured for cooled, depressurised samples using a calibrated pH meter.

5.1.2.3 Mechanical testing

Once the samples were chemically and mineralogically characterised, a series of compressive strength tests was conducted on 12 month-reacted samples. Thirty-two uniaxial compression (UCS) tests (including 4 replicates for each CO₂ injection condition) were performed on both SS and CS formations to quantify the effect of different mineralogy and injection pressures on reservoir rock strength. The compression tests were conducted according to the methods suggested in the ASTM standards (Brown, 1981). The testing was conducted at Monash University's DEERL using cylindrical sandstone samples. A SHIMADZU AG 9 300 kN compression machine with a maximum compression load capacity of 300 kN (Fig. 5.2b) was used for the experiments, the loading rate was maintained at 0.1 mm/min for all the tests and applied loads were recorded using an automatic data acquisition system.

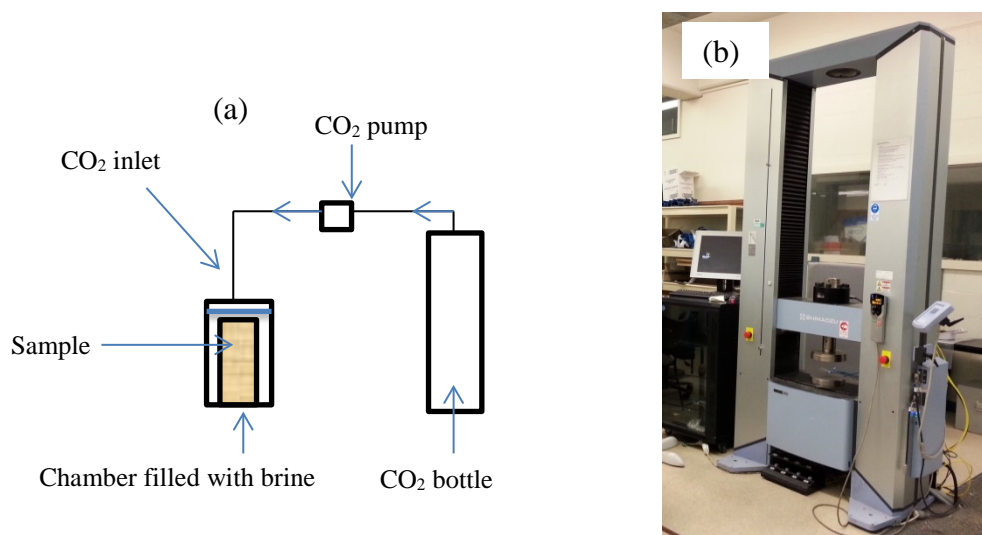


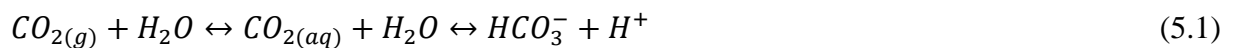
Figure 5.2. (a) Schematic diagrams of CO₂ saturation chamber and (b) The UCS testing set-up.

5.1.3 Results and discussion

The experiment series was initiated by characterising the chemical and mineralogical response of both SS and CS formations upon CO₂ exposure. The chemical response was evaluated in terms of the pH behaviour of the resulting buffer solution and mineralogical characterisation was done based on the reaction kinetics of three major rock minerals, quartz, calcite and kaolinite, because these three minerals play dominant roles in rock grain cementation in the tested rocks compared to the other rock minerals. Sections 5.1.3.1, 5.1.3.2 and 5.1.3.3 below discuss the findings of these chemical and mineralogical test series and Section 5.1.3.4 discusses the findings of mechanical testing conducted on 12 month-reacted samples under different injection pressure conditions. All of the results were used to evaluate the optimum reservoir conditions for the CO₂ sequestration process.

5.1.3.1 Reactions between the injected CO₂ with aquifer pore fluid

A typical CO₂ sequestration process in deep saline aquifers involves the pumping of captured CO₂ from the surface into the deep host formation. The dissolution of this injected CO₂ in aquifer brine is the fundamental trapping mechanism of CO₂ in the aquifer, and is called “solubility trapping” in the deep saline sequestration process (Koide et al., 1995). This solubility trapping is important, because of its ability to create a relatively fast and large sink for the captured anthropogenic CO₂. The reaction sequence of the dissolution process can be written as follows:



As shown in Eq. 5.1, the dissolution of injected CO₂ in brine consists of a series of linked reversible reactions. The rate of each is highly dependent on the in-situ pressure and temperature condition (Wiebe, 1941) and is further varied with surrounding factors, such as the fluid chemistry, pH and salinity level of the aquifer pore fluid. Wiebe and Gaddy (1940) and Wiebe (1941) showed that there is a trend of increasing CO₂ solubility in pure water with decreasing temperature and increasing pressure (see Fig. 5.3a). As mentioned previously, the other important factor that governs CO₂ solubility is the specific composition of the aquifer pore fluid, and Enick and Klara (1990) showed that CO₂ solubility decreases with increasing ionic strength of the aqueous phase (see Fig. 5.3b), mainly due to the resultant CO₂ injection-induced salting-out effect (Garrels and Christ, 1965).

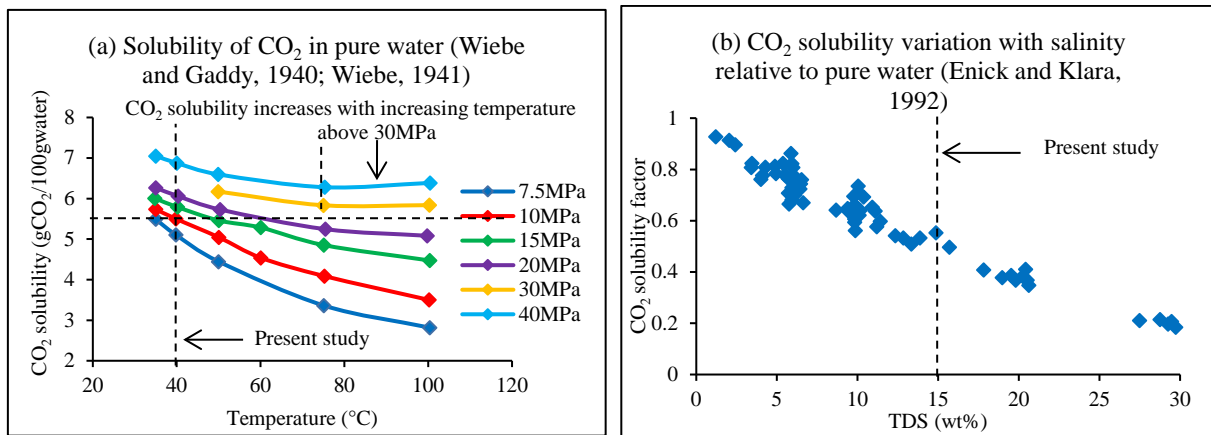


Figure 5.3. (a) Solubility of CO₂ in pure water (b) Solubility of CO₂ with salinity relative to pure water.

The dissolution of CO₂ in aquifer pore fluid can be considered as a comparatively fast process, if the CO₂ and pore fluid have a good environment for mixing well (Rochelle et al., 2004). To date, the CO₂-water reaction equilibrium and its reactive kinetics have been well documented by many researchers (Ellis and Golding, 1963; Stewart and Munjal, 1970; Bevan and Savage, 1989; Czernichowski-Lauriol et al., 1996). The experiment conducted under 20 MPa injection pressure by Czernichowski-Lauriol et al. (1996) showed that this reaction is faster than most fluid-mineral reactions. According to Czernichowski-Lauriol et al. (1996), the dissolution of CO₂ in pure water has a reaction rate of $7 \times 10^{-5} \text{ mol cm}^{-2} \text{ s}^{-1}$, which is far faster than the quartz and K-feldspar reactions in pure water (around $10^{-15} \text{ mol cm}^{-2} \text{ s}^{-1}$).

However, during the CO₂ sequestration process, this dissolution rate can be decelerated through the influence of other factors, such as the diffusional process, buoyancy-driven fluid mixing, viscous fingering, mineral reactions and mixing driven by deep groundwater flow (Rochelle et al., 2004). Of these, the influence of mineral reactions is one of the most critical factors, as it contributes considerably to the mineral sequestration process, the other dominant trapping mechanism of CO₂ in deep saline aquifers. Over a long time period, the resulting free H^+ ions made through the dissolution of injected CO₂ in the aquifer pore fluid (Eq. 5.1) can react with the host formation's minerals, altering the natural chemical composition of the aquifer pore fluid. According to past studies (Law and Bachu, 1996; Gunter et al., 2000), the interaction between the host formation and the resulting acidic environment is highly dependent on the mineral composition, mineral abundance/distribution, and reactive surface area of the host formation. In addition, mineral reaction-induced pH buffering also significantly affects CO₂

solubility over a long period. Perkins and Gunter (1995) stated that CO₂ solubility decreases with decreasing pH in the aquifer pore fluid, as it reactivates the backward reaction of Eq. 5.1 due to the enhanced H⁺ ions-induced new chemical equilibrium of the system. Interestingly, due to the linked reversible nature of the dissolution reaction of CO₂, interactions with the host formation that consume H⁺ ions tend to drive reaction (Eq. 5.1) forward, causing more CO₂ to dissolve in the aquifer pore fluid. This complex reversible CO₂ dissolution reaction is site-specific due to different mineral compositions and in-situ conditions, such as temperature and pressure (Perkins and Gunter, 1995). Therefore, detailed studies related to this complex chemical interaction of host formation are required in order to quantify the storage capacity of the host formation prior to CO₂ injection. This matter was considered in the present study.

The collected residual pore fluid samples were first characterised based on their pH variation during the reaction process. The pH values of the chamber pore fluids were measured at regular time intervals (every 5 hours) during the reaction process. The measurements were taken using a calibrated pH meter and the calibration was done using solutions of a mixture of HCl (0.1-0.001M) and NaCl (0-0.3M) with a constant ionic strength of 0.15M.

Fig. 5.4 shows the variations of the resulting pH buffer zones of the aquifer pore fluids with respect to reaction time for each pressure condition. As can be seen in Fig. 5.4, the pH of both pore fluids (SS and CS type) do not display steady variations over time, and initially drop from their natural pH value and then reach equilibrium over time. For example, after an initial drop, at 4 MPa injection pressure, the SS-reacted pore fluid showed the lowest pH value of 5.43 after 2 months of saturation and the CS-reacted pore fluid showed the lowest pH value of 5.93 after 6 months reaction time. Under the same test conditions, SS-reacted pore fluid showed the highest pH values of 5.64 after 3 and 12 months of saturation and CS-reacted pore fluid showed the highest pH value of 6.2 after 4 and 12 months saturation. These dissimilar pH variations exhibit the chemical diversity of the SS and CS formations.

The dissolution of injected CO₂ in the pore fluid causes its natural pH to be reduced due to the increased H⁺ ion concentration in the pore fluid. However, this increased pH trend confirmed that pH variation is not proportional to the H⁺ ion activity in the CO₂ solubility process and is affected by enhanced mineralogical reaction-induced new chemical equilibrium. Interestingly, in comparison with SS-reacted pore fluid, CS-reacted pore fluid showed a considerable increment in pH after initial drawdown of the pH under all the test conditions. For instance, at

4MPa injection pressure, after initial drawdown, the pH in CS-reacted pore fluid increases from 5.81 to 5.99 after 2 months, which is a considerable increase compared to SS-reacted pore fluid. Moreover, the SS formation creates a more acidic environment compared to the CS formation during the sequestration process (Fig. 5.4). This significant increment of pH in CS-reacted pore fluid compared to SS-reacted pore fluid is obviously correlated with the dissolution/precipitation of calcite rock minerals, as it disturbs the equilibrium of the buffer solution.

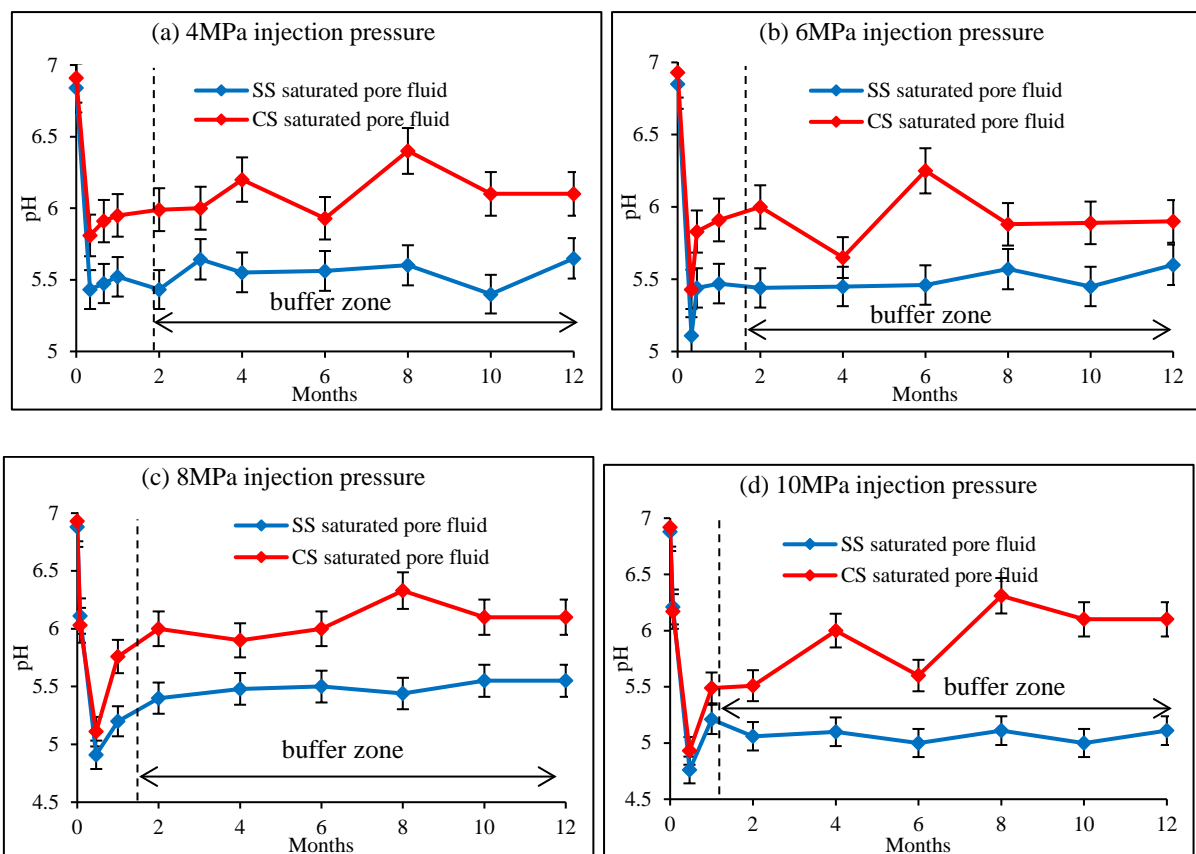


Figure 5.4. Influence of different mineralogy and injection pressure on pH buffering characteristics of the aquifer pore fluid.

A number of studies (Perkins and Gunter, 1995; Law and Bachu, 1996; Gunter et al., 2000) have shown that silicate-cemented sandstone formations are much better geological candidates for deep saline sequestration than carbonate-cemented sandstone formations, due to their better pH buffering characteristics. Good buffering solution has the ability to maintain constant pH throughout the sequestration process. As Fig. 5.4 shows, after the initial reduction of pH, SS-reacted pore fluid maintained nearly constant pH buffering characteristics compared to the CS-reacted pore fluid. This observation is consistent with past findings.

In addition, the effect of CO₂ injection pressure is crucial in creating this CO₂ dissolution-created buffer zone. As mentioned earlier, under the selected temperature condition (35°C), CO₂ dissolution increases with increasing injection pressure, which is also confirmed by Fig. 5.3a. The pH varies with different CO₂ injection pressures, as shown in Fig. 5.4 and according to this figure, in SS-reacted pore fluids, the initial drawdown of pH varies with different injection pressures, and 5.43, 5.11, 4.91 and 4.76 pH values were recorded at 4, 6, 8 and 10 MPa injection pressure conditions, respectively. The lowest pH value obtained of 4.76 under 10 MPa injection pressure confirmed the increment in CO₂ solubility with increasing injection pressures from 4 to 10 MPa. Likewise, similar pH variation was observed in CS-reacted pore fluids, where the initial pH reductions of 5.81, 5.43, 5.11 and 4.93 were observed with increasing injection pressures from 4 to 10 MPa, respectively. However, the pH reduction with increasing CO₂ injection pressure is greater for the SS-reacted pore fluid. These dissimilar pH variations confirm the significant effect of injection pressure on the chemical behaviour of both formations, as a more acidic environment is created with increasing injection pressure due to the enhanced CO₂ dissolution process.

It is now clear that SS and CS formations have unique behaviours in terms of chemical response and it is important to understand the impact of rock mineral reactions on CO₂ solubility during sequestration in deep saline aquifers.

5.1.3.2 Reaction between dissolved CO₂ and aquifer rock minerals

In deep saline sequestration, carbonate reactions (calcite, dolomite and magnesite) are very important, because their dissolution reaction consumes a considerable amount of dissolved CO₂, which in turn enhances the mineral trapping process (Pokrovsky et al., 2009). However, due to the absence of dolomite and magnesite in the studied formations, the present study considered only calcite as a potential candidate for carbonate reaction, and that was identified in terms of Ca²⁺ concentration in the chamber pore fluid. The general form of the calcite (CaCO₃) dissolution reaction can be written as follows:



Fig. 5.5 shows the variation of Ca²⁺ concentration with reaction time in SS- and CS-reacted chamber pore fluids. The measurements were taken at regular time intervals (every month)

during the reaction process and ICP-AES analysis was carried out to analyse the chemistry of the collected chamber pore fluid.

A comparison of the results obtained from SS- and CS-reacted pore fluids (Figs. 5.5) shows that the two formations have different calcite reaction kinetics under different injection pressure conditions. According to Fig. 5.5, significant calcite leachate reactions can be seen in the CS formation compared to the SS formation, and this is obviously due to the presence of a higher percentage of calcite minerals in the CS mineral structure than the SS mineral structure. For example, at 4MPa injection pressure, after 12 months of reaction, the CS-reacted pore fluid showed a calcite concentration of 112.32 mg/l and the SS-reacted pore fluid showed a calcite concentration of 56.34 mg/l under the same conditions, which is 49.84% lower than the value of the CS concentration. Similar calcite reaction trends were observed for other injection pressure conditions (Fig. 5.5).

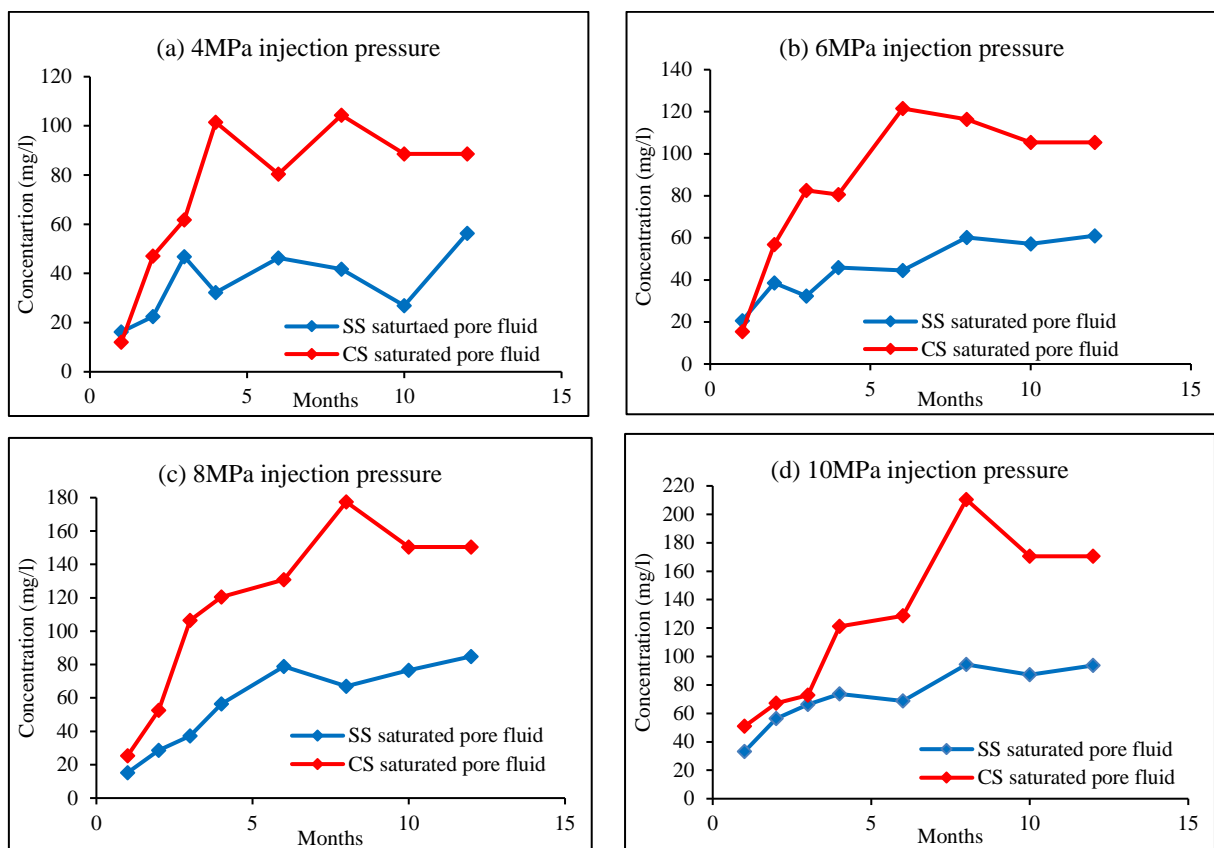


Figure 5.5. Variation of Ca^{2+} concentration in chamber pore fluids with saturation time.

Furthermore, the influence of CO_2 injection pressure on the calcite reaction can be seen in Fig. 5.5. As the figure shows, the total concentration of calcite mineral significantly changes with

increasing CO₂ injection pressure. For both chamber pore fluids, after 12 months of reaction, the total concentration of calcite minerals increases with increasing injection pressure from 4 to 10 MPa. The improved acidic environment due to the boosted solubility of CO₂/brine may be a reasonable explanation for the enhanced reaction kinetics under increased injection pressures (Kaszuba et al., 2003).

Apart from the CO₂ injection pressure, other factors like temperature, pH and other rock mineral reaction kinetics also considerably influence the calcite reaction (Pokrovsky et al., 2009). In the present study, the effect of temperature was ignored by conducting tests under the same constant temperature (35°C). According to Fig. 5.5, calcite mineral can be subjected to both dissolution and precipitation, depending on the chemical composition and pH of the pore fluid. For instance, at 4 MPa injection pressure, in CS-reacted pore fluid, the highest Ca²⁺ concentration was observed after 8 months of reaction, at which the highest pH condition in the system was recorded (see Fig. 5.4a). Interestingly, the calculated saturated index at this point revealed that sample pore fluid is close to super-saturation with respect to calcite mineral, which confirms the possibility of re-precipitation of calcite minerals under this condition. However, the SS-reacted pore fluid displayed a strongly under-saturated condition with respect to calcite minerals under the same injection pressure, probably due to the lower amount of existing Ca²⁺. Alkattan et al. (1998) showed that calcite dissolution is not simply proportional to the H⁺ activity in the system. To extract the actual behaviour of the calcite reaction, the rates should be corrected in terms of pH, injection pressure and temperature effects, and should also be correlated with other mineral and chemical reaction kinetics.

In order to fully understand the complex mixed reaction under the tested conditions, quartz and kaolinite mineral behaviours were chemically and mineralogically characterised. The quartz mineral reaction was first evaluated for both SS- and CS-reacted pore fluids in terms of Si⁴⁺ concentration in the chamber pore fluid. Normally, Si⁴⁺ concentration in the chamber fluids reflects the dissolution of quartz minerals due to the absence of other major Si⁴⁺ sources, such as illite and feldspar. However, the activation of existing kaolinite ($Al_2Si_2O_5(OH)_4$) and muscovite ($KAl_2(AlSi_3O_{10})(F,OH)_2$) minerals can also contribute some small part to changing the Si⁴⁺ ion concentration in the residual pore fluid. In order to identify the dominant reaction mechanism on Si⁴⁺ ion variation, XRD analysis was performed. According to the XRD results, minor changes (dissolution reactions) in muscovite and kaolinite minerals were observed after

12 months reaction. Therefore, considering the low reaction behaviours of those two minerals, the present study ignored the influence of the dissolution of muscovite and kaolinite minerals on Si^{4+} ion variation and only the quartz mineral was considered as a potential Si^{4+} source. The general reaction of quartz dissolution in an acidic environment can be written as follows:



In the present study, the SS formation facilitated a greater opportunity for fluid-quartz interaction due to the higher percentage of quartz minerals in the mineral structure. Hence, greater Si^{4+} ion leachability can be expected in SS-reacted chamber pore fluids compared to CS-reacted fluids. According to Fig. 5.6, a significant amount of Si^{4+} ion was leached from the SS than the CS formation during the one-year reaction period. For example, at 10MPa injection pressure, after 12 months reaction, the SS-reacted fluid showed a Si^{4+} ion concentration of 68.84mg/l and the CS-reacted fluid showed a Si^{4+} ion concentration of 20.45mg/l, which is 70.29% lower than the SS value. Due to the higher percentage of quartz mineral (90%) in SS, the potential reaction area of quartz mineral is much higher, and this offers a much greater opportunity for reaction with the resulting acidic environment compared to the CS formation.

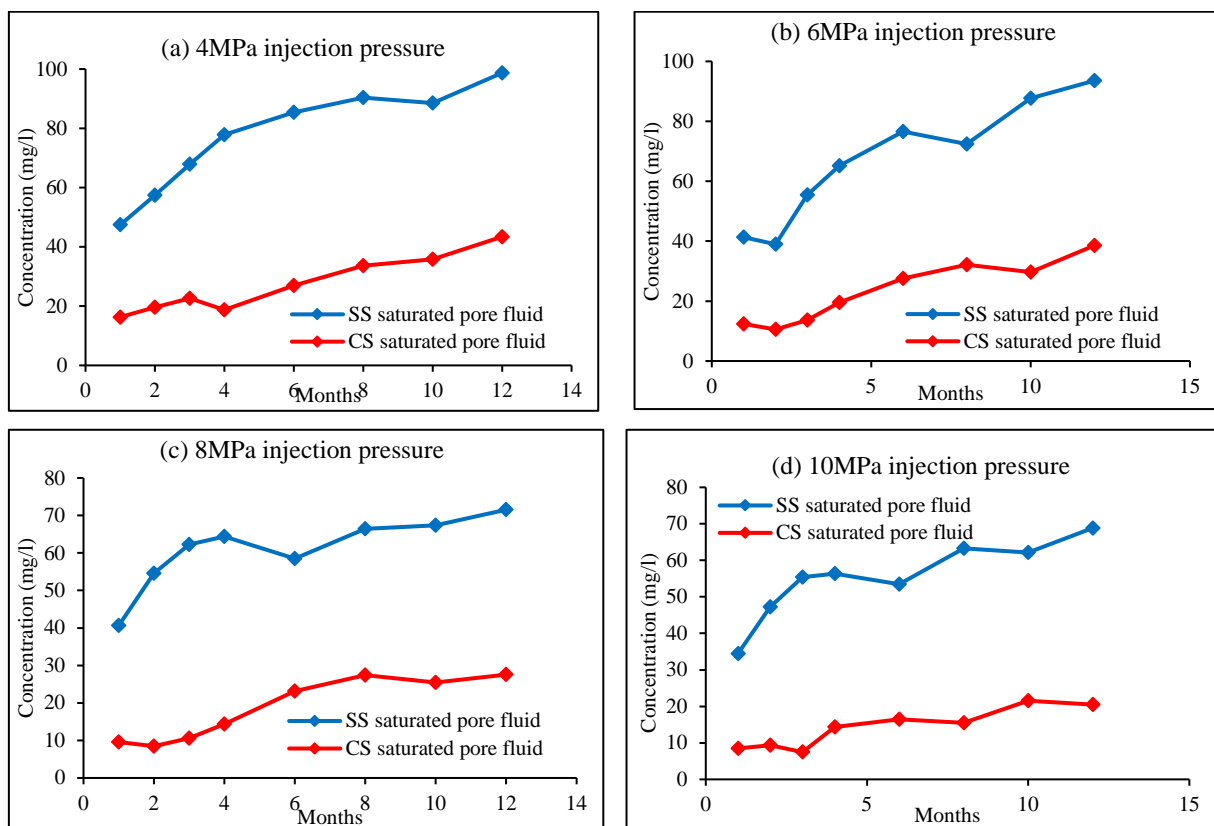


Figure 5.6. Variation of Si^{4+} concentration in chamber pore fluids with saturation time.

Fig. 5.6 clearly explains how the influence of injection pressure affects quartz mineral corrosion under both sub-critical and super-critical injection conditions. As the figure shows, the general Si^{4+} ion concentration trend of reduction with increasing injection pressure can be seen in both the SS and CS cases. For example, in the SS-reacted pore fluid, after 12 months, the Si^{4+} ion concentration has decreased from 94.71 to 68.84 mg/l with the increasing injection pressure from 4 to 10 MPa, and a similar decreasing trend can be seen in the CS-reacted pore fluid. This decreasing trend can be explained based on the phenomenon of hydrolysis of quartz (Eq. 5.4):



The solubility of CO_2 in the brine/rock system increases with increasing CO_2 pressure in the reaction chamber, creating a more acidic environment in the solution. Because of this enhanced acidity in the system, the formation of H_4SiO_4 is delayed by the new equilibrium, due to the reactivation of the backward reaction in Eq. 5.4, which consequently reduces the reaction rate of quartz mineral in the system with increasing CO_2 pressure. A similar observation was recorded by Lin et al. (2008) for quartz-cemented granite samples. According to Fig. 5.6, the phase change of CO_2 from sub-critical to super-critical also considerably affects the quartz corrosion in the SS formation, and in the 12-month-reacted pore fluid, a 23.54% reduction in Si^{4+} ion concentration occurred with the increase of the injection pressure from 6 to 8 MPa (the critical point lies at 7.13 MPa), which is significantly higher than the similar reduction observed under pure sub-critical condition (4 to 6MPa (5.22%) and pure super-critical condition (8 to 10MPa (3.77%)). Increasing the CO_2 phase condition from sub- to super-critical appears to accelerate the hydrolysis reaction, probably due to the highly chemically active nature of super-critical CO_2 (Ranjith et al., 2013). However, this phase change is not significant for the quartz reaction in the CS formation, and it is probable that the effect of the calcite reaction-induced new chemical equilibrium (specially the calcite reaction-induced high pH) may have a much greater influence on the quartz reaction than the phase change of CO_2 . To date, a limited number of studies have focused on the quartz mineral reaction in sandstone under reservoir rock conditions. However, most have considered very short exposure times, and are therefore unable to capture the real (long-term) effect of CO_2 injection on the chemical and mineral structure of reservoir rock in the field (Liu et al., 2003; Lin et al., 2008).

Finally, the kaolinite reaction was evaluated. The basic kaolinite dissolution reaction in the acidic system can be expressed as follows:

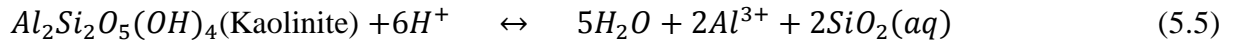
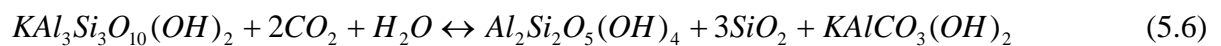


Fig. 5.7 shows the Al^{3+} ion concentration variations with respect to the injection pressure and reaction time for both the SS and CS conditions. A comparison of the results for the SS- and CS-reacted chamber fluids gives an almost identical variation of Al^{3+} ion composition in both cases. However, the Al^{3+} ion variations in chamber pore fluids (Fig. 5.7) confirmed that there is a slight influence of injection pressure, and an increasing trend was observed for both cases with increasing injection pressures. For example, for CS-reacted pore fluid, after 12 months reaction, the Al^{3+} ion concentration in the chamber increased from 1.95 to 3.85mg/l with increasing injection pressure from 4 to 10 MPa, which is quite insignificant compared to the Ca^{2+} and Si^{4+} ion variations with injection pressure. To verify the Al^{3+} source mineral, which is responsible for the above alteration, comprehensive XRD analysis was performed on 12-monthsreacted samples. According to Table 5.3, after 12 months of saturation, a considerable amount of kaolinite precipitation was observed in both the SS and CS samples. For example, in the CS formation, the initial kaolinite percentage increased from 4.37% to 4.48% with the reaction of CO_2 /brine at 4MPa injection pressure, and in the SS formation, the initial percentage increased from 2.29% to 3.05% under the same conditions. Therefore, it is now clear that the kaolinite mineral is not only the agent responsible for the observed increment in Al^{3+} ion concentration, possibly due to the activation of muscovite ($KAl_3Si_3O_{10}(OH)_2$) minerals in both cases, which was confirmed by the XRD results. In order to provide a clarification on these complex kaolinite and muscovite reactions, saturation indexes of kaolinite and muscovite were calculated and will be discussed in detail in Section 5.1.3.3. As it can be seen in Table 5.3, the muscovite minerals dissolved in the resulting acidic environment also contribute to the re-precipitation of kaolinite (aluminosilicates) minerals, and that re-precipitation process can be explained by the following reaction:



In addition, the XRD results confirmed the calcite and quartz mineral dissolution nature of the two types of sandstone samples. According to Table 5.3, after 12 months of reaction, the initial quartz mineral in the SS formation decreased by around 13.63% and 8.39% under 4 MPa and 8 MPa, injection pressures, respectively. Likewise, with respect to the initial composition, in the CS formation, around 6.8% and 4.1% reductions were observed in quartz mineral upon exposure to 4 and 8 MPa injection pressures, respectively. This reveals that, compared with the

SS formation, CS formation displayed very stable behaviour in terms of quartz mineral corrosion, but is chemically unstable due to its considerably greater calcite reactions compared to the SS formation. Therefore, the stability of the calcite mineral in an acidic environment was investigated. According to the XRD results, after 12 months of reaction with CO₂, around 48.34% and 67.17% calcite reductions in CS formation were seen at 4 and 8 MPa injection pressures, respectively. However, the SS formation did not show a significant reduction in calcite minerals compared to the CS formation, where 7.53% and 17.41% reductions were observed upon exposure to 4 and 8MPa injection pressures, respectively.

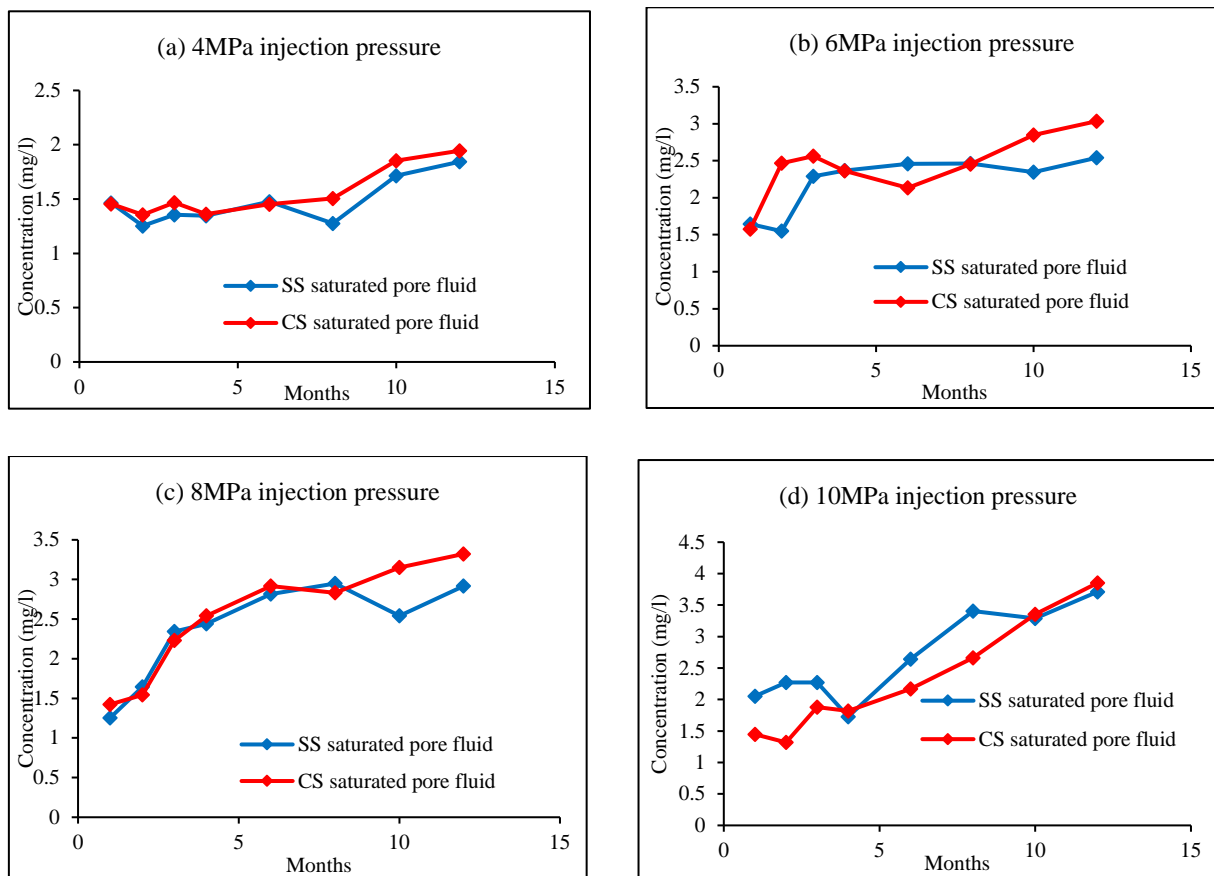


Figure 5.7. Variation of Al^{3+} concentration in chamber pore fluids with saturation time.

5.1.3.3 Chemical equilibrium and kinetic evaluation of rock mineral reaction upon exposure to CO₂

Based on the results discussed above, it is clear that that rock mineral reactions upon CO₂ injection into saline aquifers alter both the rock minerals and the pore water chemistry, and all of these alterations are dependent on the mineral structure of the aquifer rock mass. However, a deeper understanding of the rock mineral reaction process, including the equilibrium and

kinetic behaviours is very important prior to CO₂ injection into saline aquifers for effective CO₂ storage. This is considered in the following sections of the paper to provide a comprehensive image of the chemical equilibrium and kinetic behaviour of quartz, calcite and kaolinite and the influence on the CO₂ storage process under reservoir conditions. To characterise the equilibrium and reaction kinetics of each mineral, the mineral concentration data discussed above of the formation rock mass and the pore fluid were used to calculate the reaction rate (R), thermodynamic equilibrium constant (K_{sp}), ion activation product (IPA) and saturation index (SI).

Table 5.3. Results of XRD analysis (g).

	Initial composition		4MPa (After 12months)		8MPa (After 12months)	
	SS	CS	SS	CS	SS	CS
Quartz	206.06	139.91	177.97	130.44	188.78	134.24
Calcite	18.32	65.58	16.94	33.88	15.13	21.53
Kaolinite	2.29	4.37	3.05	4.48	3.63	5.15
Muscovite	2.29	2.18	0.21	1.48	0.11	0.88
Barite	-	2.18	-	1.37	-	<1
Siderite	-	2.18	-	<1	-	<1

During CO₂ sequestration in deep saline aquifers, mineral trapping plays a major role in the long-term isolation of injected CO₂ from the atmosphere through various precipitation reactions, and the permanent precipitation of carbonate minerals with CO₂ rich reservoir brine is dominant (Lin et al., 2008). The evaluation of the carbonate reaction mechanism in the sequestration environment is therefore crucial, because the deposition of carbonate minerals may negatively affect the reservoir flow performance, even creating permanent damage to reservoir flow performance for CO₂ injection (Moore et al., 2005).

According to Fig. 5.8, it is clear that the SS and CS formations exhibit different calcite reaction mechanisms, and the CS formation displays higher reaction rates than the SS formation, which is related with the greater percentage of calcite minerals in the CS formation. Interestingly, the present study observed an increasing concentration of Ca^{2+} ions in the pore fluid over the reaction time, and the calculated SI values revealed that the sample pore fluid is closer to its saturation level with respect to Ca^{2+} ion after 10 months in the CS-reacted system. This is believed to be related to the calcite mineral precipitation which occurred in the test environment.

In relation to the influence of CO₂ pressure on the calcite reaction mechanism, the calcite reaction rate increased with increasing injection pressure for both CS and SS conditions (Fig. 5.9), possibly because the higher CO₂ pressure allows the injected CO₂ to more easily penetrate tiny pores, creating a more acidic environment in the aquifer brine. Furthermore, the phase change of CO₂ from sub-critical to super-critical also appears to have a more considerable impact on the calcite reaction rate in the CS formation than the SS formation (Fig. 5.9), and in the CS formation, the calcite reaction rates display much higher values under super-critical conditions compared to sub-critical conditions. This is because, at a particular temperature, free energy associated with the calcite reaction under super-critical conditions is relatively higher than under sub-critical conditions of CO₂, and the diffusion of CO₂ into the rock pore space should therefore be much easier under super-critical conditions. However, no clear phase influence could be seen in the SS formation, probably due to the small amounts of calcite minerals in it.

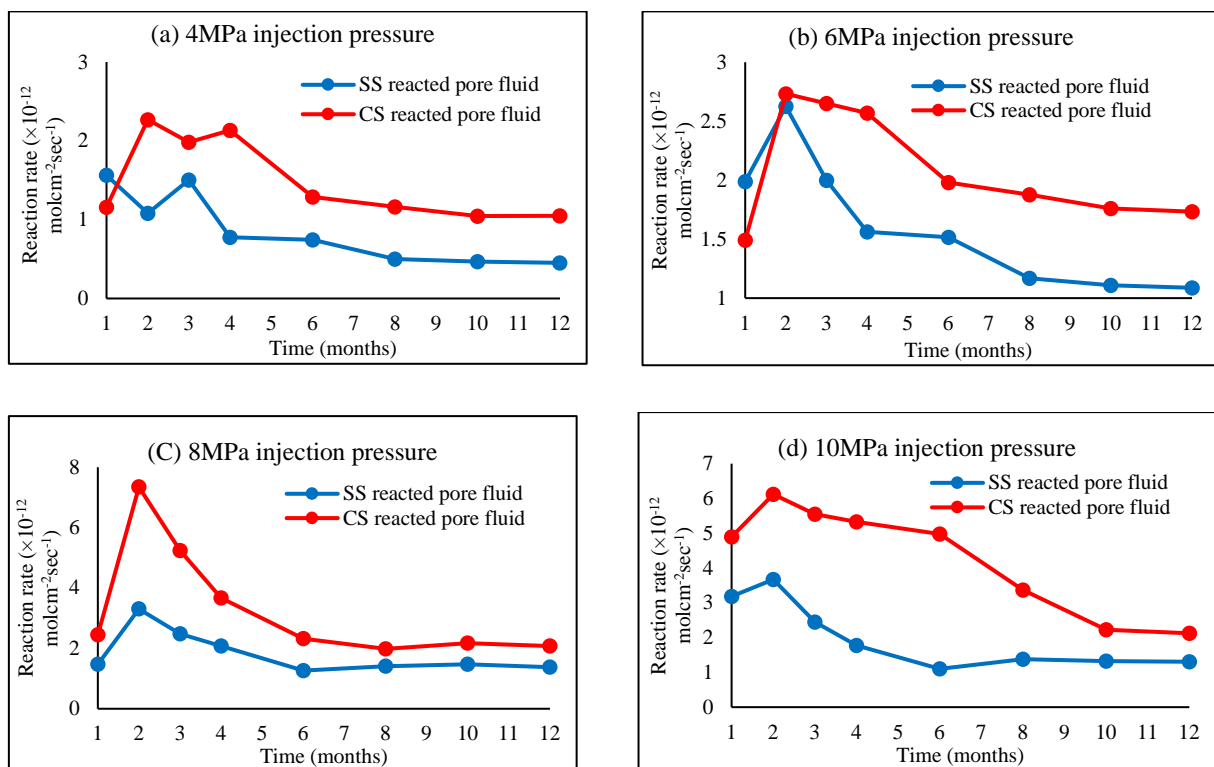


Figure 5.8. Calculated reaction rate of Ca²⁺ as a function of reaction time.

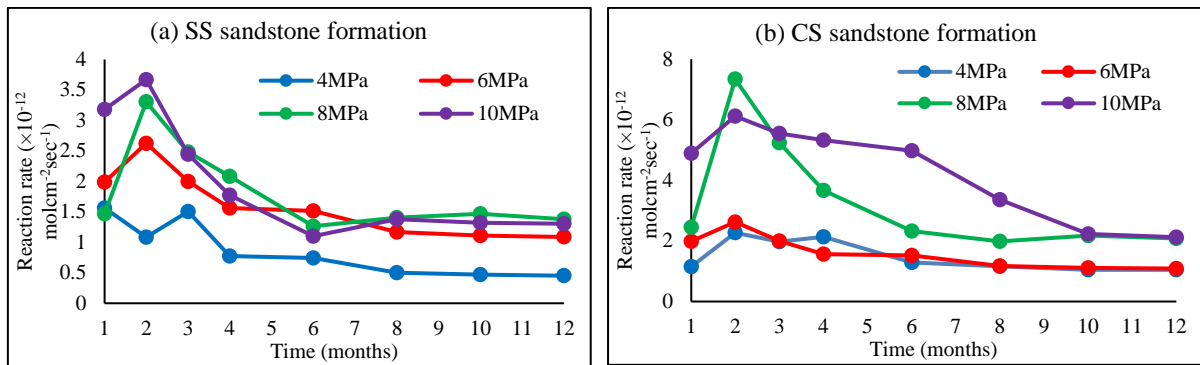


Figure 5.9. Influence of CO₂ partial pressure on Ca^{2+} reaction rate (a) silicate-cemented and (b) carbonate-cemented formation.

As mentioned earlier, apart from calcite, quartz (SiO_2) is one of the main mineral components in the selected sandstone formations, comprising 90% in the SS formation and 64% in the CS formation, respectively. According to chemical thermodynamics, quartz minerals follow zero-order kinetics as follows (Eq. 5.7):

$$R = AK_+ \quad (5.7)$$

where A is the surface area and K_+ is the rate constant.

However, in the CO₂ sequestration environment, these quartz mineral reaction kinetics need to be changed according to the pH dependent behaviour (see Section 5.1.3.1) and it is now clear that the acidic environment resulting from the CO₂ solubility process in aquifer brine has a considerable influence on quartz mineral reaction kinetics. Considering this effect, Eq. 5.7 above can be re-expressed as follows:

$$R = K_+[H^+]^n[1-SI] \quad (5.8)$$

where n is a constant.

Based on Eq. 5.8, the present study evaluated the reaction rate of Si^{4+} ions under the two different cementation conditions (Fig. 5.10). According to Fig. 5.10, the cementation (mineralogy) characteristics of the formation have a significant influence on the quartz mineral reaction rate, and compared to the carbonate-cemented formation (CS), the Si^{4+} ion reaction rate is far greater in the silicate-cemented formation (SS) under the tested injection pressure conditions, possibly due to the higher percentage of quartz mineral in the SS formation than the

CS formation. The presence of greater amounts of quartz minerals increases the potential reaction surface area of quartz mineral in the SS formation, causing enhanced reaction rates. In addition, the different buffer conditions resulting during the solubility mechanism also have a considerable influence on the quartz reaction (see Sections 5.1.3.1 and 5.1.3.2). Interestingly, in the SS formation, after 10 months of reaction, the reaction rate almost stabilised under each injection pressure condition, indicating an equilibrium state of Si^{4+} ion dissolution, which occurred at a much earlier stage in the CS formation (within 4 months). In addition, the effect of CO_2 pressure on the quartz reaction rate was also investigated, and only a slight reduction in the Si^{4+} ion reaction rate with increasing CO_2 pressure was found (see Fig. 5.11).

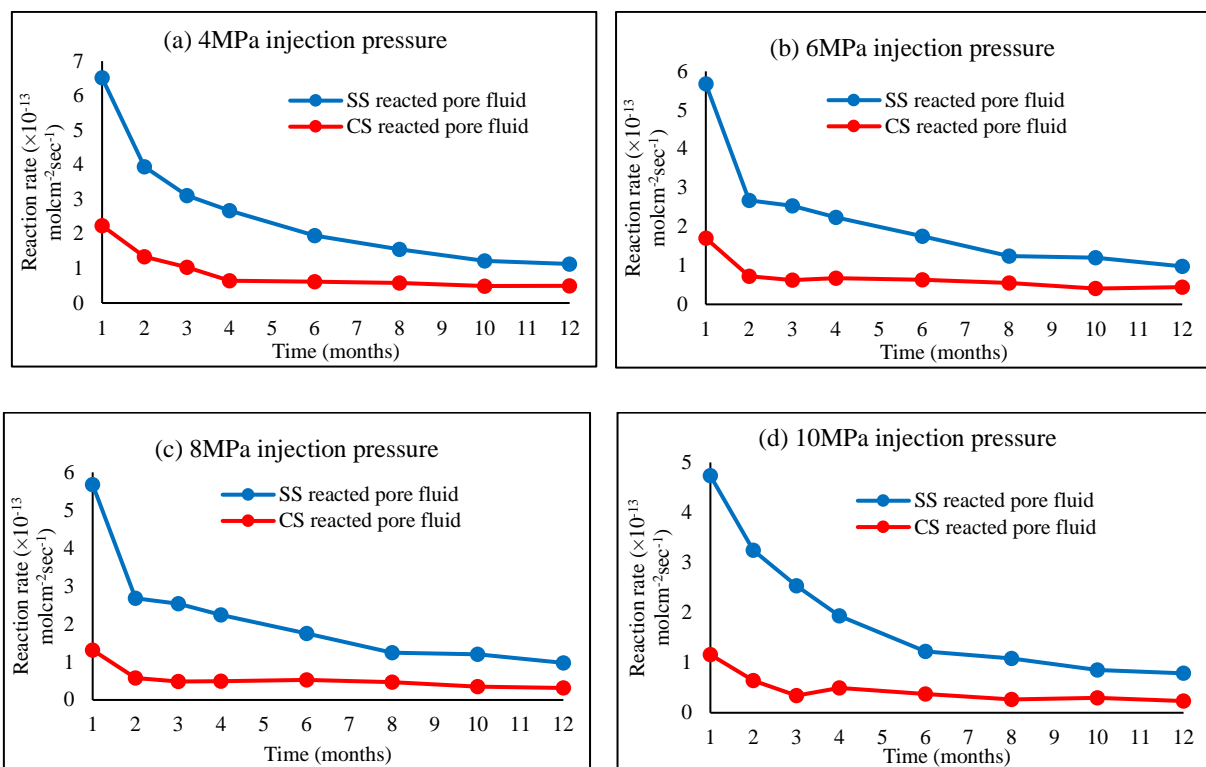


Figure 5.10. Calculated reaction rate of Si^{4+} ion as a function of reaction time.

The Al^{3+} ion reaction kinetics were finally examined to understand the chemical response of kaolinite and muscovite minerals upon exposure to CO_2 . Interestingly, the reaction rate of Al^{3+} ion seems far below the observed reaction rates of Ca^{2+} and Si^{4+} ions. For example, according to the calculated values, the reaction rates of Ca^{2+} and Si^{4+} ions are in the order of 10^{-12} and 10^{-13} , respectively, which are much higher than the Al^{3+} ion reaction rate (in the order of 10^{-16}). However, similar reaction kinetics for Al^{3+} ion reaction were seen in both the CS and SS

formations (Fig. 5.12). Fig. 5.13 shows the influence of CO₂ pressure on the Al³⁺ ion reaction rate. As the figure shows, the reaction rate increases with increasing injection pressure, probably due to the enhanced acidity in the residual fluid.

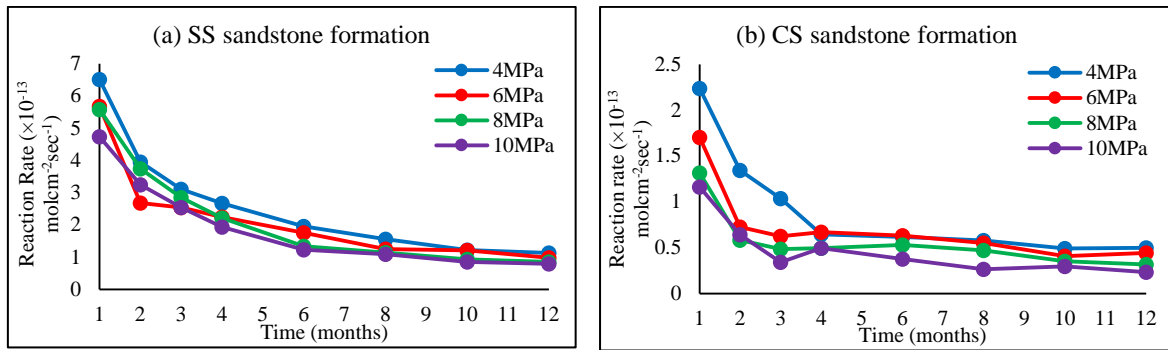


Figure 5.11. Influence of CO₂ partial pressure on Si⁴⁺ reaction rate (a) silicate-cemented and (b) carbonate-cemented formation.

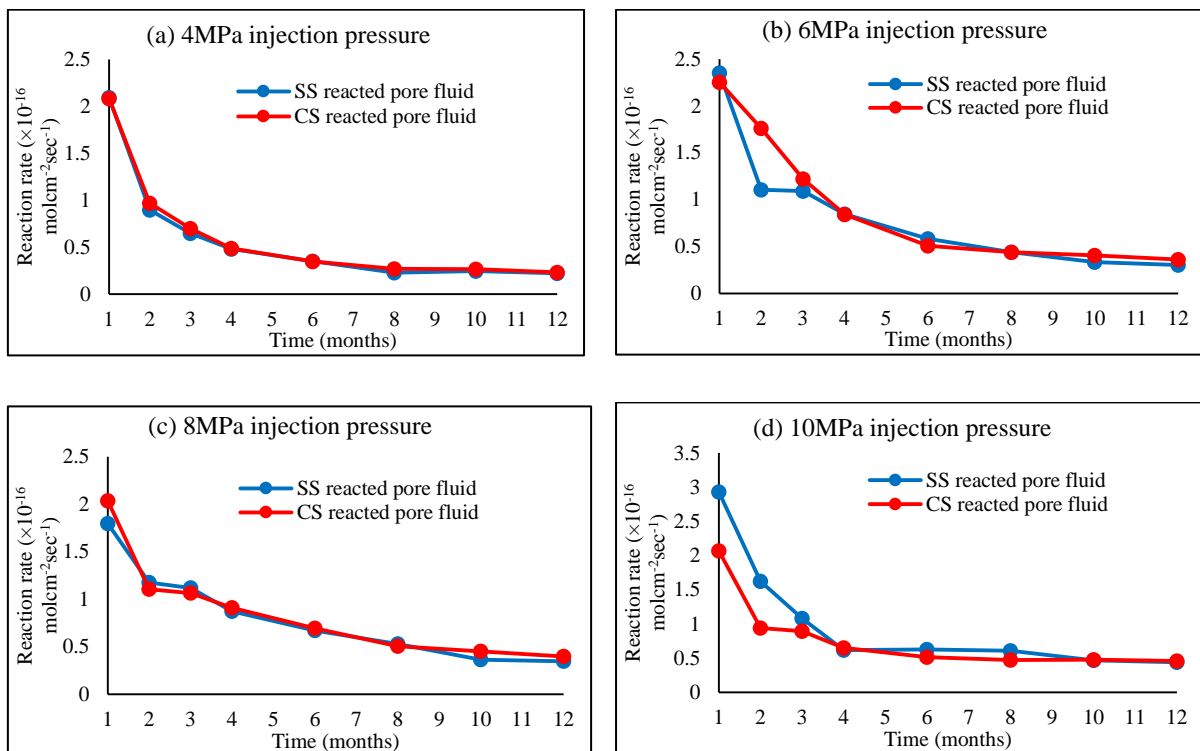


Figure 5.12. Calculated reaction rate of Al³⁺ ion as a function of reaction time.

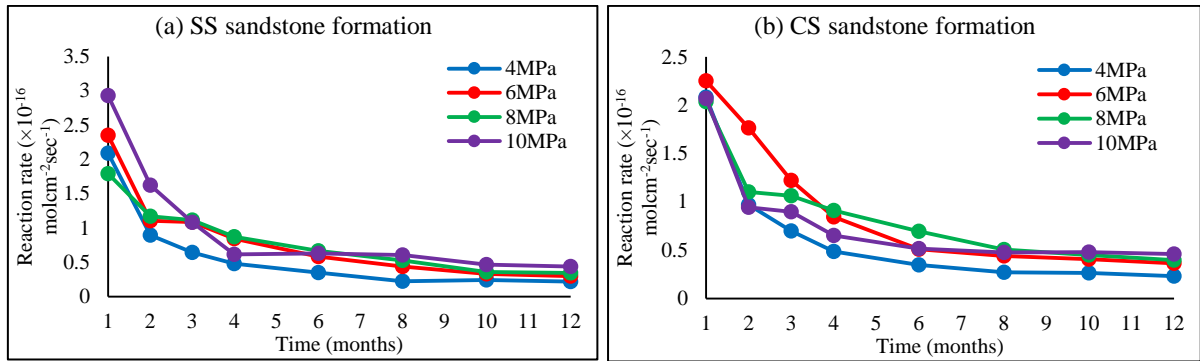


Figure 5.13. Influence of CO₂ partial pressure on kaolinite reaction rate (a) silicate-cemented and (b) carbonate-cemented formation.

In chemical thermodynamics, the dissolution/precipitation of any rock mineral is controlled by the law of mass action (Ball and Nordstrom, 1991). According to this law, a mineral A_aB_b dissolves/precipitates according to the reaction formula:



The thermodynamic equilibrium constant can then be defined as:

$$K_{sp} = \{A\}_{eq}^a \{B\}_{eq}^b \quad (5.10)$$

where, $\{ \}_{eq}$ is the activity of each ion at equilibrium.

The activity of each ion was calculated using Eq. 5.11 below:

$$\{ \} = Y_i C_i \quad (5.11)$$

where Y_i is the activity coefficient and C_i is the concentration.

According to the Debye-Huckel model (Fisher and Levin, 1993), the activity coefficient can be defined as:

$$\log Y_i = -Az_i^2 \sqrt{I} \quad (5.12)$$

where z_i is the valence of the ion i , I is the ionic strength of the ion i and A is a constant which can be calculated using the derivation below.

$$A = 1.82 \times 10^6 (\epsilon T)^{-3/2} \quad (5.13)$$

where, ε is the dielectric constant and T is the temperature.

After finding the thermodynamic equilibrium constant for each rock mineral, the ion activation product was calculated to characterise the equilibrium conditions of each rock mineral based on their SIs under the tested conditions. Generally, the ion activation product of the rock mineral reaction can be expressed as a function of each actual activity level of the corresponding ions and the SI then can be defined based on the ion activation product obtained and the thermodynamic equilibrium constant. Eqs. 5.14 and 5.15 show the expressions of the ion activation product (*IAP*) and saturation index (*SI*), respectively.

$$IPA = \{A\}_{actual}^a \{B\}_{actual}^b \quad (5.14)$$

$$SI = \log_{10} [IAP / K_{sp}] \quad (5.15)$$

The calculated SI values revealed that the residual pore fluid was rarely saturated with rock minerals, apart from calcite minerals. The calculated equilibrium mineral saturation state of the residual fluid with respect to calcite minerals at 35°C is shown in Fig. 5.14. Moreover, the SS and CS formations showed dissimilar equilibrium characteristics with respect to calcite, quartz and kaolinite minerals. In the SS-reacted pore fluid, the calculated mineral saturation state with respect to calcite clearly increases with increasing injection pressure, which is not visible in the CS-reacted pore fluid. Apart from the 8 and 10MPa reacted pressures, the SS formation-reacted pore fluid samples were under-saturated with respect to calcite mineral, and at 10MPa pressure, the pore fluid sample displayed super-saturation after 8 months of reaction, confirming the possibility of calcite precipitation. As shown in Fig. 5.14, the residual pore fluids achieved their equilibrium states with respect to calcite minerals after 12 months of reaction under 8 and 10MPa pressure conditions. However, fluid samples collected from the CS formation after 10 and 12 months revealed that the fluid samples were close to saturation with respect to calcite mineral for all the tested injection pressure conditions. In addition, the calculated mineral saturation state of the residual pore fluid under both conditions showed that kaolinite is near saturation during this reaction period, which was also confirmed by the XRD results. According to the XRD results for the samples reacted with 4 and 8MPa pressures, kaolinite mineral crystallized during the one-year reaction under both conditions. However, despite the high concentration of Si^{4+} ion concentration compared to Al^{3+} ions, since both samples were under-saturated with respect to quartz mineral, precipitation did not occur, because no quartz minerals were super-saturated under both conditions.

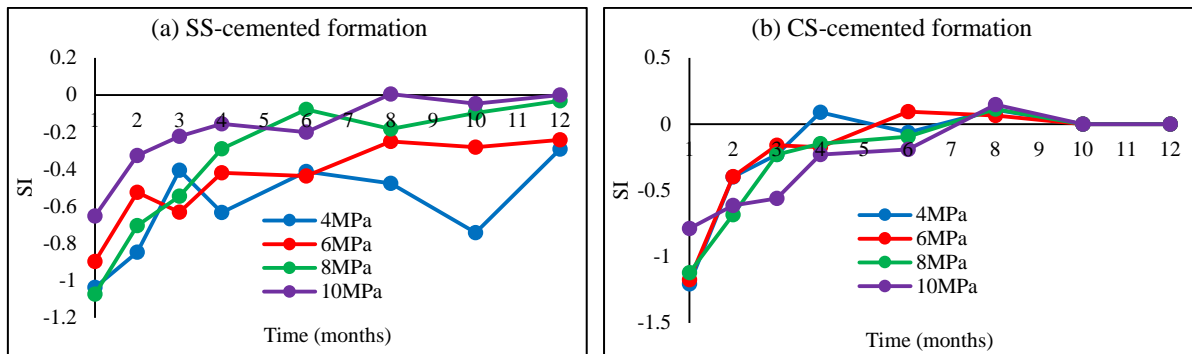


Figure 5.14. Calculated equilibrium mineral saturation state of residual fluid with respect to calcite mineral as a function of time.

It is now clear that due to the different mineralogical compositions, the role of host formation can vary for CO₂ solubility and mineral trapping processes during sequestration, and this can change in terms of chemical response and also the rate of reaction of rock minerals, consequently affecting the hydro-mechanical stability of the host formation. This is the subject of the next section.

5.1.3.4 Mineralogical alteration-induced mechanical behaviour in reservoir rock formations

After characterising the chemical and mineralogical behaviour of the two reservoir rock formations, a series of compressive strength tests was conducted to investigate the mechanical stability of the two formations upon CO₂ injection. This test series was conducted using 12 month-reacted samples, and the strength alteration in them upon CO₂ injection at each injection pressure condition was examined. To combine the observed CO₂ injection-induced chemico-mineral reactions with changes in the formation mechanical properties, the compressive strength variations were then plotted against the resulting weight loss of each sample after 12 months of reaction under the tested pressure conditions (Fig. 5.15).

As depicted in Fig. 5.15, although the strength values of the sandstone samples obtained from the two formations are mostly similar (around 22 MPa in SS and 20 MPa in CS), their response to CO₂ saturation appears to be quite different. Interestingly, the SS formation rock strength exhibits an increasing trend with increasing injection pressure, while the CS formation strength exhibits a reduction trend with increasing injection pressure. The increasing strength characteristics in the SS formation rock with increasing injection pressure may be related to the quartz mineral reaction kinetics discussed in Section 5.1.3.2 above. As discussed in Section

5.1.3.2, quartz minerals are more stable under high injection pressure conditions than in lower pressure conditions, and high compressive strength can therefore be expected in SS formations at higher injection pressures compared to lower injection pressures. For example, the SS formation strength increased from 22.15 to 23.83 MPa with the increase of injection pressure from 4 to 10 MPa. The sample weight reduction of 3.81% decreased to 2.35% when the injection pressure increased from 4 to 10 MPa, which confirms the stability of quartz minerals under high pressure conditions. However, according to the chemical and mineralogical analysis, there is a possibility of other mineral reactions occurring caused by calcite and kaolinite dissolution in the SS formation, which causes a weakening in the rock mass. Although rock mass weakening through calcite and kaolinite dissolution occurs simultaneously in the rock mineral structure in SS- type sandstone, the quartz mineral reaction seems to be dominant. This is to be expected, due to the quartz-abundant mineral structure in the SS sandstone.

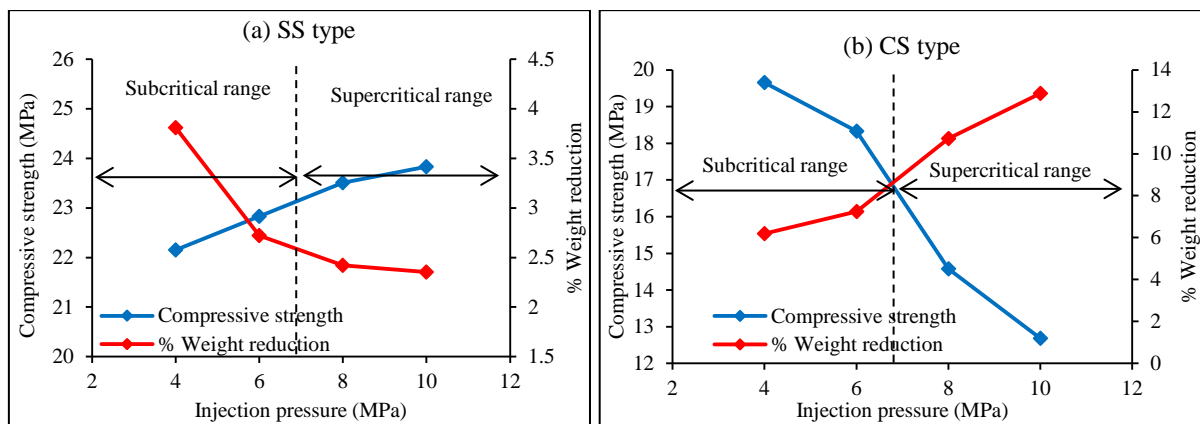


Figure 5.15. Mechanical behaviour of SS- and CS-type sandstone formations.

However, the situation in CS formation sandstone is different, as calcite minerals are dominant and therefore control the mechanical characteristics. This is clearly evident from the compressive strength reduction trend in the CS sandstone with increasing CO₂ injection pressure, as shown in Fig. 5.15. According to Fig. 5.15b, the compressive strength of the CS formation decreases from 19.66 to 13.68 MPa with increasing injection pressure from 4 to 10 MPa. This is because increased CO₂ pressure reduces the pH of the host formation, promoting the dissolution of calcite in the rock formation cementation phase, which weakens the grain-to-grain bonds and therefore the overall rock mass strength. The weight loss values for the CS formation are consistent with the above argument, and a considerable weight reduction at higher injection pressures was observed compared to lower injection pressures (Fig. 5.15b). Based on all the above results, it is clear that the SS formation has a major quartz-cemented mineral

structure compared to the calcite-cemented CS formation, and it therefore has greater potential to withstand the CO₂ sequestration process, in terms of the rock mass strength. This dissimilar strength response occurred as a result of the different mineral reaction kinetics in the two formations. Due to the different mineral reaction kinetics and chemical equilibriums, the weakening which occurs upon CO₂/brine interaction varies between the SS and the CS formation. These contradictory strength responses to SS and CS sandstones upon CO₂ injection reveal that different aquifer rock masses may respond in different ways to the CO₂ sequestration process, depending on their rock mineral structure. Therefore, a definitive conclusion on how CO₂ injection affects the long-term integrity of the CO₂ sequestration process in saline aquifers is impossible.

According to Fig. 5.15, not only CO₂ injection pressure, but also the injecting CO₂ phase condition has a considerable influence on CO₂ injection-induced strength alterations in formation rocks. As Fig. 5.15b shows, increasing the CO₂ injection pressure from 6 to 8 MPa (between which CO₂ phase transition occurs at 7.38 MPa) in the CS formation causes a quite high strength reduction of 20.5%, which is much higher than the strength reductions observed upon 4 to 6 MPa (about a 6.8% reduction) and from 8 to 10MPa (about a 6.2% reduction) increases in CO₂ injection pressures without changing the phase condition. As mentioned earlier, the more chemically-active nature of super-critical CO₂ than sub-critical CO₂ may be the reason for this, as it certainly accelerates the calcite dissolution reactions, creating a greater strength reduction in CS-type sandstone. However, such a clear phase influence could not be seen in the SS sandstone strength alteration. For example, around 2.98% strength increment was observed with a CO₂ pressure increase from 6 to 8 MPa, which is approximately equal to the strength increments observed for the same phase conditions, when an increase of CO₂ pressure from 4 to 6 MPa at sub-critical condition caused around 2.98% increment and an increase of CO₂ pressure from 8 to 10 MPa at super-critical condition caused around 1.39% increment. This is probably because the CO₂ phase has less influence on the quartz reaction kinetic. These results further reveal the greater mechanical stability of SS formations in the CO₂ sequestration process, which does not vary much with the phase transition of CO₂. This is favourable for the safety of the sequestration process.

5.1.4 Conclusions

This study was conducted to obtain a comprehensive understanding of the effect of long-term CO₂ exposure on the chemico-mineralogical structure of saline aquifer rock formations, depending on the rock mineral structure. A combined chemico-mineralogical and mechanical investigation of varyingly CO₂ saturated (1 year of saturation time) silicate-cement (SS) and carbonate-cement (CS) sandstone samples obtained from the Gosford site in the Sydney Basin enabled the following major conclusions to be drawn:

- The existence of a calcite mineral-dominant mineral structure (CS) in the aquifer rock formation causes the formation's chemical and mineral structure to be significantly affected by the injection of CO₂. This was evidenced by the greater pH buffering characteristics and the experimentally-observed chemical reaction kinetics in the calcite- dominant CS formation compared to the quartz-dominant SS formation.
- Although exposure to CO₂ also initiates considerable quartz mineral reactions, these are not as significant as calcite mineral reactions, due to the greater chemical stability of quartz compared to calcite minerals in the CO₂ environment. Apart from these major mineral reactions, some minor re-precipitation of kaolinite minerals also occurred in both sandstone formations upon CO₂ injection, due to the possible dissolution of muscovite minerals present in the rock mineral structure. However, these were at much lower rates and the effect was therefore insignificant.
- The rock mineral alterations in deep saline aquifers upon CO₂ injection have a significant influence on the strength characteristics of the reservoir rock mass, bringing an additional risk to the long-term integrity of the CO₂ sequestration process. However, these strength property alterations are clearly dependent on the aquifer rock mass mineral structure. For example, the CS formation was subjected to much greater strength property changes upon exposure to CO₂ compared to the SS formation, due to the significant calcite dissolution process compared to the quartz dissolution/precipitation process in the SS formation upon interaction with CO₂.
- Interestingly, CO₂ injection may cause a strength gain in aquifer rock mass with SS-type sandstone, due to quartz precipitation upon interaction with CO₂. In contrast, the aquifer rock mass formation made with CS-type sandstone was mostly subject to

mechanical weakening due to the dissolution of the cementation phase (calcite) among the grain-to- grain contacts upon CO₂ interaction.

- The injecting CO₂ properties also significantly affect the CO₂-brine-rock mineral interaction, creating mechanical property alterations in aquifer rock mass formations, and increasing the injecting CO₂ pressure significantly enhances the alterations due to the highly acidic environment created by the enhanced solubility of CO₂ in brine.
- In addition to the injecting CO₂ pressure, the phase of CO₂ also affects the CO₂ injection- induced mechanical property changes in reservoir rock, depending on the formation's mineral structure. For example, the influence of CO₂ phase change from sub-critical to super-critical condition is more significant for the rock mineral and associated mechanical property changes in CS sandstone than SS sandstone.
- All of these facts show the stable characteristics of SS formations compared to CS formations under the reservoir conditions present in deep saline aquifers. Based on these results, it can be concluded that the SS formation in the Gosford basin has more suitable characteristics for CO₂ sequestration than the CS formation in terms of strength and chemical stability upon exposure to a CO₂ environment.

5.1.5 References

1. Alkattan M, Oelkers EH, Dandurand JL, Schott J. An experimental study of calcite and limestone dissolution rates as a function of pH from -1 to 3 and temperature from 25 to 80°C. *Chemical Geology* 1998; 151: 199-214.
2. Bachu S, Bennion B. Effects of in-situ conditions on relative permeability characteristics of CO₂-brine systems. *Environmental Geology* 2008; 54: 1707-1722.
3. Ball JW, Nordstrom DK. WATEQ4F User's manual with revised thermodynamic data base and test cases for calculating speciation of major, trace and redox elements in natural waters. USGS Open-File Report 1991; 90: 129-185.
4. Bevan J, Savage D. The effect of organic acids on the dissolution of K-feldspar under conditions relevant to burial diagenesis. *Mineralogical Magazine* 1989; 53: 415-425.
5. Brown ET. Rock characterisation, testing and monitoring. *International Society of Rock Mechanics* 1981, 23; 81-85.
6. Czernichowski-Lauriol I, Sanjuan B, Rochelle C, Bateman K, Pearce J, Blackwell P. Analysis of the geochemical aspects of the underground disposal of CO₂. *Deep Injection Disposal of Hazardous and Industrial Wastes, Scientific and Engineering Aspects Academic Press* 1996; 26: 565-583.
7. Conolly JR. Models for Triassic deposition in the Sydney Basin. *Journal of the Geological Society of Australia* 1969; 2: 209-223.
8. Ellis AJ, Golding RM. The solubility of carbon dioxide above 100°C in water and in sodium chloride solutions. *American Journal of Science* 1963; 261: 47-60.
9. Enick RM, Klara SM. CO₂ solubility in water and brine under reservoir conditions. *Chemical Engineering Communications* 1990; 90: 23-33.
10. Fisher ME, Levin Y. Criticality in ionic fluids: Debye-Hückel theory, Bjerrum, and beyond. *Physical Review Letters* 1993; 71(23): 3826-3841.
11. Garrels RM, Christ CL. *Solutions, minerals, and equilibria*. Freeman-Cooper, San Francisco 1965, 450-467.
12. Gunter WD, Perkins EH, Hutcheon I. Aquifer disposal of acid gases: modelling of water-rock reactions for trapping of acid wastes. *Applied Geochemistry* 2000; 15: 1085-1095.

13. Kaszuba JP, Janecky DR, Snow MG. Carbon dioxide reaction processes in a model brine aquifer at 200°C and 200bars: implications for geologic sequestration of carbon. *Applied Geochemistry* 2003; 18:1065-1080.
14. Koide HG, Tazaki Y, Noguchi M. Subterranean containment and long-term storage of carbon dioxide in unused aquifers and in depleted natural gas reservoirs. *Energy Conversion and Management* 1995; 33: 619-626.
15. Law DHS, Bachu S. Hydrogeological and numerical analysis of CO₂ disposal in deep aquifers in the Alberta sedimentary basin. *Energy Conversion and Management* 1996; 37: 1167-1174.
16. Leung DYC, Caramanna G, Maroto-Valer MM. An overview of current status of carbon dioxide capture and storage technologies. *Renewable and Sustainable Energy Reviews* 2014; 39: 426-443.
17. Lin H, Fujii T, Takisawa R, Takahashi T, Hashida T. Experimental evaluation of interactions in supercritical CO₂/water/rock minerals system under geologic CO₂ sequestration conditions. *Journal of Materials Science* 2008; 43(7): 2307-2315.
18. Liu L, Suto Y, Bignall G, Yamasaki N, Hashida T. CO₂ injection to granite and sandstone in experimental rock/hot water systems. *Energy Conversion and Management* 2003; 44(9): 1399-1410.
19. Marbler H, Erickson KP, Schmidt M, Lempp C, Pollmann H. Geomechanical and geochemical effects on sandstones caused by the reaction with supercritical CO₂: an experimental approach to in situ conditions in deep geological reservoirs. *Environmental Earth Science* 2013; 69: 1981-1998.
20. MaDonnell KL. Depositional environments of the Triassic Gosford formation, Sydney basin. *Journal of the Geological Society of Australia* 1973; 21: 107-132.
21. Moore J, Adams M, Allis R, Lutz S, Rauzi S. Mineralogical and geochemical consequences of the long-term presence of CO₂ in natural reservoirs: An example from the Springerville-St. Johns field, Arizona, and New Mexico, U. S. A. *Chemical Geology* 2005; 217: 365-385.
22. Perkins EH, Gunter WD. Aquifer disposal of CO₂-rich greenhouse gases: Modelling of water-rock reaction paths in a siliciclastic aquifer. In: *Proceedings of the 8th International Symposium on Water-Rock Interaction -WR1-8*, Balkema, Rotterdam 1995: 895-898.

23. Perera MSA, Ranjith PG, Viete DR. Effects of gaseous and super-critical carbon dioxide saturation on the mechanical properties of bituminous coal from the Southern Sydney Basin. *Applied Energy* 2013; 110: 73-81.
24. Pokrovsky OS, Golubev SV, Schott J, Castillo A. Calcite, dolomite and magnesite dissolution kinetics in aqueous solutions at acid to circumneutral pH, 25 to 150°C and 1 to 55 atm pCO₂: new constraints on CO₂ sequestration in sedimentary basins. *Chemical Geology* 2009; 265(1): 20-32.
25. Ranjith PG, Perera MSA, Khan E. A study of safe CO₂ storage capacity in saline aquifers: a numerical study. *International Journal of Energy Research* 2013; 37: 189-199.
26. Rathnaweera TD, Ranjith PG, Perera MSA, Lashin A, Al Arifi N. Non-linear stress–strain behaviour of reservoir rock under brine saturation: An experimental study. *Measurement* 2015a; 71: 56-72.
27. Rathnaweera TD, Ranjith PG, Perera MSA, Haque A, Lashin A, Al Arifi N. et al. CO₂-induced mechanical behaviour of Hawkesbury sandstone in the Gosford basin: An experimental study. *Materials Science and Engineering-A* 2015b; 64: 123-137.
28. Rochelle CA, Czernichowski-Lauriol I, Milodowski AE. The impact of chemical reactions on CO₂ storage in geological formations: a brief review. Geological Society, London, Special Publications 2004; 233(1): 87-106.
29. Stewart EB, Munjal RK. The solubility of carbon dioxide in pure water, synthetic sea water and synthetic sea-water concentrates at -5 to 25°C and 10 to 45atm pressure. *Journal of Chemical and Engineering Data* 1970; 1591: 67-71.
30. Ward CR. Sedimentation in the Narrabeen group, southern Sydney basin, New South Wales. *Journal of the Geological Society of Australia* 1972; 19: 393-409.
31. White CU, Strazisar BR, Granite EJ, Hoffman JS, Pennline HW. Separation and Capture of CO₂ from Large Stationary Sources and Sequestration in Geological Formations- Coalbeds and Deep Saline Aquifers, *Journal of the Air & Waste Management Association* 2003; 53(6): 645-715.
32. Wiebe R. The binary system carbon dioxide-water under pressure. *Chemical Reviews* 1941; 29: 475-481.

33. Wiebe R, Gaddy VL. The solubility of carbon dioxide in water at various temperatures from 12 to 40°C and at pressures to 500 atmospheres. Critical phenomena. Journal of the American Chemical Society 1940; 62: 815-817.

5.2 Summary of Chapter 5

In this chapter, the behaviour of silicate- and carbonate-cemented reservoir rock was experimentally investigated by conducting comprehensive chemical, mineralogical and mechanical tests. In general, the investigated sandstones from the Sydney Basin, which have potential for the storage of CO₂, display different resistance to chemical, mineralogical and mechanical alterations by brine and CO₂ due to differences in their mineral composition.

According to the results, significant calcite mineral dissolution is observed in the carbonate-cemented formation upon exposure to CO₂. Similarly, calcite dissolution is also observed in the silicate-cemented formation, but the reaction is much lower than that for the carbonate-cemented formation. In addition, minor dissolution of quartz minerals and secondary precipitation of kaolinite minerals are observed in both formations. Interestingly, the quartz mineral reaction is minor compared to the reaction of calcite minerals in both formations, which confirms the chemical stability of quartz compared to calcite in the CO₂ sequestration environment. According to chemical analysis, higher pH conditions exist in the carbonate-cemented formation than the silicate-cemented formation, probably due to the dissolution reaction of calcite, which causes the increased alkalinity of the system. In addition, the effects of CO₂ injection pressure and CO₂ phase change on the chemical behaviour of reservoir rock were also investigated. The results show that the dissolution/precipitation reactions of rock minerals increase with increasing CO₂ injection pressures for both formations, mainly due to the enhanced solubility of CO₂ in brine with increased injection pressure. Moreover, CO₂ phase change has a more significant influence on the alteration of the carbonate-cemented formation than the silicate-cemented formation.

According to the results of strength tests, CO₂ interaction creates considerable mechanical weakening in the carbonate-cemented formation compared to the silicate-cemented formation, due to the weaker mineral grain structure in the carbonate-cemented formation. The average strength of the carbonate-cemented formation decreases with increasing injection pressure, while increased injection pressure causes the strength to increase in the silicate-cemented formation. Therefore, in a CO₂ sequestration environment, silicate-cemented formations have more stable chemical and mechanical characteristics than silicate-cemented formations.

CHAPTER 6

Experimental Investigation of Process-enhancement Technologies in Deep Saline CO₂ Storage

Declaration

One publication is included in Chapter 6 and the details of the publication are given below.

Chapter 6.1

Rathnaweera TD, Ranjith PG, Perera MSA, Haque A. Influence of CO₂-brine co-injection on CO₂ storage capacity enhancement in deep saline aquifers: An experimental study on Hawkesbury sandstone formation. *Energy and Fuel* 2016; 30: 4229-4243.

Declaration for Thesis Chapter 6

Declaration by candidate

Monash University

In the case of Chapter 6 the nature and extent of my contribution to the work was the following:

Nature of Contribution	Extent of contribution (%)
Initiation, key ideas, experimental work, analysis of data and writing up	85

The following co-authors contributed to the work. Co-authors who are students at Monash University must also indicate the extent of their contribution in percentage terms:

Name	Nature of contribution	Extent of contribution (%) for student co-authors only
Ranjith PG	Key ideas, reviewing and editing the manuscript	N/A
Perera MSA	Reviewing and editing the manuscript	N/A
Haque A	Reviewing and editing the manuscript	N/A

The undersigned hereby certify that the above declaration correctly reflects the nature and extent of the candidate's and co-authors' contributions to this work*.

Candidate's
Signature

		Date 22/07/16
--	--	------------------

Main
Supervisor's
Signature

		Date 22/07/16
--	--	------------------

*Note: Where the responsible author is not the candidate's main supervisor, the main supervisor should consult with the responsible author to agree on the respective contributions of the authors.

6 Experimental Investigation of Process-enhancement Technologies in Deep Saline Storage

6.1 Influence of CO₂-brine co-injection on deep saline storage

As a result of growing awareness of the advantages of deep saline CO₂ sequestration, extensive research is being carried out on the physical and chemical behaviour of formations throughout the world. However, research relating to technical and economic feasibility and improvement of the existing injection, storage, and monitoring technologies has been limited. Geological sites for CO₂ sequestration in deep saline aquifers must be carefully selected and generally require appropriate permeability, porosity and thickness of the reservoir rock and a cap rock with good sealing capacity. Of these features, adequate permeability in the reservoir formation is a critical issue in any deep saline sequestration process and fluid-based hydraulic fracturing has been introduced to enhance permeability in tight geological formations. However, since this practice raises many environmental issues, better alternatives are being tested in the field, among which the use of simultaneous injection of CO₂ and brine is a comparatively novel but effective method to enhance the storage process. This technique also enables field projects to reduce the extensive time required for CO₂ solubility in brine. Therefore, the influence of simultaneous injection of CO₂ and brine on sequestration in deep saline aquifers is investigated in this section of the thesis for the Hawkesbury sandstone formation. The following published journal paper reports on this part of the study.

Influence of CO₂–Brine Co-injection on CO₂ Storage Capacity Enhancement in Deep Saline Aquifers: An Experimental Study on Hawkesbury Sandstone Formation

T. D. Rathnaweera, P. G. Ranjith,* M. S. A. Perera, and A. Haque

Department of Civil Engineering, Monash University, Building 60, Melbourne, Victoria 3800, Australia

ABSTRACT: This study was conducted to identify a potential CO₂-storage-capacity-enhancement technique: enhancement of CO₂ storage through co-injection or the simultaneous injection of CO₂ and brine into saline aquifers. A series of triaxial permeability tests on brine-saturated sandstone samples for a range of injection pressures (4–10 MPa) under different confining pressures (20–35 MPa) was performed at 35 °C constant temperature. To clearly identify the sequestration-enhancement capability of the proposed novel method, conventional CO₂ injection (injection of only CO₂ into brine-saturated rock) was also carried out under the same test conditions. Both tests were subjected to comprehensive chemical analyses to evaluate the alteration of CO₂ solubility in brine caused by the proposed method. CO₂ flow behavior under conventional CO₂ injection may convert from two- to single-phase flow over time around the injection point, as a result of forced brine migration. This may create a suddenly increased advective flux sometime after injection, which negatively affects the carbonation efficiency and eventually the mineral trapping process. Such issues can be eliminated by the proposed CO₂–brine co-injection technique, because it offers significantly slower flow rates under the continuously available two-phase condition in the system. According to the results, the resulting slower flow rates under the co-injection process further enhance the mineral trapping process, allowing for additional time to activate the dissolution reaction compared to the conventional injection process. This will enable field projects to reduce the extensive time required for CO₂ solubility in brine. Importantly, the solubility enhancement resulting from the proposed co-injection is much greater for supercritical CO₂. This demonstrates the better performance expected of the proposed novel co-injection process under field conditions, because CO₂ generally exists in its supercritical state in deep saline aquifers. In addition, the results show that the resulting H⁺ ion concentration increases with an increasing confining pressure, confirming the positive influence of aquifer depth on solubility under any injection conditions. Interestingly, this depth effect on solubility enhancement appears to be greater for co-injection than conventional injection. The proposed co-injection technique is also favorable for the long-term safety of the process, because the associated reduced CO₂ relative permeability in saline aquifers also offers more opportunity for hydrodynamic trapping mechanisms.

1. INTRODUCTION

CO₂ geo-sequestration is an effective atmospheric CO₂ mitigation method,¹ and the injection of CO₂ at the largest possible rates using the smallest number of wells has recently been identified as an economically feasible option for CO₂ sequestration in deep saline aquifers.² However, the solubility of CO₂ in brine and the associated unpredictable brine and CO₂ relative permeability variations in the aquifer lead to the creation of unpredictable CO₂ injection and storage rates during the sequestration process. Precise knowledge of the multiphase flow behavior of brine and CO₂ in reservoir rock is therefore required to achieve prospective storage targets and to make appropriate operational decisions on CO₂ sequestration in deep saline aquifers.

With respect to brine–CO₂ multiphase flow behavior in deep saline aquifers during CO₂ sequestration, the concept of relative permeability plays an important role, because it offers quantitative measurement of the spatial and temporal distribution and migration of CO₂ in the aquifer. Understanding the behavior of CO₂ in the subsurface structure during the injection stage is also required to maintain the CO₂ leakage risk at a minimal level, which is one of the critical concerns in any sequestration project in terms of long-term stability. According to Juanes et al.,³ brine–CO₂ multiphase flow behavior in the reservoir has a critical influence on its capillary/residual trapping

mechanisms, which, in turn, affect the effectiveness of the other sequestration mechanisms. Furthermore, brine–CO₂ relative permeability measurements are also important in estimating and optimizing the reservoir storage capacity, because they govern the solubility trapping process.

To date, although the importance of multiphase flow measurements for reservoir performance in oil recovery has been well-documented, very few laboratory studies have been conducted on CO₂–brine systems for saline aquifers.^{4–12} Apart from experimental relative permeability studies, many numerical modeling studies have been reported, most of which show the important role played by multiphase flow behavior in CO₂ sequestration.^{3,13–18}

All of these experimental and numerical studies show the importance of precise identification of multiphase flow behavior on CO₂ sequestration in deep geological formations, including saline aquifers. However, the CO₂ storage process in saline aquifers occurs at quite a slow rate as a result of the associated slow interaction among brine–CO₂ and rock minerals, and the slow solubility of injected CO₂ in brine is one of the major

Received: January 21, 2016

Revised: April 10, 2016

Published: April 13, 2016

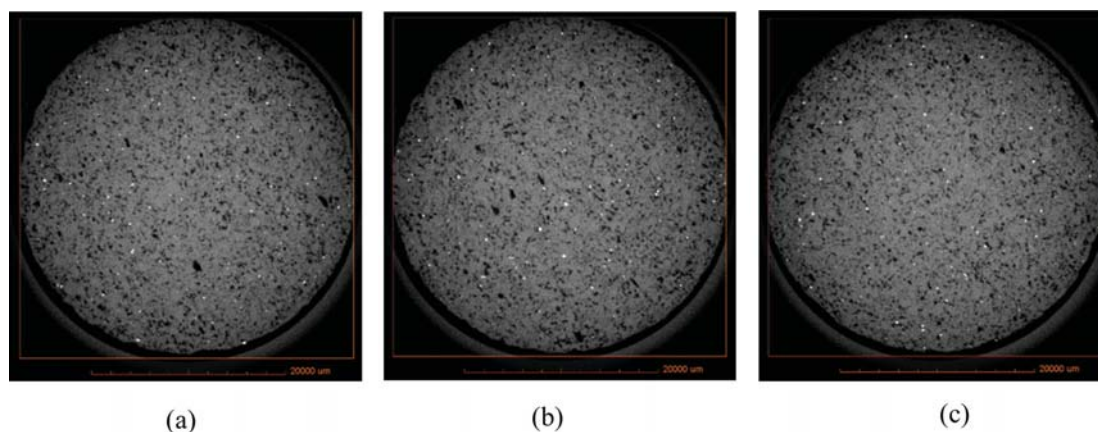


Figure 1. Results of CT scanning along the sample length: (a) top surface, (b) middle section, and (c) bottom surface.

drawbacks. Research studies have therefore been initiated to determine possible reaction-enhancement techniques, including that by Juanes et al.³ These researchers showed how the performance of the CO₂ sequestration process can be improved by injecting alternating slugs of water and CO₂ into the aquifer. According to their results, the injection of water slugs alternating with CO₂ injection has the ability to enhance sequestration, because the injecting water force causes the breaking up of large connected CO₂ plumes. This enhances the CO₂ trapping process by spreading out accumulated CO₂ at the top of the aquifer. However, according to Eke et al.,¹⁹ the use of brine for pure water has the ability to reduce the buoyancy force, the driving force for CO₂ back migration toward the surface, because CO₂ dissolved in saline water or brine creates much denser carbonic liquid formation compared to pure water. In addition, as stated by Eke et al.,¹⁹ a major drawback with CO₂–water co-injection is that it requires the injection of significant volumes of water into the formation, and unfortunately, that requires significant amounts of energy and money. More importantly, injecting the world's most precious resource “water” into deep saline formations is not a good option. This makes CO₂–brine co-injection a promising option for the enhancement of deep saline sequestration. Therefore, this novel approach was tested in the present study, by simultaneously injecting CO₂ and brine into reservoir rock samples under *in situ* stress conditions. Such CO₂–brine injection creates multiphase flow behavior inside the rock mass. The aim of this study is therefore to identify the potential CO₂-storage-capacity-enhancement mechanism in saline aquifers by applying current knowledge of CO₂–brine multiphase flow behavior in aquifers.

2. EXPERIMENTAL SECTION

2.1. Sample Preparation. Hawkesbury sandstone blocks, belonging to the Triassic geological age, were obtained from the Sydney basin, New South Wales, Australia. The mineralogy of the testing material was obtained by conducting X-ray diffraction (XRD) analysis. According to the analysis, the mineralogical structure of the tested sandstone is around 90% quartz, 6% calcite, 2% kaolinite, 1% muscovite, and <1% other clay minerals, and the main cementing phases are quartz, calcite, and kaolinite. Homogeneous sandstone blocks were first carefully selected on the basis of visual inspection (macroscopic homogeneity), and computed tomography (CT) scanning was used to ensure the microlevel homogeneity, including pore distribution, grain size, mineral distribution, and grain arrangement (Figure 1). According to the results of CT scanning, it is quite reasonable to assume a homogeneous pore arrangement in and among the tested samples. The selected blocks were

then cored into 38 mm diameter and 76 mm high samples, and finally, the sample ends were ground. The prepared samples were first oven-dried at 35 °C for 48 h (this low-temperature condition was selected to avoid microstructural damage). A total of 28 prepared samples were then placed in brine-filled (salinity: 15% NaCl by weight) desiccators and subjected to brine saturation for 2 weeks under vacuum to ensure maximum saturation, and the weights of the samples were measured regularly to ensure the steady-state full saturation condition until a constant mass was reached. The specimens were removed from the desiccators just before the tests. Later, the same NaCl concentration was used for the brine injection processes under single- and two-phase conditions.

2.2. Relative Permeability Tests. A series of steady-state permeability tests was conducted using the high-pressure triaxial setup available in the Deep Earth Energy Laboratory at Monash University under drained conditions.²⁰ The newly developed high-pressure triaxial setup used in this study²¹ and its schematic diagram are shown in Figure 2.

After the sample is placed in the pressure cell (details of the procedure can be found in ref 20), the cell was filled with oil and the required confining pressure was applied using a syringe pump (see Figure 2). The cell temperature was then adjusted to 35 °C (a typical reservoir temperature condition) using the temperature control unit and maintained for 24 h to ensure temperature equilibrium. Finally, CO₂ and brine co-injection was initiated.

The injection unit consists of two pumps connected with a set of needle valves and pressure gauges. As shown in Figure 3, a compressed air-based Haskel MS-36 liquid pump was used to inject brine and a syringe pump (Teledyne Isco, model 260D) was used to inject CO₂. This configuration provides continuous fluid delivery, and the refilling and delivery of each pump are automatically controlled by two controllers attached to each pump. Before entering the sample, the injecting CO₂ and brine were brought to the experimental temperature condition of 35 °C using the attached heating system inside the individual units, and this 35 °C temperature condition was maintained during the whole injection period (see Figure 4).

The injection was performed by simultaneously injecting CO₂ and brine into the sample under controlled pressure conditions (see Figures 2 and 3). The CO₂ pressure was first set to the required injection pressure, and the same injection pressure was then assigned to the brine. After individually obtaining the required injection pressures, the CO₂ (N/V 1) and brine (N/V 2) inlet valves (see Figure 3) were opened and kept open to achieve pressure equilibrium before the main upstream valve was opened (N/V 3), to allow for CO₂–brine to move toward the sample. Downstream CO₂ and brine flow rates were recorded until the steady-state condition was reached. The flushed-out brine was collected using a Dreshel bottle to separate CO₂ and brine in the effluent, and the corresponding effluent brine weight over time was recorded using a precision balance [an EHB + 3000 g × 0.01 g (non-trade)]. The results were then used to calculate the brine release rates. Similarly, the separate CO₂ flow rate was also measured using a digital flow meter (a digital gas

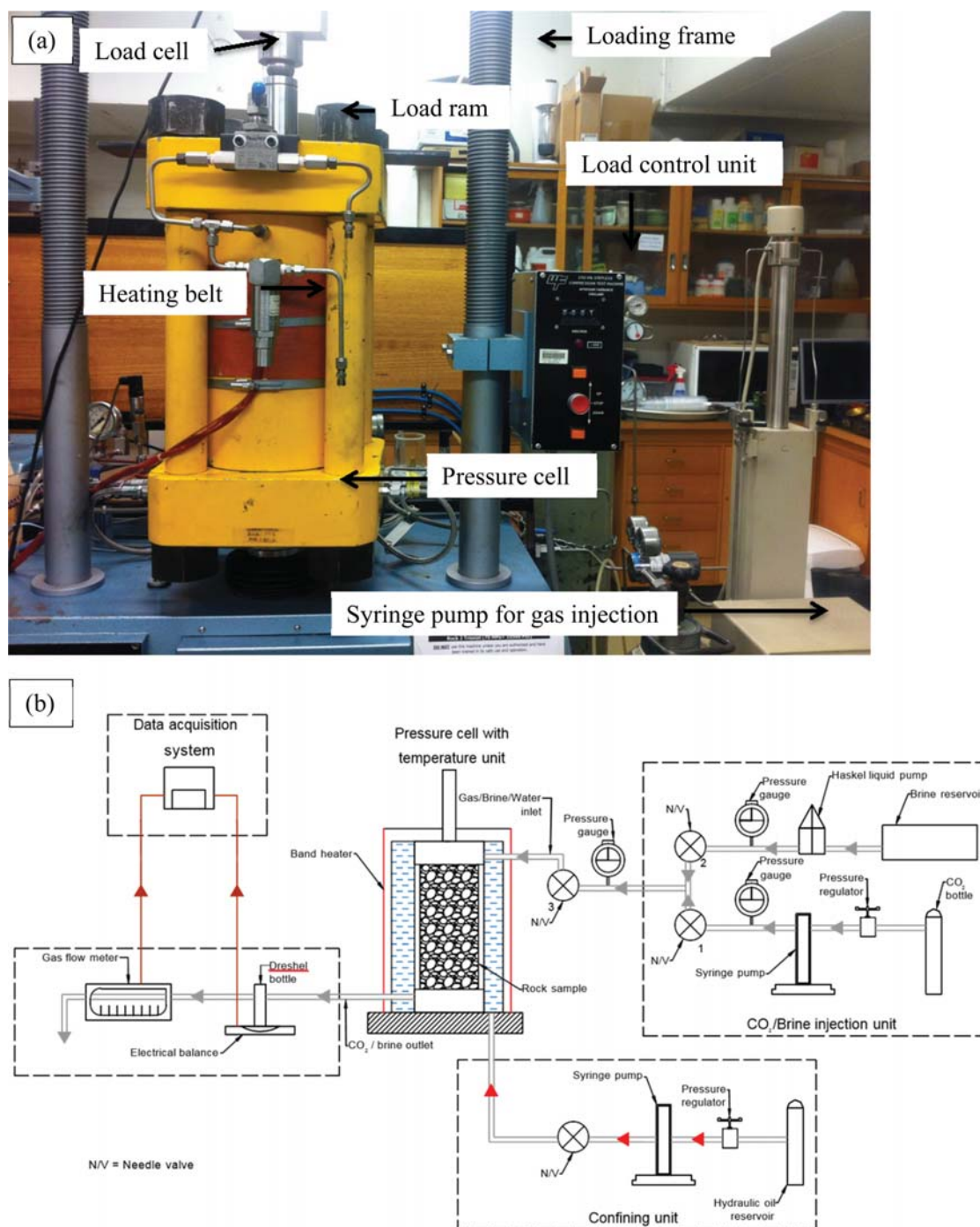


Figure 2. (a) Newly developed high-pressure triaxial setup used in this study²¹ and (b) its schematic representation.

flow meter type XFM-17 with a capacity of 1000 mL/min). The confining and CO₂–brine injection pressure conditions are shown in Table 1. The CO₂ and brine flow rates were used to calculate the effective permeability values for co-injection. Finally, on the basis of the calculated effective permeability values, relative permeability measurements were undertaken, as described in section 3.

To calculate the relative permeability characteristics of the selected sandstone, a separate set of dry reservoir rock samples was tested under single-phase conditions by separately injecting CO₂ and brine, under the same injection conditions. Apart from these two types of tests, to compare the flow characteristics of conventional injection to co-injection, a series of single-phase CO₂ injections on brine-saturated samples was

also conducted under the same test conditions. In all of the tests, the downstream CO₂ and brine flow rates were recorded as described above using a precision balance and a digital flow meter, and the results were then used to calculate effective permeability using the conventional injection process. Finally, the flow rates and effective permeability values obtained from conventional injection and co-injection were compared to identify the most effective process for CO₂ sequestration (single-phase CO₂ injection into dry samples was performed to find the single-phase permeability parameters required for the relative permeability calculations). Table 2 shows the downstream flow rates for conventional and co-injection techniques with their standard deviations for 20 and 30 MPa confining pressure conditions.

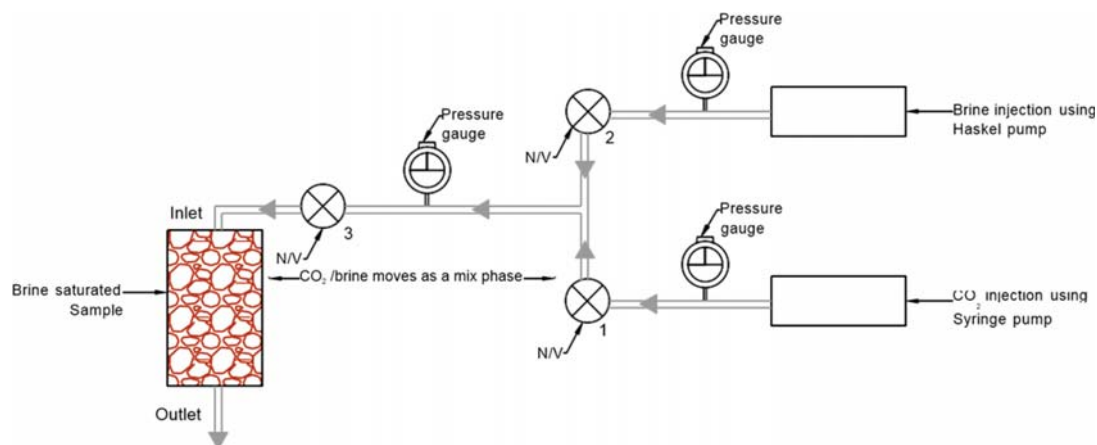


Figure 3. Schematic diagram of the injection unit.

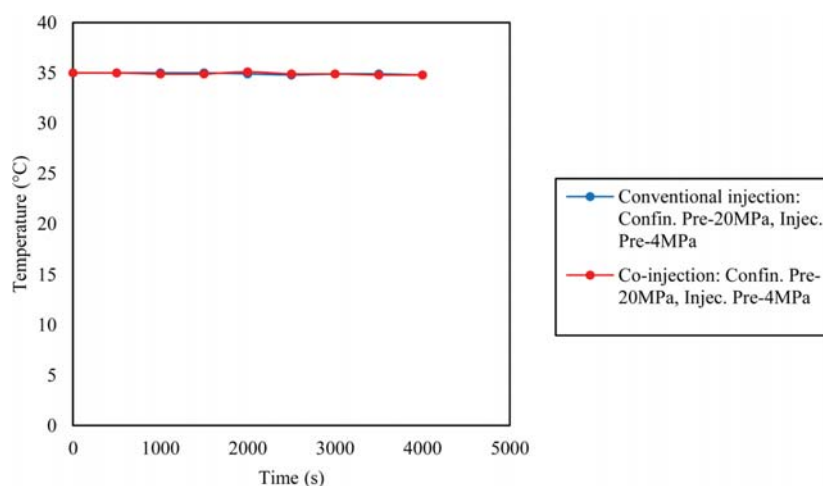


Figure 4. Temperature variation during the experiment under conventional and co-injection cases.

Table 1. Confining and CO₂–Brine Injection Pressure Conditions

confining pressure (MPa)	injection pressure (MPa)													
	test 1		test 2		test 3		test 4		test 5		test 6		test 7	
	CO ₂	brine	CO ₂	brine	CO ₂	brine	CO ₂	brine	CO ₂	brine	CO ₂	brine	CO ₂	brine
20	4	4	5	5	6	6	7	7	8	8	9	9	10	10
25	4	4	5	5	6	6	7	7	8	8	9	9	10	10
30	4	4	5	5	6	6	7	7	8	8	9	9	10	10
35	4	4	5	5	6	6	7	7	8	8	9	9	10	10

3. RESULTS AND DISCUSSION

3.1. Application of Darcy's Law and Klinkenberg Correction.

The downstream flow rate versus injection pressure graphs for all three types of tests, single-phase CO₂ and brine injection into dry samples, conventional CO₂ injection into brine-saturated samples, and CO₂–brine co-injection into brine-saturated samples, are shown in Figure 5. According to Figure 5, the downstream flow rate under each test condition follows a laminar flow behavior, exhibiting a linear variation between the flow rate and pressure. This implies the applicability of Darcy's law for each test condition considered. However, it should be noted that the applicability of Darcy's law for multiphase conditions was based on the assumption that each individual

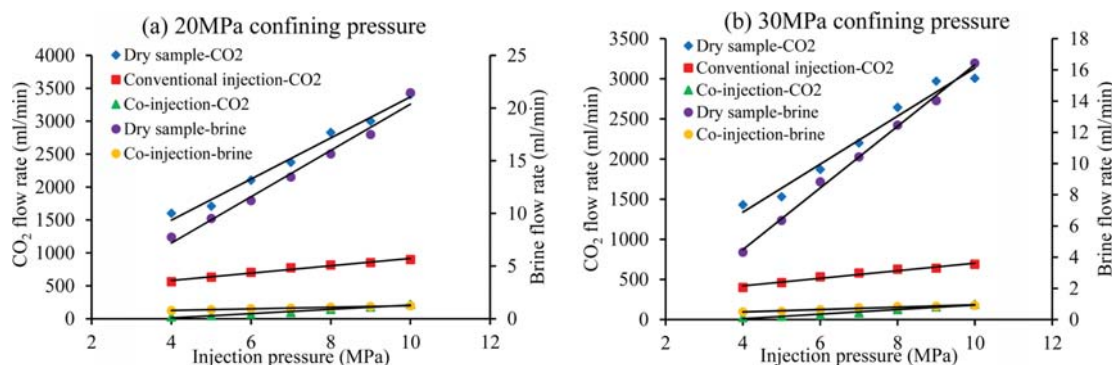
component (CO₂ or brine) in the multiphase system individually obeys Darcy's law. According to Ranjith and Moore et al.,^{22,23} the relative permeability of each individual phase in two-phase conditions can be evaluated using the following form of Darcy's equation for negligible elevation and velocity head conditions.

For the CO₂ phase (non-wetting phase), effective permeability under two-phase conditions can be expressed as follows:²²

$$k_{\text{CO}_2} = \frac{2Q_{\text{CO}_2} \mu_{\text{CO}_2} L P_{\text{atm}}}{A(P_{\text{in}}^2 - P_{\text{atm}}^2)} \quad (1)$$

Table 2. Flow Rates Values with Their Standard Deviations for 20 and 30 MPa Confining Pressure Conditions

condition	injection pressure (MPa)	20 MPa confining pressure		30 MPa confining pressure	
		mean flow rate (mL/min)	standard deviation (mL/min)	mean flow rate (mL/min)	standard deviation (mL/min)
conventional case CO ₂ flow rate	4	561.18	1.2	401.59	1.2
	5	633.43	0.93	461.63	1.32
	6	704.64	1.02	532.42	1.72
	7	774.51	0.88	581.07	0.93
	8	818.57	1.21	628.06	1.28
	9	854.19	0.73	641.23	1.47
co-injection case CO ₂ flow rate	10	898.73	2.17	688.48	1.69
	4	28.71	0.99	24.55	1.43
	5	45.22	1.23	39.5	1.05
	6	67.56	0.91	59.09	0.78
	7	94.45	1.27	83.04	1.03
	8	140.37	0.61	122.99	0.63
co-injection brine flow rate	9	176.96	1.51	157.98	1.11
	10	217.9	1.39	190.99	1.53
	4	0.78	0.092	0.49	0.024
	5	0.83	0.054	0.53	0.018
	6	0.96	0.028	0.64	0.027
	7	0.99	0.023	0.76	0.031
	8	1.1045	0.063	0.83	0.052
	9	1.156	0.013	0.86	0.018
	10	1.21	0.012	0.91	0.034

Figure 5. Obtained linear trends for CO₂ flow rate versus injection pressure.

Then, the relative permeability under each condition can be evaluated as a ratio between the two-phase effective CO₂ permeability and the single-phase CO₂ permeability.²²

$$k_{rCO_2} = \frac{2Q_{CO_2}\mu_{CO_2}LP_{atm}}{AK_{CO_2}(P_{in}^2 - P_{atm}^2)} \quad (2)$$

Similarly, for the brine phase (wetting phase), the relative permeability under each condition can be evaluated as a ratio between the two-phase effective brine permeability and the single-phase brine permeability.^{22,24,25}

$$k_{rb} = \frac{Q_b\mu_b L}{AK_b(P_{in} - P_{atm})} \quad (3)$$

On the basis of the single- and two-phase (co-injection) steady-state flow rates that we obtained, the corresponding relative permeability measurements were estimated using eqs 2 and 3. Because the viscosity of CO₂ and brine vary depending upon the pressure and temperature values,²⁶ the REFPROP database was used to calculate the appropriate viscosity values of CO₂ and brine employed during the test.

To evaluate the effect created by the Klinkenberg slip flow effect for the CO₂ single-phase injection condition, these permeability data were corrected using the Klinkenberg correction factor using eq 4.²⁷ For this purpose, CO₂ permeability was plotted against the inverse of the average pore pressure to confirm the Klinkenberg effect (Figure 6a). For all of the cases of the CO₂ single-phase condition, CO₂ permeability increases linearly with an increasing inverse of the average pore pressure, and this is consistent with Klinkenberg's eq 4. Corresponding correction factors were therefore estimated using these slopes to add the Klinkenberg correction for the measured single-phase permeability values, and the results are shown in Figure 6b. According to the figure, the corrected CO₂ permeability is considerably smaller than the measured results, which explains the strong influence of slip flow on permeability under the CO₂ single-phase condition.

$$K_{CO_2} = K_b \left[1 + \frac{2b}{P_{in} + P_{out}} \right] \quad (4)$$

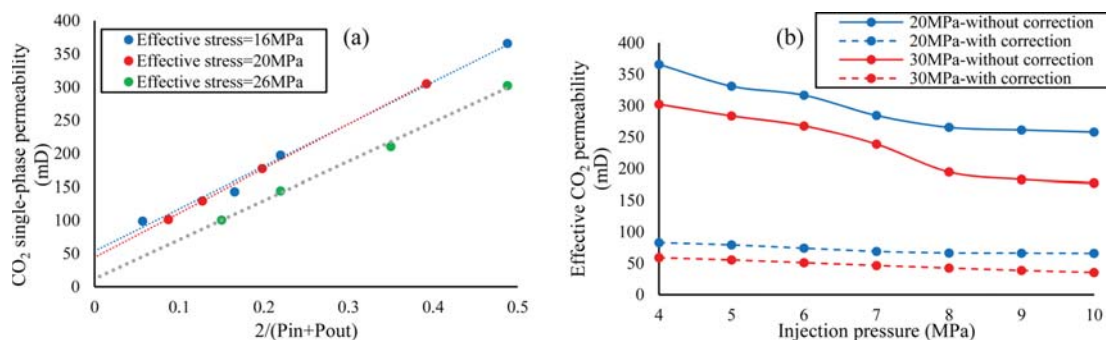


Figure 6. (a) Relationship between CO_2 permeability and inverse of the average pore pressure to confirm Klinkenberg effect in eq 4 and (b) comparison of corrected effective CO_2 permeability and experimental effective CO_2 permeability.

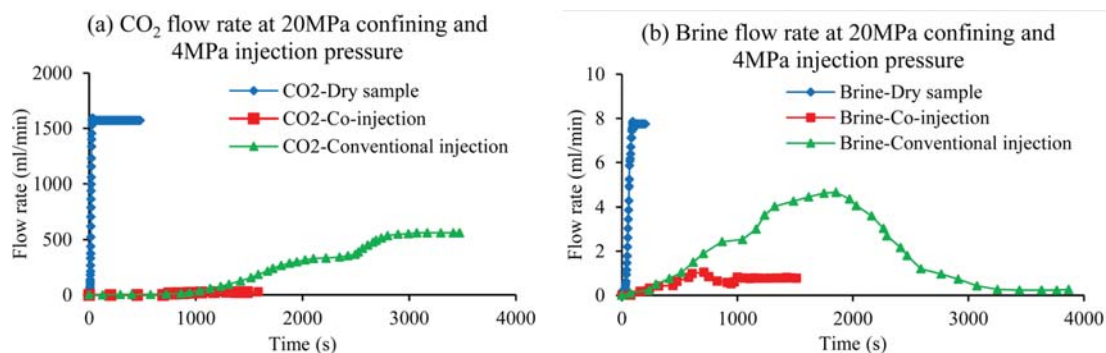


Figure 7. Comparison of dry sample, co-injection, and conventional injection flow rates for (a) CO_2 and (b) brine.

3.2. Two-Phase Flow Behaviors of CO_2 and Brine Co-injection. A close examination of Figure 7 shows a significant reduction in CO_2 and brine flow rates under co-injection (two-phase) compared to the single-phase condition, probably as a result of the mutual influence of each phase on the other. For example, at 20 MPa confining pressure and 4 MPa injection pressure (see Figure 7), the single-phase flow rates of CO_2 and brine decreased by around 98.2 and 90.4% with the change of the phase condition to two phase. The two-phase CO_2 flow rates and brine flow rates under co-injection are shown in Figures 8 and 9, respectively. According to the figures, with the simultaneous injection of CO_2 and brine into brine-saturated samples, the saturated brine begins to flush out from the samples, making a noticeable brine flow rate at the beginning of the test. Over time, the brine flow rate first increases up to a maximum value, then gradually decreases, and comes to a steady state. The initial brine flow rate increase is due to the initiation of forced brine migration inside the sample. The decrease in the brine flow rate before reaching the steady state is due to the initiation of CO_2 flow inside the reservoir pore structure, and from this point onward, the effluent has both brine and CO_2 and behaves as a two-phase system. The effluent CO_2 flow rate then gradually increases over time and eventually reaches a steady state. The flow rates of both brine and CO_2 reach the steady-state condition at around 1050 and 1350 s, respectively (Figure 10). According to Figure 10, after 12 min, the brine flow rate increases to its maximum value of 1.09 mL/min, and at the same time, CO_2 flow begins to increase. After this peak, the brine flow rate gradually decreases and reaches a steady state of 0.78 mL/min. In the case of the CO_2 flow rate, it slowly increases until it reaches a 28.78 mL/min steady-state condition. According to Figure 10, both flow rates achieve their steady-state conditions after about 20 min of

injection. Because the injecting pressures of both phases are equal, the relative flow characteristics of each phase are mainly governed by the physical properties of each and their mutual influence. As shown by past studies,^{3,17,18,22} CO_2 flow rates under single-phase conditions generally reduce with increasing confining pressure as a result of the associated pore shrinkage, which should similarly affect two-phase flows. The data in the present study also confirm this (refer to Figure 11). To prove this pore shrinkage with increasing confining pressure, the volumetric deformation, which occurred under different confining pressures, was evaluated under zero injection pressure using the syringe pump data in the confining unit. For the analysis, the control confining pressure condition was taken as 20 MPa, and with respect to 20 MPa, each volume change was calculated for 25, 30, and 35 MPa confining pressure conditions. Figure 11 shows the volumetric deformation (%) variation with respect to confining pressure, which confirms the significant effect of confining pressure on pore shrinkage in porous saline aquifer rocks.

3.3. Single- and Two-Phase Flow Behaviors of Conventional CO_2 Injection. Importantly, the CO_2 flow variations under conventional CO_2 injection display both single- and two-phase flow behaviors. In conventional injection, at the beginning, CO_2 moves in a two-phase system inside the brine-saturated rock, and this converts to single-phase flow over time after the flushing out of all of the brine from the rock sample. In such situations, CO_2 flow behaves as a single phase because there is no mobile brine inside the sample to create a two-phase condition in it. For example, according to Figures 7b and 12, the brine flow rate first gradually increases and eventually reaches a maximum value as a result of the initiation of forced brine migration from the sample with the injecting fluid. The brine flow rate then starts to decrease until there is no more brine production in the

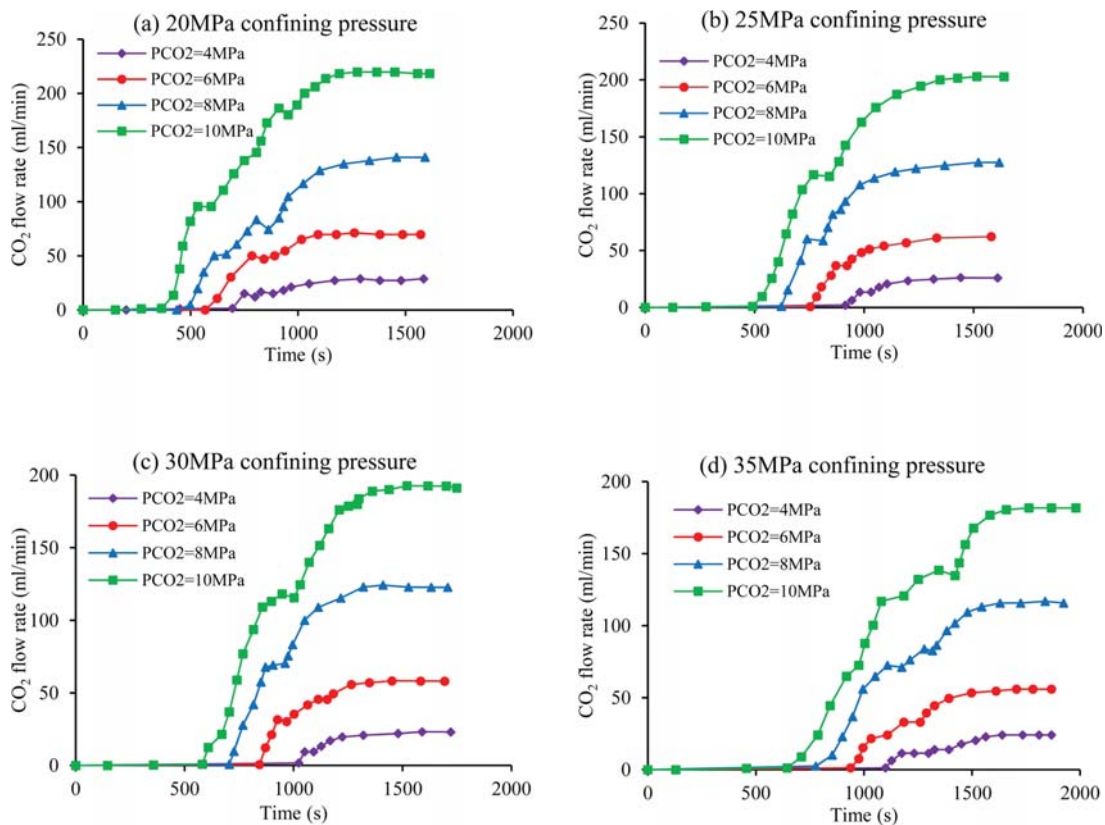


Figure 8. CO₂ two-phase flow rates for the CO₂-brine co-injection case for each confining pressure: (a) 20 MPa, (b) 25 MPa, (c) 30 MPa, and (d) 35 MPa.

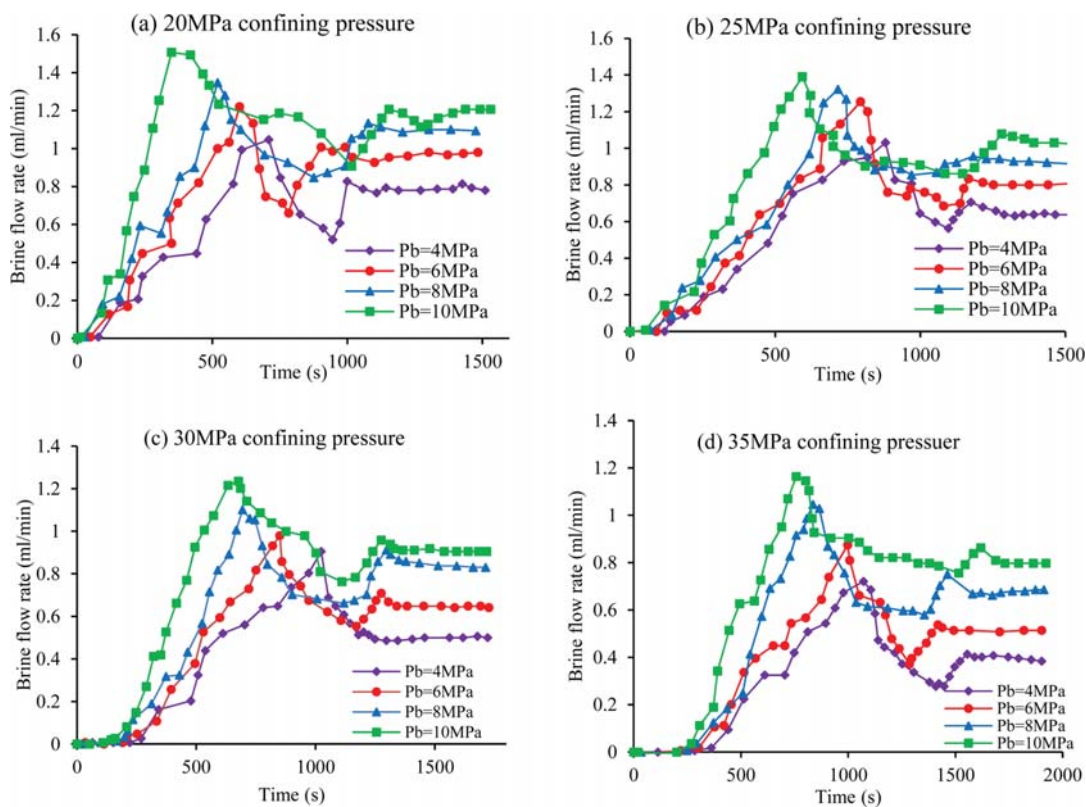


Figure 9. Two-phase flow rates for the brine phase for each confining pressure: (a) 20 MPa, (b) 25 MPa, (c) 30 MPa, and (d) 35 MPa, with co-injection.

effluent (the brine flow rate becomes zero), at which point the CO₂ inlet flow rate is equal to the outlet flow rate. For this reason, brine flow rates under conventional injection exhibit a parabolic

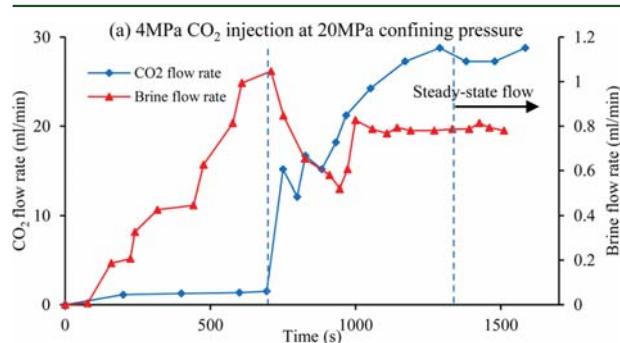


Figure 10. Behavior of brine and CO₂ flow rates under co-injection condition.

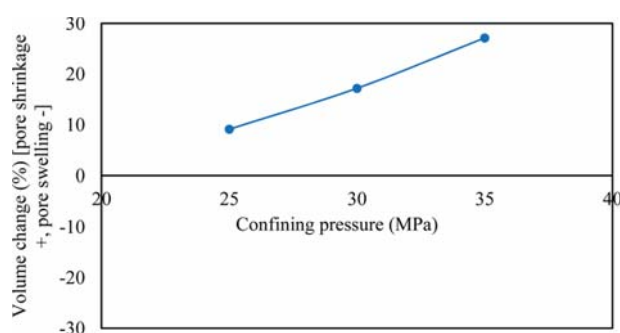


Figure 11. Variation of volumetric deformation (%) with respect to confining pressure.

variation against time. This confirms that there is no more mobile brine inside the reservoir pore structure, creating a single-phase CO₂ flow condition or movement of CO₂ through a CO₂-saturated sample. The occurrence of such full CO₂ saturation near the well bore during CO₂ sequestration in deep saline aquifers has also been recorded in the field.^{2,28}

During conventional injection, the brine in the aquifer pore space (the wetting phase) is displaced by the injecting CO₂ (the non-wetting phase), creating three noticeable regions in the aquifer: (1) the CO₂-saturated zone in the near well-bore region (high-pressure region), (2) the two-phase region, and (3) the brine-saturated region far from the well.^{2,29,30} As a result of the high-pressure conditions of the near well-bore region, brine migration initiates. In conventional CO₂ injection, it is impossible for the solubility reaction to occur in the CO₂-saturated zone as a result of the absence of aquifer brine. The solubility reaction can only occur after the two-phase region exists next to the CO₂-saturated dry zone, which, however, has much lower pressure conditions. Therefore, the solubility process here requires considerable geological time.²

Under the proposed co-injection, reservoir flow always behaves as a two-phase flow, even in the high-pressure region exits near the well bore. This offers opportunity for solubility reactions to occur in this high-pressure, near-well-bore region at much greater rates. In addition, the possibility to partially dissolve CO₂ in brine in the injection well or pipelines (before the injection) under the co-injection process also speeds up CO₂ immobilization. Considering all of these facts, it is clear that the proposed co-injection process is highly effective for the near-well-bore region compared to conventional injection.

According to Figures 8 and 13, the trends of CO₂ flow rate development for conventional injection compared to co-injection cases are quite different. This is mainly due to the transition of

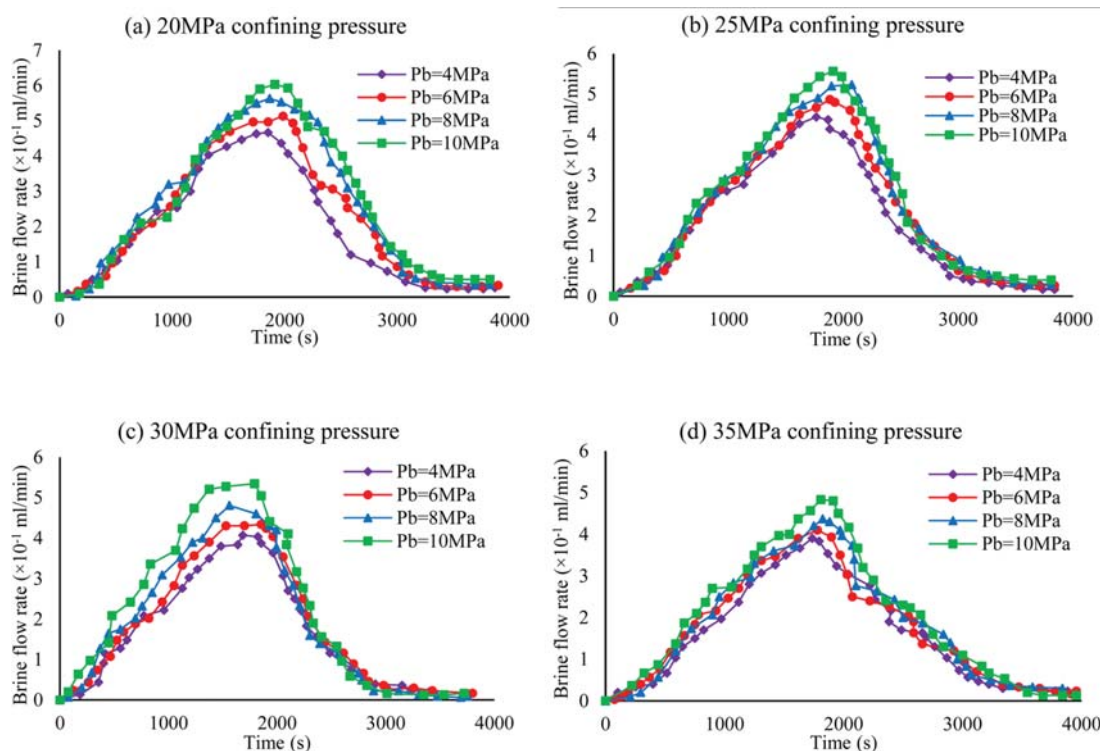


Figure 12. Flow rates for the brine phase for each confining pressure: (a) 20 MPa (b) 25 MPa, (c) 30 MPa, and (d) 35 MPa, with conventional injection.

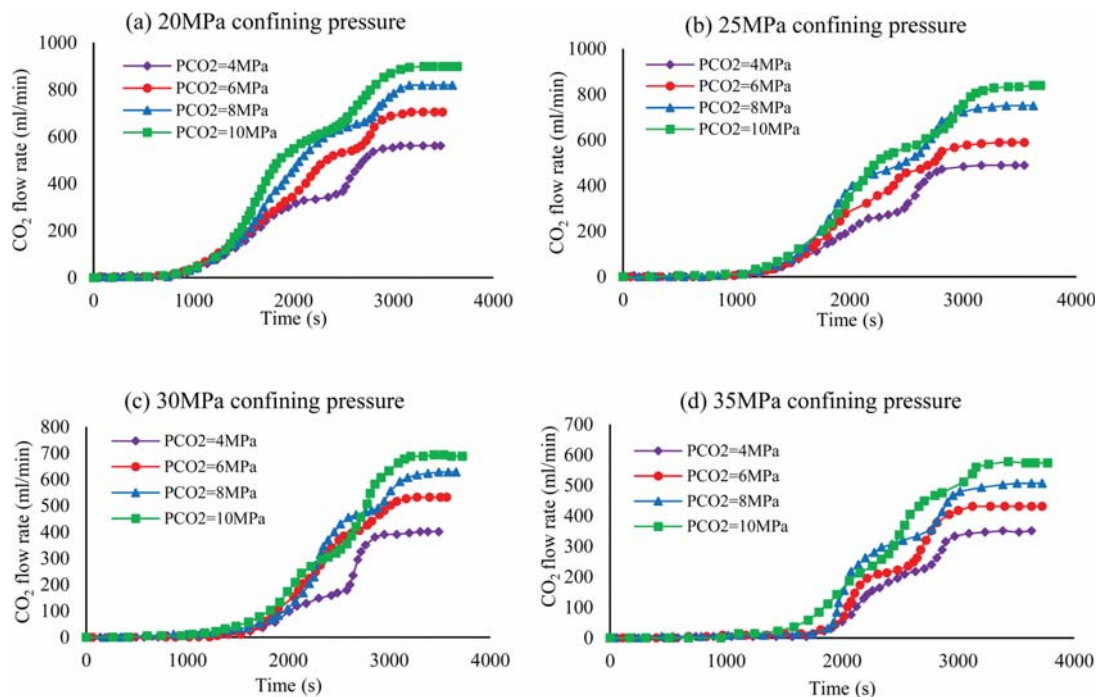


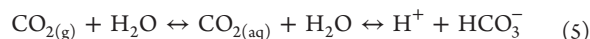
Figure 13. CO₂ two-phase flow rates for the conventional CO₂ injection case for each confining pressure: (a) 20 MPa, (b) 25 MPa, (c) 30 MPa, and (d) 35 MPa.

two-phase behavior into a single-phase flow condition in conventional injection. This leads to higher advective flux over time with conventional injection, causing a much greater CO₂ mass flow rate through the sample once the flow behavior becomes single-phase in conventional injection. For example, for 4 MPa injection and 20 MPa confining pressure, the CO₂ flow rate comes to a steady state at around 561.18 mL/min with conventional injection and at around 28.78 mL/min with co-injection, which is significantly lower. These findings imply that the CO₂ flow rate can vary significantly during conventional CO₂ injection in CO₂ sequestration in deep saline aquifers. Therefore, the influence of the CO₂ flow rate on CO₂ storage capacity is worth studying. Andreani et al.³¹ showed that a possible negative influence can be created by this expected sudden increase of CO₂ flow rate in conventional CO₂ injection, because it reduces the carbonation efficiency and eventually the mineral trapping mechanism of CO₂ injected in the reservoir.

Importantly, the novel technique tested in this study, the co-injection of brine and CO₂ into the aquifer, appears to avoid such issues, as a result of its ability to maintain a relatively low flow rate profile compared to conventional injection. This implies that, in comparison to conventional injection, co-injection has greater potential to enhance CO₂ storage capacity in saline aquifers by offering more opportunities for the mineral trapping mechanism. The other main CO₂ storage mechanism in deep saline aquifers is solubility trapping, and it is important to see how this is influenced by the co-injection process. This is the subject of the next section.

3.4. Influence of CO₂–Brine Co-injection on Solubility and Mineral Trapping in Saline Aquifers. This was studied by conducting a series of chemical analyses, where the pH variation in the effluent was used to identify the solubility performance of CO₂ in brine under each injection condition. It is well-known that the solubility reaction between injected

CO₂ and aquifer brine or the solubility trapping process provides relatively quicker and greater CO₂ storage ability in saline aquifers compared to other trapping mechanisms.³² The basic solubility reaction between injected CO₂ and aquifer brine can be expressed by eq 5, and according to this equation, this reaction releases H⁺ ions into the aquifer while reducing its pH. The performance of this solubility reaction can therefore be evaluated by checking the resulting pH of the system.



pH measurements of downstream brine samples collected under each condition were therefore taken using a calibrated pH meter [the calibration was performed using a solution of HCl (0.1–0.001 M) and NaCl (0–0.3 M) with a constant ionic strength of 0.15 M], and the results were used to calculate the H⁺ ion concentration in the effluent during each injection condition. According to the results, a significant pH reduction can be seen in the brine samples collected from co-injection tests compared to conventional injection tests. This confirms the greater amount of H⁺ ions released in the co-injection process. For example, under 4 MPa injection and 20 MPa confining pressure, co-injection leads to a 7.1 to 5.7 pH reduction compared to the 7.1 to 6.8 pH reduction observed for conventional injection. Figure 14 shows the H⁺ ion concentration in the effluent during each injection condition, which clearly indicates the significantly greater H⁺ ion production for co-injection compared to conventional injection. This confirms the possibility of enhancing mineral trapping mechanisms during CO₂ sequestration through co-injection. This exhibits the ability of the proposed novel co-injection to accelerate the CO₂ solubility trapping mechanism in saline aquifers during CO₂ sequestration. The extensive time required for CO₂ solubility in brine is one of the major drawbacks to CO₂ sequestration in saline aquifers. Therefore, addressing this issue using the novel

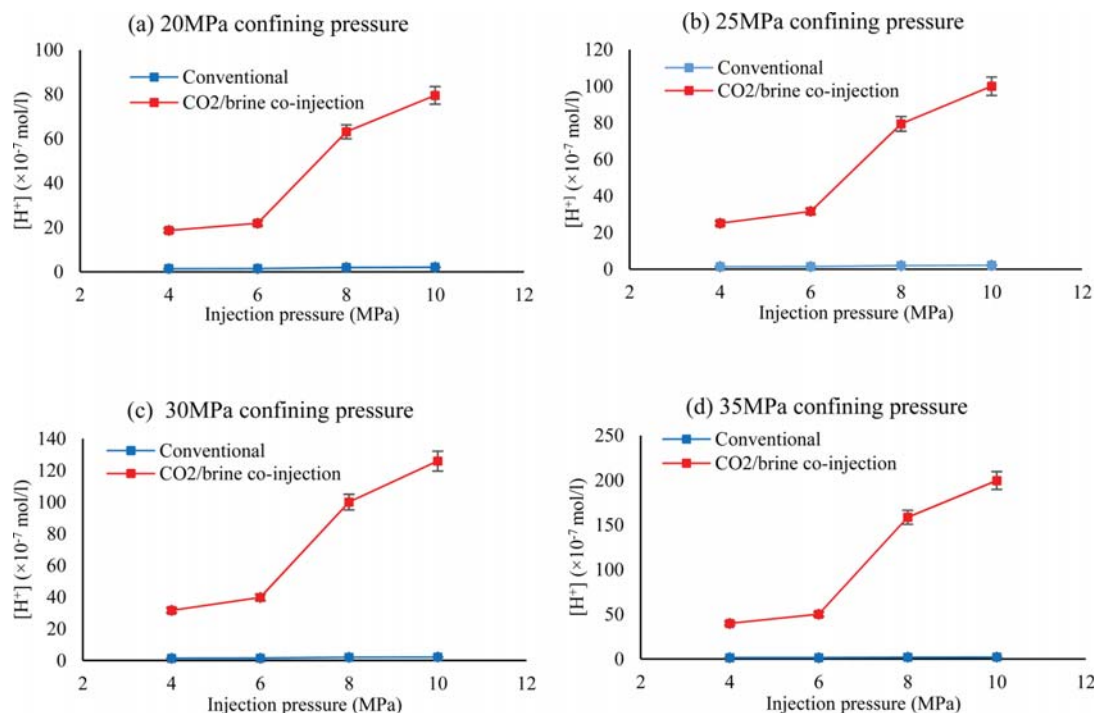


Figure 14. H^+ ion concentration variation with respect to CO_2 injection pressure for conventional and co-injection cases.

co-injection concept would be highly useful in future CO_2 sequestration field projects in saline aquifers.

On the other hand, this enhancement in the solubility trapping process also accelerates the mineral trapping process of CO_2 in the aquifer as a result of the release of greater amounts of H^+ ions (as a weak carbonic acid) in the aquifer. In addition, the resulting slower flow rates under co-injection further improve the mineral trapping process, allowing for additional time to activate the dissolution reaction compared to the conventional injection process. Although the conventional process also allows for the activation of this dissolution reaction, the resulting forced brine migration during the phase transition from two phase to single phase that occurs near the well bore reduces the time available for the reactions, negatively influencing the mineral trapping performance.

3.5. Influence of Depth and CO_2 Phase Change on Solubility and Mineral Trapping in Saline Aquifers. It is also essential to know the effect of aquifer characteristics on CO_2 storage, particularly the depth effect, before drawing final conclusions. This was tested next. Figure 14 shows how the reservoir depth (confining pressure) influences the solubility and mineral trapping enhancements with CO_2 -brine co-injection and conventional injection. According to Figure 14, the resulting H^+ ion concentration increases with increasing confining pressure, confirming the positive influence of aquifer depth on solubility under any injection condition. For example, increasing the confining pressure from 20 to 35 MPa causes the H^+ ion concentration under 4 MPa injection pressure to increase from 18.6×10^{-7} to 39.81×10^{-7} mol/L with co-injection and from 1.41×10^{-7} to 1.48×10^{-7} mol/L with conventional injection. This positive influence of aquifer depth on solubility trapping is mainly related to the effective stress effect, where increased effective stress under high confining pressures causes the rock mass to shrink, reducing its pore space. This increases the rock mass tortuosity for CO_2 movement, resulting in reduced

permeability in the rock mass. Under this reduced permeability condition, CO_2 movement through the reservoir rock decreases, offering more time for CO_2 and aqueous brine to mix well, resulting in enhanced solubility in the system. Importantly, this depth effect on solubility enhancement appears to be greater for co-injection than conventional injection. As mentioned earlier, as a result of the forced brine migration, the pore fluid (brine) closer to the injection well will be pushed out from the injecting fluid (CO_2), creating a pure injection fluid zone in the aquifer near the injection point. However, this zone has the highest pressure induced by the injecting fluid and, therefore, has greater possibility for solubility trapping. In conventional injection, because only pure CO_2 is injected, the opportunity for solubility trapping is much less, and under the proposed co-injection, as a result of the presence of both phases (CO_2 and brine), mutual solubility can occur during injection in this region. This implies that co-injection is more effective for the aquifer zone closer to the injection area. However, the fluid movement rate through any reservoir decreases with increasing depth (confining pressure increases) as a result of the associated pore shrinkage effect. Therefore, the greater the depth, the longer the intermediate zone (two-phase region) exists and, therefore, the greater the solubility enhancement ability through co-injection. For these reasons, the depth effect on solubility enhancement appears to be greater for co-injection than conventional injection. This shows that the effectiveness of the proposed co-injection process increases with increased aquifer depth, and this process is therefore preferable for deeper aquifers.

To have further insight into the effect of confining and injection pressures on the constricted pore structure, the brine retained in the samples after each test was calculated by measuring the weight of the samples before and after the permeability tests (Figure 15). According to Figure 15, the trapped brine mass percentage increases with an increasing confining pressure and decreases with an increasing injection pressure for both cases,

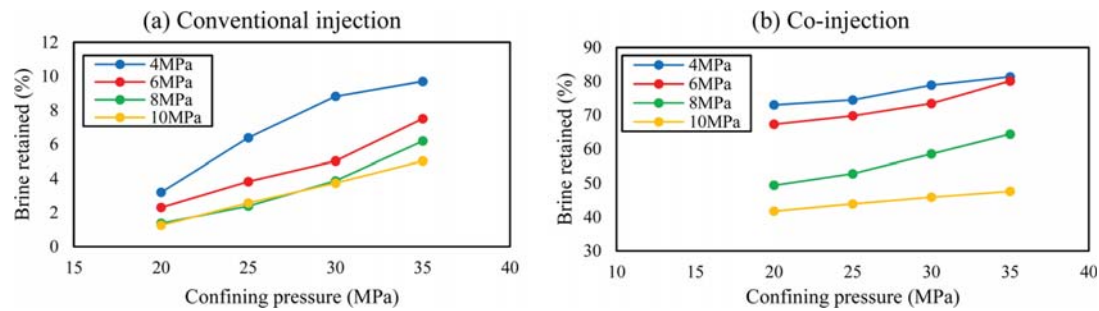


Figure 15. Trapped brine variation inside the specimens with respect to confining and injection pressure: (a) conventional and (b) co-injection cases.

which implies that the pore changes created by confining and injection pressures in the samples. If the injection pressure effect is considered, the high advective flux created by greater injection pressures enhances the brine drainage process, which reduces the brine trapping mechanism in the aquifer. On the other hand, an increased confining pressure enhances the rock mass tortuosity for CO_2 movement, which reduces the CO_2 flow-induced advective flux in saturated brine, resulting in lower brine drainage and greater trapping possibility, including solubility trapping in the system.

In addition to the influence of depth, the influence of the aquifer temperature is also worth investigation as a result of the expected high-temperature conditions in deep saline aquifers compared to the ground level. High temperatures are expected to have a negative influence on the solubility reaction, because CO_2 solubility in brine decreases with increasing temperature.³³ However, this was beyond the scope of the present study.

It is also expected that the phase change of CO_2 from sub- to supercritical also positively influences the solubility reaction in sequestration environments as a result of the greater reactivity and greater availability of the free energy of supercritical CO_2 molecules.³⁴ Figure 14 gives ample evidence for this, where sudden pH reduction and H^+ ion concentration increment can be seen at the point where the injection pressure changes from 6 to 8 MPa. According to Figure 14, supercritical injection under co-injection displays a significantly greater influence on solubility than conventional injection. For example, when the injection pressure changes from 6 MPa (subcritical) to 8 MPa (supercritical) under 20 MPa confining pressure, the H^+ ion concentration increases by around 75% with co-injection compared to only around 18% with conventional injection. This confirms that the CO_2 phase change does not have much influence on the solubility reaction in conventional injection compared to co-injection. This shows the greater applicability of co-injection under field conditions, which further demonstrates its value as a CO_2 -storage-capacity-enhancement technique.

3.6. Alteration of the Relative Permeability Behavior in Saline Aquifers through Co-injection and Its Influence on the Long-Term Stability of CO_2 Sequestration. The relative permeability variations observed for co-injection against injection and confining pressures are shown in Figure 16. According to the general rule of two-phase flow,²² when the relative permeability of one phase increases, the relative permeability of the other phase should decrease. This argument is consistent with the results of the present study for co-injection, where, when the relative permeability of the CO_2 phase increased, the relative permeability of the brine phase began to decrease (see Figure 12). For instance, at 20 MPa confining pressure, when the fluid injection pressure increases from 4 to 6 MPa, the relative permeability

of CO_2 decreases, increasing the relative permeability of the brine phase. However, with a further increase of the injection pressure, at 7 MPa, the relative permeability of CO_2 starts to increase and the relative permeability of brine starts to reduce. A similar behavior was observed for all of the confining pressure conditions (25, 30, and 35 MPa). Interestingly, this relative permeability trend transition occurs around the critical CO_2 pressure of 7.38 MPa under the temperature conditions of $35 > 31.8^\circ\text{C}$, the critical temperature of CO_2 . Therefore, the observed trends relate to the phase transition of CO_2 from sub- to supercritical. This indicates the importance of examining the influence of the CO_2 phase on the shape of the relative permeability curve, particularly in light of the current lack of knowledge of the subject as a result of the limited studies available.

3.6.1. Influence of the CO_2 Phase Change on the Relative Permeability Behavior in Saline Aquifers. It is important to know whether supercritical CO_2 has a different wetting behavior with reservoir rock compared to subcritical CO_2 in deep saline aquifer CO_2 sequestration or whether the unique physical properties of supercritical CO_2 , including its greater density, affect its relative permeability behavior in these formations. As mentioned earlier, preferable saline aquifers for CO_2 sequestration are located at great depths, at which the pressure and temperature conditions normally exceed the critical values of CO_2 (critical pressure of 7.38 MPa and temperature of 31°C). Therefore, CO_2 mostly exists in its supercritical state in deep saline aquifers. However, the influence of the CO_2 phase on its relative permeability characteristics is to date poorly understood. When CO_2 reaches its critical conditions, it becomes more and more dense with increasing pressure³⁵ and may exceed the brine density under certain pressure and temperature conditions.³⁶ The mixing of brine in supercritical CO_2 is therefore much easier than in gas CO_2 ,^{36,37} the phase condition. This has a clear influence on CO_2 solubility in brine and, therefore, the storage process. In addition, the CO_2 phase change also influences wetting and non-wetting behavior in the aquifer, because, if CO_2 is in its gas state, the brine phase acts as the wetting phase and injected CO_2 behaves as the non-wetting phase, which will change for supercritical CO_2 . This is because supercritical CO_2 may exhibit a weak wetting behavior compared to gaseous CO_2 (non-wetting behavior),³⁸ and this wettability behavior is one of the facts governing the relative permeability characteristics of reservoir rocks.³⁹ The different wettability behaviors of supercritical and gaseous CO_2 have been shown by Chalbaud et al.³⁸ based on wetting angle measurements. According to these researchers, supercritical CO_2 has much greater wetting angles in the two-phase system compared to gaseous CO_2 . This means that a CO_2 film spread on brine-wetted pores can stabilize over a larger range of capillary pressures and eventually enhance CO_2

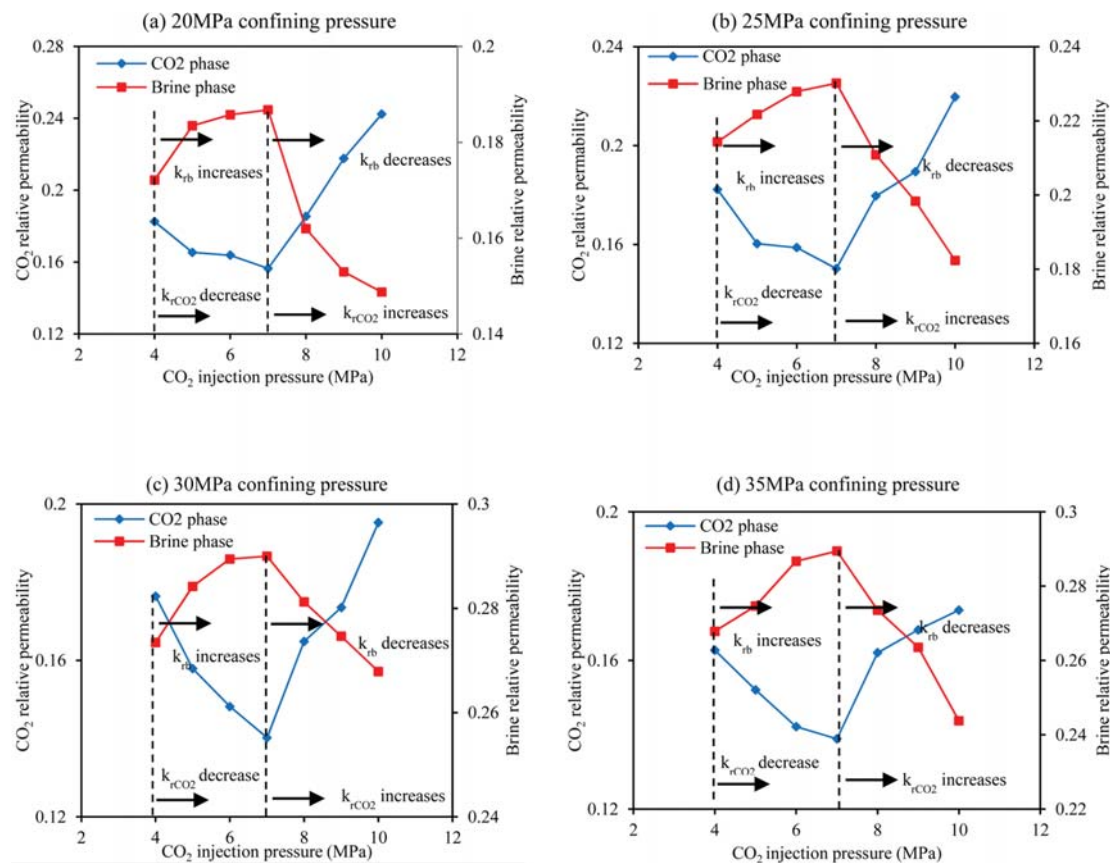


Figure 16. Relative permeability variations in CO₂ and brine phases with respect to different injection and confining pressures.

movement through the film drainage process, resulting in enhanced relative permeability characteristics compared to subcritical CO₂.⁴⁰ This enhanced wettability behavior of supercritical CO₂ compared to subcritical CO₂ is a strong reason for the observed greater relative CO₂ permeability for supercritical CO₂ beyond the critical point and the increasing relative permeability with the further increase of the injection pressure (see Figure 16). The former gas or subcritical CO₂ relative permeability reduction trend with an increasing injection pressure may relate to the Klinkenberg slip flow effect, where gas slippage at the pore wall as a result of the highly compressible nature of gas CO₂ creates lower permeability values under gas-phase CO₂. This slip flow effect increases with an increasing pore pressure or injection pressure, with the possible reduction of CO₂ permeability with an increasing injection pressure.³⁵ The combined influence of the variation of wettability characteristics and the slip flow effect may create the gas CO₂ relative permeability trend (Figure 16) with the co-injection process.

3.6.2. Influence of Other Influencing Factors on the Flow Behavior in Saline Aquifers. The effect of interfacial tension (IFT) on wettability in a two-phase system is also critical and cannot be ignored.³⁷ According to Hebach et al. and Yang and Gu,^{41,42} IFT between CO₂ and brine strongly depends upon the injection pressure and decreases with an increasing injection pressure, creating enhanced relative flow characteristics. This is because IFT creates a negative effect or barrier for CO₂ migration through the rock pore space. Importantly, this IFT varies significantly around the critical point of CO₂, and even a small variation in the pressure or temperature around this point may

lead to significant variation in IFT between CO₂ and brine.⁴³ Because of this strong influence of IFT on wettability, it also has a strong influence on relative permeability and saturation in reservoir rock formations.⁸ Viscosity governs the IFT characteristics for the two phases, and fluid movement through the pore space becomes much easier with enhanced viscosity contrast between CO₂ and brine as a result of reduced IFT.⁴⁴ Figure 17 shows the observed variation in viscosity ratios between CO₂ and brine against different injection pressures. As the figure shows, the viscosity ratio significantly increases when the subcritical CO₂ injection phase changes to the supercritical phase. For example, at 35 °C, the viscosity ratio increases from 9.67×10^{-10} to 1.19×10^{-9} when the subcritical pressure of 6 MPa changes to the supercritical pressure of 8 MPa. This enhanced viscosity contrast between CO₂ and brine in the supercritical state also causes the observed enhanced CO₂ relative permeability characteristics in the rock samples. The decreasing effective stress with increasing injection pressure may also have a significant influence on CO₂ permeability enhancement with increasing injection pressure.

To distinguish the effects of influencing factors (IFT, wettability, slip flow, and effective stress) on individual CO₂ behavior, the effective permeability values for co-injection, conventional injection, and single-phase injection were compared. Figure 18 shows the effective CO₂ permeability variations for each condition under two different confining pressure conditions (20 and 30 MPa). According to Figure 18, the single-phase CO₂ permeability values are far higher for both conventional and co-injection values. For example, under 4 MPa injection and 20 MPa confining pressure conditions, the single-phase permeability in

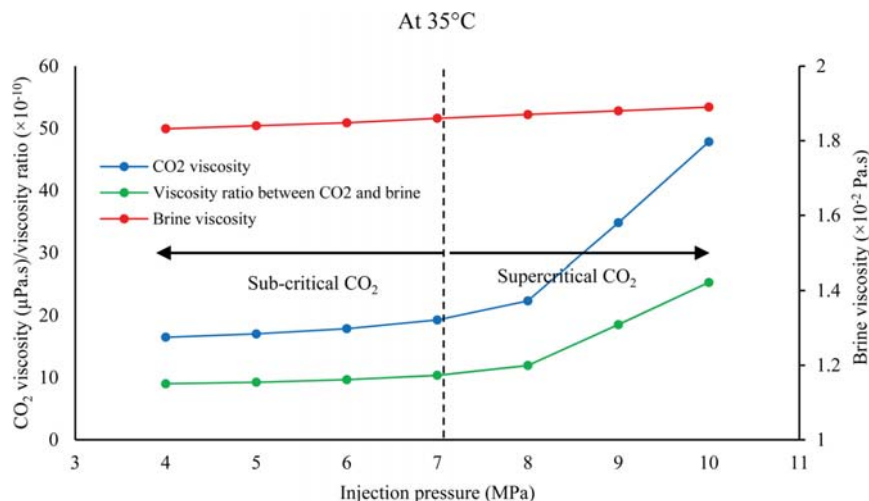


Figure 17. Behavior of the viscosity ratio between CO₂ and brine under sub- and supercritical conditions.

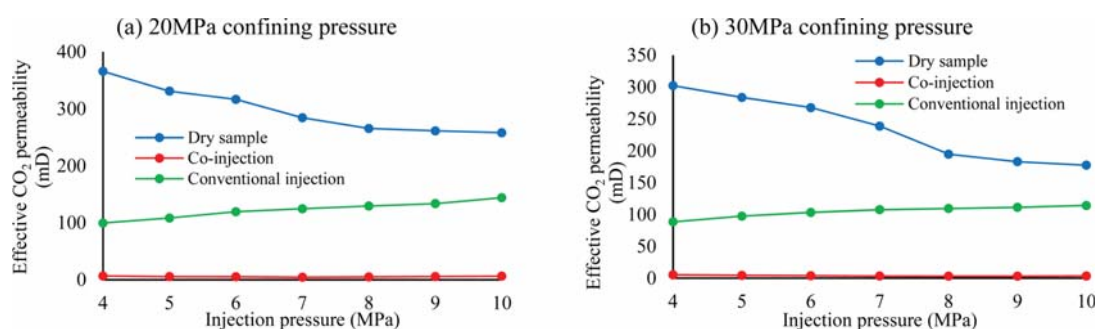


Figure 18. Effective CO₂ permeability variation with injection pressure for three different conditions: (a) 20 MPa and (b) 30 MPa confining pressure.

dry samples displays a value of 365.73 mD, which is significantly higher than that for conventional injection (99.47 mD) and co-injection (6.68 mD). This is probably as a result of the saturation effect, because brine saturation obstructs the free flow paths for CO₂ movement, resulting in reduced effective permeability conditions compared to the dry condition. As Figure 18 shows CO₂ permeability in dry reservoir rock samples decreases with an increasing injection pressure, and a similar trend was observed by Rathnaweera et al.²⁰ In contrast, the increasing effective CO₂ permeability with an increased injection pressure can be seen for conventional injection, whereas co-injection initially displayed a decreasing trend under the subcritical pressure range (4–7 MPa) and then displayed an increasing trend with a further increase of the injection pressure from 7 to 10 MPa. The decreasing permeability trend of CO₂ in a single-phase condition is related to the Klinkenberg effect,⁴⁵ and a comprehensive description of the Klinkenberg effect on dry permeability variation can be found in the study by Rathnaweera et al.²⁰ If the permeability of conventional injection and co-injection are considered, as a result of brine saturation, the slip flow effect between the solid wall and mean gas molecules is decreased as a result of the friction between brine and gas phases, resulting in a minor Klinkenberg effect for conventional and co-injection cases (both wet conditions). The observed increasing trend of effective CO₂ under conventional injection with increasing injection pressure is probably due to the effective stress influence, where the effective stress effect decreases with an increasing injection pressure and its reduction causes the rock mass to expand by increasing its

pore space. This eventually reduces rock mass tortuosity for CO₂ movement, resulting in enhanced reservoir permeability. Although this happens in dry samples, the slip flow effect may be dominant at that stage. Interestingly, co-injection displayed a unique effective CO₂ permeability variation compared to the other two conditions. In addition, the lowest permeability values were obtained for co-injection cases, probably as a result of the influence of the IFT, capillary, and wettability effects of brine and CO₂ phases compared to the conventional and single-phase conditions. In contrast, the slip flow effect significantly influences the single-phase flow behavior compared to other factors, and conventional injection is predominantly affected more by the effective stress effect than the slip flow, IFT, and wettability effects. However, co-injection displays more influence of the IFT and wettability effects, which is confirmed by the lowest permeability values compared to the conventional case. According to Ketzner et al.,³⁴ if a reservoir has a higher permeability value, the efficiency of hydrodynamic trapping decreases, facilitating the easy escape of injected CO₂ from the reservoir, which is not favorable for sequestration. Therefore, the lower permeability behavior observed under co-injection has the capability to enhance the hydrodynamic trapping mechanism compared to conventional injection, which is beneficial for long-term sequestration.

3.7. Comparison of the Co-injection Process to Other Innovative Concepts. A similar study conducted by Eke et al.¹⁹ to identify innovative concepts that can cope with the uncertainties associated with the underground geological formations

and enhance CO₂ storage in the formation found that the CO₂/brine surface mixing strategy has more advantages compared to the co-injection proposed in this present study. These researchers investigated four injection strategies, including conventional CO₂ injection, CO₂/brine surface mixing and injection, CO₂/water surface mixing and injection, and CO₂/brine co-injection. According to them, with respect to conventional CO₂ injection and CO₂/water surface mixing and injection, CO₂/brine surface mixing and CO₂/brine co-injection methods have more advantages. Among the disadvantages of CO₂/water surface mixing and injection, a major limitation is that it requires the injection of significant volumes of water into the formation. If conventional injection is considered, it mainly relies on the presence of a good sealing (caprock). In addition, it requires a sufficient capillary entry pressure to hold injected CO₂. Finally, the researchers concluded that CO₂/brine surface mixing and injection is the best of the four injection scenarios considered in their study. With respect to the CO₂/brine co-injection strategy, CO₂/brine surface dissolution in the mixing vessel proves to be the primary advantage of the CO₂/brine surface mixing and injection strategy, because it speeds up the solubility reaction, thereby reducing time required to achieve immobilization in the subsurface formation. However, according to the results of the present study, CO₂ can also dissolve in brine before release to the reservoir under co-injection, which also helps to speed up CO₂ immobilization. Furthermore, the design of a mixing vessel for surface mixing needs extra capital, because it requires more power and additional operational costs to maintain the desirable design variables, including the operating temperature and pressure of the mixing vessel.¹⁹ These limitations are well-explained by Eke et al.¹⁹ Therefore, although CO₂/brine surface mixing enhances CO₂ immobilization, the operational costs involved in the process may reduce its feasibility compared to co-injection. However, it is necessary to conduct in-depth comparative research on these two processes, considering various aspects, including the injection/extraction process, pipeline, surface equipment, and energy costs, before coming to a conclusion.

4. CONCLUSION

This study was conducted to identify a novel CO₂-storage-capacity-enhancement practice for saline aquifers, the co-injection of CO₂ and brine into saline aquifers. On the basis of the experimental results, the following major conclusions can be drawn: (1) Conventional CO₂ injection causes a sudden increase in advective flux after some time of injection. This reduces the carbonation efficiency and eventually the mineral trapping mechanism of injecting CO₂ in the reservoir and, therefore, negatively affects the CO₂ sequestration process. Such issues can be eliminated by the proposed CO₂-brine co-injection technique. (2) The proposed CO₂-brine co-injection also enhances the solubility trapping process. This is confirmed by the greater pH reductions and H⁺ accumulations observed in the effluents produced in co-injection compared to conventional injection. (3) Importantly, this enhancement of CO₂ solubility trapping by the proposed co-injection technique is aquifer-type-dependent, and its effectiveness increases with increasing aquifer depth. Therefore, the proposed technique is preferable for deeper aquifers. (4) Furthermore, supercritical injection under co-injection has a significantly greater influence on solubility than conventional injection, which is particularly important for field CO₂ sequestration projects, in which CO₂ is in its supercritical state in the aquifer. (5) CO₂-brine co-injection creates reduced

CO₂ relative permeability in saline aquifers, and the associated improved hydrodynamic trapping mechanism confirms that it is a safer CO₂ storage process in saline aquifers, with minimal risk of potential CO₂ leakage from the aquifer to surrounding freshwater aquifers. (6) The extensive time required for the CO₂ solubility process in brine is one of the major disadvantages of CO₂ sequestration in saline aquifers. Therefore, the ability to address this issue using the novel co-injection concept is a ground-breaking finding for CO₂ sequestration in saline aquifers.

■ AUTHOR INFORMATION

Corresponding Author

[REDACTED]

Notes

The authors declare no competing financial interest.

■ NOMENCLATURE

- K_b = single-phase permeability of brine
- K_{CO_2} = single-phase permeability of CO₂
- k_{rCO_2} = relative permeability of CO₂
- k_{rb} = relative permeability of brine
- k_{CO_2} = effective CO₂ permeability
- Q_{CO_2} = CO₂ flow rate
- Q_b = brine flow rate
- μ_{CO_2} = viscosity of CO₂
- μ_b = viscosity of brine
- P_{in} = inlet (injection) pressure
- P_{atm} = atmospheric pressure
- A = sample area
- L = sample length
- b = Klinkenberg correction factor

■ REFERENCES

- (1) Wanniarachchi, W. A. M.; Ranjith, P. G.; Perera, M. S. A.; Lashin, A.; Al Arifi, N.; Li, J. C. Current opinions on foam-based hydrofracturing in deep geological reservoirs. *Geomech. Geophys. Geo-energ. Geo-resour.* **2015**, *1*, 121–134.
- (2) Burton, M.; Bryant, S. L. Eliminating buoyant migration of sequestered CO₂ through surface dissolution: Implementation costs and technical challenges. *SPE Reservoir Eval. Eng.* **2009**, *12* (03), 399–407.
- (3) Juanes, R.; Spiteri, E. J.; Orr, F. M.; Blunt, M. J. Impact of relative permeability hysteresis on geological CO₂ storage. *Water Resour. Res.* **2006**, *42* (12), 12–25.
- (4) Bennion, B.; Bachu, S. Relative permeability characteristics for supercritical CO₂ displacing water in a variety of potential sequestration zones. *Proceedings of the SPE Annual Technical Conference and Exhibition*; Dallas, TX, Oct 9–12, 2005; DOI: [10.2118/95547-MS](https://doi.org/10.2118/95547-MS).
- (5) Benson, S. M.; Tomutsa, L.; Silin, D.; Kneafsey, T.; Miljkovic, L. Core Scale and Pore Scale Studies of Carbon Dioxide Migration in Saline Formations. *Proceedings of the 8th International Conference on Greenhouse Gas Control Technologies (GHGT8)*; Trondheim, Norway, June 19–22, 2006; pp 92–104.
- (6) Bachu, S.; Bennion, B. Effects of in-situ conditions on relative permeability characteristics of CO₂-brine systems. *Environ. Geol.* **2008**, *54* (8), 1707–1722.
- (7) Suekane, T.; Nobuso, T.; Hirai, S.; Kiyota, M. Geological storage of carbon dioxide by residual gas and solubility trapping. *Int. J. Greenhouse Gas Control* **2008**, *2* (1), 58–64.
- (8) Shi, J. Q.; Xue, Z.; Durucan, S. History matching of CO₂ core flooding CT scan saturation profiles with porosity dependent capillary pressure. *Energy Procedia* **2009**, *1* (1), 3205–3211.
- (9) Perrin, J. C.; Krause, M.; Kuo, C. W.; Miljkovic, L.; Charoba, E.; Benson, S. M. Core-scale experimental study of relative permeability properties of CO₂ and brine in reservoir rocks. *Energy Procedia* **2009**, *1* (1), 3515–3522.

- (10) Cole, D. R.; Chialvo, A. A.; Rother, G.; Vlcek, L.; Cummings, P. T. Supercritical fluid behaviour at nanoscale interfaces: Implications for CO₂ sequestration in geologic formations. *Philos. Mag.* **2010**, *90* (17), 2339–2363.
- (11) Levine, J. Relative permeability experiments of carbon dioxide displacing water & their implications for carbon sequestration. Ph.D. Thesis, Columbia University, New York, 2010.
- (12) Perrin, J. C.; Benson, S. An experimental study on the influence of sub-core scale heterogeneities on CO₂ distribution in reservoir rocks. *Transp. Porous Media* **2010**, *82* (1), 93–109.
- (13) Wegener, D. C.; Harpole, K. J. Determination of relative permeability and trapped gas saturation for predictions of WAG performance in the South Cowden CO₂ flood. *Proceedings of the SPE/DOE Improved Oil Recovery Symposium*; Tulsa, OK, April 21–24, 1996; DOI: 10.2523/35429-MS.
- (14) Doughty, C.; Pruess, K. Modelling supercritical carbon dioxide injection in heterogeneous porous media. *Vadose Zone J.* **2004**, *3*, 837–847.
- (15) Flett, M.; Gurton, R.; Taggart, I. The function of gas–water relative permeability hysteresis in the sequestration of carbon dioxide in saline formations. *Proceedings of the SPE Asia Pacific Oil and Gas Conference and Exhibition*; Perth, Western Australia, Australia, Oct 18–20, 2004; DOI: 10.2118/88485-MS.
- (16) Kumar, A.; Ozah, R.; Noh, M.; Pope, G. A.; Bryant, S.; Sephrnoori, K.; Lake, L. W. Reservoir simulation of CO₂ storage in deep saline aquifers. *Soc. Petro. Eng. J.* **2005**, *10* (3), 336–348.
- (17) Hesse, M. A.; Orr, F. M. J.; Tchelepi, H. A. Gravity currents with residual trapping. *J. Fluid Mech.* **2008**, *611*, 35–60.
- (18) Kopp, A.; Class, H.; Helmig, R. Investigations on CO₂ storage capacity in saline aquifers: Part I. Dimensional analysis of flow processes and reservoir characteristics. *Int. J. Greenhouse Gas Control* **2009**, *3* (3), 263–276.
- (19) Eke, P. E.; Naylor, M.; Haszeldine, S.; Curtis, A. CO₂/Brine Surface Dissolution and Injection: CO₂ Storage Enhancement. *Soc. Petro. Eng.* **2011**, *6* (1), 41–53.
- (20) Rathnaweera, T. D.; Ranjith, P. G.; Perera, M. S. A. Effect of Salinity on Effective CO₂ Permeability in Reservoir Rock Determined by Pressure Transient Methods: An Experimental Study on Hawkesbury Sandstone. *Rock Mech. Rock Eng.* **2015**, *48* (5), 2093–2110.
- (21) Shukla, R.; Ranjith, P. G.; Choi, S. K.; Haque, A. A novel testing apparatus for hydromechanical investigation of rocks: Geo-sequestration of carbon dioxide. *Rock Mech. Rock Eng.* **2012**, *45* (6), 1073–1085.
- (22) Ranjith, P. G. Analytical and numerical investigation of water and air flow through rock media. Ph.D. Thesis, Department of Civil Engineering, University of Wollongong, Wollongong, New South Wales, Australia, 2000.
- (23) Moore, J.; Adams, M.; Allis, R.; Lutz, S.; Rauzi, S. Mineralogical and geochemical consequences of the long-term presence of CO₂ in natural reservoirs: An example from the Springerville-St. Jones field, Arizona, and New Mexico, USA. *Chem. Geol.* **2005**, *217*, 365–385.
- (24) Ranjith, P. G.; Perera, M. S. A. A new triaxial apparatus to study the mechanical and fluid flow aspects of carbon dioxide sequestration in geological formations. *Fuel* **2011**, *90* (8), 2751–2759.
- (25) De Silva, P. N. K.; Ranjith, P. G. A study of methodologies for CO₂ storage capacity estimation of saline aquifers. *Fuel* **2012**, *93*, 13–27.
- (26) Fenghour, A.; Wakeham, W. A.; Vesovic, V. The viscosity of carbon dioxide. *J. Phys. Chem. Ref. Data* **1998**, *27*, 31–44.
- (27) Tanikawa, W.; Shimamoto, T. Klinkenberg effect for gas permeability and its comparison to water permeability for porous sedimentary rocks. *Hydro. Earth System Sci. Discuss.* **2006**, *3* (4), 1315–1338.
- (28) Marbler, H.; Erickson, K. P.; Schmidt, M.; Lempp, C.; Pollmann, H. Geomechanical and geochemical effects on sandstones caused by the reaction with supercritical CO₂: An experimental approach to in situ conditions in deep geological reservoirs. *Environ. Earth Sci.* **2013**, *69*, 1981–1998.
- (29) Hunt, J. R.; Sitar, N.; Udell, K. S. Non-aqueous phase liquid transport and clean up: Analysis of mechanisms. *Water Resour. Res.* **1988**, *24* (8), 1247–1258.
- (30) Noh, M. L.; Lake, L. W.; Bryant, L.; Araque-Martinez, A. Implications of coupling fractional flow and geochemistry for CO₂ injection in aquifers. *SPE Reservoir Eval. Eng.* **2007**, *10* (4), 406–411.
- (31) Andreani, M.; Luquot, L.; Gouze, P.; Godard, M.; Hoise, E.; Gibert, B. Experimental study of carbon sequestration reactions controlled by the percolation of CO₂-rich brine through peridotites. *Environ. Sci. Technol.* **2009**, *43* (4), 1226–1231.
- (32) Rathnaweera, T. D.; Ranjith, P. G.; Perera, M. S. A.; Haque, A.; Lashin, A.; Al Arifi, N.; Chandrasekharam, D.; Yang, S. Q.; Xu, T.; Wang, S. H.; Yasar, E. CO₂-induced mechanical behaviour of Hawkesbury sandstone in the Gosford basin: An experimental study. *Mater. Sci. Eng., A* **2015**, *641*, 123–137.
- (33) Duan, Z.; Sun, R.; Zhu, C.; Chou, I. An improved model for the calculation of CO₂ solubility in aqueous solutions containing Na⁺, K⁺, Ca²⁺, Mg²⁺, Cl⁻, and SO₄²⁻. *Mar. Chem.* **2006**, *98* (2), 131–139.
- (34) Ketzner, J. M.; Iglesias, R.; Einloft, S.; Dullius, J.; Ligabue, R.; de Lima, V. Water-rock-CO₂ interactions in saline aquifers aimed for carbon dioxide storage: Experimental and numerical modelling studies for the Rio Bonito formation (Permian), southern Brazil. *Appl. Geochem.* **2009**, *24*, 760–767.
- (35) Perera, M. S. A.; Ranjith, P. G.; Choi, S. K.; Airey, D. Investigation of temperature effect on permeability of naturally fractured black coal for carbon dioxide movement: An experimental and numerical study. *Fuel* **2012**, *94*, 596–605.
- (36) Spycher, N.; Pruess, K.; Ennis-King, J. CO₂-H₂O mixtures in the geological sequestration of CO₂. I. Assessment and calculation of mutual solubilities from 12 to 100°C and up to 600 bar. *Geochim. Cosmochim. Acta* **2003**, *67*, 3015–3031.
- (37) Muller, N. Supercritical CO₂-brine relative permeability experiments in reservoir rock—Literature review and recommendations. *Transp. Porous Media* **2011**, *87*, 367–383.
- (38) Chalbaud, C.; Robin, M.; Bekri, M.; Egermann, P.; Bertin, H. Wettability impact on CO₂ storage in aquifers: Visualisation and quantification using micromodels, pore network model and reservoir simulation. *Proceedings of the SCA International Symposium*; Calgary, Alberta, Canada, Sept 10–12, 2007.
- (39) Oren, P. E.; Bakke, S. Reconstruction of Berea sandstone and pore-scale modelling of wettability effects. *J. Pet. Sci. Eng.* **2003**, *39* (3), 177–199.
- (40) McDougall, S. R.; Sorbie, K. S. The impact of wettability on water flooding: Pore-scale simulation. *SPE Reservoir Eng.* **1995**, *10* (03), 208–213.
- (41) Hebach, A.; Oberhof, A.; Dahmen, N.; Kogel, A.; Ederer, H.; Dinjus, E. Interfacial Tension at Elevated Pressures—Measurements and Correlations in the Water + Carbon Dioxide System. *J. Chem. Eng. Data* **2002**, *47*, 1540–1546.
- (42) Yang, D.; Gu, Y. Interfacial Interactions of Crude Oil—Brine—CO₂ Systems under Reservoir Conditions. *Proceedings of the SPE Annual Technical Conference and Exhibition*; Houston, TX, Sept 26–29, 2004; DOI: 10.2523/90198-MS.
- (43) Chun, B. S.; Wilkinson, G. T. Interfacial Tension in High Pressure Carbon Dioxide Mixtures. *Ind. Eng. Chem. Res.* **1995**, *34*, 4371–4377.
- (44) Bennion, B.; Bachu, S. The impact of interfacial tension and pore size distribution/capillary pressure character on CO₂ relative permeability at reservoir conditions in CO₂-brine systems. *Proceedings of the SPE/DOE Symposium on Improved Oil Recovery*; Tulsa, OK, April 22–26, 2006; DOI: 10.2118/99325-MS.
- (45) Picandet, V.; Khelidj, A.; Bellegou, H. Crack effects on gas and water permeability of concretes. *Cem. Concr. Res.* **2009**, *39*, 537–47.

6.2 Summary of Chapter 6

A full understanding of storage-enhancement technologies is important for deep saline sequestration, as the extensive time required for CO₂ solubility in brine reduces the efficiency of the storage process. However, all the available studies on CO₂ sequestration-enhancement strategies are based on hydraulic fracturing technology. Therefore, the main objective of this section was to introduce a novel technology to identify a potential CO₂ storage capacity-enhancement technique: enhancement of CO₂ storage through co-injection, or the simultaneous injection of CO₂ and brine into saline aquifers.

In order to investigate this technology, a series of high-pressure triaxial permeability tests on brine-saturated sandstone samples was performed under various in situ and operational conditions, including confining pressures ranging from 20-35MPa and injection pressures ranging from 4-10MPa at 35°C constant temperature. To identify the sequestration-enhancement capability of the proposed method, conventional CO₂ injection (injection of only CO₂ into brine-saturated rock) was also carried out under the same test conditions. Finally, a comprehensive chemical analysis was carried out on both methods to identify the alteration of CO₂ solubility in brine caused by the proposed method.

According to the results, CO₂ flow behaviour under conventional CO₂ injection creates a suddenly increased advective flux sometime after injection, which negatively affects the efficiency of the mineral trapping process. This flux can be reduced by the proposed CO₂-brine co-injection technique, because it offers significantly slower flow rates under the continuously available two-phase condition in the system. In addition, this novel CO₂-brine co-injection enhances CO₂ solubility trapping in the aquifer, which is confirmed by the observed greater pH reductions in the effluents produced. This will allow field projects to reduce the extensive time required for CO₂ solubility in brine, which is one of the critical concerns in any sequestration project in terms of long-term efficiency. The proposed co-injection technique is also favourable for the long-term safety of the process, because the associated reduced CO₂ relative permeability in saline aquifers also offers more opportunities for hydrodynamic trapping mechanisms. The new method is therefore more safe and efficient for CO₂ storage in deep saline aquifers.

CHAPTER 7

Numerical Investigation of Effects of CO₂ Sequestration on Deep Saline Reservoir Hydro- mechanical Properties

7 Numerical Investigation of Effects of CO₂ Sequestration on Deep Saline Reservoir Hydro-mechanical Properties

7.1 Development of a laboratory-scale numerical model of mechanical behaviour of deep saline reservoir rock under high salinity conditions

Although there are a number of numerical studies on the mechanical behaviour of reservoir rock using different computer software programs, very few studies have been reported on the application of these programs to a laboratory-scale model. However, the validation of experimental results and the prediction of laboratory behaviour for extreme conditions, which cannot be performed under experimental conditions, are required for early decision-making in relation to deep saline sequestration projects. Therefore, the development of laboratory-scale simulations is important for research into CO₂ sequestration in deep saline aquifers. The COMSOL software, which has the capability of coupling of multi-physics, was used to implement a numerical model to simulate the mechanical behaviour of reservoir rock under high salinity conditions. Aquifer salinity is an important factor when selecting a suitable deep saline sequestration site, because it causes the mechanical properties of reservoir rock to change during the sequestration process. Therefore, three different salinity conditions, 10%, 20% and 30% NaCl concentration (% by weight), were selected to investigate the mechanical characteristics of reservoir rock under both uniaxial and triaxial stress conditions. The model was used to simulate the experimental results reported in Sections 3.2 and 3.3 in Chapter 3. The model development was carried out in three main stages. In the first stage, an appropriate failure mechanism was investigated and the basic model was developed using published experimental studies. This stage is reported in a paper entitled “*Non-linear stress-strain behaviour of reservoir rock under brine saturation: An experimental study*”. In the next stage, the developed model was validated using published experimental studies. This stage is reported in a paper entitled “*Salinity-dependent strength and stress-strain behaviour of reservoir rocks in deep saline aquifers: An experimental study*”. Finally, the model was extended to predict the mechanical behaviour of reservoir rock under different salinity conditions and high confining pressures. The results of this numerical study are presented in this section in a submitted journal paper entitled “*Development of a laboratory-scale numerical model to simulate the mechanical behaviour of deep saline reservoir rocks under varying salinity conditions in uniaxial and triaxial test environments*”.

Development of a Laboratory- scale Numerical Model to Simulate the Mechanical Behaviour of Deep Saline Reservoir Rocks under Varying Salinity Conditions in Uniaxial and Triaxial Test Environments

T. D. Rathnaweera¹, P.G. Ranjith¹, M. S. A. Perera¹

¹Department of Civil Engineering, Monash University, Building 60, Melbourne, Victoria, 3800, Australia.

Abstract

The maintenance of the long-term mechanical stability of the reservoir rock mass is essential in CO₂ sequestration in deep saline aquifers. However, it cannot be confirmed without predicting the worst-case scenarios in saline aquifers, including high salinity conditions and the complexities caused by surrounding factors such as reservoir depth. Laboratory experiments to identify all such situations are difficult due to the advanced facilities required, and the associated cost and time. Therefore, numerical models play an important role in extending laboratory measurements for such complex and extreme situations. Although numerous numerical studies have been performed to date on field-scale conditions in saline aquifers, less consideration has been given to simulating laboratory data, which is important for up-scaling the data to field conditions. This study therefore aims to develop a laboratory-scale numerical model to simulate the mechanical behaviour of brine-saturated reservoir rock under triaxial stress laboratory conditions. The model validation was performed by measuring uniaxial and triaxial laboratory test data under 10-25 MPa confining pressures and the model was then used to investigate the influence of pore fluid salinity percentage on reservoir rock strength by considering various possible salinity levels (5%, 10%, 15%, 20%, 25% and 30% NaCl) and the influence of depth using a range of confining pressures from 10- 100 MPa.

The proposed numerical model based on the stiffness degradation mechanism of reservoir rock can accurately simulate salinity-dependent stress-strain behaviour under any stress environment (uniaxial/triaxial). According to the model, both pore fluid salinity and confining stress add additional strength to the reservoir rock mass due to NaCl crystallization and pore shrinkage. Importantly, the model clearly shows a reduction of the effect of pore fluid salinity on reservoir rock strength characteristics with increasing reservoir depth or confinement, mostly due to the more significant effective stress at such extreme depths. This provides an important finding on

CO₂ sequestration in saline aquifers: salinity-dependent strength alteration is not very important for extremely deep aquifers compared to shallow aquifers. Although this model has the capability to simulate the failure of reservoir rock under extreme pressure conditions, the simulation results show a small fluctuation near the post-peak stage due to the complexity of the damage mechanism caused by strain localization.

Keywords: Laboratory- scale model, salinity, stiffness degradation, uniaxial, triaxial

7.1.1 Introduction

Numerical simulation is essential in addressing issues arising in CO₂ sequestration in deep saline aquifers, due to the extensive cost and time required (Perera et al., 2014). Generally, most laboratory-scale experiments are limited to low injection pressures, confining pressures and temperature conditions and have limitations in their applicability to real field situations. The development of appropriate laboratory-scale models eliminates such limitations, and models provide the ability to predict hydro-mechanical variations under extreme pressure and temperature conditions. The development of appropriate laboratory-scale models using user-friendly simulators is of utmost importance for research into deep saline sequestration. The present numerical study was motivated by that demand. Although a number of field-scale simulations have been developed to date using different numerical modelling software packages, including TOUGH, COMSOL, FEMLAB, RTAFF2, ECLIPSE and COMET3 (Robinson et al., 2000; Sbai and Mamora, 2005; Class et al., 2009; Wei, 2009; Perera et al., 2013; Ranjith et al., 2013), very few studies have focused on the small domains available in experimental conditions such as triaxial and uniaxial tests. The impact of CO₂ injection on hydro-mechanical behaviour in deep saline aquifers cannot be precisely understood without laboratory-scale models and the combined investigation of laboratory- and field-scale simulations is therefore required to fill the existing knowledge gaps related to the long-term physical and chemical behaviours of deep saline reservoirs.

The COMSOL 5.0 simulator with a user-friendly interface was used in this study to develop a laboratory-scale model to simulate reservoir rock mechanical behaviour in deep saline aquifers in both uniaxial and triaxial stress environments. Although this simulator has been used in the industry for field-scale simulations, to date no study has been reported on the laboratory-scale application of the simulator to salinity-dependent mechanical behaviour in reservoir rock samples. For the purpose of modelling, experimental data obtained from triaxial compression

tests on brine-saturated reservoir rock samples were used. Further, three different salinity conditions were selected (0, 10, 20 and 30% NaCl (% by weight)) to investigate the influence of salinity concentration on reservoir rock mass mechanical characteristics in the salinity conditions expected in deep saline aquifers. Here, 0% salinity or water-saturated condition was used for comparison with NaCl-saturated samples to identify the pure salinity effect on the rock mass mechanical properties. This salinity effect on the mechanical behaviour of reservoir rock is important to precisely understand the existing strength characteristics of varying-saturated reservoir rocks.

7.1.2 Stiffness degradation model for reservoir rock

7.1.2.1 Stiffness degradation mechanism

The analysis of the mechanical behaviour of reservoir rock in deep saline aquifers requires detailed knowledge of its failure characteristics. Sedimentary rocks (soft surrounding rock) in deep saline aquifers often undergo strain hardening/ softening under stress application (mechanical loading). Since this salinity-induced mechanical behaviour (strain hardening and softening behaviours) has a significant influence on the reservoir's capacity, precise understanding of the mechanical property alterations, particularly at pre-peak and post-peak stages, is important for the long-term stability of reservoirs used for sequestration.

A number of studies have been performed to date to understand stiffness degradation (Cao et al., 2007; Chen et al., 2010; Flora and Lirer, 2013), and have clearly shown the strain softening properties in rock formations underground (Hoek and Brown, 1997). Importantly, many studies have shown that the stiffness degradation mechanism of rock can be precisely modelled by simulating the stress-strain characteristics and the failure process of rocks. Zhang et al. (2013) conducted a series of triaxial tests on red sandstone to develop an elasto-plastic model to evaluate the applicability of compression laws and simulate the actual failure behaviour (pre-peak and post-peak) of red sandstone. According to the stress evaluation path model developed by Niu et al. (2012) by performing cyclic loading experiments on sandy mudstone, the strength parameters (cohesion and friction angle) in the post-peak stage reduce exponentially compared to the pre-peak stage. Martin and Chandler (1994) and Martin (1997) investigated the applicability of bond-weakening and friction-hardening models in evaluating the compression fracturing mechanism in reservoir rocks to develop some strain softening models employing the theory of continuum mechanics. Zdenek and Bazant (1984) proposed a model based on the

plastic strain-softening effect to develop a relationship between equivalent stress and equivalent plastic strain, and based on the same plastic potential theory, Zhang et al. (2008) established a relationship between strength parameters and strain softening parameters of granite by investigating the yield surface characteristics. Lu et al. (2010) carried out a numerical verification study for the attenuation rules of the strength parameters of soft rock considering the confining pressure effect, and introduced a new concept that generalizes cohesion and the friction angle to express the yield surface. On the basis of the relationship between tangent modulus and post-peak strain, Joseph and Barron (2003) attempted to predict stress-strain behaviour, and Yu et al. (2012) carried out an important study to characterise the post-peak behaviour of brittle failure based on degradation angle. These researchers proposed a strain-softening model to accurately predict the strength degradation of brittle rocks and the effect of confining pressure. Li et al. (2011) studied the post-peak behaviour of brittle rocks considering the degradation of the deformation modulus and the strength parameters and developed a strain-softening model. Chen et al. (2010) proposed a new method to determine the stability of rock formations based on a strength reduction method based on the attenuation of the deformation modulus, cohesion and the tensile strength of rocks. Wang et al. (2009) also presented an evaluation method for the internal damage mechanism of brittle rock based on the stiffness degradation phenomenon.

However, most of these studies fail to illustrate the relationship between modulus damage and strength attenuation, and therefore fail to predict the stress-strain behaviour of brittle rocks, including both the pre-peak and post-peak stages (Zhao et al., 2014). To precisely understand the existing relationship between these two parameters, Zhao et al. (2014) presented an evaluation method for the attenuation law of strength parameters of brittle rocks at the failure stage considering stiffness degradation. The present study has developed an advanced laboratory-scale numerical model to simulate the mechanical behaviour of reservoir rock under brine-saturated conditions, based on Zhao et al.'s (2014) findings. Since deep saline aquifers generally contain highly saline brine, the salinity effect on reservoir characteristics is important for the selection of feasible and effective deep saline sequestration sites. According to Bachu and Bennion (2008) and Shukla et al. (2013), NaCl concentration in saline aquifers can vary in the range of 2% to 25% (% by NaCl weight). Therefore, this study selected six different NaCl concentrations to cover the low to high salinity conditions in real reservoirs (5% to 30%).

7.1.2.2 Model development

Fig. 7.1 shows the stress-strain relationships corresponding to triaxial compression tests conducted for a reservoir rock under 10 MPa confining pressure and various saturation conditions. The figure reveals that, regardless of saturation type, the axial strain of the reservoir rock starts to decrease after the peak, indicating an occurrence of strain localization during the post-peak stage.

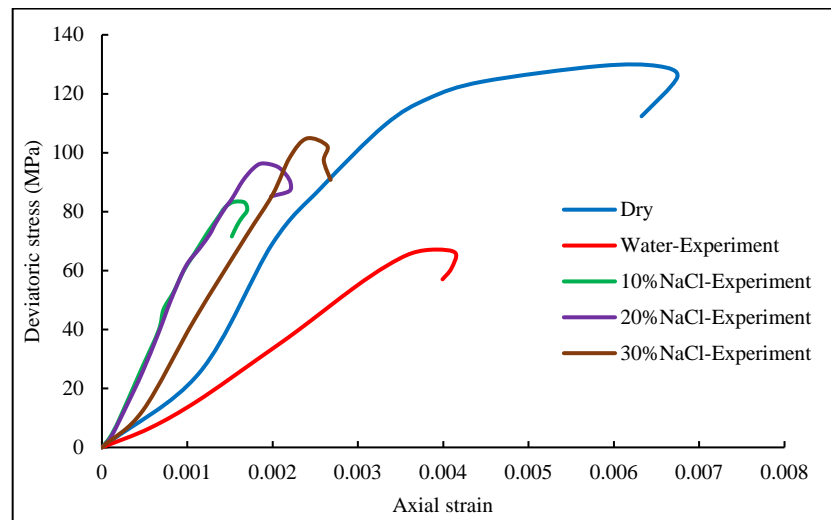


Figure 7.1. Stress-strain relations of triaxial compression tests conducted under 10MPa confining pressure for reservoir rock under different saturation conditions.

To numerically represent this actual stress-strain variation of the reservoir rock mass during loading, various phases of the stress-strain curves were simplified and analysed (Fig. 7.2). According to Fig. 7.2a, the general response of reservoir rock during triaxial loading can be explained as including an elastic region, a plastic yielding region and a stiffness degradation region, followed by a strain localization process (partial strain softening region). For the purpose of modelling, the observed strain localization process was however ignored, assuming an entirely strain softening effect after the peak point. Furthermore, due to the short yield stage (AB), the plastic yielding/ strain hardening region before the peak failure can be considered as an extension of the elastic region. The present study therefore selected the tri-linear concept to model the stress-strain behaviour of reservoir rock under different salinity conditions and confining pressures (Fig. 7.2b). In the simplified tri-linear model, the region OB indicates the initial pressurization, crack closure and micro-crack development stages that consist of the elastic region OA followed by the plastic region AB. To analyse the failure mechanism of

reservoir rock, it is important to identify the damage threshold point during the loading process, and according to Zhao et al. (2014), this damage threshold point normally coincides with the yield point. After peak point B, the reservoir rock sample undergoes stiffness degradation, inducing reductions in the stiffness and strength of the rock sample due to the extension and penetration of the crack damage stresses. As a result of this stiffness degradation, the unloading modulus at post-peak stage, E_s , is lower than the elastic modulus at pre-peak stage, E_0 . Stage CD represents the residual stage of the stress-strain curve.

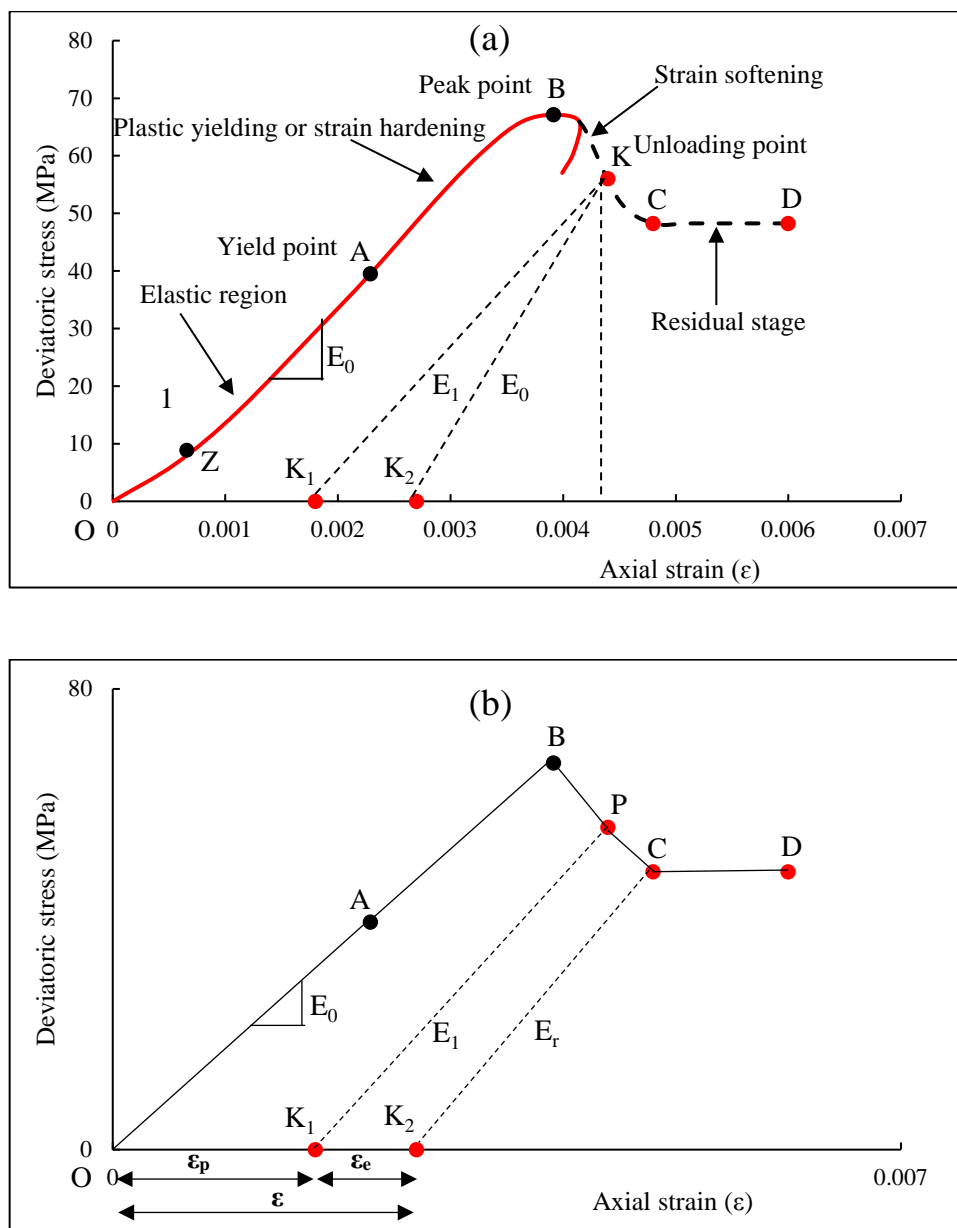


Figure 7.2. (a) Stiffness degradation of reservoir rock under triaxial compression and (b) simplified tri-linear strain softening model.

To simplify the strain behaviour of the reservoir rock mass, the stress response of reservoir rock was introduced into the model to capture the confining pressure or depth effect. This stress effect was implemented based on the equivalent stress (effective stress) applied on the rock mass and was introduced into the model as a function of axial stress (σ_1), confining pressure (σ_3) and Poisson's ratio (γ) as follows (Toshikazu, 1981):

$$\sigma_{eff} = \sigma_1 - 2\gamma\sigma_3 \quad (7.1)$$

To identify the corresponding elastic modulus at different phases of the stress-strain curve, the behaviour of the pre-peak and post-peak stages of loading was considered (Fig. 7.2), and the elastic modulus at the pre-peak and post-peak stages was calculated, based on experimental data. The calculated modulus values were then inserted into the model to simulate the pre-peak and post-peak behaviour of reservoir rock as E_0 and E_s , respectively. In addition, to mimic the post-peak failure, a special parameter called the “softening modulus”, α was introduced into the model. To derive the post-peak elastic modulus as a function of pre-peak modulus, a stiffness degradation coefficient (ω) was also included in the model and combined in the post-peak elastic modulus equation as follows:

$$E_s = (1 - \omega)E_0 + \omega E_r \quad (7.2)$$

where, E_r represents the elastic modulus at the residual stage.

After defining the pre-peak and post-peak modulus, strength parameters were incorporated to simulate the stress state at each stage by introducing elastic and plastic strains into the stress equations. Hence, the stress equation for the post peak stage (point P) can be written as:

$$\sigma_{1p} = \sigma_{1f} - \alpha(\varepsilon_{1p} - \varepsilon_{1f}) \quad (7.3)$$

where, σ_{1p} is the axial stress at post-peak stage (point P), σ_{1f} is the axial failure stress at peak point (point B), ε_{1p} is the axial strain at post-peak stage and ε_{1f} is the axial strain at failure.

According to elastic and plastic theories, the total axial strain can be defined as a combination of elastic and plastic strain. Therefore, the total axial strain at post-peak can be expressed as:

$$\varepsilon_{1p} = \varepsilon_{1pe} + \varepsilon_{1pp} \quad (7.4)$$

where, ε_{1pe} and ε_{1pp} stand for elastic and plastic strains at the post-peak stage, respectively.

For conventional triaxial compression, the elastic strain at post-peak stage can be defined as:

$$\varepsilon_{1pe} = \frac{\sigma_{eff}}{E_s} \quad (7.5)$$

Accordingly, the plastic strain at post-peak is:

$$\varepsilon_{1pp} = \varepsilon_{1f} + \frac{\sigma_{1f} - \sigma_{1p}}{\alpha} - \frac{\sigma_{eff}}{E_s} \quad (7.6)$$

Generally, the deformation of brittle rock is a coupled process of damage failure and a plastic mechanism and therefore the model is based on the assumption that the stress-state at the post-peak stage fulfils the Mohr-Coulomb yield criterion, to couple these two mechanisms.

According to the Mohr-Coulomb yield criterion, the second deviatoric strain invariant (γ^p) defines the level of plastic deformation and can be expressed as:

$$\gamma^p = \sqrt{\frac{1}{2} e_{ij} e_{ij}} \quad (7.7)$$

where, $e_{ij} = \varepsilon_{ij} - \frac{1}{3} \varepsilon_{kk} \delta_{ij}$

Based on the yield surface criteria, without considering the intermediate stress effect, the present study defined the second deviatoric strain invariant (equivalent plastic shear strain) to simulate the degradation effect of stiffness on the strength parameters (cohesion and friction angle) of reservoir rock during the post-peak stage. Therefore, the equivalent plastic strain can be defined as:

$$\varepsilon^{ps} = \sqrt{\frac{1}{2} [(\varepsilon_{1pp} - \varepsilon_{mp})^2 + (\varepsilon_{3p} - \varepsilon_{mp})^2 + \varepsilon_{mp}^2]} \quad (7.8)$$

where, ε_{mp} is the average plastic strain, which can be defined as:

$$\varepsilon_{mp} = (\varepsilon_{1pp} + \varepsilon_{3p})/3 \quad (7.9)$$

According to the irrelative plastic flow, the plastic strain at post-peak stage can also be expresses based on the dilation characteristics of the rock as follows:

$$\varepsilon_{3p} = -\eta\varepsilon_{1pp} \quad (7.10)$$

Since the present study found significant dilation characteristics in the reservoir rock during the experimental work (Rathnaweera et al., 2015), the dilatancy gradient, η was introduced into the model to simulate the corresponding dilation characteristics of the reservoir rock. For that purpose, Eqs. 7.8-7.10 were combined to obtain an equation which defines the second strain invariant function in the yield surface. Therefore, the strain function was changed to:

$$\varepsilon^{ps} = \sqrt{\frac{1+\eta+\eta^2}{3}}\varepsilon_{1pp} \quad (7.11)$$

Finally, based on Eqs. 7.3-7.5, the relationship between strength and plastic strain in the softening stage can be established as:

$$\sigma_1 = \frac{1+\frac{\alpha}{E_0}}{1+\frac{\alpha}{E_s}}\sigma_{1f} - \frac{\alpha}{1+\frac{\alpha}{E_s}}\varepsilon_{1pp} + 2\gamma\frac{\frac{\alpha}{E_s} - \frac{\alpha}{E_0}}{1+\frac{\alpha}{E_s}}\sigma_3 \quad (7.12)$$

The yield surface function, φ , where all the stress points are located, can be written as:

$$\varphi = \sigma_1 - \xi\sigma_3 - 2C\sqrt{\xi} \quad (7.13)$$

where, $\xi = (1 + \sin \phi)/(1 - \sin \phi)$, and C and ϕ denote the cohesion and friction angle, respectively. To model the initial part of the (OB) stress-strain curve, the yield surface criterion was applied by defining the initial cohesion (C_0), and fiction angle (ϕ_0) of the reservoir rock, and according to limited state theory, this initial yield surface should satisfy the Eq. 7.13 above. Therefore,

$$\varphi_0 = \sigma_{1f} - \xi_0\sigma_3 - 2C_0\sqrt{\xi_0} = 0 \quad (7.14)$$

From Eq. 7.14, the failure stress of reservoir rock can now be calculated as:

$$\sigma_{1f} = \xi_0\sigma_3 + 2C_0\sqrt{\xi_0} \quad (7.15)$$

By solving Eqs. 7.10, 7.12 and 7.15, the corresponding strength parameters can be modelled as:

$$\phi = \arcsin \frac{A_1 \xi_0 + A_2 - 1}{A_1 \xi_0 + A_2 + 1} \quad (7.16)$$

$$C = A_1 C_0 \sqrt{\frac{\xi_0}{A_1 \xi_0 + A_2}} - \frac{A_3 \varepsilon^{PS}}{N \sqrt{A_1 \xi_0 + A_2}} \quad (7.17)$$

$$\text{where, } A_1 = \frac{1 + \frac{\alpha}{E_0}}{1 + \frac{\alpha}{E_s}}, \quad A_2 = 2\gamma \frac{\frac{\alpha}{E_s} - \frac{\alpha}{E_0}}{1 + \frac{\alpha}{E_s}} \text{ and } A_3 = \frac{\alpha}{2 \left(1 + \frac{\alpha}{E_s} \right)}$$

After establishing each phase of the stress-strain behaviour of reservoir rock, the structural mechanics module in COMSOL simulator was used for modelling purposes, as it can solve problems related to structural and solid mechanics. The structural module in COMSOL has the capability of modelling the behaviour of isotropic, orthotropic, and fully anisotropic materials as well as non-linear materials and can include large deformation effects.

7.1.3 Experimental data used for model validation

This numerical study is based on the results of two published experimental studies entitled “Salinity-dependent strength and stress-strain behaviour of reservoir rocks in deep saline aquifers: An experimental study” and “Non-linear stress-strain behaviour of reservoir rock under brine saturation: An experimental study” (Rathnaweera et al., 2014; Rathnaweera et al., 2015). In these studies, the reservoir rock samples (Hawkesbury sandstone) 38 mm in diameter and 76 mm high were saturated with water, 10%, 20% and 30% NaCl concentration brine solutions in desiccators for 60 days and unconfined and triaxial compressive strength tests were performed with a displacement-controlled loading rate of 0.1mm/min. The input parameters for the modelling were obtained from the experimental results. Fig. 7.3 shows the stress-strain behaviour of reservoir rock specimens for different concentrations of NaCl in unconfined stress conditions.

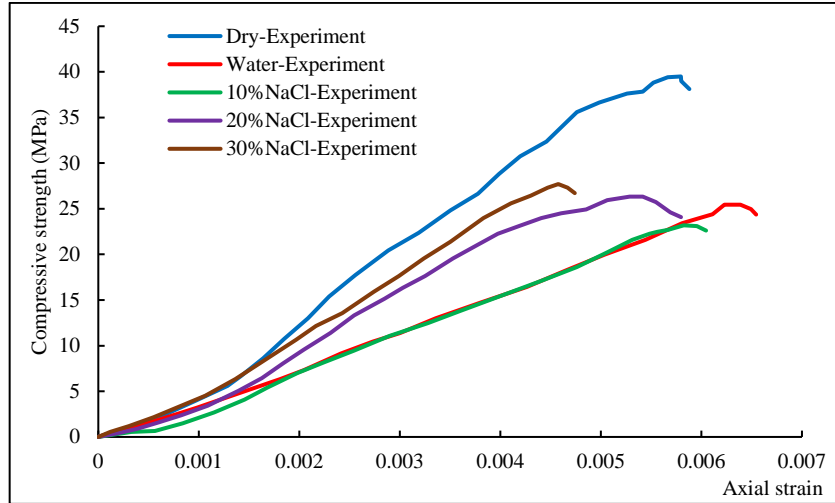


Figure 7.3. Experimental stress-strain curves for tested specimens under unconfined stress conditions.

7.1.4 Model geometry, parameters, boundary and reservoir conditions and loading

Since the experimental sample was a cylinder, a 2-D axisymmetric model was selected to simulate the uniaxial and triaxial tests on brine-saturated reservoir rock, and the model was converted to a 3-D model using the results node available under the “Model Builder” interface in the COMSOL simulator. Fig. 7.4 shows the model geometry and the finite element mesh used in this study. Table 7.1 presents the meshing parameters used in the model geometry. The input parameters of the model (Table 7.2) were obtained from experimental studies that include reservoir rock mechanical parameters such as softening modulus, Poisson’s ratio, pre-peak elastic modulus, post-peak elastic modulus, axial strain at failure, failure stress, dilatancy coefficient, initial cohesion and friction angle and density (Rathnaweera et al., 2014; Rathnaweera et al., 2015).

In the present study, to capture the salinity effect, input parameters were given as a function of salinity (c), and non-linear regression method was adopted to develop those relationships. The relationships for softening modulus, failure stress, pre-peak elastic modulus, post-peak elastic modulus, axial strain at failure, initial cohesion, friction angle and dilatancy coefficient are shown in Eqs. 7.18-7.25, respectively.

$$\alpha = \alpha(c) = 8e^{-4}c^2 - 2.3e^{-3}c + 2.132 \quad (7.18)$$

$$\sigma_{1f} = \sigma_{1f}(c) = -1.2e^{-3}c^3 + 6.5e^{-2}c^2 - 7.482e^{-1}c + 25.28 \quad (7.19)$$

$$E_0 = E_0(c) = -7e^{-4}c^3 + 3.86e^{-2}c^2 - 4.092c + 5.35 \quad (7.20)$$

$$E_s = E_s(c) = -4e^{-4}c^3 + 2.46e^{-2}c^2 - 2.607e^{-1}c + 3.51 \quad (7.21)$$

$$\varepsilon_{1f} = \varepsilon_{1f}(c) = 2e^{-5}c^3 - 8e^{-4}c^2 + 1e^{-3}c + 0.45 \quad (7.22)$$

$$C_0 = C_0(c) = 2e^{-4}c^3 - 1.01e^{-2}c^2 + 1.935e^{-1}c + 0.11 \quad (7.23)$$

$$\phi_0 = \phi_0(c) = -8e^{-4}c^3 + 6.833e^{-1}c + 29 \quad (7.24)$$

$$\eta = \eta(c) = 2e^{-5}c^3 - 2e^{-4}c^2 - 2.42e^{-2}c + 1.77 \quad (7.25)$$

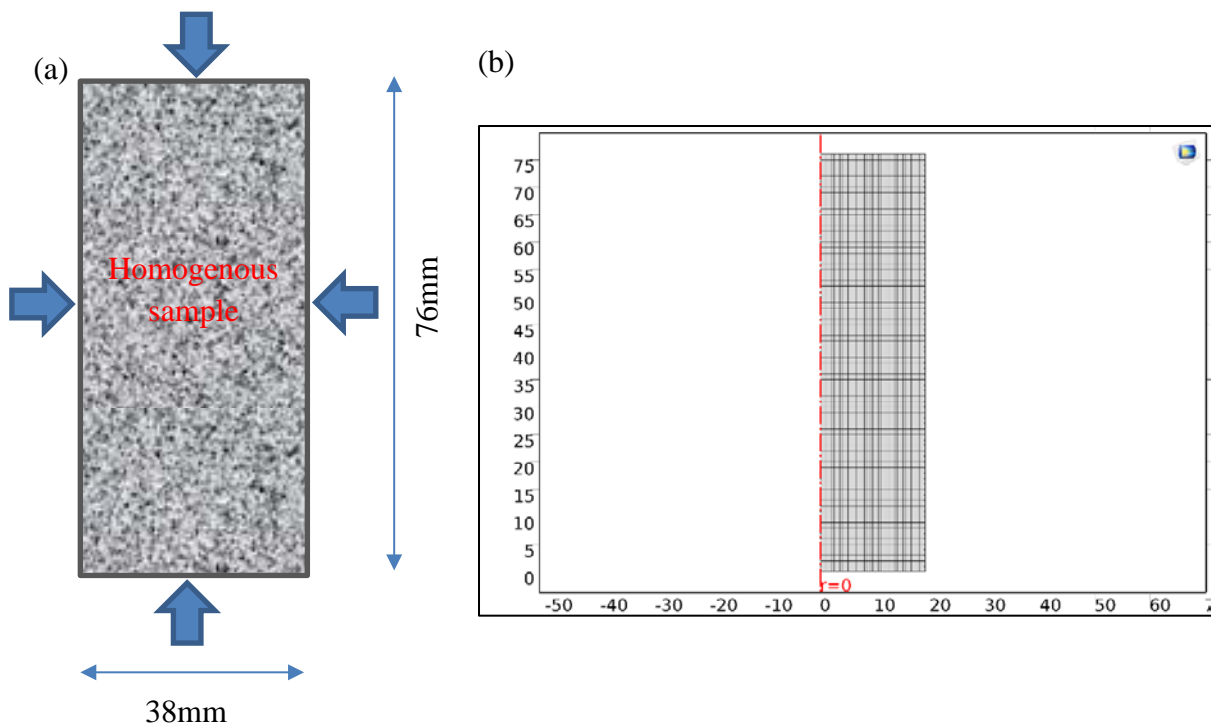


Figure 7.4. (a) Model geometry and (b) Finite element mesh for rock specimen.

Table 7.1. Meshing parameters of reservoir rock specimen model.

Property	Value
Number of degrees of freedom	45754
Number of elements (rectangular)	4127
Number of nodes	2653
Number of boundary elements	210

Table 7.2. Material properties used in laboratory-scale model under 10MPa confining pressure conditions.

Condition	α (GPa)	σ_{1f} (MPa)	E_0 (GPa)	E_s (GPa)	ε_{1f} (mm)	C_0 (MPa)	ϕ_0 (°)	η
Dry	3.21	39.52	10.29	6.73	0.36	10.75	42	1.13
Water	2.14	25.28	5.35	3.51	0.45	10.11	29	1.77
10%NaCl	2.17	23.05	4.44	2.93	0.40	11.21	35	1.52
20%NaCl	2.45	26.35	7.18	4.69	0.31	11.32	36	1.32
30%NaCl	2.82	27.72	9.50	6.22	0.30	11.46	27	1.27

To calculate the resultant vertical force, Eq. 7.26 was embedded in the model by assigning an integration operator in the component tool bar that calculates the vertical force by integrating the z component of the stress tensor at each unit area.

$$F_{res} = \int \sigma_z 2\pi r dr \quad (7.26)$$

where, F_{res} is the resultant force and r is the radius of the sample.

In order to incorporate the experimental boundary conditions in the model, the bottom boundary of the specimen was modelled as a roller support and the top boundary was modelled using boundary load (axial load), on which axial load was applied at a prescribed displacement rate until the sample reached its maximum deformation level. The right boundary was modelled as free with radial stress (confining pressure) and the left boundary was modelled using the axisymmetric condition. The right boundary condition was changed according to the test conditions (uniaxial/triaxial). Zero confinement was applied to the right boundary when the test was under uniaxial stress conditions and it was changed from 10 to 25MPa in the triaxial environment. The details of the boundary conditions are shown in Table 7.3.

Table 7.3. Boundary conditions of laboratory-scale model.

Boundary	Condition
Bottom	Roller support
Top	Free with boundary load (prescribed displacement)
Left	Axis of axisymmetry
Right	Free with boundary load (confining pressure)

The triaxial compressive strength model was developed and validated using the published experimental data of Rathnaweera et al. (2015) on the mechanical behaviour of reservoir rock under high salinity conditions at 10, 15, 20 and 25MPa confining pressures, and the accuracy of the developed triaxial model was double-checked by converting it to uniaxial stress condition and validating it using data from triaxial tests conducted under 10-25MPa confining pressures. The uniaxial model was also important for understanding the effect of pore fluid salinity level on reservoir rock mass mechanical characteristics under a simple stress condition, which in turn offers some useful information on the direct influence of pore fluid salinity on reservoir rock mass strength characteristics, eliminating the influence of depth.

7.1.5 Basic assumptions

- 1) The reservoir rock mass with a finite-difference grid-block is homogeneous.
- 2) The reservoir rock sample is at a constant uniform temperature throughout the experiment.
- 3) The reservoir rock mass is free from any matrix-level anomalies
- 4) The modelled rock domain is bounded by four boundary conditions at top, bottom, right and left boundary.
- 5) All the stress points are on the defined yield surface.

The developed model was mainly used to predict the mechanical behaviour under high confining pressure conditions.

7.1.6 Results and discussion

A comparison of stress-strain behaviours obtained from experiments and numerical modelling under various salinity conditions at 10MPa confining pressure condition is shown in Fig. 7.5. As the figure shows, the proposed model successfully reproduces the behaviour of reservoir rock tested in the experimental investigation (Rathnaweera et al., 2015). However, validation of the proposed model is required before it can be used to predict reservoir rock behaviour under high confining pressure conditions. For this purpose, zero confining pressure was assigned in the model and the results were compared with the published data of Rathnaweera et al. (2014) in a uniaxial stress environment. An overall comparison of the stress-strain curves from the experimental study and the COMSOL simulation at zero confining pressure is shown in Fig. 7.6. Based on this figure, the model results are fairly consistent with the experimental results for all the tested conditions. To confirm the consistency of the proposed model, statistical analysis, including standard deviation and coefficient of variation was carried out on the

experimental results and the numerical modelling for each test condition (Table 7.4). Once the model was validated under both triaxial and uniaxial stress conditions, the model was used to study the mechanical behaviour of reservoir rock under extreme uniaxial and triaxial conditions and under high confining pressures.

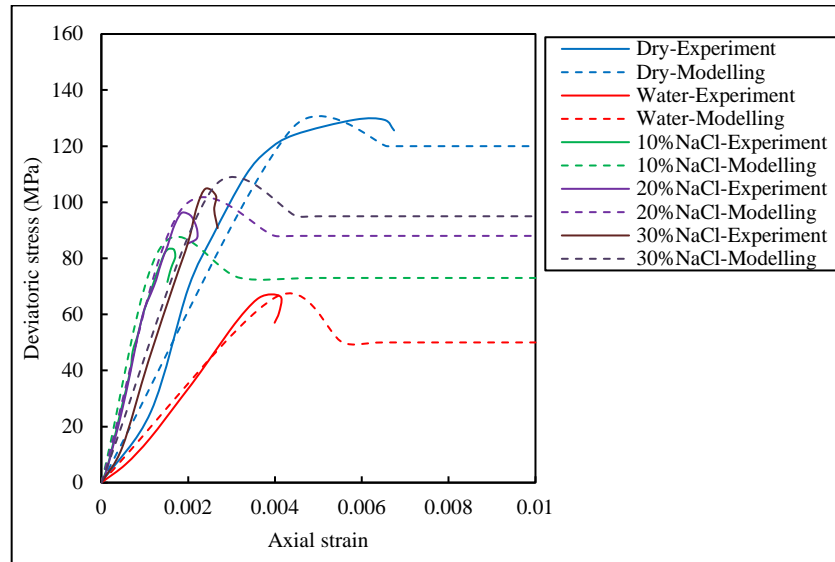


Figure 7.5. Overall comparison of stress-strain curves of reservoir rock tested under 10MPa confining pressure.

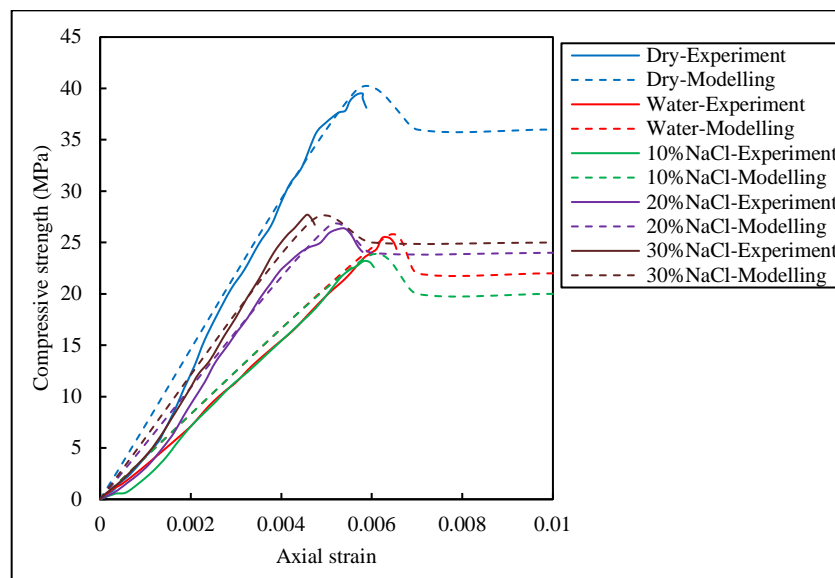


Figure 7.6. Overall comparison of stress-strain curves of reservoir rock saturated with different salinity conditions in unconfined environment.

Table 7.4. Results of statistical analysis.

Condition	Standard deviation (MPa)	Coefficient of variation (%)
dry	0.48	0.37
water	0.51	0.41
10%NaCl	0.78	0.94
20%NaCl	0.61	0.50
30%NaCl	0.35	0.27

7.1.6.1 Pore fluid salinity-dependent strength variation in reservoir rock in simplest stress environment (uniaxial compressive stress)

Prior to considering the complex triaxial stress environments in real field conditions, the simplest possible load condition or uniaxial load condition was first examined to distinguish the salinity effect from the confining effect to see the direct influence of pore salinity on reservoir strength characteristics. As shown in Fig. 7.7, first the model was validated using 10, 20 and 30% NaCl salinity conditions and then more salinity conditions (5, 15 and 25% NaCl) were predicted using the model in the salinity region expected in deep saline aquifers (<30% NaCl), in order to determine the influence of salinity on reservoir strength characteristics in a uniaxial stress environment.

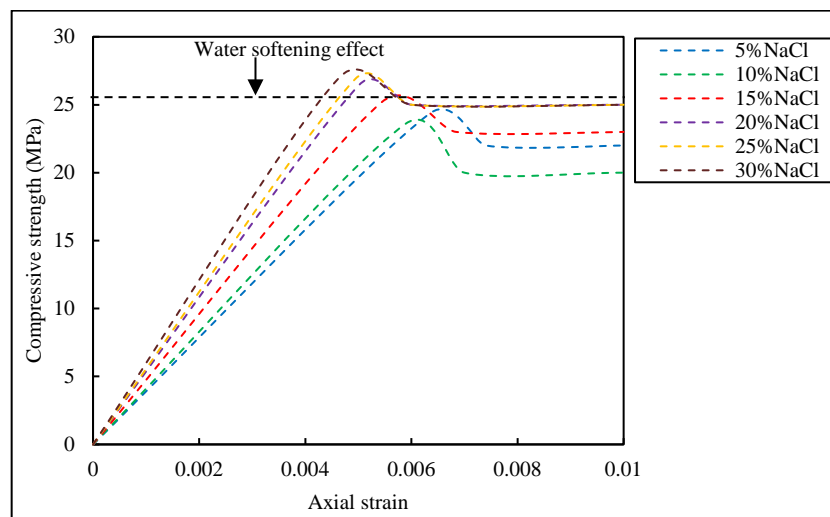


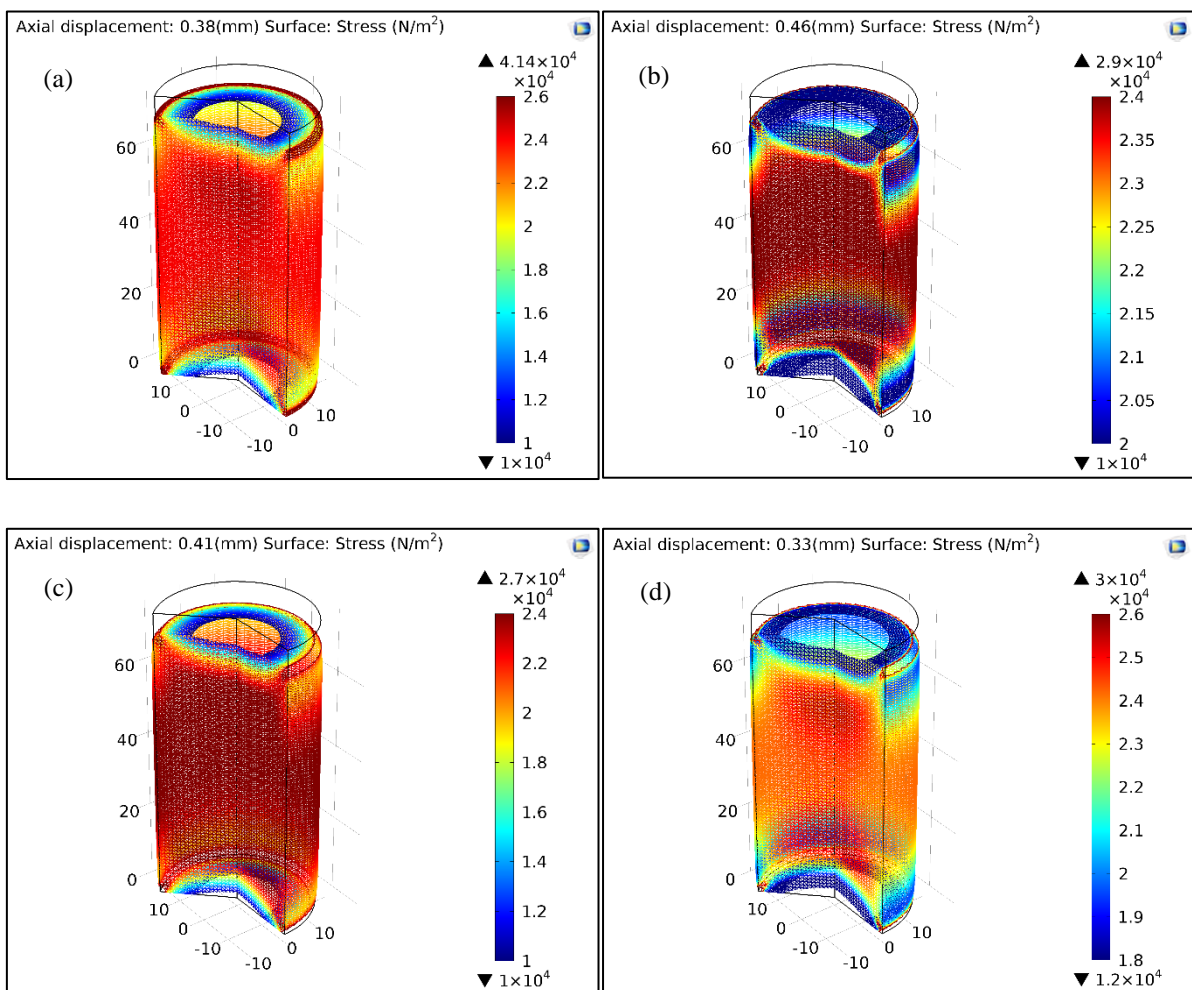
Figure 7.7. Predicted mechanical behaviour of reservoir rock under different salinity conditions.

According to Fig. 7.7, the uniaxial compressive strength of the saturated reservoir rock varies from 25.57 to 25.15MPa, 23.81MPa and 24.34MPa by changing the NaCl concentration in the

pore fluid from 0% to 15%, 10% and 5%, respectively with an increment in the trend after 10%. For example, the compressive strength increases from 23.81 to 25.15MPa by increasing the NaCl concentration from 10% to 15%. A similar trend can be seen up to 30% concentration of NaCl, and the compressive strength increases from 25.15 to 26.45MPa, 26.88MPa and 28.04MPa with increasing NaCl concentration from 15% to 20%, 20% to 25% and 25% to 30%, respectively. The uniaxial experimental study conducted on Otway Basin reservoir rocks by Shukla et al. (2013) also showed similar variation in compressive strength of reservoir rock with increasing salinity, however up to only 15%. According to Shukla et al. (2013), the compressive strength of Otway sandstone decreases from 36.27 to 35.89MPa, 36.27 to 33.03MPa and from 36.27 to 31.02MPa with increasing NaCl saturation from 0% to 15%, 0% to 10% and from 0% to 5%, respectively. According to these results, generally the water-softening effect on saturated reservoir rock is weakened by the existence of salinity in the pore water, and increasing the salinity level contributes more and more to the elimination of the softening effect, probably by the crystallisation of NaCl in the reservoir rock pore space. The enhancement of the water-softening effect at 10% (exhibited by the reduction of compressive strength with increasing salinity level from 5 to 10%) is a matter of interest and should be correlated with the NaCl ion corrosion effect (Rathnaweera et al., 2014). However, this critical point observed at 10% salinity is reservoir rock mass property-dependent. For example, the present study observed this critical NaCl concentration at 10% NaCl concentration, and the study conducted by Shukla et al. (2013) revealed this point at 5% NaCl concentration. The differences in pore geometry, including the porosity and mineral composition of the two formations in the present study and that of Shukla et al. (2013), are the main reason for these different behaviours. However, since enhancement of reservoir rock strength with increasing NaCl concentration is favourable for the long-term safety of CO₂ sequestration, this needs to be investigated prior to any fieldwork.

Fig. 7.8 shows the modelling results for the strain distribution of the reservoir rock specimens at failure under unconfined stress conditions. According to the results, the water-saturated sample exhibits the maximum axial displacement accumulation of 0.46 mm compared to the other tested conditions, probably due to the softening effect created by the water saturation. This has been demonstrated by many researchers who have shown that water softening causes elastic weakening, pore pressure increment (caused by the expanded rock matrix) and corrosive deterioration (Edmond and Paterson, 1972; Hadizadeh and Law, 1991). Interestingly, this

accumulated axial displacement appears to be reduced with increasing NaCl concentration in the reservoir rock mass. For instance, axial displacement decreases from 0.41 to 0.31 mm with increasing NaCl saturation from 10% to 30%. According to the experimental evidence of Shukla et al. (2013) and Rathnaweera et al. (2014), this strain reduction with increasing salinity is probably related to NaCl crystallization in the reservoir rock pore space under high salinity conditions. When the salinity increases, the amount of NaCl deposited in the rock pore space also increases and that in turn reduces the reservoir rock compressibility by adding additional cementation to the reservoir pore matrix. For this reason, the accumulated axial strain at failure reduces with increasing salinity.



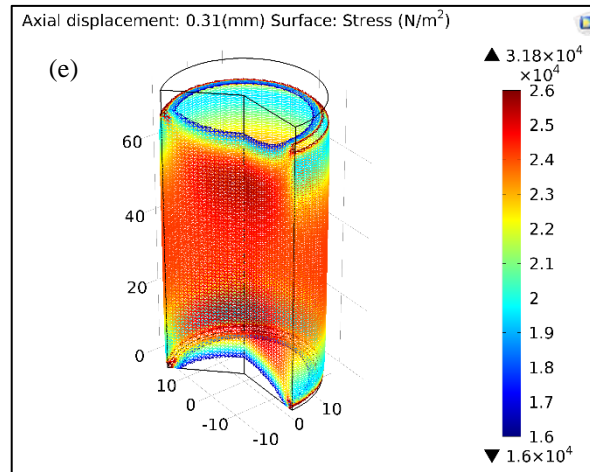


Figure 7.8. COMSOL results of strain distribution of reservoir rock specimens at failure under unconfined stress conditions (a) dry, (b) water-, (c) 10%NaCl-, (d) 20%NaCl-, and (e) 30%NaCl-saturated samples.

After obtaining a clear understanding of the influence of salinity on reservoir rock strength characteristics under the simplest possible stress condition, the more reliable triaxial stress condition was considered. The study of uniaxial and triaxial stress conditions assists in understanding the influence of reservoir depth-related in-situ stresses on pore fluid salinity in causing strength changes in deep saline aquifers.

7.1.6.2 Reservoir rock behaviour in real in-situ environment (triaxial stress)

The validated model was then used to predict the mechanical behaviour of reservoir rock in real in-situ situations in deep saline aquifers (confining stress environment) and possible extreme conditions (high confining stress). The most suitable deep saline aquifers for CO₂ sequestration are located at depths of 0.8 to 2km (Bachu and Bennion, 2008), at which confinements are around 25 to 60MPa, respectively. Therefore, to examine possible extreme conditions (or much deeper reservoir conditions), the model developed using data obtained under 10, 15, 20 and 25MPa confining pressures was used to examine the reservoir mechanical characteristics under much greater confinements (30 to 100MPa).

In general, rock becomes stronger with the application of confining pressure, due to its corresponding compacted nature. Confining pressure-dependent dry rock strength behaviour has been experimentally investigated by many researchers (Griggs, 1936; Mogi, 1966; Rathnaweera et al., 2015). According to these researchers, the failure mechanism changes from brittle to ductile with increasing confining pressure and this transitional confining pressure is

normally higher for stronger rocks. In addition, Mohr's internal friction angle decreases with increasing confining pressure (Mogi, 1966). Although the governing equations used in the present model fail to simulate this transition process (brittle to ductile) with increasing confining pressure, the model was successful in simulating the strain hardening effect after the yield point and non-linear post-peak behaviour after failure. The deviatoric stress variations obtained from the COMSOL model and experimental data under 20MPa confining pressure are shown in Fig. 7.9. According to the figure, the predicted mechanical behaviour of reservoir rock at 20MPa confining pressure successfully reproduces the measured data, confirming the model's accuracy. Under 20MPa confining pressure, the effective failure strength of the reservoir rock appears to increase with increasing salinity (NaCl concentration), which is similar to the reservoir rock behaviour in the uniaxial stress environment. For example, under 20MPa confining pressure, the failure strength increases from 110 to 125MPa and from 118 to 139MPa when the NaCl concentration of the pore fluid increases from 10 to 20% and from 20 to 30%, respectively.

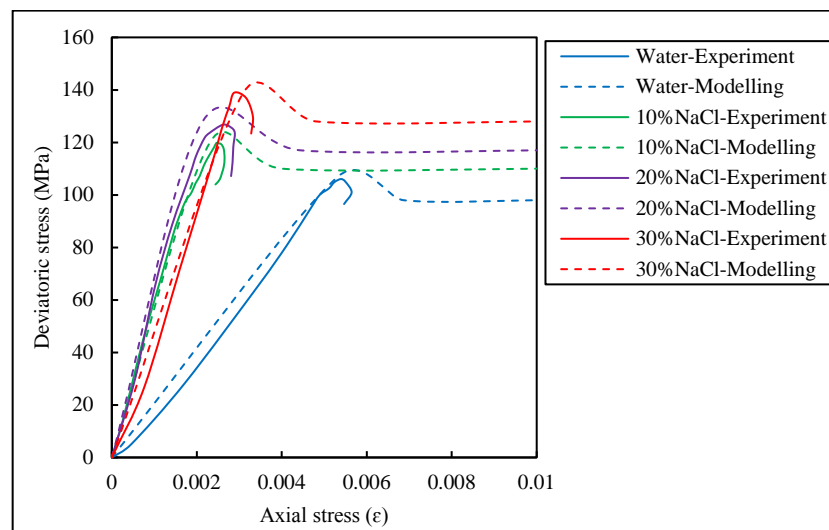
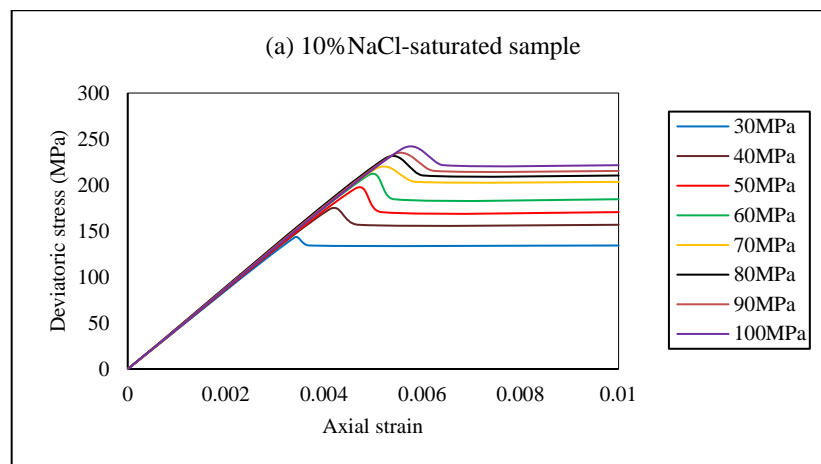


Figure 7.9. Deviatoric variations obtained from COMSOL model and experimental work for 20MPa confining pressure.

Fig. 7.10 shows the model's predicted deviatoric stress results for varyingly concentrated brine-saturated conditions at various high confining pressures. According to the figure, deviatoric stress generally increases with increasing confining pressure. For example, according to the results, increasing the confining pressure from 30 to 100MPa causes the deviatoric stress in 10%, 20% and 30% NaCl-saturated samples to increase from 143.26 to 238.56MPa, 154.34 to 241.34MPa and 165.13 to 257.35MPa, respectively. However, the rate of increment appears to

reduce with increasing confining pressure, especially after 60 MPa. For instance, in the 30% NaCl-saturated sample, when the confining pressure was increased from 30 to 40MPa, the deviatoric stress increases by 15.28%, whereas the corresponding increment for 90 to 100MPa confining pressure increment is only 1.81%, and the situation is similar for all the test conditions. A physical explanation for this phenomenon was given by Mogi (1966). According to him, at a sufficiently high confining pressure, the shear strength of a fault is eventually as high as the shear stress required to develop the fault through the intact rock. If this is the case, there is no stress drop when the fault forms. This hypothesis appears to be consistent with the findings of the present study.

The most important factor that is required to be tested in high confining pressure environments is how the salinity influences reservoir rock strength characteristics under such extreme confining conditions. As can be seen in the predicted behaviour in Fig. 7.10, the confining pressure effect dominates the mechanical behaviour of reservoir rock at such high depths compared to the salinity-dominant mechanical behaviour at shallow depths (<30MPa confinements). For example, at 30MPa confining pressure, the deviatoric stress increases from 143.26 to 190.35MPa with the increase of salinity from 10% to 30% NaCl in the pore fluid, which is a 32.87% increment. However, at 100MPa confining pressure, the deviatoric stress increases from 238.56 to only 257.35MPa with the increase of salinity from 10% to 30% NaCl in the pore fluid, which is a 7.88% increment. Therefore, it can be said that the higher the depth, the more negligible the effect of salinity on the mechanical behaviour of reservoir rock becomes compared to the depth effect (confining pressure). This provides an important finding on CO₂ sequestration in saline aquifers: salinity-dependent strength changes are not as important for extremely deep aquifers compared to shallow aquifers.



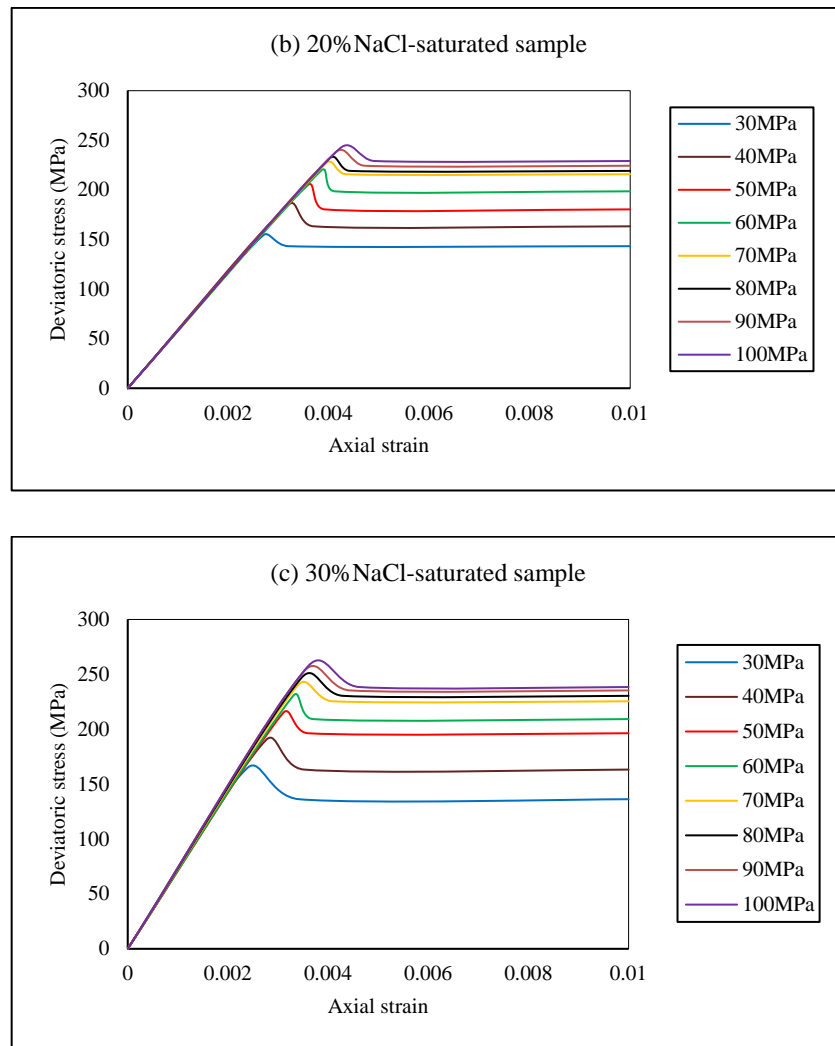


Figure 7.10. Predicted deviatoric stress results using COMSOL model for brine-saturated conditions.

Overall, the developed model successfully simulates the mechanical behaviour of reservoir rock in both uniaxial and triaxial stress environments under different salinity conditions. However, the simulation results exhibit some fluctuation near the post-peak compared to the experimental results, which might be due to the complex inhomogeneous deformation of the rock mass caused by strain localization which cannot be adequately incorporated in the model.

7.1.7 Conclusions

Pore fluid salinity and depth influences on the mechanical behaviour of reservoir rock (Hawkesbury sandstone) were numerically simulated following the development of a laboratory-scale triaxial model using the COMSOL Multiphysics simulator. The model validation was performed using measured triaxial laboratory test data under 10-25MPa

confining pressures. The model accuracy was double-checked by converting it to uniaxial test conditions by setting the confining pressure to zero and comparing the uniaxial model data with unconfined compressive strength results. The model was then used to investigate the influence of pore fluid salinity on reservoir rock strength by considering various possible salinity levels (5%, 10%, 15%, 20%, 25% and 30% NaCl) and the depth influence using a range of confining pressures (10-100MPa). The following conclusions can be drawn:

- The stiffness degradation mechanism can be used effectively to simulate the stress-strain data of Hawkesbury sandstone under brine saturation conditions. It is particularly important to identify the reservoir behaviour under extreme conditions as very high confinements are difficult situations to create in the laboratory environment.
- According to the developed laboratory-scale model, pore fluid salinity has a considerable impact on the mechanical behaviour of Hawkesbury sandstone, regardless of stress environment (uniaxial/ triaxial). This is consistent with the existing experimental findings in the field. The presence of NaCl in the aquifer pore fluid enhances the reservoir rock strength through the deposition of NaCl crystals in the rock mass pore structure, and the influence increases with increasing NaCl concentration in the pore fluid.
- The model also shows the considerable influence of confining pressure on reservoir rock mass strength, and at greater depths or confinements reservoir rocks have higher failure strengths due to their shrunken pore structure.
- Importantly, the model clearly shows the reduction of the influence of pore fluid salinity on reservoir rock strength with increasing reservoir depth or confinement, mostly due to the more significant effective stress at extreme depths. For example, the failure strength increased by only around 7.88% with increasing pore fluid salinity from 10% to 30% NaCl at 100MPa confinements and by the huge amount of around 66.54% with increasing confining pressure from 30 to 100MPa at 30% NaCl salinity. An important finding on CO₂ sequestration in saline aquifers is that salinity-dependent strength changes are not as important for extremely deep aquifers as for shallow aquifers.
- In addition, according to the model, the influence of confining stress on reservoir rock strength reduces with increasing confining stress due to limitations in pore shrinkage, particularly after around 60MPa confinement when the influence becomes negligible. For example, in 30% NaCl-saturated samples, 15.27% and 1.8% strength increments were

observed with increasing confining pressure from 30 to 40MPa and 90 to 100MPa, respectively.

- Overall, the predicted reservoir rock mass strength enhancement under elevated salinity conditions is a favourable condition for CO₂ sequestration in deep saline aquifers. However, this should be counter-checked with other factors, such as reservoir depth and temperature, CO₂ injection pressure and the chemical and mineralogical behaviour of reservoir rock in CO₂ rich environments.

7.1.8 References

1. Bachu S, Bennion B. Effects of in-situ conditions on relative permeability characteristics of CO₂-brine systems. *Environmental Geology* 2008; 54: 1707-1722.
2. Cao WG, Li X, Zhao H. Damage constitutive model for strain-softening rock based on normal distribution and its parameter determination. *Journal of Central South University of Technology* 2007; 14(5): 719-724.
3. Chen GQ, Feng XT, Jiang Q. Study of dynamic early warning method of surrounding rock deformation monitoring for large underground powerhouse considering rock degradation. *Rock and Soil Mechanics* 2010; 31(9): 3012-3018.
4. Class H, Ebigbo A, Helmig R, Dahle HK, Nordbotten JM, Celia MA, et al. A benchmark study on problems related to CO₂ storage in geological formations. *Computers and Geosciences* 2009; 13: 409-434.
5. Edmond JM, Paterson MS. Volume change during the deformation of rocks at high pressure. *International Journal of Rock Mechanics and Mining Science* 1972; 9: 161-182.
6. Flora A, Lirer S. Small strain shear modulus of undisturbed gravelly soils during undrained cyclic triaxial tests. *Geotechnical and Geological Engineering* 2013; 31(4): 1107-1122.
7. Griggs DT. Deformation of rocks under high confining pressure. *Journal of Geology* 1936; 44: 541-577.
8. Hadizadeh J, Law RD. Water weakening of sandstone and quartzite deformed at various stress and stress rates. *International Journal of Rock Mechanics and Mining Science* 1991; 221: 431-439.
9. Hoek E, Brown ET. Practical estimates of rock mass strength. *International Journal of Rock Mechanics and Mining Sciences* 1997; 34(8): 1165-1187.
10. Joseph TG, Barron K. The post-failure characteristics of rock. *CIM Bulletin* 2003; 96(1070): 66-76.
11. Li YJ, Zhang DL, Liu BG. Development and verification of strain-softening model considering deformation modulus degradation in FLAC3D. *Rock and Soil Mechanics* 2011; 32(S2): 647-659.

12. Lu YL, Wang LG, Yang F. Post-peak strain softening mechanical properties of weak rock. *Chinese Journal of Rock Mechanics and Engineering* 2010; 29(3): 640-648.
13. Lubarda VA, Mastilovic S, Knap J. Brittle-ductile transition in porous rocks by cap model. *Journal of Engineering Mechanics* 1996; 122(7): 633-642.
14. Martin CD. Seventeenth Canadian Geotechnical Colloquium: the effect of cohesion loss and stress path on brittle rock strength. *Canadian Geotechnical Journal* 1997; 34(5): 698-725.
15. Martin CD, Chandler N. The progressive fracture of Lac du Bonnet granite. *International Journal of Rock Mechanics and Mining Sciences and Geomechanics* 1994; 31(6): 643-659.
16. Mogi K. Pressure dependent of rock strength and transition from brittle fracture to ductile flow. *Bulletin of the Earthquake Research Institute* 1966; 44: 215-232.
17. Niu SJ, Jing HW, Yang XX. Experimental study of strength degradation law of surrounding rock in fractured zone of deep roadway. *Chinese Journal of Rock Mechanics and Engineering* 2012; 31(8): 1587-1596.
18. Perera MSA, Ranjith PG, Ranathunga AS, Koay AYJ, Zhao J, Choi SK. Optimization of enhanced coal-bed methane recovery using numerical simulation, *Journal of Geophysics and Engineering* 2014; 12: 90-107.
19. Perera MSA, Ranjith PG, Choi SK, and A Bouazza. A parametric study of coal mass and cap rock behaviour and carbon dioxide flow during and after carbon dioxide injection, *Fuel* 2013;106:129-138.
20. Ranjith, P.G, Perera, M.S.A., and E. Khan. A study of safe CO₂ storage capacity in saline aquifers: a numerical study, *International Journal of Energy Research* 2013; 37(3): 189-199.
21. Rathnaweera TD, Ranjith PG, Perera MSA. Salinity-dependent strength and stress-strain characteristics of reservoir rocks in deep saline aquifers: An experimental study. *Fuel* 2014; 122: 1-11.
22. Rathnaweera TD, Ranjith PG, Perera MSA, Aref Lashin, Nassir Al Arifi. Non-linear stress-strain behaviour of reservoir rock under brine saturation: an experimental study. *Measurement* 2015; 71: 56-72.
23. Robinson BA, Viswanathan HS, Valocchi AJ. Efficient numerical techniques for modelling multi-component groundwater transport based upon simultaneous solution of strongly coupled subsets of chemical components. *Advanced Water Resources* 2000; 23: 307-324.

24. Seo JG, Mamora DD. Experimental and simulation studies of sequestration of supercritical carbon dioxide in depleted gas reservoirs. *Energy and Resource Technology* 2005; 127: 234-241.
25. Shukla R, Ranjith PG, Choi SK, Haque A, Yellishetty M, Hong L. Mechanical behaviour of reservoir rock under brine saturation. *Rock Mechanics and Rock Engineering* 2013; 46 (1): 83-89.
26. Toshikazu K. An analysis of excavation in strain softening rock. *Proceedings of the Japan Society of Civil Engineers* 1981; 34: 107-117.
27. Wang XB, Pan YS, Dai SH. Stability analysis of shear-band and surrounding-rock system considering stiffness deterioration. *Journal of Disaster Prevention and Mitigation Engineering* 2009; 29(2): 147-153.
28. Wei L. Estimate CO₂ storage capacity of the Johansen formation: numerical investigation beyond the benchmarking exercise. *Computers and Geosciences* 2009; doi:10.1007/s10596-008-9122-x.
29. Yu HJ, Zhang CH, Wang LG. Post-peak strain softening model of rock based on degradation angle. *Journal of China Coal Society* 2012; 37(3): 402-406.
30. Zdenek P, Bazant F. Continuum theory for strain softening. *Journal of Engineering Mechanics* 1984; 110(12): 1666-1692.
31. Zhang F, Sheng Q, Zhu ZQ. Study of post-peak mechanical behaviour and strain-softening model of Three Gorges granite. *Chinese Journal of Rock Mechanics and Engineering* 2008; 27(S1): 2651-2655.
32. Zhang K, Zhou H, Shao JF. An experimental investigation and an elastoplastic constitutive model for a porous rock. *Rock Mechanics and Rock Engineering* 2013; 46(6): 1499-1511.
33. Zhao Z, Wang W, Gao X. Evaluation laws of strength parameters of soft rock at the post-peak considering stiffness degradation. *Applied Physics and Engineering* 2014; 15(4): 282-290.

7.2 Investigation of relative flow characteristics of Hawkesbury formation under laboratory conditions

Although CO₂ sequestration in deep saline aquifers provides a promising solution to effectively mitigate anthropogenic CO₂ emissions, the interaction between injected CO₂ and brine leads to unpredictable hydro-mechanical behaviours in the reservoir formation during storage. In particular, the relative flow behaviour of the reservoir critically affects the safety and efficiency of sequestration. Therefore, precise knowledge of this is paramount for the long-term integrity of any sequestration project. The main objective of this section is to develop a laboratory-scale relative-flow model which can simulate the relative flow behaviour of brine-saturated Hawkesbury sandstone. The proposed model was used to simulate the triaxial tests conducted on reservoir rock reported in Chapter 6. The following submitted journal paper explains the numerical simulation procedure and the outcomes.

Investigation of Relative Flow Characteristics of Brine-saturated Reservoir Rock: A Numerical Study of the Hawkesbury Formation

T. D. Rathnaweera¹, P.G. Ranjith¹, M. S. A. Perera¹

¹Department of Civil Engineering, Monash University, Building 60, Melbourne, Victoria, 3800, Australia.

Abstract

Precise knowledge of the relative flow behaviour of CO₂ and brine during CO₂ sequestration in deep saline aquifers and its impact on the sequestration process is required to ensure the safety and efficiency sequestration project. This numerical study therefore aims to identify the interaction-induced relative flow behaviour of reservoir rock. COMSOL Multiphysics numerical simulator was used to develop a laboratory-scale relative flow model to simulate the CO₂ movement and brine drainage processes in brine-saturated Hawkesbury sandstone samples. A 2-D axisymmetric pore-elastic model was developed using the pore-elastic module available in COMSOL and Buckley-Leverett flow theory was applied to the model using pre-defined partial differential equations. The proposed model was first validated using experimental permeability data conducted under triaxial drained conditions and the model was then extended to predict relative flow characteristics, such as brine and CO₂ saturation and CO₂ pressure distribution along the sample length under different injection pressures, including both sub- and super-critical conditions.

According to the results, the developed model simulates the experimental results reasonably well with less than 10% relative error. The numerical results also reveal that there is a considerable effect of CO₂ phase change on the final distribution of the CO₂ and brine saturation profiles. In addition, the CO₂ pressure distribution along the sample length shows a non-linear relationship between the CO₂ pressure and sample length.

Keywords: relative flow, COMSOL, sub-critical, super-critical, injection pressure

7.2.1 Introduction

Carbon dioxide (CO₂) sequestration in deep saline aquifers is a promising solution for the mitigation of anthropogenic CO₂ emissions (Perera et al., 2011; Rathnaweera et al., 2014). To date, growing awareness about global warming has made the effects of CO₂ sequestration on

reservoir rock hydro-mechanical behaviour a topic of great research interest. As a result, field-scale numerical studies have been reported on the hydro-mechanical behaviour of deep saline reservoir rock upon exposure to CO₂ (Andre et al., 2007; Burton et al., 2009). However, little attention has been given to how CO₂ injection is affected under laboratory-scale conditions. Therefore, the present study aims to address this gap by developing a laboratory-scale relative flow model capable of simulating reservoir rock flow behaviour in a CO₂ sequestration environment. To develop the simulation, the present study used the COMSOL Multiphysics simulator and pre-defined partial differential equations were employed to characterise the relative flow behaviour of the Hawkesbury formation under laboratory-scale conditions.

In relation to CO₂ sequestration in deep saline aquifers, a thorough understanding of the two-phase flow of CO₂ and aquifer brine through porous reservoir rock is important for both analytical and numerical simulations. Almost 160 years have passed since Darcy (1856) introduced his first theory, which is considered to be the starting point of the development of the scientific quantitative theory of flow through porous media. Since then, a considerable number of studies have been carried out to expand the basic flow theory introduced by Darcy to capture complex flow phenomena, including multi-phase flows, deformation of solid matrix, non-linear flow regimes, and other transport processes (mass, heat, etc.). In addition, the theory of two-phase flow through porous media has undergone extensive development in the last three decades due to its capability of simulating many engineering applications (Dogan, 1986). Of these applications, the interaction between aqueous brine and injected CO₂, such as the dissolution of CO₂ in brine and the adsorption of CO₂ into the rock matrix makes deep saline sequestration flow behaviour even more complex. Therefore, the identification of appropriate two-phase flow models applicable to deep saline sequestration is important for numerical and experimental investigations. To date, a considerable number of two-phase models have been proposed (Corey, 1954; Brooks and Corey, 1964; Mualem, 1976; Muller, 2011; Mitiku and Bauer, 2013; Oostrom et al., 2016), and some of these models are summarised in Table 7.5.

Table 7.5. Overview of existing two-phase flow models.

Model	Saturation-capillary pressure model ($S - P_c$)	Relative permeability-saturation model ($k_r - S$)	Remarks
VG-M(Van Genuchten-Mualem)	$\overline{S}_l = [1 + \alpha P_c^{n_v}]^{-m_v}$ or $\overline{S}_l = [1 + (\frac{P_c}{P_0})^{n_v}]^{-m_v}$	For $S_l > S_{li}$ $k_{rl} = \overline{S}_l^{-1/2} [1 - (1 - \overline{S}_l^{1/m_v})]^2$ $k_{rg} = \overline{S}_g^{-1/2} [1 - (1 - \overline{S}_l^{1/m_v})]^2$ For $S_l \leq S_{li}$ $k_{rl} = 0$ $k_{rg} = 1$	<ul style="list-style-type: none"> • Couple ($k_r - S$) and ($S - P_c$) model using same pore-geometry and m_v parameter • Widely used to predict plume behaviour
BC-B(Brooks-Corey-Burdine)	$\overline{S}_l = (\frac{P_c}{P_0})^{-\lambda}$	For $S_l > S_{li}$ $k_{rl} = \overline{S}_l^{(3+2/\lambda)}$ $k_{rg} = \overline{S}_g^2 [1 - \overline{S}_l^2]$ For $S_l \leq S_{li}$ $k_{rl} = 0$ $k_{rg} = 1$	<ul style="list-style-type: none"> • Couple and model using same pore-geometry and λ parameter • Widely used to analyse coupled wellbore-reservoir flow during injection
VG-C(Van Genuchten-Corey)	$\overline{S}_l = [1 + \alpha P_c^{n_v}]^{-m_v}$ or $\overline{S}_l = [1 + (\frac{P_c}{P_0})^{n_v}]^{-m_v}$	For $S_l > S_{li}$ $k_{rl} = \overline{S}_l^4$ $k_{rg} = \overline{S}_g^2 [1 - \overline{S}_l^2]$ For $S_l \leq S_{li}$ $k_{rl} = 0$ $k_{rg} = 1$	<ul style="list-style-type: none"> • Uncouple approach of ($k_r - S$) and ($S - P_c$) model • Used to investigate combined effects of capillary pressure and salinity and in situ thermodynamic conditions • Salt precipitation and associated pressure build up
VG-hMC(Van Genuchten-hybrid Mualem-Corey)	$\overline{S}_l = [1 + \alpha P_c^{n_v}]^{-m_v}$ or $\overline{S}_l = [1 + (\frac{P_c}{P_0})^{n_v}]^{-m_v}$	For $S_l > S_{li}$ $k_{rl} = \overline{S}_l^{-1/2} [1 - (1 - \overline{S}_l^{1/m_v})]^2$ $k_{rg} = \overline{S}_g^2 [1 - \overline{S}_l^2]$ For $S_l \leq S_{li}$ $k_{rl} = 0$ $k_{rg} = 1$	<ul style="list-style-type: none"> • Hybrid between coupled ($k_{rl} - S$) and ($S - P_c$) model and uncoupled ($k_{rg} - S$) • Most widely used model for scCO₂ injection
VG-EPL(Van Genuchten-Endpoint Power Law)	$\overline{S}_l = [1 + \alpha P_c^{n_v}]^{-m_v}$ or $\overline{S}_l = [1 + (\frac{P_c}{P_0})^{n_v}]^{-m_v}$	For $S_l > S_{l0}$ $k_{rl} = k_{rl0-EPL} \left(\frac{S_l - S_{l0}}{1 - S_{l0}} \right)^{N_{l-EPL}}$ $k_{rg} = k_{rg0-EPL} \left(\frac{S_g}{1 - S_{l0}} \right)^{N_{g-EPL}}$	<ul style="list-style-type: none"> • Difficult to use endpoint S_{l0} in the relative permeability relations which is larger than the irreducible saturation S_{li}

		For $S_l \leq S_{l0}$ $k_{rl} = 0$ $k_{rg} = 1 - \left(\frac{1 - k_{rg0-EPL}}{S_{l0}} \right) S_l$	
BC-vC(Brooks-Corey-variable Corey)	$\overline{S}_l = \left(\frac{P_c}{P_0} \right)^{-\lambda}$	For $S_l > S_{li}$ $k_{rl} = \overline{S}_l^{N_{l-vC}}$ $k_{rg} = k_{rg0-vC} \overline{S}_g^2 [1 - \overline{S}_l^{N_{g-vC}}]$ For $S_l \leq S_{li}$ $k_{rl} = 0$ $k_{rg} = 1 - \left(\frac{1 - k_{rg0-vC}}{S_{li}} \right) S_l$	<ul style="list-style-type: none"> The other model using fitted $(k_r - S)$ relations, the BC-vC model, uses variable exponents, with values depending on the fit to the experimental data

Generally, the injection of CO₂ into deep saline aquifers can be characterised by mass conservation equations for the three components, water, salt (NaCl) and CO₂. Ignoring non-isothermal effects, chemical reactions and the effects of mechanical stress, Pruess et al. (1999) introduced a three-phase system, water-salt-CO₂, following the mass conservation equation:

$$\frac{d}{dt} \int_{V_n} M^K dV_n = \int_{\Gamma_n} F^K \cdot n d\Gamma_n + \int_{V_n} q^K dV_n \quad (7.27)$$

In addition, some initial simulation studies of CO₂ injection into deep saline aquifers have been conducted with existing petroleum reservoir simulators (van der Meer, 1992; Korbol and Kaddour, 1995; Weir et al., 1995; Law, 1996; Law and Bachu, 1996). However, as mentioned earlier, a small number of studies have been undertaken on the application of these simulators to problems with small rock domains. Tang et al. (2002) conducted a numerical study to investigate the coupled behaviour of flow, stress and damage in rock failure. They proposed a flow-stress-damage (FSD) coupling model for heterogeneous rocks that takes into account the growth of existing fractures and the formation of new fractures. The simulation results of this study revealed that the nature of fluid flow in rocks varies from material to material, and strongly depends upon the heterogeneity of the rock. Kueper and Frind (1991) performed two-phase flow simulation to characterise the migration properties of a dense, non-aqueous phase liquid through heterogeneous porous rock using input parameters from laboratory measurements of capillary pressure-saturation curves. The results of this study showed the migration characteristics of non-wetting liquid strongly depend on the capillary properties of the porous medium and are also influenced by the fluid's physical properties. Mercer and Cohen

(1990) performed a numerical study on non-aqueous phase liquids and found that these non-aqueous liquids behave differently from dissolved solutes in the sub-surface. Watanabe et al. (2008) developed a numerical model to simulate the fracture permeability of artificially-developed granite. The model was basically used to characterise the fluid flow behaviour through rock fractures under confining pressures. According to these researchers, numerically obtained fracture permeability is important for understanding sub-surface flow, especially the fluid flow behaviour in aperture structures under different confining pressures. Although there are a number of studies on rock fluid interaction under laboratory conditions, a small number of laboratory-scale numerical studies have set out to identify the CO₂ sequestration effects, but their research is limited. For example, Andre et al. (2014) presented a coupled numerical approach to represent the drying mechanisms of brine-saturated reservoir rocks under laboratory conditions. According to their results, the capillary properties of reservoir rock prevent the sudden evaporation of irreducible water. Moreover, they showed that the capillary force effect can be minimised by maintaining a sufficient CO₂ injection rate. In addition, the results also revealed that brine salinity in the aquifer has a major impact on reservoir rock porosity and permeability.

A review of various two-phase relative permeability-saturation-capillary pressure models by Oostrom et al. (2016) revealed the applicability of those models to the simulation of deep saline sequestration. Six published numerical multiphase concepts, including van Genuchten-Mualem, Brooks-Corey-Burdine, van Genuchten-Corey, van Genuchten-hybrid Mualem-Corey, van Genuchten-endpoint power law and Brooks-Corey-variable Corey were analysed using data from four well-characterised sandstones (Berea, Paaratte, Tuscaloosa, Mt. Simon). According to their results, the plume extension and saturation distribution of each sandstone highly depends on the nature of the relative permeability-saturation-capillary pressure model used. Moreover, the van Genuchten-Mualem model over-estimated the CO₂ relative permeability, resulting in considerably large plume distributions during and after injection. In addition, the van Genuchten-Corey model predicted the smallest plume distribution due to the under-estimation of the aqueous phase relative permeability. Of the six models, the van Genuchten-hybrid Mualem-Corey and Buckley-Leverett models were found to be the best fit to the experimental results. Therefore, in order to have accurate flow estimations, it is necessary to select a reliable relative permeability relation when modelling deep saline sequestration process.

Therefore, the present study selected the Buckley-Leverett flow concept to develop a laboratory-scale model using the COMSOL Multiphysics simulator and the model was then validated using experimental data. The relative flow behaviour of brine-saturated Hawkesbury sandstone under triaxial laboratory conditions was simulated by injecting CO₂ at a constant pressure at one end of the sample and the drainage characteristics of both CO₂ and brine were evaluated. In addition, the influence of CO₂ injection pressure, including the phase behaviour of CO₂ on the relative flow characteristics of reservoir rock, was also investigated. The model concept and the governing equations developed are presented in the next section.

7.1.2 Model concept and governing equations

The intension of this study is to couple the relative flow model with multiphase and multicomponent equations to investigate the migration of CO₂ through brine-saturated reservoir rock under laboratory conditions. In order to fulfil this requirement, beta model (Chen, 2000), a well-known multiphase fluid flow model in reservoir engineering, was incorporated. Generally, this model deals with three phases: water, oil and gas. However, in order to apply this flow model to the simulation of the relative flow behaviour of a two-phase system which has only brine and CO₂, the present study modified the existing multiphase fluid flow equations as follows. Taking into account two-phase behaviour, the mass balance equation for a CO₂ and brine system can be written as follows:

For the brine phase:

$$\phi \frac{\partial}{\partial t} \left(\frac{S_b}{B_b} \right) + \nabla \cdot \left(\frac{1}{B_b} u_b \right) = q_b \quad (7.28)$$

For the CO₂ phase:

$$\phi \frac{\partial}{\partial t} \left(\frac{S_{CO_2}}{B_{CO_2}} + \frac{R_{sb} S_b}{B_b} \right) + \nabla \cdot \left(\frac{1}{B_{CO_2}} u_{CO_2} + \frac{R_{sb}}{B_b} u_b \right) = q_{CO_2} \quad (7.29)$$

Here, \underline{u}_b and \underline{u}_{CO_2} represent the volumetric phase velocity, which can be characterised by the two-phase Darcy law as follows:

$$\underline{u}_\alpha = - \frac{kk_{r\alpha}}{\mu_\alpha} (\nabla P_\alpha - \rho_\alpha g) ; \quad (7.30)$$

where, $\alpha = b, CO_2$

After defining the basic equations, to make the solution converge (as the system has only two equations and it contains four unknowns), two additional equations were introduced to the system as follows:

$$S_b + S_{CO_2} = 1 \quad (7.31)$$

$$P_{cbCO_2} = P_{CO_2} - P_b \quad (7.32)$$

Eqs. 7.28 and 7.29 were then combined to simplify the mass balance equation and transformed into a single pressure equation as follows:

$$\nabla \underline{u} = \sum_{\alpha=b, CO_2} B_\alpha \left[q_\alpha - \phi S_\alpha \frac{\partial}{\partial t} \left(\frac{1}{B_\alpha} \right) - \underline{u}_\alpha \cdot \nabla \left(\frac{1}{B_\alpha} \right) \right] - B_{CO_2} \left(\phi \frac{S_b}{B_b} \frac{\partial R_{sb}}{\partial t} + \frac{1}{B_b} \underline{u}_b \cdot \nabla R_{sb} \right) \quad (7.33)$$

where, total (\underline{u}) and phase velocities (\underline{u}_b and \underline{u}_{CO_2}) are given by;

$$\underline{u} = -k\lambda \left[\nabla P_b + f_{CO_2} \nabla P_{cbCO_2} - g \nabla z \sum_\alpha f_\alpha \rho_\alpha \right] \quad (7.34)$$

$$\underline{u}_b = f_b \underline{u} + k f_b \lambda_{CO_2} \left[\nabla P_{cbCO_2} - (\rho_{CO_2} - \rho_b) g \nabla z \right] \quad (7.35)$$

$$\underline{u}_{CO_2} = f_{CO_2} \underline{u} + k f_{CO_2} \lambda_b \left[-\nabla P_{cbCO_2} - (\rho_b - \rho_{CO_2}) g \nabla z \right] \quad (7.36)$$

where λ_α is the phase mobility function which defines as $\lambda_\alpha = \frac{k_{r\alpha}}{\mu_\alpha}$ and accordingly, the total

mobility (λ) can be written as, $\lambda = \sum \lambda_\alpha$. In addition, the fractional flow function (f_α) can be

expressed as $f_\alpha = \frac{\lambda_\alpha}{\lambda}$ and the total velocity can be defined as, $\underline{u} = \sum \underline{u}_\alpha$.

Finally, Buckley-Leverett relative permeability constitutive equations were introduced to the system to simulate the relative flow behaviour of reservoir rock:

$$k_{rb} = S_e^2 \quad \text{and} \quad k_{rCO_2} = (1 - S_e)^2 \quad (7.37)$$

where, S_e is the normalised saturation which is defined as:

$$S_e = \frac{S_b - S_{rb}}{1 - S_{rb} - S_{rCO_2}} \quad (7.38)$$

7.2.3 Model development

7.2.3.1 Basic assumptions

- 1) Reservoir rock was modelled as a poro-elastic material and drained matrix and isotropic properties were used to define the reservoir flow properties.
- 2) Due to the short period of injection, the reaction between CO₂ and rock minerals was assumed to be zero.
- 3) The effect of gravity was ignored.
- 4) The major fluid driving force across the reservoir rock was assumed to be the pressure gradient.
- 5) The dissolution of CO₂ in brine can be ignored due to the short period of injection.
- 6) CO₂ adsorption into reservoir rock matrix was assumed to be zero.
- 7) Residual brine saturation was assumed to be constant for all the injection pressure conditions.
- 8) In order to simulate the drained conditions, the top boundary pressure was assumed to be equal to atmospheric pressure (0.1MPa).

7.2.3.2 Geometry, boundary conditions and input parameters

The present study considered a 2-D axisymmetric porous domain 38mm in diameter and 76mm long, initially saturated with brine. CO₂ was injected at a constant pressure at the bottom end to displace brine to the other end. The model boundary conditions and the assumed mesh pattern for the study are shown in Fig. 7.11. In order to simulate the laboratory triaxial conditions, the top boundary was modelled by roller support, since in the laboratory, the bottom boundary moves upward while keeping the top boundary fixed in the axial direction and moving freely in the lateral direction. The bottom boundary was modelled by the fixed support condition and injection pressures were applied to the bottom boundary. The hydrostatic pressure condition was applied using confining pressure and the parametric sweep function was used to input different injection pressures. In addition, confining and injection pressure-induced axial load (F_v) was applied to the bottom boundary, as shown in Fig. 7.11.

The flow behaviour of reservoir rock was simulated by previously defined partial differential equations (see Section 7.2.2) and the derived equations were introduced to the model using PDE mode for time-dependent analysis in coefficient form. In addition, the poro-elastic module was incorporated to model the reservoir rock sample and mechanical boundary conditions. The

relevant input parameters were taken from the laboratory experiments and are provided in Table 7.6.

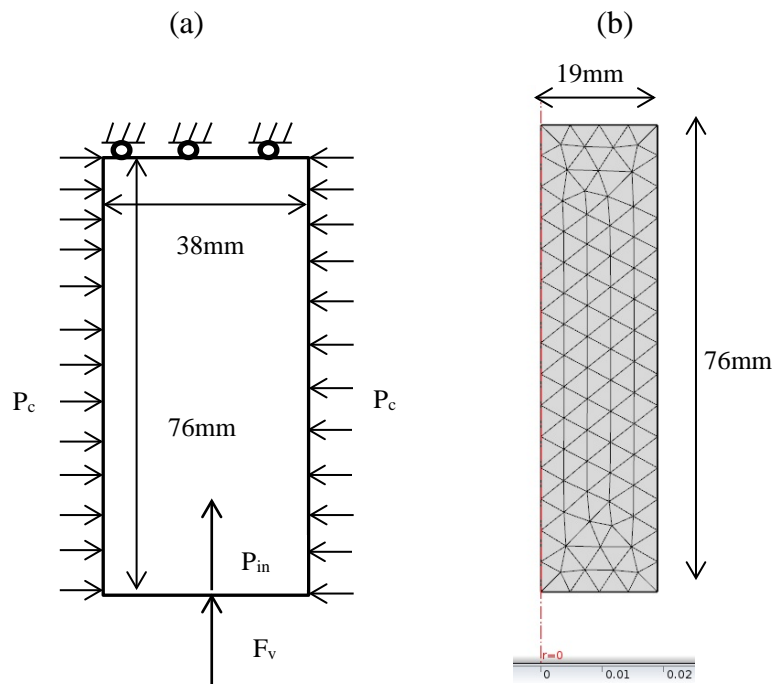


Figure 7.11. Model boundary conditions and the assumed mesh pattern for this study.

Table 7.6. Input parameters for the model.

Value	Description
6.32[GPa]	Young's modulus of sandstone
0.26	Poisson's ratio of sandstone
0.31	Porosity of sandstone
2600[kg/m ³]	Density of sandstone
0.67[GPa]	Bulk modulus of sandstone
40[MPa]	Shear modulus of sandstone
0.7	Biots-Willis coefficient
1.0×10 ⁻¹² [m ² /s]	Liquid phase diffusion coefficient
35°C	Temperature
100mD	Absolute permeability
5×10 ⁻¹¹ [MPas]	Brine viscosity
1.5×10 ⁻¹¹ [MPas]	CO ₂ viscosity
0.01	Residual brine saturation
20MPa	Confining pressure

The model was first used to discuss the influence of CO₂ injection pressure, including both sub- and super-critical, on CO₂/brine saturation in the reservoir pore structure. To include both sub- and super-critical conditions, the simulation was run for different injection pressures (1-7MPa sub-critical and 8-14MPa super-critical pressures) at a constant confining pressure of 20MPa.

7.2.3.3 Model validation using experimental data

The developed laboratory-scale model was first validated using experimental data. For the validation, the triaxial drained experimental condition was considered with two different injection scenarios: 4 and 8MPa CO₂ injection pressures at 20MPa confining pressure. The experimental results are shown in Fig. 7.12, along with the corresponding model predictions. According to Fig. 7.12, the predicted simulation results are consistent with the experimental data. In addition, Table 7.7 presents the relative error of the numerical predictions with respect to the experimental data. All two relative errors are well below 10%, which confirms the accuracy of the proposed model in predicting the relative flow behaviour of the Hawkesbury formation in a CO₂ sequestration environment.

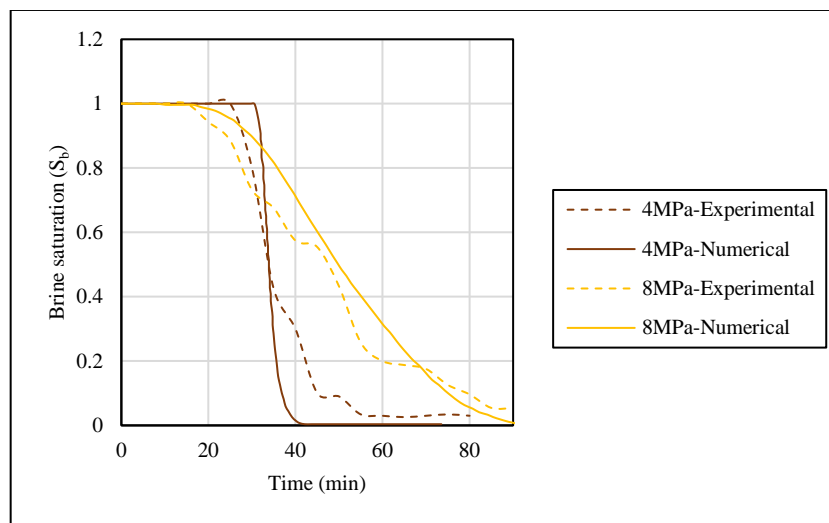


Figure 7.12. Comparison of brine saturation of reservoir rock obtained from experiments and COMSOL model (20MPa confining pressure).

Table 7.7. Relative error of numerical predictions with respect to experimental data.

Injection condition	Brine saturation
	Relative error (%)
4MPa	7.32
8MPa	6.46

The present study analysed the convergence properties of the liquid-phase diffusion coefficient, for precise quantification of the required accuracy of model predictions. To date, ample studies have confirmed the requirement of estimating convergence properties of diffusion coefficients for accurate simulation results (Diaz-Viera et al., 2008). Therefore, four different diffusion coefficients were considered. Fig. 7.13 shows the numerical solutions of the flow problem with varying diffusion coefficients. As expected, the predictions of the simulation strongly depend on the diffusion coefficient. For values of the diffusion coefficient between 10^{-10} - 10^{-13} m^2/s , the numerical predictions converged. As Fig. 7.13 shows, the best trade-off in terms of efficiency and accuracy for the diffusion coefficient has the value of 10^{-12} m^2/s . This value was taken and considered for the modelling to simulate the relative flow behaviour of the Hawkesbury formation. The results are presented and discussed in the following section.

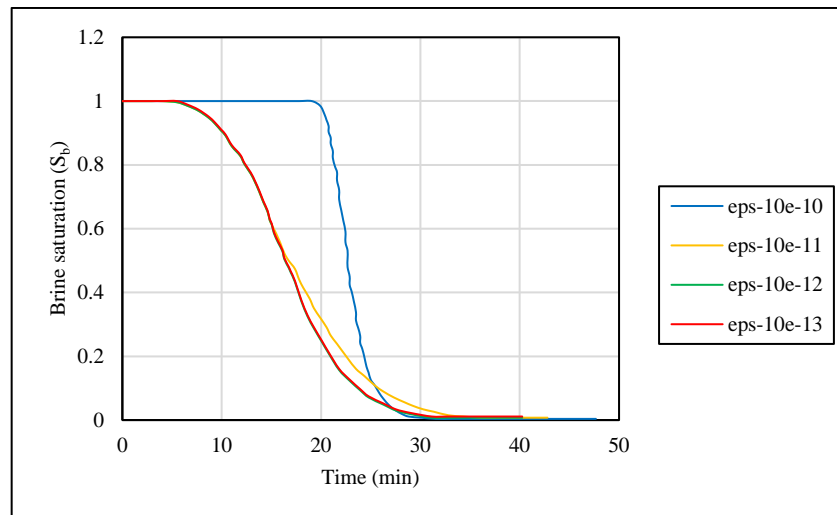


Figure 7.13. Numerical solution results for varying liquid-phase diffusion coefficients (14MPa injection pressure and 20MPa confining pressure).

7.2.4 Results and discussion

The first part of this section discusses the influence of CO_2 injection pressure, including both sub- and super-critical on CO_2 /brine saturation in the reservoir pore structure using the simulation results. The model was run for different CO_2 injection pressures, including sub-critical pressures of 1-7MPa and super-critical pressures of 8-14MPa. Figs. 7.14 and 7.15 show the saturation profiles of the brine and CO_2 phases, respectively. As Figs. 7.14 and 7.15 indicate, during CO_2 flooding, brine saturation decreases with time and CO_2 saturation increases as it invades the reservoir pore space. The importance of the relative CO_2 /brine saturation has been

well illustrated by Doughty and Pruess (2004) and Hovorka et al. (2004). According to these researchers, precise knowledge of relative-phase saturation (CO_2 and brine) is important in the deep saline storage process, mainly for trapping mechanisms. In addition, the present study found that CO_2 /brine saturation of reservoir rock and the resulting fluid flow are greatly affected by CO_2 injection pressure. As shown in Fig. 7.14a, in sub-critical CO_2 flow conditions, the time required to complete the brine-drainage process decreases with the increase of CO_2 injection pressure. For example, when CO_2 injection pressure increases from 1 to 7MPa, the time required to complete the brine-drainage process reduces from 58 minutes to 22 minutes. A similar trend can be seen for super-critical CO_2 injection pressures, as illustrated in Fig. 7.14b. In relation to variation of CO_2 saturation, the time required to reach full CO_2 saturation also reduces with increasing CO_2 injection pressure for both sub- and super-critical injection conditions, as shown in Fig. 7.15. This is mainly due to the higher pushing force created by the higher injection pressures. Physically, this high injection pressure is responsible for the non-wetting CO_2 invading smaller pores, which have higher capillary entry pressures. Juanes et al. (2006) investigated how the performance of CO_2 sequestration projects is affected by high CO_2 injection pressures. According to these researchers, high injection pressures cause snap-off to occur (Valvatne and Blunt, 2004) in smaller pores during imbibition, resulting in increased macroscopic trapping, which is favourable for deep saline storage.

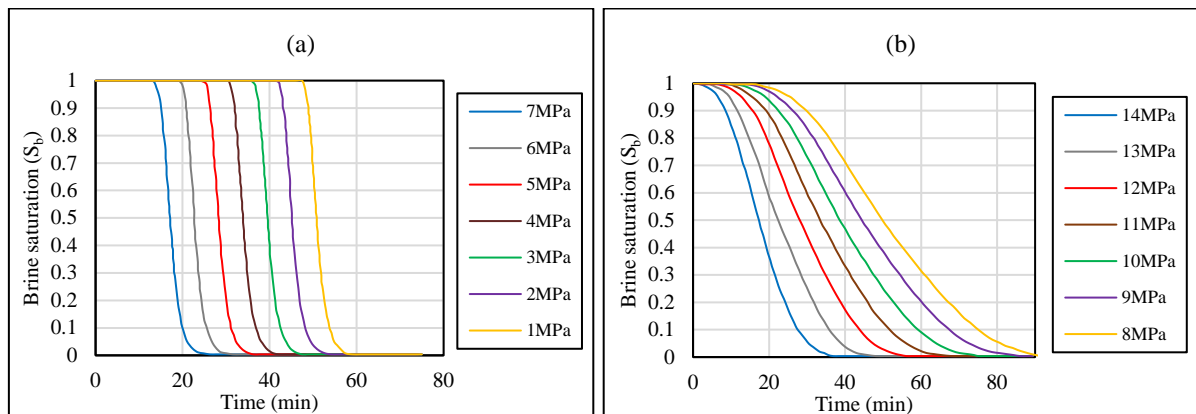


Figure 7.14. Results of brine saturation profile with time (20MPa confining pressure).

However, the results of the present study reveal that CO_2 -phase change has a significant influence on the final distribution of brine and CO_2 saturation in the reservoir rock sample, and this can be simply identified by comparing the shapes of the saturation profiles obtained under both sub- and super-critical conditions (Figs. 7.14 and 7.15). According to Fig. 7.14, compared to sub-critical condition, brine saturation starts to decrease relatively quickly under super-

critical pressure conditions. However, super-critical conditions take relatively more time to reach residual conditions compare to sub-critical conditions. This behaviour is also true for CO₂ saturation, as can be clearly seen in Fig. 7.15. For example, brine saturation takes 18 minutes to decrease at 7MPa injection pressure (sub-critical), while it only takes 3 minutes at 8MPa injection pressure (super-critical). As discussed by Diaz-Viera et al. (2008), the observed different behaviours of brine and CO₂ saturation under sub- and super-critical CO₂ pressure conditions are probably due to the effect of the viscosity ratio.

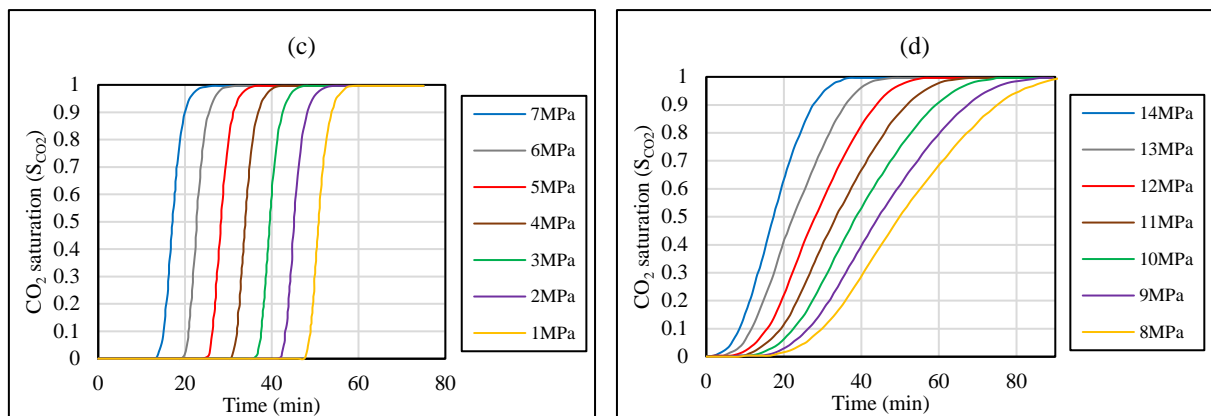


Figure 7.15. Results of CO₂ saturation profile with time (20MPa confining pressure).

The CO₂ concentration distribution along the sample length at different injection pressures was also modelled, and the CO₂ concentration profiles up to 40min of CO₂ injection at 4MPa and up to 80min of CO₂ injection at 8MPa injection pressures are shown in Figs. 7.16 and 7.17, respectively. As the figures show, the CO₂ mass travels along the sample with time due to diffusion and flushes the existing brine from the sample. According to the results, at 4MPa injection pressure, the maximum concentration at the injection boundary of the rock sample increases from 0.09 to 37.4kg/m³ after 0-40min of CO₂ injection, while the concentration at the drainage boundary increases from 0 to 35.2kg/m³ during the same period of time. Fig. 7.18 shows the CO₂ concentration distribution in reservoir rock after 40min of CO₂ injection at 4MPa and 80min of CO₂ injection at 8MPa injection pressure, respectively. As expected, for a given confining pressure, CO₂ concentration increases with increasing CO₂ injection pressure, and the results are consistent with the results shown in Figs. 7.16 and 7.17. For instance, CO₂ concentration at the injection boundary increases from 37.4 to 45.5kg/m³ as the injection pressure is increased from 4 to 8MPa. Similarly, CO₂ concentration at the drainage boundary increases from 35.2 to 42.7kg/m³ as the injection pressure is increased from 4 to 8MPa.

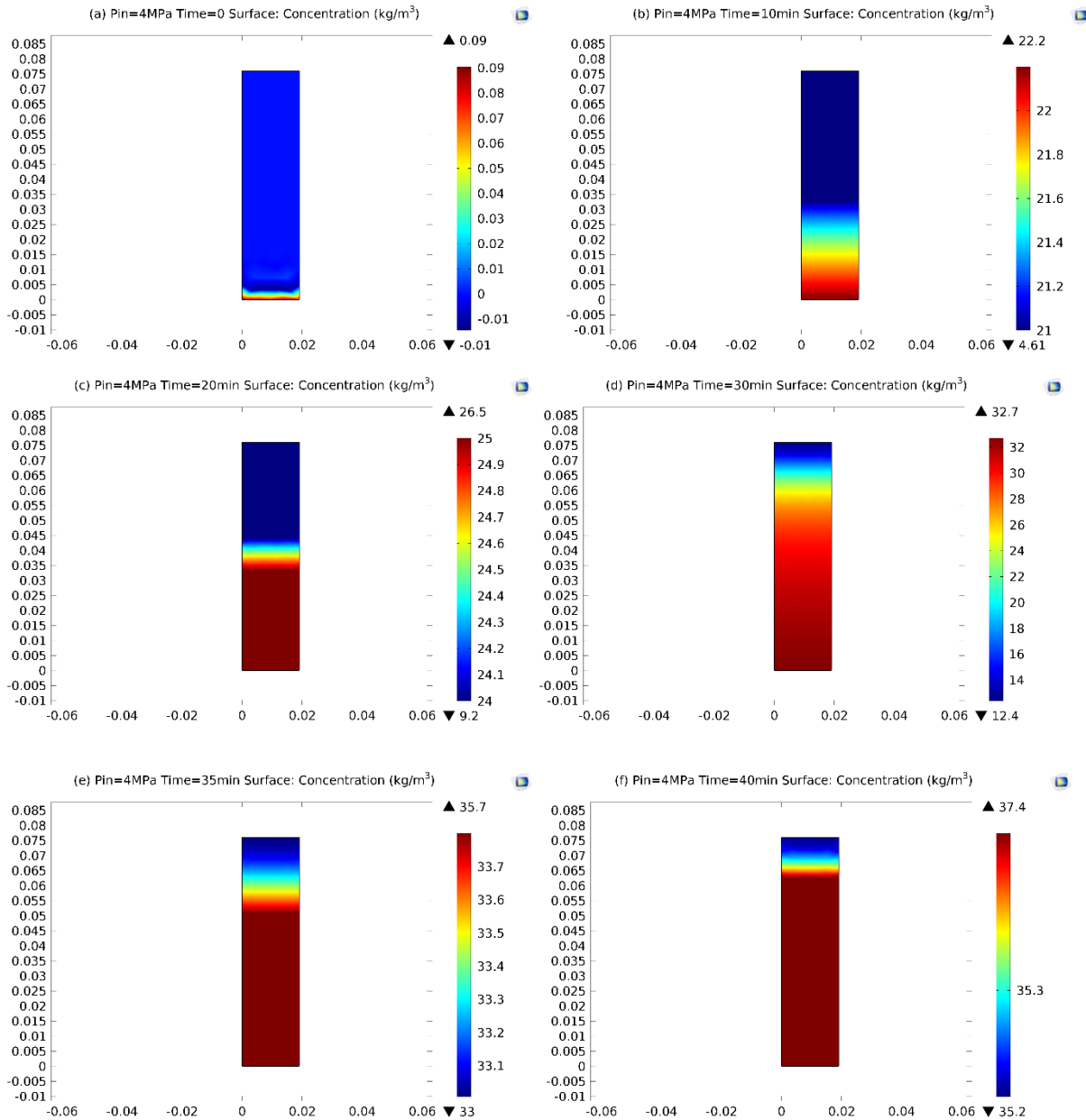


Figure 7.16. CO₂ concentration profiles up to 40 minutes of CO₂ injection at 4MPa injection pressure (20MPa confining pressure).

The CO₂ pressure in the reservoir rock at steady state was plotted for different injection pressures. Fig. 7.19 shows the CO₂ pressure distributions along the sample length at steady state. According to the results, the CO₂ pressure gradient along the sample length displays a non-linear relationship, and CO₂ pressure reduces non-linearly along the length of the sample at any injection pressure. For example, at steady state, at 4MPa injection pressure, the CO₂ pressure in the reservoir rock decreases exponentially from 4 to 2.32MPa along the sample length between 0-58mm, and a sudden drop from 2.32 to 0.1MPa (atmospheric pressure) can be seen

in the sample length between 58-65mm. This type of evaluation is essential for flow estimation analyses in deep saline sequestration, because under laboratory conditions it is difficult to define the flow behaviour of CO₂, especially under super-critical conditions.

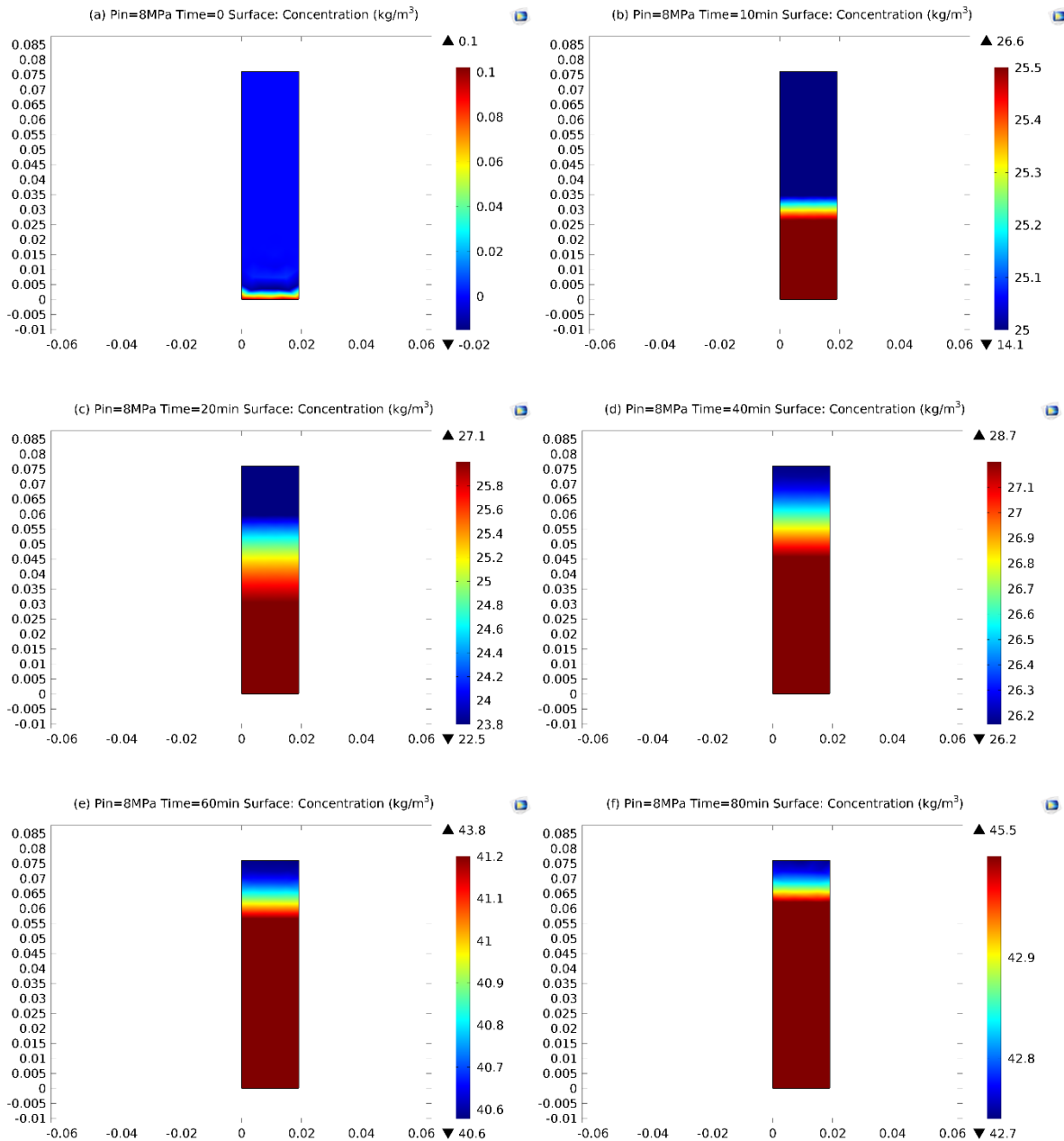


Figure 7.17. CO₂ concentration profiles up to 80 minutes of CO₂ injection at 8MPa injection pressure (20MPa confining pressure).

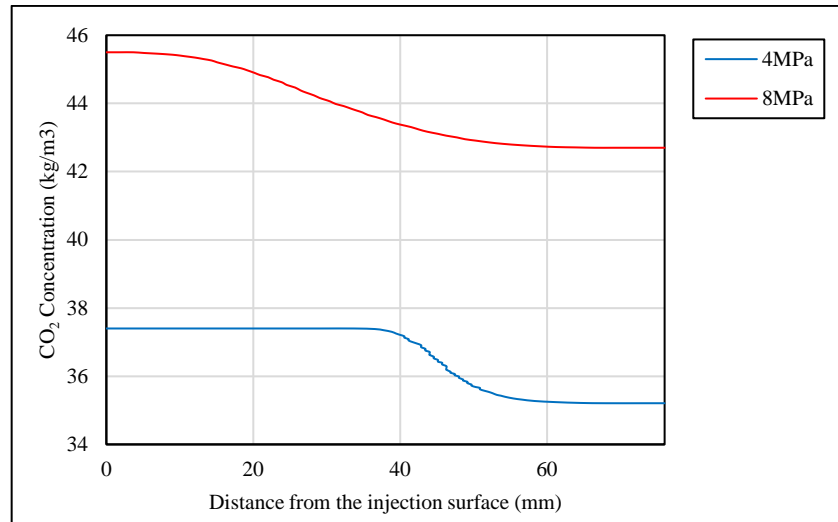


Figure 7.18. CO₂ concentration distribution in reservoir rock after 40min of CO₂ injection at 4MPa and 80min of CO₂ injection at 8MPa injection pressures (20MPa confining pressure).

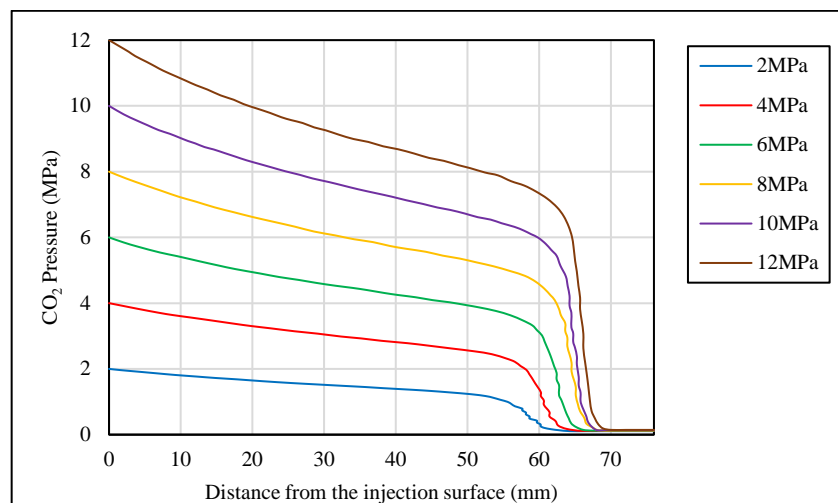


Figure 7.19. CO₂ pressure distributions along the sample length at steady-state (20MPa confining pressure).

7.2.5 Conclusions

A laboratory-scale numerical study was carried out on brine-saturated Hawkesbury sandstone to simulate the relative flow characteristics of brine and CO₂ during the drainage process in deep saline sequestration. COMSOL Multiphysics software was used to develop the numerical simulation. Pre-defined partial differential equations were used to characterise the relative flow behaviour using the Buckley-Leverett concept and the poro-elastic module was used to define the mechanical behaviour of reservoir rock under laboratory conditions. The results of

experimental work, in which triaxial drained permeability testing was conducted on brine-saturated reservoir rocks, were used to validate the developed model. The simulation was then extended to investigate the effect of different injection pressures, including both sub- and super-critical CO₂ pressure conditions. According to the results, the Buckley-Leverett flow concept successfully reproduces results that are relatively close to the experimental data. In addition, the liquid-phase diffusion coefficient plays a considerable role in defining the final distribution of brine and CO₂, and convergence analysis found that the best value varies between 10⁻¹⁰-10⁻¹³ m²/s.

As observed under sub- and super-critical flow conditions, CO₂ storage capacity in deep saline aquifers can be significantly enhanced by increasing the injection pressure. The simulation results show that the relative flow of reservoir rock varies significantly with the phase change of CO₂, probably due to the effect of the viscosity ratio. In addition, CO₂ pressure distributions under different CO₂ injection pressures reveal the non-linear behaviour of the pressure gradient along the sample length.

7.2.6 Nomenclature

M^K = Accumulation term

V_n = Volume of arbitrary sub-domain

F^K = Component of mass flux

q^K = Specific mass source rate

n = Unit normal vector

Γ_n = Interface area

b = Brine-phase

CO_2 = Carbon dioxide phase

α = b and CO_2 phases

\underline{u}_α = Volumetric phase velocity

ϕ = Porosity

k = Absolute permeability

S_α = Saturation

μ_α = Viscosity

ρ_α = Density

P_α = Pressure

B_α = Formation volume

$k_{r\alpha}$ = Relative permeability

R_{sb} = Gas solubility

P_{CbCO_2} = CO₂-brine capillary pressure

S_{rb} = Residual brine saturation

S_{rCO_2} = Residual CO₂ saturation

7.2.7 References

1. Andre L, Audigane P, Azaroual M, Menjoz A. Numerical modelling of fluid-rock chemical interactions at the supercritical CO₂-liquid interface during CO₂ injection into a carbonate reservoir, the Dogger aquifer (Paris Basin, France). *Energy Conversion and Management* 2007; 48(6): 1782-1797.
2. Andre L, Peysson Y, Azaroual M. Well injectivity during CO₂ storage operations in deep saline aquifers-Part 2: Numerical simulations of drying, salt deposit mechanisms and role of capillary forces. *International Journal of Greenhouse Gas Control* 2014; 22: 301-312.
3. Arias I, Knap J, Chalivendra VB, Hong S, Ortiz M, Rosakis AJ. Numerical modelling and experimental validation of dynamic fracture events along weak planes. *Computer Methods in Applied Mechanics and Engineering* 2007; 196: 3833-3840.
4. Brooks RH, Corey AT. *Hydraulic Properties of Porous Media*. Hydrology Papers 3. Colorado State University, Fort Collins, CO, 1964.
5. Burton M, Kumar N, Bryant SL. Why relative permeability matters as much as absolute permeability. *Energy Procedia* 2009; 1: 3091-3098.
6. Chen Z. Formulations and numerical methods of the black oil model in porous media. *Journal of Numerical Analysis* 2000; 38: 489-514.
7. Corey AT. The interrelation between gas and oil permeabilities. *Producer's Monthly* 1954; 19 (1): 38-42.
8. Dagan G. Statistical theory of groundwater flow and transport: Pore to laboratory, laboratory to formation, and formation to regional scale. *Water Resources Research* 1986 ; 22(9S) : 12-27.
9. Darcy HPG. *Les Fontaines Publiques de la Ville de Dijon, Exposition et Applications de Principes a Suivre et des Formules a Employer dans les Questions de Distribution D'eau*, Victor Dalmont, Paris, 1856.
10. Diaz-Viera MA, Lopez-Falcon DA, Moctezuma-Berthier A, Ortiz-Tapia A. COMSOL implementation of a multiphase fluid flow model in porous media. In *Proceedings of the COMSOL Conference*, 2008.
11. Doughty C, Pruess K. Modelling supercritical carbon dioxide injection in heterogeneous porous media. *Journal of Vadose Zone* 2004; 3: 837-847.

12. Hovorka SD, Doughty C, Holtz MH. Testing efficiency of storage in the subsurface: Frio brine pilot experiment, paper presented at International Conference on Greenhouse Gas Control Technologies (GHGT-7), Int. Energy Agency, Vancouver, B. C., Canada, 2004.
13. Juanes R, Spiteri EJ, Orr FM, Blunt MJ. Impact of relative permeability hysteresis on geological CO₂ storage. *Water Resources Research* 2006; 42(12): 32-45.
14. Korbol R, Kaddour A. Sleipner Vest CO₂ disposal-injection of removed CO₂ into the Utsira Formation. *Energy Conversion and Management* 1995; 36: 509-512.
15. Kueper BH, Frind EO. Two-phase flow in heterogeneous porous media: 2. Model application. *Water Resources Research* 1991; 27(6): 1059-1070.
16. Law D. Injectivity studies. In: Hitchon B (ed.) *Aquifer disposal of carbon dioxide*. Geoscience Publishing, Alberta, Canada 1995: 59-92.
17. Law DHS, Bachu S. Hydrogeological and numerical analysis of CO₂ disposal in deep aquifers in the Alberta sedimentary basin. *Energy Conversion and Management* 1996; 37:1167-1174.
18. Mercer JW, Cohen RM. A review of immiscible fluids in the subsurface: properties, models, characterization and remediation. *Journal of Contaminant Hydrology* 1990; 6(2): 107-163.
19. Mitiku AB, Bauer S. Optimal use of a dome-shaped anticline structure for CO₂ storage: a case study in the North German sedimentary basin. *Environmental and Earth Science* 2013; 70 (8): 3661-3673.
20. Mualem Y. New model for predicting hydraulic conductivity of unsaturated porous-media. *Water Resources Research* 1976; 12 (3): 513-522.
21. Muller N. Supercritical CO₂-brine relative permeability experiments in reservoir rocks-literature review and recommendations. *Transport in Porous Media* 2011; 87: 367-383.
22. Oostrom M, White MD, Porse SL, Krevor SCM, Mathias SA. Comparison of relative permeability-saturation-capillary pressure models for simulation of reservoir CO₂ injection. *International Journal of Greenhouse Gas Control* 2016; 45: 70-85.
23. Perera MSA, Ranjith PG, Choi SK, Airey D. Numerical simulation of gas flow through porous sandstone and its experimental validation. *Fuel* 2011; 90(2): 547-554.

24. Pruess K, Garcia J. Multiphase flow dynamics during CO₂ disposal into saline aquifers. *Environmental Geology* 2002; 42(2-3): 282-295.
25. Rathnaweera TD, Ranjith PG, Perera MSA. Salinity-dependent strength and stress–strain characteristics of reservoir rocks in deep saline aquifers: An experimental study. *Fuel* 2014; 122: 1-11.
26. Rathnaweera TD, Ranjith PG, Perera MSA, Haque A, Lashin A, Al Arifi N, et al. CO₂-induced mechanical behaviour of Hawkesbury sandstone in the Gosford basin: An experimental study. *Material Science and Engineering A* 2015; 641: 123-137.
27. Rathnaweera TD, Ranjith PG, Perera MSA. Experimental investigation of geochemical and mineralogical effects of CO₂ sequestration on flow characteristics of reservoir rock in deep saline aquifers. *Nature Scientific reports* 2016; 6: 19362.
28. Tang CA, Tham LG, Lee PKK, Yang TH, Li LC. Coupled analysis of flow, stress and damage (FSD) in rock failure. *International Journal of Rock Mechanics and Mining Sciences* 2002; 39(4): 477-489.
29. Valvatne PH, Blunt MJ. Predictive pore-scale modelling of two-phase flow in mixed wet media. *Water Resources Research* 2004; 40: 190-205.
30. van der Meer LGH. Investigations regarding the storage of carbon dioxide in aquifers in the Netherlands. *Energy Conversion and Management* 1992; 33(5): 611-618.
31. Watanabe N, Nobuo H, Noriyoshi T. Determination of aperture structure and fluid flow in a rock fracture by high-resolution numerical modelling on the basis of a flow-through experiment under confining pressure. *Water Resources Research* 2008; 44(6): 123-136.
32. Weir GJ, White SP, Kissling WM. Reservoir storage and containment of greenhouse gases. In: Pruess K (ed.) *Proceedings, TOUGH Workshop 95, 20-22 March 1995, Berkeley, CA, Lawrence Berkeley National Laboratory Rep LBL-37200: 33-238*

7.3 Development of a field-scale numerical model of hydro-mechanical, mineralogical and geochemical behaviour of deep saline reservoir rock

Modelling the injection and storage of CO₂ in deep saline formations has provided valuable insights into flow, mechanical and geochemical behaviours and has proved useful for planning and monitoring activities during pilot projects. Therefore, numerical simulation work was carried out using the COMSOL Multiphysics simulator to investigate the long-term effect of CO₂ sequestration on the hydro-mechanical, mineralogical and geochemical behaviours of the Hawkesbury formation. In order to develop the flow behaviour, the equations proposed under laboratory-scale conditions (see Section 7.2) were extended to field-scale conditions by coupling geochemical and mineralogical reactions. The following submitted journal paper entitled “*Injection and storage of CO₂ in deep saline aquifers: A numerical study on Hawkesbury formation*” explains the numerical procedure and the results.

Injection and Storage of CO₂ in Deep Saline Aquifers: A Numerical Study on Hawkesbury Formation

T. D. Rathnaweera¹, P.G. Ranjith¹, M. S. A. Perera¹

¹Department of Civil Engineering, Monash University, Building 60, Melbourne, Victoria, 3800, Australia.

Abstract

In recent years, researchers have focused on mitigation options which can be used to reduce anthropogenic CO₂ emissions, and CO₂ sequestration in deep saline aquifers has been identified as an effective and feasible method. However, lack of understanding concerning the hydro-mechanical and geochemical phenomena that occur when CO₂ is injected into deep saline aquifers may adversely affect the long-term integrity of sequestration. These considerations have made the effect of CO₂ sequestration a topic of great numerical research interest, but to date most studies have focused on the geochemical consequences, with little attention to the combined hydro-mechanical and geochemical effects. Therefore, the present study aims to identify the combined interaction-induced reservoir behaviour by developing a field-scale numerical model which can simulate the hydro-mechanical, mineralogical and geochemical behaviours of deep saline aquifers under CO₂ sequestration conditions. The COMSOL Multi physics numerical simulator was employed to investigate the behaviour of the Hawkesbury formation upon exposure to CO₂ sequestration. The PDE interface available in the COMSOL (mathematical module) Multiphysics simulator was used to define the governing processes in reservoirs using partial differential equations. After developing the model, data from the Dogger aquifer in the Paris basin were used to validate the model and finally the model was extended to simulate the Hawkesbury formation. According to the results, the long-term interaction of CO₂ causes Hawkesbury formation's pore structure to significantly change.

Keywords: CO₂ sequestration, COMSOL Multiphysics, hydro-mechanical, geochemical

7.3.1 Introduction

CO₂ sequestration in deep saline aquifers offers a promising solution to reduce the global emission of anthropogenic CO₂ into the atmosphere. Over the past 20 years, several pilot and commercial projects for CO₂ sequestration in deep saline aquifers have been launched. For example, the Sleipner Field project in the North Sea, the first field project of CO₂ injection into

a deep saline aquifer, has been successfully underway since 1996 (Korbol and Kaddour, 1995). However, the injection of CO₂ into a deep saline aquifer causes its natural properties to be changed, altering the hydro-mechanical and geochemical equilibriums between the reservoir rock and the formation water. Therefore, in-depth knowledge regarding the consequences arising from these changes is required for the clarification of safety, feasibility and economic issues in a particular sequestration project during its preparation, operation and after-injection stages. In addition, a better understanding of the mechanisms and geochemistry involved in deep saline sequestration is needed for further improvement of the technology. For example, the estimation of the amount of CO₂ which a given formation can safely store is an important issue which must be addressed before beginning CO₂ injection into an aquifer. Such estimation cannot be done only with laboratory test results, and requires a complete field-scale numerical model which can couple all these mechanisms and the geochemistry involved in deep saline sequestration.

Several mechanisms and geochemistry reactions are involved, in deep saline reservoirs during and after storage, and require consideration, due to safety concerns, especially the potential leakage of injected CO₂ to the atmosphere. Of these, the phase change of injected super-critical CO₂ due to changes in temperature and/or pressure and/or chemical interaction with rock minerals and brine is a critical concern, as it can increase the upward pressure on the reservoir and caprock. Ultimately, this increased pressure can cause tension or compression cracking in the reservoir and the caprock, and may reactivate pre-existing non-transmissive faults and joints, increasing the possibility of leakage of injected CO₂ through the reservoir and caprock (Van Ruth et al., 2006). In addition, reservoir permeability can either increase or decrease, depending on the geochemistry involved in the interaction of injected CO₂, aquifer brine and reservoir rock (Zerai et al., 2006; Kristinof et al., 2010). Once CO₂ is injected into a reservoir, it is trapped in the reservoir by different trapping mechanisms, including structural, hydrodynamic, mineral, residual, adsorption and solubility trapping (Ozah et al., 2005). Solubility, structural and residual trapping are the most effective and fast CO₂ trapping mechanisms during and immediately after the injection phase, whereas mineral trapping is an extremely slow mechanism which usually has a time frame of thousands of years after injection. In order to accurately estimate the effective CO₂ storage capacity, it is necessary to select the appropriate description of these relevant storage mechanisms and for more realistic estimation, reservoir heterogeneous behaviour must be incorporated in the calculation of storage capacity (Kopp et

al., 2008). To date, a number of numerical studies have been carried out to understand the behaviour of deep saline reservoir rock during and after the injection of CO₂ (Andre et al., 2007; Burton et al., 2009; Bacci et al., 2011; Oldenburg et al., 2011). According to these studies, the selected numerical model should be able to simulate the subsequent migration of the injected CO₂, the spreading of CO₂ including gravity fingering and plume development, and other processes, such as CO₂ dissolution in aquifer brine, temperature changes and mineral dissolution/precipitation.

Alonso et al. (2012) conducted a numerical study to simulate the coupled hydro-mechanical behaviour of reservoir rock on the basis of critical-state theory, which includes a non-linear hypo-elastic law, and a brittle/ductile yield criterion. Navarro et al. (2010) also performed a simulation study to characterize the hydro-mechanical behaviour of reservoir rock, incorporating the shearing and dilation behaviour of porous rocks, According to these researchers, the proposed model yielded a realistic description of the mechanical behaviour of reservoir rock. Goerke et al. (2011) also developed a numerical simulation to characterise CO₂ injection-induced multi-phase hydro-mechanical processes in deep saline aquifers. The conceptual model was derived based on the balance laws of mass and momentum, the constitutive relations of the fluid and solid, as well as their mutual interaction. However, they neglected the solubility and possible rock mineral reaction effects which occur due to the mutual interaction between CO₂ and aquifer brine. Despite the importance of knowledge of the mechanical behaviour of reservoir rock, as yet few numerical modelling studies have considered the coupled behaviour of hydro-mechanical and geochemical reactions that occur when super-critical CO₂ is in contact with the aquifer brine and the reservoir rock at the temperatures and pressures found in geological reservoirs. However, number of numerical studies have been conducted on the geochemical and mineralogical changes in reservoir rock under deep saline conditions without coupling the actual hydro-mechanical variations. For example, Andre et al. (2007) carried out a numerical modelling study on CO₂-rock chemical interaction at the super-critical CO₂-brine interface during CO₂ injection. They envisaged two injection scenarios, including the injection of CO₂-saturated brine and the injection of pure CO₂ in a super-critical state. The results revealed the high reactivity of CO₂-saturated brine, which can dramatically change the reservoir pore structure. According to their results, the injection of CO₂-saturated brine causes reservoir rock porosity to increase by up to 90%, associated with strong carbonate mineral dissolution, and by about 5% to 7% in most parts of the reservoir due

to the injection of pure CO₂, revealing less reactivity of pure CO₂ compared to CO₂-saturated brine. Xu et al. (2004) also evaluated the consequences of deep saline sequestration on the chemical and mineralogical behaviour of reservoir rocks, modelling three different aquifer mineral compositions under batch reaction conditions. The model considered three major criteria: (1) the kinetics of chemical interactions between the reservoir rock minerals and the aqueous phase, (2) CO₂ solubility dependence on pressure, temperature and salinity of the system, and (3) redox processes that may be important in deep sub-surface environments. They found that mineral trapping efficiency varies considerably with rock type (mineral composition), and the accumulation of carbonate minerals in the rock matrix leads to a considerable decrease in porosity, adversely affecting permeability and fluid flow in the aquifer. Johnson et al. (2001) simulated the large-scale injection of CO₂ at Statoil's Sleipner project, analysing the mechanisms responsible for structural, solubility and mineral trapping. White et al. (2001) introduced a reactive chemical transport model, which can quantify the effectiveness of mineral sequestration of CO₂ in saline aquifers. McPherson and Lichtner (2001) proposed a mathematical sedimentary model, including multiphase flow of CO₂ and interaction between aquifer brine and CO₂, to evaluate the resident time and migration patterns of injected CO₂ in the sequestration site located in the Powder River Basin of Wyoming. A batch geochemical numerical study carried out by Gunter et al. (1997) illustrated that mineral trapping may take tens to hundreds of thousands of years to complete the reactions.

Although there have been a number of studies on geochemical and mineralogical variations of deep saline reservoir rocks, little attention has been given to how reservoir flow is influenced by these changes. The behaviour of deep saline aquifers can only be appreciated by the combined investigation of geochemical, mineralogical and hydro-mechanical changes with CO₂ sequestration. However, no such comparison has been undertaken in previous simulation studies in deep saline aquifers. The present numerical study is motivated by this gap in knowledge. This study aims to develop a numerical simulation which can couple the hydro-mechanical, geochemical and mineralogical behaviour of reservoir rock in CO₂ sequestration environments. The model was developed using the COMSOL Multiphysics simulator and the developed model was finally used to investigate the behaviour of Hawkesbury sandstone in the Sydney Basin under deep saline sequestration conditions.

7.3.2 Model development

7.3.2.1 COMSOL Multiphysics

COMSOL Multiphysics is a FEM-based software package for the modelling and simulation of any physics-based system, and it uses a MATLAB-based script language. A particular strength of this simulator is its ability to account for multiphysics phenomena and the optional modules available add additional value to it. The present study selected COMSOL as a platform to develop the simulation because of its capability of modelling processes governed by different partial differential equations, which enables researchers to harness its powerful simulation environment for geotechnical and civil engineering applications. In order to simulate the impact of CO₂ sequestration on the reservoir formation, its flow, mechanical and chemical behaviours were specified through the setting of individual partial differential equations using the mathematics modulus available in the COMSOL simulator. First, the model was used to couple the mechanical and flow behaviour of reservoir rock without combining any geochemical and mineralogical effects. For that purpose, a solid mechanics interface and the Mualem and Corey flow model were utilised. The governing hydro-mechanical equations were derived based on the basic laws of force equilibrium, mass conservation and two-phase fluid dynamics and input into the COMSOL model in coefficient form using the PDE interface. After evaluating the reservoir hydro-mechanical performance, geochemical and mineralogical effects were coupled with the model by developing a set of kinetic and equilibrium mineral reaction equations. Table 7.8 shows summary of the coupling process used in this study. Finally, the coupled equations were numerically solved using the finite element method (FEM) implemented in COMSOL.

Table 7.8. Coupled processes description.

Main process	Coupled with	Brief description
Mechanical	Flow behaviour	Poro-elastic deformation
Flow behaviour	Mechanical	Poro-elastic deformation-induced porosity and relative permeability variation
Chemical	Flow and mechanical	Diffusion and dispersion effect
Flow and mechanical	Chemical	Mineral reaction-induced poro-elastic deformation, porosity and relative permeability

7.3.2.2 Governing equations

The reservoir formation was taken as a linear-elastic material and Biot's effective stress principle was adopted for the modelling. This assumption is proposed by other researchers (Hudson et al., 2005) to study the impact of CO₂ sequestration on reservoir rocks, and a similar method has been applied by others (Neaupane et al., 1999; Chan et al., 2005). Eq. 7.39 below is used to model the mechanical equilibrium of the reservoir formation.

$$G \frac{\partial^2 u_i}{\partial x_i \partial y_j} + (G + \lambda) \frac{\partial^2 u_j}{\partial x_i \partial y_j} - \alpha \frac{\partial P}{\partial x_i} - \beta K_D \frac{\partial T}{\partial x_i} + F_i = 0 \quad (7.39)$$

The mechanical behaviour was then coupled with the flow module via the volumetric deformation and porosity change. Eqs. 7.40 and 7.41 were introduced to the model to link the flow behaviour of reservoir rock based on the conservation of total mass (CO₂ and brine).

$$\frac{\partial \phi p_\alpha S_\alpha}{\partial t} = \frac{\partial}{\partial x_i} \left[\frac{p_\alpha k_{ra} k_{ij}}{\mu_\alpha} \left(\frac{\partial p_\alpha}{\partial x_j} - p_\alpha g \frac{\partial D}{\partial x_j} \right) \right] + q_\alpha P_\alpha^* + Q_{ad} \quad (7.40)$$

$$\frac{\partial (\phi p_\alpha S_\alpha)}{\partial t} = p_\alpha S_\alpha \frac{\partial \phi}{\partial p_\alpha} \frac{dP_\alpha}{dt} + \phi S_\alpha \frac{\partial p_\alpha}{\partial P_\alpha} \frac{dP_\alpha}{dt} + \phi p_\alpha \frac{\partial S_\alpha}{\partial P_c} \frac{dP_c}{dt} \quad (7.41)$$

where, subscript α represents the CO₂ and brine phases, separately.

In assigning flow equations, the dispersion and diffusion term was defined based on the concentration of each species in α phase (rock minerals) as follows:

$$Q_D = \sum_{l=1}^{n_{nw}} \left\{ \frac{\partial}{\partial x_i} \left[\phi \left(D_{nwij}(S_{nw}) + D_{nwm}(S_{nw}) \right) \frac{\partial C_{nwl}}{\partial x_j} \right] M_l \right\} \quad (7.42)$$

where, subscript w and nw represent the wetting and non-wetting phases, respectively.

The estimated porosity change can then be expressed as Eq. 7.43:

$$\phi = \phi_r + c_c (P_w - P_{wr}) \quad (7.43)$$

To define relative-permeability characteristics of CO₂ and brine phases, the Van Genuchten's capillary pressure curve model was introduced as follows:

$$S_w = 1 - S_{mw} = \left[\frac{1}{1 + (\alpha_v H_c)^N} \right]^M = \frac{\theta_w - \theta_{wres}}{\theta_{ws} - \theta_{wres}} \quad (7.44)$$

Next, the specific capacity of water/brine phase was introduced as Eq. 7.45:

$$C_P = \frac{dS_w}{dP_c} = \frac{\alpha_v (N-1)(1 - S_{wres})(\alpha_v P_c)^{(N-1)}}{(1 + (\alpha_v P_c)^N)^{(2N-1)/N}} \quad (H_c > 0) \quad \text{and} \quad C_P = 0 \quad (H_c < 0) \quad (7.45)$$

The Van Genuchten's capillary pressure model and the Mualem and Corey model were finally connected to simulate the relative flow behaviour of reservoirs.

$$k_{rw} = S_w^L [1 - (1 - S_w^{1/M})^M]^2 \quad \text{and} \quad k_{mww} = (1 - S_w^2)(1 - S_w)^2 \quad (7.46)$$

After interconnecting the mechanical and relative permeability characteristics, the solute transport equation was derived, assuming that solute transport properties are governed only by diffusion and mechanical dispersion:

$$p_\alpha \phi S_\alpha \frac{\partial C_{al}}{\partial t} + \frac{\partial S_l}{\partial t} = \frac{\partial}{\partial x_i} [\phi (D_{\alpha ij}(S_\alpha) + D_{cm}(S_\alpha)) \frac{\partial C_{al}}{\partial x_j}] - \frac{\partial}{\partial x_i} (V_{\alpha i} C_n) - K_{cn} \phi C_{cn} - K_{sn} S_n + q_\alpha C_{cn}^* \quad (7.47)$$

The mechanical dispersion coefficient in CO₂ or the brine phase can be written as:

$$D_{ij} = \alpha_T V \delta_{ij} + (\alpha_L - \alpha_T)(V_i V_j / V) \quad (7.48)$$

Accordingly, molecular diffusion in α phase in reservoir can be defined as:

$$D_{cm} = \delta D_{cm0} / \tau^2 \quad (7.49)$$

By combining the saturation effect of each phase, the dispersion coefficient and molecular coefficient can be simplified as:

$$D_{\alpha ij}(S_\alpha) = S_\alpha D_{\alpha ij} \quad ; \quad D_{cm}(S_\alpha) = S_\alpha D_{cm} \quad (7.50)$$

Assuming the adsorption/desorption processes are reversible, the kinetic equilibrium between rock and α phase can be written as follows:

$$\frac{\partial S_l}{\partial t} = k_{al}(k_{dl} C_{al} - S_l) - r_{sl} \quad (7.51)$$

$$\frac{\partial C_{al}}{\partial t} = k_{al}(k_{dj}C_{al} - S_l) - r_{al} \quad (7.52)$$

The main thermodynamic properties needed to model the flow behaviours of CO₂ and brine in reservoirs are density, viscosity, and the specific enthalpy of the fluid phases as a function of temperature and pressure. Brine density was calculated using the method proposed by Battistelli et al. (1997). According to the correlation proposed by Andersen et al. (1992), the density of the aqueous phase with dissolved CO₂ can be calculated, assuming the additivity of the volumes of brine and dissolved CO₂. Aqueous viscosity was obtained from the correlation presented by Phillips et al. (1981), and the specific enthalpy of the aqueous phase was calculated from the correlation developed by Lorenz et al. (2000). The solubility of CO₂ and brine was modelled according to the mass law described by Xu et al. (2004). Equilibrium between the CO₂ and brine phases was assumed for the CO₂ dissolution calculation.



where, subscripts *sc* and *aq* denote super-critical and aqueous CO₂, respectively.

According to Henry's mass-action law, the dissolution of CO₂ in the aqueous phase can be calculated as:

$$K \tau P = \gamma C \quad (7.54)$$

where, *K* is the equilibrium constant depending on the temperature, *P* is the partial pressure of CO₂, *γ* is the aqueous CO₂ activity coefficient calculated using the Debye-Huckel model (Helgeson et al., 1981) and *τ* is the fugacity parameter of aqueous CO₂ depending on pressure and temperature.

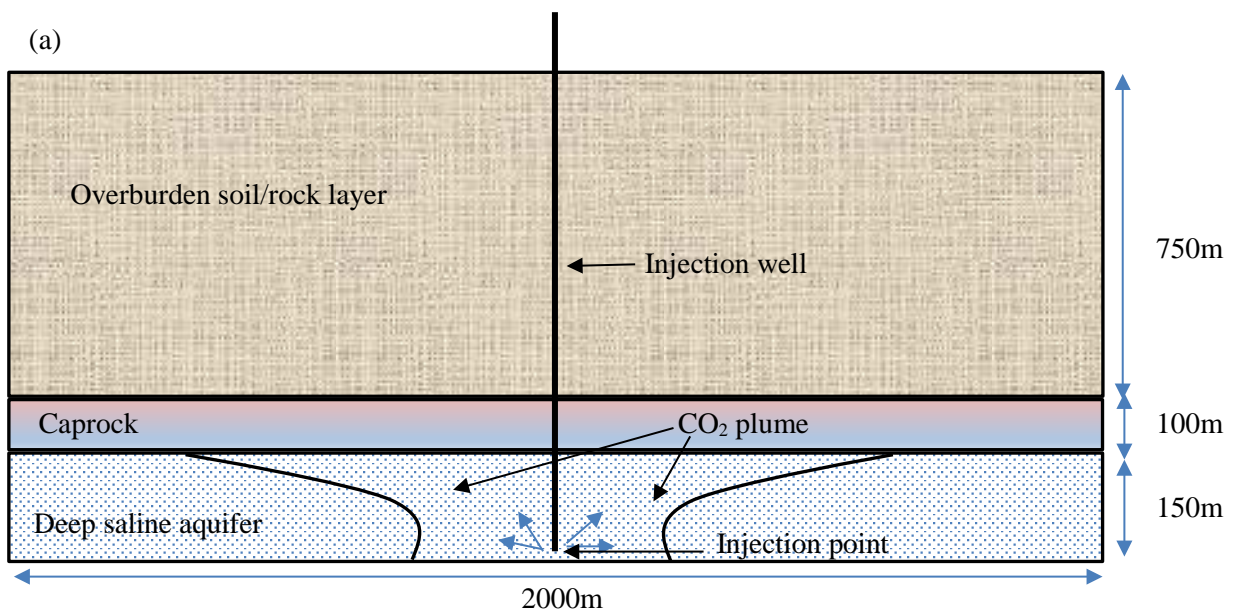
Finally, kinetic mineral reactions were assigned to the model and kinetic mineral dissolution/precipitation reactions were modelled according to the kinetic rate law of Lasaga (1984) as follows:

$$r_m = -sbn \left[\log \left(\frac{Q_m}{K_m} \right) \right] k_m A_m \left[\left(\frac{Q_m}{K_m} \right)^\mu - 1 \right]^n \quad (7.55)$$

where, r_m is the dissolution/precipitation rate of the mineral m , where positive values indicate dissolution, and negative values indicate precipitation, A_m is the specific reactive surface area, K_m is the equilibrium constant for the mineral-CO₂-brine reaction, Q_m is the ion activity product, k_m is the rate constant, and the parameters μ and n are two positive numbers (usually taken as equal to unity). The expression $sbn \left[\log \left(\frac{Q_m}{K_m} \right) \right]$ was incorporated to ensure that the correct sign is enforced when μ and n are not equal to unity.

7.3.2.3 Model geometry and boundary conditions

A 2-D axisymmetric model, which couples the fluid flow, mechanical deformation and chemical and mineralogical reactions that occur in deep saline reservoir formations was used for the study. A schematic representation of the model is shown in Fig. 7.20a. This model simulates an intact sandstone reservoir that is free of any faults, joints or fractures. In addition, the model includes an intact caprock and an overburden soil/rock layer. The reservoir lies 850m below the surface with the water table assumed to be at the ground level. The caprock and the reservoir formation are 100 and 150m thick, respectively. CO₂ is injected from the injection well 10m above the reservoir base for 50 years at a constant injection rate of $1.5 \times 10^{-3} \text{ m}^3/\text{s}$ at an injection pressure of 20MPa. Fig. 7.20b shows the finite element mesh of the proposed reservoir model. A radial zone of 2km diameter was investigated for 100 years including 50 years of CO₂ injection and 50 years of storage.



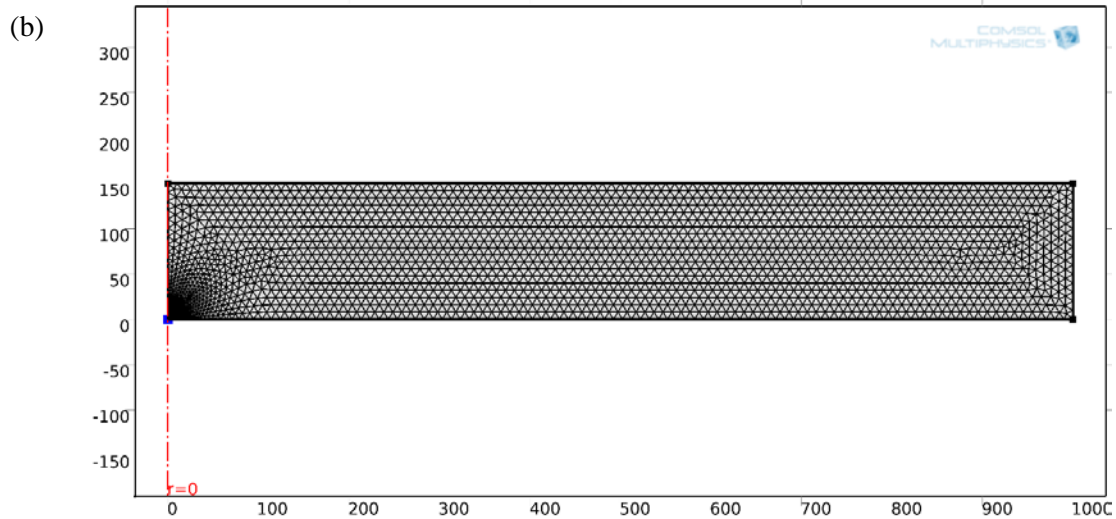


Figure 7.20. (a) Schematic representation of the 2-D axisymmetric model and (b) model geometry in mesh mode.

Boundary conditions were assigned separately considering the initial conditions of pressure, flow and solute concentration of the reservoir formation. The initial pressure condition of the reservoir was taken as:

$$P(x, y, z, 10) = P_0 \quad (7.56)$$

Accordingly, the pressure boundary was defined as:

$$P(x, y, z, t) = \bar{P}(x, y, z, t) \quad (7.57)$$

The initial flow boundary condition was modelled as follows:

$$-k_g k_{r\alpha} / \mu_\alpha (\partial P / \partial x_j + p_\alpha g k_{i3}) n_l = I_f(x, y, z, t) \quad (7.58)$$

where, the velocity vector of α phase was derived as:

$$V_{\alpha i} = -\frac{k_{\alpha r} k_{ij}}{\mu_\alpha} \left(\frac{\partial P_\alpha}{\partial x_j} + p_\alpha g \frac{\partial D}{\partial x_j} \right) \quad (7.59)$$

After assigning the initial boundary conditions of the mechanical and flow modulus, chemical species transport boundary conditions were introduced into the model. First, the initial solute concentration in α (CO_2 and brine) phase was defined and Eq. 7.60 represents the initial solute concentration in α phase:

$$C_{\alpha L}(X, Y, Z, C_{oi}) = C_{\alpha i0} \quad (7.60)$$

Then, the initial solute concentration in reservoir rock phase was introduced:

$$S_l(x, y, z, 0) = S_{l0} \quad (7.61)$$

Finally, the flux boundary conditions of solutes were defined:

$$\frac{\partial}{\partial x_i} \left\{ \phi S_a [D_{aij}(S_w) + D_{am}(S_w)] \frac{\partial C_{cl}}{\partial x_j} \right\} = I_c(x, y, z, t) \quad (7.62)$$

More details of selected geometrical boundary conditions are presented in Table 7.9.

Table 7.9. Boundary setting for the reservoir formation.

Boundary	Boundary condition
Bottom	Fixed
Far right	Roller
Left	Axisymmetric
Injection well	Axisymmetric

7.3.2.3 Model parameters and variables

The input parameters for the model include the reservoir's physical, chemical and mineralogical conditions. In addition, three stages were used to input parameters into the model. In the initial stage, the model was developed using the physical properties of the Dogger aquifer in the Paris Basin reported by Andre et al. (2007) and the model was validated by comparing the results with Andre et al.'s (2007) findings. Table 7.10 shows the physical properties of the Dogger aquifer. The validated model was then modified to simulate the behaviour of the Hawkesbury formation in a CO₂ sequestration environment, and the input physical parameters are shown in Table 7.11. Here, in the second stage, the conversion of the initial model to the Hawkesbury formation was carried out without coupling kinetic mineral reactions, and apart from flow behaviour, the model considered only the longitudinal and transverse dispersion of injected CO₂ in aqueous brine. In a later stage, mineral reaction coupling was carried out and the input geochemical and kinetic reaction parameters are illustrated in Tables 7.12-7.16.

Table 7.10. Physical properties of the Dogger aquifer (Andre et al., 2007).

Porosity (%)	12	Molecular diffusion coefficient brine phase (m ² /s)	1×10 ⁻⁹
Permeability coefficient(mD)	100	Residual brine content, θ_{bres}	0.199
Longitude dispersion coefficient (m)	0.025	Saturate brine content, θ_{bs}	1.0
Transverse dispersion coefficient (m)	0.0025	VG constant, a_v (m ⁻¹)	1.8
CO ₂ molecular diffusion coefficient (cm ² /s)	2.8×10 ⁻⁵	VG constant, N	2.5

Table 7.11. Basic hydraulic properties of the Hawkesbury formation.

Porosity (%)	31	Molecular diffusion coefficient brine phase (m ² /s)	1×10 ⁻⁹
Permeability coefficient(mD)	100	Residual brine content, θ_{bres}	0.01
Longitude dispersion coefficient (m)	0.05	Saturate brine content, θ_{bs}	0.30
Transverse dispersion coefficient (m)	0.005	VG constant, a_v (m ⁻¹)	1.8
CO ₂ molecular diffusion coefficient (m ² /s)	2.0×10 ⁻⁹	VG constant, N	1.84

Table 7.12. Input parameters for the geochemical coupling.

D CO_2	2.0e ⁻⁹ [m ² /s]	Diffusion coefficient of CO_2
D H_2CO_3	1.96e ⁻⁹ [m ² /s]	Diffusion coefficient of H_2CO_3
D HCO_3^-	1.105e ⁻⁹ [m ² /s]	Diffusion coefficient of HCO_3^-
D CO_3^{2-}	0.92e ⁻⁹ [m ² /s]	Diffusion coefficient of CO_3^{2-}
D H^+	9.312e ⁻⁹ [m ² /s]	Diffusion coefficient of H^+
D Ca^{2+}	7.43.26e ⁻¹⁰ [m ² /s]	Diffusion coefficient of Ca^{2+}
D Si^{4+}	2.24e ⁻¹¹ [m ² /s]	Diffusion coefficient of Si^{4+}
D Al^{3+}	1.06e ⁻¹² [m ² /s]	Diffusion coefficient of Al^{3+}
D Mg^{2+}	3.41e ⁻¹⁰ [m ² /s]	Diffusion coefficient of Mg^{2+}

$D_{Fe^{2+}}$	$0.72e^{-9}[\text{m}^2/\text{s}]$	Diffusion coefficient of Fe^{2+}
$D_{Ba^{2+}}$	$4.76e^{-12}[\text{m}^2/\text{s}]$	Diffusion coefficient of Ba^{2+}
D_{Na^+}	$1.37e^{-9}[\text{m}^2/\text{s}]$	Diffusion coefficient of Na^+
D_{K^+}	$6.16e^{-10}[\text{m}^2/\text{s}]$	Diffusion coefficient of K^+
D_{Cl^-}	$1.52e^{-9}[\text{m}^2/\text{s}]$	Diffusion coefficient of Cl^-
$D_{SO_4^{2-}}$	$0.12e^{-9}[\text{m}^2/\text{s}]$	Diffusion coefficient of SO_4^{2-}
T	50 [C°]	Operating temperature
pH	6.7	Operating pH
I	0.136	Ionic strength in molar
P	25MPa	Operating pressure in MPa
P_{CO_2}	20MPa	Partial pressure of CO_2 in MPa
c_unit	1000[mol/m ³]	Unit activity concentration
$C[Ca^{2+}]$	0.733 [mol/m ³]	Initial concentration of Ca^{2+}
$C[Si^{4+}]$	1.13[mol/m ³]	Initial concentration of Si^{4+}
$C[Al^{3+}]$	0.59 [mol/m ³]	Initial concentration of Al^{3+}
$C[Mg^{2+}]$	1.45 [mol/m ³]	Initial concentration of Mg^{2+}
$C[Fe^{2+}]$	0.72 [mol/m ³]	Initial concentration of Fe^{2+}
$C[Ba^{2+}]$	0.09 [mol/m ³]	Initial concentration of Ba^{2+}
$C[Na^+]$	869.57 [mol/m ³]	Initial concentration of Na^+
$C[K^-]$	5.92 [mol/m ³]	Initial concentration of K^-
$C[Cl^-]$	571.43 [mol/m ³]	Initial concentration of Cl^-
$C[SO_4^{2-}]$	21.88 [mol/m ³]	Initial concentration of SO_4^{2-}
h	200[m]	Formation thickness
v	0.00002[m/s]	Aquifer pore fluid velocity
rho_sandstone	2600[kg/m ³]	Density of reservoir formation
c_unit	1000[mol/m ³]	Unit activity concentration

Table 7.13. Chemical composition of aqueous phase in deep saline formation.

Context	Na^+	K^+	Mg^{2+}	Ca^{2+}	SO_4^{2-}	HCO_3^-	Cl^-	TDS
Content (mol/m ³)	869.57	5.92	1.45	0.733	21.88	37.71	571.43	3.2g/l

Table 7.14. Specific surface area (SSA) data.

Mineral	SSA (m ² /g)
Quartz (SiO_2)	0.01133
Calcite ($CaCO_3$)	0.01107
Kaolinite ($Al_2Si_2O_5(OH)_4$)	0.01156
Siderite ($FeCO_3$)	0.00167
Illite ($KAl_2Si_4O_{10}(OH)_2$)	0.01043

Table 7.15. Kinetic rate parameters used in reactive transport simulations.

Mineral	Intrinsic rate constant, k_0	Activation energy, E_a
	(mol.m ⁻² .s ⁻¹)	(J.mol ⁻¹)
Quartz	-13.9	87500
Calcite	-8.78	41870
Kaolinite	-13	62760
Siderite	-9.22	41870
Illite	-14	58620

Table 7.16. Equilibrium reactions used in reactive transport simulations.

Equilibrium reaction	Log equilibrium coefficient
$CO_{2(aq)} + H_2O = HCO_3^- + H^+$	-6.27
$CaCO_{3(aq)} + H^+ = Ca^{2+} + HCO_3^-$	6.54
$CaHCO_3^+ = Ca^{2+} + HCO_3^-$	-1.13
$SiO_2 + 4H^+ = Si^{4+} + 2H_2O$	-12.19

$HSiO_3^- + H^+ = SiO_{2(aq)}$	9.55
$Al_2Si_2O_5(OH)_4 + 2H^+ = 2Al^{3+} + 2H_2SiO_4 + H_2O$	-11.31
$KAl_2Si_4O_{10}(OH)_2 + H^+ = AlSi_3O_5^{4+} + SiO_2 + KAlCO_3(OH)_2$	-11.85
$FeCO_3 + H^+ = Fe^{2+} + HCO_3^-$	2.35
$Fe_{(aq)}^{2+} + HCO_3^- = H^+ + FeCO_{3(aq)}$	-1.03

With the injection of CO₂, CO₂ begins to dissolve in the aqueous phase and this reaction gives an acid solution, pH close to 3-5 (Andre et al., 2007). In this study, the dissolution reaction of CO₂ in aqueous phase was assumed to be controlled by Henry's law (Lasaga, 1984). The input variables for the model including dissociation of injected CO₂ process are shown in Table 7.17. A sequential iteration approach was used for the coupling between flow, geochemical and mineral reactions. The chemical diffusion, dispersion and reactions were iteratively solved until convergence.

Table 7.17. Kinetic reactions used in reactive transport simulations.

Kinetic reaction	Log kinetic equilibrium coefficient
$SiO_{2(s)} = SiO_{2(aq)}$	-3.54
$CaCO_3 + 2H_2O + 2CO_2 = Ca^{2+} + 3HCO_3^- + H^+$	1.42
$Al_2Si_2O_5(OH)_4 + 2H^+ = 2Al^{3+} + 2H_2SiO_4 + H_2O$	-3.21
$KAl_2Si_4O_{10}(OH)_2 + H^+ = AlSi_3O_5^{4+} + SiO_2 + KAlCO_3(OH)_2$	-2.15
$FeCO_3 + 2H_2O + 2CO_2 = Fe^{2+} + 3HCO_3^- + H^+$	0.67

7.3.3 Model validation

The model was validated using the Dogger aquifer data presented by Andre et al. (2007). In their study, the researchers considered two injection scenarios: the injection of CO₂-saturated water and the injection of pure super-critical CO₂. Of these two scenarios, the present study selected only one injection scenario for the purposes of model verification, and that considers the realistic injection of pure super-critical CO₂. To simulate the aquifer behaviour, the model was developed based on the physical properties of the Dogger formation and included all other

parameters, including reservoir temperature, mineralogy, chemical composition and injection rate.

After running the Dogger aquifer simulation, the results were compared with those of Andre et al. (2007). Fig. 7.21 shows the comparison of the results from present study and Andre et al. (2007). Here, two variations have been compared with Andre et al.'s (2007) results: porosity change in the aquifer, and pH variation of the aquifer due to 10 years of CO₂ injection. As can be seen in Fig. 7.21, the proposed model soundly reproduced the behaviour of the Dogger aquifer as presented by Andre et al. (2007). In practice, it is difficult to expect similar variations in both studies for various reasons. The main reason is that two different numerical platforms were used to derive the aquifer behaviour. Andre et al. (2007) used the TOUGHREACT simulator, which is completely different from the COMSOL simulator, and includes flow and transport equations and has a framework of reactive geochemistry. For this reason, some additional input parameters are required to simulate the flow behaviour of reservoirs using COMSOL, such as the diffusion coefficient and the dispersion coefficient. To verify the consistency of the proposed model, statistical analysis, including standard deviation and coefficient of variation was carried out on Andre et al.'s (2007) and the present study data to evaluate the variability of the results. As expected, the standard deviations and coefficients of variation obtained for both cases did not show good relationships, especially for pH variations. However, the porosity variations showed good agreement, and the proposed model almost fits Andre et al.'s (2007) data. When the validation was completed, the model was used to study the behaviour of the Hawkesbury formation under CO₂ sequestration conditions.

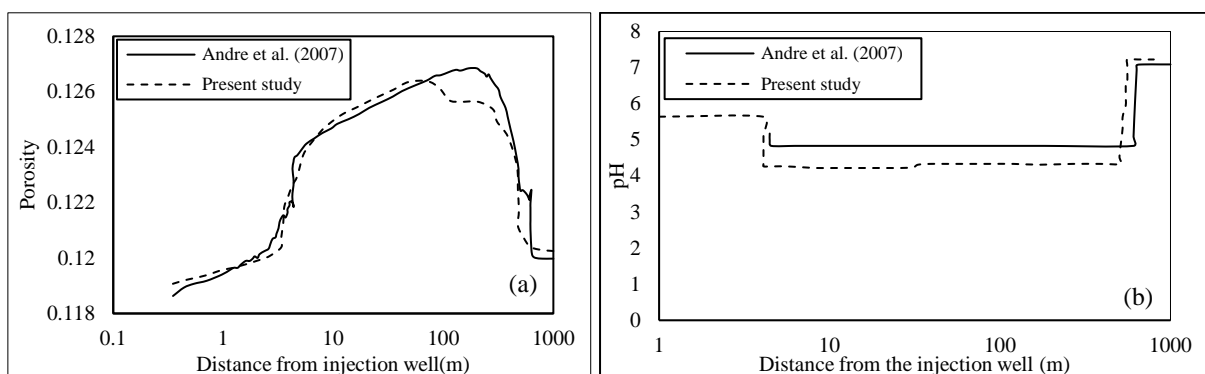


Figure 7.21. Model validation using Dogger aquifer data (a) porosity profile and (b) pH variation after an injection of 10 years.

7.3.4 Results and discussion

7.3.4.1 Chemical and mineralogical response of Hawkesbury formation upon exposure to CO₂

Precise knowledge relating to the behaviour of injected CO₂ in reservoir formations in in-situ environments is important in deep saline sequestration, because the injected CO₂ encounters diverse geochemical and mineralogical processes during the injection and storage stages. The interaction between injected CO₂ and aqueous brine can be considered as the primary chemical reaction in deep saline sequestration. This process, which is well-known as the dissolution of CO₂ in aqueous brine, can be described in three stages in Eqs. 7.63-7.65:



Under reservoir conditions, CO₂ and aqueous brine can be considered as two immiscible fluids. With the interaction between the two fluids, the dissolution of CO₂ into the brine phase and of brine into the CO₂, can take place. Over the past two decades, many research studies have investigated the behaviour of CO₂/brine systems, including their thermodynamic, equilibrium and kinetic properties (Duan et al., 1995; Kiepe et al., 2002; Duan and Hu, 2004). According to these studies, the behaviour of the CO₂-brine mixture can be modelled using the equation of state theory. In order to investigate how CO₂ dissolution influences CO₂ sequestration in the Hawkesbury formation, CO₂ solubility in the aqueous phase was first considered. To simulate the solubility reaction of CO₂, the equation state for the CO₂-NaCl system developed by Duan et al. (1995) was incorporated as follows:

$$\ln m_{CO_2} = \ln y_{CO_2} \phi_{CO_2} P - \frac{\mu_{CO_2}}{RT} - 2\lambda_{CO_2-Na^+} (D_{Na^+} + D_{K^+} + 2D_{Ca^{2+}} + 2D_{Mg^{2+}}) - \xi_{CO_2-NaCl} D_{Cl^-} (D_{Na^+} + D_{K^+} + D_{Ca^{2+}} + D_{Mg^{2+}}) + 0.07D_{SO_4^{2-}} \quad (7.66)$$

Table 7.12 shows the model input parameters that were used to simulate the dissolution of injected CO₂ in the brine phase. For the modelling, the reservoir was assumed to be saturated with a highly saline brine (20% NaCl concentration by weight), with the chemical composition

given in Table 7.13. Fig. 7.22 shows the variation of $CO_{2(g)}$, $H_2CO_{3(aq)}$, $H^+_{(aq)}$ and $HCO^-_{3(aq)}$ ion concentrations during 50 years of injection and 50 years of storage.

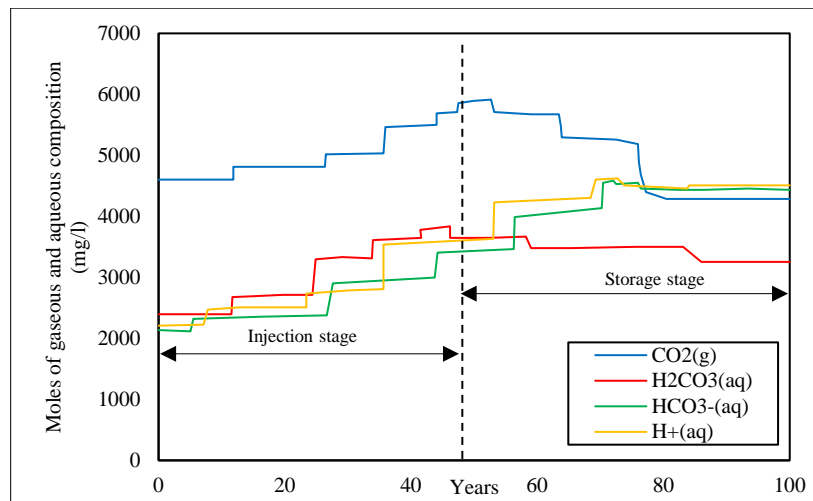


Figure 7.22. Evaluation of $CO_{2(g)}$, $CO_{2(aq)}$ and $HCO^-_{3(aq)}$ in the system with time.

According to the results, during the injection stage, the process of CO_2 dissolution continues as long there is $CO_{2(g)}$ phase and that results in increasing the $H_2CO_{3(aq)}$ phase in the aquifer. However, due to the chemical instability of the resulting $H_2CO_{3(aq)}$, the forward reaction of Eq. 7.64 initiates, and as a result, $H^+_{(aq)}$ and $HCO^-_{3(aq)}$ ion concentrations increase, resulting in an acidic medium in the reservoir. As can be seen in Fig. 7.22, when the injection stops, the $CO_{2(g)}$ phase in the reservoir begins to decrease, and as a result, the $H_2CO_{3(aq)}$ phase gradually decreases. For example, the $H_2CO_{3(aq)}$ ion concentration in the aquifer decreases from 3874.36 to 3286.71mg/l over the storage period of 50 years. According to Eq. 7.64, the reduction of the $H_2CO_{3(aq)}$ ion concentration should activate the backward reaction and should reduce the production of $H^+_{(aq)}$ and $HCO^-_{3(aq)}$ ions. However, as can be seen in Fig. 7.22, after injection, $H^+_{(aq)}$ and $HCO^-_{3(aq)}$ ion concentrations first increase up to a maximum value and then gradually decrease and come to a steady state. This unusual behaviour of $H^+_{(aq)}$ and $HCO^-_{3(aq)}$ ion concentrations may be due to the initiation of mineral reactions, which consume the resulting $H^+_{(aq)}$ and $HCO^-_{3(aq)}$ ions in the aquifer, activating the forward reaction of Eq. 7.65. Accordingly, rock minerals start to dissolve as long there is sufficient $H^+_{(aq)}$ in the system and increases the

rock ions in the system, such as Ca^{2+} , Mg^{2+} , Fe^{2+} , Al^{3+} , Ba^{2+} and Si^{4+} . Finally, the ions generated by the rock mineral dissolution process start to react with free HCO_3^- ions and re-precipitate as secondary minerals. Fig. 7.23 provides a closer view of this.

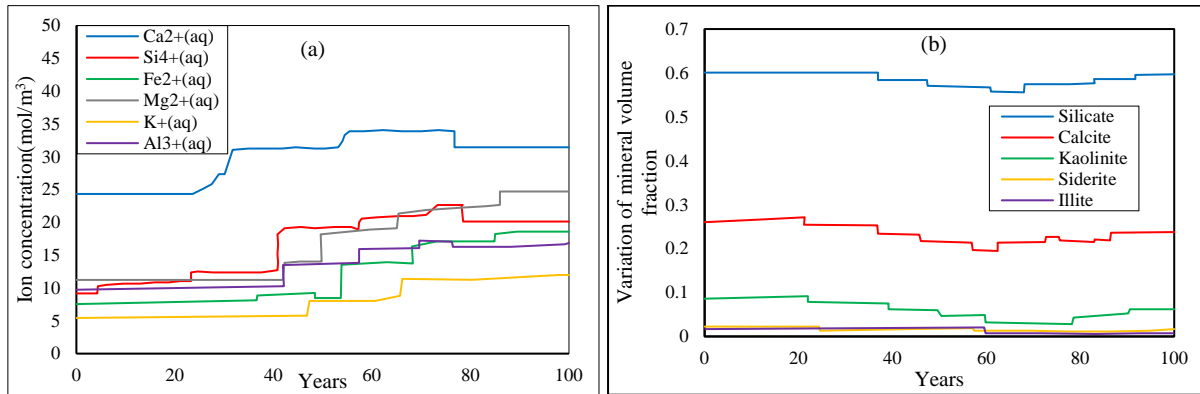


Figure 7.23. (a) Variation of ion composition and (b) variation of mineral volume fraction with time.

As shown in Fig. 7.23a, the resulting acidic environment reacts with rock minerals and increases ion concentrations in the aquifer. Table 7.14 shows the initial mineral composition of the Hawkesbury formation and it consists mainly of silicate and calcite (60% and 26% by volume, respectively) with some minor amounts of kaolinite, siderite, barite and illite. According to Fig. 7.23a, it is clear that the chemical response of the Hawkesbury formation upon exposure to CO_2 can be summarised as serial and parallel reactions, as shown in Tables 7.16 and 7.17. The reservoir fluid composition was analysed for major (Si^{4+} , Ca^{2+} , Al^{3+}) and some minor (Mg^{2+} , K^+ , Fe^{2+}) cations. To date, a number of studies have been carried out to investigate the chemical and mineral responses of sandstone formations upon exposure to CO_2 (Azaroual et al., 1997; Brosse et al., 2005; Andre et al., 2007). The studies have found that this CO_2 injection-induced mineral alteration process (mineral trapping) is truly a long-term phenomenon. The results of the present study are consistent with those of previous studies, revealing the long-term characteristics of the mineral trapping mechanism of the Hawkesbury formation. According to the results, it took more than 30 years to initiate early mineral trapping reactions under simulated reservoir conditions. In order to understand the geochemical behaviour of each rock mineral, the variation of ion concentrations in the aquifer was analysed. According to the results, the Ca^{2+} ion concentration in the aquifer increases at the very beginning of the injection process (after 23 years of injection), where the initial concentration of 24.33mg/l increases to 31.27mg/l after 23years and further increases to 33.89mg/l after the injection stops. Generally,

the increase of Ca^{2+} ion concentration in the aquifer provides basic identifying evidence for calcite mineral dissolution, which is confirmed by Fig. 7.23b. According to this figure, the calcite in the Hawkesbury formation begins to react with dissolved free H^+ ions after 30 years of injection and that is responsible for the enhanced Ca^{2+} ion concentration in the aquifer, as seen in Fig. 7.23a. The calcite dissolution continues after injection for 70 years and then begins to re-precipitate in the simulated environment. Similar variation can be seen in the Al^{3+} ion concentration, which starts to increase after 40 years of injection and continues until 75 years after injection, and then starts to decrease. In this formation, the increase in Al^{3+} ion concentration is probably caused by the dissolution of clay minerals such as illite and kaolinite. As can be seen in Fig. 7.23b, the resulting acid solution starts to dissolve kaolinite after 20 years and illite after 60 years, respectively. Moreover, the numerical results also show some enrichment patterns in the Mg^{2+} and K^+ ions, and these are believed to be related to the dissolution of illite minerals from the reservoir formation. However, no illite or siderite is formed throughout the simulation time. In addition to these reactions, Si^{4+} ion concentration can be expected to increase due to the dissolution of silicate, kaolinite and illite minerals in the formation during CO_2 sequestration.

The other important parameter in the geochemical behaviour of the Hawkesbury formation is the aquifer pH. The pH of the aquifer is controlled first by the dissolution of CO_2 in the brine phase, which reduces to a value 4.2 after 20 years of injection and then by calcite dissolution, which increases the pH to 5.1 after injection by consuming H^+ ions in the system. Fig. 7.24 shows the variations of the resulting pH buffer region of the reservoir with respect to simulation time (injection and storage).

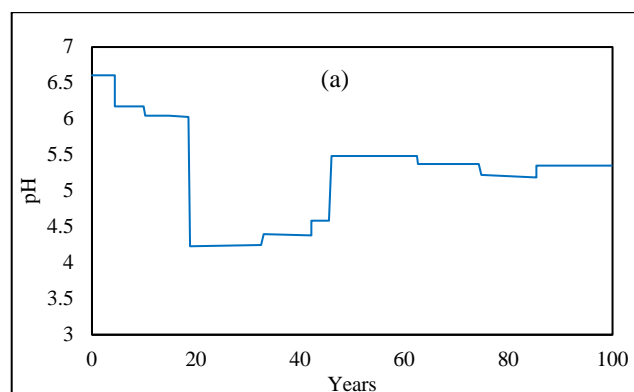
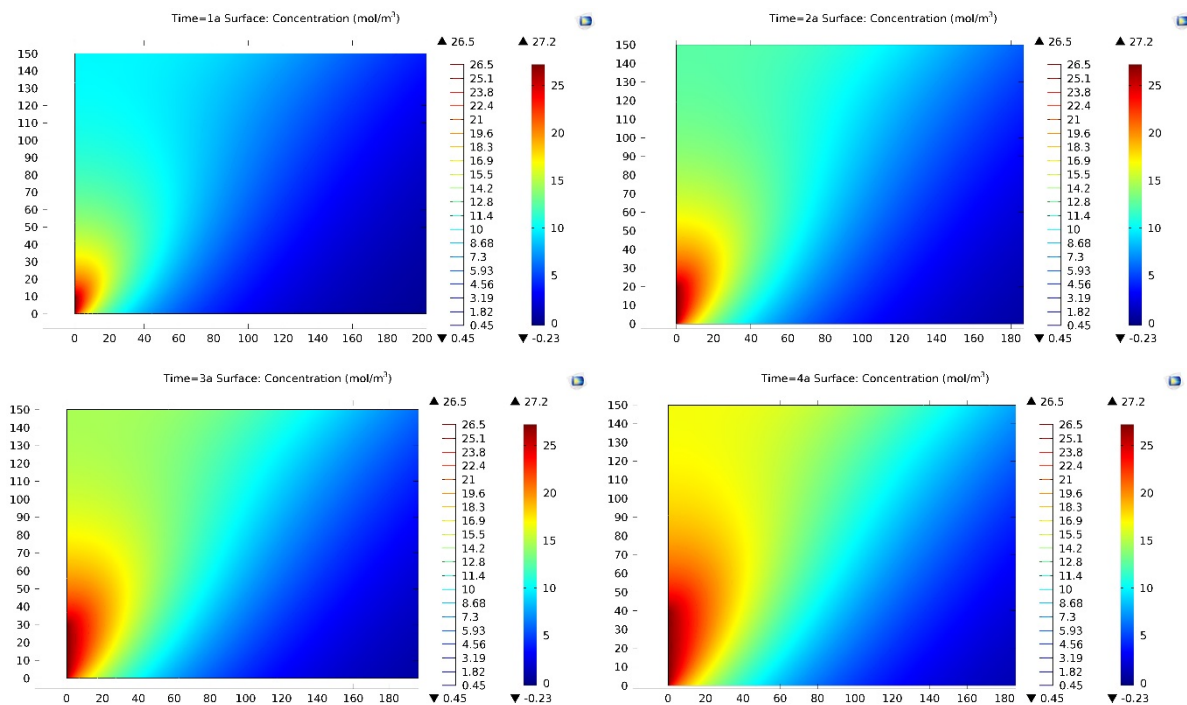


Figure 7.24. The variations of the resulted pH buffer regions of the reservoir with respect to the simulation time.

The CO₂ plume development near the injection well throughout the injection period of 50 years is presented in Fig. 7.25. The most important question addressed in this study is how far the CO₂ plume travels through the reservoir formation, and addressing this issue will provide useful information to minimize the risks associated with CO₂ sequestration. According to the results, even if injection is stopped after 50 years, the migration of the CO₂ plume continues for some time. As can be seen in Fig. 7.25, after 1, 2, 3, 4, 5, and 20 years, the CO₂ plume front reaches an extension of 60, 100, 120, 160, 180 and 400m, respectively. In addition, three different saturation regions can be identified in the aquifer during the injection stage: 1) a CO₂-saturated region (red), 2) a two-phase or partially-saturated region (light blue) and 3) a brine-saturated region (dark blue). A similar observation was reported by Noh et al. (2007) and Burton et al. (2009). According to these researchers, these regions can be modelled as two fronts separately by assigning different boundary conditions. Burton et al. (2009) proposed a mathematical solution to simulate these three regions, based on the relationship between phase mobility and relative permeability and pressure drop and flow rate.



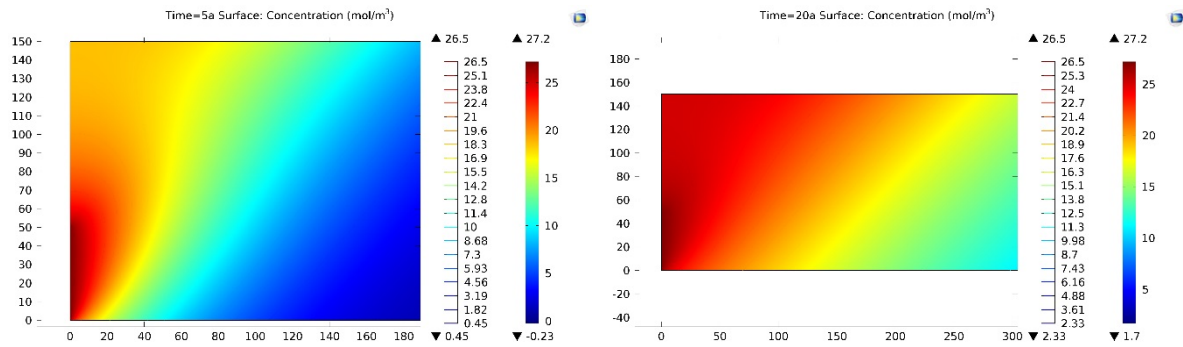


Figure 7.25. CO₂ plume development in Hawkesbury formation (a) 1 year (b) 2 years (c) 3 years (d) 4 years (e) 5 years and (f) 20 years.

The effective implementation of CO₂ injection in deep saline aquifers requires adequate porosity and permeability. According to the findings of the present study, rock mass mineralogical change causes the porosity of the formation to significantly change during and after injection. As Fig. 7.26 shows, the initial porosity of the Hawkesbury formation starts to increase after around 40 years and it reaches its maximum value of 0.35 after 75 years. However, at the end of the simulation time (around 90 years), the porosity of the formation starts to decrease and it reaches 0.33. In relation to the initial increment of porosity, CO₂ sequestration may cause it to be enhanced by around 12.9%. According to past studies (Rochelle et al., 2004; Rathnaweera et al., 2016), even such a small alteration in porosity may have a considerable effect on the effectiveness of the sequestration process.

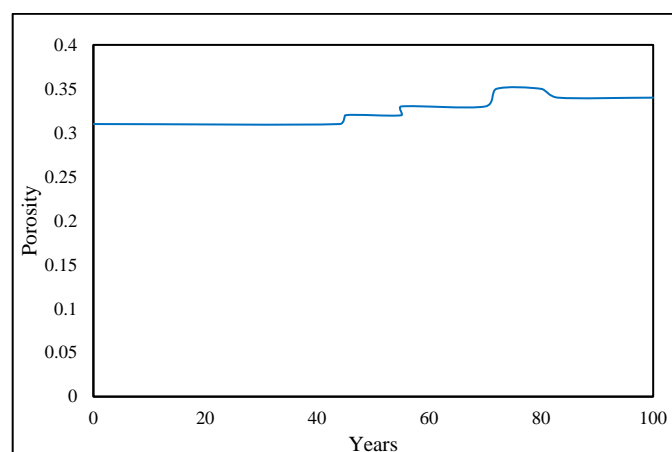


Figure 7.26. Porosity variation with respect to simulation time.

However, as can be seen in Fig. 7.26, the reservoir porosity starts to change at the end of the injection stage and therefore, the effect of porosity may not adversely affect the injectivity of

the process. Although the process is safe in terms of injectivity, the CO₂ sequestration-created porosity increment in the Hawkesbury formation enhances the movement of the CO₂ plume into upper layers, increasing the high risk of CO₂ leakage during storage. Furthermore, if CO₂ moves from the reservoir to the caprock it will start to react with the caprock and create major changes in the caprock structure, including the dissolution of the caprock's sealing properties. If this happens, it will lead to the formation of new flow pathways for CO₂, creating a major leakage risk. This is a serious issue, and should be considered before beginning CO₂ sequestration in the Hawkesbury formation.

7.3.4.2 CO₂ sequestration-induced hydro-mechanical behaviour of Hawkesbury formation

Effective CO₂ injection into a deep saline aquifer generally depends on various hydro-mechanical parameters. This section therefore deals with the parameters that may cause hydro-mechanical failure during CO₂ sequestration in deep saline aquifers. Of the various parameters, CO₂ sequestration-induced reservoir pressure is critical. As discussed in Ranjith et al. (2013), excessive reservoir pressures may cause irreversible mechanical changes, resulting in hydraulic fracture or shear failure in both the aquifer and caprock. Therefore, it is of utmost importance to evaluate the reservoir pressure during and after CO₂ injection to ensure that such issues are minimized. The present study therefore simulated and analysed the reservoir pressure upon exposure to CO₂ for two scenarios: 1) without and 2) with coupling geochemical and mineralogical effects. Here, the second scenario was selected to understand the long-term geochemical and mineralogical alteration effects (discussed in the previous section) on the mechanical and flow behaviour of Hawkesbury sandstone.

For the first scenario, the reservoir pressure was determined by assigning an injection pressure of 10MPa while maintaining the depth (confining pressure) and temperature effects without coupling rock mineral alterations. The results are shown in Fig. 7.27a. After evaluating the first case, the model was coupled with geochemical and mineralogical rock alterations to determine how rock mineral alteration influences the hydro-mechanical behaviour of the Hawkesbury formation. These results are shown in Fig. 7.27b. According to Fig. 7.27, there is a significant influence of CO₂ injection-induced rock mineral alteration on reservoir pressure. As the figure shows, the reservoir pressure increases for both cases during the injection stage. For instance, in scenario 1, reservoir pressure increases from 10 to 17.46MPa, whereas in scenario 2 it increases from 10 to 18.23MPa. It is now clear that the reservoir pressure induced by CO₂

injection in the first scenario (without considering geochemical and mineralogical reactivity between reservoir minerals and injected CO₂) is much lower than in the second injection scenario. According to the results, the global rock mineral reactivity leads to a maximum reservoir pressure increase of about 82.3%, while scenario 1 leads to a maximum reservoir pressure increase of about 71.3%, which is 11% lower than the second scenario. However, when the injection stops, the reservoir pressure begins to dissipate for both cases. Interestingly, this pressure dissipation rate appears to be much higher in the second scenario than the first. For example, in scenario 1, the reservoir pressure decreases from 17.46 to 17.05MPa after 60 years, which is a 2.35% reduction compared to that for 50 years (a reduction rate of 0.041MPa/year). However, in scenario 2, the reservoir pressure decreases from 18.23 to 17.01MPa after 60 years, which is 6.67% reduction compared to that for 50 years (a reduction rate of 0.122MPa/year).

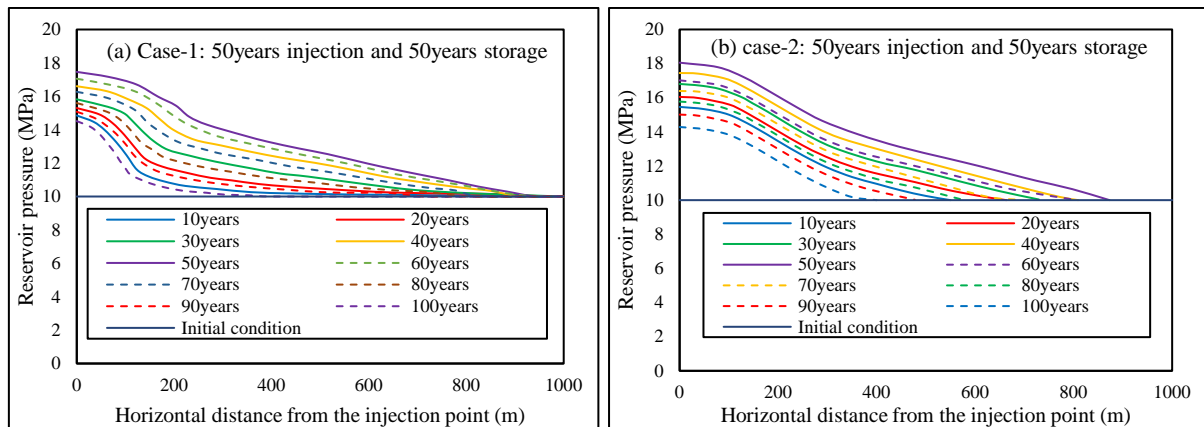


Figure 7.27. Variation of reservoir pressure along the horizontal distance from injection point (a) case 1 and (b) case 2.

The high reservoir pressure accumulation observed in the second scenario is probably due to the rock mineral alteration-induced pore structural modification. Reservoirs with larger porosity yield larger CO₂ plumes during deep saline sequestration due to the easy movement of injected CO₂ through the modified larger pore network (Oostrom et al., 2016). The results of this study confirm that there is a modification in the porosity of the reservoir, which is clearly seen in Fig. 7.26. In order to identify the effect of porosity change on the reservoir CO₂ saturation profile, the variations of CO₂ saturation with time were recorded at two points 10m and 30m away from the injection point and evaluated under both scenarios, with and without coupling rock mineral alteration. The results are depicted in Fig. 7.28. As the figure shows, a higher CO₂ saturation profile can be seen in the simulation that includes the coupling of both hydro-mechanical and geochemical processes, revealing the significance of rock mineral changes on reservoir porosity.

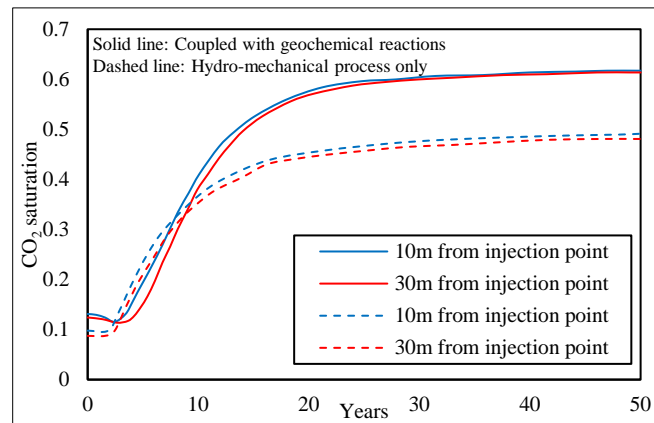


Figure 7.28. Time evaluation of CO₂ saturation profile at 10 and 30m from injection point.

7.3.5 Conclusions

CO₂ sequestration in deep saline aquifers and its effect on the reservoir's hydro-mechanical, geochemical and mineralogical behaviours can be successfully modelled using the COMSOL Multiphysics numerical simulator. Therefore, the present study incorporated COMSOL software to simulate the behaviour of Hawkesbury sandstone in a CO₂ sequestration environment. The mathematical module available in COMSOL was used to input pre-defined partial differential equations which govern the hydro-mechanical, geochemical and mineralogical behaviour of reservoir rock. In addition, in order to identify the influence of rock mineral alteration on the overall performance of the formation, two scenarios, 1) with and 2) without coupling rock mineral alteration with hydro-mechanical behaviour, were considered. According to the results of the field-scale model, the following conclusions can be drawn:

- The injection of CO₂ into Hawkesbury sandstone causes its hydro-mechanical, geochemical and mineralogical characteristics to change considerably. According to the results, the porosity of the aquifer is significantly affected by rock mineral alteration. After 40 years of injection, the reservoir porosity begins to increase and it keeps increasing until it starts to decrease in 80 years. This observed porosity alteration is probably due to the precipitation/dissolution of rock minerals and this is confirmed by the mineral reactions observed.
- According to the numerical results, considerable amounts of calcite, silicate and kaolinite minerals start to dissolve at the early stage of injection. However, after injection stops, there is a possibility of re-precipitation of calcite, silicate and kaolinite.

- The proposed model also illustrates the importance of considering geochemical and mineralogical reactions when evaluating the integrity of any deep saline sequestration project. According to the results, rock mineral alteration appears to play a considerable role in reservoir pressure and CO₂ plume movement, and causes the reservoir pressure to increase over time.
- The CO₂ saturation profiles obtained for the two scenarios also reveal the significance of rock mineral alteration, and higher saturation profiles were obtained for the first scenario than the second scenario. This is due to the modified porosity properties of the reservoir upon exposure to CO₂, which enhance the movement of CO₂ by increasing the saturation profile.

7.3.6 Nomenclature

α =Phase of fluid (wetting (*w*) or non-wetting (*nw*) phase)

ρ_{α} =Density of α -phase fluid

μ_{α} =Viscosity of α -phase fluid

P_{α} =Pressure of α -phase fluid

k_{ij} =Absolute permeability tensor of reservoir rock

k_{ar} =Relative permeability of α -phase

X_{nw} =Mass fraction of CO₂ in the aqueous phase

ρ_{nw} =Partial density of dissolved CO₂

ϕ =Porosity of reservoir

ϕ_0 =Initial porosity condition

D =Direction vector of gravity

θ_{α} =Volumetric content of α -phase fluid

ρ_{α}^* =Density of α -phase fluid in source term

q_{α} =Flux of α -phase fluid in source term, including chemical changes

S_α = Saturation of α -phase in reservoir rock

g = Gravity term

c_r = Compressibility of reservoir rock

n_α = Total number of chemical species in α -phase

Q_D = Flux in source term caused by dispersion and diffusion

M_l = Molar weight of species l in CO_2 phase

$C_{\alpha l}$ = Concentration of solute l in α -phase

S_l = Concentration of solute l on solid phase

$V_{\alpha i}$ = Flow velocity of α -phase in i^{th} direction

$K_{\alpha n}$ = Reaction rate of n^{th} solute in α -phase

$K_{s n}$ = Reaction rate of n^{th} solute on solid phase

$D_{\alpha ij}(S_w)$ = Mechanical dispersion tensor of α -phase

$D_{\alpha m}(S_w)$ = Molecular diffusion coefficient of α -phase

$C_{\alpha l} = l^{\text{th}}$ species concentration in α -phase in source term

δ_{ij} = Kronecker delta

α_L = Longitudinal dispersion coefficient

α_T = Transverse dispersion coefficient

V_i = Velocity component in i^{th} direction

V = Absolute average velocity of fluid

D_{mo} = Molecular diffusivity of solute

$D_{\alpha m}$ = Pore molecular diffusivity of solute

τ = tortuosity factor

δ = Constrictivity

$C_{\alpha i}$ = i^{th} species in α -phase

S_i = i^{th} species on solid phase

k_i = adsorption rate of i^{th} species

k_{dl} = Linear distribution coefficient of i^{th} species between solid and fluid phases

r_{si} = Chemical reaction rate of i^{th} species on solid phase

$r_{\alpha i}$ = Chemical reaction rate of i^{th} species in α -phase

$k_{s_{mwi}}$ = Solubility rate if i^{th} species in CO₂ phase

$S_{\alpha i}$ = Saturated concentration of i^{th} species in α -phase

p_c = Capillary pressure

H_c = Capillary pressure head

C_p = Specific capacity of water

θ_{ares} = Residual volumetric content of α -phase

$\theta_{\alpha s}$ = Saturated volumetric content of α -phase

α_v = Van Genuchten's model constant

M = Van Genuchten's model constant

N = Van Genuchten's model constant

L = Van Genuchten's model constant

r_m = Reaction rate

k = Intrinsic rate constant

A = Specific reactive area

θ = pH power law constant

η = pH power law constant

K_m = Equilibrium constant for the chemical reactions

Q_m = Reaction quotient

7.3.7 References

1. André L, Audigane P, Azaroual M, Menjöz A. Numerical modelling of fluid–rock chemical interactions at the supercritical CO₂–liquid interface during CO₂ injection into a carbonate reservoir, the Dogger aquifer (Paris Basin, France). *Energy Conversion and Management* 2007; 48(6): 1782-1797.
2. Andersen G, Probst A, Murray L, Butler S. An Accurate PVT Model for Geothermal Fluids as Represented by H₂O-NaCl-CO₂ Mixtures, *Proceedings of the 17th Workshop on Geothermal Reservoir Engineering*, Stanford, CA, 1992: 239-248.
3. Alonso J, Navarro V, Calvo B, Asensio L. Hydro-mechanical analysis of CO₂ storage in porous rocks using a critical state model. *International Journal of Rock Mechanics and Mining Sciences* 2012; 54: 19-26.
4. Azaroual M, Fouillac C, Matray JM. Solubility of silica polymorphs in electrolyte solutions, II. Activity of aqueous silica and solid silica polymorphs in deep solutions from the sedimentary Paris Basin. *Chemical Geology* 1997; 21: 167-79.
5. Bacci G, Korre A, Durucan S. An experimental and numerical investigation into the impact of dissolution/precipitation mechanisms on CO₂ injectivity in the wellbore and far field regions. *International Journal of Greenhouse Gas Control* 2011; 5(3): 579-588.
6. Battistelli A, Calore C, Pruess K. The Simulator TOUGH2/EWASG for Modeling Geothermal Reservoirs with Brines and Non-Condensable Gas. *Geothermics* 1997; 26: 437-464.
7. Brosse E, Magnier C, Vincent B. Modelling fluid-rock interaction induced by the percolation of CO₂-enriched solutions in core samples: the role of reactive surface area. *Oil and Gas Science Technology* 2005; 60(2): 287-305.
8. Burton M, Kumar N, Bryant SL. Why relative permeability matters as much as absolute permeability. *Energy Procedia* 2009; 1: 3091-3098.
9. Chan T, Stanchell FW. Subsurface hydro-mechanical (HM) impacts of glaciation: sensitivity to transient analysis, HM coupling, fracture zone connectivity and model dimensionality. *International Journal of Rock Mechanics and Mining Sciences* 2005; 42(5-6): 828-49.
10. Duan Z, Moller N, Weare JH. Equation of state for the NaCl-H₂O-CO₂ system: prediction of phase equilibrium and volumetric properties. *Geochim Cosmochim Acta* 1995; 59: 2869-2882.

11. Duan Z, Hu J. A new cubic equation of state and its applications to the modelling of vapour-liquid equilibria and volumetric properties of natural fluids. *Geochim Cosmochim Acta* 2004; 68(14): 2997-3009.
12. Goerke UJ, Park CH, Wang W, Singh AK, Kolditz O. Numerical simulation of multiphase hydro-mechanical processes induced by CO₂ injection into deep saline aquifers. *Oil and Gas Science and Technology-Revue d'IFP Energies Nouvelles* 2011; 66(1): 105-118.
13. Gunter WD, Wiwchar B, Perkins EH, Aquifer disposal of CO₂-rich greenhouse gases: extension of the time scale of experiment for CO₂-sequestering reactions by geochemical modelling. *Mineralogy and Petrology* 1997; 59: 121-140.
14. Helgeson HC, Murphy WM, Aagaard P. Thermodynamic and kinetic constraints on reaction rates among minerals and aqueous solutions. II. Rate constants, effective surface area, and the hydrolysis of feldspar. *Geochim. Cosmochim Acta* 1981; 48: 2405-2432.
15. Hudson JA, Stephansson O, Andersson J. Guidance on numerical modeling of thermo-hydro-mechanical coupled processes for performance assessment of radioactive waste repositories. *International Journal of Rock Mechanics and Mining Sciences* 2005; 42(5-6): 850-70.
16. Johnson JW, Nitao JJ, Steefel CI, Knaus KG. Reactive transport modelling of geologic CO₂ sequestration in saline aquifers: the influence of intra-aquifer shales and the relative effectiveness of structural, solubility, and mineral trapping during prograde and retrograde sequestration, In *Proceedings of the 1st National Conference on Carbon Sequestration*. Washington, DC, 2001.
17. Kiepe JS, Horstmann K, Fischer K, Gmehling J. Experimental determination and predictions of gas solubility data for CO₂-H₂O mixtures containing NaCl or KCl at temperatures between 313 and 393K and pressure up to 10MPa. *Industrial Engineering and Chemical Research* 2002; 41: 4393-4398.
18. Kopp A, Class H, Helmig R. Investigations on CO₂ storage capacity in saline aquifers: Part 1. Dimensional analysis of flow processes and reservoir characteristics. *International Journal of Greenhouse Gas Control* 2008; 3(3): 263-276.
19. Korbol R, Kaddour A. Sleipner vest CO₂ disposal injection of removed CO₂ into the Utsira Formation. *Energy* 1995; 36: 509-512.

20. Kristinof R, Ranjith PG, Choi SK. Finite element simulation of fluid flow in fractured rock media. *Journal of Environmental Earth Sciences* 2009; 60(4): 765-773.
21. Lasaga AC. Chemical kinetics of water-rock interactions. *Journal of Geophysics Research* 1984; 89: 4009-4025.
22. Lorenz S, Maric D, Rirschl C. Eine analytische Funktion zur Bestimmung der Enthalpie wässriger NaCl Lösungen, draft report, Institut für Sicherheitstechnologie, Köln, Germany, April 2000.
23. McPherson BJOL, Lichtner PC. CO₂ sequestration in deep aquifers, In *Proceedings of the 1st National Conference on Carbon Sequestration*. Washington, DC, 2001.
24. Navarro V, Alonso J, Calvo B, Sanchez J. A constitutive model for porous rock including effects of bond strength degradation and partial saturation. *International Journal of Rock Mechanics and Mining Science* 2010; 47(8):1330-1338.
25. Neaupane KM, Yamabe T, Yoshinaka R. Simulation of a fully coupled thermos-hydro-mechanical system in freezing and thawing rock. *International Journal of Rock Mechanics and Mining Sciences* 1999; 36(5): 563-80.
26. Noh M L, Bryant L, Araque-Martinez A. Implication of coupling fractional flow and geochemistry for CO₂ injection in aquifers. In *SPE/DOE Symposium on Improved Oil Recovery*. Society of Petroleum Engineers 2007; 10(4): 406-411.
27. Oldenburg CM, Doughty C, Peters CA, Dobson PF. Simulations of long-column flow experiments related to geologic carbon sequestration: effects of outer wall boundary condition on upward flow and formation of liquid CO₂. *Greenhouse Gases: Science and Technology* 2011; 2(4): 279-303.
28. Oostrom M, White MD, Porse SL, Krevor SCM, Mathias SA. Comparison of relative permeability-saturation-capillary pressure models for simulation of reservoir CO₂ injection. *International Journal of Greenhouse Gas Control* 2016; 45: 70-85.
29. Ozah R, Lakshminarasimhan S, Pope G, Sepehrnoori K, Bryant S. Numerical simulation of the storage of pure CO₂ and CO₂-H₂S gas mixtures in deep saline aquifers. In *SPE Annual Technical Conference and Exhibition* 2005: 12-21.
30. Phillips, Christopher J, Timothy RHD. Determining rheological parameters of debris flow material. *Geomorphology* 1981; 4(2): 101-110.

31. Ranjith PG, Perera MSA, Khan E. A study of safe CO₂ storage capacity in saline aquifers: a numerical study. *International Journal of Energy Research* 2013; 37: 189-199.
32. Rathnaweera TD, Ranjith PG, Perera MSA. Experimental investigation of geochemical and mineralogical effects of CO₂ sequestration on flow characteristics of reservoir rock in deep saline aquifers. *Nature Scientific Reports* 2016; 6: 19362-19372.
33. Rochelle CA, Czernichowski-Lauriol I, Milodowski AE. The impact of chemical reactions on CO₂ storage in geological formations: a brief review. *Geological Society, London, Special Publications* 2004; 233: 87-106.
34. Van Ruth PJ, Nelson EJ, Hillis RR. Fault reactivation potential during CO₂ injection in the Gippsland Basin, Australia. *Exploration Geophysics* 2006; 37: 50-59.
35. White SP, Weir GJ, Kissling WM. Numerical simulation of CO₂ sequestration in natural CO₂ reservoirs on the Colorado Plateau. In *Proceedings of the 1st National Conference on Carbon Sequestration*, Washington, DC, 2001.
36. Xu T, John AA, Pruess K. Numerical simulation of CO₂ disposal by mineral trapping in deep aquifers. *Applied Geochemistry* 2004; 19: 917-936.
37. Zerai B, Beverly ZS, Matisoff G. Computer simulation of CO₂ trapped through mineral precipitation in the Rose Run Sandstone Ohio. *Applied Geochemistry* 2006; 21: 223-240.

7.4 Summary of Chapter 7

This chapter has presented the details of a numerical study conducted under laboratory- and field-scale conditions using the COMSOL Multiphysics simulator. Numerical simulations which can characterise the deep saline sequestration process are important for the clarification of safety, feasibility and economic issues of a particular sequestration project during the preparation, operation and post-injection stages. In addition, a precise knowledge of the mechanisms and geochemistry involved in deep saline sequestration is needed for further improvement of the sequestration process.

Although there have been many numerical studies on field-scale conditions using different simulators, few studies have been reported on the application of these simulators to laboratory conditions. Therefore, a natural aquifer's mechanical behaviour was first simulated by developing a laboratory-scale model under both uniaxial and triaxial stress conditions. According to the results, the proposed model based on tri-linear stress can reasonably reproduce the salinity-dependent mechanical behaviour of reservoir rock, as reported in Chapter 3.2 and 3.3.

The relative flow model developed using the Buckley-Leverett flow theory revealed the importance of liquid diffusion coefficients when defining the flow behaviour of deep saline sequestration. According to the results, the developed model predicts the experimental results reasonably well, with less than 10% relative error. The numerical results also revealed that there is a significant influence of CO₂ phase change on the final saturation profiles of CO₂ and brine. In addition, the CO₂ pressure gradient along the sample length showed that the pressure gradient has a non-linear relationship with sample length.

The results of the field-scale model illustrated the importance of coupling hydro-mechanical, mineralogical and geochemical behaviours in deep saline sequestration. The model was developed by extending the governing equations proposed for the laboratory-scale flow model reported in Section 7.2. The CO₂ saturation profiles obtained for two scenarios 1) with and 2) without coupling rock mineral alteration with hydro-mechanical behaviour) showed the significance of the rock mineral alteration, and higher CO₂ saturation profiles were obtained for the first scenario than the second scenario. This is probably due to the modified porosity properties of the reservoir upon exposure to CO₂ which enhance the movement of CO₂ by increasing the CO₂ saturation profile.

CHAPTER 8

Conclusions and Suggestions for Future Research

8 Conclusions and Suggestions for Future Research

8.1 Conclusions

The main objective of this thesis was to investigate the chemical, mineralogical and hydro-mechanical behaviour of reservoir rock in deep saline CO₂ sequestration. In order to achieve the above main objective, the present study selected the Gosford Hawkesbury sandstone formation as a potential reservoir for deep saline sequestration due to its favourable geological and petrophysical properties for long-term CO₂ storage. Experimental and numerical modelling studies were conducted on the Hawkesbury formation and this thesis reports them in a structured manner. This thesis comprises eight major chapters, of which five are dedicated to the presentation of the major findings of the thesis, while the other three chapters provide the introduction, literature review and conclusions. In addition, each chapter has been subdivided into inter-related sections to meet the specific sub-objectives to achieve the main goal of this thesis. The major conclusions drawn from each relevant chapter are presented in the following sub-sections.

8.1.1 Conclusions regarding mechanical behaviour of deep saline reservoir rock in natural and CO₂-sequestered environments

8.1.1.1 Experimental work

The mechanical behaviour of reservoir rock in deep saline aquifers in natural and CO₂-induced environments was investigated using experimental and numerical approaches. First, natural aquifer mechanical behaviour was evaluated under unconfined and confined stress conditions. Generally, deep saline aquifers contain highly saline brine and their salinity increases with aquifer depth. The salinity also changes from aquifer to aquifer (the aquifer-specific parameter). Therefore, precise knowledge of the salinity-induced mechanical behaviour of reservoir rock is crucial for the selection of effective and safe CO₂ storage sites. In addition, it is expected that the mechanical properties of deep saline reservoir rock will be completely different from its dry and water-saturated properties. A comprehensive mechanical study was therefore conducted on brine-saturated Hawkesbury sandstone (saturated for one month) for a range of salinity levels (0, 10, 20 and 30% NaCl) using a series of compressive strength tests and integrating the use of AE and ARAMIS technologies. Finally, SEM analysis was carried out to investigate the brine-induced microstructural changes in the reservoir pore space. However, the effect of

salinity on the mechanical behaviour of reservoir rock can only be fully understood following the combined investigation of mechanical behaviour in both unconfined and confined stress environments, because preferable saline aquifers for CO₂ storage are generally located very deep underground (0.8-2km), where the rock is highly confined (20-30MPa). Therefore, in order to evaluate the real-field effect on the mechanical behaviour of natural reservoir rock, it is necessary to conduct tests under different confining pressures. Therefore, a series of triaxial strength tests was conducted on brine-saturated samples (0-30% NaCl) for a range of confining pressures (5-20MPa). After obtaining the triaxial results, the applicability of the conventional Mohr-Coulomb failure criterion to brine-saturated reservoir rock was also studied. The test results of both studies revealed the following behaviours.

1. Water saturation (pore fluid with 0% of NaCl) appears to play a significant role in reservoir rock strength, and causes the dry rock mass strength to be reduced by around 36%.
2. The samples saturated with 10% NaCl showed a reduction in compressive strength (8.82%) and the samples saturated with higher percentages of NaCl (20% and 30%) showed an enhancement in compressive strength (4.23% and 9.65%), compared to water-saturated specimens.
3. The brittleness of reservoir rock increases with increasing NaCl concentration in the aquifer pore fluid. The Young's modulus reduction due to water saturation reduces with the addition of NaCl, and increasing the NaCl concentration from 20% and 30% causes the Young's modulus to increase by 34.21% and 77.57%, respectively.
4. According to the AE results, the increased salinity of the pore fluid causes the crack initiation stress threshold to increase. However, samples saturated with 10% NaCl showed a reduction in crack initiation stress (9.75MPa) and those saturated with 20% and 30% NaCl showed an enhancement in crack initiation stress (11.32 and 15.73MPa), compared to water-saturated samples (11.04MPa).
5. The physical phenomenon causing this altered mechanical behaviour was identified by performing SEM analysis. According to the results, high salinity conditions (20 and 30% NaCl) cause NaCl crystals to crystallise in the reservoir pore structure. This reduces the number of voids, resulting in improved reservoir rock strength. However, low salinity brine-saturated samples (10% NaCl) did not show such behaviour, and the observed mechanical weakening process in low salinity brine-saturated samples is probably due to the chemically corrosive

nature of NaCl ions. Although this happens in rock samples with higher percentages of NaCl (20% and 30%), the NaCl crystallization effect is the dominant influence on mechanical behaviour compared to the chemically corrosive effect.

6. The presence of highly saline brine as a pore fluid enhances the shear strength parameters (friction angle and cohesion) of the reservoir rock. The friction angle and cohesion of the studied Hawkesbury sandstone increase by around 22%, 25% and 32% and 3.5%, 4% and 5.6% in the presence of 10%, 20% and 30% NaCl concentration in the pore fluid. The friction angle enhancement is probably due to the crystallisation of NaCl in the rock pore structure, as crystallised NaCl enhances the friction between the grain-to-grain contacts of the grain-supported rock matrix. The observed cohesion gain in the reservoir rock with the presence of NaCl in the pore fluid is due to the clay mineral precipitation by NaCl, which was confirmed by XRD results.

7. The presence of NaCl in the pore fluid enhances the dilatancy strength of reservoir rock by reducing post-peak dilation, and the effect increases with increasing brine concentration in the pore fluid. This is because the deposition of NaCl crystals in the rock pore space reduces its porosity and consequently enhances the micro- and macro-fracturing resistivity of the rock mass.

8. When the pore fluid has a higher degree of salinity, the conventional linear Mohr-Coulomb failure criterion creates a considerable deviation from the measured triaxial stress data of Hawkesbury sandstone under brine saturation conditions. In addition, the measured data deviate from the Mohr-Coulomb criterion at high confining pressures.

9. Based on triaxial strength data, a modified Mohr Coulomb failure criterion was proposed to predict the strength variation of brine-saturated reservoir rocks under high confinements. The performance of the proposed criterion in terms of the accuracy of the predictions was tested, and the results revealed that the model can satisfactorily predict the strength variation of brine-saturated Hawkesbury sandstone.

10. The mechanical analysis of natural reservoir rock (brine-saturated Hawkesbury sandstone) in unconfined and confined stress environments indicates the mechanical strengthening action of high salinity brine on reservoir rock strength. This is favourable for the long-term integrity of CO₂ sequestration in deep saline aquifers, as it leads to enhanced fracturing resistivity, resulting in reduced risk of CO₂ back-migration into the atmosphere.

After investigating mechanical behaviour of natural reservoir formations, the mechanical behaviour of the CO₂+brine-reacted (at 10MPa CO₂ pressure and 35°C temperature) Hawkesbury formation was evaluated in both unconfined and confined stress environments. First, different saturation conditions, dry, water- and brine-saturated Hawkesbury sandstone with and without CO₂ reaction, were considered in the unconfined stress environment to obtain an understanding of the influence of CO₂ injection on the mechanical properties of reservoir rock. In addition, SEM, XRD and XRF analyses were employed to identify the chemical and mineralogical changes that occur in reservoir rocks during CO₂ injection. Next, a study was conducted on CO₂-reacted Hawkesbury sandstone under in-situ stress and temperature conditions to characterise the behaviour of reservoir rock upon exposure to scCO₂ (supercritical CO₂). Finally, a comprehensive chemical and mineralogical analysis was carried out on CO₂-reacted samples to precisely identify the chemically-coupled mechanical behaviour of reservoir rock. The following conclusions are drawn based on these studies.

1. The injection of CO₂ into brine-saturated Hawkesbury sandstone causes a considerable strength reduction due to mineralogical alteration-induced mechanical weakening in the grain contacts.
2. The altered reservoir pore geometry due to CO₂ injection is affected the effective stress patterns acting on the rock matrix, and a significant increase in effective stress coefficient was observed in the tested brine+CO₂-reacted sandstone samples (compared to brine-saturated and dry samples). This creates a pore pressure-dominant (compared to mean total stress) mean effective stress field in the formation.
3. The slip tendency of brine+CO₂-reacted reservoir rock is increased with increasing injection pressure and this reveals the fate of the resulting pore pressure-dominant effective stress field during CO₂ injection.
4. In addition, the Mohr-Coulomb failure lines deviate from linear to non-linear when the sample condition changes from dry to brine and dry to brine+CO₂-reacted.
5. The mechanical analysis of CO₂-induced reservoir rock in unconfined and confined stress environments revealed mechanical weakening in the reservoir pore structure. This is not favourable for the long-term integrity of CO₂ sequestration in deep saline aquifers, because it leads to reduced rock strength, resulting in enhanced risk of CO₂ back-migration into the atmosphere.

Next, the influence of carbonate and silicate cementation on deep saline sequestration was considered. The main aim of this study was to identify the influence of different mineral compositions on the mechanical behaviour of reservoir rock in a deep saline CO₂ sequestration environment. First, natural samples (carbonate- and silicate-cemented sandstone) were reacted with brine+CO₂ under different injection pressures, including sub-critical (4, 6MPa) and super-critical (8, 10MPa) pressure conditions under a constant temperature of 35°C. Next, the chemical and mineralogical behaviours were investigated by performing comprehensive chemical and mineralogical analyses (including ICP-AES and XRD) on the samples and the reacted pore fluids, and the mineralogical characterisation was carried out based on three dominant rock minerals: quartz, calcite and kaolinite. Finally, the influence of silicate and carbonate cementation on the mechanical behaviour of reservoir rock was investigated by performing a series of strength tests on 12-month reacted samples in an unconfined stress environment. According to the results, the following conclusions can be drawn:

1. The presence of calcite minerals as a major cement significantly changes the chemical response of the reservoir formation upon exposure to CO₂. The pH variations obtained for silicate- and carbonate-cemented sandstones clearly confirm the above argument, showing higher pH buffering characteristics in calcite-dominant carbonate-cemented formations compared to quartz-dominant silicate-cemented formations.
2. In the CO₂ sequestration environment, carbonate-cemented sandstone reservoirs are more geochemically active than silicate-cemented formations.
3. In addition, the chemical and mineralogical results show the possibility of the occurrence of quartz mineral reaction in both formations. However, the quartz mineral reaction is be minor compared to the reaction of calcite minerals observed in both formations. This confirms the chemical stability of quartz compared to calcite in the CO₂ sequestration environment.
4. According to the mechanical test results, carbonate-cemented sandstone shows the lowest strength characteristics compared to silicate-cemented sandstone upon exposure to CO₂.
5. Finally, it can be concluded that silicate-cemented sandstone in the Gosford basin has more suitable characteristics than carbonate-cemented sandstone in terms of strength and chemical stability upon exposure to CO₂. These two different behaviours should be carefully considered during the site selection process.

8.1.1.2 Numerical work

The development of laboratory-scale simulations is essential for research studies of CO₂ sequestration in deep saline aquifers. The COMSOL software, which has the capability to couple multi-physics, was used to implement a numerical model to simulate the mechanical behaviour of reservoir rock under high salinity conditions. Finally, the model was extended to predict the mechanical behaviour of reservoir rock under high confining pressure conditions. According to the basic model developed:

1. The stiffness degradation approach can be successfully used to simulate the measured stress-strain data of Hawkesbury sandstone under brine saturation conditions, especially at high confinements, which cannot be experimentally investigated under existing laboratory conditions.

8.1.2 Conclusions regarding flow behaviour of deep saline reservoir rock in natural and CO₂-sequestered environments

8.1.2.1 Experimental work

The present study conducted a number of experiments to identify the combined geochemical, mineralogical and permeability effects on long-term sequestration in deep saline aquifers. This experiment study started by investigating the natural aquifer (only brine-saturated without CO₂ reaction) flow behaviour under different salinity conditions. A series of high-pressure triaxial experiments was, therefore, performed to investigate the effect of salinity, injection pressure including CO₂ phase change, and confining pressure on effective CO₂ permeability in Hawkesbury sandstone. The selected brine concentrations were 0, 10, 20 and 30% NaCl by weight and the experiments were conducted for a range of CO₂ injection (2-12MPa) and confining (20-35MPa) pressures at a temperature of 35°C. The following conclusions can be drawn based on these studies:

1. The presence of high concentrations of NaCl in the aquifer pore fluid causes the Hawkesbury rock's permeability to be reduced, and this effect increases with increasing NaCl concentration in the pore fluid. The observed permeability reduction with increasing salinity is due to NaCl crystallisation in the rock pore structure, which reduces the reservoir's effective permeability by obstructing the flow paths.

2. The effective CO₂ permeability of reservoir rock decreases significantly with increasing confining pressure due to the closure of some internal fractures and inter-connected flow pathways under increased effective stress.
3. The effective CO₂ permeability of reservoir rock increases with increasing injection pressure under any confining pressure conditions due to the opening of existing pores and new flow pathways for CO₂ movement.
4. The resulting NaCl crystallisation process alters the pore geometry, causing the simple effective stress law for permeability to be inapplicable to saline aquifers. The effective stress coefficient for saline aquifer permeability decreases with increasing salinity level.

After identifying the natural aquifer behaviour without CO₂ reaction, a comprehensive chemical, mineralogical and permeability investigation was carried out to combine the chemical and mineralogical changes on the long-term flow behaviour of reservoir rock. Hawkesbury sandstone samples were first reacted to a mixture of brine and super-critical CO₂ and the changes caused by CO₂ were identified by comparison with samples exposed to plain brine and brine-saturated with N₂. According to the results:

1. The interaction between injected CO₂ and aquifer brine causes a carbonic acid to form, which causes a significant pH drop in the aquifer pore fluid. The resulting acidic environment then reacts with reservoir rock minerals.
2. Long-term CO₂ reaction causes significant rock mineral alterations to occur in the reservoir pore structure. The CO₂+brine reaction in this study caused significant dissolution of some rock minerals, including calcite, siderite, quartz and barite minerals. Of these, the dissolution of calcite and quartz dissolution was prominent.
3. The significant rock mass mineralogical and pore structure alterations caused by long-term CO₂ interaction with the Hawkesbury formation causes its permeability to be enhanced by around 10%.
4. The pore structure alterations caused by CO₂ interaction also affect the effective stress response of the aquifer rock mass, and a significant increase in effective stress coefficient from around 0.95 to 3.5 was observed in this study.

5. Although present study observed mineral dissolution-dominant enhanced flow behaviour in the Hawkesbury formation, there may be completely different behaviours (such as mineral precipitation-dominant reduced flow behaviours) in different aquifer formations, depending on the reactivity of the rock minerals. Therefore, it is important to investigate the influence of different mineral compositions on the flow behaviour of reservoir rock in deep saline aquifers, because geochemical and mineralogical responses upon exposure to CO₂ can significantly change from aquifer to aquifer.

In addition, a comprehensive study was carried out on CO₂-reacted Hawkesbury sandstone to identify the influence of overburden load variations on the long-term flow performance of CO₂ storage in deep saline aquifers. High-pressure triaxial strength and permeability tests, coupled with acoustic emission (AE) and scanning electron microscopy (SEM) analyses, were conducted. The following conclusions can be drawn based on this study:

1. Increasing the stress applied on the aquifer causes its flow ability to reduce to some extent due to pore matrix compaction. Further increasing of the overburden pressure may accelerate the aquifer's flow performance due to dilation-induced pore opening
2. However, dilation-induced pore opening may create sudden leakage (exceeding the acceptable rate proposed by many regulatory frameworks) of injected CO₂ from the reservoir, causing pollution of surrounding freshwater aquifers.

Finally, a study was conducted to identify a potential CO₂ storage capacity-enhancement technique: enhancement of CO₂ storage through co-injection, or the simultaneous injection of CO₂ and brine into saline aquifers. A series of triaxial permeability tests on brine-saturated sandstone samples for a range of injection pressures (4-10MPa) under different confining pressures (20-35MPa) was performed at 35°C constant temperature. To clearly identify the sequestration-enhancement capability of the proposed method, conventional CO₂ injection (injection of only CO₂ into brine-saturated rock) was also performed under the same test conditions. Both tests were subjected to comprehensive chemical analyses to evaluate the alteration of CO₂ solubility in brine caused by the proposed method. Based on the experimental results, the following major conclusions can be drawn:

1. The resulting sudden increase in advective flux after some time of conventional CO₂ injection reduces the carbonation efficiency and eventually the mineral trapping mechanism, and

therefore negatively affects the CO₂ storage process. Such issues can be eliminated by the proposed CO₂-brine co-injection technique.

2. The proposed CO₂-brine co-injection also enhances solubility trapping. This is confirmed by the greater pH reduction and H^+ accumulation observed in the effluent produced in co-injection compared to conventional injection.

3. CO₂-brine co-injection creates reduced CO₂ relative permeability in saline aquifers, and the associated improved hydrodynamic trapping mechanism confirms that it is a safer CO₂ storage process in saline aquifers, with minimal risk of potential CO₂ leakage from the aquifer to surrounding freshwater aquifers.

4. The extensive time required for CO₂ solubility in brine is one of the major disadvantages of CO₂ sequestration in saline aquifers. Therefore, the ability to address this issue using the novel co-injection concept is a ground-breaking finding for CO₂ sequestration in saline aquifers.

8.1.2.2 Numerical work

As the first step in the development of the field-scale flow model, a basic laboratory-scale flow model was developed using the COMSOL Multiphysics simulator to simulate CO₂ flow through reservoir rock samples. A 2-D axisymmetric poro-elastic model was developed using the poro-elastic module available in COMSOL and the Buckley-Leverett flow theory was applied to the model using pre-defined partial differential equations. The developed model was first validated using experimental permeability data conducted under triaxial drained conditions and the model was then extended to predict the relative flow characteristics. According to the results:

1. The Buckley-Leverett flow concept can be successfully used to simulate the relative flow behaviour of brine-saturated Hawkesbury formation, and the results are relatively close to the experimental data with less than 10% relative error.

2. The liquid-phase diffusion coefficient plays a considerable role in defining the final distribution of brine and CO₂ and convergence analysis found that the best value lies between 10^{-10} - 10^{-13} m²/s.

Finally, the developed laboratory-scale flow model was extended into a field-scale model to predict the behaviour of Hawkesbury sandstone under field conditions. After developing the

model, the model was validated using data from the Dogger aquifer in the Paris basin and finally, the model was extended to simulate the Hawkesbury formation. According to the results, the following major conclusion can be drawn:

1. The developed model reveals the importance of considering geochemical and mineralogical reactions when evaluating the integrity of any deep saline sequestration project. According to the results, rock mineral alteration appears to play a considerable role in reservoir pressure distribution and CO₂ plume movement.

8.2 Suggestions for future research

1. It is proposed to perform hydro-mechanical tests on much larger specimens (about 1m in height and 0.5m in diameter). This will help to understand the influence of the heterogeneous nature of deep saline reservoir rock, which is highly relevant to our understanding of the actual behaviour of reservoir rock in deep saline aquifers. This could possibly be carried out using the triaxial set-up available in the Deep Earth Energy Laboratory in the Civil Engineering Department at Monash University.

2. In this study the effects of different mineralogical compositions on reservoir hydro-mechanical properties were investigated only for sandstones composed of quartz, calcite and kaolinite (major rock minerals). However, the presence of other major rock minerals in the reservoir rock matrix could significantly affect hydro-mechanical behaviour observed in the present study. Therefore, it is important to investigate the influence of other mineral combinations, such as quartz and feldspar, quartz and albite, and quartz and microcline, to better understand deep saline reservoir behaviour during CO₂ sequestration.

3. In relation to strength tests, in this study the influence of sub- and super-critical CO₂ reactions on reservoir mechanical properties were evaluated only by performing unconfined compressive strength tests. However, in order to understand the real field effects on reservoir mechanical properties, it is important to conduct triaxial experiments in a confining environment. Therefore, it is proposed to repeat the strength tests under triaxial test conditions and evaluate the influence of sub- and super-critical CO₂ on reservoir mechanical properties under confining stress conditions.

4. In this study the effect of the CO₂ reaction on reservoir permeability characteristics was investigated only for samples reacted at 10MPa CO₂ injection pressure under super-critical

conditions. Therefore, it is also proposed to conduct permeability tests for CO₂-reacted samples under different injection pressure conditions, including both sub- and super-critical conditions.